

U.S. DEPARTMENT OF
ENERGY

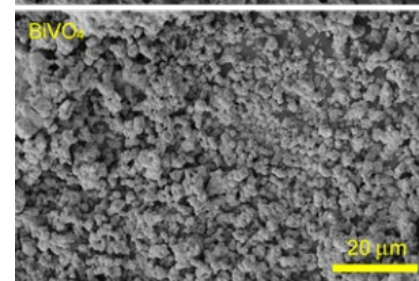
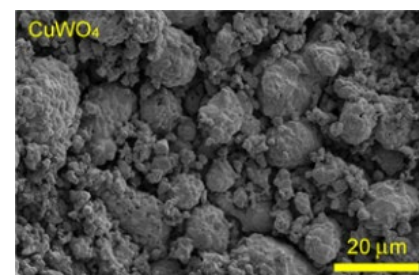
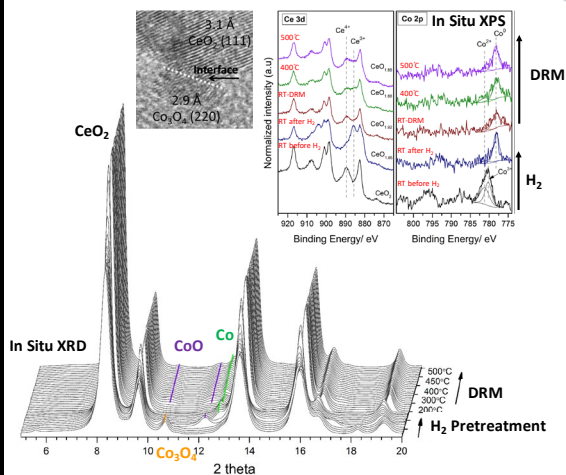
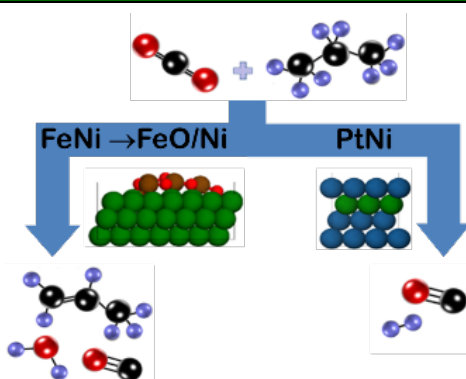
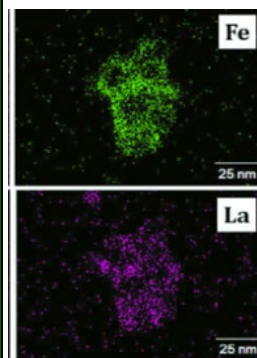
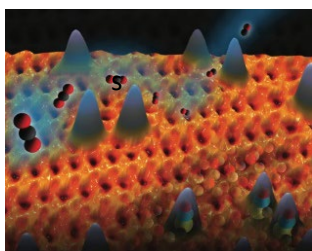
Office of
Science

2018 Catalysis Science PI Meeting
Harnessing Complexity in Catalysis

Gaithersburg Marriot Washingtonian Center

Gaithersburg, MD

July 30-August 1, 2018



Program and Abstracts for the

2018 BES/Catalysis Science Research PI Meeting: *“Harnessing Complexity in Catalysis”*



U.S. DEPARTMENT OF
ENERGY

Office of
Science

Gaithersburg Marriott Washingtonian Center
Gaithersburg, Maryland
July 30-August 1, 2018

The research grants and contracts described in this document are supported by the U.S. Department of Energy, Office of Science/Basic Energy Sciences, as part of the Catalysis Science Program within the Chemical Sciences, Geosciences and Biosciences Division.

FOREWORD

The 2018 Catalysis Science Research PI Meeting is sponsored by the Division of Chemical Sciences, Geosciences and Biosciences, Office of Basic Energy Sciences (BES), U.S. Department of Energy. It is being held on July 30–August 1, 2018, at the Marriott Washingtonian Hotel in Gaithersburg, Maryland. The purposes of this meeting are to discuss the recent advances in the chemical, physical, and biological bases of catalysis science, to foster exchange of ideas and cooperation among BES/Catalysis Science Program PIs, and to discuss the new science challenges and opportunities recently emerging in catalytic technologies for energy production and use.

Catalysis research activities within BES emphasize fundamental research aimed at understanding reaction mechanisms and, ultimately, controlling the chemical conversion of natural and artificial feedstocks to useful energy carriers. The long-term goals of this research are to discover fundamental scientific principles, and to produce insightful approaches for the prediction of catalyst structure-reactivity behavior. Such knowledge, integrated with advances in chemical and materials synthesis, *in-situ* and *operando* analytical instrumentation, chemical kinetics and dynamics measurements, and computational chemistry methods, will allow the control of chemical reactions along desired pathways. This new knowledge will impact the efficiency of conversion of natural resources into fuels, chemicals, materials, or other forms of energy, while minimizing the impact to the environment.

This year's meeting pursues the continuing goal of highlighting the potential advances in catalysis science of special relevance to the energy, economic and environmental future of the U.S., with the theme of the "*Harnessing Complexity in Catalysis*". Indeed, catalytic processes continue to account for ~90% of chemical manufacturing, with more than 20% of all industrial products employing catalytic processes in their manufacture. Also significant are the continuing contributions of catalysis for processes leading to cleaner air and water. This year's program includes special sessions on Synergistic Crosscutting Division Themes and their Role in Catalysis, Data Science in Catalysis, in addition to 18 oral and 55 poster presentations by BES/Catalysis Science PIs.

Special thanks go to the program investigators and their students, postdocs, and collaborators for their dedication to the continuous success and visibility of the BES/Catalysis Science Program. We also thank Teresa Crockett³, and the Oak Ridge Institute for Science and Education staff (Connie Lansdon and Linda Severs) for the logistical and web support of the meeting. Finally very special thanks go to Raul Miranda³ for his longstanding and continuing contributions to the BES/Catalysis Science Program, now from his role as Team Lead for Chemical Transformations in the BES/Chemical Sciences, Geosciences and Biosciences Division.

Bill Jones¹, Daniel Resasco², Viviane Schwartz³, and Chris Bradley³

¹University of Rochester

²University of Oklahoma

³Catalysis Science Program - Office of Basic Energy Sciences - U.S. Department of Energy

2018 Catalysis Science PI Meeting Harnessing Complexity in Catalysis

July 30-August 1, 2018
Marriott Washingtonian, Gaithersburg, MD

Program chairs: Bill Jones and Daniel Resasco

Monday Morning, July 30

7:30-8:30 am **Registration and Breakfast**

OPENING SESSION

Session Chairs: **Bill Jones and Daniel Resasco**

8:30-9:00 am Welcoming Remarks and Program Updates

Viviane Schwartz and Chris Bradley, DOE/BES/Catalysis Science Program

9:00-9:10 am PI Meeting Theme – *“Harnessing Complexity in Catalysis”*

Bill Jones, University of Rochester and **Daniel Resasco**, University of Oklahoma

9:10-9:30 am BES Update

Raul Miranda, Team Lead, DOE/BES/Chemical Sciences, Geosciences and Biosciences Division

PLENARY SESSION I – Synergistic Theme Crosscuts

Session Chairs: **Bill Jones**, University of Rochester and **Daniel Resasco**, University of Oklahoma

9:30-10:10 am *“Atomic Precision Studies of Molecular Catalyst Reactions using X-Ray Lasers”*

Amy Cordones-Hahn, SLAC

10:10-10:20 am Discussion

10:20-10:35 am **Coffee Break**

10:35-11:15 am *“Accessing the Reactive Intermediates of Enzymes that Catalyze H₂ and N₂ Activation”*

Paul King, NREL

11:15-11:25 am Discussion

11:25 am-12:05 pm “High Throughput Experimentation and Data-driven Understanding of Fundamental Processes at the Intersection of Materials and Catalysis Sciences”

John Gregoire, JCAP

12:05-12:15 pm Discussion

12:15-1:30 pm **Working Lunch**

Monday Afternoon, July 30

PI SESSION I – Design of Catalysts Beyond the Binding Site

Session Chair: **Alex Katz**, UC Berkeley

1:30-2:00 pm “Bio-inspired Oxyanion Reduction”

Alison Fout, University of Illinois Urbana-Champaign

2:00-2:10 pm Discussion

2:10-2:40 pm “Computational Catalysis at the Solid-liquid Interface and Approaches for Coping with Complexity”

Andreas Heyden, University of South Carolina

2:40-2:50 pm Discussion

2:50-3:20 pm “Positioning Active Sites in Catalytic Materials – From Cooperative Catalysis to Cascade Catalysis in Multicompartment Nanoreactors”

Chris Jones, Georgia Tech

3:20-3:30 pm Discussion

3:30-3:45 pm **Coffee Break**

PI SESSION II – Addressing Selectivity in Catalysis

Session Chair: **Bob Waymouth**, Stanford University

3:45-4:15 pm “Approaches to Selectivity in Catalysis”

Melanie Sanford, University of Michigan

4:15-4:25 pm Discussion

4:25-4:55 pm “Complexity in Synthesis and Selective Oxidation Catalysis”

Steve Suib, University of Connecticut

4:55-5:05 pm Discussion

5:05-7:00 pm **Dinner (on your own)**

Monday Evening, July 30

Poster SESSION I

7:00-9:00 pm (Odd numbers)

Tuesday Morning, July 31

7:30-8:30 am **Breakfast**

PI SESSION III – Transformations Involving Carbon Dioxide

Session Chair: **Jingguang Chen**, Columbia

8:30-9:00 am “The Effect of Lewis Acid Co-Catalysts on the Reversible Hydrogenation of Carbon Dioxide to Formic Acid and Methanol”

Wes Bernskoetter, University of Missouri- Columbia

9:00-9:10 am Discussion

9:10-9:40 am “Bio-Inorganic Approaches to Molecular Electrocatalysis”

Chris Chang, LBNL/UC Berkeley

9:40-9:50 am Discussion

9:50-10:20 am “Using Free Energies for H⁺ and H⁻ Transfers to Design Catalysts for the Reduction of CO₂”

Aaron Appel, PNNL

10:20-10:30 am Discussion

10:30-10:45 am **Coffee Break**

PI SESSION IV – Data Science in Catalysis

Session Chair: **Manos Mavrikakis**, University of Wisconsin

10:45-11:15 am “Towards Modeling Complexity in Catalysis with Density Functional Theory, Machine Learning, and Molecular Simulation”

John Kitchin, Carnegie Mellon University

11:15-11:25 am Discussion

11:25-11:55 am “Machine Learning Acceleration of Computational Catalysis Studies”

Thomas Bligaard, SLAC

11:55-12:05 am Discussion

12:05-1:00 pm **Working Lunch**

Tuesday Afternoon, July 31

Panel Session – Opportunities for Data Science in Catalysis

Session Chairs: **Viviane Schwartz** and **Chris Bradley**, DOE/BES/Catalysis Science Program

1:00-3:00 pm Panel Discussion

3:00-3:15 pm **Coffee Break**

PI SESSION V – Reaction Networks and Complex Catalytic Environments

Session Chair: **Dan Mindiola**, Penn

3:15-3:45 pm “Homogeneous Catalysis Meets Heterogeneous Catalysis: Alkanes and Alkenes Transformations”

Max Delferro, Argonne National Laboratory

3:45-3:55 pm Discussion

3:55-4:25 pm “Kinetic and Spectroscopic Studies of Catalytic Mechanisms: Hydrodeoxygenation of Biomass Feedstocks on Transition Metal Phosphides”

Ted Oyama, Virginia Tech

4:25-4:35 pm Discussion

4:35-5:05 pm “Carbenes as Powerful Ligands for Transition Metal Catalysts and as Small Molecule Activators on their Own Rights”

Guy Bertrand, UC-San Diego

5:05-5:15 pm Discussion

5:15-7:30 pm **Dinner (on your own)**

Tuesday Evening, July 31

Poster SESSION II

7:30-9:30 pm (Even numbers)

Wednesday Morning, August 1

7:30-8:30 am **Breakfast**

PI SESSION VI – Dynamic Evolution of Catalysts

Session Chair: **Abhaya Datye**, University of New Mexico

8:30-9:00 am “Pathways for Methanol Synthesis from the Conversion of C-H bonds over Well-defined Metal-Oxide Surfaces”

Sanjaya Senanayake, Brookhaven National Laboratory

9:00-9:10 am Discussion

9:10-9:40 am "Nanoparticle Catalyst and Other Particle Formation—*Disproof-based, Minimalistic*—Mechanisms: Extracting Broadly Applicable Simplicity from Nature’s Complexity”

Rick Finke, Colorado State University

9:40-9:50 am Discussion

9:50-10:20 am “Single Metal Atoms in Alloys and Oxides as Catalysts for Chemicals Production”

Charlie Sykes, Tufts University

10:20-10:30 am Discussion

10:30-10:45 am **Coffee Break**

PI SESSION VII – Reaction Networks and Complex Catalytic Environments II

Session Chair: **Yuriy Román**, MIT

10:45-11:15 am “The Catalytic Science of Making Up and Breaking Up Nitrogen”

Bill Schneider, University of Notre Dame

11:15-11:25 am Discussion

11:25-11:55 am “Unique Local Catalytic Environments in Cellulose Depolymerization”

Matthew Neurock, University of Minnesota

11:55 am-12:05 pm Discussion

Closing Session

12:05-12:15 pm Final Remarks

Bill Jones, Daniel Resasco, Viviane Schwartz, and Chris Bradley

12:15 pm Adjourn

Poster Sessions

Monday, July 30, 2018

Dave Cox
Tom Jaramillo, SLAC
Manos Mavrikakis
Eric McFarland
Will Medlin
Dan Mindiola
Buddie Mullins
Eranda Nikolla
Jack Norton
Colin Nuckolls
Marek Pruski, Ames
Daniel Resasco
Fabio Ribeiro
Jose Rodriguez, BNL
Yuriy Roman
Aaron Sadow, Ames
Annabella Selloni
Wendy Shaw, PNNL
Carsten Sievers
Igor Slowing, Ames
Mitch Smith
Jin Suntivich
Yogi Surendranath
Steve Tait
Bin Wang
Bob Waymouth
Mike White, BNL
Ross Widenhoefer
Zili Wu, ORNL
Bingjun Xu
Ye Xu

Tuesday, July 31, 2018

Simon Bare, SLAC
Bart Bartlett
Suzanne Blum
Charlie Campbell
Jingguang Chen
Miaofeng Chi, ORNL
Dick Crooks
Abhaya Datye
Zdenek Dohnalek, PNNL
Melis Duyar, SLAC
Dan Ess
Josh Figueroa
Bruce Gates
Vanda Glezakou, PNNL
Ray Gorte
Lars Grabow
Oliver Gutierrez-Tinoco, PNNL
Nilay Hazari
Stepan Irle, ORNL
Seung Soon Jang
Mike Janik
Bill Jones
Alex Katz
Cong Liu, ANL
Ping Liu, BNL
Raul Lobo
Matt Neurock

TABLE OF CONTENTS

TITLE PAGE	i
FOREWORD	ii
AGENDA	iii
TABLE OF CONTENTS	x
ABSTRACTS.....	1
<u>Plenary Session Abstracts</u>	
<i>Atomic Precision Studies of Molecular Catalyst Reactions using X-Ray Lasers</i> Amy Cordones-Hahn (SLAC)	3
<i>Accessing the Reactive Intermediates of Enzymes that Catalyze H₂ and N₂ Activation</i> Paul King (NREL)	4
<i>High Throughput Experimentation and Data-driven Understanding of Fundamental Processes at the Intersection of Materials and Catalysis Sciences</i> John Gregoire (JCAP/CalTech).....	5
<u>Principal Investigator Abstracts</u>	
<u>Oral Sessions</u>	
<i>Bio-inspired Oxyanion Reduction</i> Alison Fout (University of Illinois-Urbana Champaign)	7
<i>Theoretical Investigation of Heterogeneous Catalysis at the Solid-Liquid Interface for the Conversion of Lignocellulosic Biomass Model Molecules</i> Andreas Heyden (University of South Carolina)	8
<i>Positioning Active Sites in Catalytic Materials – From Cooperative Catalysis to Cascade Catalysis in Multicompartment Nanoreactors</i> Chris Jones (Georgia Tech).....	11
<i>Ion Exchange Approach for Incorporating Cations in Metal Organic Frameworks: Challenges and Opportunities</i> Melanie Sanford (University of Michigan).....	20
<i>Selective Oxidation Catalysis</i> Steve Suib (University of Connecticut)	24
<i>The Effect of Lewis Acid Co-Catalysts on the Reversible Hydrogenation of Carbon Dioxide to Formic Acid and Methanol</i> Wesley Bernskoetter (University of Missouri).....	36
<i>Bio-Inorganic Approaches to Molecular Electrocatalysis</i> Chris Chang (UC Berkeley and LBNL)	40

<i>Using Free Energies for H⁺ and H⁻ Transfers to Design Catalysts for the Reduction of CO₂</i> Aaron Appel (PNNL)	42
<i>Designing single-atom alloys with DFT, machine learning and atomistic simulations</i> John Kitchin (Carnegie Mellon University).....	43
<i>Machine Learning Acceleration of Computational Catalysis Studies</i> Thomas Bligaard (SLAC)	**
<i>Homogeneous Catalysis Meets Heterogeneous Catalysis: Alkanes and Alkenes Transformations</i> Max Delferro (ANL)	46
<i>Kinetic and Spectroscopic Studies of Catalytic Mechanisms: Hydrodeoxygenation of Biomass Feedstocks on Transition Metal Phosphides</i> Ted Oyama (Virginia Tech)	47
<i>Novel Stable Carbenes and their Applications in Catalysis</i> Guy Bertrand (UC San Diego)	51
<i>Pathways for Methanol Synthesis from the Conversion of C-H bonds over Well-defined Metal-Oxide Surfaces</i> Sanjaya Senanayake (BNL)	56
<i>Dust Effects On Nucleation Kinetics and Resultant Catalytic Nanoparticle Product Size-Distributions: An Illustrative Case Study of a Prototype, Catalytically Active Ir(O)_n Transition-Metal Nanoparticle Formation System</i> Rick Finke (Colorado State University)	57
<i>Single metal atoms in alloys and oxides as catalysts for chemicals production</i> Charlie Sykes (Tufts University).....	61
<i>Modeling and Exploiting Non-idealities in Nitrogen Catalysis</i> Bill Schneider (University of Notre Dame)	67
<i>Unraveling the Catalytic Transformations Drive the Activation of Cellulose</i> Matthew Neurock (University of Minnesota).....	70

** Talk was given, but no abstract was provided.

Poster Sessions

<i>Development of in-situ/operando Catalyst Characterization Capabilities as SSRL: Progress Report</i> Simon Bare (SUNCAT/SLAC National Accelerator Laboratory)	73
<i>Exploring Nanoparticle Photocatalysts for Room Temperature, Aerobic Organic Oxidations</i> Bart Bartlett (University of Michigan)	74
<i>Single Turnover at Molecular Catalysts</i> Suzanne Blum (UC Irvine).....	77
<i>Supported Metal Nanoparticles: Correlating Structure with Catalytic Function through Energetics</i> Charlie Campbell (University of Washington).....	80

<i>Metal Carbides and Bimetallic Alloys as Low-cost Electrocatalysts</i> Jingguang Chen (Columbia University)	84
<i>Elucidating Chemical and Electronic Interactions of Metal-Support Interfaces via STEM</i> Miaofeng Chi (ORNL)	90
<i>MnO(100): Initial Experimental Benchmarks for Adsorption and Co-Adsorption on the Ordered Surface and Oxidation to Mn³⁺ Surface Compounds</i> David Cox (Virginia Polytechnic Institute and State University)	91
<i>Electrocatalytic Reduction of Oxygen on Metal Nanoparticles in the Presence and Absence of Interactions with Metal-Oxide Supports</i> Richard Crooks (University of Texas, Austin)	95
<i>Sub Nanometer Sized Clusters for Heterogeneous Catalysis</i> Abhaya Datye (University of New Mexico)	99
<i>Catalytic Chemistry of Oxide Supported Single Palladium Atoms</i> Zdenek Dohnalék (Pacific Northwest National Laboratory)	106
<i>Discovery and Development of Heterogeneous Catalysts for Higher Alcohol Synthesis</i> Melis Duyar (SLAC)	107
<i>Theory, Simulation, and Design of High-Oxidation State Main-Group Metal Catalysts for Hydrocarbon C-H Functionalization</i> Dan Ess (BYU)	108
<i>Twists to the Cluster-Surface Analogy: New Strategies for the Synthetic Manipulation of Strong-Field Metal-Carbonyl Clusters</i> Joshua Figueroa (UC San Diego)	112
<i>Supported Molecular Metal Catalysts: Single-Sites to Pair-Sites to Metal Clusters</i> Bruce Gates (University of California, Davis)	116
<i>Complexity in catalysis through the lens of large scale molecular simulations</i> Vanda Glezakou (PNNL)	122
<i>Fabrication of Nano-Structured Catalyst Supports by ALD</i> Ray Gorte (University of Pennsylvania)	123
<i>Tailoring surface oxygen affinity for selective reduction reactions</i> Lars Grabow (University of Houston)	126
<i>Mechanism and energetic landscapes of acid-catalyzed alcohol dehydration in condensed phases: towards understanding confinement and solvent effects</i> Oliver Y. Gutierrez-Tinoco (PNNL)	131

<i>The Rational Design of Improved Base Metal Catalysts for Carbon Dioxide Valorization and Hydrogen Production</i> Nilay Hazari (Yale University)	132
<i>Performance evaluation of the density-functional tight-binding method for catalysis applications</i> Stephan Irle (ORNL)	136
<i>Positioning Active Sites in Catalytic Materials – From Cooperative Catalysis to Cascade Catalysis in Multicompartment Nanoreactors</i> Seung Soon Jang (Georgia Tech)	138
<i>N₂ electroreduction catalysis – design of the near surface environment for enhanced selectivity</i> Michael Janik (Penn State).....	139
<i>Transition Metal Activation and Functionalization of C-H and C-C Bonds</i> Bill Jones (University of Rochester)	142
<i>Confinement of Supported Molecular Active Sites in Cups: A Comparative Study of Homogeneous, Amorphous, and Crystalline Catalysts</i> Alex Katz (UC Berkeley).....	146
<i>Computational Studies of Bimetallic Nano-Cluster for Non-Oxidative Dehydrogenation of Light Alkanes</i> Cong Liu (Argonne National Laboratory)	150
<i>Reforming of Methane on Single Site Catalysts</i> Ping Liu (Brookhaven National Laboratory)	151
<i>CO₂-Assisted Ethane Dehydrogenation and Aromatization over Zn-Containing Zeolites</i> Raul Lobo (University of Delaware).....	152
<i>Atomic-scale Design of Metal and Alloy Catalysts: A Combined Theoretical and Experimental Approach</i> Manos Mavrikakis (University of Wisconsin).....	156
<i>Fundamental Mechanisms of C-X bond Transformations on Complex Molten Surfaces</i> Eric McFarland (University of California, Santa Barbara)	163
<i>Tuning Selectivity on Metal Oxide Catalysts and Supports with Organic Monolayers</i> J. Will Medlin (University of Colorado, Boulder).....	169
<i>Expounding the Chemistry of Molecular Nitrides and Phosphides in Groups 3 and 5 Transition Metals and the Selective Catalytic Monoborylation of Methane</i> Daniel Mindiola (University of Pennsylvania)	173
<i>Surface Chemistry Experiments Related to Fischer-Tropsch Synthesis on Cobalt Deposited on Au(111)</i> C. Buddie Mullins (University of Texas, Austin)	176
<i>Elucidating and Controlling Active Sites and their Environments in the Electrocatalytic Reduction of CO₂ over Post Transition Metals</i> Matthew Neurock (University of Minnesota).....	180

<i>Efficient Oxygen Electrocatalysis by Nanostructured Mixed-Metal Oxides</i>	
Eranda Nikolla (Wayne State University).....	182
<i>Effect of Polarity Matching on Kinetics of Hydrogen Atom Transfer from Transition-Metal Hydrides to Trityl Radicals</i>	
Jack Norton (Columbia University).....	186
<i>Designing Catalytic Spaces in Organic Semiconductors</i>	
Colin Nuckolls (Columbia University)	190
<i>Functionalization of oxide and zeolite catalysts to improve tolerance to hot liquid water</i>	
Daniel Resasco (University of Oklahoma)	194
<i>Fundamental Studies of Oxidation Reactions on Model Catalysts: Product Inhibition and Mechanism for Propylene Epoxidation on Au/TS-1</i>	
Fabio Ribeiro (Purdue University)	199
<i>Demystifying atomic environments within heteroatom substituted zeolite frameworks with solid-state nuclear magnetic resonance</i>	
Yuriy Roman-Leshkov (MIT)	202
<i>Structural evolution of titanium dioxide during reduction in high pressure hydrogen</i>	
Annabella Selloni (Princeton University)	206
<i>Cooperativity of the outer coordination sphere with the active site for molecular catalysts for small molecule conversions</i>	
Wendy Shaw (PNNL).....	210
<i>Conversion of Methane over NiO/Ce_xZr_{1-x}O₂ Catalysts</i>	
Carsten Sievers (Georgia Institute of Technology).....	211
<i>Electrocatalytic ammonia splitting at ambient temperatures</i>	
Milton R. Smith, III (Michigan State University).....	215
<i>Measurements of the Oxygen Electroadsorption on Well-defined IrO₂ and RuO₂: A Discussion of the Scaling Relation and Sabatier Principle</i>	
Jin Suntivitch (Cornell University).....	216
<i>Graphite-Conjugated Catalysis</i>	
Yogesh Surendranath (MIT)	217
<i>Platinum Single-site Centers through Metal-ligand Self-assembly on Powdered Metal Oxide Supports and their Selective Catalytic Activity</i>	
Steven L. Tait (Indiana University).....	222
<i>Water Trapped at the Interface of Hydrophobized Catalysts for C-C Coupling Reactions</i>	
Bin Wang (University of Oklahoma)	227

<i>Selective Catalytic Oxidations: Scope and Mechanism</i> Robert Waymouth (Stanford University).....	228
<i>Size-Selected Metal Oxide Clusters as Model Inverse Catalysts</i> Michael G. White (Brookhaven National Laboratory and Stony Brook University).....	232
<i>Force/Activity Relationships in Transition Metal-Catalysis</i> Ross Widenhoefer (Duke University)	233
<i>Electrochemical Nitrogen Reduction Reaction on Metal Nitrides</i> Bingjun Xu (University of Delaware).....	236
<i>Interaction of Hydrogen with CoCrFeNi High Entropy Alloys</i> Ye Xu (LSU)	239
<i>Interfacial catalysts for transformations of oxygenates: construction, characterization, catalytic activity and reaction mechanisms</i> Aaron Sadow (Ames FWP)	240
<i>Tunable Single-Site Catalysts for Selective Functionalization of Alkanes</i> Max Delferro (ANL FWP).....	250
<i>In-situ Studies for the Conversion of C-O Bonds on Complex Metal-Oxide Interfaces</i> José A. Rodriguez (BNL FWP)	258
<i>Fundamentals of Catalysis and Chemical Transformations</i> Zili Wu (ORNL FWP)	270
<i>Transdisciplinary Approaches to Realize Novel Catalytic Pathways to Energy Carriers</i> Johannes Lercher (PNNL FWP).....	282
<i>Catalyzing electrochemical transformations involving H₂O, O₂, H₂, and H₂O₂</i> Thomas Jaramillo (SUNCAT FWP).....	306
LIST OF PARTICIPANTS	319

ABSTRACTS

Atomic Precision Studies of Molecular Catalyst Reactions using X-Ray Lasers

Amy Cordones-Hahn
PULSE Institute, SLAC National Laboratory Accelerator

Presentation Abstract

Electronic excitation of molecular catalysts has the potential to drive their catalytic reactions, which include multiple changes in charge distribution and nuclear structure. Photo-induced redox process may be highly localized or delocalized over the full molecule and photo-induced structural changes may include reactant bonding that occurs at metal or ligand sites. The atomic precision of x-ray spectroscopy enables the real-time mapping of charge distribution and bond making/breaking processes during multi-step reactions, and has the potential to directly probe and resolve catalytic reaction mechanisms. For molecular catalysts based on first row transition metals and redox-active ligands, the localization of redox or bonding changes on metal or ligand sites often cannot be determined by traditional experimental methods. For this class of systems, multi-edge X-ray absorption spectroscopy tuned to selectively probe metal or ligand core level transitions has the potential to resolve transient changes in charge or bonding at metal and ligand atomic sites during photoinduced catalytic reactions.

In this presentation, I will discuss how LCLS-II will enable time-resolved multi-edge soft x-ray studies aimed at resolving the specific role of metal and ligand atomic sites in molecular photocatalysts with redox active ligands. I will present an example highlighting how multi-edge transient x-ray absorption enables determination of detailed photochemical reaction mechanisms, in the context of previous studies of a photochromic Ruthenium-sulfoxide complex. I will also present preliminary x-ray spectroscopic results for a class of Ni-centered hydrogen evolution electro- and photo-catalysts with redox active ligands. Static soft x-ray absorption tuned to the central Ni and ligand S atom edges was used to map the delocalization of the electron accepting orbitals that participate in the reduction reactions of these catalysts. These results support ligand-dependent differences in the proposed electrochemical reaction mechanisms of the catalysts. Preliminary transient hard x-ray spectroscopy on the hundred picosecond timescale will also be presented, with the goal to resolve photochemical product formation upon photoexcitation of the catalyst in the presence of electron and proton sources.

Accessing the Reactive Intermediates of Enzymes that Catalyze H₂ and N₂ Activation

Paul W. King^a, Jacob H. Artz^a, David W. Mulder^a, Katherine A. Brown^a, Derek F. Harris^b, Jesse Ruzicka^c, Lance C. Seefeldt^b, Gordana Dukovic^c, John W. Peters^d

^a Biosciences Center, National Renewable Energy Laboratory, Golden, CO 80401

^d Department of Chemistry and Biochemistry, Utah State University, Logan, UT 84322

^c Department of Chemistry and Biochemistry, University of Colorado Boulder, Boulder, CO 80309

^d Institute of Biological Chemistry, Washington State University, Pullman, WA 99163

Presentation Abstract

Reduction-oxidation (redox) enzymes catalyze the interconversion of electrochemical potential energy with chemical bonds in reactions that cover a wide range of small molecule activation chemistry. Understanding the guiding principles by which redox enzymes function can provide a foundation to help advance development of catalysts for conversion of abundant solar and wind energy into chemicals. Towards this goal, our work is addressing the mechanisms of enzymes that catalyze reactions that are critical to developing renewable energy economies, the reversible activation of H₂ by hydrogenase and the (photochemical) reduction of N₂ to NH₃ by nitrogenase. Our work on hydrogenases has shown enzymes that otherwise share a common catalytic cofactor have extremely different reactivity that span a wide range of reaction bias. Biophysical studies indicate that each enzyme varies in stabilization of different cofactor oxidation states implying they each operate in a distinct catalytic regime. Work on nitrogenase has focused on coupling the enzyme to light harvesting by nanoparticles for photochemically driven N₂ reduction to ammonia. This system is being developed to enable photo-trapping of reaction intermediates and to understand the relationship between electron flux and potential in the N₂ activation reaction. A summary of our research progress on these topics will be presented.

Plenary Session Abstracts

John M. Gregoire

High throughput experimentation and data-driven understanding of fundamental processes at the intersection of materials and catalysis sciences

John M. Gregoire

Joint Center for Artificial Photosynthesis (JCAP), California Institute of Technology

Presentation Abstract

The physical sciences increasingly leverage advances in modern computing, in particular catalysis science where ab initio methods enable many fundamental advancements science and machine learning methods have recently augmented computational chemistry. To realize the full potential of these methods, commensurate and complementary advancements in experimental catalysis science are needed. The Joint Center for Artificial Photosynthesis houses a concerted effort to develop high throughput experimental methods to meet this need, with efforts concentrated on heterogeneous (photo)electrocatalysis of solar fuels reactions such as the oxygen evolution reaction. Rapid synthesis and screening of material libraries enables evaluation of candidate materials proposed by high throughput computational screening, and as of this year, the majority of metal oxide photoanodes with visible band gap have been discovered by this type of theory-experiment integrated discovery pipeline. Some experiments produce datasets that are too large and complex to be interpreted by standard techniques or even expert researchers, motivating the deployment of machine learning methods and/or the development of artificial intelligence algorithms. Knowledge obtained from this integration of experiments and data science includes fundamental insights as well as guiding principles for directing future research efforts. In addition to highlighting several experiment-data science-theory research modalities that have proved successful, the presentation will also survey the suite of experimental and data management capabilities built particularly for these research purposes.

Monday PI

Oral Presentations

Bioinspired Oxyanion Reduction

Alison R. Fout, Courtney L. Ford, Yun Ji Park, Michael J. Drummond, and Tabitha Miller
University of Illinois at Urbana-Champaign

Presentation Abstract

The uses of nitrogen and chlorine oxyanions are both extensive and varied, with notable applications in bleaching agents, propellants, fertilizers, and explosives. Because of their high solubility and mobility in water, they have become pervasive contaminants in many sources of drinking water and pose a significant health risk. While remediation of these pollutants by traditional means is difficult, the metalloenzymes (per)chlorate reductase and chlorite reductase efficiently reduce (per)chlorate and chlorite, respectively, to benign products. Inspired by these biological systems, we designed a non-heme iron system featuring a secondary coordination sphere to facilitate the reduction of these oxyanions to more innocuous products. Addition of these oxyanions to the iron(II) system furnished an iron(III)-oxo complex which could be rendered catalytic with the addition of protons and electrons to release water. The catalytic reduction of perchlorate by the non-heme iron(II) system was also demonstrated. We propose that the non-covalent secondary coordination sphere interactions imparted by the ligand periphery stabilized intermediates and promoted deoxygenation of the oxyanions.

DE-SC0016026 : Bio-inspired Catalysts Featuring Earth Abundant Metals and Secondary Coordination Sphere Interactions for the Reduction of Oxyanions

Student(s): Courtney L. Ford, Yun Ji Park, Michael J. Drummond, and Tabitha Miller

Affiliations(s): (*include only if different from above*)

Publications Acknowledging this Grant in 2015-2018

1. Gordon, Z.; Drummond, M. J.; Bogart, J. A.; Schelter, E. J.; Lord, R. L.; Fout, A. R. "Tuning the Fe(II/III) Redox Potential in Non-heme Fe(II)-Hydroxo Complexes through Primary and Secondary Coordination Sphere Modifications." *Inorg. Chem.*, **2017**, *56*, 4852-4863.
2. Ford, C. L.;* Park, Y.;* Matson, E. M.; Gordon, Z.; Fout, A. R. "A bio-inspired iron catalyst for nitrate and perchlorate reduction." *Science*, **2016**, *354*, 741-743. *authors contributed equally. Highlighted in Halford, B. (2016, November). Iron complex reduces oxyanion pollutants. *C&EN*, 10, 94(45), p.10, and Brennan, M. (2017, January). Nitrate NO more. *Nature Chemistry* 9, p.8.
3. Matson, E. M.;* Park, Y.;* Bertke, J. A.; Fout, A. R. Synthesis and characterization of M(II) (M = Mn, Fe and Co) azafulvene complexes and their X₃⁻ derivatives. *Dalton. Trans.* 2015, 10377-10384. * authors contributed equally
4. Park, Y.;* Matson, E. M.;* Nilges, M.J.; Fout A. R. Exploring Mn–O Bonding in the Context of an Electronically Flexible Secondary Coordination Sphere: Synthesis of a Mn(III)-Oxo. *Chem. Comm.* **2015**, 5310-5313. * authors contributed equally

Theoretical Investigation of Heterogeneous Catalysis at the Solid-Liquid Interface for the Conversion of Lignocellulosic Biomass Model Molecules

Andreas Heyden
University of South Carolina, Department of Chemical Engineering

Presentation Abstract

The overall goal of this research program is the development and validation of a hierarchy of multi-scale methods for computing activation and reaction free energies of elementary processes occurring at metal-liquid interfaces that are only up to two orders of magnitude slower than current conventional catalysis tools for catalytic gas-solid studies. As a result, these novel tools will permit within a decade computational metal catalysis studies at solid-liquid interfaces with similar ease to current gas-metal catalysis studies (assuming a similar growth in computing infrastructure as seen in the past couple of decades). Our hierarchy of novel multi-scale methods starts with (i) the use of implicit solvation models to approximately describe solvation effects on elementary reactions at metal surfaces, (ii) the application of our hybrid quantum mechanics (QM) and molecular mechanics (MM) solvation scheme for computing free energies of reactions at metal-liquid interfaces, and (iii) the inclusion of solvent coordinates in the reaction coordinate when computing free energies with our QM/MM approach. As model systems for our computational study, we present recent results on the reductive deoxygenation of ethylene glycol over metal catalysts under aqueous-phase processing (APP) conditions.

DE-SC0007167: Theoretical Investigation of Heterogeneous Catalysis at the Solid-Liquid Interface for the Conversion of Lignocellulosic Biomass Model Molecules

Student(s): Mohammad Saleheen, Subrata Kundu, Adam Yonge, Mehdi Zare, Anand Verma

RECENT PROGRESS

Explicit solvation model for solid surfaces implementation, validation, and application

We continued our parameterization study of our explicit solvation model for metal surfaces (eSMS) method to improve its efficiency and better understand our error bars. Specifically, in collaboration with Dr. Michael Shirts from the University of Colorado, we improved upon our exponential averaging in our free energy calculations. Also, by using forward and reverse averaging (using BAR) and repeating each calculation at least 5 times (using a new ensemble), we are now able to provide reliable 95% confidence intervals for our free energy estimations. More importantly, we have been able to reduce the uncertainty in the prediction of free energies of activation and reaction in solution to below 0.1 eV (often +/- 0.05 eV). Significant phase space sampling is necessary for this reduction in uncertainty which is practically only possible with our QM/MM approach. Next, we applied our eSMS approach to the C-H and O-H bond cleavage of ethylene glycol on Pt(111) under aqueous-phase reforming conditions to explain the counter-

intuitive (and likely wrong) result of implicit solvation models that predict hardly any aqueous solvent effect in O–H bond cleavage (likely due to the inability of implicit solvation models to properly consider hydrogen bonding). Explicit solvation effect calculations (eSMS) agree with the implicit solvation models for C–H bond cleavage where they both predict a small solvation effect (~0.1-0.2 eV free energy barrier reduction and practically no effect on the free energy of reaction - the good agreement likely originates from a lack of changes in hydrogen bonding along the reaction coordinate). In contrast and unlike the implicit solvation models, our explicit solvation model predicts a larger solvent stabilization of both the transition state and product state in O–H bond cleavage due to its ability to approximately describe hydrogen bonding (0.4-0.5 eV reduction in activation free energy and 0.3-0.4 eV increase in the exergonicity of the reaction). As a result, O–H bond dissociations are significantly favored over C–H bond dissociations under aqueous processing conditions of biomass and aqueous solvation effects significantly change the reaction mechanism. Interestingly, we also showed that solvation effects on the enthalpy of reaction are significantly larger (roughly twice as large) than on the free energy of reaction most relevant for catalysis. Non-harmonic entropic effects significantly reduce the solvation effect. This conclusion has significant consequences for modeling solvation effects, as it means that any brute force DFT approach, microsolvation or bilayer adsorption/ice models (all of them do not permit extensive phase space sampling) are only appropriate whenever the system temperature is low enough or the solvent–solute interaction strong enough that entropic effects along the reaction coordinate can be described accurately by the harmonic approximation. In fact, under biomass conversion conditions, there is a very high risk that due to a lack of extensive configuration space sampling, these models significantly overestimate solvent effects (because the harmonic approximation breaks down under biomass conversion conditions). Likely, these models are more appropriate for predicting enthalpies of solvation than free energies of solvation; however, for catalysis applications free energies of solvation are needed.

Investigation of the deoxygenation of lignocellulosic biomass model molecules over transition metal surfaces

Our hierarchical multiscale modeling approach for understanding and designing heterogeneous metal catalysts for the deoxygenation of lignocellulosic biomass model molecules is based on first investigating a network of elementary reaction steps at the gas-metal and implicit solvent-metal interface before studying key reactions with our eSMS methodology. In the last allocation period, we investigated the liquid-phase (implicit solvation model) hydrodeoxygenation of guaiacol over Pt(111) and Ru(0001). In addition, we studied the HDO and hydrogenation of phenol over Pt(111), Pd(111), and Ru(0001). Our objective has been understanding solvation effects on various C-H, O-H, and C-OH bond dissociations. In particular, we are interested if aromatic alcohols (commonly present in lignin) possess different solvation effects to aliphatic alcohols and acids. Finally, we started the generation of volcano plots for the HDO of propanoic acid. We already possessed all (low coverage) gas phase DFT numbers for 5 transition metals (Pt, Pd, Ni, Rh, Ru - plus all ground state data for Re, Cu, Ag) and we started generating both high coverage data and solvation effect data. The objective here has been to illustrate how solvation effects modify the top of the volcano curve.

Publications Acknowledging this Grant in 2015-2018

Please classify your publications into three categories according to the source of support for the work published:

(I) Exclusively funded by this grant;

1. Lu, J.; Behtash, S.; Mamun, O.; Heyden, A. Theoretical Investigation of the Reaction Mechanism of the Guaiacol Hydrogenation over a Pt(111) Catalyst. *ACS Catalysis* **2015**, *5*, 2423-2435.
2. Lu, J.; Heyden, A. Theoretical Investigation of the Reaction Mechanism of the Hydrodeoxygenation of Guaiacol over a Ru(0001) Model Surface. *J. Catal.* **2015**, *321*, 39-50.
3. Lu, J.; Wang, M., Zhang, X., Heyden, A., Wang, F. α -O-4 bond cleavage mechanism for lignin model compounds over Pd catalysts identified by combination of first-principles calculations and experiments. *ACS Catalysis* **2016**, *6*, 5589-5598.
4. Faheem, M., Saleheen, M., Lu, J., Heyden, A. Ethylene glycol reforming on Pt(111): first-principles microkinetic modeling in vapor and aqueous phases. *Catal. Sci. Tech.* **2016**, *6*, 8242-8256.
5. Saleheen, M., Heyden, A. Liquid phase modeling in heterogeneous catalysis. *ACS Catalysis* **2018**, *8*, 2188-2194.

(II) Jointly funded by this grant and other grants with leading intellectual contribution from this grant;

1. Behtash, S.; Lu, J.; Mamun, O.; Williams, C. T.; Monnier, J. R.; Heyden, A. Solvation Effects in the Hydrodeoxygenation of Propanoic Acid over a Model Pd(211) Catalyst. *J. Phys. Chem. C* **2016**, *120*, 2724-2736.
2. Behtash, S.; Lu, J.; Walker, E.; Heyden, A. Solvent Effects in the Liquid Phase Hydrodeoxygenation of Methyl Propionate over a Pd(111) Catalyst Model. *J. Catal.* **2016**, *333*, 171-183.

(III) Jointly funded by this grant and other grants with relatively minor intellectual contribution from this grant;

1. Lu, J.; Faheem, M.; Behtash, S.; Heyden, A. Theoretical Investigation of the Decarboxylation and Decarbonylation Mechanism of Propanoic Acid over a Ru(0001) Model Surface. *J. Catal.* **2015**, *324*, 14-24.
2. Mamun, O., Walker, E., Faheem, M., Bond, J. Q., Heyden, A. Theoretical investigation of the hydrodeoxygenation of levulinic acid to α -valerolactone over Ru(0001). *ACS Catalysis* **2017**, *7*, 215-228.
3. Mamun, O., Saleheen, M., Bond, J. Q., Heyden, A. Importance of angelica lactone formation in the hydrodeoxygenation of levulinic acid to α -valerolactone over a Ru(0001) model surface. *J. Phys. Chem. C* **2017**, *121*, 18746-18761.

Positioning Active Sites in Catalytic Materials – From Cooperative Catalysis to Cascade Catalysis in Multicompartment Nanoreactors

Seung Soon Jang,¹ Marcus Weck,² Christopher W. Jones¹
¹Georgia Institute of Technology, ²New York University

Presentation Abstract

At any given moment, the cell is carrying out a large number of non-orthogonal (and competing) catalytic transformations simultaneously. This is made possible by compartmentalizing these transformations and catalysts, thereby shielding them from each other. Currently, synthetic analogs to such chemical reaction diversity do not widely exist, though there is significant interest in one-pot, multistep strategies to supersede intermediate work-up procedures. In particular, synthetic multicompartment systems – where individual catalyst particles are tailored to contain multiple, distinct zones or compartments within a single particle that isolate specific active sites, reagents or reactions - are in their infancy. Furthermore, reports of combining non-orthogonal transformations in one pot have been limited to a few examples, none of them allowing for multiple non-orthogonal and enantioselective transformations. An interdisciplinary research team that can probe all aspects of the design, synthesis and characterization of compartmentalizable, catalyst-containing nanoreactors is exploring this topic from both experimental and theoretical points of view. Our prior work began with the design of cooperative catalysts, where multiple active sites work in tandem on a single substrate to catalyze a reaction, and now focuses on cascade catalysis. In particular, researchers at GT and NYU are developing new platforms for use as multicompartment nanoreactors to support a library of catalysts, both transition metal based and organocatalysts, for tandem or multi-step catalysis. Using these model systems, we seek fundamental principles that can be used to understand and design future classes of supported, cooperative and/or tandem catalysts.

DE-FG02-03ER15459: Multi Compartment Nanoreactors as Supports for Incompatible Molecular Catalysts

PIs: Christopher W. Jones, Marcus Weck, Seung Soon Jang

Postdoc(s): Hung Vu Tran, Li-Chen Lee, Tyler Womble

Student(s): Caroline Hoyt, Aaron Cohen, Michael Küpfert, Peiyuan Qu, Connor Callaway, Jacob Cleveland

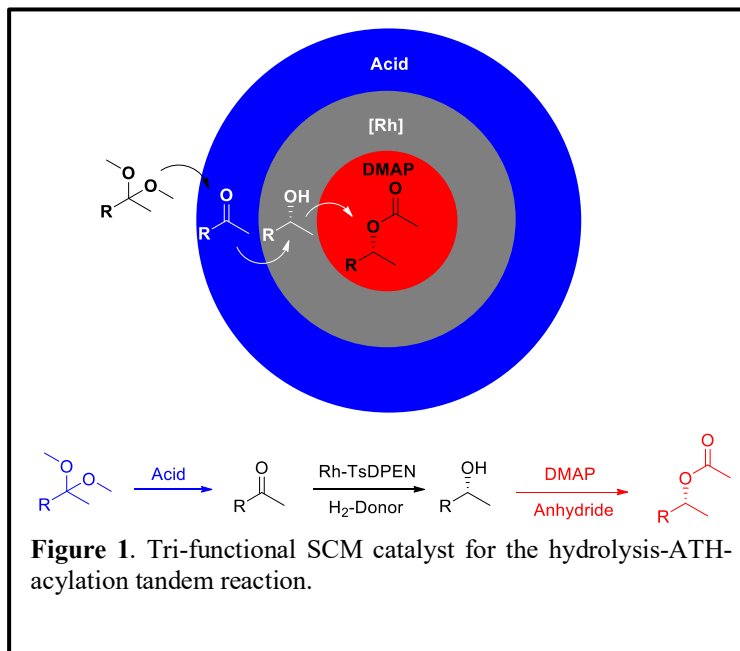
RECENT PROGRESS

Shell Cross-linked Micelles (SCMs) As Nanoreactors for Tandem Catalysis – Transition Metal Catalysts

The research team has previously utilized shell cross-linked micelles (SCM)s as catalytic support structures to facilitate two step non-orthogonal tandem reactions in one pot. This was enabled through site isolation of each catalyst in the corona and the core of the micelle. We are increasing the complexity of the system by incorporating a third catalyst in the cross-linked shell of the SCM

to facilitate a three step tandem reaction sequence (Figure 1). The reaction sequence that is targeted is the acid catalyzed ketal hydrolysis followed by Rh-TsDPEN catalyzed asymmetric transfer hydrogenation (ATH) and subsequent acylation by DMAP.

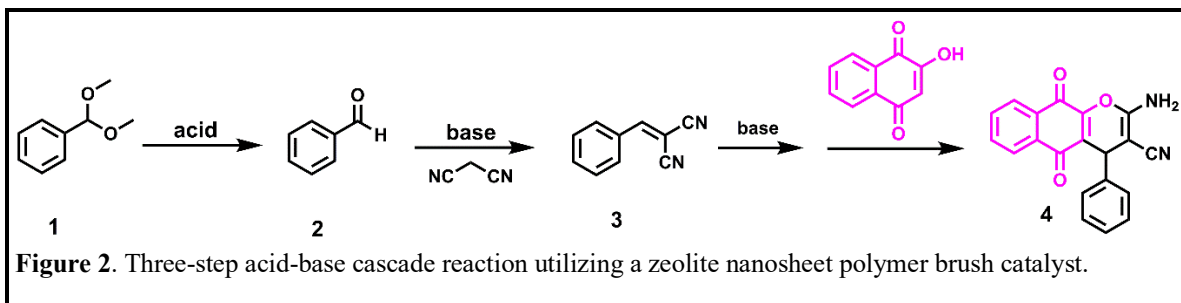
This SCM design is based on poly(2-oxazoline)s. The self-assembly of the tri-functional SCM nanoreactor **COOH-Rh-DMAP** into spherical micelles was confirmed by SEM and dynamic light scattering (DLS) in water. A series of catalytic tests using this nanoreactor in combination with mono- and bifunctional micelles as well as the analogous homogenous systems as controls revealed that the unsupported acid catalyzed hydrolysis is incompatible with the ATH reaction conditions and DMAP. However, in the micellar system, the carboxylic acid sites in the corona are spatially separated from the other two catalysts and quantitative conversion of the ketal to the chiral alcohol was obtained within 36 hrs. This demonstrates the compatibility of the first two reaction steps in tandem.



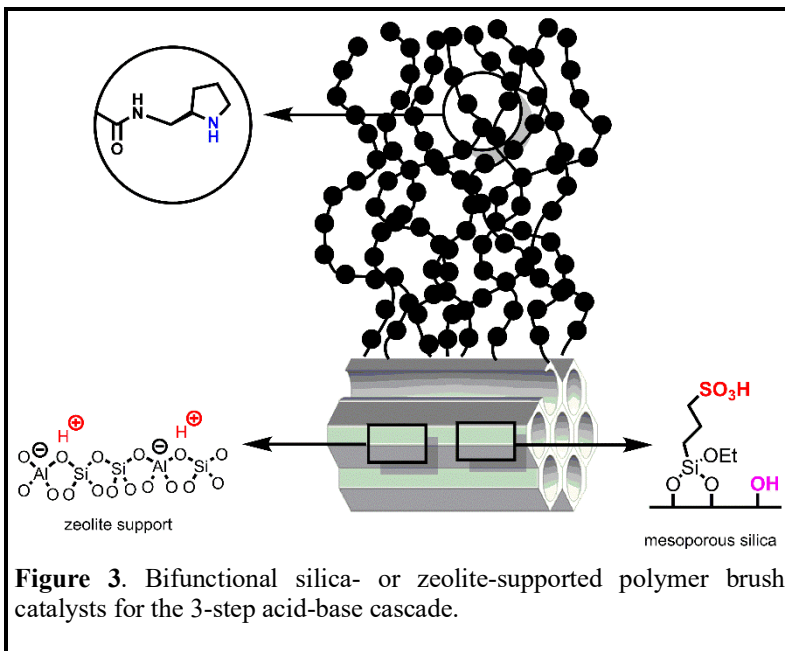
tandem. Homogenous catalytic tests of the ATH showed that Rh-TsDPEN gets partially deactivated in the presence of DMAP, as the pH of the aqueous reaction solution is increased. On the contrary, the SCM nanoreactor contains DMAP catalysts at the polymer chain end with adjacent tridecanyl- side chains forming the micelle core that provide sufficient spacing apart from the Rh-TsDPEN in the cross-linked shell. Despite the failures of the homogeneous control reactions, the three step tandem reaction catalyzed by **COOH-Rh-DMAP** resulted in 60% conversion to the ester product with 98% ee with the rest of the substrate being completely converted to the intermediate chiral alcohol. This demonstrates the viability of our micelle support strategy to enable a three step non-orthogonal tandem reactions in one reaction vessel.

Porous Oxide-supported Pyrrolidine Polymer Brushes for 3-Step Cascade Catalysis

The research team has demonstrated the use of shell cross-linked micelles for several different two step and now 3 step (above) cascade reactions. The example above used a poly(2-oxazoline) based triblock copolymer. In a new direction, we seek to broaden the scope of multi-compartment reactor building blocks by incorporating porous oxide domains with the polymeric structures. Furthermore, we hypothesize that by including oxide domains that allow for shape-selectivity, we can begin direct the diffusion of species down a specific path, as a cell does, rather than allowing random diffusive transport in all directions. We have synthesized a oxide-supported polymer brush catalyst to incorporate acid sites within the oxide support, and active base sites on the polymer brush chains to catalyze a three-step cascade. The cascade reaction includes an acid-catalyzed ketal hydrolysis, followed by a Knoevenagel condensation and a Michael addition catalyzed by the same basic pyrrolidine catalyst, as shown below in Figure 2.



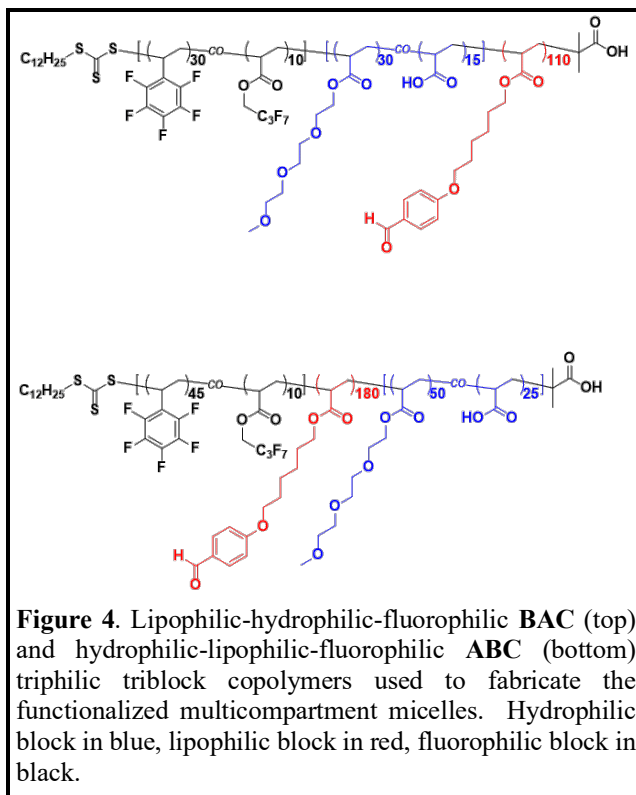
Two different acidic support structures were investigated for the acid-catalyzed step to elucidate the impact of their structures on the full reaction cascade (mesoporous silica, zeolite nanosheets). Use of 2D zeolite nanosheets as the oxide support allows for good acid/base domain separation while allowing for the additional advantage of shape-selectivity. 2D zeolite nanosheet structures are relatively new, being originally described in the literature in 2009. Our zeolite support contains both meso- and micropores, with surface areas comparable to mesoporous silica. Use of this support allowed for high catalytic activity, with excellent active site accessibility to the microporous acid sites easily achieved. The base-catalyzed Knoevenagel and Michael addition proceed to quantitative yields in 24 h at room temperature. With the utilization of the microporous acid sites, the starting protected benzaldehyde dimethyl acetal (1) is hydrolyzed to benzaldehyde (2) and further condensed to create a larger product (3) (Figure 2). Because of the size of this product, it remains in the polymer brush and bulk solution and cannot diffuse back into the zeolite core. As a result, the product 3 interacts with the pink reagent in Figure 2 and the base-catalyzed Michael addition further expands the product to produce a sterically large chromene (4) which has pharmaceutical applications. Initial experiments with the full cascade demonstrate 80% conversion of the first step with 5 mol% acid sites, and 80% yield of chromene (4) over the course of 24 h, even at room temperature.



Functionalized Multicompartment Micelles as Catalytic Nanoreactors

The research team has made significant progress in the preparation of functionalized multicompartment micelles (MCMs), a system we are utilizing as next-generation catalytic nanoreactors for multistep non-orthogonal chemical transformations. The use of MCMs allows for an additional level of microphase separation by extending the block-copolymer structures, for example using aqueous self-assembly of a triphilic triblock copolymer with mutually incompatible hydrophilic, lipophilic, and fluorophilic blocks. In contrast to literature reports of MCMs made with polymers lacking reactive groups, we have prepared linear triphilic triblock copolymers that contain orthogonal “handles” on each polymer block, enabling the system to undergo targeted post-polymerization reactions with a series of functionalized small molecules to introduce various active sites.

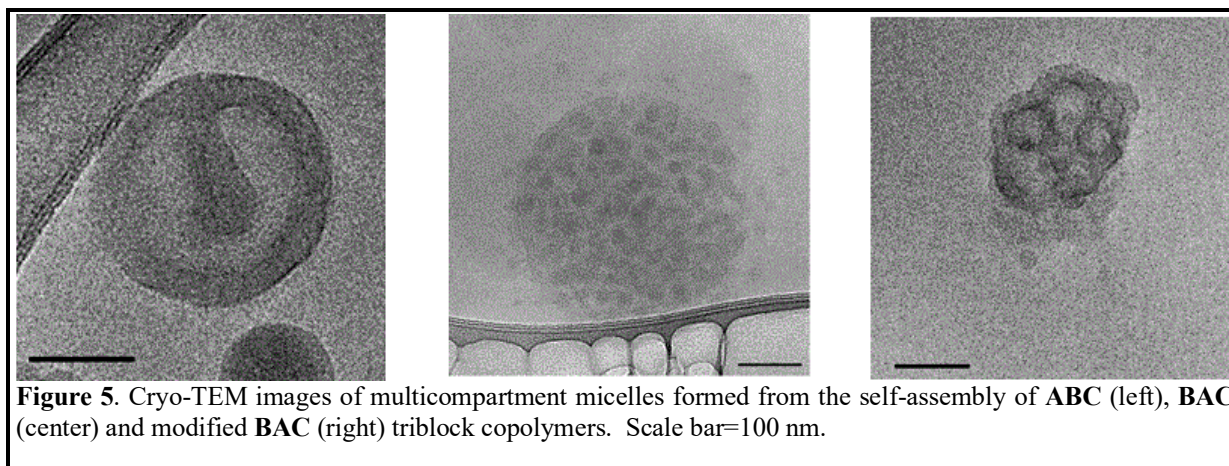
The research team has prepared linear lipophilic-hydrophilic-fluorophilic **BAC** and hydrophilic-lipophilic-fluorophilic **ABC** triblock copolymers, which are shown in Figure 4. Each block contains an orthogonal “handle” that can be selectively targeted using a series of post-polymerization reactions. The formation of MCMs was confirmed using cryogenic-transmission electron microscopy (cryo-TEM). The **ABC** triblock copolymer self-assembled to form core-shell-corona “onions” (Figure 5, left) while the **BAC** triblock copolymer self-assembled to form “raspberries,” in which the electron-dense fluorophilic domain appears as darkened patches on the hydrophobic core (Figure 5, center). Each block of the **BAC** triblock copolymer could be selectively modified using functionalized small molecules. The resulting modified **BAC** triblock copolymer forms MCMs upon aqueous self-assembly (Figure 5, right), highlighting the potential of this system for more advanced catalytic applications. The research team is currently exploring the potential of functionalized MCMs for preliminary two-step non-orthogonal chemical transformations.



Morphological Studies of BAC Triblock Copolymers: An Experimental and Computational Collaboration

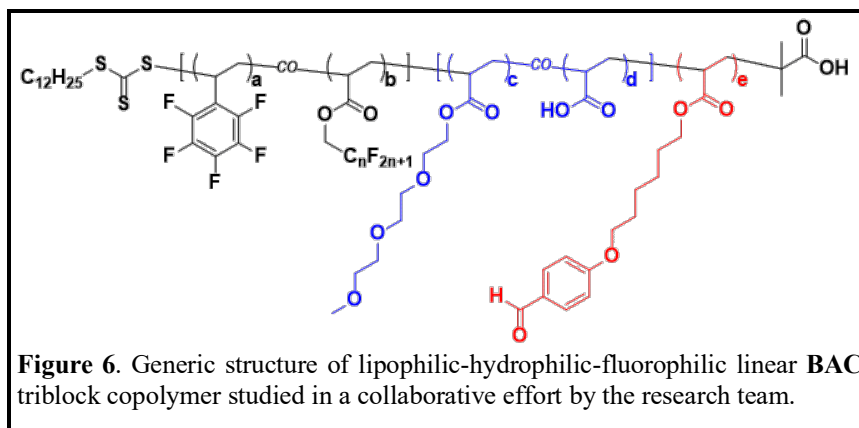
The research team is combining experimental and computational techniques to model the micellar morphologies formed via the aqueous self-assembly of linear lipophilic-hydrophilic-fluorophilic **BAC** triblock copolymers (Figure 6). Because of the central position of the hydrophilic block in this particular sequence, **BAC** triblock copolymers tend to self-assemble in an aqueous environment to form complex “raspberry” multicompartment micellar morphologies, whereas **ABC** triblock copolymers give rise to simpler core-shell-corona “onions,” as we have shown earlier in this report. Because the synthesis of a triblock copolymer can often be a time-intensive

process, computational simulations are widely employed to quickly model a large library of polymeric systems. In this collaborative effort, **BAC** triblock copolymers are prepared synthetically, self-assembled, and imaged using cryo-TEM, whilst simultaneously modeling them computationally using dissipative particle dynamics (DPD) simulation method. The work aims to determine the accuracy of computational approaches to model a complex, self-assembled, triphilic polymeric system, while providing an aid to predict and precisely generate new multicompartment micellar morphologies for future work.



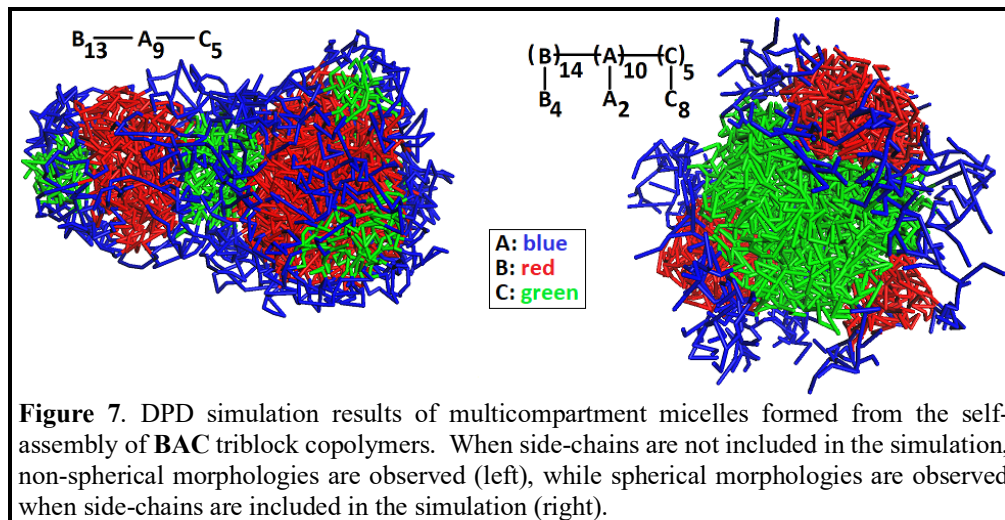
Experimentally, the research team has synthesized a large number of **BAC** triblock copolymers and imaged the self-assembled structures using cryo-TEM. Variations were made in the block length ratio of the three blocks or in the composition of the fluorophilic block **C**. Spherical morphologies are generated at all levels of hydrophilic content. We also investigated modifications to the fluorophilic block **C**. By decreasing the amount of bulky perfluorinated aliphatic monomer in the fluorophilic block, the volume of this block is significantly reduced and more complex multicompartment micellar morphologies are formed. Starting with a single lipophilic-hydrophilic “parent” **BA** diblock copolymer, we can generate “onions” and patchy morphologies with large and small patches as the volume of the fluorophilic block is incrementally decreased. We view this as a simple strategy to quickly prepare a diverse library of multicompartment micellar morphologies for use in catalysis.

Computational simulations were also performed for the same **BAC** linear triblock copolymers to assess the accuracy in modelling such a complex polymeric system using *in silico* methods (Figure 7). Simulations were performed through the DPD simulation method, a coarse-grained method for



studying systems with total particle numbers on the order of 10^4 or more. These studies implemented various levels of coarse-graining, ranging from simplified linear **BAC** triblock

copolymers to branched polymers consisting of bulky side chains. Most noteworthy were the morphological differences between the computational models and experimental results when explicit side chains were not included in the computational models. In particular, by not including side chains in the DPD simulations, a larger number of non-spherical morphologies were observed, a result that is inconsistent with the experimental data. However, by explicitly including side-chains in the DPD simulations, spherical morphologies were primarily generated, providing a far higher level of accuracy with the experimental results. These results highlight the challenges of simulating a complex triphilic polymeric system and provide a useful tool in predicting and developing new multicompartment micellar morphologies.



Computational Block-Length Tunability of Multicompartment Micelle Structures

Based on the success with DPD simulation noted above, we examined the dependence of MCM morphology on the lengths and length ratios of the hydrophilic, lipophilic, and fluorophilic copolymer blocks. In our follow-up DPD simulation study, the effect of polymer architecture of an HLF (hydro-lipo-fluoro) triblock copolymer on the resultant aqueous MCM morphology was examined as a function of the length and length ratio of the three polymer blocks. A detailed study of the BAC system highlights the dependence of the micelle structure on the lipophilic-to-fluorophilic block length ratio. This ratio is defined for a purely linear chain as $\mathcal{R}_l = \tilde{b}_L / \tilde{b}_F$, where \tilde{b}_L and \tilde{b}_F represent the reduced DPD block lengths corresponding to a real polymer of lipophilic and fluorophilic block lengths b_L and b_F . The micelle structure variation as a function of \mathcal{R}_l was studied at several fixed hydrophilic block lengths. Repulsion parameters for this study were assigned to ensure immiscibility between the A, B, and C blocks. The exact values were based first on χ -values calculated via the miscibility analysis method developed previously, converted to repulsion parameters, and finally adjusted to allow for distinct three-phase separation upon self-assembly.

Simulation results are presented in Figure 8a, where the horseshoe-like shape highlights the structural similarities at either extreme of \mathcal{R}_l . For improved clarity, due to the thickness of the hydrophilic shell, visibility of the hydrophilic block is disabled in Figure 8b. It is clear that the preference for the formation of a strongly spheroidal morphology increases as \mathcal{R}_l becomes further from unity. Patches of the deficient species surround the core in these extremes (regimes I and III). As \mathcal{R}_l approaches unity, however, these patches become larger; near $\mathcal{R}_l = 1$, the micelle becomes decidedly non-spheroidal (regime II). This phenomenon is especially evident in Figure 8b, where segmented worm-like morphologies arise for $B_4A_{18}C_5$ and $B_5A_{18}C_4$.

It should not be overlooked that adding side-chains to one or more of the copolymer blocks is expected to result in morphological changes similar to directly increasing the lengths of the corresponding blocks. This prediction is based on the fact that volume free energy contributions will arise from both main-chain and side-chain species. As such, the parameter \mathcal{R}_l presented here should be applied only to systems of micelles composed of triblock copolymers that may be approximately represented as purely linear. For systems of triblock copolymers with bulky side-chains, intuition suggests that there exists a natural extension of the structural parameter \mathcal{R}_l into a more general form \mathcal{R} that does not require the aforementioned assumption of copolymer linearity. Precise determination of the quantitative relationship between block length, side-chain length, and micelle structure is the focus of ongoing study by the research team.

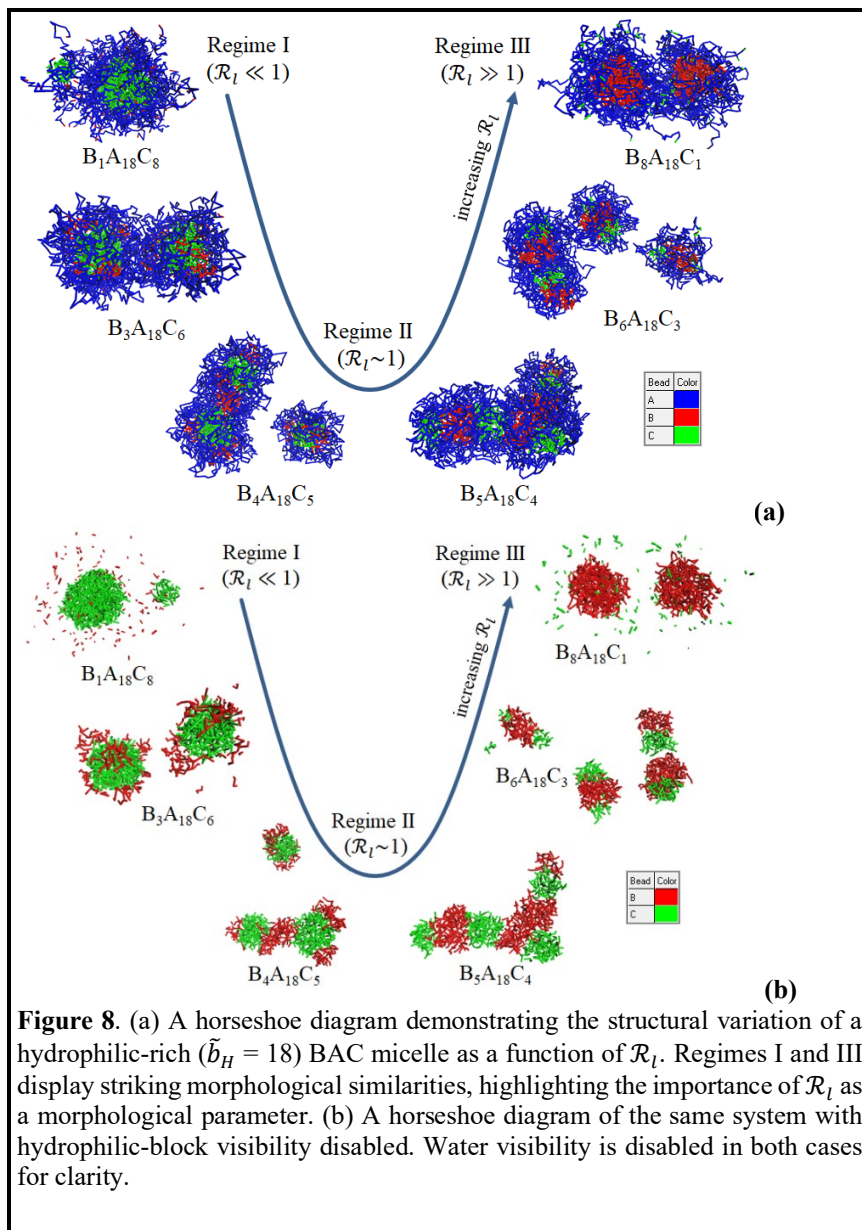


Figure 8. (a) A horseshoe diagram demonstrating the structural variation of a hydrophilic-rich ($\bar{b}_H = 18$) BAC micelle as a function of \mathcal{R}_l . Regimes I and III display striking morphological similarities, highlighting the importance of \mathcal{R}_l as a morphological parameter. (b) A horseshoe diagram of the same system with hydrophilic-block visibility disabled. Water visibility is disabled in both cases for clarity.

Publications Acknowledging this Grant in 2015-2018

Category 1: Sole funding from DOE-BES and this Specific Grant

1. "Spatial Arrangement and Acid Strength Effects on Acid-Base Cooperativity." J. Lauwaert; E.M. Moschetta; P. van der Voort; J. Thybaut; C.W. Jones; G. B. Marin; *J. Catal.* **2015**, *325*, 19-25.
2. "Compartmentalization of Non-orthogonal Catalytic Transformations for Tandem Catalysis." J. Lu; J. Dimroth; M. Weck; *J. Am. Chem. Soc.* **2015**, *137*, 12984-12989.
3. "Co-Salen Complexes as Catalysts for the Asymmetric Henry Reaction - Reversed Enantioselectivity through Simple Ligand Modification." J. Dimroth; M. Weck; *RSC Adv.* **2015**, *5*, 29108-29113.
4. "Reaction-Dependent Heteroatom Modification of Acid-Base Catalytic Cooperativity in Aminosilica Materials." E. Moschetta; N.A. Brunelli; C.W. Jones; *Appl. Catal. A. Gen.* **2015**, *504*, 429-439.
5. "Post-Grafting Amination of Alkylhalide-Functionalized Silica for Applications in Catalysis, Adsorption and ¹⁵N NMR Spectroscopy." E.M. Moschetta; M.A. Sakwa-Novak; J.L. Greenfield; C.W. Jones; *Langmuir* **2015**, *31*, 2218-2225.
6. "Co(III) Complexes of Tetradentate X₃L Type Ligands: Synthesis, Electronic Structure, and Reactivity." Y. Feng; L. Burns; L.-C. Lee; C.R. Murdock; C.D. Sherrill; C.W. Jones; *Inorg. Chim. Acta* **2015**, *430*, 30-35.
7. "Molecular Dynamics Simulation Study of Sodium Dodecyl Sulfate Micelle: Water Penetration and Sodium Dodecyl Sulfate Dissociation." B.J. Chun; J.I. Choi; S.S. Jang; *Colloids Surf. A* **2015**, *474*, 36-43.
8. "Characterization of Molecular Association of Poly(2-oxazoline)s-based Micelles with Various Epoxides and Diols via the Flory-Huggins Interaction Parameter: A Molecular Dynamics Simulation Approach." B.J. Chun; J. Lu; M. Weck; S. S. Jang; *PhysChemChemPhys* **2015**, *17*, 29161-29170.
9. "Counterion and Substrate Effects on Barrier Heights of the Hydrolytic Kinetic Resolution of Terminal Epoxides Catalyzed by Co(III)-salen." M. R. Kennedy, L. A. Burns, C. D. Sherrill, *J. Phys. Chem. A.* **2015**, *119*, 403-409.
10. "Kinetic and Mechanistic Examination of Acid-Base Bifunctional Aminosilica Catalysts in Aldol and Nitroaldol Condensations." V.E. Collier; N.C. Ellebracht; G. I. Lindy; E.G. Moschetta; C.W. Jones; *ACS Catal.* **2016**, *6*, 460-468.
11. "Acid-Base Bifunctional Shell Cross-Linked Micelle Nanoreactor for One-Pot Tandem Reaction." L. -C. Lee; J. Lu; M. Weck; C.W. Jones; *ACS Catal.* **2016**, *6*, 784-787.
12. "Dissipative Particle Dynamics Simulation Study of Poly(2-Oxazoline)-based Multicompartment Micelle Nanoreactor." B.J. Chun; C.C. Fisher; S.S. Jang; *PhysChemChemPhys* **2016**, *18*, 6284-6290.
13. "Micelle-based Nanoreactors Containing Ru-porphyrin for the Epoxidation of Terminal Olefins in Water." J. Lu; L. Liang; M. Weck; *J. Mol. Catal. A Chem.* **2016**, *417*, 122-125.

14. “Molecular Dynamics Simulations of Aldol Condensation Catalyzed by Alkylamine-Functionalized Crystalline Silica Surfaces.” K.C. Kim; E.M. Moschetta; C.W. Jones; S.S. Jang; *J. Am. Chem. Soc.* **2016**, *138*, 7664-7672.
15. “Bifunctional Polymer Architectures for Cooperative Catalysis: Tunable Acid-Base Polymers for the Aldol Condensation.” C.B. Hoyt; L.-C. Lee; A. E. Cohen; M. Weck; C.W. Jones; *ChemCatChem* **2017**, *9*, 137-143.
16. “Molecular Modeling Approach to Determine Flory-Huggins Interaction Parameter for Polymer Miscibility Analysis.” C. P. Callaway, K. Hendrickson, N. Bond, S. M. Lee, P. Sood, S.S. Jang, *ChemPhysChem* **2018**, doi.org/10.1002/cphc.201701337
17. “Multicompartment Micelles Synthesized From Functionalizable Triphilic Triblock Copolymers.” A.E Cohen, W. Tong, K. Dancel Manning, M. Weck, **2018**, manuscript submitted.

Ion Exchange Approach for Incorporating Cations in Metal Organic Frameworks: Challenges and Opportunities

Melanie S. Sanford, Bryant James, Danielle Samblanet, Douglas Genna, Antek G. Wong-Foy,
Adam J. Matzger

Presentation Abstract

This presentation will discuss ion exchange as a method for supporting cations in anionic metal organic frameworks (MOFs). We will present detailed studies of the ion exchange process using alkali metal cations, including optimization of the exchange conditions to maximize ion loading, while minimizing decomposition of the MOF support. We will then describe our work supporting Rh and Ir hydrogenation catalysts in various MOFs. Approaches for using the MOF support to modulate both catalyst activity and selectivity will be described. Finally, strategies for characterization of these materials both pre- and post-catalysis will be discussed.

Grant Number/Title: DE-FG02-08ER15997: MOF-Supported Metal Catalysts for Alkene Hydrogenation and C–H Functionalization

Lead PI: Prof. Melanie Sanford; co-PI: Prof. Adam Matzger

Research Scientist: Dr Antek Wong-Foy

Post-doc: Dr. Douglas Genna, Dr. Yiyang Liu

Student(s): Bryant James, Jake Boissonnault, Mark Mantell

RECENT PROGRESS

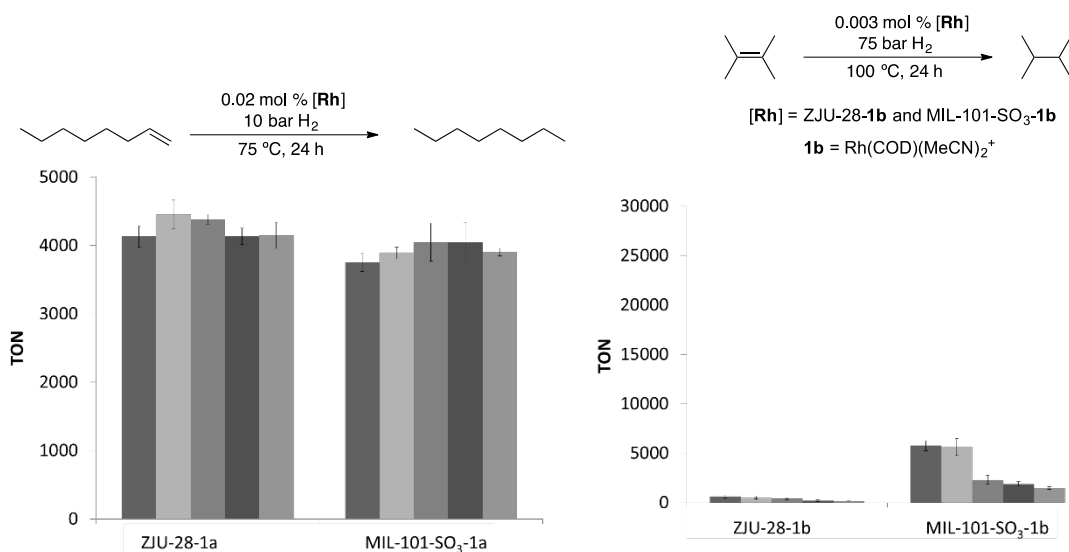
Ion Exchange of Rh Alkene Hydrogenation Catalysts: Impact of MOF Support on Catalysis

Over the past several years, metal organic frameworks (MOFs) have been widely targeted as supports for catalysts. We aimed to exploit the well-defined and highly tunable pore structures of these materials to modulate the stability, reactivity, and selectivity of alkene and carbonyl hydrogenation catalysts. Our initial studies focused on supporting cationic hydrogenation catalysts in anionic MOFs via ion exchange. Importantly, ion exchange has been used previously to introduce diverse cations into MOFs but has not, to our knowledge, previously been employed in MOF catalysis. In principle, this approach would enable well-defined immobilization of cationic catalysts based on a simple balancing of charged sites. It would avoid the requirement for covalent tethering and would enable us to support diverse catalysts without altering their chemical structures.

We first developed a method for supporting cationic metal complexes in different MOFs that bear an anionic charge (e.g., ZJU-28 and MIL-101-SO₃). The cationic Rh complex (dppe)Rh(COD)BF₄ (**1a**) was loaded into ZJU-28 and MIL-101-SO₃ via ion exchange, by shaking suspensions of the corresponding MOF immersed in a 0.015 M DMF solution of **1a** for 3 days.

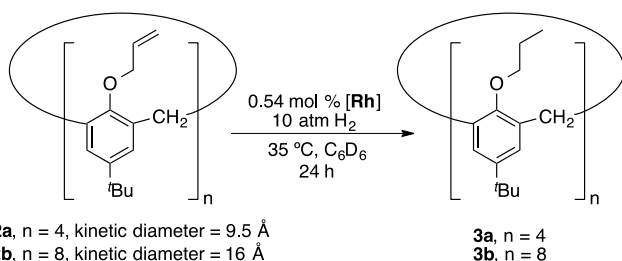
The resulting materials were then washed with DMF, dried at room temperature under vacuum, and characterized using ICP-OES, powder X-ray diffraction (PXRD), and gas sorption.

These two materials, ZJU-28-**1a** and MIL-101-SO₃-**1a**, were examined as catalysts for the hydrogenation of 1-octene. With this substrate, they afforded comparable results, providing ~4000 turnovers of 1-octene to *n*-octane in each case (theoretical maximum is 5000). Both materials could be recycled at least 4 times, and the recycled materials afforded comparable TON (~4000) after 24 h. The reactions were also monitored via *in situ* Raman spectroscopy, which showed that hydrogenation catalysis is significantly faster with MIL-101-SO₃-**1a** as compared to that with ZJU-28-**1a**, both before and after recycling. We hypothesize that this is due, at least in part, to the significantly larger pore sizes and pore windows of the MIL-101-SO₃ support compared to those of ZJU-28.



We also compared the same two materials for the hydrogenation of the more challenging substrate 2,3-dimethylbutene. With this substrate, the nature of the support dramatically impacted activity. For example, ZJU-28-**1a** afforded low initial reactivity, providing a TON of just 1500 (out of a theoretical maximum TON of 30,000). Furthermore, significant loss of activity was observed with each subsequent recycle of ZJU-28-**1a**, and after 4 recycles, this catalyst afforded just 289 turnovers. In marked contrast, MIL-101-SO₃-**1a** was a much more effective catalyst for the hydrogenation of 2,3-dimethylbutene, affording 8800 turnovers after 24 h. Furthermore, upon recycling, the activity of MIL-101-SO₃-**1a** nearly doubled to 13500 turnovers. This enhanced activity was largely maintained over three additional recycles.

Finally, we examined the ZJU-28-**1a** and MIL-101-SO₃-**1a** catalyzed hydrogenation of the calixarene-tethered alkene substrates **2a** and **2b**. These two substrates have very large kinetic diameters (9.5 and 16 Å, respectively). Since the pore windows of ZJU-28 and MIL-101-SO₃ are 9 × 9 Å and 16 × 14 Å, respectively, we anticipated that these materials should exhibit size-selective catalysis. Indeed, with MIL-101-SO₃-

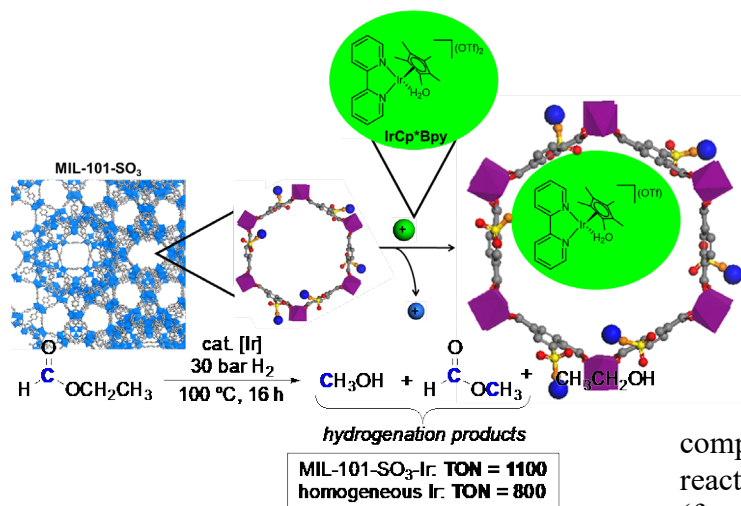


1a, full conversion (TON = 185) was obtained with the smaller calixarene substrate **2a**. However, the larger substrate **2b**, which has a kinetic diameter close to the pore window of the MOF, afforded only partial hydrogenation (TON = 52) after 24 h. In addition, with ZJU-28-**1a** as the catalyst (which has a pore window that is smaller than the kinetic diameter of both of the calixarenes), no hydrogenation of either **2a** or **2b** was detected. These results demonstrate that size-selective catalysis can be achieved by supporting the same catalyst in two structurally different metal organic frameworks.

Overall, these initial studies showed that the nature of the MOF support impacts various aspects of catalysis, including: (i) the rate of 1-octene hydrogenation; (ii) the activity (as measured by TON) and recyclability of the catalyst in 2,3-dimethylbutene hydrogenation; and (iii) the size selectivity of the catalyst in the hydrogenation of alkenes appended to calixarenes.

Ion Exchange of Ir Ester Hydrogenation Catalysts: Enhanced Catalyst Performance but Poor Recyclability

We used analogous methods to supporting the cationic ester hydrogenation catalyst $\text{Cp}^*\text{Ir}(\text{bipy})(\text{H}_2\text{O})^{2+}$ in MIL-101-SO₃. MIL-101-SO₃ suspended in a THF solution of $\text{Cp}^*\text{Ir}(\text{bipy})(\text{H}_2\text{O})^{2+}$ was shaken for 4 d. The resulting material was then washed with THF, dried at room temperature under vacuum, and characterized using ICP-OES, powder X-ray diffraction (PXRD), and gas sorption.



The supported Ir complex was examined as a catalyst for the hydrogenation of methyl formate and compared to the homogeneous analogue. This reaction produces a mixture of methanol (from hydrogenation), methyl formate (from

hydrogenation followed by transesterification), and ethanol (from hydrogenation plus transesterification). The hydrogenation products were quantified with each catalyst, and the supported catalyst was found to afford an almost 40% increase in activity under analogous conditions relative to the homogeneous system (TON = 1100 versus 800, respectively). However, despite this significant increase in activity, the supported catalyst showed poor recyclability. Filtering the resulted in a TON of only 70. This suggests that either: (i) the supported catalyst is undergoing deactivation during the initial catalysis experiment or (ii) the catalyst is leaching from the support during catalysis/recycling. Detailed experiments have been conducted to distinguish these possibilities

Detailed Studies and Optimization of Ion Exchange Process

In both of the catalysis studies described above, methods for characterization of the spent catalysts would provide crucial information about the structures of the [Rh]/[Ir] complexes following hydrogenation. We hypothesized that ion exchange would provide a simple route to remove and characterize remaining single site catalysts from the MOF. To achieve this, we first focused on optimizing the ion exchange process using alkali metal salts as model systems. These

studies revealed that, under appropriately selected conditions, MIL-101-SO₃ undergoes quantitative incorporation of Li⁺, Na⁺, K⁺, Rb⁺, and Cs⁺ (incorporating 1 equiv of M⁺ per SO₃⁻ in the framework). Several factors were identified as crucial for achieving fast rates and high K_{eq} of this ion incorporation process. First, pre-treatment of the parent, as-synthesized MOF with a weak base is essential for fully deprotonating the sulfonic acid linkers and thus facilitating ion incorporation. The choice of base (aqueous NaHCO₃) and pre-treatment time (10 min) were both crucial to limit competing decomposition of the framework. Subsequent treatment with aqueous MCl resulted in quantitative conversion to the MIL-101-SO₃-M structure without degradation of the crystallinity of the MOF. Furthermore, the parent material MIL-101-SO₃H was obtained quantitatively by reaction with aqueous HCl. Ion exchange between the alkali metal supported MOFs was also examined. These studies revealed that quantitative exchange occurs when MIL-101-SO₃-M is treated with 20 equiv of M⁺Cl. This approach is currently being explored as a means to characterize the supported catalysts both pre- and post-catalysis.

MOF Catalysts for Methane C–H Functionalization

Another set of studies has focused on developing MOF-supported catalysts for the C–H functionalization of the light alkanes methane and ethane. The development of catalysts for the selective C–H functionalization of methane (the primary component of natural gas) is a long-standing goal in the field of catalysis. The C–H bonds of methane are highly kinetically inert, particularly compared to those of most reaction solvents and methane functionalization products (CH₃X; X = new functional group). Thus, developing strategies to achieve the selective functionalization of CH₄ in the presence of CH₃X, solvent, and other components of natural gas (e.g., ethane) remains major challenge. To accomplish this goal, we sought to leverage work by Hartwig, Smith and others in the development of catalysts for the C–H borylation of heavier, liquid hydrocarbons to achieve methane/ethane C–H borylation reactions. Our initial studies in this area identified Ir, Rh and Ru catalysts ligated with Cp and/or bipyridine ligands that catalyze methane C–H borylation reaction with varied levels of selectivity for mono- versus di-borylation. Ongoing efforts are underway to support these ligands/catalysts in MOFs in order to explore: (i) the impact of site isolation and MOF structure on catalyst activity and selectivity as well as to (ii) implement these catalysts in flow reactor systems.

Publications Acknowledging this Grant in 2015-2018

I. Exclusively funded by this grant:

1. Genna, D. G.; Pfund, L. Y.; Samblanet, D. C.; Wong-Foy, A. G.; Matzger, A. J.; Sanford, M. S. “Rhodium Hydrogenation Catalysts Supported in Metal Organic Frameworks: Influence of the Framework on Catalytic Activity and Selectivity,” *ACS Catal.* **2016**, *6*, 3569-3574.
2. James, B. R.; Boissonnault, J. A.; Wong-Foy, A. G.; Matzger, A. J.; Sanford, M. S. “Structure Activity Relationships in Metal-Organic Framework Catalysts for the Synthesis of Propylene Carbonate from CO₂ and Propylene Oxide,” *RSC Adv.* **2018**, *8*, 2132-2137.

II. Jointly funded by this grant and other grants with leading intellectual contribution from this grant

1. Cook, A. K.; Schimler, S. D.; Matzger, A. J.; Sanford, M. S. “Catalyst-Controlled Selectivity in the C–H Borylation of Methane and Ethane,” *Science* **2016**, *351*, 1421-1424.

Selective Oxidation Catalysis

Steven L. Suib

Departments of Chemistry, Chemical and Biomolecular Engineering, and Institute of Materials Science, University of Connecticut

Presentation Abstract

Porous transition metal oxides and their role in selective catalytic oxidations are the focus of our research. Micropores (< 2 nm), mesopores (2-50 nm), macropores (> 50 nm), and sometimes combinations of these are important in control of mass transport and selectivity. The control of particle size in the nanometer regime can lead to enhanced activity in some reactions. Such nano-size materials can have markedly different properties than similar bulk materials (m and above). Control of morphologies of porous transition metal oxides such as hollow spheres, rods, helices, spirals, and many other shapes is also a factor in the control of catalytic activity, selectivity, and stability. Numerous other variables in the design of selective oxidation catalysts besides the above-mentioned properties may be significant such as mixed valency, surface area, thermal stability, chemical stability, electronic effects, active sites, and others.

One key area that needs further exploration is the detection and potential correlation of reactive oxygen species (ROS) in heterogeneous catalytic selective oxidations. Only one detection method is often used to study ROS where multiple methods may provide a more thorough understanding of such catalysts. Reasons why researchers have focused on a few methods are that such ROS species on oxides are difficult to track; methods used to study ROS are quite complicated, expensive, and time consuming. No one method can reliably monitor the multitude of species (O, OH, OOH, $^1\text{O}_2$, O_2^{2-} , O_2^- and others). Monitoring oxygen vacancies and their importance in heterogeneous catalysis is also critical.

Grant or FWP Number: Porous Transition Metal Oxides: Synthesis, Characterizations, and Catalytic Activity

PI: Steven L. Suib

Postdoc(s): Ben Liu

Student(s): Biswanath Dutta, Laura Achola, Peter Kerns

RECENT PROGRESS

A major recent focus of this research project is to continue to develop the best methods to characterize ROS, to carry out thorough detection of all such species, and to do so during *in operando* conditions when possible. **Table 1** outlines methods that will be used to characterize these ROS. In addition, new methods will be developed to study such ROS as well as DFT computational modeling studies.

Table 1, Names, Formulas and Methods of Detection of Reactive Oxygen Species (ROS).

Name	Formula	Methods	References
Superoxide	O ₂ ⁻	<i>In operando</i> FTIR, EPR, UV-VIS.	19
Peroxy	OOH	EPR, (Ultraviolet Visible (UV-VIS) Spectroscopy.	20
Hydroxyl	OH	XPS, <i>in operando</i> FTIR and/or Raman, TG-MS, UV-VIS.	21
Singlet Oxygen	¹ O ₂	Temperature Programmed (TP) Emission, EPR Trapping.	22
Atomic Oxygen	O	Electron Paramagnetic Resonance (EPR)	23
Oxygen Radicals	O [•]	EPR, ¹⁸ O Uptake/Mass Spectrometry (MS).	24
Lattice Oxygen	O ²⁻	¹⁸ O Exchange, TP Methods, X-ray Photoelectron Spectroscopy (XPS).	25
Oxygen Vacancies	O _v	¹⁸ O Uptake/MS, XPS, Thermogravimetric Analysis (TG).	26

Clearly though, ROS are not the only important species and parameters that control selective oxidations. Methods will also be used and developed to study distributions of oxidation states, compositions, particle size, structure, porosity, surface species, dopants, stability, and others. The determination and correlation of all of these parameters with catalytic activity, selectivity, and stability will be critical in our major focus to determine detailed mechanisms and kinetics; to elucidate the bonding, insertion, or bond breaking steps as influenced by nanostructures and steric constraints; and to determine how various parts of the inorganic catalyst structure activate the different functionalities of multifunctional organic species in either a concerted or un-concerted manner.

Unique catalysts that are developed under controlled conditions are central to these missions. Synthetic control of catalysts comes from specific methods such as use of templates, structure directors, surfactants, core shells, self-assembly, epitaxial growth, size reduction, capping agents, sol gel, and other methods. Morphologies can be controlled by compositions including dopants. The conditions during syntheses such as use of heat, light, pH, point of zero charge, stirring, high pressure, and others are also clearly important.

For many years our focus has been selective oxidations using microporous transition metal oxides, in particular manganese oxide based materials that have been shown to have excellent selectivities for small substrates. Use of mesoporous transition metal oxides in the area of selective oxidations has been limited due to compositional limitations and stability of such materials. Titanium oxide materials and doped silica and alumina based mesoporous materials are exceptions. Catalytic studies with pure single metal oxides that are well ordered and thermally stable transition metal oxide mesoporous materials of groups 7B, 8B, 1B and 2B as well as groups IIIA, IVA, and lanthanides with monomodal (uniform, sharp) pore size distributions have been extremely limited. The availability of such mesoporous materials has recently been developed by our group and unique selective catalytic oxidations (*vide infra*) important in the production of new fuels, chemicals, pharmaceuticals, medicines, and others.

The primary *hypothesis of this research* is that if mesoporous systems with specific reactive oxygen species can be prepared then enhanced catalytic activity and selectivity will result from better transport, tuned active sites, and control of catalyst properties (Oxide Composition,

Nanostructure, Porosity, and Oxidation State). A *related hypothesis* is that if synthetic and characterization methods can lead to control of mixed valency, structure, porosity, stability, and related parameters, then the mechanisms and kinetics of such catalysts can be further understood. Computational modeling studies will also provide a guide for understanding such systems.

The DOE Basic Energy Sciences website describes interest in novel developments in many areas including identification of the elementary steps of catalytic mechanisms and kinetics; studies of structure-reactivity relationships of solution phase or supported inorganic or mixed inorganic/organic hybrid materials on solids; dynamics of the structure of catalysts and their stability; use of novel spectroscopic techniques and structural probes for *in situ* and *in operando* studies, synthesis of reproducible catalysts used under working conditions; design of various structures for structural flexibility and chemical specificity which might influence catalytic properties of inorganic catalysts; controlled syntheses and fundamental understanding of the chemistry of unique inorganic, organic, and hybrid catalysts; new strategies for design and synthesis of selective catalysts for fuels and chemicals; activation of CO₂ and multifunctional molecules; and determination of catalytic mechanisms. This project has efforts in many of those areas.

Many studies of nano-size materials these days focus on control of size and shape of particles. This proposal concerns control of size and shape of nano-size materials as well as control of pores and structures. Such structural control of transition metal oxides is unique. The ability to control pore size and obtain monomodal uniform pores for transition metal, lanthanide, and nonmetal oxide mesoporous materials is rare. Such uniform pores will allow better control of confinement and encapsulation of large moieties such as the organic substrates given above as well as enzymes, related biomolecules, and large inorganic clusters. This research is transformative since whole families of new mesoporous materials with controlled properties can be synthesized and used in a variety of areas of science and engineering.

A fundamental understanding of the catalytic sites and mechanisms of reaction in selective oxidation catalysis is important for the design and use of better catalysts. Preliminary data for selective oxidations suggest that rates of reactions can be markedly enhanced by using well-ordered crystalline monomodal uniform mesopore sized materials. Uses of *in situ* and *in operando* conditions for determining the nature of ROS and studying catalytic reactions with new methods like DART-MS are in their infancy. Combined FTIR/Raman studies of the same catalyst in the same catalytic cell can provide complementary information to understand catalytic intermediates. Ancillary EPR, ¹⁸O labeling, D labeling, and other methods will focus on exact determinations of ROS. Rationale for choosing the specific catalytic reactions are that some have not ever been reported, all are environmentally friendly, all targets are both fundamentally and commercially significant, and all involve new inexpensive scaleable catalysts and processes.

Publications Acknowledging this Grant in 2015-2018

(I) *Exclusively funded by this grant;*

1. Kuo, C. H.; Mosa, I.; Poyraz, A. S.; Biswas, S.; El-Sawy, A.; Song, W.; Luo, Z.; Chen, S. Y.; Rusling, J.; He, J.; Suib, S., Robust Mesoporous Manganese Oxide Catalysts for Water Oxidation, *ACS Catalysis*, 2015, 5, 1693-1699.
2. Njagi, E.; Genuino, H. C.; Kuo, C. H.; Dharmarathna, S.; Gudz, A.; Suib, S.L., High-Yield Selective Conversion of Carbohydrates to Methyl Levulinate Using Mesoporous Sulfated Titania-based Catalysts, *Micr. Mesopor. Mat.*, 2015, 202, 68-72.

3. Kuo, C. H.; Li, W.; Pahalagedara, L.; El-Sawy, A. M.; Kriz, D.; Genz, N.; Guild, C.; Ressler, T.; Suib, S. L.; He, J., Understanding the Role of Gold Nanoparticles in Enhancing the Catalytic Activity of Manganese Oxides in Water Oxidation Reactions, *Ang. Chem. Int. Ed.*, 2015, 54, 2345–2350.
4. Luo, Z.; Poyraz, A. S.; Kuo, C. H.; Miao, R.; Meng, Y.; Chen, S. Y.; Jiang, T.; Wenos, C.; Suib, S.; Crystalline Mixed Phase (Anatase/Rutile) Mesoporous Titanium Dioxides for Visible Light Photocatalytic Activity, *Chem. Mat.*, 2015, 27, 6-17.
5. Hay, S.; Obee, T.; Luo, Z.; Jiang, T.; Meng, Y.; He, J.; Murphy, S.; Suib, S., The Viability of Photocatalysis for Air Purification, *Molecules*, 2015, 20, 1319-1356.
6. Wasalathanthri, N.; Poyraz, A. S.; Biswas, S.; Meng, Y.; Kuo, C. H.; Kriz, D.; Suib, S. L., High-Performance Catalytic CH₄ Oxidation at Low Temperatures: Inverse Micelle Synthesis of Amorphous Mesoporous Manganese Oxides and Mild Transformation to K_{2-x}Mn₈O₁₆ and ε-MnO₂, *J. Phys. Chem. C*, 2015, 119, 1473-1482.
7. Biswas, S.; Poyraz, A. S.; Meng, Y.; Kuo, C. H.; Guild, C.; Tripp, H.; Suib, S. L. Ion induced promotion of activity enhancement of mesoporous manganese oxides for aerobic oxidation reactions, *Appl. Catal., B: Env.*, 2015, 165, 731-741.
8. Jiang, T.; Poyraz, A.; Iyer, A.; Zhang, Y.; Luo, Z.; Zhong, W.; Miao, R.; El-Sawy, A.; Guild, C.; Sun, Y.; Kriz, D.; Suib, S., L., Synthesis of Mesoporous Iron Oxides by an Inverse Micelle Method and Their Application in the Degradation of Orange II under Visible Light at Neutral pH, *J. Phys. Chem.*, 2015, 119, 10454-10468.
9. Jafari, T.; Noshadi, I.; Khakpash, N.; Suib, S. L., Superhydrophobic and Stable Mesoporous Polymeric Adsorbent for Siloxane Removal: D4 Super-Adsorbent, *J. Mat. Chem. A*, 2015, 3, 5023-5030.
10. Garces, L.; Hincapie, B.; Zenger, R.; Suib, S., The Effect of Temperature and Support on the Reduction of Cobalt Oxide: An *In Situ* XRD Study, *J. Phys. Chem.*, 2015, 119, 5484-5490.
11. Kuo, C. H.; Mosa, I. M.; Thanneeru, S.; Sharma, V.; Zhang, L.; Biswas, S.; Aindow, M.; Alpay, S. P.; Rusling, J. F.; Suib, S. L.; He, J., Facet-dependent catalytic activity of MnO electrocatalysts for oxygen reduction and oxygen evolution reactions, *J. C. S. Chem. Comm.*, 2015, 51, 5951-5954.
12. Najafpour, M.; Suib, S. L., Nano-sized Mn oxide as a true catalyst for alcohol oxidation by a mononuclear manganese(II) complex, *Dalton Trans.*, 2015, 44, 15121-15125.
13. Jiang, T.; Du, S.; Jafari, T.; Zhong, W.; Sun, Y.; Song, W.; Luo, Z.; Hines, W. A.; Suib, S., Synthesis of mesoporous gamma-Fe₂O₃ supported palladium nanoparticles and investigation of their roles as magnetically recyclable catalysts for nitrobenzene hydrogenation, *Appl. Catal. A: Gen.*, 2015, 502, 105-113.
14. Zhang, Y.; Jin, L.; Sterling, K.; Luo, Z.; Jiang, T.; Miao, R.; Guild, C.; Suib, S. L., Potassium modified layered Ln₂O₂CO₃ (Ln: La, Nd, Sm, Eu) materials: Efficient and stable heterogeneous catalysts for biofuel production, *Green Chem.*, 2015, 17, 3600-3608.
15. Jin, J.; Hines, W. A.; Kuo, C. H.; Perry, D. M.; Poyraz, A. S.; Xia, Y.; Zaidi, T.; Nieh, M. P.; Suib, S. L., Magnetic Studies of Mesoporous Nanostructured Iron Oxide Materials Synthesized by One-Step Soft-Templating, *Dalton Trans.*, 2015, 44, 11943 - 11953.
16. Zou, J. P.; Ma, J.; Luo, J. M.; Yu, J.; He, J.; Meng, Y.; Luo, Z.; Bao, S. K.; Liu, H. L.; Long, L.; Sheng, L.; Suib, S. L., Fabrication of Novel Few layered WS₂-Bi₂WO₆/Bi_{3.84}W_{0.16}O_{6.24} Composites with Enhanced Photocatalytic Performance, *Appl. Catal. B*, 2015, 179, 220-228.
17. Biswas, S.; Dutta, B.; Mullick, K.; Kuo, C. H.; Poyraz, A.; Suib, S. L., Efficient Aerobic Oxidation of Amines to Imines by Cesium Promoted Mesoporous Manganese Oxide, *ACS Catal.*,

2015, 5, 4394-4403.

18. Liu, B.; Kuo, C. H.; Chen, J.; Luo, J.; Thanneeru, S.; Li, W.; Song, W.; Biswas, S.; Suib, S. L.; He, J., Ligand-Assisted Co-Assembly Approach toward Mesoporous Hybrid Catalysts of Transition-Metal Oxides and Noble Metals: Photochemical Water Splitting, *Ang. Chem., Int. Ed.*, 2015, 54, 9061-9065.

19. Poyraz, A. S.; Biswas, S.; Kim, E., Meng, Y.; Suib, S. L., Mesoporous Multivalent Transition Metal Oxides (V,Cr,Mn,Fe, and co) in Catalysis, in Comprehensive Guide for Mesoporous Materials, Properties and Development, Nova Publishers, 2015, 3, 285-314.

20. Liu, B.; Luo, Z.; Federico, A.; Song, W.; Suib, S.; He, J., Colloidal amphiphile-templated growth of highly crystalline mesoporous non-siliceous oxides, *Chem. Mat.*, 2015, 27, 6173-6176.

21. Jain, R.; Poyraz, A. S.; Gamliel, D. P.; Valla, J.; Suib, S. L.; Maric, R., Comparative study for low temperature water-gas shift reaction on Pt/ceria catalysts: role of different ceria supports, *Appl. Catal. A*, 2015, *Appl. Catal., A:Gen.*, 2015, 507, 1-13.

22. Chen, C. H.; Njagi, E.; Chen, S. Y.; Horvath, D.; Xu, L.; Morey, A.; Mackin, C.; Joesten, R.; Suib, S. L., Structural Distortion of Molybdenum-doped Manganese Oxide Octahedral Molecular Sieves for Enhanced Catalytic Performance, *Inorg. Chem.*, 2015, 54, 10163-71.

23. Dutta, B.; Biswas, S.; Sharma, V.; Savage, N. O.; Alpay, S. P.; Suib, S. L., Mesoporous Manganese Oxide Catalyzed Aerobic Oxidative Coupling of Anilines to Aromatic Azo Compounds, *Ang. Chem. Int. Ed.*, 2016, 55, 2171-2175.

24. El-Sawy, A.; Suib, S. L., Controlling the Active Sites of Sulfur Doped Carbon Nanotube-Graphene Nanolobes for Highly Efficient Oxygen Evolution and Reduction Catalysis, *Adv. Energy Mat.*, 2016, 6,

25. Poyraz, A.; Meng, Y.; Biswas, S.; Suib, S. L., Mesoporous TM Oxide Materials by Surfactant-Assisted Soft templating, in Perovskites and Mixed Metal Oxides, Granger, P., Parvulescu, V. I.; Kaliaguine, S. I.; Prellier, W., Eds., Wiley VCH, NY, 701-714.

26. Acquah, C.; Cagnetta, M.; Achenie, L. E. K.; Suib, S. L.; Karunanithi, A., Effect of Solvent Topography and Steric Hindrance on Crystal Morphology, *Ind. & Eng. Chem. Res.*, 2015, 54, 12108-12113.

27. Mosa, I. M.; Biswas, S.; El-Sawy, A. M.; Botu, V.; Guild, C.; Song, W.; Ramprasad, R.; Rusling, J. F.; Suib, S. L., Tunable mesoporous manganese oxide for high performance oxygen reduction and evolution reactions, *J. Mat. Chem. A*, 2016, 4, 620 – 631.

28. Zou, J. P.; Wu, D. D.; Bao, S. K.; Luo, J.; Luo, X. B.; Lei, S.; Liu, H. L.; Du, H. M.; Luo, S.; Au, C. T.; Suib, S. L., Hydrogen Evolution from Water Coupled with the Oxidation of As(III) in a Photocatalytic System, *ACS Appl. Mat. Int.*, 2015, 7, 28429-28437.

29. Botu, V.; Mhadeshwar, A.; Suib, S. L.; Ramprasad, R., Optimal Dopant Selection for Water Splitting With Cerium Oxides: Mining and Screening First Principles, in Information Science for Discovery and Design, Springer Ser. Materials, 2016, 225, 157-171.

30. Wang, Z.; Yu, J.; Zhang, X.; Li, N; Liu, B.; Li, Y.; Wang, Y.; Wang, W.; Li, Y.; Zhang, L.; Dissanayake, S.; Suib, S. L.; Sun, L., Large Scale and Controllable Synthesis of Graphene Quantum Dots from Rice Husk Biomass: A Comprehensive Utilization Strategy, *ACS Appl. Mat. Int.*, 2016, 8, 1434-1439.

31. Pahalegedara, M.; Pahalegedara, L.; He, J.; Miao, R.; Gottlieb, B.; Rathnayake, D.; Suib, S. L., Room Temperature Selective Reduction of Nitrobenzene to Azoxybenzene over Magnetically Separable Urchin-like Ni /Graphene Nanocomposites, *J. Catal.*, 2016, 336, 41-48.

32. Miao, R.; Luo, Z.; Zhong, W.; Chen, S. Y.; Jiang, T.; Dutta, B.; Nasr, Y.; Zhang, Y.; Suib, S. L., Mesoporous TiO₂ Modified with Carbon Quantum Dots as a High-Performance Visible Light

- Photocatalyst, *Appl. Catal. B, Env.*, 2016, 189, 26-38.
33. Pahalagedara, M. N.; Pahalagedara, L. R.; Kriz, D.; Chen, S. Y.; Beaulieu, F.; Thalaspitiya, W.; Suib, S. L., Copper Aluminum Mixed Oxide (CuAl MO) Catalyst: A Green approach for the One-pot Synthesis of Imines under Solvent-free Conditions, *Appl. Catal. B*, 2016, 188, 227-234.
34. Correa-Baena, J. P.; Kriz, D. A.; Giotto, M.; Suib, S. L.; Agrios, A. G., Fluoride additive in epoxide-initiated sol-gel synthesis enables thin-film applications of SnO₂ aerogels, *RSC Adv.*, 2016, 6, 21326-21331.
35. He, J.; Liu, Y.; Meng, Y.; Sun, X.; Biswas, S.; Shen, M.; Luo, Z.; Miao, R.; Zhang, L.; Mustain, W. E.; Suib, S. L., High-rate long-life of Li-ion batteries using reduced graphene oxide/Co₃O₄ as anode materials, *RSC Adv.*, 2016, 6, 24320 - 24330.
36. Luo, Z.; Cetegen, S. A.; Miao, R.; Jiang, T.; Chen, S. Y.; Jafari, T.; Zhang, Y.; Suib, S. L., Structure-Property Relationships of Copper Modified Mesoporous TiO₂ Materials on Alkyne Homocoupling Reactions, *J. Catal.*, 2016, 338, 94-103.
37. Liu, B.; Yao, H.; Song, W.; Jin, L.; Mosa, I. M.; Rusling, J. F.; Suib, S. L.; He, J., Ligand-Free Noble Metal Nanocluster Catalysts on Carbon Supports 2 via “Soft” Nitriding, *J. Am. Chem. Soc.*, 2016, 138, 4718-4721.
38. Liu, B.; Mosa, I. M.; Song, W.; Zheng, H.; Kuo, C. H.; Rusling, J. F.; Suib, S. L.; He, J., Unconventional structural and morphological transitions of nanosheets, nanoflakes and nanorods of AuNP@MnO₂, *J. Mat. Chem. A*, 2016, 4, 6447-6455.
39. Zou, J. P.; Wang, L. C.; Luo, J.; Nie, Y. C.; Xing, Q. J.; Luo, X. B.; Du, H. M.; Luo, S.; Suib, S. L., Synthesis and Efficient Visible Light Photocatalytic H₂ Evolution of A Metal-free g-C₃N₄/Graphene Quantum Dots Hybrid Photocatalyst, *Appl. Catal. B: Env.*, 2016, 193, 103-109.
40. Liu, B.; Yao, H.; Daniels, R. A.; Song, W.; Zheng, H.; Jin, L.; Suib, S. L.; He, J., A facile synthesis of Fe₃C@mesoporous carbon nitride nanospheres with superior electrocatalytic activity, *Nanoscale*, 2016, 8, 5441-5445.
41. Luo, Z.; Huan, T. D.; Mosa, I. M.; Poyraz, A. S.; Miao, R.; Zhong, W.; Cloud, J.; Kriz, D.; Thanneeru, S.; Ramprasad, R.; Suib, S. L., Mesoporous, Blue MoO_{3-x} Material as Efficient Electrocatalyst for Hydrogen Evolution Reaction, *Adv. Energy Mat.*, 2016, 6,
42. Jafari, T.; Moharreri, E.; Amin, A. S.; Miao, R.; Song, W.; Suib, S. L., Photocatalytic Water Splitting-The Untamed Dream: A Review of Recent Advances, *Molecules*, 2016, 21, 900/1-900/29.
43. Zou, J. P.; Liu, H. L.; Luo, J.; Xing, Q. J.; Du, H. M.; Jiang, X. H.; Luo, X. B.; Luo, S. L.; Suib, S. L., Three-Dimensional Reduced Graphene Oxide Coupled with Mn₃O₄ for Highly Efficient Removal of Sb(III) and Sb(V) from Water, *ACS Appl. Mat. Int.*, 2016, 8, 18140-18149.
44. Biswas, S.; Mullick, K.; Chen, S. Y.; Kriz, D. A.; Shakil, M. D.; Kuo, C. H.; Angeles-Boza, A. M.; Rossi, A. R.; Suib, S. L., Mesoporous Copper/Manganese Oxide Catalyzed Coupling of Alkynes: Evidence for Synergistic Cooperative Catalysis, *ACS Catal.*, 2016, 6, 5069-5080.
45. Song, W.; Ren, Z.; Chen, S. Y.; Meng, Y.; Biswas, S.; Nandi, P.; Elsen, H.; Gao, P. X.; Suib, S. L., Ni and Mn-Promoted Mesoporous Co₃O₄: a Stable Bifunctional Catalyst with Surface Structure Dependent Activity for Oxygen Reduction Reaction and Oxygen Evolution Reaction, *ACS Applied Materials & Interfaces*, 2016, 8, 20802-20813.
46. Wasalathanthri, N.; SantaMaria, T. M.; Kriz, D. A.; Dissanayake, S. L.; Kuo, C. H.; Biswas, S.; Suib, S. L., Mesoporous Manganese Oxides for NO₂ Assisted Catalytic Soot Oxidation, *Appl. Catal. B*, 2016, 201, 543-551.
47. Zou, J. P.; Wu, D. D.; Luo, J.; Xing, Q. J.; Luo, X. B.; Dong, W. H.; Luo, S.; Du, H. M.; Suib, S. L., A Strategy for One-Pot Conversion of Organic Pollutants into Useful Hydrocarbons through

Coupling Photodegradation of MB with Photoreduction of CO₂, *ACS Catalysis*, 2016, 6, 6861-6867.

48. Pahalagedara, L.; Kriz, D.; Wasalathanthri, N.; Weerakkodi, C.; Meng, Y.; Dissanayake, S.; Pahalagedara, M.; Luo, Z.; Suib, S. L.; Nandi, P.; Benchmarking of Manganese Oxide Materials with CO Oxidation as Catalysts for Low Temperature Selective Oxidation, *Appl. Catal. B*, 2017, 204, 411-420.

49. Yin, S.; Sauyet, T.; Guild, C.; Suib, S. L.; Jain, M., Magnetic properties of pure and Fe doped HoCrO₃ thin films fabricated via a solution route, *J. Magnet. Magn. Mat.*, 2017, 428, 313-319.

50. Miao, R.; He, J.; Sahoo, S.; Luo, Z.; Zhong, W.; Chen, S. Y.; Guild, C.; Jafari, T.; Dutta, B.; Cetegen, S.; Wang, M.; Alpay, S. P.; Suib, S., Reduced Graphene Oxide Supported Nickel-Manganese-Cobalt Spinel Ternary Oxide Nanocomposites and Their Chemical-Converted Sulfide Nanocomposites as Efficient Electrocatalysts for Alkaline Water Splitting, *ACS Catalysis*, 2016, 7, 819-832.

51. Mullick, K.; Biswas, S.; Angeles-Boza, A. M.; Suib, S. L., Heterogeneous Mesoporous Manganese Oxide Catalyst for Aerobic and Additive-Free Oxidative Aromatization of N-Heterocycles, *Chem. Comm.*, 2017, 53, 2256-2259.

52. Liu, L.; Luo, Y.; Tan, W.; Liu, F.; Suib, S. L., Zhang, Y.; Qiu, G., Zinc removal from aqueous solution using deionization pseudocapacitor with high-performance nanostructured birnessite electrode, *Env. Sci. : Nano*, 2017, 4, 811-823.

53. Jafari, T.; Moharreri, E.; Toloueinia, P.; Amin, A. S.; Sahoo, S.; Khakpash, N.; Noshadi, I.; Alpay, S. P.; Suib, S. L., Microwave Assisted Synthesis of Amine Functionalized Mesoporous Polydivinylbenzene for CO₂ Adsorption, *J. CO₂ Util.*, 2017, 19, 79-90.

54. Iyer, A.; Kuo, C. H.; Dharmarathna, S.; Luo, Z.; Rathnayake, D.; He, J.; Suib, S. L., An ultrasonic atomization assisted synthesis of self-assembled manganese oxide octahedral molecular sieve nanostructures and their application in catalysis and water treatment, *Nanoscale*, 2017, 9, 5009-5018.

55. Liu, B.; Jiang, T.; Zheng, H.; Dissanayake, S.; Song, W.; Federico, A.; Suib, S. L.; He, J., Nanoengineering of Aggregation-Free and Thermally-Stable Gold Nanoparticles in Mesoporous Frameworks, *Nanoscale*, 2017, 9, 6380-6390.

56. Liu, B.; Wang, P.; Lopes, A.; Jin, L.; Zhong, W.; Pei, Y.; Suib, S., L.; He, J, Au-carbon electronic interaction mediated selective oxidation of styrene, *ACS Catal.*, 2017, 7, 3483-3488.

57. Liu, G.; Liu, J.; Li, W.; Liu, C.; Wang, F.; He, J.; Guild, C.; Jin, J.; Kriz, D.; Suib, S. L., Aerobic oxidation of alcohols over Ru-Mn-Ce and Ru-Co-Ce catalysts: The effect of calcination temperature, *Appl. Catal., A: Gen.*, 2017, 535, 77-84.

58. Najafpour, M. M.; Shirazi A. A.; Balaghi, S. E.; Deljoo, B.; Mousazade, Y.; Jafari, T.; Aindow, M.; Suib, S. L., Transformation of La_{0.65}Sr_{0.35}MnO₃ in Electrochemical Water Oxidation, *Int. J. Hydrogen Energy*, 2016, 42, 8560-8568.

59. Biswas, S.; Mullick, K.; Chen, S. Y.; Gudz, A.; Carr, D. M.; Mendoza, C.; Angeles-Boza, A. M.; Suib, S. L., Facile Access to Versatile Functional Groups from Alcohols by Single Multifunctional Reusable Catalysts, *Appl. Catal., B: Env.*, 2017, 203, 607-614.

60. Zhong, W.; Jiang, T.; Jafari, T.; Poyraz, A. S.; Wu, W.; Kriz, D. A.; Du, S.; Biswas, S.; Pettes, M. T.; Suib, Steven L., Modified Inverse Micelle Synthesis for Mesoporous Alumina with a High D4 Siloxane adsorption Capacity, *Micropor. Mesopor. Mat.*, 2017, 239, 328-335.

61. Xing, Y.; Liu, Z.; Wu, D.; Guo, X.; Qu, X.; Fang, S.; Suib, S. L.; Self-assembly synthesis of Mn₃O₄ hierarchical micro/nano architectures as supercapacitor electrodes, *J. Mat. Sci.*, 2017, 28, 12004-12014.

62. Suib, S. L., A Review of Recent Developments of Mesoporous Materials, *Chem. Record*, 2017, 17, 1169-1183.
63. Jafari, T.; Meguerdichian, A.; Jiang, T.; El-Sawy, A.; Suib, S. L., Non-precious Metal Oxide and Metal-free Catalysts for Energy Storage and Conversion, in *Advanced Electrode Materials*, Ashutosh Tiwari, Filiz, Kuralay, Lokman Uzun, Eds., 2016, Chapter 7, 243-320, Wiley-Scrivener, Beverly, MA.
64. Xing, Y.; Guo, X.; Wu, D.; Liu, Z.; Fang, S.; Suib, S. L., Construction of macroscopic 3D foams of metastable manganese oxides via a mild templating route: Effects of atmosphere and calcination, *J. Alloys Comp.*, 2017, 719, 22-29.
65. Kuo, C.H.; Kriz, D. A.; Gudz, A.; Suib, S. L., Biosynthesis of size-controlled metal and metal oxide nanoparticles by bacteria, in *Bio-Nanoparticles*, Edited by Singh, O. V., 2015, 123-140.
66. Liu, L.; Qiu, G.; Suib, S. L.; Liu, F.; Zheng, L.; Tan, W.; Qin, L., Enhancement of Zn²⁺ and Ni²⁺ removal performance using a deionization, *Chem. Eng. J.*, 2017, 328, 464-473.
67. Sahoo, S.; Suib, S. L.; Alpay, S. P., Graphene Supported Single Atom Transition Metal Catalysts for Methane Activation, *ChemCatChem*, 2018, in press.
68. Mullick, K.; Biswas, S.; Kim, C.; Ramprasad, R.; Angeles-Boza, A. M.; Suib, S. L., Ullmann Reaction Catalyzed by Heterogeneous Mesoporous Copper Manganese Oxide: A Kinetic and Mechanistic Analysis, *Inorg. Chem.*, 2017, 56, 10290-10297.
69. Pardakhti, M.; Moharrerri, E.; Wanik, D.; Suib, S. L.; Srivastava, R., Machine learning using combined structural and chemical descriptors for prediction of methane adsorption performance of metal organic frameworks (MOFs), *ACS Comb. Sci.*, 2017, 19, 640-645.
70. Liu, Z.; Wu, D.; Guo, X.; Fang, S.; Wang, L.; Xing, Y.; Suib, S. L., Robust Macroscopic 3D Sponges of Manganese Oxide Molecular Sieve, *Chem. Eur. J.*, 2017, 23, 16213 – 16218.
71. Miao, R.; Dutta, B.; Sahoo, S.; He, J.; Zhong, W.; Cetegen, S.; Jiang, T.; Alpay, S. P.; Suib, S. L., Mesoporous Iron Sulfide for Highly Efficient Electrocatalytic Hydrogen Evolution, *J. Am. Chem. Soc.*, 2017, 139, 13604-13607.
72. Weerakkody, C.; Biswas, S.; Song, W.; He, J.; Wasalathanthri, N.; Dissanayake, S.; Kriz, D. A.; Dutta, B.; Suib, S. L., Controllable Synthesis of Mesoporous Cobalt Oxide for Peroxide Free Catalytic Epoxidation of Alkenes under Aerobic Conditions, *Appl. Catal., B*, 2017, 221, 681-690.
73. Biswas, S.; Dutta, B.; Mannodi-Lanakithodi, A.; Clarke, R.; Song, W.; Ramprasad, R.; Suib, S. L., Heterogeneous Mesoporous Manganese/Cobalt Oxide Catalyst for Selective Oxidation of 5-hydroxymethylfurfural to 2,5-diformylfuran, *Chem. Comm.* 2017, 53, 11751-11754.
74. Zhong; W.; Jiang; T.; Dang; Y.; He, J.; Chen, S. Y.; Kuo, C. H.; Kriz, D.; Meng, Y.; Meguerdichian, A.; Suib, S. L., Mechanism studies on methyl orange dye degradation by perovskite-type LaNiO₃ under dark ambient conditions, *Appl. Catal. A*, 2018, 554, 54-63.
75. Dutta, B.; Sharma, Sharma; Sassu, N.; Dang, Y.; Weerakkody, C.; Macharia, J.; Miao, R.; Howell, A. R.; Suib, S. L., Cross Dehydrogenative Coupling of N-Aryltetrahydroisoquinolines (sp³ C-H) with Indoles (sp² C-H) Using Heterogeneous Mesoporous Manganese Oxide Catalyst, *Green Chemistry*, 2017, 19, 5350 – 5355.
76. He, J.; Wang, M.; Wang, W.; Miao, R.; Zhong, W.; Chen, S. Y.; Poges, S.; Jafari, T.; Song, W.; Liu, J.; Suib, S. L., Hierarchical Mesoporous NiO/MnO₂@PANI Core-Shell Microspheres Highly Efficient and Stable Bifunctional Electrocatalysts for Oxygen Evolution and Reduction Reactions, *ACS Appl. Mat. Int.*, 2017, 9, 42676-42687.
77. Zhong, W.; Jiang, T.; Dang, Y.; He, J.; Chen, S. Y.; Kuo, C. K.; Kriz, D.; Meng, Y.;

- Meguerdichian, A. G.; Suib, S. L., Mechanism studies on Methyl Orange dye degradation by perovskite-type $\text{LaNiO}_{3-\delta}$ under dark ambient conditions, *Appl. Catal., A: Gen.*, 2018, 549, 302-309.
78. Liu, B.; Jin, L.; Zhong, W.; Lopes, A.; Suib, S. L.; He, J., Ultrafine and Ligand-Free Precious Metal (Ru, Ag, Au, Rh and Pd) Nanoclusters Supported on Phosphorus-Doped Carbon, *Chem. Eur. J.*, 2018, 24, 2565-2569.
79. Moharreri, E.; Hines, W.; Biswas, S.; Perry, D.; He, J.; Murray-Simmons, D.; Suib, S. L., Comprehensive Magnetic Study of Nanostructured Mesoporous Manganese Oxide Materials and Implications for Catalytic Behavior, *Chem. Mat.*, 2018, 30, 1164-1177.
80. Meguerdichian, A.; Jafari, T.; Shakil, M. M.; Miao, R.; Achola, L.; Macharia, J.; Shirazi, A. A.; Suib, S., Synthesis and Electrocatalytic Activity of Ammonium Nickel Phosphate, $\text{NH}_4\text{NiPO}_4 \cdot 6\text{H}_2\text{O}$ and β -Nickel Pyrophosphate, $\beta\text{-Ni}_2\text{P}_2\text{O}_7$ Catalysts for Electrocatalytic Decomposition of Urea, *Inorg. Chem.*, 2018, 57, 1815-1823.
81. Luo, Z.; Kriz, D. A.; Miao, R.; Kuo, C. H.; Zhong, W.; Guild, C.; He, J.; Willis, W.; Dang, Y.; Suib, S. L.; Nandi, P., TiO_2 Supported Gold-Palladium Catalyst for Effective Syngas Production from Methane Partial Oxidation, *Appl. Catal. A.*, 2018, 554, 54-63.
82. Hincapie, B.; Llano, S. M.; Garces, H. F.; Espinal, D.; Suib, S. L.; Garces, L. J., Epoxidation of Cyclopentene by a Low Cost and Environmentally Friendly Bicarbonate/Peroxide/Manganese System, *Ads. Sci. & Tech.*, 2018, 36, 9-22.
83. Yin, S.; Zhong, W.; Guild, C. J.; Shi, J.; Suib, S. L.; Cotica, L. F.; Jain, M., Effect of Gd Substitution on the structural, magnetic, an magnetocaloric Properties of HoCoO_3 , *J. Appl. Phys.*, 2018, 123, 053904/1-053904/6.
84. Nie, Y. C.; Yu, F.; Wang, L. C.; Xing, Q. J.; Liu, X.; Pei, Y.; Zou, J. P.; Dai, W. L.; Li, Y.; Suib, S. L., Photocatalytic Degradation of Organic Pollutants Coupled with Simultaneous Photocatalytic H_2 Evolution over Graphene Quantum $\text{TiO}_2\text{-g-C}_3\text{N}_4$ Composite Catalysts: Performance and mechanism, *Appl. Catal., B: Env.*, 2018, 227, 312-321.
85. Liu, C.; Luo, W.; Liu, J.; Sun, L.; Yang, Y.; Liu, G.; Wang, F.; Zhong, W.; Guild, C.; Suib, S. L., Pt/Ferric Hydroxyphosphate: An Effective Catalyst for the Selective Hydrogenation of α,β -Unsaturated Aldehydes (Ketones) into α,β -Unsaturated Alcohols, *Catal. Lett.*, 2018, 148, 555-563.
86. Ouyang, J.; Zheng, C.; Gu, W.; Zhang, Y.; Yang, H.; Suib, S. L. Textural properties determined CO_2 capture of tetraethylenepentamine loaded SiO_2 nanowires from α -sepiolite *Chem. Eng. J.*, 2018, 337, 342-350.
87. Poges, S.; Dutta, B.; Khanna, H.; Moharreri, E.; Aindow, M.; Suib, S. L., Cross Sectional Analysis of Cation Doped Transition Metal Oxide Mesoporous Catalyst Materials, *Microsc. Microanal.*, 2017, 23, 292-293.
88. King'onde, C. K.; Garces, H. F.; Suib, S. L., Nano-Structures & Nano-Objects, End to End and Side by Side Alignment of Short Octahedral Molecular Sieve (OMS-2) Nanorods into Long Microyarn Superarchitectures and Highly Flexible Membranes, *Nano-Str. Nano-Obj.*, 2018, 14, 49-56.

(II) *Jointly funded by this grant and other grants with leading intellectual contribution from this grant;*

1. Guild, C. J.; Kriz, D.; Vovchok, D.; Llorca, J.; Xu, W.; Bruix, A.; El-Sawy, A.; Biswas, S.; Suib, S. L.; Sennayake, S. D., In situ Studies of cerium Oxide Nanoparticles During the Water Gas Shift Reaction, *Preprints – ACS, Div. Energy & Fuels*, 2015, 60, 136.

2. Jiang, T.; Zhong, W.; Jafari, T.; Du, S.; He, J.; Fu, Y. J.; Singh, P.; Suib, S. L., Siloxane adsorption by mesoporous aluminosilicates, *Chem. Eng. J.*, 2016, 289, 356-364.
3. Jafari, T.; Jiang, T.; Zhong, W.; Khakpash, N.; Deljoo, B.; Aindow, M.; Singh, P.; Suib, S. L., Modified Mesoporous Silica for Efficient Siloxane Capture, *Langmuir*, 2016, 32, 2369-2377.
4. Chen, S. Y.; Song, W.; Lin, H. J.; Wang, S.; Biswas, S.; Mollahosseini, M.; Kuo, C. H.; Gao, P. X.; Suib, S. L.; Manganese Oxide Nano-Array Based Monolithic Catalysts: Tunable Morphology and High Efficiency for CO Oxidation, *ACS Appl. Mat. & Int.*, 2016, 8, 7834-7842.
5. Noshadi, I.; Kanjilal, B.; Jafari, T.; Moharreri, E.; Khakpash, N.; Jiang, T.; Suib, S. L., Hydrophobic Mesoporous Adsorbent based on Cyclic Amine - Divinylbenzene Copolymer for Highly Efficient Siloxane Removal, *RSC Adv.*, 2016, *RSC Advances*, 2016, 6, 77310 – 77320.
6. Guild, C.; Vovchok, D.; Kriz, D. A.; Bruix, A.; Hammer, B.; Llorca, J.; Xu, W.; El-Sawy, A.; Biswas, S.; Rodriguez, J. A.; Senanayake, S. D.; Suib, S. L.; Water Gas Shift over Metal-Free Nanocrystalline Ceria: An Experimental and Theoretical Study, *ChemCatChem*, 2017, 9, 1373-1377.
7. Vovchok, D.; Guild, C. J.; Llorca, J.; Xu, W.; Jafari, T.; Toloueinia, P.; Kriz, D.; Waluyo, I.; Palomino, R. M.; Rodriguez, J. A.; et al, Cu supported on mesoporous ceria: water gas shift activity at low Cu loadings through metal-support interactions, *Phys. Chem. Chem. Phys.*, 2017, 19, 17708-17717.
8. Palmieri, A.; Liu, Y.; He, J.; Meng, Y.; Suib, S. L.; Mustain, W. E., Metal Oxide/Reduced Graphene Oxide Anodes or Lithium batteries, *ECS Transactions*, 2015, 66, (9, Lithium-Ion Batteries and Beyond), 47-55.

(III) *Jointly funded by this grant and other grants with relatively minor intellectual contribution from this grant;*

1. Bhakta, S.; Seraji, S.; Suib, S.; Rusling, J., Antibody-like Biorecognition Sites for Proteins from Surface Imprinting on Nanoparticles, *ACS Appl. Mat. Interf.*, 2015, 7, 28197–28206.
2. Dey, S.; Chen, S.; Thota, S.; Shakil, M. M. ; Suib, S.; Zhao, J., Effect of Gradient Alloying on Photoluminescence Blinking of Single CdS_xSe_{1-x} Nanocrystals, *J. Phys. Chem. C*, 2016, 120, 20547-20554.
3. Liu, Y.; Palmieri, A.; He, J.; Meng, Y.; Beauregard, N.; Suib, S. L.; Mustain, W., Highly Conductive In-SnO₂/RGO Nano-Heterostructures with Improved Lithium-Ion Battery Performance, *Sci. Rep.*, 2016, 6, 25860.
4. Bhakta, S.; Dixit, C. K.; Bist, I.; Jalil, K. A.; Suib, S. L.; Rusling, J. F., Sodium hydroxide catalyzed monodispersed high surface area silica Nanoparticles, *Mat. Res. Expr.*, 2016, 3, 075025/1-075025/8.
5. Dixit, C. K.; Bhakta, S.; Kumar, A.; Suib, S. L.; Rusling, J. F., Fast Nucleation for Silica Nanoparticle Synthesis in Sol-Gel Method, *Nanoscale*, 2017, 9, 5009-5018.
6. Wang, W.; Wang, Z.; Liu, J.; Luo, Z.; Suib, S. L.; He, P.; Ding, G.; Zhang, Z.; Sun, L., Single-step One-pot Synthesis of TiO₂ Nanosheets Doped with Sulfur on Reduced Graphene Oxide with Enhanced Photocatalytic Activity, *Sci. Reports*, 2017, 7, 46610.
7. Sharafeldin, M.; Bishop, G. W.; Bhakta, S.; El-Sawy, A.; Suib, S. L.; Rusling, J. F., Fe₃O₄ nanoparticles on graphene oxide sheets for isolation and ultrasensitive amperometric detection of cancer biomarker proteins, *Biosens. Bioelectr.*, 2017, 91, 359-366.
8. Yu, J.; Liu, J.; Clearfield, A.; Sims, J. E.; Speigle, M. T.; Suib, S. L.; Sun, L., Synthesis of layered Double Hydroxide Single-Layer Nanosheets in Formamide, *Inorg. Chem.*, 2016, 55, 12036-12041.

9. Bhakta, S.; Dixit, C. K.; Bist, I.; Macharia, J.; Shen, M.; Kadimisetty, K.; He, J.; Dutta, B.; Suib, S. L.; Rusling, J. F., Albumin Removal from Human Serum using Surface Nanopockets on Silica-coated Magnetic Nanoparticles, *Chem. Comm.*, 2017, 53, 9254-9257.
10. Dey, S.; Zhou, Y.; Sun, Y.; Jenkins, J. A.; Kriz, D.; Suib, S. L.; Chen, O.; Zou, S.; Zhao, J., Excitation wavelength dependent photon anti-bunching/bunching from single quantum dots near gold nanostructures, *Nanoscale*, 2018, 10, 1038-1046.

Tuesday PI Oral Presentations

The Effect of Lewis Acid Co-Catalysts on the Reversible Hydrogenation of Carbon Dioxide to Formic Acid and Methanol

Nilay Hazari and Wesley H. Bernskoetter
Yale University; University of Missouri

Presentation Abstract

The steady decline in the world's fossil fuel reserves and the potential environmental consequences of continued fossil fuel use has spawned considerable interest in the utilization of renewable carbon sources. Carbon dioxide is a particularly attractive feedstock owing to its high abundance, low cost and toxicity, and relative ease of transport. In addition, the reversible hydrogenation of carbon dioxide offers the potential to store hydrogen, a clean energy source, in a transportable liquid form which can be released by dehydrogenation at the point of use. This presentation will describe the project's latest advances in understanding the catalytic transformations associated with the use of formic acid and methanol as liquid molecules for chemical hydrogen storage. Particular emphasis is placed on the significant role Lewis acid and other co-catalysts play in catalytic activity. The application a series of pincer supported iron catalysts for the (de)hydrogenative syntheses of several valuable commercial chemicals is also discussed.

DE-SC0018222: Elucidating the Role of Lewis Acid Co-Catalysts in Base Metal Promoted CO₂ Hydrogenation and Related Processes

Postdoc(s): Name(s) Upul Jayarathne

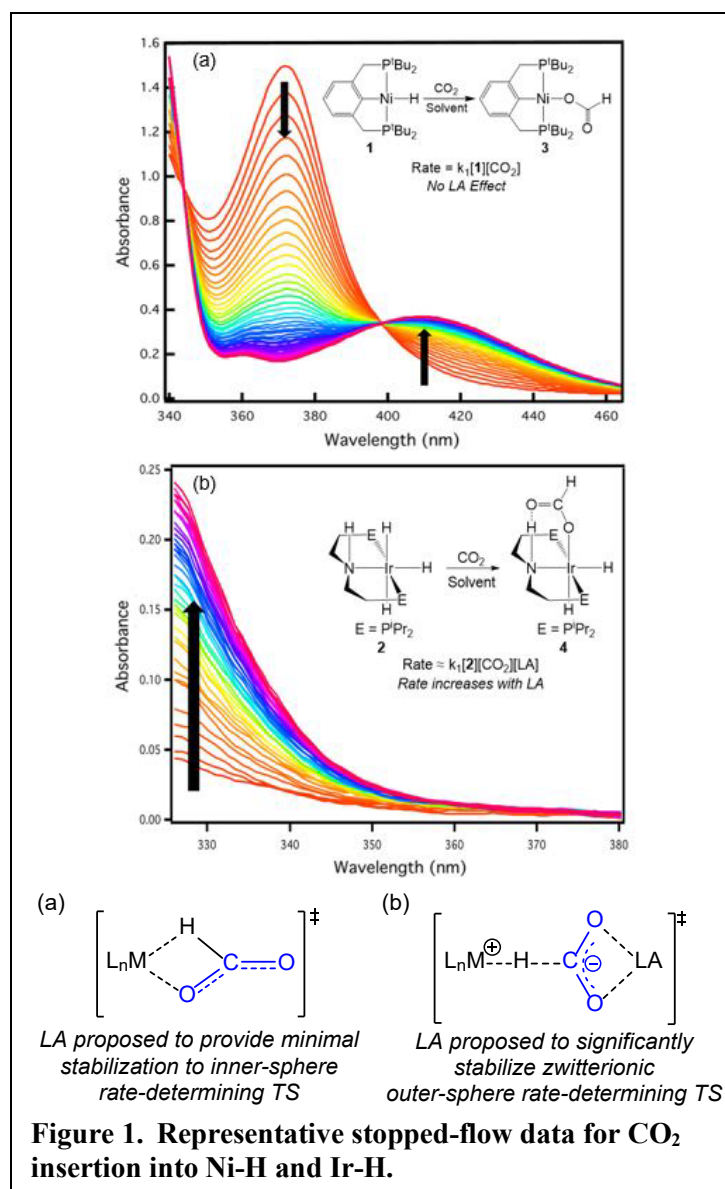
Student(s): Elizabeth M. Lane; Jessica E. Heimann; Nicholas E. Smith; Julia Curley

RECENT PROGRESS

Research progress toward the elucidation reversible transition metal/LA co-catalyzed CO₂ hydrogenation and related reactions is summarized below for selected areas.

Lewis acid (LA) and solvent-dependent kinetics of CO₂ insertion

The insertion of CO₂ into metal hydrides (or other ligands) is fundamental to most metal mediated CO₂ reduction catalysis. Our project has recently begun using stopped-flow methods to examine the kinetics of this reaction of inner-sphere (meaning the electrophile pre-coordinates to the metal) and outer-sphere (meaning no pre-coordination of the electrophile to the metal) CO₂ insertions into metal hydride complexes. The preliminary results indicate that species which utilize an outer-sphere pathway (such as the Ir-H species in Figure 1) exhibit a significant rate enhancement with LA, while those that proceed via an inner-sphere mechanism are unaffected by the presence of LA (like the Ni-H species in Figure 1). Our current hypothesis is that this influence originates from LA stabilization of the carboxylate anionic charge build up in the transition structure of the outer-sphere pathway, which is not required in the inner-sphere pathway. Additionally, a notable solvent



reduction of $[(^i\text{PrPnP})\text{FeH}(\text{CO})]$ (**1**) ($^i\text{PrPnP} = \text{N}\{\text{CH}_2\text{CH}_2(\text{P}^i\text{Pr}_2)\}_2$) to generate the zerovalent iron dicarbonyl species $[(^i\text{PrPnP})\text{Fe}(\text{CO})_2]$, which we hypothesize forms via reductive H_2 elimination from a transient iron hydride species, $[(^i\text{PrPN}^{\text{H}}\text{P})\text{Fe}(\text{H})_2(\text{CO})]$, followed by species degradation and capture of emitted CO (Figure 2). More recently, we have observed and characterized two analogous zerovalent iron dicarbonyl species produced from the N-methylated catalyst analog $[(^i\text{PrPN}^{\text{Me}}\text{P})\text{FeH}(\text{CO})(\text{BH}_4)]$ (**2**) ($^i\text{PrPN}^{\text{Me}}\text{P} = \text{MeN}\{\text{CH}_2\text{CH}_2(\text{P}^i\text{Pr}_2)\}_2$) (Figure 2). The first new deactivation product, $[(^i\text{PrPN}^{\text{Me}}\text{P})\text{Fe}(\text{CO})_2]$, was identified during the catalyzed N-formylation of amines by CO_2 and H_2 . Unlike many other iron promoted CO_2 hydrogenation reaction, the presence of Lewis acid Li salts lowered catalyst productivity. This atypical result originates from the acceleration of a second catalyst deactivation pathway to form a cationic iron dicarbonyl species, $[(^i\text{PrPN}^{\text{Me}}\text{P})\text{Fe}(\text{H})(\text{CO})_2]\text{OTf}$ (Figure 2). While formation of these iron dicarbonyl complexes is obviously deleterious to catalysis, their identification is a significant first step toward developing longer lived, more productive catalytic systems. We are currently working

effect has been observed for the rate of CO_2 insertion into a Ni-H species which utilizes the inner-sphere mechanism. Significantly, this provides another tool for rationally enhancing the kinetics of CO_2 insertion in cases where LA co-catalysts are less effective. Investigating a range of solvent effects has demonstrated a rough correlation between rate enhancement and solvent acceptor number, which is itself a measure of the Lewis acidity of the solvent. As may be expected on the basis of the proposed transition structures in the lower section of Figure 1, a strong solvent influence was observed in the outer-sphere CO_2 insertion as well, though incompatibility between our Ir-H complex and several target solvents has slowed a more complete analysis within this domain of CO_2 insertion reactions.

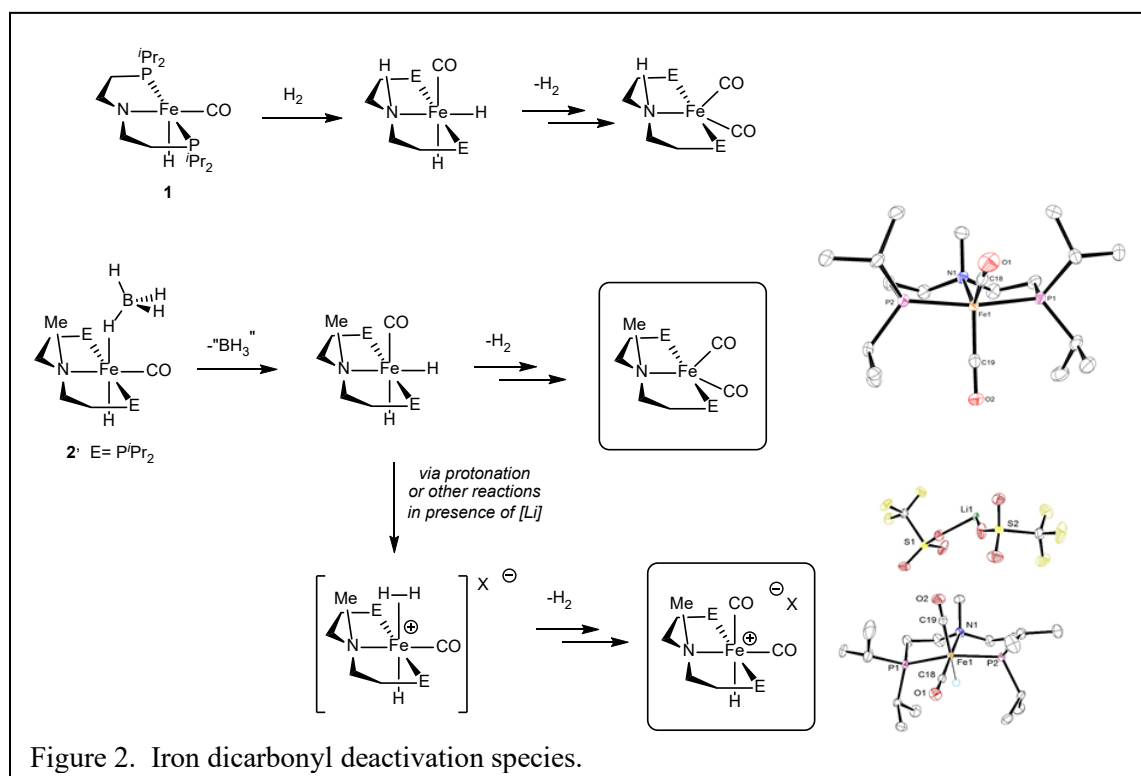
Deactivation pathways for catalytic Iron-Lewis Acid systems:

Our investigations into base metal catalysis have identified several catalyst deactivation species relevant to Fe/LA co-catalyzed CO_2 hydrogenation reactions. We have previously observed the deactivating

with computational experts Profs. Ainara Nova, David Ballcells (both at Oslo) and Martin Jaraiz (Valladolid) to better understand these deactivation reactions and other mechanistic cornerstones of CO₂ hydrogenation.

Sequential hydrogenation of CO₂ to methanol

Our prior research efforts have validated the ability of catalyst **1** to mediate both steps of a proposed CO₂ to MeOH conversion, namely, N-formylation using CO₂ and formamide hydrogenation to generate MeOH (Figure 3). Both of these reactions occur using the same catalyst under similar solvent, temperature, and pressure conditions, suggesting that a single stage CO₂ to MeOH conversion is feasible. Our recent efforts to realize this potential have identified several remaining obstacles to integrating these two catalytic processes. The most significant barrier



appears to be the incomplete consumption of all CO₂ in the first phase of the process, which permits generation of an iron formate complex, [(ⁱPr⁺PN^HP)FeH(CO)HCO₂⁻] (Figure 3). The iron formate species has been previously characterized and is known to be an intermediate in the reversible hydrogenation of CO₂ to formic acid, however, under the conditions of amide hydrogenation it appears to provide a thermodynamic sink. Therefore, we have taken an interim step of conducting the CO₂ to MeOH conversion in a one pot, two stage reaction in which the excess CO₂ is vented prior to the amide hydrogenation step. Additionally, the presence of molecular sieves to remove the water by-product and/or filtration of carbamate salts to remove latent CO₂ sources further enhance the conversion to MeOH. Admittedly, this current manifestation of the process is less than ideal, however, the two step reaction does provide TONs for MeOH as high as 650, on par with the few known precious metal catalysts, and the first high-functioning earth abundant metal catalyst for this process.

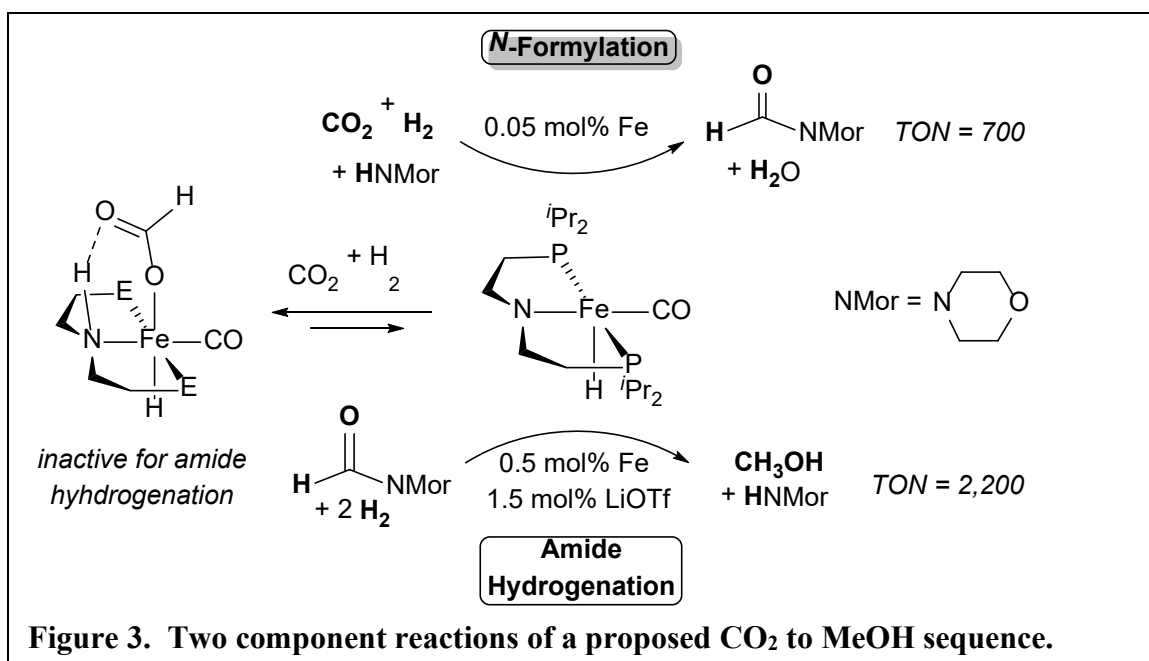


Figure 3. Two component reactions of a proposed CO₂ to MeOH sequence.

Publications Acknowledging this Grant in 2015-2018

(I) Exclusively funded by this grant;

Jayarathne, U.; Hazari, N.; Bernskoetter, W. H. "Selective Iron-Catalyzed N-Formylation of Amines using Dihydrogen and Carbon Dioxide" *ACS Catal.* **2018**, *8*, 1338-1345.

Lane, E. M.; Hazari, N.; Bernskoetter, W. H. "Iron-catalyzed Urea Synthesis: Dehydrogenative Coupling of Methanol and Amines" *Chem. Sci.* **2018**, *9*, 4003-4008.

Bio-Inorganic Approaches to Molecular Electrocatalysis

Christopher J. Chang
Chemical Sciences Division, Lawrence Berkeley National Laboratory, Department of Chemistry,
University of California, Berkeley

Presentation Abstract

Rising energy demands and the changing climate at the global scale motivate the invention of new technologies for solar-to-chemical conversion for sustainable use of limited carbon resources. To meet this challenge, we have initiated a program to develop new molecular catalysts for generating hydrogen from water and fixing carbon dioxide, with particular interest in bio-inorganic systems that operate in green aqueous media with sustainable electrical energy input. This talk will present our latest work on molecular platforms for water and hydrogen and carbon dioxide reduction that utilize concepts and components from materials and biological catalyst systems.

FWP #CH030201: Harnessing Complexity for Catalytic Efficiency

PI: John F. Hartwig

RECENT PROGRESS

Publications Acknowledging this Grant in 2015-2018

13. Cao, Z.; Derrick, J. S.; Xu, J.; Gao, R.; Gong, M.; Nichols, E. M.; Smith, P. T.; Liu, X.; Wen, X.; Coperet, C.; Chang, C. J.; "Chelating N-Heterocyclic Carbene Ligands Enable Tuning of Electrocatalytic CO₂ Reduction to Formate and Carbon Monoxide through Surface Organometallic Chemistry", *Angew. Chem. Int. Ed.* **2018**, *57* 4981-4985. (I)
12. Nichols, E. M.; Derrick, J. S.; Nistanaki, S. K.; Smith, P. T.; Chang, C. J.; "Positional effects of second-sphere amide pendants on electrochemical CO₂ reduction catalyzed by iron porphyrins", *Chem. Sci.* **2018**, *9*, 2952-2960. (I)
11. Diercks, C. S.; Lin, S.; Kornienko, N.; Kapustin, E. A.; Nichols, E. M.; Zhu, C.; Zhao, Y.; Chang, C. J.; Yaghi, O. M. "Reticular Electronic Tuning of Porphyrin Active Sites in Covalent Organic Frameworks for Electrocatalytic Carbon Dioxide Reduction", *J. Am. Chem. Soc.* **2018**, *140*, 1116-1122. (I)
10. Gong, M.; Cao, Z.; Liu, W.; Nichols, E. M.; Smith, P. T.; Derrick, J. S.; Liu, Y. S.; Liu, J.; Wen, X.; Chang, C. J.; "Supramolecular Porphyrin Cages Assembled at Molecular–Materials Interfaces for Electrocatalytic CO Reduction", *ACS Central Science* **2017**, *3*, 1032-1040. (I)
9. Lin, S.; Yang, X.; Jia, S.; Weeks, A. M.; Hornsby, M.; Lee, P. S.; Nichiporuk, R. V.; Iavarone, A. T.; Wells, J. A.; Toste, F. D.; Chang, C. J. "Redox-based reagents for chemoselective methionine bioconjugation", *Science* **2017**, *355*, 597-602. (II)
8. Kashif, M. K.; Milhuisen, R. A.; Nippe, M.; Hellerstedt, J.; Zee, D. Z.; Duffy, N. W.; Halstead, B.; De Angelis, F.; Fantacci, S.; Fuhrer, M. S.; Chang, C. J.; Cheng, Y.-B.; Long, J. R.; Spiccia,

- L.; Bach, U. "Cobalt Polypyridyl Complexes as Transparent Solution-Processable Solid-State Charge Transport Materials", *Adv. Energy Mater.* **2016**, 1600874. (III)
7. Cao, Z.; Kim, D.; Yu, Y.; Xu, J.; Lin, S.; Wen, X.; Nichols, E. M.; Jeong, K.; Reimer, J. A.; Yang, P.; Chang, C. J. "A Molecular Surface Functionalization Approach to Tuning Nanoparticle Electrocatalysts for Carbon Dioxide Reduction", *J. Am. Chem. Soc.* **2016**, *138*, 8120-8125. (I)
 6. Kornienko, N.; Zhao, Y.; Kley, C. S.; Zhu, C.; Kim, D.; Lin, S.; Chang, C. J.; Yaghi, O. M.; Yang, P. "Metal–Organic Frameworks for Electrocatalytic Reduction of Carbon Dioxide", *J. Am. Chem. Soc.* **2015**, *137*, 14129-14135. (II)
 5. Nichols, E. M.; Gallagher, J. J.; Liu, C.; Su, Y.; Resasco, J.; Yu, Y.; Sun, Y.; Yang, P.; Chang, M. C. Y.; Chang, C. J. "Hybrid bioinorganic approach to solar-to-chemical conversion", *Proc. Natl. Acad. Sci. USA* **2015**, *112*, 11461-11466. (I)
 4. Lin, S.; Diercks, C. S.; Zhang, Y.; Kornienko, N.; Nichols, E. M.; Zhao, Y.; Paris, A. R.; Kim, D.; Yang, P.; Yaghi, O. M.; Chang, C. J. "Covalent organic frameworks comprising cobalt porphyrins for catalytic CO₂ reduction in water", *Science* **2015**, *346*, 1208-1213. (I)
 3. Jurss, J. W.; Khnayzer, R. S.; Panetier, J. A.; El Roz, K. A.; Nichols, E. M.; Head-Gordon, M.; Long, J. R.; Castellano, F. N.; Chang, C. J. "Bioinspired design of redox-active ligands for multielectron catalysis: effects of positioning pyrazine reservoirs on cobalt for electro- and photocatalytic generation of hydrogen from water", *Chem. Sci.* **2015**, *6*, 4954-4972. (I)
 2. Chantarojsiri, T.; Sun, Y.; Long, J. R.; Chang, C. J. "Water-Soluble Iron(IV)-Oxo Complexes Supported by Pentapyridine Ligands: Axial Ligand Effects on Hydrogen Atom and Oxygen Atom Transfer Reactivity", *Inorg. Chem.* **2015**, *54*, 5879-5887. (I)
 1. Liu, C.; Gallagher, J. J.; Sakimoto, K. K.; Nichols, E. M.; Chang, C. J.; Chang, M. C. Y.; Yang, P. "Nanowire–Bacteria Hybrids for Unassisted Solar Carbon Dioxide Fixation to Value-Added Chemicals", *Nano Lett.* **2015**, *15*, 3634-3639. (II)

Using Free Energies for H⁺ and H⁻ Transfers to Design Catalysts for the Reduction of CO₂

Aaron M. Appel,^a Eric S. Wiedner,^a John C. Linehan,^a David A. Dixon^b
^a Pacific Northwest National Laboratory, Institute for Integrated Catalysis
^b University of Alabama, Department of Chemistry & Biochemistry

Presentation Abstract

The wide spread and efficient use of intermittent and distributed energy sources, including solar and wind, would be facilitated by the storage of electrical energy in the form of high energy density fuels. The design of catalysts for the relevant chemical transformations is essential for this approach to energy storage. While hydrogen is a suitable target for some applications, the reduction of carbon oxygenates can be advantageous as a result of the potential for producing liquid fuels for use in transportation. In our work, we aim to develop knowledge of the parameters required for designing catalysts with exceptional performance for these multistep transformations. In particular, we have focused on the use of thermodynamic parameters to enable catalyst design by matching the free energies of catalytic intermediates throughout the catalytic cycle. With this focus in mind, we are pursuing different routes to controlling the relative free energies of catalytic intermediates, especially for the reduction of CO₂ through the transfer of a hydride (H⁻) as a reducing equivalent. In addition to the design of the primary coordination sphere of catalysts, we have shifted our attention to understanding the impact of solvent upon the free energy for hydride transfer as well as the resulting catalyst performance. Studies of phosphine complexes of cobalt, nickel, and copper hydrides will be presented, and the role of solvents will be highlighted for the relevant catalysts.

FWP-47319: Low-Temperature Catalytic Routes for Energy Carriers via Spatial and Chemical Organization

PI: Johannes Lercher

Designing single-atom alloys with DFT, machine learning and atomistic simulations

John R. Kitchin
Carnegie Mellon University
Department of Chemical Engineering

Presentation Abstract

Single atom alloys are metal alloys where one component is sufficiently dilute that it exists as isolated atoms (i.e. surrounded only by unlike atoms) in the alloy. Some of these systems show enhanced or unique reactivity that is unexpected from the pure metal components. We have identified a class of these materials, and some features of their electronic structure that may explain the origin of the unique properties. We are currently developing strategies to facilitate the design of these materials using combinations of density functional theory, machine learning and atomistic simulations. Our goal is to be able to design single atom alloy nanoparticle catalysts that have a maximal density of single atom sites at the surface under reaction conditions. Density functional theory (DFT) is too expensive to use directly for this, but it is the most reliable method to estimate the energetics of nanoparticle catalysts. We are using machine learning to develop atomistic potentials from DFT calculations that are as accurate, but considerably cheaper computationally. These potentials can then be used to explore more of the configuration space of alloy nanoparticles to identify the most probable particle geometries. They can also be coupled with atomistic simulations such as Monte Carlo simulations to estimate the surface composition of alloy surfaces accounting for segregation and temperature effects. Together, these methods should expand the reach of DFT to larger systems, and longer time scales of catalytic phenomena, and increase our understanding of these materials.

DE-SC0018187: Enhanced selectivity in the single atom alloy limit: C=C versus C=O hydrogenation

Student(s): Mingjie Liu

Affiliations(s): Chemical Engineering, Carnegie Mellon University

RECENT PROGRESS

Single atom alloy catalysts

Single atom alloys are a class of metal alloys in which one component is in a dilute limit where it only interacts with atoms of the majority type. These materials have gained interest as catalysts, because the dilute atoms may act as isolated sites with unique properties. It does not appear that any alloy in the dilute limit will show unique properties, but that in particular one needs a dilute reactive metal in a noble metal host. In this scenario, the d-orbitals of the reactive metal are unable to fully hybridize with those of the noble metal host, leading to a sharpening of the reactive metal d-states (see Figure 1). This leads to a balance of competing effects at the active site that include the interactions of adsorbates with the sharpened d-states and the interactions with the broad sp-band of the noble metals.

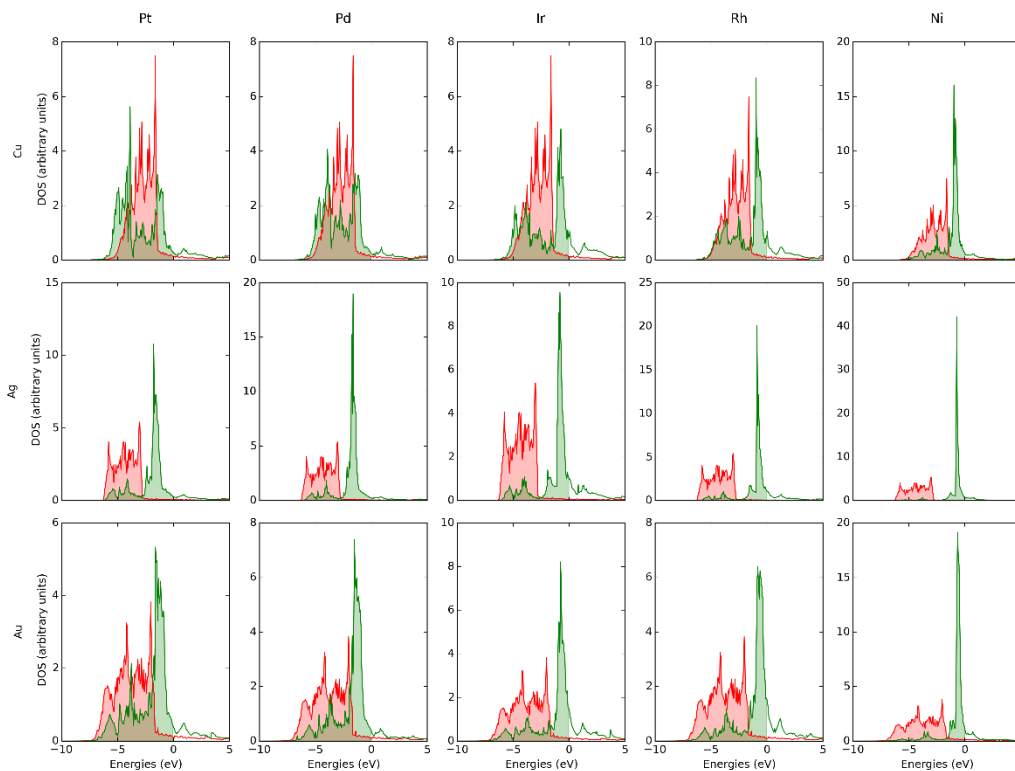


Figure 1. The d-band density of states of single atom alloys. In each case, the single atom shows a sharp density of states near the Fermi level.

The balance of these interactions can lead to apparent deviations from the often observed scaling relations observed on typical transition metal alloys. This is illustrated in Figure 2, where the dissociative adsorption of hydrogen is shown for a large number of single atom alloy systems. These variations lead to a wide range of deviations in the barriers of reactions in many classes of reactions, leading to the opportunity to find new materials with better catalytic properties than conventional alloys.

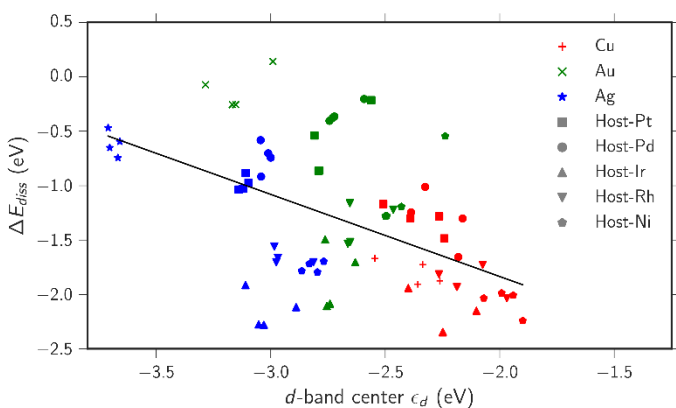


Figure 2. Dissociative adsorption energies of hydrogen on single atom alloy catalysts.

Together, these results illustrate the potential for single atom alloys to be useful catalytic materials, but they do not show how one might design one that has a large concentration of active sites while

maintaining the single atom alloy behavior, or how the activity might change in a lower coordination environment such as a nanoparticle.

Modeling segregation in metal alloys

A key challenge in understanding the reactivity of alloy surfaces is predicting the surface composition under reaction conditions. In earlier work¹, we made an approximation that the surface was a random alloy in equilibrium with a bulk alloy, and we estimated the surface composition in the presence of hydrogen. This mean-field approach neglected short-range order and local site composition effects on adsorption, but was reasonably effective at explaining some trends in reactivity for H₂-D₂ exchange on Cu-Pd alloys. We developed a new approach to modeling segregation using DFT to build a machine-learned potential that could be used with Monte Carlo simulations.² This new approach provided quantitative agreement of the surface composition of a Au-Pd alloy (111) surface across composition space. In addition, since we used an atomistic simulation we could also show the extent of short-range order and show that while a random alloy is not a perfect model for these alloys, it is not too wrong.

Future work

The approach to build a DFT data-driven, machine-learned potential for alloys appears to be very promising. We are currently extending the idea to alloy nanoparticles with the goal of modeling size dependent alloy nanoparticle segregation behavior, eventually including the effects of adsorbates. This should provide the means to design these materials with desired properties.

Publications Acknowledging this Grant in 2015-2018

- (I) *Exclusively funded by this grant;*
Thirumalai, H., & Kitchin, J. R., Investigating the reactivity of single atom alloys using density functional theory, *Topics in Catalysis* **2018**, 61(5-6), 462-474.
<http://dx.doi.org/10.1007/s11244-018-0899-0>.
- (II) *Jointly funded by this grant and other grants with leading intellectual contribution from this grant;*
N/A
- (III) *Jointly funded by this grant and other grants with relatively minor intellectual contribution from this grant;*
N/A

¹ Boes, J. R., Gumuslu, G., Miller, J. B., Gellman, A. J., & Kitchin, J. R., Estimating bulk-composition-dependent H₂ adsorption energies on Cu_xPd_{1-x} alloy (111) surfaces, *ACS Catalysis*, 5(2), 1020–1026 (2015).
<http://dx.doi.org/10.1021/cs501585k>.

² Boes, J. R., & Kitchin, J. R., Modeling segregation on AuPd(111) surfaces with density functional theory and Monte Carlo simulations, *The Journal of Physical Chemistry C*, 121(6), 3479–3487 (2017).
<http://dx.doi.org/10.1021/acs.jpcc.6b12752>.

Homogeneous Catalysis Meets Heterogeneous Catalysis: Alkanes and Alkenes Transformations

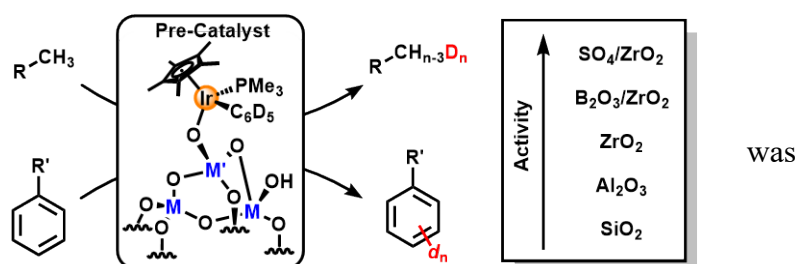
David M. Kaphan,¹ Rachel C. Klet,¹ Cong Liu,¹ Magali Ferrandon,¹ Jeremy Kropf,¹ Frederic A. Perras,² Marek Pruski,² Adam Hock,^{1,3} and Massimiliano Delferro¹

¹Chemical Sciences and Engineering Division, Argonne National Laboratory. ²Ames Laboratory. ³Department of Chemistry, Illinois Institute of Technology.

delferro@anl.gov

Systematic study of the interactions between organometallic catalysts and metal oxide support materials is essential for the realization of rational design in heterogeneous catalysis. Herein we describe the stoichiometric and catalytic chemistry of a [Cp*(PMe₃)Ir(III)] complex chemisorbed on a variety of acidic metal oxides as a multifaceted probe for stereoelectronic communication between the support and organometallic center. Electrophilic bond activation was explored in the context of stoichiometric hydrogenolysis as well as catalytic H/D exchange. Further information was obtained from the observation of processes related to dynamic exchange between grafted organometallic species and those in solution. The supported organometallic species were characterized by a variety of spectroscopic techniques including DNP solid-state NMR spectroscopy, DRIFT, and XAS. Strongly acidic modified metal oxides such as sulfated zirconia engender high levels of activity toward electrophilic bond activation of both sp² and sp³ C–H bonds, including the rapid deuteration of methane at room temperature; however, the global trend for the supports studied here does not suggest a direct correlation between activity and surface Brønsted acidity, and more complex metal surface interactions are at play. One such interaction was identified as an unexpected

redox event between the organometallic species and the modified oxide surfaces. Evidence of oxidative mechanism provided by studying the analogous homogeneous reactivity of the organometallic precursors toward [Ph₃C]⁺, a Lewis acid known to effect formal hydride abstraction by one electron oxidation followed by hydrogen abstraction. Organometallic deuterium incorporation, a result of the surface redox process, was found to be correlated with surface sulfate concentration, as well as the extent of dehydration under thermal activation conditions of sulfated alumina and sulfated zirconia supports. Surface sulfate concentration dependence, in conjunction with a computational study of surface electron affinity, indicates an electron deficient pyrosulfate species as the redox active moiety. These results provide further evidence for the ability of sulfated metal oxides to participate in redox chemistry not only toward organometallic complexes, but also in the larger context of their application as catalysts for the transformation of light alkanes.



Kinetic and Spectroscopic Studies of Catalytic Mechanisms: Hydrodeoxygenation of Biomass Feedstocks on Transition Metal Phosphides

S. Ted Oyama
Virginia Tech, Department of Chemical Engineering
Blacksburg, VA 24061

Presentation Abstract

The study of mechanisms of reaction is an active area of chemical kinetics, even though it is generally held that mechanisms cannot be proven on the basis of kinetics alone. This work shows that reactivity, spectroscopic, and transient data can be combined to give a unified picture of a reaction mechanism. The reaction studied is the hydrodeoxygenation of a pyrolysis liquid model compound, gamma-valerolactone (GVL). Use is made of in situ Fourier transform infrared spectroscopy and in situ x-ray absorption near-edge spectroscopy to probe adsorbed species and the nature of the catalyst surface at reaction studies.

The application of the work is in the conversion of pyrolysis liquids derived from biomass, whose high oxygen content (~40 wt.%) results in low heating value (about half that of petroleum liquids), high acid content (leading to corrosion problems), and low stability (resulting in increasing viscosity with storage). The catalyst studied is a member of a new family of catalysts, the transition metal phosphides, which have outstanding activity for removal of heteroatoms such as sulfur, nitrogen, and oxygen, from hydrocarbon feedstreams.

A contact time study allowed the determination of a reaction sequence for GVL HDO on Ni₂P/SiO₂ and it was found that C-O bond cleavage of the lactone ring to generate n-pentanoic acid was the rate-determining step. This was followed by hydrogen transfer steps to produce oxygen free compounds, n-pentane or n-butane. Fitting of the results using a rake mechanism that considers adsorbed intermediates indicates that the surface species from the pentanoic acid are majority species. In situ infrared and in situ x-ray absorption near-edge spectroscopy measurements support this reaction mechanism.

Grant or FWP Number: DEFG0296ER14669

Grant Title: Kinetics and Mechanism of Hydrodeoxygenation on Metal Phosphides

Postdoc(s): Gwang-Nam Yun, Phuong Bui

Affiliations(s): Virginia Tech

RECENT PROGRESS

Mechanism Studies

The hydrodeoxygenation (HDO) mechanism of the cyclic five-membered ester γ -valerolactone (GVL-C₅H₈O₂) as a model compound for pyrolysis oil derived from biomass was studied on a Ni₂P/MCM-41 catalyst. Reaction tests for the HDO of GVL were conducted in a fixed-bed continuous flow reactor at 300 °C and 0.5 MPa. A contact time analysis determined the reaction

pathway, and it was found that ring-opening of GVL to produce pentanoic acid was the rate-determining step. This was followed by formation of pentanal and decarbonylation to generate n-butane or hydrogenation to form n-pentane. The results are shown in Fig. 1.

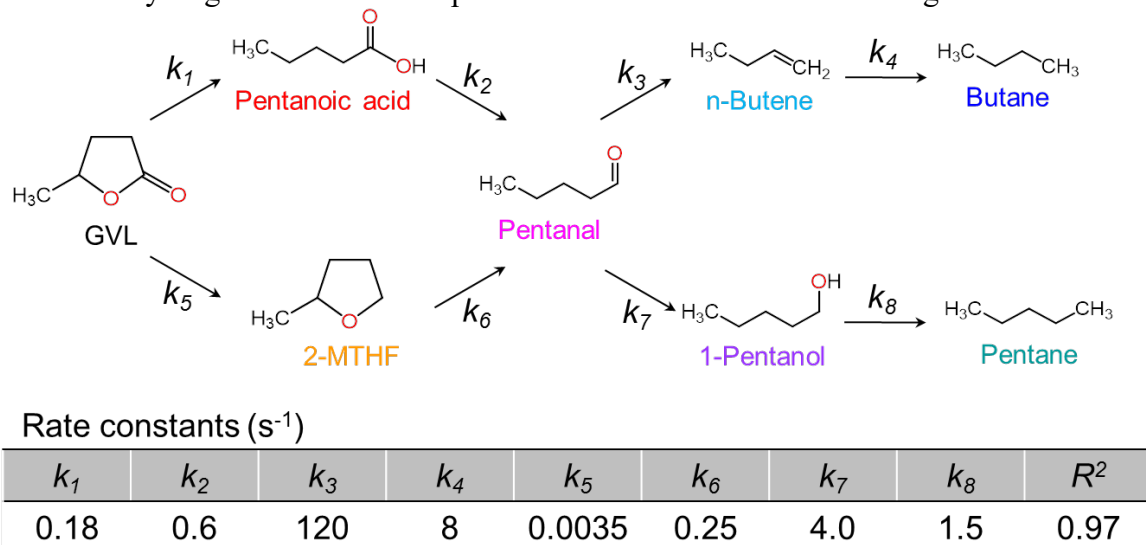


Fig. 1. Reaction Network for the Hydrodeoxygenation of γ -Valerolactone

A partial pressure analysis of H_2 and GVL was consistent with a rate equation derived from a Langmuir-Hinshelwood (L-H) mechanism. The kinetic analysis allowed calculation of coverages. The results are shown in Fig. 2.

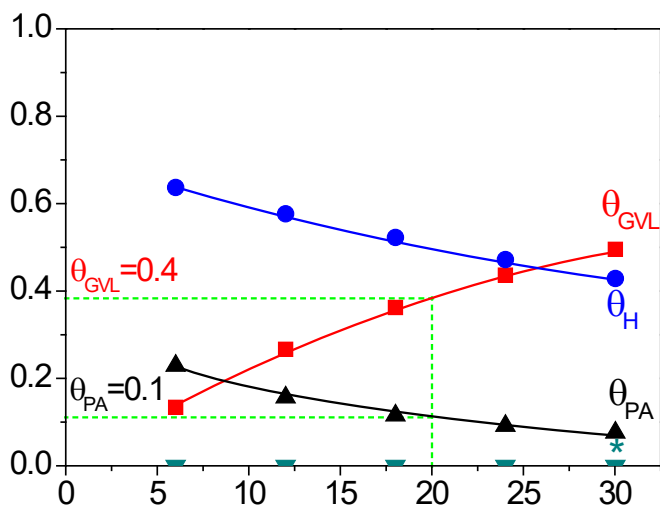


Figure 2. Coverages Calculated from Kinetic Parameters for the HDO of GVL

In situ infrared measurements under reactive H_2 and inert N_2 confirmed a reaction mechanism with ring-opening to form pentanoic acid, in which the number of CH_2 groups in adsorbed species increased under H_2 flow. Furthermore, in situ quick X-ray absorption fine structure measurements showed the participation of $Ni^{\delta+}$ species in the reaction as would be expected for the adsorption of

electron withdrawing oxygenated species like carboxylic acids. The data are shown in Fig. 3. The results allowed the establishment of a complete picture of the reaction mechanism.

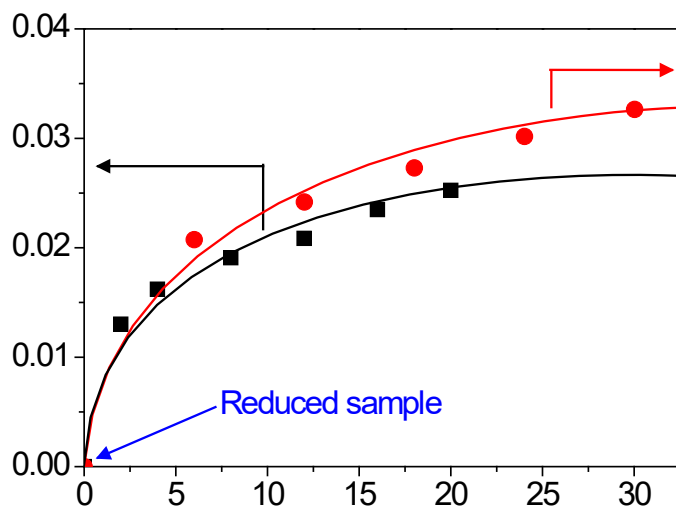


Figure 3. Comparison of NEXAFS Absorbance and GVL Coverage

Publications Acknowledging this Grant in 2016-2018

Please classify your publications into three categories according to the source of support for the work published:

(I) Exclusively funded by this grant;

(1) Bui, P. P.; Takagaki, A.; Kikuchi, R.; Oyama, S. T. Kinetic and Infrared Spectroscopy Study of Hydrodeoxygenation of 2-Methyltetrahydrofuran on a Nickel Phosphide Catalyst at Atmospheric Pressure, *ACS Catal.* **2016**, 6, 7701–7709.

(2) Bui, P.P.; Oyama, S.T., Takagaki, A.; Carrow, B.P.; Nozaki, K., Reactions of 2-Methyltetrahydropyran on Silica-Supported Nickel Phosphide in Comparison with 2-Methyltetrahydrofuran, *ACS Catal.* **2016**, 6, 4549–4558.

(3) Iino, A.; Takagaki, A.; Kikuchi, R.; Oyama, S.T.; Bando K.K., Combined in situ XAFS and FTIR study of the Hydrodeoxygenation Reaction of 2-Methyltetrahydrofuran on Ni₂P/SiO₂, *J. Phys. Chem. C.* **2018**, In press

(II) Jointly funded by this grant and other grants with leading intellectual contribution from this grant;

(1) Koike, N.; Hosokai, S.; Takagaki, A.; Nishimura, S.; Kikuchi, R.; Ebitani, K.; Suzuki, Y.; Oyama, S. T., Upgrading of pyrolysis bio-oil using nickel phosphide catalysts *J. Catal.* **2016**, 333, 115-126.

- (2) Yun, G.-N.; Ahn, S.-J.; Takagaki, A.; Kikuchi, R.; Oyama, S. T., Hydrodeoxygenation of γ -valerolactone on bimetallic NiMo phosphide catalysts G.-N. Yun, S.-J. Ahn, A. Takagaki, R. Kikuchi, S. T. Oyama
J. Catal. **2017**, 353, 141-151.
- (3) Zhang, J.; Matsubara, G.-N.; Zheng, H.; Takagaki, A.; Kikuchi, R.; Oyama, S.T., Comparison of phosphide catalysts prepared by temperature-programmed reduction and liquid-phase methods in the hydrodeoxygenation of 2-methylfuran
Appl. Catal. A: Gen. **2017**, 548, 39-46.

Guy Bertrand

Novel Stable Carbenes and their Applications in Catalysis

Guy Bertrand

UCSD-CNRS Joint Research Laboratory (UMI 3555), Department of Chemistry and Biochemistry, University of California, San Diego, La Jolla, California 92093-0358

Presentation Abstract

The preparation of cyclic (alkyl)(amino)carbenes with a six-membered backbone will first be discussed. Compared to their five-membered analogues, they feature increased % V_{bur} and enhanced donor and acceptor properties, as evidenced by the observed $n \rightarrow \pi^*$ transition trailing into the visible region. The high ambiphilic character even allows for the intramolecular insertion of the carbene into an unactivated $C(\text{sp}^3)\text{-H}$ bond. To assess the differences between CAAC-5 and CAAC-6, and more importantly to prove the superiority of the later as ligand for transition metal catalysts, we will present the results obtained in the palladium-mediated α -arylation of propiophenone with arylchlorides.

In the second part, we will present our results concerning the reduction of CO_2 into the conjugate base of formic acid, using dihydrogen. While catalysts based on noble metals have shown high turnover numbers (TONs), the use of abundant first-row metals is underdeveloped. We found a catalytic system, involving a stable copper hydride, activating CO_2 , working in tandem with a Lewis pair, heterolytically splitting H_2 ; unprecedented TONs for copper are obtained.

Lastly, we will show that a bicyclic CAAC is able to activate CO without metals, and to transfer it to organic substrates.

DE-SC0009376: Transition-metal-catalyzed functionalization of ammonia, hydrazine, and basic anilines

Postdoc(s): E. Tomás-Mendivil, R. Jazzar.

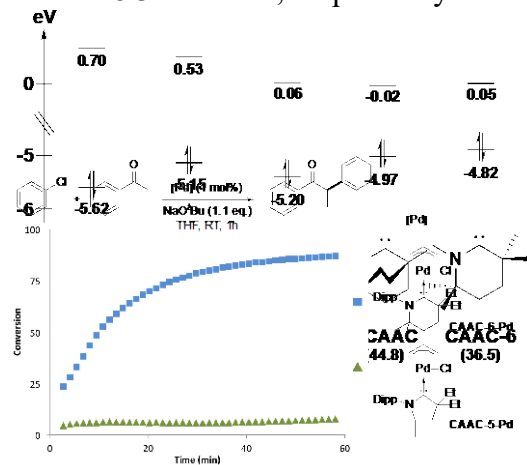
Student(s): E. A. Romero; C. M. Weinstein.

RECENT PROGRESS

Synthesis of stable six-membered cyclic (alkyl)(amino)carbenes and palladium catalysis

Since their discovery in 2005, five-membered cyclic (alkyl)(amino)carbenes (**CAAC-5**) have been widely used. CAACs are excellent ligands for transition metals and their complexes have found applications in catalysis, especially for the hydroamination of alkynes and allenes with NH_3 and NH_2NH_2 , and also in material science. The advantages of **CAAC-5** over NHCs can be traced back to their higher nucleophilicity (higher HOMO, more σ -donating) and electrophilicity (lower LUMO, more π -accepting), and consequently to their smaller singlet-triplet gap (ΔE_{ST}). It is well established that increasing the carbene bond angle of NHCs induces greater p character of both the HOMO and LUMO of the carbene, effectively shrinking the ΔE_{ST} . Based on these results, we decided to prepare six-membered cyclic (alkyl)(amino)carbenes (**CAAC-6**). Indeed, DFT calculations at the B3LYP/def2-TZVPP level of theory found that expanding the ring size of NHCs

from five to six decreases the HOMO-LUMO gap and ΔE_{ST} by 0.64 eV and 13.3 kcal/mol, respectively. Similarly, the HOMO-LUMO gap and the ΔE_{ST} of **CAAC-6** were found to be smaller than those of **CAAC-5** by 0.39 eV and 11.8 kcal/mol. To our delight, calculations also show that **CAAC-6** has a smaller HOMO-LUMO gap and ΔE_{ST} than the recently reported **BICAAC** by 0.08 eV and 8.3 kcal/mol, respectively. This can be rationalized by the accessible low energy chair conformation of the triplet **CAAC-6**, compared to the strained triplet state of **BICAAC**.

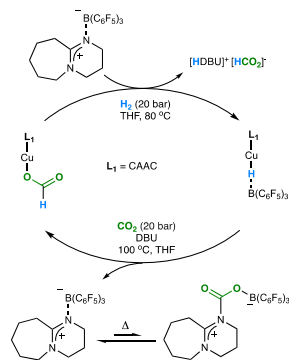


To assess the differences between **CAAC-5** and **CAAC-6**, and more importantly to prove the superiority of the later as ligand for transition metal catalysts, we considered the palladium-mediated α -arylation of propiophenone with arylchlorides. The figure herewith clearly demonstrates the advantages of **CAAC-6**.

It is safe to predict that a variety of **CAAC-6** metal complexes will feature very strong metal-carbene bonds, which will allow for catalysis under harsh conditions, as requested for hydroamination reactions with NH_3 .

Tandem Copper Hydride - Lewis Pair Catalyzed Reduction of Carbon Dioxide into Formate with Dihydrogen

The reduction of CO_2 into formic acid or its conjugate base, using dihydrogen, is a particularly attractive process. While catalysts based on noble metals have shown high turnover numbers (TONs), the use of abundant and inexpensive first-row metals is underdeveloped. The key steps of the reaction are the CO_2 insertion into a metal-hydride, and the regeneration of the latter with H_2 with concomitant formation of the formate. For the first step, copper is known as one of the most efficient metals, as shown by the numerous copper-catalyzed carboxylation reactions, but has difficulties activating H_2 . From this analysis, we envisaged that a system involving a stable copper hydride activating CO_2 , working in tandem with a dihydrogen activator, would bring together an ideal synergy for the catalytic reduction of CO_2 with H_2 . As a dihydrogen activator, we chose amine-borane frustrated Lewis pairs (FLPs) pioneered by Stephan, Erker and others. Note that in the presence of H_2 , FLPs are also known to reduce CO_2 , but the subsequent cleavage of the boron-oxygen bond to regenerate the FLP is extremely endergonic thereby preventing this process from being catalytic. We found that in the presence of DBU, $(\text{CAAC})\text{CuH}-\text{B}(\text{C}_6\text{F}_5)_3$ complexes achieve CO_2 conversion to formate with TONs up to 1881. Through stoichiometric reactions, we have been able to postulate a reasonable catalytic cycle (Figure herewith).



Publications Acknowledging this Grant in 2015-2018

(I) Exclusively funded by this grant

1. Dielmann, F. ; Bertrand, G. Reactivity of a Stable Phosphinonitrene towards Small Molecules. *Chem. Eur. J.* **2015**, 21, 191-198.

2. Tolentino, D. R.; Jin, L.; Melaimi, M.; Bertrand, G. Mesoionic Carbene-Gold(I) Catalyzed Bis-Hydrohydrazination of Alkynes with Parent Hydrazine. *Chem. Asian J.* **2015**, *10*, 2139-2142.
3. Jin, L.; Tolentino, D. R.; Melaimi, M.; Bertrand, G. Isolation of Bis(copper) Key Intermediates in Cu-Catalyzed Azide-Alkyne “Click Reaction” *Sci. Adv.* **2015**, *1*, e1500304.
4. Jin, L.; Romero, E. A.; Melaimi, M.; Bertrand, G. The Janus Face of the X Ligand in the Copper Catalyzed Azide Alkyne Cycloaddition. *J. Am. Chem. Soc.* **2015**, *137*, 15696-15698.
5. Peltier, J. L.; Jazzar, R.; Melaimi, M.; Bertrand, G. Ancillary Ligand-Free Copper Catalyzed Hydrohydrazination of Terminal Alkynes with NH₂NH₂. *Chem. Commun.* **2016**, *52*, 2733 – 2735.
6. Hu, X.; Martin, D.; Bertrand, G. Room temperature hydroamination of alkynes with anilines catalyzed by anti-Bredt di(amino)carbene gold(I) complexes. *New J. Chem.* **2016**, *40*, 5993-5996.
7. Romero, E. A.; Peltier, J. L.; Jazzar, R.; Bertrand, G. Catalyst-Free Dehydrocoupling of Amines, Alcohols, and Thiols with Pinacol Borane and 9-Borabicyclononane (9-BBN). *Chem. Commun.* **2016**, *52*, 10563-10565.
8. Kleinhans, G.; Hansmann, M. M.; Guisado-Barrios, G.; Liles, D. C.; Bertrand, G.; Bezuidenhout, D. I. Nucleophilic T-shaped (LXL)Au(I)-Pincer Complexes: Protonation and Alkylation. *J. Am. Chem. Soc.* **2016**, *138*, 15873-15876.
9. Romero, E. A.; Jazzar, R.; Bertrand, G. (CAAC)CuX-catalyzed hydroboration of terminal alkynes with pinacolborane directed by the X-ligand. *J. Organomet. Chem.* **2017**, *829*, 11-13.
10. Romero, E. A.; Peltier, J. L.; Jazzar, R.; Bertrand, G. Copper-Catalyzed Dehydrogenative Borylation of Terminal Alkynes with Pinacolborane. *Chem. Sci.* **2017**, *8*, 165-168.
11. Romero, E. A.; Olsen, P. M.; Jazzar, R.; Soleilhavoup, M.; Gembicky, M.; Bertrand, G. Spectroscopic Evidence for a Monomeric Copper(I) Hydride, and Crystallographic Characterization of a Monomeric Silver(I) Hydride. *Angew. Chem. Int. Ed.* **2017**, *56*, 4024-4027.
12. Tomás-Mendivil, E.; Hansmann, M. M.; Weinstein, C. M.; Jazzar, R.; Melaimi, M.; Bertrand, G. Bicyclic (Alkyl)(amino)carbenes (BICAACs): Stable Carbenes more Ambiphilic than CAACs. *J. Am. Chem. Soc.* **2017**, *139*, 7753-7756.
(II) *Jointly funded by this grant and other grants with leading intellectual contribution from this grant;*
13. Marx, V. M.; Sullivan, A. H.; Melaimi, M.; Virgil, S. C.; Keitz, B. K.; Weinberger, D. S.; Bertrand, G.; Grubbs, R. H. Cyclic Alkyl Amino Carbene (CAAC) Ruthenium Complexes as Remarkably Active Catalysts for Ethenolysis. *Angew. Chem. Int. Ed.* **2015**, *54*, 1919-1923.
14. Bidal, Y. D.; Lesieur, M.; Melaimi, M.; Cordes, D. B.; Slawin, A. M. Z.; Bertrand, G.; Cazin, C. S. J. A simple access to transition metal cyclopropenyliidene complexes. *Chem. Commun.* **2015**, *51*, 4778 – 4781.
15. Hu, X.; Soleilhavoup, M.; Melaimi, M.; Chu, J.; Bertrand, G. Air-Stable (CAAC)CuCl and (CAAC)CuBH₄ Complexes as Catalysts for Hydrolytic Dehydrogenation of BH₃NH₃. *Angew. Chem. Int. Ed.* **2015**, *54*, 6008-6011.
16. Soleilhavoup, M.; Bertrand, G. Cyclic (Alkyl)(Amino)Carbenes (CAACs): Stable Carbenes on the Rise, *Acc. Chem. Res.* **2015**, *48*, 256-266.
17. Martin, D.; Marx, V. M.; Grubbs, R. H.; Bertrand, G. A Ruthenium Catalyst for Olefin Metathesis Featuring an Anti-Bredt N-Heterocyclic Carbene Ligand. *Adv. Synth. Catal.* **2016**, *358*, 965-969.

- 18 Kleinhans, G.; Guisado-Barrios, G.; Liles, D. C.; Bertrand, G.; Bezuidenhout, D. I. A Rhodium(I) Oxygen Adduct as a Selective Catalyst for One-Pot Sequential Alkyne Dimerization-Hydrothiolation Tandem Reactions. *Chem. Commun.* **2016**, 52, 3504-3507.
- 19 Bidal, Y. D.; Santoro, O.; Melaimi, M.; Cordes, D. B.; Slawin, A. M. Z.; Bertrand, G.; Cazin, C. S. J. Generalization of the Copper to Late Transition Metal Transmetalation to Carbenes beyond N-Heterocyclic Carbenes. *Chem. Eur. J.* **2016**, 22, 9404-9409.
- 20 Chu, J.; Munz, D.; Jazzar, R.; Melaimi, M.; Bertrand, G. Synthesis of Hemilabile Cyclic (Alkyl)(amino)carbenes (CAACs) and Applications in Organometallic Chemistry. *J. Am. Chem. Soc.* **2016**, 138, 7884-7887.
- 21 Melaimi, M.; Jazzar, R.; Soleilhavoup, M.; Bertrand, G. Cyclic (Alkyl)(Amino)Carbenes (CAACs): Recent developments. *Angew. Chem. Int. Ed.* **2017**, 56, 10046-10068.

(III) Jointly funded by this grant and other grants with relatively minor intellectual contribution from this grant;

- 22 Jin, L.; Melaimi, M.; Kostenko, A.; Karni, M.; Apeloig, Y.; Moore, C. E.; Rheingold, A. L.; Bertrand, G. Isolation of cationic and neutral (allenylidene)(carbene) and bis(allenylidene)gold Complexes. *Chem. Sci.* **2016**, 7, 150-154.
- 23 Pranckevicius, C.; Liu, L.; Bertrand, G.; Stephan, D. Synthesis of a Carbodicyclopropenylidene: A Carbodicarbene based Solely on Carbon. *Angew. Chem. Int. Ed.* **2016**, 55, 5536-5540.
- 24 Soleilhavoup, M.; Bertrand, G. Borylenes: an Emerging Class of Compounds. *Angew. Chem. Int. Ed.* **2017**, 56, 10282-10292.

Wednesday PI Oral Presentations

Pathways for Methanol Synthesis from the Conversion of C-H bonds over Well-defined Metal-Oxide Surfaces

Sanjaya D. Senanayake, Feng Zhang, Zongyuan Liu, Robert Palomino,
Ping Liu, Jose A. Rodriguez

Chemistry Department, Brookhaven National Laboratory, Upton, NY 11973 (USA)

Methane remains a valuable yet underutilized resource. Our recent studies indicate that, in spite of the high stability of methane, systems such as Ni-CeO₂(111) and CeO₂-Cu(111) can break C-H bonds even at room temperature, through careful manipulation of interfaces and metal-support interactions, using C1 oxidants (CO₂, O₂/H₂O). Our approach is to rely on *in-situ* studies, using real time in situ measurements with XRD, XAFS, XPS, infrared spectroscopy and TEM/STM coupled with DFT to study powder and model systems to elucidate C-H activation and conversion steps that produce CH₃OH and CO+H₂.

We have employed Dry Reforming of Methane (DRM: CH₄+CO₂→2CO+2H₂) conditions to establish benchmark steps for low temperature oxidative conversion of C-H bonds (using CO₂) on Ni-CeO_x, where the active species and reaction mechanism are complex while a strong interaction between small Ni nanoparticles (Ni⁰/Ni²⁺) and reduced CeO_x surfaces (Ce⁴⁺/Ce³⁺)

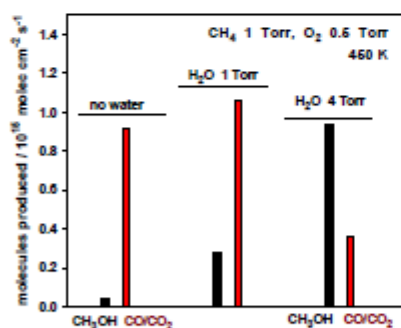


Figure 2. Production of methanol and CO/CO₂ as a function of water pressure on a CeO₂/Cu₂O/Cu(111) catalyst in which ~ 40% of the Cu₂O was covered by ceria. The samples were exposed to 1 Torr of CH₄, 0.5 Torr of O₂ and 0, 1 or 4 Torr of H₂O at 450 K.

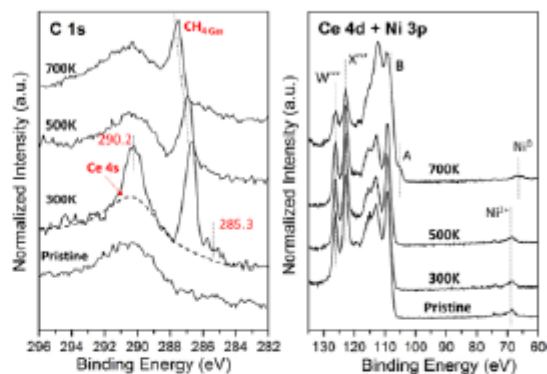


Figure 1. C 1s and Ce 4d + Ni 3p spectra of the Ni/CeO₂(111) (Θ_{Ni} ≈ 0.1 ML) surface under 100 mTorr of CH₄ at 300, 500 and 700 K.

prevail (Figure 1). We have also started to develop a method for the direct conversion of methane to methanol building on these studies. We have found that a CeO₂/Cu₂O/Cu(111) inverse system is able to activate methane at room temperature and then, with the help of water, performs a highly selective catalytic cycle, for the production of methanol (Figure 2). The interfacial interaction between CeO_x-CuO_x is crucial while the pressure of water has a strong effect on the selectivity towards the production of methanol. We have made comparison also to Ni-CeO_x systems that appear to enable pathways where H₂O acts as a promoter and site blocker for improved methanol synthesis.

1. Liu et al. *Angewandte Chemie* (2016) 128 (26), 7581-7585.
2. Lustemberg et al. *ACS Catalysis* (2016) 6 (12), 8184-8191.
3. Zuo et al. *JACS* (2016) 138 (42), 13810-13813.
4. Liu et al. *Angewandte Chemie* (2017) 56 (42) 13041-13046.
5. Zhang et al. *ACS Catalysis* (2018) 8 (4), 3550-3560.
6. Lustemberg et al. *JACS* (2018) 140 (24), 7681-7687.

Dust Effects On Nucleation Kinetics and Resultant Catalytic Nanoparticle Product Size-Distributions: An Illustrative Case Study of a Prototype, Catalytically Active Ir(0)_n Transition-Metal Nanoparticle Formation System

Richard G. Finke¹, Saim Özkar²

¹ Department of Chemistry, Colorado State University, Fort Collins, CO 80523 USA,

² Department of Chemistry, Middle East Technical University, 06800 Ankara, Turkey.

Abstract

The question is addressed if dust is kinetically important in the nucleation and growth of Ir(0)_n nanoparticles formed from [Bu₄N]₅Na₃(1,5-COD)Ir^I•P₂W₁₅Nb₃O₆₂ (hereafter [(COD)Ir•POM]⁸⁻), reduced by H₂ in propylene carbonate solvent. Following a concise review of the (often neglected) literature addressing dust in nucleation phenomena dating back to the late 1800s, the nucleation and growth kinetics of the [(COD)Ir•POM]⁸⁻ precatalyst system are examined for the effects: of 0.2 μm microfiltration of the solvent and precatalyst solution, of rinsing the glassware with that microfiltered solvent, of silanizing the glass reaction vessel, for the addition of <0.2 μm □-Al₂O₃ (inorganic) dust, for the addition of flame-made carbon-based (organic) dust, and as a function of the starting, microfiltered [(COD)Ir•POM]⁸⁻ concentration. Efforts to detect dust and its removal by dynamic light scattering and by optical microscopy are also reported. The results yield a list of 8 important findings and conclusions as detailed in the Results section which follows.

DE-FG02-03ER15453: Nanoparticle Catalysts: Nucleation Mechanistic Studies Plus Mechanism-Enabled Population Balance Modeling En Route to Nanoparticle Size and Size-Distribution Understanding and Control

PI: Professor Richard G. Finke

Postdoc(s): Dr. Saim Özkar

RECENT PROGRESS

Overview of Publications

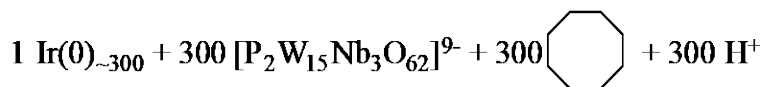
Thirteen publications to date have been produced under our DOE support since 2015; a list of their titles follows and provides a concise description of the contents of those publications. The publications provide results in 5 areas: (i) nanoparticle catalyst formation kinetics and nucleation and growth mechanisms^{Error! Bookmark not defined.,Error! Bookmark not defined.,}; (ii) supported-nanoparticle heterogeneous catalyst synthesis and formation mechanisms^{Error! Bookmark not defined.,}; (iii) nanoparticle catalyst sintering mechanisms^{Error! Bookmark not defined.,Error! Bookmark not defined.,}; (iv) studies aimed at determining the true catalyst in catalytic reactions—a key endeavor since *all* catalytic properties of interest depend on the precise chemical composition and structure of the

actual, often hidden, kinetically dominant catalyst^{Error! Bookmark not defined.}; and (v) other synthetic and kinetics and mechanistic studies important in chemical catalysis.^{Error! Bookmark not defined..Error! Bookmark not defined.} All of the 13 publications listed have been funded exclusively by our DOE grant.

Poster Presentation Focusing on: Dust Effects On Nucleation Kinetics and Catalytic Nanoparticle Product Size-Distributions: The Illustrative Case Study of a Prototype Ir(0)_n Transition-Metal Nanoparticle Formation System

The poster presentation at the annual contractor’s meeting will focus on an intriguing study this past grant year^{Error! Bookmark not defined.} of what turn out to be the profound effects of omnipresent room dust, and its removal by microfiltration, on nanoparticle catalyst formation and how—simply by μm filtration—one can narrow nanoparticle product size distributions by more than a factor of two.

The system studied is a prototype Ir(0)_{~300} nanoparticle catalyst formation system that starts from ca. 300 equivalents of a [(1,5-COD)Ir•P₂W₁₅Nb₃O₆₂]⁸⁻ precursor (hereafter = (COD)Ir•POM⁸⁻) and then reduces this precatalyst under hydrogen according to the overall, experimentally demonstrated^{Error! Bookmark not defined.} stoichiometry in the scheme below:



The four most noteworthy results out of 8 total conclusions summarized in a 2017 *Langmuir* paper^{Error! Bookmark not defined.} are: (i) that the nucleation apparent rate “constant” $k_{1\text{obs}(\text{bimol})}$ is shown to be slowed by a factor of ~5 to ~7.6, depending on the precise experiment and its conditions, by just filtration of the precatalyst solution using a 0.20 μm filter *and* rinsing the glassware surface with 0.20 μm filtered propylene carbonate solvent; (ii) that simply employing a 0.20 μm filtration step narrows the size-distribution of the resulting Ir(0)_n nanoparticles *by a factor of 2.4 from ±19% to ±8%*, a remarkable result; (iii) that this narrower size-distribution can be accounted for by the slowed nucleation rate constant, $k_{1\text{obs}(\text{bimol})}$ and by the unchanged autocatalytic growth rate constant, $k_{2\text{obs}(\text{bimol})}$, that is, by the increased ratio of $k_{2\text{obs}(\text{bimol})}/k_{1\text{obs}(\text{bimol})}$ that further separates nucleation from growth in time for filtered, vs unfiltered, solutions; and (iv) five lines of evidence indicate that the filterable component of the solution, which is having the nucleation rate-enhancing, and size-dispersion broadening, effects, is dust.

The broader impact and importance of the study of (the striking!) dust effects in the formation mechanism of catalytically active nanoparticles is that the dominant hypothesis going forward, for nucleation studies anywhere in nature where dust is (omni)present, needs to be that dust is a kinetically important component of both the nucleation process *and* the observed particle-size and size-distribution.

Publications Acknowledging this Grant in 2015-2018

- (I) *Exclusively funded by this Grant:*
- (II) Bayram, E.; Lu, J.; Aydin, C.; Browning, N. D.; Özkar, S.; Gates, B. C.; Finke, R. G. Agglomerative Sintering of an Atomically Dispersed Ir₁/Zeolite Y Catalyst: Compelling Evidence Against Ostwald Ripening But for Bimolecular and

- Autocatalytic Agglomeration Catalyst Sintering Steps. *ACS Catalysis*, **2015**, *5*, 3514-3527.
- (III) ¹Kent, P. D.; Mondloch, J. E.; Finke, R. G. Syntheses of Heterogeneous Ir(0)₋₆₀₀₋₉₀₀/γ-Al₂O₃ From One-Pot vs Isolated Preparations of the Precatalyst Ir(1,5-COD)Cl/γ-Al₂O₃: Discovery of Two, Competing, Trace “Ethyl Acetate Effects on the Key, Nucleation Step and Resultant Product. *ACS Catalysis*, **2016**, *6*, 5449-5461.
- (IV) ¹. Bayram, E.; Linehan, J. C.; Fulton, J. L.; Szymczak, N. K.; Finke, R. G., Determining the True Catalyst Derived from the [RhCp*Cl₂]₂ Precatalyst System: Is it Single-Metal RhCp*-Based, or a Sub-nanometer Rh₄ Cluster-Based, Cyclohexene Hydrogenation Catalysis at Room Temperature and Mild Pressures?. *ACS Catalysis* **2015**, *5*, 3876-3886.
- (V) ¹. Laxson, W. W.; Özkar, S.; Folkman, S.; Finke, R. G. The Story of a Mechanism-Based Solution to an Irreproducible Synthesis Resulting in an Unexpected Closed-System Requirement for the LiBEt₃H-Based Reduction: the Case of the Novel Subnanometer Cluster, [Ir(1,5-COD)(μ-H)₄], and the Resulting Improved, Independently Repeatable, Reliable Synthesis. *Inorg. Chim Acta.*, **2015**, *432*, 250-257.
- (VI) ¹. Özkar, S.; Finke, R. Palladium(0) Nanoparticle Formation, Stabilization, and Mechanistic Studies: Pd(acac)₂ as a Preferred Precursor, [Bu₄N]₂HPO₄ Stabilizer, Plus the Stoichiometry, Kinetics, and Minimal, 4-Step Mechanism of the Palladium Nanoparticle Formation and Subsequent Agglomeration Reactions. *Langmuir*, **2016**, *32*, 3699-3716.
- (VII) ¹. Crooks, A.; Yih, K.-H.; Li, L.; Yang, J. C.; Özkar, S.; Finke, R. G. Unintuitive Inverse Dependence of the Apparent Turnover Frequency, TOF_{app}, on Precatalyst Concentration: A Quantitative Explanation in the Case of Ziegler-type Nanoparticle Catalysts Made from [(1,5-COD)Ir(μ-O₂C₈H₁₅)₂] and AlEt₃. *ACS Catalysis* **2015**, *5*, 3342-3353.
- (VIII) ¹. Bentea, L.; Watzky, M. A.; Finke, R. G. Sigmoidal Nucleation and Growth Curves Across Nature Fit by the Finke-Watzky Model of Slow Continuous Nucleation and Autocatalytic Growth: Explicit Formulas for the Lag and Growth Times Plus Other Key Insights. *J. Phys. Chem. C.*, **2017**, *121*, 5302-5312.
- (IX) ¹. Özkar, S.; Finke, R. Nanoparticle Nucleation is Termolecular and Involves Hydrogen: Evidence for a Kinetically Effective Nucleus of Three, {Ir₃H₂•P₂W₁₅Nb₃O₆₂}⁶⁻, in Ir(0)_n Nanoparticle Formation From [(1,5-COD)Ir^I•P₂W₁₅Nb₃O₆₂]⁸⁻ Plus Hydrogen. *J. Am. Chem. Soc.* **2017**, *139*, 5444-5452.
- (X) ¹. Özkar, S.; Finke, R. Dust Effects On Nucleation Kinetics and Nanoparticle Product Size-Distributions: The Illustrative Case Study of a Prototype Ir(0)_n Transition-Metal Nanoparticle Formation System, *Langmuir*, **2017**, *33*, 6550-6562. DOI: 10.1021/acs.langmuir.7b01219.
- (XI) ¹. Özkar, S.; Finke, R. G. Silver Nanoparticles Synthesized by Microwave Heating: A Kinetic and Mechanistic Re-Analysis and Re-Interpretation, *J. Phys. Chem. C*, **2017**, *121*, 27643-2765.
- (XII) ¹. Finney, E. E.; Finke R. G. Catalyst Sintering Kinetic Data: Is There a Minimal Chemical Mechanism Underlying Kinetics Previously Fit by Empirical

Power-Law Expressions—and if So, What Are Its Implications?, *Industrial & Eng. Chem. Res.*, **2017**, *56*, 10271-10286.

- (XIII) ¹. Özkar, S.; Finke, R. G. A Classic, Azo-Dye Agglomeration System: Evidence for Slow, Continuous Nucleation, Autocatalytic Agglomerative Growth, Plus the Effects of Dust-Removal by Microfiltration on the Kinetics, *J. Phys. Chem. A*, **2017**, *121*, 7071-7078.
- (XIV) ¹. Watzky, M. A.; Finke, R. G. Gold Nanoparticle Formation Kinetics and Mechanism: A Critical Analysis of the Putative “Redox-Crystallization” Mechanism, *ACS Omega*, **2018**, *3*, 1555-1563.

E. Charles. H. Sykes

Single metal atoms in alloys and oxides as catalysts for chemicals production

E. Charles. H. Sykes¹ and Maria Flytzani-Stephanopoulos²

¹Department of Chemistry, ²Department of Chemical and Biological Engineering,
Tufts University, Medford, MA

Presentation Abstract

Supported single metal atoms are a new class of catalyst in which precious metals can be used at the ultimate efficiency limit. While great strides have been made in demonstrating the potential of single-atom catalysts for many industrial reactions, there remains much debate in the literature over the nature of the active sites. Using state of the art surface analysis and microscopy techniques, we have developed a system in which the atomic structure of copper oxide supported single atom Pt sites can be measured and related to their ability to oxidize CO at low temperatures, a key transformation in, for example, the next generation of automotive catalysts. We unambiguously show that single Pt atoms can perform this chemistry efficiently around room temperature, and further elucidate the mechanism with theory. The reaction was also studied at ambient pressure on partially oxidized single-atom alloys (SAAs) of Pt/Cu (Cu_xO) prepared as unsupported nanoparticles. Similar results were found, effectively bridging the surface science and catalysis findings. Both model and real catalysts have high activity and selectivity for the CO PROX reaction in that CO oxidation proceeds but hydrogen is not oxidized. The stability in the real gas mixture was excellent. Selective dehydrogenation of alkanes is also catalyzed by the Pt/Cu SAAs. The activity is much higher than that of Cu, while the catalyst is coke-resistant under realistic conditions, unlike monometallic Pt. Coke-free C-H activation was shown for dehydrogenation of n-butane to butene at 400°C without catalyst deactivation after 50h on-stream. Exploiting these promising new catalysts for the above and other reactions is a main objective of the project.

DE-FG02-05ER15730: Atomically dispersed supported metal species as catalysts for alcohol conversion, and hydrogen and chemicals production

PI: Maria Flytzani-Stephanopoulos

Student(s): Jilei Liu, Andrew Therrien, Sufeng Cao, Mengyao Ouyang, Alex Schilling, George Giannakakis

Collaborators: Manos Mavrikakis (U. Wisconsin), Sungsik Lee (ANL), Lawrence F. Allard (ORNL); Guido Busca (U. Genoa), Jean-Sabin McEwen (WSU)

RECENT PROGRESS

1. An atomic-scale view of single-site Pt catalysis for low-temperature CO oxidation

Low-temperature CO oxidation is industrially and environmentally important, and despite recent reports of facile conversion on single metal sites, debate over the nature and function of these sites exists. Due to the inherent complexity of heterogeneous catalysts, it is difficult to fully characterize the structure and environment surrounding single atoms in a supported catalyst, which are critical for accurate modeling, understanding, designing new single metal atom catalysts. For this reason, we use model studies of supported single atoms to investigate the atomic-scale geometric and electronic properties that define their catalytic behavior.^{7,8,12-14} Figure 1 shows an overview of low-temperature CO oxidation on a well-defined Cu₂O thin film model system in which the reaction sites can be imaged with atomic resolution and the reaction mechanism understood with isotope labelling TPR, RAIRS and DFT. When small amounts of Pt are added to the “29” oxide surface, they remain atomically dispersed, as found by RAIRS and high-

resolution STM¹³ shown in Fig. 1a-c. The RAIRS data in Fig. 1a show CO stretching bands for various Pt coverages at 265 K, at which temperature CO has completely desorbed from the oxide support and all the signal is due to CO on Pt sites. These spectra serve as benchmarks for understanding what supported Pt structures give rise to which IR features, a critical issue in the catalysis community. In order to probe the reaction mechanism, the “29” oxide support was labeled with ¹⁸O, shown in Fig. 1d. Pt atoms at a concentration of 1% ML were deposited onto the support and the surface saturated with C¹⁶O. The resulting desorption products were monitored and the CO₂ formed was exclusively m/z 46, which is direct evidence of a Mars and van Krevelen oxidation mechanism in which a single lattice oxygen from the Cu₂¹⁸O-like support is extracted by C¹⁶O to form C¹⁶O¹⁸O as shown schematically in Figure 1e. Both CO desorption and oxidation occurs at similar temperatures with a 33 ± 2% conversion to CO₂. Our XPS results, not shown, indicate that single supported Pt atoms exist in a neutral charge state, not previously considered to be present at the single atom limit on an oxide support. However, a thicker layer of Cu₂O will be constructed next to eliminate potential electron transfer to Pt from the underlying Cu (111) crystal.

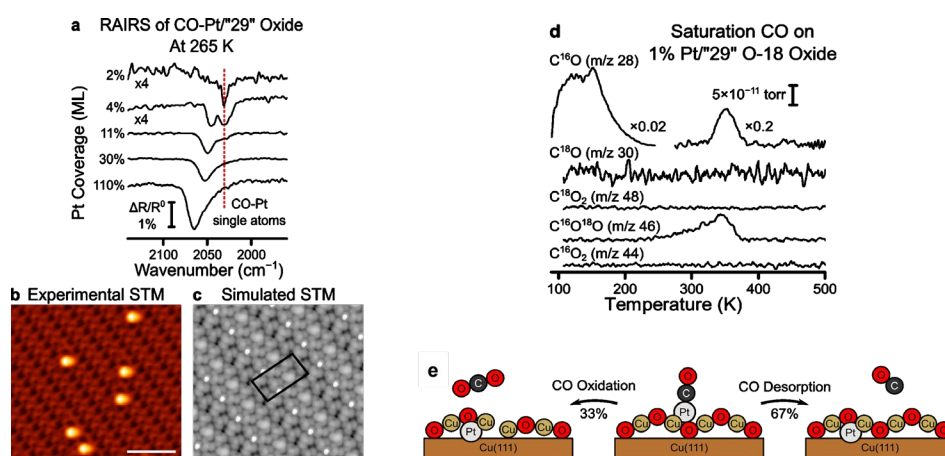


Figure 1 | CO Oxidation on single Pt atoms. **a**, RAIRS data of the CO stretch at various Pt coverages at 265 K. **b**, High-resolution STM of 0.5% ML Pt on the “29” copper oxide after adding CO and annealing to 250 K, the scale bar is 5 nm. **c**, Simulated STM image at -0.5 V of the DFT model with a CO-Pt complex in each unit cell, highlighted by the black parallelogram. RAIRS data from an initial CO saturation coverage annealed to various temperatures on **d**, TPD after saturation CO exposure on 1% ML Pt supported on an ¹⁸O labeled “29” oxide. **e**, schematic of the competing pathways for CO oxidation and CO desorption.¹³

2. Activity, Stability, and Selectivity of SAA Pt/Cu (Cu_xO) for CO Oxidation and PROX

To investigate Pt/Cu Single-Atom Alloys (SAAs) in an unsupported form, we prepared nanoporous Cu formats, np-Cu, using the sacrificial support (SiO₂) method. Galvanic replacement was subsequently used to deposit isolated Pt atoms in the np-Cu surface. The nanoporous copper particles were oxidized under KOH treatment, which allows for the thermodynamically favorable formation of cuprous oxide (Cu₂O), ultimately forming an oxidized surface layer. BET measurements indicated the formation of a catalyst with moderately high surface area (10m²/g), while the formation of an oxidized surface was verified via XRD (Fig. 2a) to mimic the surface science model with top Cu₂O layer on bulk Cu⁸. TEM imaging provided further proof for a predominant Cu₂O surface, based on the lattice spacing of 0.25nm (Fig. 2c). The atomic dispersion of Pt was verified via CO-DRIFTS, which clearly shows the absence of bridged CO and only yields a peak centered at 2097cm⁻¹ that is attributed to positively charged Pt (Fig. 2b).

Figs 3a and 3b show that Pt-np-Cu_xO is more active for the CO oxidation than np-Cu_xO regardless of the presence of hydrogen in the feed gas stream. It is also noteworthy that the “light-off” temperature was similar for the two reactions, indicating a similar reaction mechanism. For the Pt doped np-Cu_xO, conversion of CO started at 60°C, while for the bare support at temperatures higher than 90°C. This difference held at 50% and 100% CO conversion as well.

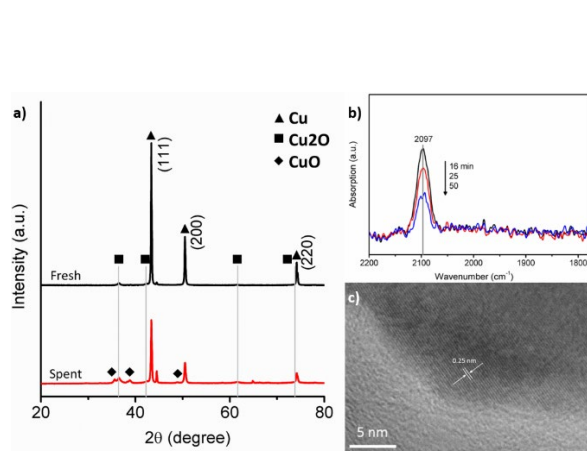


Figure 2. a) XRD measurements for the fresh (upper) and spent catalyst after CO oxidation reaction for 15 h (lower) Pt-np-Cu_xO. b) CO DRIFTS of fresh Pt-np-Cu_xO c) TEM image of as prepared Pt-np-Cu_xO

Another important aspect of this catalyst is its excellent selectivity under PROX conditions, which was maintained throughout the temperature range and even at 100% of CO at 170°C (Fig. 3b) for Pt-np-Cu_xO. Even at the highest temperature tested, the conversion of H₂ to H₂O remained below 5%. The absence of CO poisoning¹⁶, along with the negligible coking of the Pt doped materials, as confirmed by TPO, and the mild temperature of operation verified catalyst stability, even after prolonged reaction times (Fig. 3c). Thus, we have discovered a new Pt catalyst comprising Pt atoms stabilized in Cu_xO surfaces capable of CO oxidation and CO PROX reaction. The work, still in progress, demonstrates yet another successful bridging of surface science, microscopy and catalysis.

3. Inorganometallic single site Au/Pt oxo-clusters stabilized by alkali ions as catalysts for the non-oxidative methanol coupling

In situ CH₃OH IR and DFT study of methanol dehydrogenation over Au₁-O_x-Na₉-(OH)_y

A novel and practical method to prepare inorganometallic oxo-clusters of single gold and platinum atoms in alkaline solutions was developed in our lab. For gold, Au(OH)₃ was dissolved in NaOH or KOH solutions at ~80°C, with 9-10:1 ratio of Na/K to Au. Up to 1.2 wt.% loading of atomic gold was achieved by incipient wetness impregnation of titania with these solutions. This is one of the highest loadings of single gold atoms on any support reported to date. EXAFS analyses indicate that Au is coordinated with -O in the first shell and with Na or K as the sheath for Au₁-O_x-Na/K₉-(OH)_y. Non-oxidative dehydrogenation of methanol (2CH₃OH → HCOOCH₃ + 2H₂) to methyl formate (MF, coupled product) and hydrogen with 100% selectivity even at high conversions took place over Au₁-O_x-Na₉-(OH)_y/TiO₂. Interestingly, and most importantly, the intact complex could be washed out of the support in water, and re-used to impregnate the support without loss of activity. This finding led us to prepare unsupported catalysts, i.e. the same complex after drying. The unsupported material was active and as selective, as shown by our catalytic tests, and by several characterization methods. Thus, the support plays no role in the reaction.

The experimental results (capturing catalytic sites, and intermediate/spectator species identified by *in situ* DRIFTS) were complemented by theoretical studies aimed at gaining further mechanistic insight into the catalytic activity of the [Au₁-O_x]- species toward MF production. To this end, our collaborators at Wisconsin performed a detailed study of the thermochemistry of relevant steps, using density functional theory (DFT), to efficiently screen active cluster candidates.

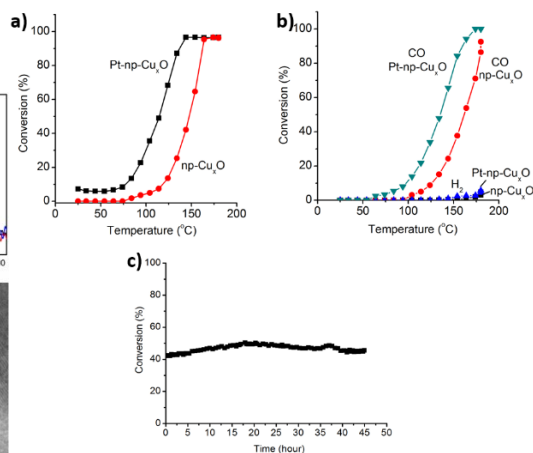


Figure 3. a) Second cycle TPSR data for CO oxidation over Pt-np-Cu_xO and np-Cu_xO, 50 mL/min, 2% O₂, 2% CO, bal. He, 500 mg sample b) TP-PROX on Pt-np-Cu_xO and np-Cu_xO, 50 mL/min, 2% O₂, 2% CO, 40% H₂, bal. He, 500 mg sample c) Steady-state PROX at 130°C on Pt-np-Cu_xO, 50 mL/min, 2% O₂, 2% CO, 40% H₂, bal. He, 500 mg sample

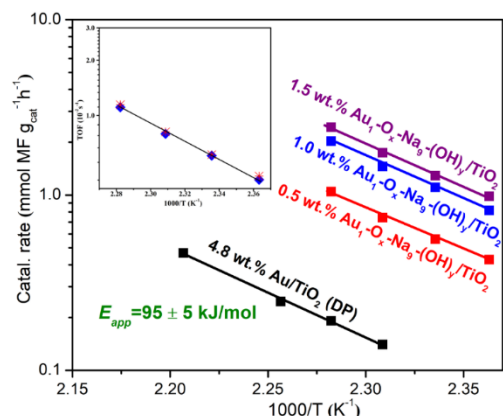


Fig. 4. Non-oxidative methanol dehydrogenation activity and stability of gold: Arrhenius-type plots of methanol dehydrogenation to MF over various Au-O_x catalysts. TOF is shown in the inset, in MF molecules produced per gold atom per sec.

Three new cluster models, permanently decorated with HCOO, were evolved from previously examined spectator-free models: Au₁-O₃-Na₉-(OH)₉, Au₁-O₇-Na₉-(OH)₅, and Au₁-O₉-Na₉-(OH), the last two being permanently decorated with two HCOO groups, while the first with a single HCOO. This agrees with the identification of HCOO as a spectator species in methanol dehydrogenation by *in situ* DRIFTS.

4. PtCu single-atom alloy catalysts for coke resistant C-H activation and selective dehydrogenation of n-butane

In another part of the project, we investigated Pt/Cu SAAs for the dehydrogenation of alkanes to produce alkenes²⁰, which are precursors to commodity polymers. Preventing coking is an active, yet challenging area of current C-H chemistry research. We have now demonstrated that Pt/Cu SAAs activate C-H bonds with significantly improved activity over Cu, while avoiding coking that occurs on catalysts with extended Pt ensembles due to the ability of Cu to facilitate C-C coupling chemistry.²⁰ We conducted EXAFS and FTIR studies to confirm the formation of Cu NPs with embedded isolated Pt atoms.¹⁵ Encouraged by the success in the coke resistant B-D scrambling, Fig. 5, we explored the nonoxidative dehydrogenation of butane with SAA catalysts. At 400 °C, Pt_{0.01}Cu-SAA stably converts butane to butene for at least 52 h without any deactivation. The high stability of Pt_{0.01}Cu-SAA in butane dehydrogenation results from a lack of Pt ensembles that are easily coked.²⁰ Therefore, we have demonstrated the SAA Pt/Cu alloy as a most promising catalyst for alkane dehydrogenation. Work is continuing to rank order other M/Cu SAAs (M: Pt, Pd, Rh, Ni, ...) and improve our mechanistic understanding of these systems.

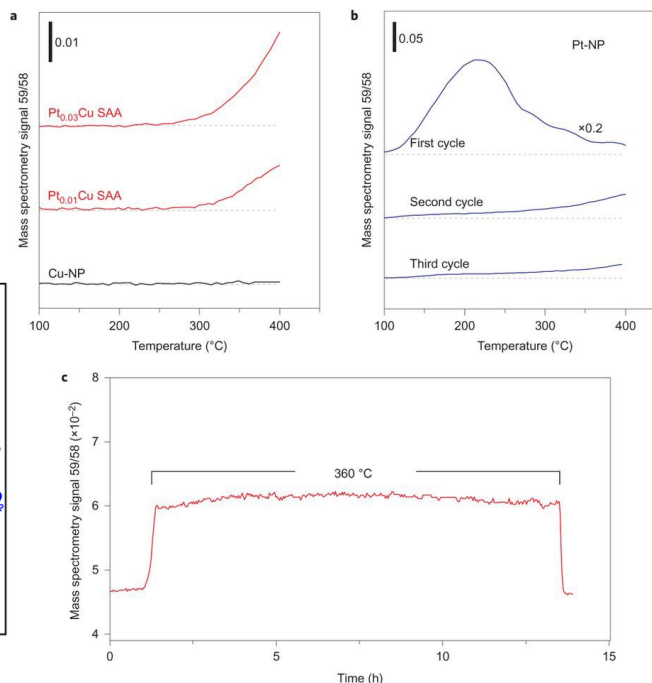


Figure 5. TPSR data for the B-D scrambling reaction over (a) Pt_{0.03}Cu-SAA, Pt_{0.01}Cu-SAA and Cu-NP catalysts and (b) Pt-NP catalysts, monitored by mass spectrometry. The data in (a) are from the second reaction cycle. First, second and third cycles of TPSR are shown for Pt-NP (b); (c) 12-h test for the Pt_{0.01}Cu-SAA catalyst at 360°C showing stability over time. The catalyst was at RT at the beginning and end of the test, 50 mL/min, 5% butane, 2% deuterium, bal. Ar, 100 mg sample.²⁰

Publications Acknowledging this Grant in 2015-2018

(I) Exclusively funded by this grant

1. Garbarino, G.; Wang, C.; Valsamakis, I.; Chitsazan, S.; Riani, P.; Finocchio, E.; Flytzani-Stephanopoulos, M.; Busca, G. A study of Ni/Al₂O₃ and Ni-La/Al₂O₃ catalysts for the steam reforming of ethanol and phenol, *Applied Catalysis B: Envir.* **2015**, 174-175, 21–34
2. Yang, M.; Liu, J.; Lee, S.; Zugic, B.; Huang, J.; Allard, L.F.; Flytzani-Stephanopoulos, M. A Common Single-Site Pt(II)–O(OH)_x– Species Stabilized by Sodium on 'Active' and 'Inert' Supports Catalyzes the Water-Gas Shift Reaction, *J. Am. Chem. Soc.* **2015**, 137 (10), 3470–3473
3. Lucci, F. R.; Marcinkowski, M. D.; Lawton, T. J.; Sykes, E. C. H., H₂ Activation and Spillover on Catalytically Relevant Pt-Cu Single Atom Alloys. *J. Phys. Chem. C.* **2015**, 119, 24351-24357
4. Yi, N.; Flytzani-Stephanopoulos, M., Gold-Ceria: the making of a robust catalyst for fuel processing and hydrogen production, **2015**, Chapter 5 in *Catalysis by Materials with Well-Defined Structures* (Edited by Wu and Overbury). Elsevier Science, ISBN: 9780128012178
5. Wang, C.; Garbarino, G.; Allard, L. F.; Wilson, F.; Busca, G.; Flytzani-Stephanopoulos, M., Low-Temperature Dehydrogenation of Ethanol on Atomically Dispersed Gold Supported on ZnZrO_x. *ACS Catal.* **2016**, 6, 210–218
6. Wang, C.; Yang, M.; Flytzani-Stephanopoulos, M. Single Gold Atoms Stabilized on Nanoscale Metal Oxide Supports Are Catalytically Active Centers for Various Reactions. *AIChE J.* **2016**, 62, 429–439
7. Hensley, A. J. R.; Therrien, A. J.; Zhang, R.; Marcinkowski, M. D.; Lucci, F. R.; Sykes, E. C. H.; McEwen, J. S. CO Adsorption on the “29” Cu_xO/Cu(111) Surface: An Integrated DFT, STM, and TPD Study. *J. Phys. Chem. C* **2016**, 120, 25387–25394
8. Therrien, A. J.; Zhang, R.; Lucci, F. R.; Marcinkowski, M. D.; Hensley, A. J. R.; McEwen, J. S.; Sykes, E. C. H. Structurally Accurate Model for the “29”-Structure of Cu_xO/Cu(111): A DFT and STM Study. *J. Phys. Chem. C.* **2016**, 120, 10879-10886
9. Yang, M.; Flytzani-Stephanopoulos, M. Design of Single-Atom Metal Catalysts on Various Supports for the Low-Temperature Water-Gas Shift Reaction. *Catal. Today* **2017**, 298, 216–225
10. Flytzani-Stephanopoulos, M. Supported Metal Catalysts at the Single-Atom Limit - A Viewpoint. *Chinese J. Catal.* **2017**, 38, 1432–1442
11. Garbarino, G.; Wang, C.; Valsamakis, I.; Chitsazan, S.; Riani, P.; Finocchio, E.; Flytzani-Stephanopoulos, M.; Busca, G. Acido-Basicity of Lanthana/Alumina Catalysts and Their Activity in Ethanol Conversion. *Appl. Catal. B Environ.* **2017**, 200, 458–468

12. Therrien, A. J.; Hensley, A. J. R.; Zhang, R.; Pronschinske, A.; Marcinkowski, M. D.; McEwen, J.-S.; Sykes, E. C. H. Characterizing the Geometric and Electronic Structure of Defects in the “29” Copper Surface Oxide. *J. Chem. Phys.* **2017**, *147*, 224706

13. Therrien, A. J.; Hensley, A. J. R.; Marcinkowski, M. D.; Zhang, R.; Lucci, F. R.; Coughlin, B.; Schilling, A. C.; McEwen, J.-S.; Sykes, E. C. H. An Atomic-Scale View of Single-Site Pt Catalysis for Low-Temperature CO Oxidation. *Nat. Catal.* **2018**, *1*, 192–198 [Cover Art]

(II) *Jointly funded by this grant and other grants with leading intellectual contribution from this grant;*

14. Therrien, A. J.; Groden, K.; Hensley, A. J. R.; Schilling, A. C.; Hannagan, R. T.; Marcinkowski, M. D.; Pronschinske, A.; Lucci, F. R.; Sykes, E. C. H.; McEwen, J. S. Water Activation by Single Pt Atoms Supported on a Cu₂O Thin Film. *J. Catal.* **2018**, *364*, 166–173

15. Lucci, F.; Liu, J.; Marcinkowski, M. D.; Yang, M.; Flytzani-Stephanopoulos, M.; Sykes, E.C.H. Selective hydrogenation of butadiene on platinum copper alloys at the single atom limit. *Nat. Commun.* **2015**, *6*, 8550

16. Liu, J.; Lucci, F. R.; Yang, M.; Lee, S.; Marcinkowski, M. D.; Therrien, A. J.; Williams, C. T.; Sykes, E. C. H.; Flytzani-Stephanopoulos, M. Tackling CO Poisoning with Single-Atom Alloy Catalysts. *J. Am. Chem. Soc.* **2016**, *138*, 6396–6399

(III) *Jointly funded by this grant and other grants with relatively minor intellectual contribution from this grant;*

17. Li, Z.; Potapenko, D. V.; Rim, K. T.; Flytzani-Stephanopoulos, M.; Flynn, G. W.; Osgood, R. M.; Wen, X.-D.; Batista, E. R. Reactions of Deuterated Methanol (CD₃OD) on Fe₃O₄(111). *J. Phys. Chem. C* **2015**, *119*, 1113–1120

18. Shan, J.; Lucci, F. R.; Liu, J.; El-Soda, M.; Marcinkowski, M. D.; Allard, L. F.; Sykes, E. C. H.; Flytzani-Stephanopoulos, M. Water Co-Catalyzed Selective Dehydrogenation of Methanol to Formaldehyde and Hydrogen. *Surf. Sci.* **2016**, *650*, 121–129

19. Marcinkowski, M. D.; Liu, J.; Murphy, C. J.; Liriano, M. L.; Wasio, N. A.; Lucci, F. R.; Flytzani-Stephanopoulos, M.; Sykes, E. C. H. Selective Formic Acid Dehydrogenation on Pt-Cu Single-Atom Alloys. *ACS Catal.* **2017**, *7*, 413–420

20. Marcinkowski, M. D.; Darby, M. T.; Liu, J.; Wimble, J. M.; Lucci, F. R.; Lee, S.; Michaelides, A.; Flytzani-Stephanopoulos, M.; Stamatakis, M.; Sykes, E. C. H. Pt/Cu Single-Atom Alloys as Coke-Resistant Catalysts for Efficient C-H Activation. *Nat. Chem.* **2018**, *10*, 325–332

21. Gates, B. C.; Flytzani-Stephanopoulos, M.; Dixon, D. A.; Katz, A. Atomically Dispersed Supported Metal Catalysts: Perspectives and Suggestions for Future Research. *Catal. Sci. Technol.* **2017**, *7*, 4259–4275

22. Zhao, Y.; Yang, K. R.; Wang, Z.; Yan, X.; Cao, S.; Ye, Y.; Dong, Q.; Zhang, X.; Thorne, J. E.; Jin, L.; Materna, K. L.; Trimpalis, A.; Bai, H.; Fakra, S. C.; Zhong, X.; Wang, P.; Pan, X.; Guo, J.; Flytzani-Stephanopoulos, M.; Brudvig, G. Q.; Batista, V. S.; Wang D. Stable Iridium Dinuclear Heterogeneous Catalysts Supported on Metal-Oxide Substrate for Solar Water Oxidation. *Proc. Natl. Acad. Sci.* **2018**, 20172213.

Modeling and Exploiting Non-idealities in Nitrogen Catalysis

William F. Schneider
University of Notre Dame

Presentation Abstract

Among the most significant developments in heterogeneous catalysis in the last 20 years is the emergence of microkinetic models, often parameterized from density functional theory (DFT) calculations, used to quantify observed catalyst performance and to guide the discovery of new catalytic materials. While DFT directly reports binding energies and elementary step activation energies, the free energies that enter into microkinetic models must be computed from additional approximations. Frequently these free energy approximations assume ideal behavior—that adsorbates do not interact with one another, or that adsorbates are immobile or vibrate harmonically about a binding site. These assumptions can and do have an impact on predicted catalyst performance and potentially even on predicted trends.

In this presentation I discuss our work related to three categories of non-idealities, presented in the context of nitrogen oxidation and reduction catalysis. I describe our strategy for calculation of adsorbate translational free energy, the contribution least well described by conventional models, and compare the exact results to standard approximations. I briefly describe computational models of adsorbate-adsorbate interactions, examine the implications of their incorporation into explicit, lattice-based microkinetic models, and describe recent advances in mean-field descriptions of this coverage-dependence. Lastly, I describe recent work to explore the kinetic consequences of the most fundamental assumption of all—that of energy equipartition—in an effort to rationalize and guide plasma-enhanced catalysis.

DE-FG02-06ER15839: Towards Realistic Models of Heterogeneous Catalysis: Simulations of Oxidation Catalysis from First Principles

Postdoc(s): Dr. Hanyu Ma

Student(s): Anshumaan Bajpai, Prateek Mehta

RECENT PROGRESS

Adsorbate Translational Free Energies

The free energy of a system is determined by the volume of phase space the system explores at a given temperature. An adsorbate at a surface may be immobile, in which case the translational contribution to its free energy vanishes, or it may freely translate, in which case the translational contribution to its free energy is proportional to area. In reality neither limit is correct, as the energy landscape an adsorbate experiences as it translates is corrugated. This corrugation can be approximately represented using analytical models, such as the harmonic oscillator. In principle, however, these potential energy landscapes are computable, and thus the translational free energies knowable without approximation.

Figure 1 shows DFT-computed translational potential energy surfaces for a variety of atomic adsorbates on Au(100) and Pt(100). The differences in preferred adsorption site across adsorbates and energy corrugation across metals are evident. By solving the two-dimensional Schrödinger equation on these potentials, we extract translational densities of states and, from the corresponding partition functions, the translational free energy.

Figure 2 shows representative results for O on Au(100). The exact (PES) solution is intermediate between the harmonic oscillator (HO) and hindered (HT) or free translator (FT). Absolute differences are on the order of 0.1 eV at 800 K, arguably small relative to the underlying DFT uncertainty. By comparing across systems, we find that the errors associated with conventional models are highly case specific, and further that common strategies for selecting particular models may compound rather than ameliorate errors. Further, we find that in the cases studied the PES is to a good approximation separable, and thus that the problem reduces to solving two 1-dimensional Schrödinger equations. Thus, the full PES solution can be applied with introduction of minimal additional computational expense relative to the standard models. We are working to extend these models to more corrugated surfaces and more complex adsorbates.

Catalytic Consequences of Adsorbate-Adsorbate Interactions

In the conventional approach, adsorbate-surface binding energies are computed at a fixed coverage, say in a 2×2 or 3×3 supercell of a particular metal facet. Such an approach is appropriate for comparing energies across facets, between metals, or even between adsorbates. Under catalytic conditions, however, adsorption energies can deviate significantly from the ideal, coverage-independent limit because of ubiquitous adsorbate-adsorbate interactions.

We have used lattice-based, DFT-parameterized cluster expansions (CE) to represent coverage-dependent adsorption energies and have developed techniques to simplify their construction for multi-adsorbate systems. While the CE is accurate, it becomes increasingly cumbersome to parameterize with increasing numbers and types of adsorbates. We have developed analytical expressions for coverage-dependent adsorption that nicely reproduce the CE results.

Figure 3 shows predicted adsorbate coverages during steady-state NO oxidation on Pt(111) computed using the full CE, two literature analytical models (linear and piece-wise linear), and a new, activity-inspired model (act). The activity model performs well over a wide range of conditions and coverages. Figure 4 reports the corresponding NO oxidation rates. The activity model best matches the CE at low temperatures, where coverages are the highest. At high temperatures all models deviate from the CE, a consequence of underlying mean-field assumption in the analytical models.

Catalytic Ammonia Oxidation

The NO oxidation systems is a practically important model, but our goal is to extend these models to more complicated catalysis. Ammonia oxidation is technologically important and is interesting because of selectivity issues between N_2 , NO, and NH_3 . While the thermodynamic N_2 selectivity is larger than 99% at conditions relevant to ammonia slip catalysis (ASC), the observed selectivities of platinum group metals (PGMs) are often less than 80%, insufficient to meet

emission regulations. To date, there is no self-consistent comparison of intrinsic selectivity over PGM, and the relation between surface coverage and product selectivity remain unclear.

We have computed all reaction steps relevant to ammonia oxidation on Pt, Pd and Rh(111). We find that direct N-H bond dissociation has high activation barriers on the metal terraces but that activation energies are diminished by reaction with co-adsorbed O* and OH*. Figure 5 shows the results of a mean-field microkinetic model of ammonia oxidation at a representative ASC condition, parameterized from the DFT results, and plotted as a Sankey diagram to compare the net rates of the parallel reaction steps. The diagrams show that N₂ selectivity follows Pt > Rh > Pd and it highlights the relative importance of O* and OH* activated NH_x* dehydrogenation.

An analysis of these coverage-independent microkinetic results shows that, at low temperature and low O₂/NH₃ ratios, the most abundant surface intermediate is N and N₂ selectivity is high; in contrast, at high temperature and high O₂/NH₃ ratios, O becomes the most abundant surface intermediate and selectivity switches towards NO and N₂O. These observations are consistent with experimental observations. The work highlights the relationship between coverage and selectivity and motivates further development of coverage-dependent models.

Publications Acknowledging this Grant in 2015-2018

(I) Exclusively funded by this grant;

J. M. Bray and W. F. Schneider, "First-Principles Analysis of Structure Sensitivity in NO Oxidation on Pt," *ACS Catal.*, **2015**, 5, 1087-1099.

L. M. Herder, J. M. Bray, and W. F. Schneider, "Comparison of Cluster Expansion Fitting Algorithms for Interactions at Surfaces," *Surf. Sci.*, **2015**, 640, 104-111.

A. Bajpai, K. Frey, and W. F. Schneider, "Binary Approach to Ternary Cluster Expansions: NO–O–Vacancy System on Pt(111)," *J. Phys. Chem. C*, **2017**, 121, 7344-7354.

A. Bajpai, P. Mehta, K. Frey, A. Lehmer, and W. F. Schneider, "Benchmark First Principles Calculations of Adsorbate Free Energies," *ACS Catalysis* **2018**, 8, 1945-1954.

(III) Jointly funded by this grant and other grants with relatively minor intellectual contribution from this grant;

P. Mehta, P. Barboun, F. A. Herrara, J. Kim, P. Rumbach, D. B. Go, J. C. Hicks, and W. F. Schneider, "Overcoming Ammonia Synthesis Scaling Relations with Plasma-enabled Catalysis," *Nature Catal.* **2018**, 1, 269-275.

Unraveling the Catalytic Transformations Drive the Activation of Cellulose

Matthew Neurock, Paul Dauenhauer, Greg Facas, Vineet Maliekkal, Saurabh Maduskar
Department of Chemical Engineering and Materials Science, University of Minnesota,
Minneapolis, MN, 421 Washington Ave. SE, Minneapolis, MN 55455

Presentation Abstract

Cellulose, the most abundant biopolymer in lignocellulosic biomass, can be transformed into value added chemicals and fuels through thermochemical as well as biochemical routes. In fast pyrolysis, cellulose is rapidly heated to 400-600 °C where it liquefies and depolymerizes to form anhydro-oligomers including levoglucosan, furans, anhydrosugar and light oxygenates that make up bio-oil as well as gas and char. Pyrolysis results in a complex array of thousands of different species. The complexity of following the reactivity of this multicomponent three-phase system presents significant challenges for reaction systems that can track the kinetics for individual species while eliminating heat and mass transfer effects as well as for modeling the elementary transformations. As such, most of the kinetic models for the cellulose pyrolysis are lumped empirical models devoid of the fundamental chemistry. While ab initio simulations have provided unique insights into elementary bond breaking/making steps, most reported studies examine the reactivity of a single model molecule in absence of the complex reaction environment.

Herein we have developed and used a novel reactor system (Pulse-Heated Analysis of Solid/Surface Reactions (PHASR)) together with in-situ analytical methods that allow us to rapidly heat and cool samples to control the reaction progress and capture time-resolved kinetics. These efforts are coupled with detailed ab initio simulations and kinetic Monte Carlo simulations that follow the molecular transformations of cellulose within their complex solid and liquid environments. We examine in detail the reactions within the solid and liquid that form during pyrolysis and show that the local environment can, in some cases, significantly promote the reactivity by catalyzing particular reactions. More specifically we examine the molecular transformations in the initial depolymerization of cellulose to form Levoglucosan, a primary product formed via glycosidic bond cleavage, and explore the catalytic effects of hydroxyl groups as well as metal ions such as Ca and Mg present within biomass. Experiments show two different kinetic regimes for the thermal decomposition of cellulose that operate via different mechanisms. The high temperature regime has a high activation barrier and proceeds via the mid-chain scission of cellulose whereas the low temperature regime has a low barrier and extensive chain-end scission. At low temperatures, inter-sheet hydroxyl groups act as catalysts to promote the lower energy reaction pathways. At higher temperatures, the paths are predominantly thermal and proceed with higher barriers. The specific addition of Ca, as well as other alkaline or alkaline earth cations, appear to catalyze low temperature intra-chain scission. Simulations suggest that Ca disrupts the intra-plane hydrogen bonding and stabilizes the transition state for transglycosylation.

DE-SC0016346: Promoted Cellulosic Pathways and Mechanisms via Impregnated Natural Metal Catalysts (2016-2019)

PI: Paul J. Dauenhauer **Co-PI:** Matthew Neurock

Student(s): Greg Facas, Vineet Maliekkal

Publications Acknowledging this Grant in 2015-2018

- [1] Krumm, C.; Pfaendtner, J.; Dauenhauer, P.J. Millisecond Pulsed Films Unify the Mechanisms of Cellulose Fragmentation. *Chem. Materials* **2016**, 28(9), 3108-3114. (Exclusively funded by this grant)
- [2] Zhu, C.; Krumm, C.; Facas, G.; Neurock, M.; Dauenhauer, P.J. Energetics of Cellulose and Cyclodextrin Glycosidic Bond Cleavage. *Reaction Chem. and Eng.* **2017**, 2, 201-214. (Partially funded by this grant)
- [3] Maduskar, S.; Maliekkal, V.; Neurock, M.; Dauenhauer, P.J. Yield of Levoglucosan from Cellulose Pyrolysis, *ACS Sustainable Chem. and Eng.*, **2018** 6 (5), 7017-7025 (Exclusively funded by this grant)
- [4] Zhu, C.; Maduskar, S.; Paulsen, A.D.; Dauenhauer, P.J. Alkaline Earth Metal Catalyzed Thin-Film Pyrolysis of Cellulose, *ChemCatChem* **2016**, 8(4), 818-829. (Exclusively funded by this grant)
- [5] Maduskar, S.; Maliekkal, V.; Saxon, D.J.; Nasiri, M.; Reineke, T.M., Neurock, M.; Dauenhauer, P.J. Activation of Cellulose via Cooperative Hydroxyl-Catalyzed Transglycosylation of Glycosidic Bonds. In preparation, 2018. (Exclusively funded by this grant)
- [6] Facas, G.; Maliekkal, V.; Neurock, M.; Dauenhauer, P.J.; Activation of Cellulose with Alkaline Earth Metals. In preparation, 2018. (Exclusively funded by this grant)

Poster Session Abstracts

Development of *in-situ/operando* Catalyst Characterization Capabilities at SSRL: Progress Report

Simon R. Bare¹, Adam S. Hoffman¹, Alexey Boubnov¹
¹SSRL, SLAC National Accelerator Laboratory

Presentation Abstract

Accessible and versatile *in-situ/operando* experimental capabilities are the lifeblood of a catalysis-related synchrotron beam line. These capabilities allow critical experiments to be performed on working catalysts and provide detailed information on the atomic-level structure (geometric and electronic) of the active site, allowing structure-property relationships to be developed, and ultimately leading to the discovery of new catalysts. This poster highlights some of the synchrotron catalyst characterization capabilities that have recently been implemented and are currently under development at SSRL. The initial focus has been on the infrastructure necessary for the study of thermal heterogeneous catalysts. Results will be presented on: (i) Versatile experimental infrastructure (gas delivery and *in-situ* cells) for safe and reliable operations (temperatures up to 700°C, pressures up to 70 bar) for XRD and XAFS, using cobalt-based catalysts for higher alcohol synthesis from syngas as an example; (ii) Long-term studies, e.g. deactivation phenomena in Fischer-Tropsch catalysts; (iii) Time-resolved spectroscopy using quick-scanning and continuous-scanning XAFS. This capability will be illustrated with a study of ligand-exchange kinetics in supported molecular catalysts; (iv) Combined *in-situ* FTIR/XAFS capability, and (v) The use of FEFF9 XANES spectral simulations based upon DFT-optimized structures to both predict experimental observations and for enhanced data analysis.

SUNCAT FWP

SLAC National Accelerator Laboratory

PI: Jens Norskov

Postdoc(s): Adam S. Hoffman, Alexey Boubnov

Exploring Nanoparticle Photocatalysts for Room Temperature, Aerobic Organic Oxidations

Bart M. Bartlett*, John L. DiMeglio, Kori D. McDonald, Aaron D. Proctor, and Shobhana Panuganti
University of Michigan, Department of Chemistry

Presentation Abstract

The aerobic photochemical oxidation of benzylamine to *N*-benzylidenebenzylamine and benzyl alcohol to benzaldehyde have been carried out on CdS nanowires as well as on the oxides WO₃, CuWO₄, and BiVO₄ as test proton-coupled-electron-transfer reactions in acetonitrile. CdS undergoes photocorrosion that accompanies photocatalysis, hinting that the radical intermediates formed during catalysis lead to corrosion, similar to what has been observed with hydroxy radical in water. The oxides are significantly more stable, and particle size is a key parameter for maximizing reaction rate. For example, 20 nm particles of WO₃ generated by microwave synthesis from WCl₆ yield an order of magnitude enhancement in rate for photocatalytic benzylamine coupling (rate constant 2.5 h⁻¹ g⁻¹ WO₃) under 3-sun simulated solar radiation. Current efforts include assessing the scope of this reactivity to non-benzylic substrates.

DE-SC0006587: Exploring Photoelectrochemical and Photocatalytic Oxidations on Semiconductor Nanostructures

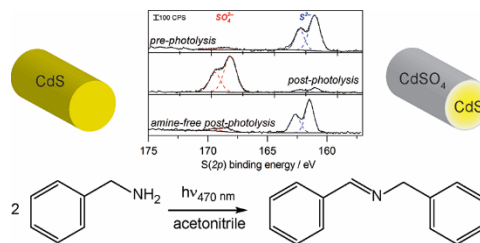
Postdoc(s): Dr. John L. DiMeglio

Student(s): Andrew G. Breuhaus-Alvarez, Kori D. McDonald, Aaron D. Proctor, Shobhana Panuganti

RECENT PROGRESS

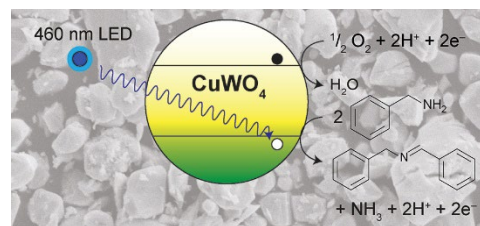
The Interplay of Corrosion and Photocatalysis During Non-Aqueous Benzylamine Oxidation on Cadmium Sulfide. (Chem. Mater. 2017, 29, 7579-7586.)

Bulk, nanowire, and chemical bath deposits of cadmium sulfide (CdS) have been evaluated for their propensity to oxidize benzylamine to *N*-benzylidenebenzylamine (*N*-BB) in acetonitrile both photocatalytically and photoelectro-chemically. During the reaction, the surface morphology of CdS (SEM imaging) and the chemical composition of the surface (XPS analysis) change. These two changes are accompanied by Cd²⁺ leaching into solution (ICP-OES analysis) and by H₂S gas evolution (chemical test) to unveil surface corrosion. This corrosion is linked to amine reactivity directly; control experiments show that CdS is quite stable during substrate-free photolysis even under prolonged irradiation. Moreover, photoelectrochemical experiments show that oxygen as well as trace water are essential reactants in CdS photocorrosion.



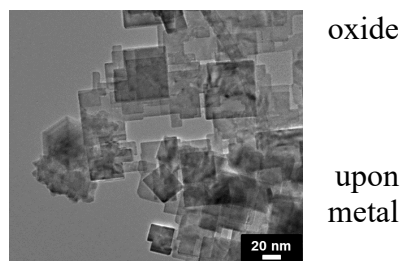
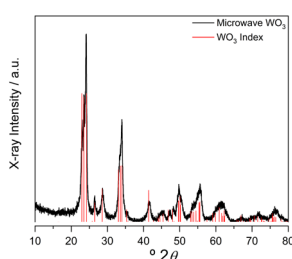
CuWO₄ as a Photocatalyst for Room Temperature Aerobic Benzylamine Oxidation. (Chem. Commun. 2018, 54, 1101-1104.)

Oxidation of benzylamine carried out on the ternary oxides CuWO₄ and BiVO₄ under aerobic conditions shows quantitative conversion to *N*-BB with initial rate constants 0.34 h⁻¹ g⁻¹ and 0.70 h⁻¹ g⁻¹ for CuWO₄ and BiVO₄ respectively. Moreover, the catalytic semiconductor particles can be washed and recycled 5 times with no loss in activity.



Synthesis of Oxide Nanoparticle Catalysts by Microwave Methods (Work in progress)

Tuning particle size and composition in synthesis is complicated in aqueous solution because fast diffusion and hydrolysis rates give rise to large, low surface area particles that often sinter annealing. Using organic solvents with halide precursors in high boiling point solvents gives crystalline phase-pure nanomaterials that do not require annealing. For example, WO₃ nanoplatelets can be synthesized from WCl₆ in benzyl alcohol as the solvent in 30 minutes using 20 – 30 W microwave power. The average particle size is on the order of 20 nm, and the initial rate for benzylamine oxidation on these nanoparticles is the fastest observed in our photocatalysis experiments yet, 2.5 h⁻¹ g⁻¹ WO₃.

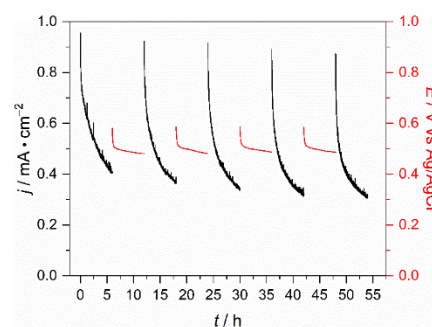


oxide
upon
metal

For example, WO₃ nanoplatelets can be synthesized from WCl₆ in benzyl alcohol as the solvent in 30 minutes using 20 – 30 W microwave power. The average particle size is on the order of 20 nm, and the initial rate for benzylamine oxidation on these nanoparticles is the fastest observed in our photocatalysis experiments yet, 2.5 h⁻¹ g⁻¹ WO₃.

Kinetics and Faradaic Efficiency of Oxygen Evolution on Reduced H_xWO₃ (Work in progress)

Instability in the observed photocurrent density during photoelectrochemical water oxidation on WO₃ has previously been attributed to formation of destructive peroxytungstate intermediates. Tungsten oxide electrodes have been synthesized by spin coating from an ammonium metatungstate sol followed by annealing. Under constant illumination, repeated cycles of poisoning these WO₃ electrodes at 0.98 V vs Ag/AgCl in pH 1 sulfate solution followed by measuring the open circuit potential for several hours show reversibility in the photocurrent decay. This behavior is attributed to photochromic H_xWO₃ generated at low concentration within the electrode, which serves to increase the donor density. Mott-Schottky analysis of electrochemical impedance spectroscopy (EIS) measurements before and after performing the oxygen evolution reaction (OER) exhibit a decrease in donor density from 2.6(8) × 10²⁰ cm⁻³ to 7(2) × 10¹⁹ cm⁻³. Measuring the OER rate by gas chromatography during water oxidation shows concurrent recovery of catalytic activity, illustrating the role of H_xWO₃ during photocatalysis.



Publications Acknowledging this Grant in 2015-2018

(I) Exclusively funded by this grant; (undergraduate co-authors underlined)

1. Brancho, J. J.; Bartlett B. M.* Challenges in Co-Alloyed Titanium Oxynitrides, a Promising Class of Photochemically Active Materials. *Chem. Mater.* **2015**, *27*, 7207-7217. (Up-and-coming series)
2. Lhermitte, C. R.; Verwer, J. G.; Bartlett B. M.* Improving the Stability and Selectivity for the Oxygen-Evolution Reaction on Semiconducting WO₃ Photoelectrodes with a Solid-State FeOOH Catalyst. *J. Mater. Chem. A* **2016**, *4*, 2960-2968. (Water Splitting and Photocatalysis themed issue)
3. Lhermitte, C. R.; Bartlett, B. M.* Advancing the Chemistry of CuWO₄ for Photoelectrochemical Water Oxidation. *Acc. Chem. Res.* **2016**, *49*, 1121–1129.
4. Esarey, S. L.; Holland, J. C.; Bartlett, B. M.* Determining the Fate of a Non-Heme Iron Oxidation Catalyst Under Illumination, Oxygen, and Acid. *Inorg. Chem.* **2016**, *55*, 11040–11049.
5. DiMeglio, J. L.; Bartlett, B. M.* The Interplay of Corrosion and Photocatalysis During Nonaqueous Benzylamine Oxidation on Cadmium Sulfide. *Chem. Mater.* **2017**, *29*, 7579-7586.
6. Brancho, J. J.; Proctor, A. D.; Panuganti, S.; Bartlett, B. M.* Urea-glass Preparation of Titanium Niobium Nitrides and Subsequent Oxidation to Photoactive Titanium Niobium Oxynitrides. *Dalton Trans.* **2017**, *46*, 12081-12087.
7. Proctor, A. D.; Panuganti, S.; Bartlett, B. M.* CuWO₄ as a Photocatalyst for Room Temperature Aerobic Benzylamine Oxidation. *Chem. Commun.* **2018**, *54*, 1101-1104.
8. Esarey, S. L.; Bartlett, B. M.* pH-Dependence of Binding Constants and Desorption Rates of Phosphonate- and Hydroxamate-Anchored [Ru(bpy)₃]²⁺ on TiO₂ & WO₃. *Langmuir* **2018**, *34*, 4535-4547.

Single Turnover at Molecular Catalysts

Prof. Suzanne A. Blum*, Quinn T. Easter, Dr. Nozomi Saito
Chemistry Department, University of California, Irvine, USA 93697-2025

Presentation Abstract

Catalytic cycles are typically depicted as possessing time-invariant steps with fixed rates. Yet the true behavior of individual catalysts with respect to time is unknown, hidden by the ensemble averaging inherent to bulk measurements. Herein, focused on a ring-opening metathesis polymerization reaction catalyzed by the second-generation Grubbs' ruthenium catalyst, we show evidence for variable chemical kinetics at individual catalysts with fluorescence microscopy possessing sufficient sensitivity for the detection of single chemical reactions. Insertion reactions in submicron regions likely occur at groups of many (not single) catalysts, yet not so many that their unique kinetic behavior is ensemble averaged.

DE-SC0016467: Single-Molecule Fluorescence Tools at the Interface of Homogeneous and Heterogeneous Catalysis

Postdoc(s): Dr. Nozomi Saito

Student(s): Quinn T. Easter

RECENT PROGRESS

Evidence for Dynamic Chemical Kinetics at Individual Molecular Ruthenium Catalysts.

The experiments in this area provided evidence for dynamic chemical kinetics at individual molecular polymerization catalysts. Although the rates of monomer insertion at single catalysts were not measured, real-time chemical kinetics information could nevertheless be measured without the averaging that occurs in a traditional ensemble measurement. The sensitivity to detect single fluorophores from individual ROMP reactions enabled estimation of quantitative kinetics of polymerization at subparticle, submicron regions of polymer aggregates. These data unexpectedly showed that regions of polymer aggregates change catalytic chemical reactivity abruptly and that distinct kinetics dominate within a subparticle region. Broadly, such changing kinetic states plausibly affect the macroscopic properties of resulting polymers (e.g., through regionally differing amounts of comonomer incorporation in block copolymers). Key details about chemical kinetics are generally hidden by ensemble measurements, and this fluorescence microscopy approach provides a way to gain insight into the dynamic behavior of molecular catalysts and thus redefine the dogmatic view of catalytic cycles.

The First Single-Turnover Fluorescence Imaging of Any Molecular Catalyst

Multiple active individual molecular ruthenium catalysts were pinpointed within growing polynorbornene, revealing reaction dynamics and location information that is unavailable through traditional ensemble experiments. These experiments are the first single-turnover fluorescence microscopy imaging at any molecular (chemo)catalyst and achieve the detection of individual monomer reactions at an industrially important molecular ruthenium ring-opening metathesis polymerization (ROMP) catalyst under synthetically relevant catalytic conditions (e.g., unmodified industrial catalyst, ambient pressure, condensed phase, ~ 0.03 M monomer). These results further establish the key fundamentals of this imaging technique for characterizing the reactivity and location of active molecular catalysts even when they are the minor components.

Catalysis is a multibillion-dollar world-wide industry, yet the determination of the phase and local environment of active catalysts is a long-standing analytical challenge. This is especially true in reactions at the homogenous/heterogeneous interface where the (unknown) phase and locations of the active catalyst can have a profound effect on its local environment and thus reactivity and selectivity. Herein we employ fluorescence microscopy with single-monomer insertion reaction sensitivity under catalytic conditions at individual molecular catalysts. Resultant imaging data revealed phase and spatiotemporally resolved individual active molecular ruthenium catalysts within growing polymers for the first time, providing information that is unavailable through traditional ensemble techniques. The industrially important monomer norbornene and catalyst 1 were selected for initial studies. The molecular ruthenium catalyst “Grubbs II” is inactive when phosphine is coordinated; thus, the presence of ruthenium does not imply catalytic activity and new analytical techniques are needed to pinpoint the origin and distribution of reactivity.

While well-known in biological systems, zeolite, and nanoparticle catalysis, this is the first example of achieving the single-turnover detection limit with a molecular catalyst by single-molecule fluorescence microscopy. Given that molecular catalysts make up a significant portion of all catalysis, imaging turnover in these systems at the single-molecule level holds great potential to reveal reactivity information hidden by ensemble averaging like it has in biological, zeolite, and nanoparticle systems.

The added challenge with molecular catalysts is that their small size means they diffuse rapidly in solution, precluding imaging. Approaches with stoichiometric reactions of molecular species chemically tethered to glass to reduce their motion and make them sufficiently stationary for imaging have not yet yielded catalytic turnover. In contrast, we demonstrate a strategy wherein experiments employ unmodified catalyst which is widely employed in industrial syntheses of polymers, pharmaceutical candidates, and complex molecules. No tethering to an artificial surface, which may alter its reactivity, is necessary. Instead, the experiments herein harness the changing solubility and large size of growing polymers in a precipitation polymerization reaction to aid in imaging individual active molecular catalysts; such catalysts, derived from 1 within precipitated polymers were sufficiently stationary for successful imaging of single ROMP reactions. Unlike AFM techniques that study individual catalyst sites, this technique does not require atomically smooth model surfaces.

Kinetics of the Same Reaction over Nine Orders of Magnitude in Concentration: When Are Unique Subensemble and Single-Turnover Reactivity Displayed?

Essentially no information is known about the behavior of individual molecular catalysts under reaction conditions, due to the averaging inherent to traditional analytical techniques. In this study, a combined fluorescence microscopy and ^1H NMR spectroscopy approach reveals that unique (that is, non-ensemble averaged) time-variable kinetics from molecular ruthenium catalysts within growing polynorbornene occur and are detectable between 10^{-9} M and, surprisingly, 10^{-6} M of substrate, just 1000-fold less concentrated than a typical laboratory bench-scale reaction. The kinetic states governing single-turnover events are determinable by overlay of the signal arising from individual monomer insertion reactions with that from polymer growth from neighbouring catalysts.

Publications Acknowledging this Grant in 2015-2018
(This grant started in 2016)

(I) Exclusively funded by this grant:

1. Kazuhiro, K.; Blum, S. A. "Structure–Reactivity Studies of Intermediates for Mechanistic Information by Subensemble Fluorescence Microscopy." *ACS Catal.* **2017**, *7*, 3786–3791.
2. Easter, Q. T.; Blum, S. A. "Single Turnover at Molecular Polymerization Catalysts Reveals Spatiotemporally Resolved Reactions." *Angew. Chem. Int. Ed.* **2017**, *56*, 13772–13775.
(Highlighted in *Angew. Chem. Int. Ed.* **2018** "Kinetics in the Real World.")
3. Easter, Q. T.; Blum, S. A. "Evidence for Dynamic Chemical Kinetics at Individual Molecular Ruthenium Catalysts." *Angew. Chem. Int. Ed.* **2018**, *57*, 1572–1575.

**Supported Metal Nanoparticles:
Correlating Structure with Catalytic Function through Energetics**

Charles T. Campbell
University of Washington, Departments of Chemistry and Chemical Engineering

Presentation Abstract

Many important catalysts and electro-catalysts for energy and environmental technologies involve late transition metal nanoparticles dispersed across the surface of some oxide support. The activity and long-term stability of these materials depend strongly on particle size below 5 nm, and, in this size range, upon the nature of the oxide support. The relationships between the energetic stability of late transition metal particles on oxide supports and their structural, electronic, chemisorption and catalytic properties have been analyzed in detail. We will show predictive correlations amongst the calorimetrically-measured energy of the metal atoms in these nanoparticles (i.e., the metal-atom chemical potential) and their particle size as well as their adhesion energy to the oxide surface (E_{adh}). Measurements of the metal / oxide adhesion energy reveal that E_{adh} increases with: (1) increasing oxophilicity of the metal (estimated from the heat of formation of the oxide of the metal from metal gas plus O_2), (2) decreasing oxophilicity of the oxide support (estimated from the heat of reduction of the metal oxide support to its next lower oxide), and (3) increasing density of coordinatively-unsaturated O atoms on the surface of the oxide. The strength with which oxide-supported metal particles bond adsorbates, their catalytic kinetics and their sintering rates also correlate with this metal-atom chemical potential, and thus it helps explain particle size and support effects in catalysis.

**Grant No. DE-FG02-96ER14630: Supported Metal Nanoparticles:
Correlating Structure with Catalytic Function through Energetics**

Postdoc(s): none

Student(s): Griffin Ruehl, Jack Rumpitz, Zhongtian Mao, Wei Zhang, Ziareena Almualem, John Ehren Eichler.

RECENT PROGRESS

Metal vapor adsorption calorimetry: trends in adsorption and adhesion energies

Nanoparticles on surfaces are ubiquitous in nanotechnologies, especially in catalysis where metal nanoparticles anchored to oxide supports are widely used to produce and use fuels and chemicals, and in pollution abatement. We continued our calorimetric studies of the adsorption energies of metal atoms as they grow nanoparticles on oxide supports, which provides the metal atom chemical potential versus particle size. We published a detailed study of the energetics of 2D and 3D gold nanoparticles on MgO(100). From this and other studies, we realized new ways to predict these energetics, as described below.

We proved that for hemispherical metal particles of the same diameter, D , the chemical potentials of the metal atoms in the particles (μ_M) differ between two supports by approximately -

$2(E_{\text{adh,A}} - E_{\text{adh,B}})V_m / D$, where $E_{\text{ad},i}$ is the adhesion energy between the metal and support i , and V_m is the molar volume of the bulk metal. This is consistent with calorimetric measurements of metal vapor adsorption energies onto clean oxide surfaces where the metal grows as 3D particles, which proved that μ_m increases with decreasing particle size below 6 nm, and, for a given size, decreases with E_{adh} . Since catalytic activity and sintering rates correlate with metal chemical potential, it is thus crucial to understand what properties of catalyst materials control metal/oxide adhesion energies. Trends in how E_{adh} varies with the metal and the support oxide were discovered. For a given oxide, E_{adh} increases linearly from metal to metal with increasing heat of formation of the most stable oxide of the metal (per mole metal), or metal oxophilicity, suggesting that metal-oxygen bonds dominate interfacial bonding. For the two different stoichiometric oxide surfaces that we studied with multiple metals (MgO(100) and CeO₂(111)), the slopes of these lines was found to be the same, but their offset is large (~ 2 J/m²). Adhesion energies were found to increase as: MgO(100) \approx TiO₂(110) $<$ α -Al₂O₃(0001) $<$ CeO₂(111) \approx Fe₃O₄(111).

Based on the above results and our other calorimetric measurements of metal adsorption energies, we discovered a method for estimating the metal atom chemical potential oxide-supported metal nanoparticles as a function of particle size for different metal / oxide combinations. We proved that this chemical potential for later transition metals is well approximated for a particle of diameter D by $\mu(D) = [(3\gamma_m - E_{\text{adh}})(1 + D_o/D)](2V_m / D)$, where γ_m is the surface energy of the bulk metal, E_{adh} is the adhesion energy at the bulk metal / oxide interface, and D_o is ~ 1.5 nm, and V_m is the molar volume of the bulk metal. We further showed that E_{adh} increases with: (1) increasing heat of formation of the most stable oxide of the metal from metal gas atoms plus O₂(gas) per mole of metal atoms, (2) decreasing enthalpy of reduction of the oxide to its next lower oxidation state plus O₂(gas), per mole of oxygen atoms, and (3) increasing density of surface oxygen atoms on the oxide surface. The linear scaling of E_{adh} with these properties allows estimations if E_{adh} for a variety of metal / oxide combinations. Using this E_{adh} estimate in the above equation with known values for γ_m allows estimates of metal chemical potential versus particle size for late transition metals on various oxide supports.

The above relationships and trends predicted that E_{adh} on a given oxide would be much larger for Ni particles than for any other metal particles we had studied so far. So we measured E_{adh} on MgO(100) and CeO₂(111) and confirmed those predictions with quantitative accuracy.

This new predictive ability to estimate metal chemical potential for different catalyst nanomaterials improves our ability to understand structure-property relations in catalysis and design better catalysts. We also wrote a review article about making sinter-resistant catalysts with Younan Xia at Georgia Tech.

In collaboration with Tom Mallouk's group at Penn State, we measured heats of adsorption of Ag and Cu atoms onto the basal plane of calcium niobate nanosheets. This is the first such measurement ever performed in the world on any mixed metal oxide. These results are being analyzed to determine their chemical potentials versus particle size and adhesion energies.

Catalytic Reaction Kinetics and Mechanisms

We also studied catalytic reaction kinetics. In collaboration with Johannes Lercher's PNNL team, we studied both electrocatalytic hydrogenation (ECH) and thermal catalytic hydrogenation (TCH) of phenol by carbon-supported Pt and Rh. These both showed a roll-over in rate with increasing temperature without changing the principal reaction pathways. The negative effect of temperature for aqueous-phase phenol TCH and ECH on Pt and Rh is deduced to be from dehydrogenated phenol adsorbates, which block active sites. ECH and TCH rates increase

similarly with increasing hydrogen chemical potential whether induced by applied potential or H₂ pressure, both via increasing H coverage, and indirectly by removing site blockers, a strong effect at high temperature. This enabled us to achieve rates of phenol TCH rates at 60-100 °C that are much higher than ever reported.

The Degree of Rate Control

The “degree of rate control” (DRC) is a mathematical approach for analysing multi-step reaction mechanisms that has proven very useful in catalysis research. It was invented by the PI. It identifies the “rate-controlling transition states and intermediates” (i.e., those whose DRCs are large in magnitude). Even in mechanisms with over 30 intermediates and transition states, these are generally just a few distinct chemical species whose energies, if they could be independently changed, would achieve a faster net reaction rate to the product of interest. For example, when there is a single “rate-determining step”, the DRC for its transition state (TS) is 1, which means (by definition) that if this TS’s energy could be decreased by $k_B T$ (where k_B is Boltzmann’s constant and T is temperature), the net rate would increase by a factor of e . Since the (relative) energies of these key adsorbed intermediates and transition states can be adjusted by modifying the catalyst or solvent, or even a reactant’s molecular structure, the DRC values provide important ideas for catalyst improvement. The species with large DRCs are also the ones whose energetics must be most accurately measured or calculated to achieve an accurate kinetic model for any reaction mechanism. We published an invited tutorial on DRC analysis, the calculation of DRCs, and examples of the applications of DRCs in catalysis research is presented here. It summarizes the applications of DRC analysis, including: clarifying reaction kinetics, improving the accuracy of computational models, improving reaction conditions, improving choice of oxidant in selective oxidation, incorporation in algorithms which calculate net reaction rates of multistep mechanisms without solving the differential equations involved, and high-throughput computational screening of catalyst materials. We also showed there that, since DRC values can be determined experimentally, a full microkinetic model is not required to take advantage of DRC analysis.

Publications Acknowledging this Grant in 2015-2018

A. Publications Resulting from this DOE Grant Support alone.

1. The Energetics of Cu Adsorption and Adhesion onto Reduced CeO₂(111) Surfaces by Calorimetry, T. E. James, S. L. Hemmingson, T. Ito and C. T. Campbell, *J. Physical Chemistry C* **2015**, 119, 17209-17217.
2. The Energy of Supported Metal Catalysts: from Single Atoms to Large Metal Particles, T. E. James, S. L. Hemmingson and C. T. Campbell, *ACS Catalysis* **2015**, 5, 5673–5678. (highlighted in *Chemical and Engineering News*, **93** (35) p. 33, September 7, 2015, and also as *Editor’s Choice* in *ACS Catalysis*).
3. Adsorption and Adhesion of Au on Reduced CeO₂(111) Surfaces at 300 K and 100 K, S. L. Hemmingson, T. E. James, G. M. Feeley, A. M. Tilson and C. T. Campbell, *J. Physical Chemistry C* **2016**, 120, 12113–12124.
4. Calorimetric Measurement of Adsorption and Adhesion Energies of Cu on Pt(111), T. E. James, S. L. Hemmingson, J. R.V. Sellers and C. T. Campbell, *Surface Science* **2017**, 657, 58–62. (Selected as *Editor’s Choice*.)
5. Trends in Adhesion Energies of Metal Nanoparticles on Oxide Surfaces: Understanding Support Effects in Catalysis and Nanotechnology, S. L. Hemmingson and C. T. Campbell, *ACS Nano* **2017**, 11, 1196-1203 (2017)..

6. Correction to: “Trends in Adhesion Energies of Metal Nanoparticles on Oxide Surfaces: Understanding Support Effects in Catalysis and Nanotechnology”, S. L. Hemmingson and C. T. Campbell, *ACS Nano* **2017**, 11, 1196-1203, *ACS Nano* 11, 4373 (2017).
7. Energetics of 2D and 3D Gold Nanoparticles on MgO(100): Influence of Particle Size and Defects on Gold Adsorption and Adhesion Energies, S. L. Hemmingson, G. M. Feeley, N. J. Miyake and C. T. Campbell, *ACS Catalysis* **2017**, 7, 2151-2163.
8. The Degree of Rate Control: A Powerful Tool for Catalysis Research, C. T. Campbell, *ACS Catalysis (Invited Viewpoint)* **2017**, 7, 2770-2779 (2017).
9. The Chemical Potential of Metal Atoms in Supported Nanoparticles: Dependence upon Particle Size and Support, C. T. Campbell and Z. Mao, *ACS Catalysis* **2017**, 7, 8460-8466.

B. Publications jointly funded by this DOE grant and other grants of the PI and/or his co-authors, with a leading intellectual contribution from this grant.

10. Surface Bound Intermediates in Low Temperature Methanol Synthesis – Participants and Spectators, Y. Yang, D. H. Mei, C.H.F. Peden, C.T. Campbell and C.A. Mims, *ACS Catalysis* **2015**, 5, 7328–7337.
11. The physical chemistry and materials science behind sinter-resistant catalysts, Y. Q. Dai, P. Lu, C. T. Campbell and Y. Xia, *Chemical Society Reviews* **2018**, 47, 4314-4331.

C. Publications jointly funded by this DOE grant and other grants of the PI and/or his co-authors, with relatively minor intellectual contribution from this grant;

12. Towards Benchmarking in Catalysis Science: Best Practices, Opportunities, and Challenges, T. Bligaard, R. M. Bullock, C. T. Campbell, J. G. Chen, B. C. Gates, R. J. Gorte, C. W. Jones, W. D. Jones, J. R. Kitchin, S. L. Scott, *ACS Catalysis (Perspective)*, **2016**, 6, 2590–2602. (featured as *ACS Editor’s Choice*).
13. Electrocatalytic Hydrogenation of Phenol over Platinum and Rhodium: Unexpected Temperature Effects Resolved, N. Singh, Y. Song, O. Y. Gutiérrez, D. M. Camaioni, C. T. Campbell, J. A. Lercher, *ACS Catalysis* **2016**, 6, 7466–7470.

Metal Carbides and Bimetallic Alloys as Low-cost Electrocatalysts

Jingguang G. Chen
Department of Chemical Engineering, Columbia University

Presentation Abstract

It is well known that the electronic and catalytic properties of transition metals can be modified by alloying either with carbon or with another metal. The resulting metal carbides or bimetallic alloys often demonstrate properties that are distinctively different from those of the parent metals. The goal of our research program is to identify carbide and bimetallic catalysts to either substantially reduce or completely replace Pt-group metals in electrocatalysis. Many electrochemical devices, such as electrolyzers, fuel cells and photoelectrochemical cells, currently require Pt-group metals (Pt, Pd, Ir, Rh, Ru) as electrocatalysts. The high costs and limited supplies of these precious metals create potentially prohibitive barriers to market penetration and scale-up production of devices requiring large catalyst loadings.

Our research efforts involve three parallel approaches: (1) UHV experiments and DFT calculations on single crystal surfaces to predict general trends, (2) synthesis and characterization of the corresponding polycrystalline films and powder catalysts, and (3) electrocatalytic evaluation of these materials as low-cost alternatives to replace Pt-group metal catalysts. In the past year we utilized these approaches to investigate the hydrogen evolution reaction (HER) and the CO₂ reduction reaction (CO₂RR).

DE-FG02-13ER16381: Metal Carbides and Bimetallic Alloys as Low-cost Electrocatalysts

PI: Jingguang Chen

Student(s): Brian Tackett; Tyra Zhang (3 months); Steven Denny (3 months);

RECENT PROGRESS

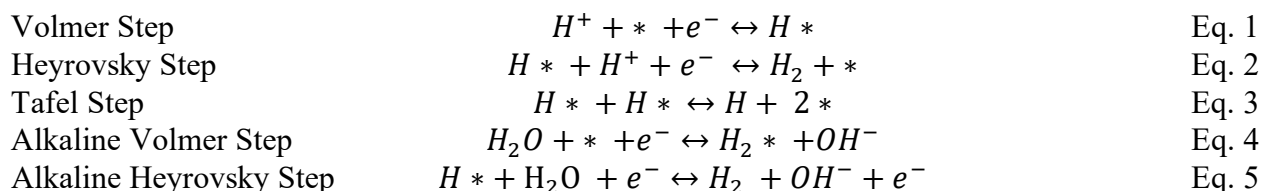
A. Metal-Modified Carbides as HER Electrocatalysts in Acid and Alkaline Electrolytes

The motivation is to identify alternative electrocatalysts using a combination of theoretical and experimental methods. Fuel cells, electrolyzers, and photoelectrochemical cells are electrochemical devices that are commonly considered as core technologies in a clean energy future. Central to the operation of all of these devices are catalysts, more specifically electrocatalysts, which mediate charge transfer processes between the electrolyte and device electrodes with minimal losses in efficiency. Unfortunately, many state-of-the-art catalysts used in the aforementioned technologies are comprised of expensive Pt-group metals (Pt, Ru, Rh, Ir, and Pd). The high prices and limited supplies of these precious metals create potentially prohibitive barriers to market penetration and scale-up production of devices requiring large catalyst loadings for efficient operation.

Understanding descriptors and trends for HER can provide insight into reaction mechanisms and help predict new active catalysts. For example, Norskov et al. used the well-

established experimental correlation between the M-H bond energy on a metal surface and its HER activity to develop a database of density functional theory (DFT)-calculated hydrogen binding energies (HBEs) for monometallic catalysts. This resulted in a volcano curve when plotted with experimentally measured exchange current density. Their work provided new thermodynamic data about the adsorbed hydrogen intermediate being involved in the acidic Volmer-Heyrovsky-Tafel HER mechanism (Eq. 1- 3), which consists of the Volmer step followed by either the Heyrovsky or the Tafel step. This approach also allowed the DFT-calculated HBE to be used as a screening tool for other acid HER catalysts. This was especially useful for developing low-cost electrocatalysts with single atom-thick layers (monolayers) of Pt supported on transition metal carbides (TMCs). Later, Sheng et al. showed that a similar volcano correlation existed between DFT-calculated HBEs and experimental alkaline HER activity on monometallic catalysts. A subsequent study revealed that HBE on Pt was dependent on the pH value of the electrolyte, which correlated HBE with HER activity over a wide pH range. Although it is unclear whether such DFT calculations will be useful for Pt-modified TMCs, which are important for reducing Pt loading in alkaline HER.

During the past funding cycle we have extended the DFT-calculated HBE correlation to metal-modified TMCs to determine the utility of using HBE for this class of materials in alkaline HER. We then explore the relationship between DFT-calculated hydroxyl binding energy (OHBE) and alkaline HER activity on metal-modified TMCs. The hydroxyl group appears in the alkaline Volmer step (Eq. 4) and Heyrovsky step (Eq. 5), so it likely impacts HER kinetics more than in the acidic case. As stated above, alkaline HER is not completely described by HBE alone, and recent studies have aimed to describe the exact role of the hydroxyl for alkaline HER (mostly on Pt surfaces). Some conclude that adsorbed OH directly participates in the Volmer step, while others state that hydroxyl only indirectly impacts HER kinetics through competitive adsorption^[13] or hydrogen stabilization. Whatever the case, clearly hydroxyl binding energy should be understood to describe alkaline HER. This is especially true for TMC surfaces, which are typically more oxophilic, and should bind hydroxyl more strongly, than Pt.



The HER electrochemical testing was performed to obtain HER activity, specified by their exchange current density (i_0). DFT calculations were performed to determine the free energy change of adsorbed hydrogen (ΔG_H) and hydroxyl group (ΔG_{OH}) for each surface, directly correlating to HBE and hydroxyl binding energy (OHBE), as shown in Table 1. To ensure the validity of the obtained HER activity, sample stability was examined by electrochemical stability testing coupled with XPS characterization before and after electrochemical testing. The correlation was then established between the calculated HBEs and OHBEs and their acid and alkaline HER activity (i_0).

Table 1. DFT calculations of ΔG_H on Pt, Pd, Au, Ag-modified carbides, Pt(111), Pd(111), Au(111), Ag(111) and unmodified carbides surfaces

Category	Surfaces	ΔG_H (eV)	ΔG_{OH} (eV)
Pt/carbides	Pt/Mo ₂ C(0001)	0.01	-2.39
	Pt/NbC(111)	-0.28	-2.41
	Pt/TaC(111)	-0.07	-2.51
	Pt/TiC(111)	-0.03	
	Pt/VC(111)	0.02	-2.26
	Pt/W ₂ C(0001)	0.09	
	Pt/WC(0001)	-0.13	-2.81
Pd/carbides	Pd/Mo ₂ C(0001)	-0.03	
	Pd/NbC(111)	-0.19	
	Pd/WC(0001)	-0.19	
Au/carbides	Au/Mo ₂ C(0001)	0.48	-2.39
	Au/NbC(111)	0.57	-2.31
	Au/TaC(111)	0.47	-2.51
	Au/VC(111)	0.51	
	Au/WC(0001)	0.14	
Ag/carbides	Ag/NbC(111)	0.44	
Bulk metals	Ag(111)	0.37	
	Au(111)	0.36	
	Pd(111)	-0.36	-2.34
	Pt(111)	-0.26	-2.21
Unmodified-carbides	Mo ₂ C(0001)	-0.75	-4.6
	NbC(111)	-0.90	-4.85
	TaC(111)	-0.99	-4.96
	TiC(111)	-0.96	
	VC(111)	-0.84	-4.91
	W ₂ C(0001)	-0.60	
	WC(0001)	-0.81	-4.19

Although it is well established that the HBE values can be used as a descriptor for the HER activity in acid, the descriptor for alkaline HER has been under debate due to the differences in proposed mechanisms in acid and alkaline electrolytes. Therefore, the Gibbs free energy change of the adsorbed hydroxyl group (ΔG_{OH}) was also calculated and summarized in Table 1. The alkaline HER activity for metal-modified TMCs forms a volcano-shaped relationship with ΔG_H , as shown in Figure 1a. This indicates that ΔG_H is, indeed, an important descriptor for alkaline HER activity on metal-modified carbides. According to Fig. 1a, the best HER activity in alkaline, obtained on the Pt surface, should correspond to the most appropriate ΔG_H located at the apex. Based on the Sabatier principle, when hydrogen atoms were bound to surfaces more strongly than Pt ($\Delta G_H < \Delta G_H^{Pt}$), the desorption process was less favored thus causing the decrease in HER activity. The trend was illustrated by unmodified TaC, Mo₂C, NbC, VC, and TaC. When hydrogen atoms

were bound to surfaces less strongly than Pt ($\Delta G_{\text{H}} > \text{Pt}$), the hydrogen surface coverage was relatively lower. As a result, higher energy (higher overpotential) was required to reach the same alkaline HER activity. The trend was formed by the electrocatalysts of Au-modified NbC, TaC and Mo₂C.

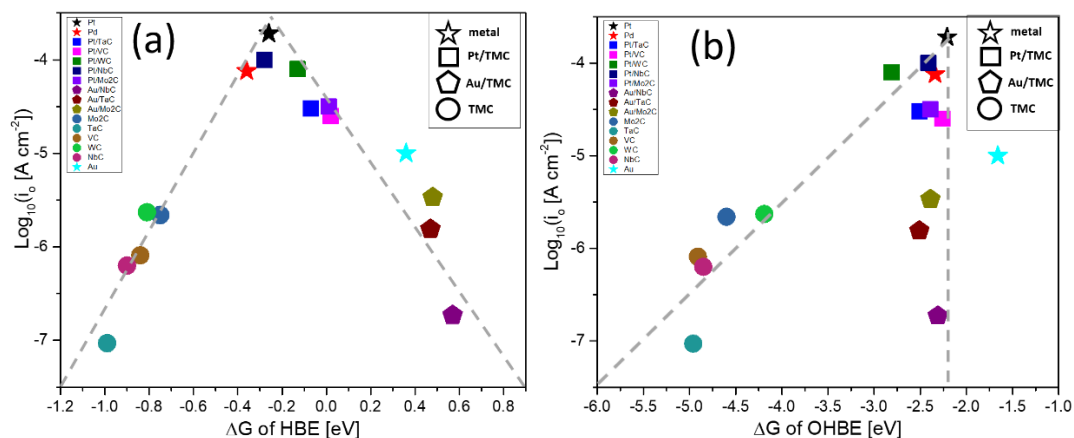


Figure 1: $\log_{10}(i_0)$ for unmodified, Pt- or Au-modified TMCs, Pt and Pd as a function of respective ΔG_{H} (a) or ΔG_{OH} (b) in 0.1 M KOH.

Unlike the volcano-shaped relationship formed with ΔG_{H} , ΔG_{OH} shows a much weaker correlation with alkaline HER activity (Figure 1b). Au-modified TMCs have similar OHBEs as Pt and Pt-modified TMCs, but the Au/TMCs alkaline exchange current densities are 2 or 3 orders of magnitude lower than their Pt counterparts. This indicates that OHBE is not a good descriptor for alkaline HER on TMCs and metal-modified TMCs. It also suggests that the adsorbed hydroxyl group does not play a direct role in the rate determining step of alkaline HER kinetics on these surfaces. Therefore, as compared to ΔG_{H} , ΔG_{OH} should be considered as a less effective descriptor for alkaline HER of examined TMC-based catalysts. Thus, the decreased HER activity for metal-modified TMCs in alkaline compared to acid cannot be attributed to HBE and OHBE alone. Instead it is likely that the alkaline environment influences the water structure or hydrogen stability, as suggested by other studies on Pt surfaces. This is the first example of a volcano trend on metal-modified TMCs for alkaline HER, and it shows that HBE is a good descriptor for this class of materials under both alkaline and acid conditions. These combined experimental and DFT results reveal that the adsorbed hydroxyl group does not directly participate in the rate determining step of the alkaline HER.

B. Investigation of CO₂ Electrochemical Reduction to Synthesis Gas (CO + H₂)

During the past funding cycle we have explored the electrochemical CO₂ reduction reaction (CO₂RR) to simultaneously produce carbon monoxide (CO) and hydrogen (H₂) on carbon supported palladium (Pd/C) nanoparticles in an aqueous electrolyte. The synthesis gas product has a CO to H₂ ratio between 0.5 and 1, which is in the desirable range for thermochemical synthesis of methanol and Fischer-Tropsch reactions using existing industrial processes. *In situ* X-ray absorption spectroscopy in both near-edge (XANES) and extended regions (EXAFS) and *in situ* X-ray diffraction show that Pd has transformed into β -phase palladium hydride (β -PdH) during the CO₂RR. Density functional theory (DFT) calculations demonstrate that the binding energies of both adsorbed CO and H are significantly weakened on PdH than on Pd surfaces, and that these

energies are potential descriptors to facilitate the search for more efficient electrocatalysts for syngas production through the CO₂RR. Our electrochemical study, combined with *in situ* XANES, EXAFS, and XRD measurements and DFT calculations unravel the origin of CO selectivity on Pd to be the *in situ* formation of β -PdH under the CO₂RR conditions. The formation of PdH significantly lowers the binding energies of both adsorbed *CO and *H, and in turn tunes the selectivity towards simultaneously produced CO and H₂ during the CO₂RR. The current study indicates that CO and H binding energies can be used as the reaction descriptors, and tuning the relative adsorption strength of CO and H should offer the opportunity to control the relative reaction rates of the CO₂RR and HER, and in turn tune the syngas composition. This design strategy should open up more options for identifying highly efficient electrocatalysts for high purity syngas production through the CO₂RR.

Based on the promising results on β -PdH catalysts, we have explored the utilization of Pd-M bimetallic systems and Pd/TMC catalysts to reduce the Pd loading while maintaining the same CO₂RR activity and selectivity. Using the same experimental and theoretical approaches, with *in situ* XANES, EXAFS, and XRD measurements and DFT calculations, we have identified several promising Pd-M bimetallic and Pd/TMC catalysts that also produce the β -PdH phase resulting in the desired CO to H₂ ratio between 0.5 and 1 with comparable total current density while achieving a significant reduction in Pd loading.

Publications Acknowledging this Grant in 2015-2018

(II) Exclusively funded by this grant;

1. B.M. Tackett, W. Sheng, S. Kattel, S. Yao, B. Yan, K.A. Kuttiyiel, Q. Wu and J.G. Chen*, “Reducing Iridium Loading in Oxygen Evolution Reaction Electrocatalysts Using Core-shell Particles with Nitride Cores”, *ACS Catalysis*, 8 (2018) 2615-2621.
2. Z. Jiang, Q. Zhang, Z. Liang and J.G. Chen*, “Pt-modified TaC as an Efficient Electrocatalyst for Ethanol Oxidation in Acid and Alkaline Electrolytes”, *Applied Catalysis B: Environmental*, 234 (2018) 329-336.
3. B.M. Tackett, W. Sheng and J.G. Chen*, “Opportunities and Challenges in Utilizing Metal-modified Transition Metal Carbides as Low-cost Electrocatalysts”, *Joule*, 1 (2017) 253-263
4. W. Sheng, S. Kattel, S. Yao, B. Yan, C.J. Hawxhurst, Q. Wu and J.G. Chen*, “Electrochemical Reduction of CO₂ to Synthesis Gas with Controlled CO/H₂ Ratios”, *Energy & Environmental Science*, 10 (2017) 1180-1185.
5. W. Wan, B.M. Tackett and J.G. Chen*, “Reactions of water and C1 molecules on carbide and metal-modified carbide surfaces”, *Chemical Society Reviews*, 46 (2017) 1807-1823.
6. L. Lin, W. Sheng, S. Yao, D. Ma* and J.G. Chen*, “Pt/Mo₂C/C-cp as a Highly Active and Stable Catalyst for Ethanol Electrooxidation”, *Journal of Power Sources*, 345 (2017) 182-189.
7. E.G. Mahoney, W. Sheng, M. Cheng, K.X. Lee, Y. Yan and J.G. Chen, “Analyzing the electrooxidation of ethylene glycol and glucose over platinum-modified gold electrocatalysts in alkaline electrolyte using in-situ infrared spectroscopy”, *Journal of Power Sources*, 305 (2016) 89-96.
8. Q. Zhang, B.M. Tackett, Q. Wu and J.G. Chen*, “Trends in Hydrogen Evolution Activity of Metal-Modified Molybdenum Carbides in Alkaline and Acid Electrolytes”, *ChemElectroChem*, 3 (2016) 1686-1693.

9. B.M. Tackett, Y.C. Kimmel and J.G. Chen*, “Metal-Modified Niobium Carbides as Low-Cost and Impurity-Resistant Electrocatalysts for Hydrogen Evolution in Acidic and Alkaline Electrolytes”, *International Journal of Hydrogen Energy*, 41 (2016) 5948-5954.
 10. M.D. Porosoff, B. Yan and J.G. Chen*, “Catalytic reduction of CO₂ by H₂ for synthesis of CO, methanol and hydrocarbons: Challenges and opportunities”, *Energy & Environmental Science*, 9 (2016) 62-73.
 11. L. Wang, E.G. Mahoney, S. Zhao, B. Yang and J.G. Chen, “Low Loading of Platinum on Transition Metal Carbides for Hydrogen Oxidation and Evolution Reactions in Alkaline Electrolyte”, *Chemical Communications*, 52 (2016) 3697-3700.
 12. Q. Lu, G.S. Hutchings, W. Yu, Y. Zhou, R.V. Forest, R. Tao, J. Rosen, B.T. Yonemoto, Z. Cao, H. Zheng, J.Q. Xiao, F. Jiao* and J.G. Chen*, “Highly Porous Non-precious Bimetallic Electrocatalysts for Efficient Hydrogen Evolution”, *Nature Communications*, 6 (2015) 6567.
 13. L. Yang, Y.C. Kimmel, Q. Lu and J.G. Chen*, “Effect of pretreatment on the particle size and oxygen reduction activities of low-loading platinum on titanium carbide powder electrocatalysts”, *Journal of Power Sources*, 287 (2015) 196-202.
 14. W. Sheng, Z. Zhuang, M. Gao, J. Zheng, J.G. Chen* and Y. Yan*, “Correlating hydrogen oxidation/evolution reaction activity on platinum at different pH with measured hydrogen binding energy”, *Nature Communications*, 6 (2015) 5848.
- (III) *Jointly funded by this grant and other grants with leading intellectual contribution from this grant;*
15. L. Wang, S. Zhu, N. Marinkovic, S. Kattel, M. Shao, B. Yang and J.G. Chen, “Insight into the Synergistic Effect between Nickel and Tungsten Carbide for Catalyzing Urea Electrooxidation in Alkaline Electrolyte”, *Applied Catalysis B: Environmental*, 232 (2018) 365-370.
 16. J. Wang, S. Kattel, Z. Wang, J.G. Chen, and C. Liu, “L-Phenylalanine Templated Platinum Catalyst with Enhanced Performance for Oxygen Reduction Reaction”, *ACS Applied Materials & Interfaces*, (2018) accepted.
 17. J. Wang, W. Wang, Z. Wang, J.G. Chen* and C.-J. Liu*, “Porous MS₂/MO₂ (M=W, Mo) Nanorods as Efficient Hydrogen Evolution Reaction Catalysts”, *ACS Catalysis*, 6 (2016) 6585-6590.
 18. Y. Zhou, Q. Lu, Z. Zhuang, G.S. Hutchings, S. Kattel, Y. Yan, J.G. Chen, J.Q. Xiao and F. Jiao, “Oxygen Reduction at Very Low Overpotential on Nanoporous Ag Catalysts”, *Advanced Energy Materials*, 5 (2015) 1500149.
- (IV) *Jointly funded by this grant and other grants with relatively minor intellectual contribution from this grant;*
19. M. Dunwell, Q. Lu, J.M. Heyes, J. Rosen, J.G. Chen, Y. Yan, F. Jiao, and B. Xu, “The Central Role of Bicarbonate in the Electrochemical Reduction of CO₂ on Gold”, *Journal of the American Chemical Society*, 139 (2017) 3774-3783.
 20. K.A. Kuttiyiel, K. Sasaki, G-G. Park, M.B. Vukmirovic, L. Wu, Y. Zhu, J.G. Chen and R.R. Adzic, “Janus Structured Pt-FeNC Nanoparticles as Catalyst for the Oxygen Reduction Reaction”, *Chemical Communications*, 53 (2017) 1660-1663.

Elucidating Chemical and Electronic Interactions of Metal-Support Interfaces via STEM

Miaofang Chi,¹ Felipe Polo Garzon,² De-en Jiang,³ Huiyuan Zhu,² Sheng Dai,² Zili Wu²

¹Center for Nanophase Materials Sciences, ²Chemical Sciences Division, Oak Ridge National Laboratory; ³Department of Chemistry, University of California, Riverside

An aim of our BES program titled “Fundamentals of Catalysis and Chemical Transformations (ERKCC96)” is to fundamentally understand how synergism can be tailored at the metal-oxide interface to control catalytic activity and selectivity. Synergistic interactions between metal centers and oxide supports provide ample flexibility to tune catalytic activity and/or selectivity of supported metal nanoparticles (NPs). Various interactions can occur at a metal-oxide interface, e.g., interfacial anchoring via vacancies, impurities, and/or elemental inter-diffusion, formation of interfacial interphases, encapsulation of NPs by the support material, atomic structural rearrangement at the interfaces and surfaces, and/or charge transfer between the NP and support, each of which impacts reactivity and selectivity. In many cases, multiple interactions co-exist and interact with each other, making characterization of interfacial phenomena extremely complicated and challenging. At the microscopic level, each of these interfacial interactions is represented by chemistry, structure, and charge. Our work is to provide mechanistic insight at the single atom and electron levels into the design of high-performance metal-oxide interfaces by revealing chemistry, structure, charge, and their interplay at model interfaces. In particular, our work is focused on answering several fundamental questions: How do different surface atomic terminations and oxygen vacancies affect the chemical bonding and charge transfer behavior at interfaces? How can post-synthesis treatments be used to tailor interfacial interactions? How do the various interfacial interactions evolve upon catalytic reactions?

This poster presentation highlights our recent efforts toward understanding the complex chemical and electronic interactions of metal-oxide interfaces by using novel scanning transmission electron microscopy (STEM) techniques. Two recent studies will be highlighted; (1) tuning the interfacial structures of Au/Fe₂O₃ core-shell NPs towards high catalytic activity, which demonstrates that multiple interfacial features, e.g. crystallinity, strain, and vacancies, can be tuned and integrated in individual core-shell particles to maximize activity for the oxygen reduction reaction; (2) advancing and utilizing 4D-STEM-based differential phase contrast (DPC) imaging to map the interfacial charge transfer with sub-Å resolution. This work is driven by the fact that interfacial charge transfer often presents at metal-oxide interfaces and is believed to impact the catalytic activity and selectivity. In this presentation, preliminary DPC results acquired for Au single atoms dispersed on SrTiO₃ will illustrate how charge transfer could occur at a metal center and the oxide support interface, and how the catalytic activity and selectivity of the Au/SrTiO₃ may be affected.

Research supported by the U.S. Department of Energy, Office of Science, Basic Energy Sciences, Chemical Sciences, Geosciences, and Biosciences Division. This research is part of FWP ERKCC96: Fundamentals of Catalysis and Chemical Transformations. For a full description of recent progress see Extended Abstract for ERKCC96. Electron Microscopy performed at the Center for Nanophase Materials Sciences, which is a U.S. DOE Office of Science User Facility.

MnO(100): Initial Experimental Benchmarks for Adsorption and Co-Adsorption on the Ordered Surface and Oxidation to Mn³⁺ Surface Compounds

Han Chen, Xu Feng and David F. Cox

Department of Chemical Engineering, Virginia Polytechnic Institute and State University,
Blacksburg, VA 24060

Presentation Abstract

Work has been undertaken to establish experimental benchmarks for adsorption and reaction on surfaces of transition metal oxides with highly correlated electronic structures which pose difficulties for modeling with DFT. A variety of probe molecules have been examined that are acidic (CO₂), basic (NH₃), can donate charge and backbond (CO) or have a tendency to dissociate on oxide surfaces (H₂O). For all adsorbates examined, DFT (as opposed to DFT+U) gives unrealistic adsorption geometries with long-range surface reconstructions or dramatic local bonding rearrangements even for very weakly adsorbed molecules. DFT+U gives more realistic geometries. The adsorption energy of the probe molecules on MnO(100) terraces has been determined experimentally with TPD and computationally with DFT+U. For weakly adsorbed molecules, simulation methods for incorporating van der Waals interactions are important for giving the best match with experiment. We have examined a variety of approaches for handling van der Waals interactions, and those based on the D3 method of Grimme give the best agreement with experiment for our particular systems.

The preparation of a surface oxide with Mn³⁺ cations from MnO(100) has also been examined to allow a future investigation of the chemistry of Mn³⁺ (3d⁴) for comparison to previous work showing differences in selectivity for hydrocarbon conversion on Cr³⁺ (3d³) and Fe³⁺ (3d⁵) which vary from dehydrogenation and C-C coupling reactions over Cr₂O₃ to nonselective oxidation over Fe₂O₃ single crystal surfaces. Oxidation of clean and Na-precovered MnO(100) was investigated by X-ray photoelectron spectroscopy (XPS), temperature programmed desorption (TPD) and low energy electron diffraction (LEED). XPS results indicate that a Mn₃O₄-like and a Mn₂O₃-like surfaces can be formed by various oxidation treatments of clean and nearly-stoichiometric MnO(100), while a NaMnO₂-like surface was produced by oxidation of the MnO(100) pre-covered with a high coverage of metallic Na. Water TPD results suggest that water adsorption is sensitive to the surface Mn oxidation states on these different material surfaces.

DE-FG02-97ER14751: Hydrocarbon Oxidation, Dehydrogenation and Coupling over Model Transition Metal Oxide Surfaces

Student(s): Han Chen, Xu Feng (graduated)

RECENT PROGRESS

Adsorption Benchmarks on MnO(100)

Experimental work has been completed for CO, CO₂, NH₃ and H₂O adsorption on MnO(100) using temperature programmed desorption (TPD). The primary desorption features for CO, CO₂, NH₃ and H₂O all exhibit first-order desorption kinetics and are attributed to molecular adsorbates on flat terraces. Experimental values of the adsorption energy are extracted from the activation energy for desorption measured in TPD. CO adsorbs molecularly, and desorbs with a primary feature at 130 K attributed to desorption from terraces, with additional contributions in a broad tail that extends to over 300 K and is attributed to desorption from defects. CO₂ adsorbs molecularly, and desorbs from 200 - 500 K from surface defect sites and at 150 K from terraces. NH₃ adsorbs molecularly, and desorbs with a primary feature at 235 K attributed to desorption from terraces, with additional contributions in a broad tail that extends to over 500 K and is attributed to desorption from defects. Water adsorbs molecularly on terraces and desorbs with a peak maximum at 260 K at low coverages. Water also dissociates on surface defects with desorption temperatures ranging between 300 and 600 K. For water and CO₂ coadsorption, TPD shows that when water is adsorbed prior to CO₂, water blocks the uptake of CO₂ on both terrace and defect sites. When CO₂ is adsorbed prior to water, water displaces pre-adsorbed CO₂ from terrace sites, but stabilizes CO₂ adsorption around defect sites through the formation of bicarbonate.

Our computational work on MnO(100) has examined DFT (PBE-GGA) and DFT+U (PBE-GGA+U). We find that for MnO(100) the DFT (PBE-GGA) functional gives a poor representations of the surface structure in the presence of all the adsorbates we have considered so far. Even adsorbates that interact very weakly with the surface give rise to nonphysical long-range reconstructions or dramatic local modifications of the Mn-O bonding in the surface layer. DFT+U gives a more believable surface structure devoid of long-range reconstructions for all adsorbates, so DFT+U has been our primary tool for examining the MnO(100) surface chemistry.

As part of our computational examination of the adsorption energy of probe molecules, we have looked at six separate methods for approximating van der Waals interactions in DFT: (1) the D2 method of Grimme,¹ (2) the D3 method of Grimme (D3),² (3) the D3 method with Becke-Johnson damping (D3BJ),³ (4) the Tkatchenko-Scheffler method,⁴ (5) the Tkatchenko-Scheffler method with iterative Hirshfeld partitioning,⁵ and (6) the dDsC dispersion correction method.⁶⁻⁷ For the limited systems we have studied to date, vdW corrections based on the D3 method of Grimme give the best agreement with experiment.

A comparison of our experimental results to DFT+U and the vdW correction that gives the best agreement experiment is given in Table 1 for adsorption on MnO(100) *terraces*.

Table 1. Comparison of Experimental and DFT Molecular Adsorption Energies on MnO(100) Terraces

Adsorbate on MnO(100) terrace sites	Experimental Adsorption Energy (kJ/mol)	Best vdW correction	PBE+U-vdW Adsorption Energy (kJ/mol)	ΔE (exp - DFT) (kJ/mol)
CO	-36.0	D3BJ	-36.4	0.4
CO ₂	-41.8	None	-47.3	5.5
NH ₃	-67.4	D3	-65.3	-2.1
H ₂ O	-61.9	D3	-57.3	-4.6

For adsorption at defects, steps and isolated oxygen vacancies have been examined for the four adsorbates. While neither of these defects are a good match for the experimental data, they all predict more strongly bound adsorbates as seen experimentally. DFT also predicts a CO₂-H₂O complex at surface steps, similar to the bicarbonate formation at surface defects suggested from experiment.

MnO(100) Oxidation and Compound Formation

Oxidation of clean and Na-precovered MnO(100) was investigated by X-ray photoelectron spectroscopy (XPS), temperature programmed desorption (TPD) and low energy electron diffraction (LEED). XPS results indicate that Mn₃O₄-like and a Mn₂O₃-like surfaces can be formed by various oxidation treatments of clean and nearly-stoichiometric MnO(100), while a NaMnO₂-like surface can be produced by oxidation of the MnO(100) pre-covered with a high coverage of metallic Na. LEED shows no long range order for these modifications of the MnO(100) surface. TPD indicates that water can be used as a probe molecule to distinguish between surface Mn²⁺ and Mn³⁺ surface cations. These surface preparations will be used in the next phase of our work to investigate the reactions of hydrocarbon fragments on surface Mn cations with different oxidation states.

References

1. Grimme, S., Semiempirical GGA-type density functional constructed with a long-range dispersion correction. *Journal of Computational Chemistry* **2006**, *27* (15), 1787-1799.
2. Grimme, S.; Antony, J.; Ehrlich, S.; Krieg, H., A consistent and accurate ab initio parametrization of density functional dispersion correction (DFT-D) for the 94 elements H-Pu. *The Journal of Chemical Physics* **2010**, *132* (15), 154104.
3. Johnson, E. R.; Becke, A. D., A post-Hartree-Fock model of intermolecular interactions: Inclusion of higher-order corrections. *The Journal of Chemical Physics* **2006**, *124* (17), 174104.
4. Tkatchenko, A.; Scheffler, M., Accurate molecular van der Waals interactions from ground-state electron density and free-atom reference data. *Physical Review Letters* **2009**, *102* (7), 073005.
5. Bultinck, P.; Van Alsenoy, C.; Ayers, P. W.; Carbó-Dorca, R., Critical analysis and extension of the Hirshfeld atoms in molecules. *The Journal of Chemical Physics* **2007**, *126* (14), 144111.
6. Steinmann, S. N.; Corminboeuf, C., A generalized-gradient approximation exchange hole model for dispersion coefficients. *The Journal of Chemical Physics* **2011**, *134* (4), 044117.
7. Steinmann, S. N.; Corminboeuf, C., Comprehensive benchmarking of a density-dependent dispersion correction. *Journal of Chemical Theory and Computation* **2011**, *7* (11), 3567-3577.

Publications Acknowledging this Grant in 2014-2018

I) Exclusively funded by this grant;

1. Feng, X.; Cox, D. F.. Oxidation of MnO(100) and NaMnO₂ formation: Characterization of Mn²⁺ and Mn³⁺ Surfaces via XPS and Water TPD. *Surface Science* **2018**, *675*, 47-53.
2. X. Feng, X.; Cox, D. F. Na Deposition on MnO(100). *Surface Science* **2016**, *645*, 23-29.

3. Dong, Y.; Brooks, J. D.; Chen, T. L.; Mullins, D. R.; Cox, D. F. Reactions of methyl groups on a non-reducible metal oxide: the reaction of iodomethane on stoichiometric α -Cr₂O₃(0001). *Surface Science* **2015**, *641*, 148-153.
 4. Dong, Y.; Brooks, J. D.; Chen, T. L.; Mullins, D. R.; Cox, D. F. Methylene migration and coupling on a non-reducible metal oxide: the reaction of dichloromethane on stoichiometric α -Cr₂O₃(0001). *Surface Science* **2015**, *632*, 28-38.
- II) *Jointly funded by this grant and other grants with leading intellectual contribution from this grant;*
5. Gibbs, G. V.; Ross, N. L.; Cox, D. F. Sulfide Bonded Atomic Radii. *Physics and Chemistry of Minerals*, **2017**, *44*, 561-566.
 6. Gibbs, G. V.; Ross, N. L.; Cox, D. F. Bond length estimates for oxide crystals with a molecular power law expression. *Physics and Chemistry of Minerals* **2015**, *42*, 587-593.
 7. Gibbs, G. V.; Ross, N. L.; Cox, D. F.; Rosso, K. M. Insights into the crystal chemistry of earth materials rendered by electron density distributions: Pauling's rules revisited. *American Mineralogist* **2014**, *99*, 1071-1084.
 8. Gibbs, G. V.; Ross, N. L.; Cox, D. F.; Rosso, K. M.; Iversen, B. B.; Spackman, M. A. Pauling Bond Strength, Bond Length and Electron Density Distributions. *Physics and Chemistry of Minerals* **2014**, *41*, 17-25.

Electrocatalytic Reduction of Oxygen on Metal Nanoparticles in the Presence and Absence of Interactions with Metal-Oxide Supports

Richard M. Crooks, Graeme Henkelman, Zhiyao Duan, and Nevena Ostojic

The University of Texas at Austin, Department of Chemistry

Presentation Abstract

Here we report that density function theory (DFT) can be used to accurately predict how Au nanoparticle (NP) catalysts cooperate with underlying SnO_{1.7} and SnO_{2.0} substrates to carry out the oxygen reduction reaction (ORR). Experimental samples were prepared by immobilizing dendrimer-encapsulated AuNPs (Au DENs) onto tin oxide supports. Dendrimers were then removed using a previously developed UV/O₃ method, allowing direct interactions between AuNPs and the underlying supports.

Experimental electrocatalysis studies indicated a two-fold improvement in the ORR kinetics and *positive shifts in the onset potential by 0.320 V and by 0.280 V when the AuNPs were in direct contact with the underlying SnO_{1.7} and SnO_{2.0} supports, respectively. These experimental results are in good agreement with the theoretically predicted onset potential shift of 0.30 V. Direct interactions between AuNPs and either SnO_{1.7} or SnO_{2.0} support also had beneficial effects on the ORR pathway. Specifically, the number of electrons involved in the ORR (n_{eff}) improved from 2.1 ± 0.2 to 2.9 ± 0.1 , when Au NPs interacted with SnO_{1.9} support, and from 2.2 ± 0.1 to 3.1 ± 0.1 , when Au NPs interacted with SnO_{2.0} substrate. According to our theoretical calculations, this activity enhancement is attributed to the existence of anionic Au arising from electron transfer from surface oxygen vacancies of SnO_x. This prediction was confirmed using X-ray photoelectron spectroscopy (XPS).*

DE-SC0010576: Testing the Predictive Power of Theory for Determining the Structure and Activity of Nanoparticle Electrocatalysts

PI: Richard M. Crooks

Co-PI: Graeme Henkelman

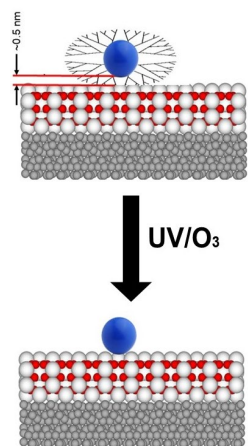
Postdoc: Zhiyao Duan

Graduate Student: Nevena Ostojic

RECENT PROGRESS

Introduction

The objective of our combined experimental and theoretical study is to develop a deeper understanding of how nanoparticle (NP) catalysts cooperate with underlying substrates to carry out both simple and complex electrocatalytic reactions. As shown in Scheme 1, the catalyst model consists of well-defined 1-2 nm metallic NPs atop ultrathin metal oxide surfaces prepared by atomic layer deposition (ALD). The ALD layer is deposited onto a pyrolyzed photoresist carbon film (PPF). This construct is electroactive and can be used to study electrocatalytic reactions taking



Scheme 1. Deposition of metal NP on thin oxide support by removing the dendrimer host via UV/O₃ treatment.

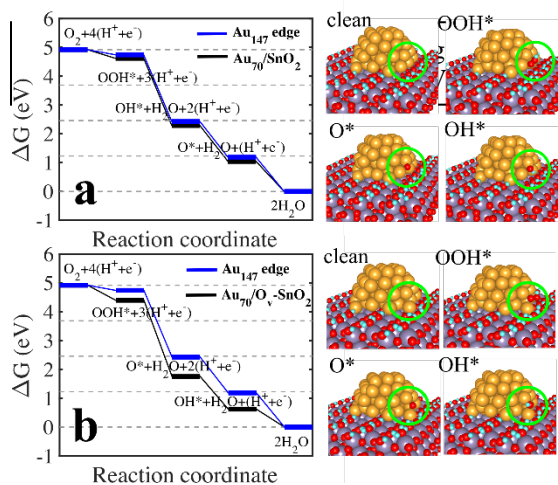
place at the DEN surface. The bottom frame of Scheme 1 shows that a UV/O₃ treatment can be used to remove the dendrimer without changing the DEN composition or morphology. In this case, the DEN is in direct contact with the oxide surface. Hence, it is possible to study electrocatalytic reactions at the NP surface in the absence or presence of substrate effects.

Importantly, the NPs in our study are small enough that 100% of their atoms can be incorporated into first-principles calculations. Our main interest is focused on the interface between the NPs and their supports, and how this region accelerates (or not) electrochemical reactions by changing the structure or electronic properties of the NPs, or by providing key reactants. The project consists of two concurrent phases. In Phase 1, density function theory (DFT) calculations are used to design catalysts having desirable properties. In Phase 2, the theoretical predictions are tested experimentally. In other words, we have shifted our scientific approach to “theory first”.

This presentation is focused specifically on the effect of SnO_{2-x}/AuNP interactions on the oxygen reduction reaction (ORR). The research was conducted in two parts. The first was using density function theory (DFT) to understand interactions between Au NPs and tin metal oxide supports. The second involved testing the theoretical prediction experimentally. This consist of immobilization of dendrimer-encapsulated AuNPs (Au DENs) onto thin metal oxide support layers deposited by ALD, subsequent removal of the dendrimers, and then electrocatalytic testing of the resulting construct (Scheme 1).

Theoretical Findings

Figure 1 shows the DFT-calculated free-energy profile along the reaction coordinates for the ORR



under standard conditions at an applied potential of $U=0$ V for stand-alone Au₁₄₇ and supported Au/SnO₂ systems. Clearly, Au₁₄₇ NPs are not good electrocatalysts for the ORR because of the weak binding of OOH*, which leads to a theoretical overpotential as high as 1 V. Keeping our previous theoretical work regarding the Au/TiO₂ system in mind, we hoped that combining AuNPs with SnO₂ supports could lead to strengthening of OOH* adsorption at the interface due to electronic effects. DFT calculations predicted that rutile SnO₂(110) surface prefers forming a water-dissociated surface structure under the operating conditions of the ORR. Thus, we modeled the hybrid Au/SnO₂ system by placing a hemispherical Au₇₀ NP on top of the water-

dissociated SnO₂(110) surface slab. As shown in Figure 1a, when Au₇₀ NP is supported on stoichiometric SnO₂, improvement in the ORR activity is not observed as compared to the ORR activity of the naked Au₁₄₇.

It is well known that SnO₂ is structurally nonstoichiometric. This is caused by the low formation energy of the oxygen vacancy and tin interstitial, and the strong mutual attraction between them. Accordingly, we introduced a surface oxygen vacancy beneath an Au atom at the edge of the Au₇₀ nanoparticle. As a result, the Au atom above the vacancy was reduced to yield anionic Au, which possesses -0.38e according to the Bader charge analysis. DFT calculations, based on the defect model, revealed an overpotential reduction of about 0.30 V as compared to unsupported Au₁₄₇ (Figure 1b). The important point is that our calculations revealed that the beneficial SnO₂/Au interaction observed for the ORR is due to electron transfer from O vacancies in the SnO_{2-x} support to the supported Au particle. The anionic Au is more oxophilic than metallic Au in the unsupported AuNP, and hence it stabilizes the OOH* and achieves better ORR activity. We have also investigated other possible active sites such as the interfacial Au/Sn site. However, the interfacial site suffers from the poisoning effect of adsorbed OH⁻ atop Sn.

Experimental Findings

To understand how interactions between metal NPs and their metal-oxide supports affect the ability of the NPs to electrocatalyze reactions, both reaction kinetics and mechanism were studied simultaneously. This was done by utilizing a custom-designed microelectrochemical flow cell.

We found that the onset potential for the ORR shifts in the positive direction by 0.32 V when AuNPs are in direct contact with the underlying SnO_{1.9} ALD support. Similarly, for the AuNPs immobilized at the SnO_{2.0} electrode, the onset potential shifts by 0.28 V in the positive direction. These values are very close to the theoretically predicted value of 0.30 V determined by DFT and discussed in the previous section. We also found that when AuNPs are in direct contact with the SnO_{1.9} ALD support, there is a ~50% decrease in the amount of peroxide generated compared to when the AuNPs remain in the dendrimer and hence are not in direct contact with the substrate.

Summary and Conclusions

We used DFT calculations to predict the nature of SnO_x/AuNP interactions and the effect that these interactions have on the ability of AuNPs to electrocatalyze the ORR. *The key finding is that after the removal of the dendrimers, improvements in the onset potential, kinetics, and mechanism of the ORR are observed. More specifically, the onset potential shifts positive by 0.320 V and by 0.280 V when the Au NPs are in a direct contact with the underlying SnO_{1.9} and SnO_{2.0} ALD supports, respectively. These shifts almost exactly match the theoretically predicted value of 0.30 V. Therefore, this is an unusual case of first-principles theory correctly predicting experimental results.*

Publications Acknowledging this Grant in 2016-2018

Category I Publications

1. Chen, J. G.; Crooks, R. M.; Seefeldt, et al. Beyond Fossil-Fuel-Driven Nitrogen Transformations. *Science* **2018**, *360*, 873 (per guidance from DOE, this publication acknowledges DOE generally but not this specific grant).
2. Huang, K.; Clausmeyer, J.; Luo, L.; Jarvis, K.; Crooks, R. M. Shape-controlled Electrodeposition of Single Pt Nanocrystals onto Carbon Nanoelectrodes. *Faraday Discuss.* **2018** (published on the RSC website).

3. Trindell, J. A.; Clausmeyer, J.; Crooks, R. M. Size Stability and H₂/CO Selectivity for Au Nanoparticles during Electrocatalytic CO₂ Reduction. *J. Am. Chem. Soc.* **2017**, *139*, 16161-16167.
4. Anderson, M. J.; Crooks, R. M. Microfluidic Surface Titrations of Electroactive Thin Films. *Langmuir* **2017**, *33*, 7053-7061.
5. Duan, Z.; Henkelman, G. Calculations of CO Oxidation over a Au/TiO₂ Catalyst: A Study of Active Sites, Catalyst Deactivation, and Moisture Effects. *ACS Catal.* **2018**, *8*, 1376-1383.
6. Luo, L; Duan, Z.; Li, H; Kim, J.; Henkelman, G; Crooks, R. M. Calculations of CO Oxidation over a Au/TiO₂ Catalyst: A Study of Active Sites, Catalyst Deactivation, and Moisture Effects. *J. Am. Chem. Soc.* **2017**, *139*, 5538-5546.
7. Anderson, M. J.; Ostojic, N.; Crooks, R. M. A Microelectrochemical Flow Cell for Studying Electrocatalytic Reactions on Oxide-Coated Electrodes. *Analytical Chemistry* **2017**, *89*, 11027-11035.
8. Ostojic, N.; Crooks, R. M. Electrocatalytic Reduction of Oxygen on Platinum Nanoparticles in the Presence and Absence of Interactions with the Electrode Surface. *Langmuir* **2016**, *32*, 9727-9735.
9. Ostojic, N.; Thorpe, J. H.; Crooks, R. M. Electron Transfer Facilitated by Dendrimer Encapsulated Pt Nanoparticles Across Ultrathin, Insulating Oxide Films. *J. Am. Chem. Soc.* **2016**, *138*, 6829-6837.
10. Duan, Z.; Henkelman, G. O₂ activation at the Au/MgO(001) interface boundary facilitates CO oxidation. *Phys. Chem. Chem. Phys.* **2016**, *18*, 5486-5490.

Eleven additional Category 1 articles were published in 2015 but are omitted due to space limitations.

* These publications may include acknowledgements to our endowment from the Welch Foundation, the funding of collaborators, and/or instrumentation grants.

Category II Publications

1. Liu, H.; An, W.; Li, Y.; Frenkel, A. I.; Sasaki, K.; Koenigsmann, C.; Su, D.; Anderson, R. M.; Crooks, R. M.; Adzic, R. R.; Liu, P.; Wong, S. S. In Situ Probing of the Active Site Geometry of Ultrathin Nanowires for the Oxygen Reduction Reaction. *J. Am. Chem. Soc.* **2015**, *137*, 12597-12609.

Sub Nanometer Sized Clusters for Heterogeneous Catalysis

Abhaya Datye¹ and Yong Wang²

¹University of New Mexico and ²Washington State University

Presentation Abstract

The focus of this project is the synthesis, characterization and reactivity of transition metal moieties ranging from single atoms to clusters of about 1 nm in diameter that are present on high surface area supports. A major barrier in the utilization of sub-nm clusters is that they are subject to Ostwald ripening, leading to growth in size to form nanoparticles. Our recent work suggests that trapping single atoms on the support could help to slow the rates of ripening. Hence, one of the goals of this project is the understanding of anchoring sites on high surface area catalyst supports. Conventional (non-reducible) oxide supports provide only limited number of sites to anchor ionic species. Reducible oxides, such as ceria provide many more sites for anchoring due to the presence of defects. But reducible oxides are often not available in high surface area form, and they may not be as robust (can react to form carbonates, for example, or sinter easily) compared to the commonly-used high surface area supports such as silica, alumina, or carbon. Increasing atomic trapping sites on conventional catalyst supports is therefore important for improving the stability of sub-nm metal clusters on a supported catalyst. Another goal of this project is to expand the applicability of single atom catalysts to a broader class of catalyzed reactions. Transition metals in ionic form are perfectly situated for further manipulation of their catalytic activity by use of ligands, as in homogeneous catalysis. Understanding the principles that help in the design of robust single atom catalysts is one of the research challenges that is addressed in this project.

DOE grant # DE-FG02-05ER15712

Sub Nanometer Sized Clusters for Heterogeneous Catalysis

Post-docs: Andrew DeLaRiva and Haifeng Xiong (UNM), Junming Sun (WSU)
Graduate Students: Chris Riley (UNM), Xavier Isidro Pereira Hernández, Jianghao Zhang & Hannah Kim (WSU)

RECENT PROGRESS

1) Activation of surface lattice oxygen in single-atom Pt/CeO₂ for low-temperature CO oxidation

To improve fuel efficiency, advanced combustion engines are being designed to minimize the amount of heat wasted in the exhaust. Hence, future generations of catalysts must perform at temperatures that are 100°C lower than current exhaust-treatment catalysts. Achieving low-temperature activity, while surviving the harsh conditions encountered at high engine loads,

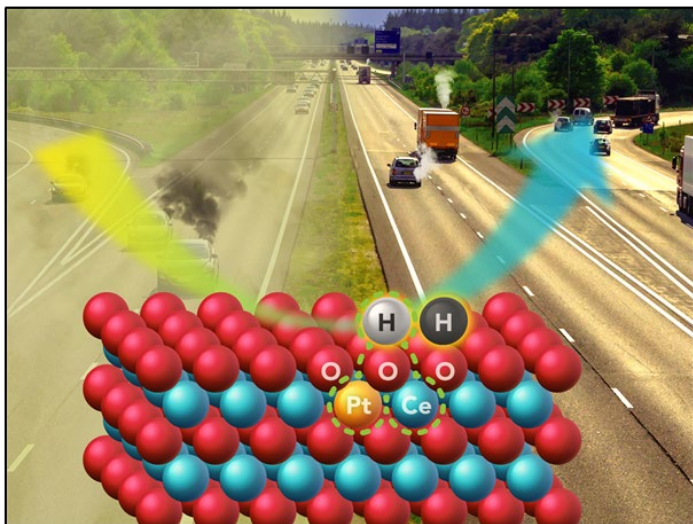


Figure 1 A new type of active site (dashed green circles) meets the dual challenge of achieving high activity and thermal stability in single atom catalysts. (L.Nie, D.Mei, H.Xiong, B.Peng, Z.Ren, X.Hernandez, A.DeLaRiva, M.Wang, M.H. Engelhard, L. Kovarik, A.K. Datye, Y.Wang, "Activation of surface lattice oxygen in single-atom Pt/CeO₂ for low-temperature CO oxidation", *Science*, 2017, 358, 1419-1423).

remains a formidable challenge. In this study, we demonstrated how atomically dispersed ionic platinum (Pt²⁺) on ceria (CeO₂), which is already thermally stable, can be activated via steam treatment (at 750°C) to simultaneously achieve the goals of low-temperature carbon monoxide (CO) oxidation activity while providing outstanding hydrothermal stability. A new type of active site is created on CeO₂ in the vicinity of Pt²⁺, which provides the improved reactivity. These active sites are stable up to 800°C in oxidizing environments (see Fig. 1).

2) Mechanistic Understanding of Methanol Carbonylation: Interfacing Homogeneous and Heterogeneous Catalysis via Carbon Supported Ir-La

The creation of heterogeneous analogs to homogeneous catalysts is of great importance to many industrial processes. Acetic acid synthesis via the carbonylation of methanol is one such process

and it relies on a difficult-to-separate homogeneous Ir-based catalyst. Using a combination density functional theory (DFT) and attenuated total reflectance-Fourier transform infrared (ATR-FTIR) spectroscopy, we determine the structure and mechanism for methanol carbonylation over a promising single-site Ir-La/C heterogeneous catalyst replacement. Here, the Ir center the active site with the rate limiting step being the reductive elimination of acetyl iodide. Furthermore, the La atomically disperses the Ir and as a Lewis acid site. In fact, the promoter in the Ir-La/C catalyst was found to behave similarly to homogeneous promoters by abstracting an iodine from the Ir center and accelerating the CO insertion step. Overall, this work

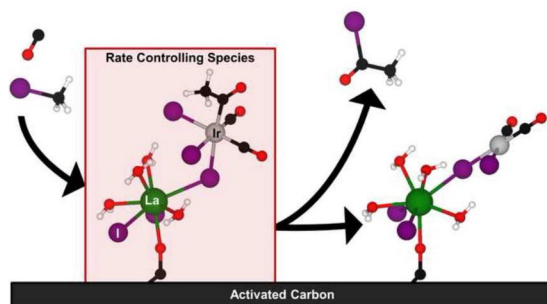


Figure 2 The Ir center is the active site with the rate limiting step being the reductive elimination of acetyl iodide in methanol carbonylation on Ir-La/C catalysts. (A.J.R.Hensley, J.Zhang, I.Vincon, X.P.Hernandez, D.Tranca, G.Seifert, J.S.McEwen, Y.Wang, "Mechanistic understanding of methanol carbonylation: interfacing homogeneous and heterogenous catalysis via carbon supported Ir-La", *J.Catal.*, 2018).

of is both acts La

provides key insight into the atomistic nature of the Ir-La/C single-site catalyst and allows for the further design and optimization of single-site heterogeneous catalysts.

3) Thermally Stable and Regenerable Platinum–Tin Clusters for Propane Dehydrogenation Prepared by Atom Trapping on Ceria

Our research team developed a new approach to synthesize thermally stable single atom catalysts (Jones et al., *Science*, 2016). We now apply this approach to reactions of interest to the DOE. Here, we explored the reactivity and stability of single atom Pt species for the industrially important reaction of light alkane dehydrogenation. The single atom Pt/CeO₂ catalysts are stable during propane dehydrogenation, but we observe no selectivity towards propene. DFT calculations show strong adsorption of the olefin produced, leading to further unwanted reactions. In contrast, when Sn is added to ceria, the single atom Pt catalyst undergoes an activation phase where it transforms into Pt-Sn clusters under reaction conditions. Formation of small Pt-Sn clusters allows the catalyst to achieve high selectivity towards propene, due to facile desorption of the product. The CeO₂-supported Pt-Sn clusters are very stable, even during extended reaction at 680 °C. By adding water vapor to the feed, coke formation can almost completely be suppressed. Furthermore, the Pt-Sn clusters can be readily transformed back to the atomically dispersed species on ceria via oxidation, making Pt-Sn/CeO₂ a fully regenerable catalyst. This work involved a collaboration with the group of Bert Weckhuysen at Utrecht University in the Netherlands.

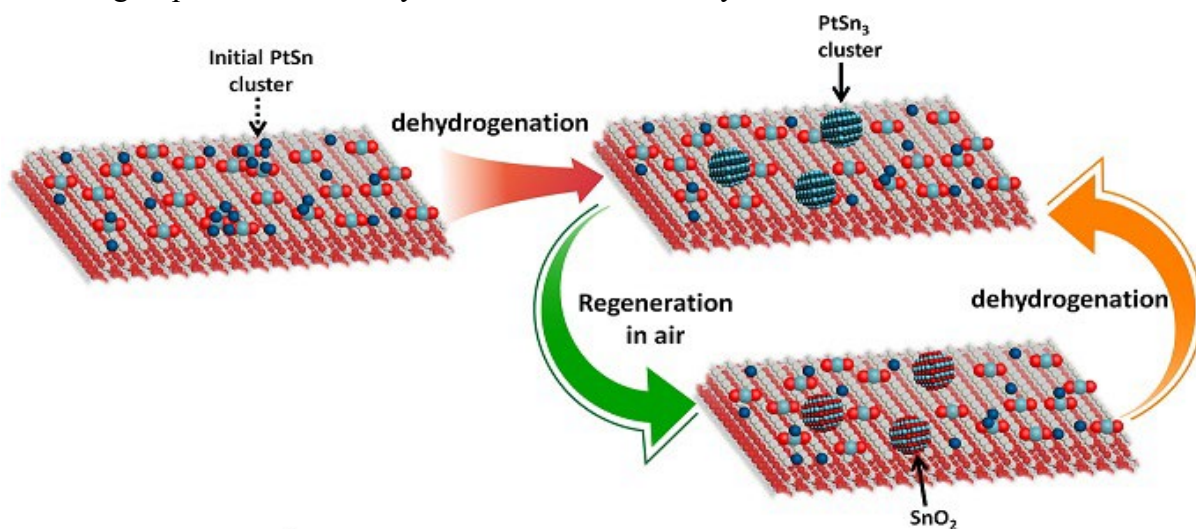


Figure 3 Schematic diagram showing how a Pt-Sn single atom catalyst is activated to form sub-nanometer clusters of PtSn₃ which after regeneration reform the Pt single atoms leaving behind SnO₂ nanoparticles. (H.F. Xiong, S. Lin, J. Goetze, P. Pletcher, H. Guo, L. Kovarik, K. Artyushkova, B.M. Weckhuysen, and A.K. Datye, *Thermally Stable and Regenerable Platinum-Tin Clusters for Propane Dehydrogenation Prepared by Atom Trapping on Ceria* *Angewandte Chemie-International Edition* 56 (31) (2017) 8986-8991)

4) Atomically dispersed Pd-O species on CeO₂(111) as highly active sites for low-temperature CO oxidation

Building on our success in generating single atom Pt catalysts, we next explored the performance of single atom Pd catalysts. Unlike their Pt counterpart, we find the Pd to be active in the single atom form, leading to exceptional activity for ceria-supported Pd for CO oxidation which is

relevant to environmental clean-up reactions. Pd loaded onto a nanorod form of ceria exposing predominantly (111) facets is already active at 50°C. Here we reported a combination of CO-FTIR spectroscopy and theoretical calculations that allows assigning different forms of Pd on the CeO₂(111) surface during reaction conditions. Single Pd atoms stabilized in the form of PdO and PdO₂ in a CO/O₂ atmosphere are involved in a catalytic cycle involving very low activation barriers for CO oxidation. The presence of single Pd atoms on the Pd/CeO₂-nanorod, corroborated by aberration-corrected TEM and CO-FTIR spectroscopy, is considered pivotal to its high CO oxidation activity.

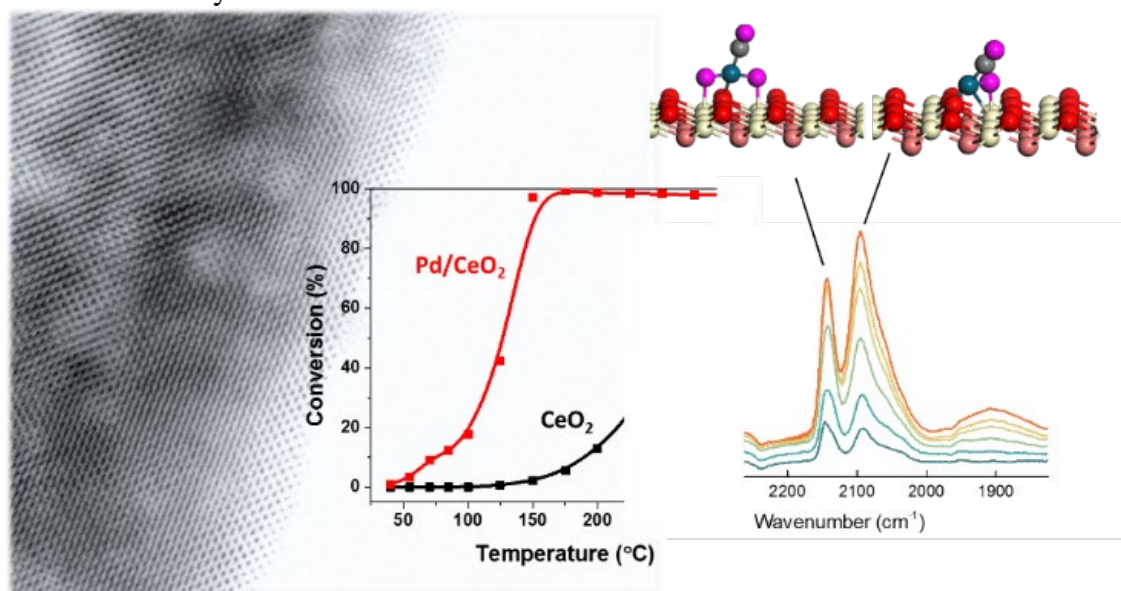


Figure 4 A composite diagram showing an AC-STEM image of Pd/CeO₂ along with the CO oxidation reactivity and the two states of the catalyst which constitute the catalytic cycle on this single atom catalyst. (G. Spezzati, Y.Q. Su, J.P. Hofmann, A.D. Benavidez, A.T. DeLaRiva, J. McCabe, A.K. Datye, and E.J.M. Hensen, *Atomically Dispersed Pd-O Species on CeO₂(111) as Highly Active Sites for Low-Temperature CO Oxidation* ACS Catal. 7 (10) (2017) 6887-6891).

Publications Acknowledging this Grant in 2015-2018

I) Exclusively funded by this grant;

1. Sun, J.; Karim, A. M.; Mei, D.; Engelhard, M.; Bao, X.; Wang, Y., New insights into reaction mechanisms of ethanol steam reforming on Co-ZrO₂. *Applied Catalysis B-Environmental* 2015, 162, 141-148.
2. Sun, J. M.; Karim, A. M.; Mei, D. H.; Engelhard, M.; Bao, X. H.; Wang, Y., New insights into reaction mechanisms of ethanol steam reforming on Co-ZrO₂. *Applied Catalysis B-Environmental* 2015, 162, 141-148.
3. Sun, J. M.; Zhang, H.; Yu, N.; Davidson, S.; Wang, Y., Effect of Cobalt Particle Size on Acetone Steam Reforming. *ChemCatChem* 2015, 7 (18), 2932-2936.
4. Wei, Z.; Karim, A. M.; Li, Y.; King, D. L.; Wang, Y., Elucidation of the roles of Re in steam reforming of glycerol over Pt-Re/C catalysts. *Journal of Catalysis* 2015, 322, 49-59.

5. Wei, Z. H.; Karim, A.; Li, Y.; Wang, Y., Elucidation of the Roles of Re in Aqueous-Phase Reforming of Glycerol over Pt-Re/C Catalysts. *ACS Catalysis* 2015, 5 (12), 7312-7320.
6. Wei, Z. H.; Karim, A. M.; Li, Y.; King, D. L.; Wang, Y., Elucidation of the roles of Re in steam reforming of glycerol over Pt-Re/C catalysts. *Journal of Catalysis* 2015, 322, 49-59.
7. Xiong, H. F.; DeLaRiva, A.; Wang, Y.; Datye, A. K., Low-temperature aqueous-phase reforming of ethanol on bimetallic PdZn catalysts. *Catalysis Science & Technology* 2015, 5 (1), 254-263.
8. Zhang, H.; Sun, J. M.; Liu, C. J.; Wang, Y., Distinct water activation on polar/non-polar facets of ZnO nanoparticles. *Journal of Catalysis* 2015, 331, 57-62.
9. Davidson, S. D.; Sun, J. M.; Wang, Y., The effect of ZnO addition on H₂O activation over Co/ZrO₂ catalysts. *Catalysis Today* 2016, 269, 140-147.
10. Hong, Y. C.; Hensley, A.; McEwen, J. S.; Wang, Y., Perspective on Catalytic Hydrodeoxygenation of Biomass Pyrolysis Oils: Essential Roles of Fe-Based Catalysts. *Catalysis Letters* 2016, 146 (9), 1621-1633.
11. Jones, J.; Xiong, H. F.; Delariva, A. T.; Peterson, E. J.; Pham, H.; Challa, S. R.; Qi, G. S.; Oh, S.; Wiebenga, M. H.; Hernandez, X. I. P.; Wang, Y.; Datye, A. K., Thermally stable single-atom platinum-on-ceria catalysts via atom trapping. *Science* 2016, 353 (6295), 150-154.
12. Liu, C. J.; Sun, J. M.; Brown, H. M.; Marin-Flores, O. G.; Bays, J. T.; Karim, A. M.; Wang, Y., Aqueous phase hydrodeoxygenation of polyols over Pd/WO₃-ZrO₂: Role of Pd-WO₃ interaction and hydrodeoxygenation pathway. *Catalysis Today* 2016, 269, 103-109.
13. Pham, H. N.; Sattler, J. J. H. B.; Weckhuysen, B. M.; Datye, A. K., Role of Sn in the Regeneration of Pt/ γ -Al₂O₃ Light Alkane Dehydrogenation Catalysts. *ACS Catalysis* 2016, 6 (4), 2257-2264.
14. Wang, W. Y.; Wu, K.; Liu, P. L.; Li, L.; Yang, Y. Q.; Wang, Y., Hydrodeoxygenation of p-Cresol over Pt/Al₂O₃ Catalyst Promoted by ZrO₂, CeO₂, and CeO₂-ZrO₂. *Industrial & Engineering Chemistry Research* 2016, 55 (28), 7598-7603.
15. Yu, N.; Zhang, H.; Davidson, S. D.; Sun, J. M.; Wang, Y., Effect of ZnO facet on ethanol steam reforming over Co/ZnO. *Catalysis Communications* 2016, 73, 93-97.
16. Chen, J. X.; Sun, J. M.; Wang, Y., Catalysts for Steam Reforming of Bio-oil: A Review. *Industrial & Engineering Chemistry Research* 2017, 56 (16), 4627-4637.
17. Hong, Y. C.; Wang, Y., Elucidation of reaction mechanism for m-cresol hydrodeoxygenation over Fe based catalysts: A kinetic study. *Catalysis Communications* 2017, 100, 43-47.
18. Hong, Y. C.; Zhang, S. R.; Tao, F. F.; Wang, Y., Stabilization of Iron-Based Catalysts against Oxidation: An In Situ Ambient-Pressure X-ray Photoelectron Spectroscopy (AP-XPS) Study. *ACS Catalysis* 2017, 7 (5), 3639-3643.
19. Nie, L.; Mei, D. H.; Xiong, H. F.; Peng, B.; Ken, Z. B.; Hernandez, X. I. P.; DeLaRiva, A.; Wang, M.; Engelhard, M. H.; Kovarik, L.; Datye, A. K.; Wang, Y., Activation of surface lattice oxygen in single-atom Pt/CeO(2) for low-temperature CO oxidation. *Science* 2017, 358 (6369), 1419-+.
20. Spezzati, G.; Su, Y. Q.; Hofmann, J. P.; Benavidez, A. D.; DeLaRiva, A. T.; McCabe, J.; Datye, A. K.; Hensen, E. J. M., Atomically Dispersed Pd-O Species on CeO(2)(111) as

- Highly Active Sites for Low-Temperature CO Oxidation. *Acs Catalysis* 2017, 7 (10), 6887-6891.
21. Xiong, H. F.; Lin, S.; Goetze, J.; Pletcher, P.; Guo, H.; Kovarik, L.; Artyushkova, K.; Weckhuysen, B. M.; Datye, A. K., Thermally Stable and Regenerable Platinum-Tin Clusters for Propane Dehydrogenation Prepared by Atom Trapping on Ceria. *Angewandte Chemie-International Edition* 2017, 56 (31), 8986-8991.
 22. Flensley, A. J. R.; Wang, Y.; Mei, D. H.; McEwen, J. S., Mechanistic Effects of Water on the Fe-Catalyzed Hydrodeoxygenation of Phenol. The Role of Bronsted Acid Sites. *ACS Catalysis* 2018, 8 (3), 2200-2208.
 23. Yu, N.; Rahman, M. M.; Chen, J.; Sun, J.; Engelhard, M.; Hernandez, X. I. P.; Wang, Y., Steam reforming of simulated bio-oil on K-Ni-Cu-Mg-Ce-O/Al₂O₃: The effect of K. *Catalysis Today* 2018.

II) Jointly funded by this grant and other grants with leading intellectual contribution from this grant;

1. Xiong, H.; DeLaRiva, A.; Wang, Y.; Datye, A. K., Low-temperature aqueous-phase reforming of ethanol on bimetallic PdZn catalysts. *Catalysis Science & Technology* 2015, 5 (1), 254-263.
2. Hensley, A. J. R.; Zhang, J. H.; Vincon, I.; Hernandez, X. P.; Tranca, D.; Seifert, G.; McEwen, J. S.; Wang, Y., Mechanistic understanding of methanol carbonylation: Interfacing homogeneous and heterogeneous catalysis via carbon supported Ir-La. *Journal of Catalysis* 2018, 361, 414-422.
3. Bossola, F.; Pereira-Hernandez, X. I.; Evangelisti, C.; Wang, Y.; Dal Santo, V., Investigation of the promoting effect of Mn on a Pt/C catalyst for the steam and aqueous phase reforming of glycerol. *Journal of Catalysis* 2017, 349, 75-83.
4. Jones, J.; Xiong, H. F.; Delariva, A. T.; Peterson, E. J.; Pham, H.; Challa, S. R.; Qi, G. S.; Oh, S.; Wiebenga, M. H.; Hernandez, X. I. P.; Wang, Y.; Datye, A. K., Thermally stable single-atom platinum-on-ceria catalysts via atom trapping. *Science* 2016, 353 (6295), 150-154.
5. Carrillo, C.; Xiong, H.; DeLaRiva, A. T.; Kunwar, D.; Peterson, E. J.; Challa, S. R.; Qi, G.; Oh, S.; Wiebenga, M. H.; Hernandez, X. I. P.; Wang, Y.; Datye, A. K., Designing Catalysts for Meeting the DOE 150 °C Challenge for Exhaust Emissions. *Microscopy and Microanalysis* 2017, 23 (S1), 2028-2029.
6. Rahman, M. M.; Davidson, S. D.; Sun, J. M.; Wang, Y., Effect of Water on Ethanol Conversion over ZnO. *Topics in Catalysis* 2016, 59 (1), 37-45.
7. Xiong, H.; Wiebenga, M. H.; Carrillo, C.; Gaudet, J. R.; Pham, H. N.; Kunwar, D.; Oh, S. H.; Qi, G.; Kim, C. H.; Datye, A. K., Design considerations for low-temperature hydrocarbon oxidation reactions on Pd based catalysts. *Applied Catalysis B: Environmental* 2018, 236, 436-444.

III) Jointly funded by this grant and other grants with relatively minor intellectual contribution from this grant;

1. Hensley, A. J. R.; Schneider, S.; Wang, Y.; McEwen, J. S., Adsorption of aromatics on the (111) surface of PtM and PtM₃ (M = Fe, Ni) alloys. *Rsc Advances* 2015, 5 (104), 85705-85719.
2. Hensley, A. J. R.; Wang, Y.; McEwen, J. S., Phenol Deoxygenation Mechanisms on Fe(110) and Pd(111). *ACS Catalysis* 2015, 5 (2), 523-536.
3. Sun, J. M.; Karim, A. M.; Li, X. S.; Rainbolt, J.; Kovarik, L.; Shin, Y.; Wang, Y., Hierarchically structured catalysts for cascade and selective steam reforming/hydrodeoxygenation reactions. *Chemical Communications* 2015, 51 (93), 16617-16620.
4. Hensley, A. J. R.; Wang, Y.; McEwen, J. S., Adsorption of guaiacol on Fe (110) and Pd (111) from first principles. *Surface Science* 2016, 648, 227-235.
5. Karim, A. M.; Al Hasan, N.; Ivanov, S.; Siefert, S.; Kelly, R. T.; Hallfors, N. G.; Benavidez, A.; Kovarik, L.; Jenkins, A.; Winans, R. E.; Datye, A. K., Synthesis of 1 nm Pd Nanoparticles in a Microfluidic Reactor: Insights from in Situ X-ray Absorption Fine Structure Spectroscopy and Small-Angle X-ray Scattering. *Journal of Physical Chemistry C* 2015, 119 (23), 13257-13267.

Catalytic Chemistry of Oxide Supported Single Palladium Atoms

Nassar Doudin,^a Jin-Cheng Liu,^b Matthew D. Marcinkowski,^a Manh Thuong Nguyen,^a Vassiliki-Alexandra Glezakou,^a Jun Li,^b Bruce D. Kay,^a Roger Rousseau,^a and Zdenek Dohnálek^{a,c}

^a Pacific Northwest National Laboratory, Physical and Computational Sciences Directorate and Institute for Integrated Catalysis, Richland, WA 99354, USA

^b Department of Chemistry, Tsinghua university, Beijing 100084, China

^c Voiland School of Chemical Engineering and Bioengineering, Washington State University, Pullman, Washington 99163, USA

Presentation Abstract

Single-atom catalysts have recently attracted great attention due to the promise of novel properties and their ultimate metal utilization. However, at the atomic level, little is known about their stabilities, interactions with the support, and mechanisms by which they operate. Recently the reconstructed Fe₃O₄(001) surface with subsurface cationic vacancies has been shown to stabilize single metal atoms to temperatures as high as 700 K, making it a promising support for model catalytic studies. Here, we follow the adsorption and reactions of molecular hydrogen and methanol on supported single Pd atoms using a combination of scanning tunneling microscopy, temperature programmed desorption, and x-ray photoelectron spectroscopy. Density functional theory investigations provide further mechanistic understanding of elemental reaction steps. We show that at 300 K H₂ dissociates and spills over onto the Fe₃O₄(001). With increasing H₂ dose, the initially isolated hydroxyl species start to form a locally ordered overlayer. At highest coverages, the surface reconstruction is lifted, and the Pd atoms become destabilized. Theoretical studies reveal that H₂ dissociates heterolytically, with hydroxyls being the final, energetically most stable species. For methanol, we find that single Pd atoms lower the dehydrogenation barrier of methoxy species to formaldehyde by almost a factor of two allowing for its room temperature formation. These studies demonstrate unique catalytic properties of single Pd atoms supported on Fe₃O₄(001).

Discovery and Development of Heterogeneous Catalysts for Higher Alcohol Synthesis

Melis S. Duyar, Eduardo Valle, Amber Janda, Alessandro Gallo, Jonathan L. Snider,
Ches Upham, Thomas F. Jaramillo

Department of Chemical Engineering, Stanford University, Stanford, CA
SUNCAT Center for Interface Science and Catalysis, SLAC National Accelerator Laboratory

Presentation Abstract

The development of new catalysts for converting synthesis gas ($\text{CO}/\text{CO}_2/\text{H}_2$) and CO_2/H_2 mixtures can unlock diverse feedstocks for the production of conventionally petroleum-derived chemicals. Synthesis gas can be produced from biomass, natural gas and other sources and CO_2 can be collected from combustion and industrial processes to be hydrogenated to high value products.

This poster will present recent research on new classes of catalysts as well as new mechanistic insights for alcohol synthesis from syngas and CO_2 . Development of new metal phosphide catalysts for methanol and higher alcohol synthesis will be discussed. Highlights from in-situ and operando characterization studies (XAS, XRD, DRIFTS) will also be presented.

Theory, Simulation, and Design of High-Oxidation State Main-Group Metal Catalysts for Hydrocarbon C-H Functionalization

Daniel H. Ess

Department of Chemistry and Biochemistry, Brigham Young University, Provo, UT 84602

Poster Abstract

This poster will showcase our use and development of standard and non-standard density functional theory (DFT) calculations to determine the potential of 5th-row and 6th-row high-oxidation state p-block, main-group compounds as catalysts in hydrocarbon C-H functionalization reactions. Featured will be completed studies on: 1) Thermodynamics and kinetic pathways for Tl-alkyl functionalization reactions in aqueous solvent using an explicit/continuum solvent model. 2) The mechanism of Hg-mediated methane and ethane amination. 3) Quantitative survey/prediction of C-H activation and functionalization reactions between In^{III}, Tl^{III}, Sn^{IV}, Pb^{IV}, and Sb^V carboxylate complexes with methane, which resulted in the prediction and experimental verification of a relatively active Sb complex. This poster will also display our development of an explicit solvation approach for carboxylic acid solvents that we are implementing in our direct molecular dynamics program called DynSuite.

Grant Number: DE-SC0018329 (Theory of Main-Group, p-Block Hydrocarbon Functionalization Reactions)

PI: Daniel H. Ess

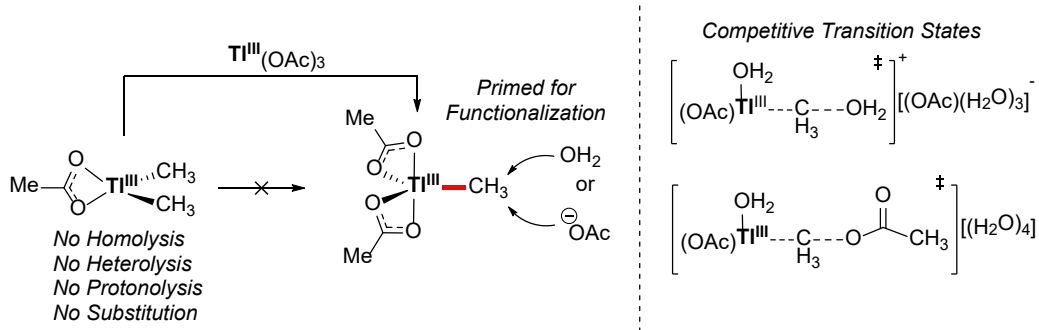
Postdoc: Samantha Gustafson

Students: Clinton King, Nathan Wohlgemuth, Lily Hamill, Nick Rollins, Ashley Holdaway, Jordan Jenkins

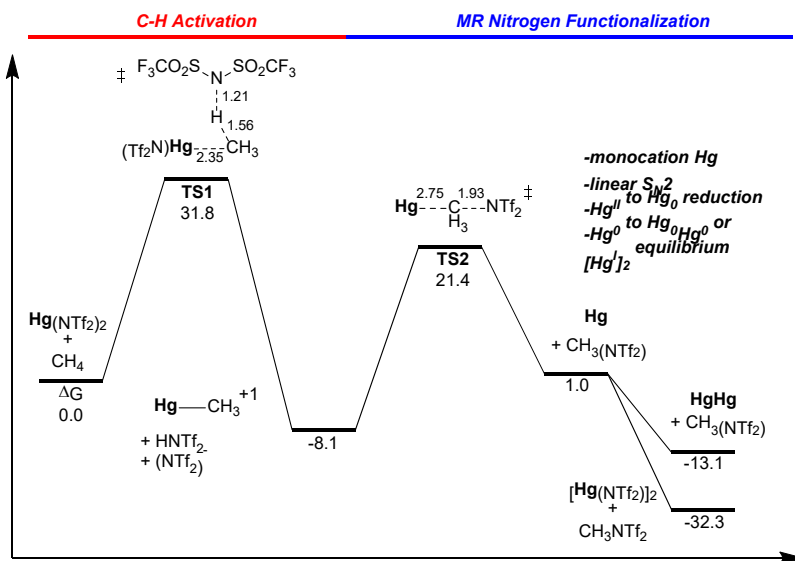
RECENT PROGRESS

Mechanisms of Main-Group Metal-Alkyl Functionalization Reactions

Metal-mediated C-H activation reactions generate metal-alkyl intermediates that can be converted into carbon-oxygen bonds through reductive functionalization reactions. While the mechanisms and reactivity of C-H activation reactions have been computationally well established, little is known about functionalization reactions, especially for p-block, main-group metal-alkyl complexes. We have completed a DFT study examining reaction thermodynamics and kinetic pathways for Tl^{III}-methyl functionalization reactions in aqueous solvent using a combination of continuum and explicit/continuum solvent models. This study examined oxygen functionalization of (OAc)Tl^{III}(CH₃)₂ and (OAc)₂Tl^{III}(CH₃) that both give methyl acetate and methanol. Our calculations revealed that (OAc)Tl^{III}(CH₃)₂ is thermodynamically and kinetically stable (e.g. bond homolysis, heterolysis, protonolysis, and reductive elimination). Functionalization is only possible after methyl anion group transfer to Tl^{III}(OAc)₃ to give (OAc)₂Tl^{III}(CH₃). This monomethyl structure is functionalized by competitive water and acetate nucleophilic reductive functionalization transitions states (see diagram below).



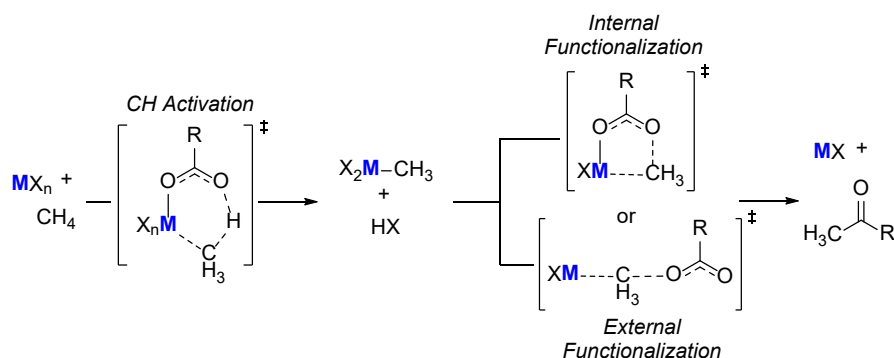
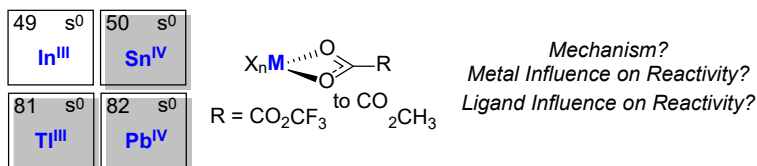
We also completed a DFT study of $\text{Hg}(\text{NTf}_2)_2$ mediated methane and ethane C-H amination. Experimentally, the Periana group at Scripps-Florida has discovered that $\text{Hg}(\text{NTf}_2)_2$ induces stoichiometric C-H functionalization of methane and ethane in nitrogen acid solvents to the corresponding alkyl amines. Our DFT study using a combination of continuum and explicit/continuum HNTf_2 solvent models examined a variety of mechanisms, including radical fragmentation, electron transfer, proton-coupled electron transfer, and hydride abstraction. None of these mechanisms are as viable as C-H activation and metal-alkyl amino functionalization. Our study also explains the selective monofunctionalization preference over difunctionalization for ethane.



Impact and Design of High-Oxidation State Main-Group Metal and Ligands on Alkane C-H Activation and Functionalization Reactions

While high-oxidation state p-block, main-group metal complexes are potential alternative catalysts to transition metals for alkane C-H functionalization reactions there is essentially nothing known on how selection of the metal and ligand impact alkane C-H activation and functionalization thermodynamics and reactivity. We completed a DFT study that determined qualitative and quantitative features of C-H activation and metal-methyl functionalization energy landscapes for reaction between In^{III} , Tl^{III} , Sn^{IV} , and Pb^{IV} carboxylate complexes with methane. We discovered that the metal influences the C-H activation barrier height to a modest extent, and

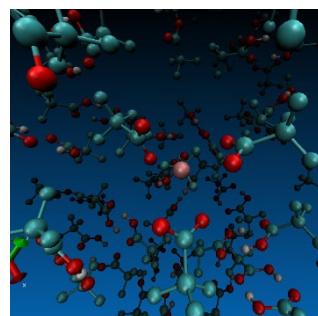
in a periodic manner, but the carboxylate ligand has a much larger quantitative impact on C-H activation. For metal-methyl functionalization reactions, the main-group metal dramatically influences activation barriers, which were correlated to bond heterolysis energies as a model two-electron reduction energies.



This study set the stage for our understanding and prediction of which main-group metals and carboxylate ligands could be useful for methane functionalization systems that utilize C-H activation and metal-alkyl functionalization reactions. We then computationally examined other 5th-row and 6th-row main-group complexes in search of complexes that showed C-H activation and functionalization barriers of <30 kcal/mol, which would be low enough for experimental examination. Our calculations identified that Sb(TFA)₅ in trifluoroacetic acid fit this design criterion. Experiments by the Periana group at Scripps-Florida have realized this prediction. Sb(TFA)₅ in TFAH was generated in situ and reacts with methane and ethane to give the corresponding mono and/or diol trifluoroacetate esters. We also completed a DFT study of this reaction mechanism, and confirmed that the most viable pathway, especially for methane, is C-H activation and metal-alkyl functionalization, rather than carbocation or radical pathways.

Development of Software and Protocol for Main-Group Mechanistic Modeling in Complete Carboxylic Acid Solvent

To date, the most useful catalysts for alkane C-H functionalization operate in strong acids. For p-block, main-group metals most active complexes react in carboxylic acid solvents. Because carboxylic acid solvents are relatively nonpolar, but induce significant hydrogen bonding, to more accurately determine mechanisms and catalytic cycles we are developing protocols to model reactions with explicit solvent.



We are currently connecting the program Packmol with our in-house direct dynamics program DynSuite, which interfaces with the electronic structure program Gaussian. This connection provides solute-solvent packing. We now have the ability to generate a solvated box or sphere of carboxylic acid solvent around main-group metal complexes and run either static DFT calculations

or DFT direct dynamics. However, there remain several practical challenges to finalize this solvation protocol, such as realistic treatment of the solvent box/sphere boundary.

Publications Acknowledging this Grant in 2015-2018

- (1) Gustafson, S. J.; Konnick, M. M.; Periana, R. A.; Ess, D. H. "Mechanisms and Reactivity of Tl(III) Main-Group Metal-Alkyl Functionalization in Water" *Under Review*; King, C. R.; Rollins, N.; Holdaway, A.; Konnick, M. M.; Periana, R. A.; Ess, D. H. "Electrophilic Impact of High-Oxidation State Main-Group Metal and Ligands on Methane C-H Activation and Functionalization Reactions" *Under Review*

Twists to the Cluster-Surface Analogy: New Strategies for the Synthetic Manipulation of Strong-Field Metal-Carbonyl Clusters

Joshua S. Figueroa and Myles J. Drance

Department of Chemistry and Biochemistry, University of California, San Diego

Presentation Abstract

When considering mechanistic and structural models for heterogeneous catalysts, there has been a long-standing conceptual analogy between discrete, molecular strong-field metal carbonyl clusters and surface active sites, especially those of bulk metals. While this analogy has been promulgated for decades, it is also well recognized that there are significant limitations with the degree to which strong-field metal carbonyl clusters can mimic the function of such heterogeneous catalysts. These limitations are especially apparent in the reactivity profile molecular cluster compounds. Indeed, the most notable break down of this comparison originates from the fact that the CO ligands themselves, due to their strong π -acidity, often play a deactivating role to multinuclear clusters relative to bulk-metal active sites. We reasoned that isolobal replacement of CO with isocyanide ligands, which are stronger σ -donors and weaker π -acids, may provide for the activation of strong-field metal carbonyl clusters a novel manner. Presented here is a synthetic study on isocyanide-for-CO replacement on the tetra-iron nitro cluster $[\text{Fe}_4(\mu_4\text{-N})(\text{CO})_{12}]^-$. We show that substitution of four CO ligands with the *m*-terphenyl isocyanide $\text{CNAr}^{\text{Mes}_2}$ ($\text{Ar}^{\text{Mes}_2} = 2,6\text{-}(2,4,6\text{-Me}_3\text{C}_6\text{H}_3)_2\text{C}_6\text{H}_3$) significantly activates the nucleophilicity of the interstitial nitrogen atom relative to the all-carbonyl congener. This electronic activation allows the cluster framework to be systematically manipulated with electrophilic substrates. A highlight of this work is the development of cluster-expansion reactions that incorporate high-spin metal centers into an otherwise low-spin, strong-field cluster system. This electronic perturbation affords new clusters that react with substrates in a manner for more similar to bulk-metal active sites, while also showing metal-metal redox cooperativity that are the hallmark of such heterogeneous systems.

DE-SC0018243: Small-Molecule Catalysis by Transition-Metal Isocyanide Monomers, Clusters and Materials

RECENT PROGRESS

Synthesis and Reaction Chemistry of Tetra-Iron Nitrido Clusters supported by *m*-Terphenyl Isocyanide Ligands. We have been interested in the ability of *m*-terphenyl isocyanides to modify the electronic properties – and ultimately the reactivity profile – of strong-field metal carbonyl clusters. There has been a long-standing conceptual analogy between discrete, strong-field metal carbonyl clusters and active sites of bulk metal surfaces. However, in many cases this conceptual analogy has fallen short, as metal carbonyl clusters rarely exhibit the reactivity patterns exhibited by metal surfaces or other heterogeneous catalysts. The origin of this discrepancy has been proposed to arise from a deactivating effect of the strongly π -acidic CO ligands on the low-valent metal centers that make up such clusters. Notably, this idea has not been resoundingly confirmed

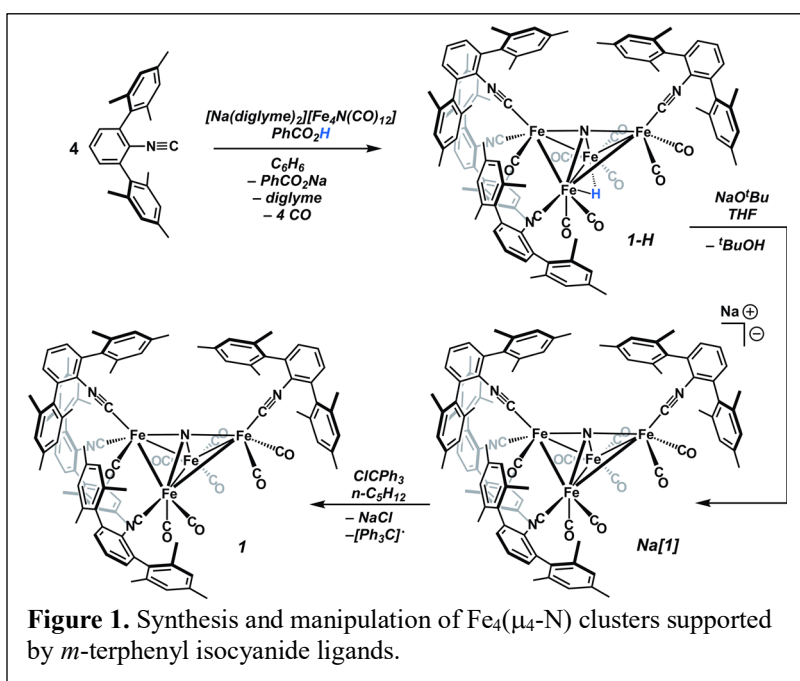
by either experimental or theoretical means. In addition, there is still a lack of general synthetic methods for the elaboration of strong-field metal carbonyl clusters, especially those that led to significant reactivity-profile enhancement. For these reasons, we postulated that CNR-for-CO replacement could deliver electronically enhanced metal clusters due to the weaker π -acceptor and stronger σ -donor nature of isocyanides relative to CO. The main goal of this study was to prepare metal cluster complexes that more actually mimic the reactivity profiles of catalytically active surface sites.

Our initial investigations focused on electronic modification of the tetra-iron nitrido cluster, $[\text{Fe}_4(\mu_4\text{-N})(\text{CO})_{12}]^-$, as this species has a notoriously unreactive interstitial nitride ligand. This cluster was originally prepared and studied as a model for

adsorbed nitrogen on Haber-Bosch catalytic surfaces. However, it does not allow for multiple protonation events at the interstitial nitrogen atom, nor does it provide a pathway for ready release of ammonia equivalents. More recently, Berben has shown that this cluster is active in HER and CO_2 -to- $[\text{HCO}_2]^-$ electrocatalysis, but the basic cluster framework is difficult to modify in a systematic manner.

Our synthetic access point to isocyanide-substituted tetra-iron nitrido clusters is outlined in Figure 1. We discovered that the cleanest CNR-for-CO replacement of $[\text{Fe}_4(\mu_4\text{-N})(\text{CO})_{12}]^-$ by *in-situ* protonation/substitution using benzoic acid (PhCO_2H) and the *m*-terphenyl isocyanide $\text{CNAr}^{\text{Mes}_2}$ ($\text{Ar}^{\text{Mes}_2} = 2,6\text{-}(2,4,6\text{-Me}_3\text{C}_6\text{H}_3)_2\text{C}_6\text{H}_3$). This produced the tetra-isocyanide nitride/hydride cluster $[\text{Fe}_4(\mu_4\text{-N})(\mu_2\text{-H})(\text{CO})_8(\text{CNAr}^{\text{Mes}_2})_4]$, which has an asymmetric distribution of isocyanide ligands on the four Fe centers as determined by X-ray diffraction. Notably, several attempts to add additional $\text{CNAr}^{\text{Mes}_2}$ ligands or obtain a symmetrically distributed Fe_4 product were unsuccessful. However, the asymmetric distribution found in the solid-state for $[\text{Fe}_4(\mu_4\text{-N})(\mu_2\text{-H})(\text{CO})_8(\text{CNAr}^{\text{Mes}_2})_4]$ is persistent in solution, as determined by the fact that its ^1H NMR spectrum does not reveal any changes indicative of fluxional behavior up to 80°C .

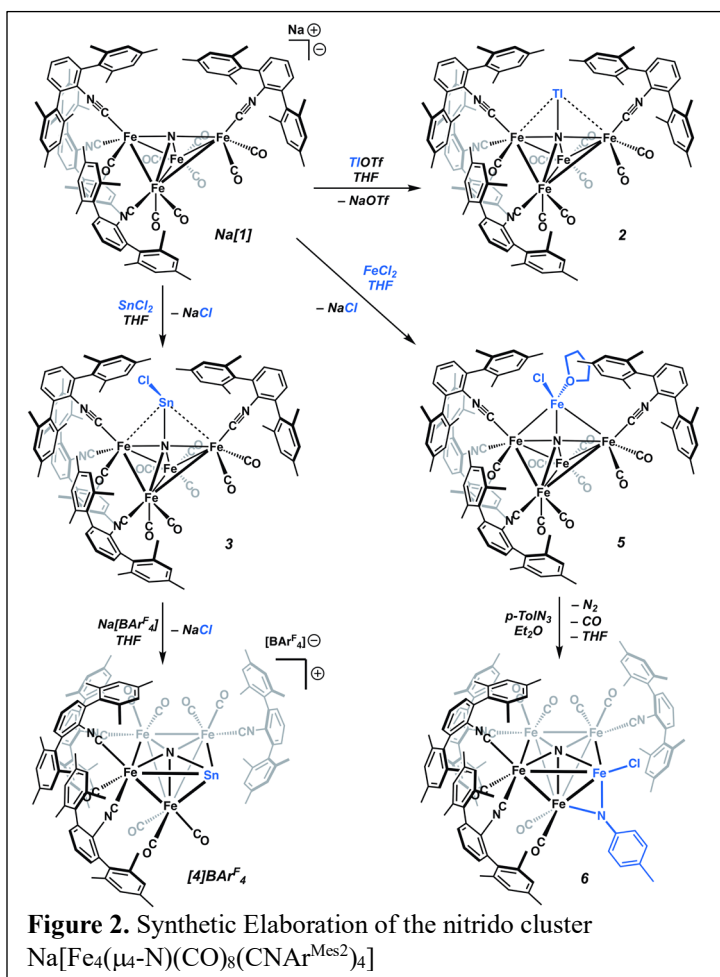
The nitrido-hydride cluster $[\text{Fe}_4(\mu_4\text{-N})(\mu_2\text{-H})(\text{CO})_8(\text{CNAr}^{\text{Mes}_2})_4]$ serves as a convenient starting material for additional cluster derivatives with this mixed $\text{CO}/\text{CNAr}^{\text{Mes}_2}$ substitution pattern. For example, deprotonation of $[\text{Fe}_4(\mu_4\text{-N})(\mu_2\text{-H})(\text{CO})_8(\text{CNAr}^{\text{Mes}_2})_4]$ with $\text{NaO}-t\text{-Bu}$ affords the salt $\text{Na}[\text{Fe}_4(\mu_4\text{-N})(\text{CO})_8(\text{CNAr}^{\text{Mes}_2})_4]$ (Figure 1), the anionic portion of which serves as a direct analogue of the all-carbonyl cluster $[\text{Fe}_4(\mu_4\text{-N})(\text{CO})_{12}]^-$. There are two critical aspects of $\text{Na}[\text{Fe}_4(\mu_4\text{-N})(\text{CO})_8(\text{CNAr}^{\text{Mes}_2})_4]$ that foreshadow its differential properties relative to salts of $[\text{Fe}_4(\mu_4\text{-N})(\text{CO})_{12-n}(\text{L})_n]^-$ with L-for-CO substitution greater than $n = 2$. We believe this is due to an important electronic effect in this system. More than likely, as strongly σ -donating L-type ligands



are added, the remaining CO ligands become less labile on account of increased π -backbonding interactions. While, isocyanides are strong σ -donors, their π -acid properties can accommodate excess electron density while still providing for CO labilization. Second, and more interestingly, $\text{Na}[\text{Fe}_4(\mu_4\text{-N})(\text{CO})_8(\text{CNAr}^{\text{Mes}_2})_4]$ is an extremely air and water sensitive material, whereas the all-carbonyl derivative $[\text{Fe}_4(\mu_4\text{-N})(\text{CO})_{12}]^-$ is prepared in H_2O . This qualitative observation indicates that $\text{CNAr}^{\text{Mes}_2}$ substitution leads to a more electron-rich system with a potentially novel reactivity profile. Indeed, this latter fact is borne out by the finding that simple oxidation of $\text{Na}[\text{Fe}_4(\mu_4\text{-N})(\text{CO})_8(\text{CNAr}^{\text{Mes}_2})_4]$ with ClCPh_3 leads to the neutral, radicaloid cluster $\text{Fe}_4(\mu_4\text{-N})(\text{CO})_8(\text{CNAr}^{\text{Mes}_2})_4$, which is stable under ambient conditions and has been structurally characterized. In contrast, the analogous radical $\text{Fe}_4(\mu_4\text{-N})(\text{CO})_{12}$ decomposes readily in solution and has only been detected conclusively using electrochemical methods. This difference strongly suggests that the stronger σ -donor profile of the isocyanides provides for a more electron-rich environment that is capable of stabilizing electron-deficient clusters.

Additional evidence that isocyanide ligation provides a more electron-rich cluster framework, and one that diverges significantly from the all-carbonyl homologue, is provided by the reactivity of the $\text{Na}[\text{Fe}_4(\mu_4\text{-N})(\text{CO})_8(\text{CNAr}^{\text{Mes}_2})_4]$ with electrophilic substrates. As shown in Figure 2, $\text{Na}[\text{Fe}_4(\mu_4\text{-N})(\text{CO})_8(\text{CNAr}^{\text{Mes}_2})_4]$ reacts with TiOTf , SnCl_2 and FeCl_2 with salt elimination to provide the novel cluster expansion products **2**, **3** and **5**. In each case, the incoming main group or transition metal fragment adds to the interstitial N atom of the cluster, thereby indicating that $\text{CNAr}^{\text{Mes}_2}$ ligation allows for an electronic threshold for the nitride nucleophilicity to be met. Most importantly, the all-carbonyl cluster $[\text{Fe}_4(\mu_4\text{-N})(\text{CO})_{12}]^-$ does not react with any of these electrophilic substrates under identical conditions, which is consistent with the traditional view of this cluster as possessing a non-nucleophilic interstitial nitrogen atom. These results represent a significant development in this project. The ability to systematically expand strong-field clusters with electronically diverse fragments creates an avenue for enhanced reactivity, especially those that more fully parallel reactive heterogeneous catalyst sites where surface reconstruction, promoter-antagonist interactions and metal-metal cooperativity are common place.

To more fully demonstrate this idea, we carried out additional synthetic studies of the expanded clusters **3** and **5**. For the stannylene cluster **3**, simple treatment with $\text{Na}[\text{BAR}^{\text{F}_4}]$ resulted



in NaCl elimination and production of the cationic cluster **4**, in which an Sn cation has formally entered the cluster framework. Electrochemical analysis of this new Sn-included cluster showed that Sn incorporation results in a ca. 700 mV anodic shift of the reduction potential of the framework relative to the parent all-carbonyl cluster $[\text{Fe}_4(\mu_4\text{-N})(\text{CO})_{12}]^-$. This effect is similar to that of Ca^{2+} ions on the OEC Mn_4 -subunit in Photosystem II and shows that tuning of cluster properties is possible with the judicious electronic modification enabled by isocyanide-for-CO substitution.

For FeCl-incorporated cluster **5**, it is important to note isocyanide-for-CO substitution provides a means of adding a high-spin metal center to an otherwise low-spin, strong-field metal carbonyl cluster. Moreover, we believe the mixed electronic profile of cluster **5** provides a far more accurate representation of surface defect sites than a strong-field cluster alone. Indeed, we found that treatment of that cluster **5** with simple organic azides results in formation of bridging imido cluster species (**6**), where the new FeCl fragment was clearly the initial point of reactivity. This result showed that the reactivity properties of cluster complexes can be enhanced by our approach and also demonstrated changes in the electronic profile of strong-field clusters can initiate cooperative effects between metal centers in the cluster framework. Investigations into this system are ongoing, with the aim of uncovering additional stoichiometric and catalytic transformations that can be mediated by these modified and elaborated cluster species.

Publications Acknowledging this Grant in 2015-2018

I) Exclusively funded by this grant:

- 1) Drance, M. J.; Mokhtarzadeh, C. C.; Melaimi, M.; Agnew D. W.; Moore, C. E.; Rheingold, A. L.; Figueroa, J. S. "Controlled Expansion of a Strong-Field Iron-Nitride Cluster: Multi-Site Ligand Substitution as a Strategy for Activating Interstitial Nitride Nucleophilicity" *Angew. Chem. Int. Ed.* **2018**, *57*, Early View.
DOI: 10.1002/anie.201801206

**Supported Molecular Metal Catalysts:
Single-Sites to Pair-Sites to Metal Clusters**

Bruce C. Gates, Erjia Guan, Adam Hoffman, Louise Debeve, University of California, Davis, Departments of Chemical Engineering and Materials Science & Engineering; Feng-Shou Xiao, Zhejiang University, Key Laboratory of Applied Chemistry of Zhejiang Province, Department of Chemistry; David A. Dixon, Department of Chemistry, University of Alabama; Alexander Katz, Department of Chemical and Biomolecular Engineering, University of California, Berkeley; J.-M. Basset, Catalysis Center, KAUST, Maria Flytzani-Stephanopoulos, Tufts University, Department of Chemical Engineering; Alper Uzun, Koç University, Department of Chemical Engineering

Presentation Abstract

We report a family of precisely synthesized supported molecular catalysts as well as novel methods to control the stability of supported metal nanocluster catalysts. The topic covers uniform single-site supported catalysts, catalysts incorporating metal pair-sites, catalysts incorporating site-isolated promoters, and some of the simplest supported metal clusters—as well as sinter-resistant nanoparticles encapsulated in zeolites. The catalysts have been characterized by IR and X-ray absorption spectroscopies, STEM, performance evaluation, and other techniques.

Grant Number De-FG02-04ER15513

Student(s) from University of California, Davis: Louise Debeve, Chia-Yu Fang, Erjia Guan, Adam Hoffman, Kimberly Justl, Andrew Palermo, Jorge Perez-Aguilar

RECENT PROGRESS

We wrote a perspective on atomically dispersed supported metal catalysts, with the following summary: Catalysts consisting of metal atoms that are atomically dispersed on supports are gaining wide attention because of the rapidly developing understanding of their structures and functions and the discovery of new, stable catalysts with new properties. Our goals in this essay are to summarize the classes of these catalysts, to state key questions about them, to point out crucial methods for their characterization, and to suggest directions for future research. Most of the catalysts in this class incorporate supports that are inorganic materials such as metal oxides and zeolites, and the list of supports has recently been expanded to include small assemblies of metal atoms within molecular metal clusters, as well as the surfaces of bulk metals, including single crystals and supported nanoparticles. Scanning transmission electron microscopy and scanning tunneling microscopy have recently provided numerous images of isolated metal atoms on support surfaces, and complementary spectroscopic results have provided evidence of the metal oxidation states (usually positive, unless the support is a metal), metal–support bonding, and the ligands

present on the metal. Catalysts in this class have been found to have activity for numerous reactions, including hydrogenations, oxidations, and the water gas shift. Some offer exciting new catalyst selectivities associated with the isolation of the metal centers within controllable environments. Some atomically dispersed supported metal catalysts, exemplified by those supported on zeolites, have nearly uniform arrays of metal sites that are considered to be nearly ideal catalytic sites, and these are excellently suited to investigation by theory, such as density functional theory, to fill in gaps left by experiment, to predict new properties, and to help guide future research.

Investigating mononuclear organoiridium species made from the precursor $\text{Ir}(\text{C}_2\text{H}_4)_2(\text{acac})$ on highly crystalline MgO powder, we have made catalysts with a wide range of metal loadings and differentiated among the MgO surface sites for iridium bonding, learning how to synthesize highly uniform supported single-site catalysts. Each Ir atom (as shown in STEM images) that was present at low loading (0.01 wt%) was bonded to three oxygen atoms of the MgO surface, as shown by EXAFS spectroscopy. These species are distinct from iridium on MgO at higher loadings, in terms of structure and catalytic activity and stability (they are resistant to sintering). These catalysts are nearly ideal in the sense of having almost all the Ir atoms at equivalent surface sites, and they are modeled accurately with density functional theory (collaboration with David Dixon). The results open the door to the precise synthesis of families of single-site catalysts.

To synthesize supported metal pair-sites in high yields and minimize inhibition of catalysis by the stabilizing ligands present in the precursor, we synthesized rhodium pair-sites on MgO from $\text{Rh}_2(\mu\text{-OMe})_2(\text{COD})_2$ (OMe = methoxy; COD = cyclooctadiene) and modified the ligands by mild hydrogenation (353 K for 1 h). The surface pair sites were retained when the organic ligands were removed, giving catalysts that facilitate H_2 dissociation much more rapidly than single-site rhodium and catalyze ethylene hydrogenation ~40 times faster than single-site rhodium on MgO at 298 K.

Working with the group of Prof. F.-S. Xiao, we extended the class of single-site catalysts to incorporate atomically dispersed metal atoms as promoters. The promoters are single-site Sn on TiO_2 supports that incorporate metal nanoparticle catalysts. Represented as $\text{M}/\text{Sn}-\text{TiO}_2$ (M = Au, Ru, Pt, Ni), these catalysts decidedly outperform the unpromoted supported metals, even for hydrogenation of nitroarenes substituted with various reducible substituents. The high activity and selectivity of these catalysts result from the creation of oxygen vacancies on the TiO_2 surface by single-site Sn, which leads to efficient, selective activation of the nitro group coupled with a reaction involving hydrogen atoms activated on the metal nanoparticles.

In work with Prof. A. Uzun of Koç University, we presented a new class of supported single-site catalyst—those modified with ionic liquid coatings. 1,3-Dialkylimidazolium ionic liquid coatings act as electron donors, increasing the selectivity for partial hydrogenation of 1,3-butadiene catalyzed by iridium complexes supported on high-surface-area $\gamma\text{-Al}_2\text{O}_3$. High-energy-resolution fluorescence detection X-ray absorption near-edge structure (HERFD XANES) measurements were used to quantify the electron donation and are correlated with the catalytic activity and selectivity. The results demonstrate broad opportunities to tune electronic environments and catalytic properties of atomically dispersed supported metal catalysts.

Supported metal nanoparticle catalysts are widely used in industry but suffer from deactivation resulting from metal sintering and coke deposition at high reaction temperatures. In further work with the Xiao group, we showed that the adsorption of molecules on metal nanoparticles can be sterically controlled through the use of zeolite crystals, by fixing the metal nanoparticles (Pt, Pd, Rh, and Ag) on zeolite crystals surrounded by a sheath of zeolite crystals. The resulting materials are sinter-resistant at 600-700 °C, and the uniform zeolite micropores allow for the diffusion of reactants enabling contact with the metal nanoparticles in the interior of each catalyst particle. These catalysts exhibit long lifetimes, outperforming conventional supported metal catalysts and commercial catalysts consisting of metal nanoparticles on the surfaces of conventional solid supports in the catalytic conversion of C₁ molecules, including the water-gas shift, CO oxidation, oxidative reforming of methane, and CO₂ hydrogenation as well as selective hydrogenation of more complicated molecules than C₁ molecules, such as substituted nitroarenes with multiple reducible groups.

Publications Acknowledging this Grant in 2015-2018

- (I) "Mononuclear iridium dinitrogen complexes bonded to zeolite HY," D. Yang, M. Chen, C. Martinez-Macias, D. A. Dixon, and B. C. Gates, *Chem. Eur. J.*, **2015**, *21*, 631-640.
- (II) "Agglomerative Sintering of an Atomically Dispersed Ir₁/Zeolite Y Catalyst: Compelling Evidence Against Ostwald Ripening but for Bimolecular and Autocatalytic Agglomeration Catalyst Sintering Steps," E. Bayram, J. Lu, C. Aydin, N. D. Browning, S. Ozkar, E. Finney, B. C. Gates, and R. Finke, *ACS Catal.*, **2015**, *5*, 3514-3527.
- (III) "Imaging Individual Lanthanum Atoms in Zeolite Y by Scanning Transmission Electron Microscopy: Evidence of Lanthanum Pair Sites," P. Xu, J. Lu, C. Aydin, L. Debeve, N. D. Browning, C. Y. Chen, and B. C. Gates, *Micropor. Mesopor. Mater.*, **2015**, *213*, 95-99.
- (IV) "From Catalyst Preparation toward Catalyst Synthesis," B. C. Gates, *J. Catal.*, **2015**, *328*, 72-74.
- (V) "Genesis of Delaminated-Zeolite Morphology: 3-D Characterization of Changes by STEM Tomography," I. Arslan, J. D. Roehling, I. Ogino, K. J. Batenburg, S. I. Zones, B. C. Gates, and A. Katz, *J. Phys. Chem. Lett.*, **2015**, *6*, 2598-2602.
- (VI) "Structures, Relative Energies, and Ligand Dissociation Energies of Iridium Carbonyl Phosphine Clusters," S. Zhang, A. Katz, B. C. Gates, and D. A. Dixon, *Comp. Theor. Chem.*, **2015**, *1069*, 18-35.
- (VII) "Single-Site Zeolite-Anchored Organoiridium Carbonyl Complexes: Characterization of Structure and Reactivity by Spectroscopy and Computational Chemistry," C. Martinez Macias, M. Chen, D. A. Dixon, and B. C. Gates, *Chem. Eur. J.*, **2015**, *21*, 11825-11835.
- (VIII) "Isostructural Zeolite-Supported Rhodium and Iridium Complexes: Tuning Catalytic Activity and Selectivity by Ligand Modification," C. Martinez-Macias, P. Serna, and B. C. Gates, *ACS Catal.*, **2015**, *5*, 5647-5656.

- (IX) "Molecular Models of Site-Isolated Cobalt, Rhodium, and Iridium Catalysts Supported on Zeolites: Ligand Bond Dissociation Energies," M. Chen, P. Serna, J. Lu, B. C. Gates, and D. A. Dixon, *Comp. Theor. Chem.*, **2015**, *1074*, 58-72.
- (X) "Migration of Single Iridium Atoms and Tri-iridium Clusters on MgO Surfaces: Aberration-Corrected STEM Imaging and Ab Initio Calculations," C. W. Han, H. Iddir, A. Uzun, L. A. Curtiss, N. D. Browning, B. C. Gates, and V. Ortolan, *J. Phys. Chem. Lett.*, **2015**, *6*, 4675-4679.
- (XI) "Controlling the Hydrogenolysis of Silica-Supported Tungsten Pentamethyl Leads to a Class of Highly Electron Deficient Partially Alkylated Metal Hydrides," N. Maity, S. Barman, E. Callens, M. K. Samantaray, E. Abou-Hamad, Y. Minenkov, V. D'Elia, A. S. Hoffman, C. M. Widdifield, L. Cavallo, B. C. Gates, and J.-M. Basset, *Chem. Sci.*, **2016**, *7*, 1558-1568.
- (XII) "Surface Metal Complexes and their Applications," J. D. Kistler, P. Serna, K. Asakura, and B. C. Gates, in "X-Ray Absorption and X-Ray Emission Spectroscopy: Theory and Applications," J. van Bokhoven and C. Lamberti, editors, Wiley, Chichester, 2016, pp. 773-808.
- (XIII) "Rhodium pair-sites on magnesium oxide: Synthesis, characterization, and catalysis of ethylene hydrogenation," D. Yang, P. Xu, E. Guan, N. D. Browning, and B. C. Gates, *J. Catal.*, **2016**, *338*, 12-20.
- (XIV) "Toward Benchmarking in Catalysis Science: Best Practices, Challenges, and Opportunities," T. Bligaard, R. M. Bullock, C. T. Campbell, J. G. Chen, B. C. Gates, R. J. Gorte, C. W. Jones, W. D. Jones, J. R. Kitchin, and S. L. Scott, *ACS Catal.*, **2016**, *6*, 2590-2602.
- (XV) "Concluding remarks: Progress toward design of solid catalysts," *Faraday Discuss.*, **2016**, *188*, 591-602.
- (XVI) "Transmission and Fluorescence X-ray Absorption Spectroscopy Cell/Flow Reactor for Powder Samples under Vacuum or in Reactive Atmospheres," A. S. Hoffman, L. M. Debeve, A. Bendjerious-Sedjerari, S. Ould Chikh, S. R. Bare, J.-M. Basset, and B. C. Gates, *Rev. Sci. Instrum.*, **2016**, *87*, 073108.
- (XVII) "Tracking Rh Atoms in Zeolite HY: First Steps of Metal Cluster Formation and Influence of Metal Nuclearity on Catalysis of Ethylene Hydrogenation and Ethylene Dimerization," D. Yang, P. Xu, N. D. Browning, and B. C. Gates, *J. Phys. Chem. Lett.*, **2016**, *7*, 2537-2543.
- (XVIII) "Homogeneity of Surface Sites in Supported Single-Site Metal Catalysts: Assessment with Band Widths of Metal Carbonyl Infrared Spectra," A. S. Hoffman, Chia-Yu Fang, and B. C. Gates, *J. Phys. Chem. Lett.*, **2016**, *7*, 3854-3860.
- (XIX) "Supported Catalysts," I. Ogino, P. Serna, and B. C. Gates, in R. Dronskowski, S. Kikkawa, and A. Stein, editors, "Handbook of Solid State Chemistry," Wiley, New York, vol. 6, pp. 313-337 (2016).

- (XX) "Single-site osmium catalysts on MgO: reactivity and catalysis of CO oxidation," D. Yang, S. Zhang, P. Xu, N. D. Browning, D. A. Dixon, and B. C. Gates, *Chem. Eur. J.*, **2017**, *23*, 2532-2536.
- (XXI) "High-Energy Resolution X-Ray Absorption Spectroscopy for Identification of Reactive Surface Species on Supported Single-Site Catalysts," A. S. Hoffman, D. Sokaras, S. Zhang, L. M. Debeve, C.-Y. Fang, A. Gallo, T. Kroll, D. A. Dixon, S. R. Bare, and B. C. Gates, *Chem. Eur. J.*, **2017**, *23*, 14760-14768.
- (XXII) "From single-site tantalum complexes to nanoparticles of Ta_xN_y and TaO_xN_y supported on silica: elucidation of synthesis chemistry by dynamic nuclear polarization surface enhanced NMR spectroscopy and X-ray absorption spectroscopy," J. C. Mohandas, E. Abou-Hamad, E. Callens, M. K. Samantaray, D. Gajan, A. Gurinov, T. Ma, S. Ould-Chikh, A. S. Hoffman, B. C. Gates, and J.-M. Basset, *Chem. Sci.*, **2017**, *8*, 5650-5661.
- (XXIII) "Single-site osmium catalysts on MgO: reactivity and catalysis of CO oxidation," D. Yang, S. Zhang, P. Xu, N. D. Browning, D. A. Dixon, and B. C. Gates, *Chem. Eur. J.*, **2017**, *23*, 2532-2536.
- (XXIV) "Dialing in single-site reactivity of a supported calixarene-protected tetrairidium cluster catalyst," A. Palermo, A. Solovyov, D. Ertler, A. Okrut, B. C. Gates, and A. Katz, *Chem. Sci.*, **2017**, *8*, 4951-4960.
- (XXV) "Role of N-Heterocyclic Carbenes as Ligands in Iridium Carbonyl Clusters," S. J. Zhang, S. D. Foyle, A. Okrut, A. Solovyov, A. Katz, B. C. Gates, and D. A. Dixon, *J. Phys. Chem. A*, **2017**, *121*, 5029-5044.
- (XXVI) "From single-site tantalum complexes to nanoparticles of Ta_xN_y and TaO_xN_y supported on silica: elucidation of synthesis chemistry by dynamic nuclear polarization surface enhanced NMR spectroscopy and X-ray absorption spectroscopy," J. C. Mohandas, E. Abou-Hamad, E. Callens, M. K. Samantaray, D. Gajan, A. Gurinov, T. Ma, S. Ould-Chikh, A. S. Hoffman, B. C. Gates, and J.-M. Basset, *Chem. Sci.*, **2017**, *8*, 5650-5661.
- (XXVII) "A Pd@Zeolite Catalyst for Nitroarene Hydrogenation with High Product Selectivity by Sterically Controlled Adsorption in the Zeolite Micropores," J. Zhang, L. Wang, Y. Shao, Y. Wang, B. C. Gates, and F.-S. Xiao, *Angew. Chem. Int. Ed.*, **2017**, *56*, 9747-9751.
- (XXVIII) "Tuning the Selectivity of Single-Site Supported Metal Catalysts with Ionic Liquids," M. Babucci, C.-Y. Fang, A. S. Hoffman, S. R. Bare, B. C. Gates, and A. Uzun, *ACS Catal.*, **2017**, *7*, 6969-6972.
- (XXIX) "Atomically dispersed supported metal catalysts: perspectives and suggestions for future research," B. C. Gates, M. Flytzani-Stephanopoulos, D. A. Dixon, and A. Katz, *Catal. Sci. Technol.*, **2017**, *7*, 4259-4275.
- (XXX) "Beyond Ordered Materials: Understanding Catalytic Sites on Amorphous Solids," B. R. Goldsmith, B. Peters, J. K. Johnson, B. C. Gates, and S. L. Scott, *ACS Catal.*, **2017**, *7*, 7543-7557.

(XXXI) "Stable Rhodium Pair Sites on MgO: Influence of Ligands and Rhodium Nuclearity on Catalysis of Ethylene Hydrogenation and H-D Exchange in the Reaction of H₂ with D₂," E. Guan and B. C. Gates, *ACS Catal.*, **2018**, *8*, 482-487.

(XXXII) "A Silica-Supported Monoalkylated Tungsten Dioxo Complex Catalyst for Olefin Metathesis," N. Maity, S. Barman, Y. Minenkov, S Ould-Chikh, E Abou-Hamad, T. Ma, Z. S. Qureschi, L. Cavallo, V. D'Elia, B. C. Gates, and J.-M. Basset, *ACS Catal.*, **2018**, *8*, 2715-2729.

(XXXIII) "Single-site catalyst promoters accelerate metal-catalyzed nitroarene hydrogenation," L. Wang, W. Guan, J. Zhang, J. Yang, Y. Zhu, Y. Han, M. Yang, C. Cen, G. Fu. B. C. Gates, and F.-S. Xiao, *Nat. Commun.*, **2018**, *9*, 1362-1370.

(XXXIV) "Beating Heterogeneity of Single-Site Catalysts: MgO-Supported Iridium Complexes," A. S. Hoffman, L. M. Debeve, S. Zhang, J. E. Perez-Aguilar, E. T. Conley, K. R. Justl, I. Arslan, D. A. Dixon, and B. C. Gates, *ACS Catal.*, **2018**, *8*, 3489-3498.

(XXXV) "Sinter-Resistant Metal Nanoparticle Catalysts Achieved by Immobilization within Zeolite Crystals via Seed-Directed Growth," J. Zhang, L. Wang, B. Zhang, H. Zhao, U. Kolb, Y. Zhu, L. Liu, Y. Han, G. Wang, C. Wang, D. Su, B. C. Gates, and F.-S. Xiao, *Nat. Catal.*, in press (2018).

(XXXVI) "Supported Cluster Catalysts Synthesized to be Small, Simple, Selective, and Stable," E. Guan, C.-Y. Fang, D. Yang, L. Wang, F.-S. Xiao, and B. C. Gates, *Faraday Discuss.*, in press (2018).

Complexity in catalysis through the lens of large scale molecular simulations

Vassiliki-Alexandra Glezakou and Roger Rousseau
Pacific Northwest National Laboratory, Richland WA 99354

Presentation Abstract

Advances in theory, computational algorithms and computer hardware have opened the window to *ab initio* molecular dynamics (AIMD), combined with enhanced sampling techniques, to discover and track novel phenomena resulting from chemical complexity. Nowhere is this more needed than in catalysis, where models including support materials, catalysts, reactants, and products need to be studied together at experimentally relevant temperatures and pressures. Global and local anharmonicities on the potential energy surface can lead to unanticipated phenomena that often go unaccounted for in many theoretical studies. Theory and simulation can inherently access atomic level details that can help us trace these intricacies. In this presentation, we will illustrate the capabilities of modern computational methods with examples drawn from the chemistry of metal particles on reducible supports, Brønsted acid chemistry in confined spaces and reactivity at solid-liquid interfaces.

In the context of metal nanoparticles supported on reducible metal oxides (such as TiO₂, CeO₂, and RuO₂), we have found that a strong coupling between the redox state of the support and the redox properties of the nanoparticle induces unique catalytic processes including the dynamic formation of transient catalytic single atoms. Similar methods can be used to investigate the confinement effect in zeolites and its effects on the free energetics of acid catalysis in confined media. Finally, as we consider catalysis at solid-liquid interfaces, we find that competitive adsorption of species leads to an interfacial layer that is appreciably different in speciation and dynamic time scales from the bulk liquid. Comparison with detailed experimental studies is provided for each of these systems confirming the discoveries.

Grant or FWP Number: Low-Temperature Catalytic Routes for Energy Carriers via Spatial and Chemical Organization, 47319

PI: Johannes Lercher

Fabrication of Nano-Structured Catalyst Supports by ALD

R. J. Gorte
Chemical & Biomolecular Engineering
University of Pennsylvania
Philadelphia, PA 19104

Interactions between a transition-metal catalyst and its support can strongly alter the stability and activity of the catalyst. Important examples include support effects with ceria and the so-called “Intelligent Catalysts” in which the metal can be redispersed by reversible ex-solution from a perovskite lattice. However, the surface areas of these functional supports are often too low or unstable; and, in the case of perovskites, the length scales for ingress and egress may be too long to take advantage of the effect. We are addressing these issues by depositing very thin films of various functional oxides, ~0.5 to 1-nm thick, onto high-surface-area supports, including Al_2O_3 and MgAl_2O_4 , by Atomic Layer Deposition. We have demonstrated that a wide range of oxides can be deposited as dense, uniform, conformal films on various supports. The films exhibit surprisingly good thermal stability and provide catalytic properties similar to observed with bulk oxides, but with higher surface areas.

DE-FG02-13ER16380: Nano-Structured Catalysts for Improved Oxide-Metal Interactions

Students: Tzia Ming Onn, Chao Lin, Xinyu Mao

RECENT PROGRESS

Smart Pd Catalyst with Improved Thermal Stability Supported on High-Surface-Area LaFeO_3 Prepared by Atomic Layer Deposition:

The concept of self-regenerating or “smart” catalysts, developed to mitigate the problem of supported metal particle coarsening in high-temperature applications, involves redispersing large metal particles by incorporating them into a perovskite-structured support under oxidizing conditions and then exsolving them as small metal particles under reducing conditions. Unfortunately, the redispersion process does not appear to work in practice because the surface areas of the perovskite supports are too low and the diffusion lengths for the metal ions within the bulk perovskite too short. Here, we demonstrate reversible activation upon redox cycling for CH_4 oxidation and CO oxidation for Pd supported on high-surface-area LaFeO_3 prepared as a thin conformal coating on a porous MgAl_2O_4 support using Atomic Layer Deposition (ALD). The LaFeO_3 film, less than 1.5-nm thick, was shown to be initially stable to at least 900 °C. The activated catalysts exhibit stable catalytic performance for methane oxidation after high-temperature treatment.

Improved Coking Resistance of “Intelligent” Ni Catalysts Prepared by Atomic Layer Deposition:

Conformal CaTiO_3 films were deposited onto MgAl_2O_4 by Atomic Layer Deposition (ALD) and then examined as an “intelligent” catalyst support for Ni in the steam and CO_2 reforming of methane. 1-nm CaTiO_3 films were characterized by scanning transmission electron microscopy and XRD and shown to be stable to at least 1073 K. Catalysts with 1- and 20-wt% Ni were studied and it was found that, following calcination at 1073 K, the Ni- $\text{CaTiO}_3/\text{MgAl}_2\text{O}_4$ catalysts required high-temperature reduction to achieve activities comparable to that of their Ni/ MgAl_2O_4 counterparts. However, the CaTiO_3 catalysts exhibited dramatically improved tolerance towards carbon-whisker formation. The carbon content on the 1-wt% Ni catalyst on $\text{CaTiO}_3/\text{MgAl}_2\text{O}_4$ was small even after heating the catalyst in a dry, 10% CH_4 -He mixture at 1073 K for 12 h.

Investigation of the Thermodynamic Properties of Surface Ceria and Ceria-Zirconia Solid Solution Films prepared by Atomic Layer Deposition on Al_2O_3 :

The properties of 20-wt% CeO_2 and 21-wt% $\text{Ce}_{0.5}\text{Zr}_{0.5}\text{O}_2$ films, deposited onto a $\gamma\text{-Al}_2\text{O}_3$ by Atomic Layer Deposition (ALD), were compared to bulk $\text{Ce}_{0.5}\text{Zr}_{0.5}\text{O}_2$ and $\gamma\text{-Al}_2\text{O}_3$ -supported samples on which 20-wt% CeO_2 or 21-wt% $\text{CeO}_2\text{-ZrO}_2$ were deposited by impregnation. Following calcination to 1073 K, the ALD-prepared catalysts showed much lower XRD peak intensities, implying that these samples existed as thin films, rather than larger crystallites. Following the addition of 1-wt% Pd to each of the supports, the ALD-prepared samples exhibited much higher rates for CO oxidation due to better interfacial contact between the Pd and ceria-containing phases. The redox properties of the ALD samples and bulk $\text{Ce}_{0.5}\text{Zr}_{0.5}\text{O}_2$ were measured by determining the oxidation state of the ceria as a function of the $\text{H}_2:\text{H}_2\text{O}$ ratio using flow titration and coulometric titration. The 20-wt% CeO_2 ALD film exhibited similar thermodynamics to that measured previously for a sample prepared by impregnation. However, the sample with 21-wt% $\text{Ce}_{0.5}\text{Zr}_{0.5}\text{O}_2$ on $\gamma\text{-Al}_2\text{O}_3$ reduced at a much higher P_{O_2} and showed evidence for transition between the $\text{Ce}_{0.5}\text{Zr}_{0.5}\text{O}_2$ and $\text{Ce}_{0.5}\text{Zr}_{0.5}\text{O}_{1.75}$ phases.

Stabilization of ZrO_2 Powders by ALD of CeO_2 and ZrO_2 :

ZrO_2 powders were modified by Atomic Layer Deposition (ALD) with CeO_2 and ZrO_2 , using $\text{Ce}(\text{TMHD})_4$ and $\text{Zr}(\text{TMHD})_4$ as the precursors, in order to determine the effect of ALD films on the structure, surface area, and catalytic properties of the ZrO_2 . Growth rates were measured gravimetrically and found to be 0.017 nm/cycle for CeO_2 and 0.031 nm/cycle for ZrO_2 . Addition of 20 ALD cycles of either CeO_2 or ZrO_2 was found to stabilize the surface area of the ZrO_2 powder following calcination to 1073 K and to suppress the tetragonal-to-monoclinic transition. Shrinkage of ZrO_2 wafers was also suppressed by the ALD films. When used as a support for Pd in CO oxidation, the CeO_2 -modified materials significantly enhanced rates due to interactions between the Pd and the CeO_2 .

Atomic Layer Deposition on Porous Materials: Problems with Conventional Approaches to Catalyst and Fuel Cell Electrode Preparation:

Atomic Layer Deposition (ALD) offers exciting possibilities for controlling the structure and composition of surfaces on the atomic scale in heterogeneous catalysts and Solid Oxide Fuel Cell (SOFC) electrodes. However, while ALD procedures and equipment are well developed for applications involving flat surfaces, the conditions required for ALD in porous, high-surface-area

materials need to be very different. The materials that are of interest for catalytic applications will also be different. For flat surfaces, rapid cycling, enabled by high carrier-gas flow rates, is necessary in order to rapidly grow thicker films. By contrast, ALD films in porous materials rarely need to be more than 1 nm thick. Elimination of diffusion gradients, efficient use of precursors, and ligand removal with less reactive precursors are the major factors that need to be controlled. In this work, we developed criteria for successful use of ALD in porous materials.

Publications Acknowledging this Grant in 2015-2018

Exclusively funded by this grant (for RJG)

1. Lin, C.; Jang, J.-B.; Zhang, L.; Stach, E. A.; Gorte, R. J. Improved Coking Resistance of “Intelligent” Ni Catalysts Prepared by Atomic Layer Deposition, submitted.
2. Onn, T. M.; Kungas, R.; Fornasiero, P.; Huang, K.; Gorte, R. J. Atomic Layer Deposition on Porous Materials: Problems with Conventional Approaches to Catalyst and Fuel Cell Electrode Preparation, *Inorganics*, **2018**, *6*, 34.
3. Onn, T. M.; Monai, M.; Dai, S.; Fonda, E. Montini, T.; Pan, X.Q.; Graham, G. W.; Fornasiero, P.; Gorte, R. J. Smart Pd Catalyst with Improved Thermal Stability Supported on High-Surface-Area LaFeO₃ Prepared by Atomic Layer Deposition, *J. Amer. Chem. Soc.*, **2018**, *140*, 4841-48.
4. Onn, T. M.; Mao, X.; Lin, C.; Wang, C.; Gorte, R. J. Investigation of the Thermodynamic Properties of Surface Ceria and Ceria-Zirconia Solid Solution Films prepared by Atomic Layer Deposition on Al₂O₃, *Inorganics*, **2017**, *5*, 69.
5. Lin, C.; Mao, X.; Onn, T. M.; Jang, J.-B.; Gorte, R. J. Stabilization of ZrO₂ Powders by ALD of CeO₂ and ZrO₂, *Inorganics*, **2017**, *5*, 65.
6. Onn, T. M.; Dai, S.; Chen, J.; Pan, X.Q.; Graham, G. W.; Gorte, R. J. High-surface area Ceria-Zirconia Films Prepared by Atomic Layer Deposition, *Catalysis Letters*, **2017**, *147*, 1465-70.
7. Onn, T. M.; Monai, M.; Dai, S.; Arroyo-Ramirez, L.; Zhang, S.; Ye, X.; Pan, X.Q.; Graham, G. W.; Fornasiero, P.; Gorte, R. J. High-Surface-Area, Iron-Oxide Films Prepared by Atomic Layer Deposition on γ -Al₂O₃, *Applied Catalysis A* **2017**, *534*, 70-77.
8. Onn, T. M.; Zhang, S.; Arroyo-Ramirez, L.; Ye, X.; Wang, C.; Pan, X. Q.; Graham, G. W.; Gorte, R. J. High-Surface-Area Ceria Prepared By ALD on Al₂O₃ Support, *Applied Catalysis B*, **2017**, *201*, 430-437.
9. Onn, T. M.; Zhang, S.; Arroyo-Ramirez, L.; Chung, Y.-C.; Graham, G. W.; Pan, X. Q.; Gorte, R. J. Improved Thermal Stability and Methane-Oxidation Activity of Pd/Al₂O₃ Catalysts by Atomic Layer Deposition of ZrO₂, *ACS Catalysis*, **2015**, *5*, 5696-5701.
10. Arroyo-Ramirez, L.; Chen, C.; Cargnello, M.; Murray, C. B.; Gorte, R. J. A Comparison of Hierarchical Pt@CeO₂/Si-Al₂O₃ and Pd@CeO₂/Si-Al₂O₃, *Catalysis Today*, **2015**, *253*, 137-141.
11. Cargnello, M.; Chen, C.; Diroll, B.; Doan-Nguyen, V.; Gorte, R. J.; Murray, C. B. Efficient Removal of Organic Ligands From Supported Nanocrystals by Fast Thermal Annealing Enables Catalytic Studies on Well Defined Active Phases, *Journal of the American Chemical Society*, **2015**, *137*, 6906-11.
12. Cargnello, M.; Sala, D.; Chen, C.; D’Arienzo, M.; Gorte, R. J.; Murray, C. B. Structure, morphology and catalytic properties of pure and alloyed Au-ZnO hierarchical nanostructures, *RSC Advances*, **2015**, *5*, 41920-33.

Tailoring surface oxygen affinity for selective reduction reactions

Lars C. Grabow, Sashank Kasiraju, Yuying Song, Purnima Kharidehal, Xiao Li
University of Houston, Chemical and Biomolecular Engineering, Houston, TX

Presentation Abstract

The selective reduction or catalytic upgrade of small oxygenated compounds from bio-oil is often as challenging as the selective oxidation of hydrocarbons. While complete reduction is feasible, it requires excess hydrogen, and thus, fares unfavorable in techno-economic analyses. Through extensive computational studies and close collaborations with experimental groups we propose that by controlling the oxygen affinity of metal or metal-oxide surfaces the catalytic yield towards partially reduced products can be significantly improved. In particular, molybdenum-oxide can be promoted with transition metals to improve the kinetics and thermodynamics of oxygen vacancy formation akin to cobalt and nickel promotion of molybdenum-sulfide for hydrodesulfurization catalysis. Alloying copper with palladium creates catalytic sites that combine the activity of palladium with the selectivity of copper for the selective dehydrogenation of small primary alcohols as required for the Guerbet coupling reaction. Similarly, the oxygen affinity of palladium-based catalysts can be increased with indium to create bifunctional reduction sites that boost the rate of nitrate reduction. In all three examples the catalytic performance is attributed to the existence of sites with dual functionality and optimized oxygen affinity that stabilizes a key reaction intermediate.

DE-SC0011983: Unifying principles for catalytic hydrotreating processes

Postdoc(s): Purnima Kharidehal, Unmesh Menon

Student(s): Sashank Kasiraju, Xiao Li

RECENT PROGRESS

Transfer of catalyst optimization strategies from hydrodesulfurization to hydrodeoxygenation

Molybdenum-oxide (MoO_3) is a promising catalyst candidate for hydrodeoxygenation (HDO) of pyrolysis vapor or liquefaction products to renewable fuels or value-added chemicals. We used density functional theory to study the mechanism and active site requirements for HDO of furan over the $\text{MoO}_3(010)$ facet and contrast our results with prior work on hydrodesulfurization (HDS) of thiophene over MoS_2 model catalysts. Using a constrained *ab-initio* thermodynamic approach we find that surface or subsurface hydroxyls are available on $\text{MoO}_3(010)$ under reaction conditions of high hydrogen and water partial pressure, but the concentration of oxygen defect sites needed

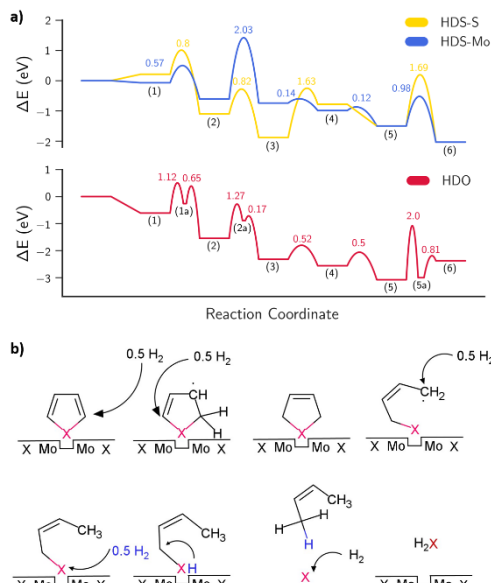


Figure 3 Hydrotreating mechanisms. (a) PED comparing HDS on thiophene on the S (yellow) and Mo (blue) edge of MoS₂, and HDO of furan (red) on MoO₃(010). (b) Schematic representation of intermediates that form during the HDO of furan and HDS of thiophene.

formation can be optimized for HDO applications. An excessive increase in surface reducibility, however, could lead to the loss of C-O bond cleavage ability and rigorous optimization of the type and concentration of promoter atoms will be needed to strike the right balance between vacancy formation and C-O bond scission activity. Overall, this work sheds some light on the atomic similarities exhibited by the well-studied S-edge of MoS₂ and MoO₃(010) for hydrotreating reactions. Through the identification of such analogies between related catalytic systems we expect to derive universal design principles for hydrotreating catalysts such that the future discovery of improved catalytic materials for hydrotreating processes will be greatly accelerated.

Selectivity tuning over bimetallic (de-)hydrogenation catalysts

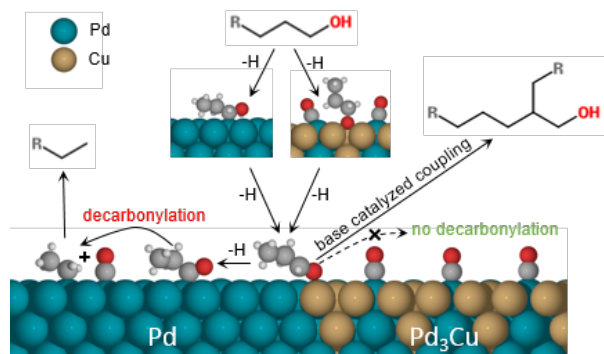


Figure 4 Simplified reaction scheme for Guerbet coupling over Pd and Pd₃Cu catalysts.

to catalyze the deoxygenation steps is limited. Despite the structural differences between MoO₃ and MoS₂, we find that the reaction mechanisms for HDO of furan over MoO₃(010) and HDS of thiophene on the S-edge of MoS₂ follow a similar sequence of elementary steps (Figure 1). Moreover, the C-O/C-S cleavage and ring opening reactions are facile on vacancy defect sites once they are formed.

As reported for the S-edge of MoS₂, the MoO₃(010) surface is also resistant to surface reduction with hydrogen, due to its inability to catalyze H₂ activation and the endothermic defect formation enthalpy. In HDS catalysis, this is remedied by transition metal promotion of MoS₂, and we were able to adopt this strategy for MoO₃(010) surfaces. The incorporation of promoter metals such as Fe, Co, Ni, Cu and Zn in the top surface layer of MoO₃(010) greatly improves the thermodynamic tendency to form O defects, even in the absence of hydrogen atmosphere at 673 K. At the same time, these surface modifications also lower the activation barrier for H₂ splitting, suggesting that the rate of vacancy

The efficacy of tandem dehydrogenation–condensation catalysts for the upgrade of bio-derived intermediates is largely determined by their relative (de-)hydrogenation and decarbonylation activity (Figure 2). For example, the Guerbet and aldol condensation reactions are of interest since they allow for C–C bond formation and give higher molecular weight oxygenates. An initial study identified Pd-supported on hydrotalcite as an active catalyst for the transformation, although this catalyst showed extensive undesirable decarbonylation. A catalyst containing Pd and Cu in a 3:1 ratio dramatically decreased decarbonylation, while preserving the high catalytic rates seen with Pd-

based catalysts. We explain this phenomenon by proposing a segregated Pd₃Cu surface model with a Cu-rich surface, consistent with a combination of experimental characterization techniques, including XRD, EXAFS, TEM, CO chemisorption and TPD.

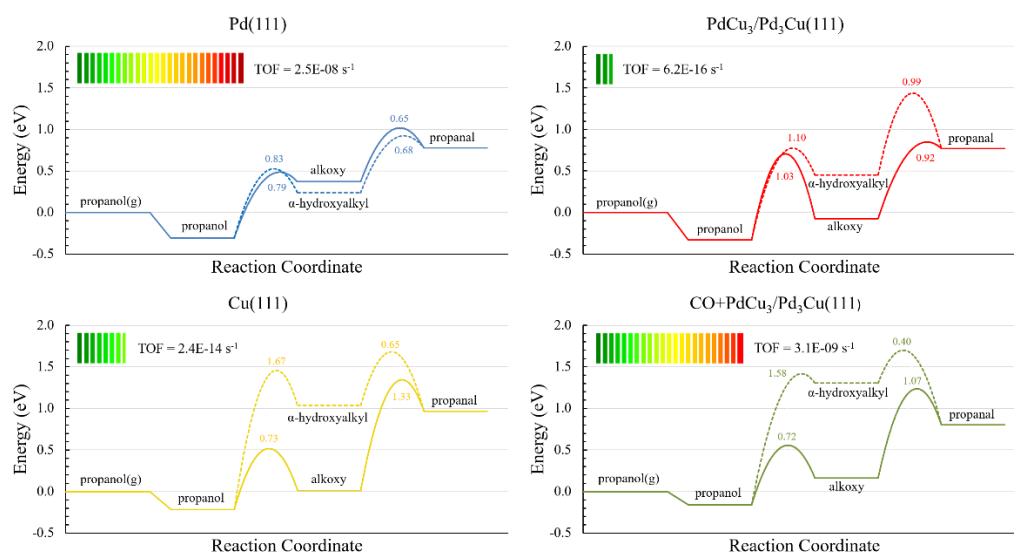


Figure 5 Potential energy diagrams for the metal catalyzed sequential dehydrogenation of propanol to propanal. The solid lines correspond to the O-bound alkoxy intermediate ($\text{CH}_3\text{CH}_2\text{CH}_2\text{O}$), whereas the dashed lines refer to the stability of the C-bound α -hydroxyalkyl intermediate ($\text{CH}_3\text{CH}_2\text{CHOH}$). The horizontal bar illustrates a turnover frequency (TOF) estimate in logarithmic scale from a microkinetic model at 503 K, 0.9 bar propanol, and 0.1 bar CO.

Density functional theory and kinetic modeling studies suggest that the surface segregation of Cu atoms in the bimetallic alloy catalyst produces Cu sites with increased reactivity, while the Pd sites responsible for unselective decarbonylation pathways are selectively poisoned by CO (Figure 3, bottom right panel). The formation of the Pd₃Cu alloy raises the d-band center of Cu significantly, leading to increased reactivity of Cu for the dehydrogenation reaction, but does not provide favorable binding sites for decarbonylation intermediates that bind through their carbon atoms. The suppression of the decarbonylation reaction is consistent with the high selectivity toward the base-catalyzed Guerbet and ABE (acetone, butanol, ethanol) coupling reactions observed experimentally. Thus, even with large excess of Pd in the catalyst, the catalytic centers are surface Cu atoms with a modified electronic structure due to interactions with Pd.

Selectivity control can also be achieved using the PdCu nanocluster size. Smaller nanoparticles favor the C–CO bond scission step of the decarbonylation reaction, due to the stronger binding of CO and alkyl species to sites of lower coordination. CO-induced segregation of reactive Pd atoms to under-coordinated step/edge sites also amplifies the geometric effect on the catalytic behavior.

Insights into nitrate reduction over indium-decorated palladium nanoparticles

Nitrate (NO_3^-) is an ubiquitous groundwater contaminant, and is detrimental to human health. Bimetallic palladium-based catalysts have been found to be promising for treating nitrate (and nitrite, NO_2^-) contaminated waters. Those containing indium (In) are unusually active, but the mechanistic explanation for catalyst performance remains largely unproven. We report that In deposited on Pd nanoparticles (NPs) show room-temperature nitrate catalytic reduction activity that varies with volcano-shape dependence on In surface coverage. The most active catalyst had

an In surface coverage of 40%, with a pseudo-first order normalized rate constant of $k_{cat} \sim 7.6 \text{ L g}_{\text{surface-metal}}^{-1} \text{ min}^{-1}$, whereas monometallic Pd NPs and In_2O_3 have nondetectable activity for nitrate reduction. X-ray absorption spectroscopy (XAS) results indicated that In is in oxidized form in the as-synthesized catalyst; it reduces to zerovalent metal in the presence of H_2 and re-oxidizes following NO_3^- contact. Selectivity in excess of 95% to nontoxic N_2 was observed for all the catalysts.

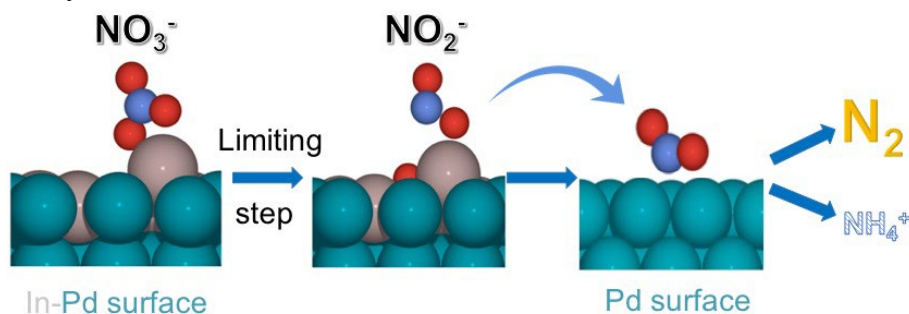


Figure 6 Schematic representation of the proposed bifunctional mechanism for nitrate reduction over In-decorated Pd nanoparticles.

DFT simulations and a lumped kinetic model showed that small In ensembles with high oxygen affinity strongly favor nitrate reduction and can remain reduced via hydrogen spillover from adjacent Pd sites, while the reduction of large In ensembles is prohibitively difficult, which is in agreement with the experimentally observed In-dependent volcano-shaped activity. A Bader charge analysis indicated an increase in oxidation of In atoms during the nitrate reduction reaction and is consistent with *in situ* XANES experiments which showed oxidation of In in nitrate solution. Based on the experimental and computational evidence, we propose a mechanism in which In oxidatively adsorbs nitrate, while Pd activates hydrogen to further reduce formed nitrite and to regenerate In sites (Figure 4). This improved understanding of the In active site expands the prospects of improved denitrification using metal-on-metal catalysts.

Publications Acknowledging this Grant in 2015-2018

(I) *Exclusively funded by this grant;*

1. Kasiraju, S.; Grabow, L. C. Learning from the Past: Are Catalyst Design Principles Transferrable between Hydrodesulfurization and Deoxygenation? *AIChE J.* **2018**.

(II) *Jointly funded by this grant and other grants with leading intellectual contribution from this grant;*

2. Nelson, R. C.; Baek, B.; Ruiz, P.; Goundie, B.; Brooks, A.; Wheeler, M. C.; Frederick, B. G.; Grabow, L. C.; Austin, R. N. Experimental and Theoretical Insights into the Hydrogen-Efficient Direct Hydrodeoxygenation Mechanism of Phenol over Ru/TiO₂. *ACS Catal.* **2015**, 5 (11), 6509–6523.
3. Goulas, K. A.; Sreekumar, S.; Song, Y.; Kharidehal, P.; Gunbas, G.; Dietrich, P. J.; Johnson, G. R.; Wang, Y. C.; Grippo, A. M.; Grabow, L. C.; et al. Synergistic Effects in

Bimetallic Palladium–Copper Catalysts Improve Selectivity in Oxygenate Coupling Reactions. *J. Am. Chem. Soc.* **2016**, *138* (21), 6805–6812.

4. Omotoso, T. O.; Baek, B.; Grabow, L. C.; Crossley, S. P. Experimental and First-Principles Evidence for Interfacial Activity of Ru/TiO₂ for the Direct Conversion of m-Cresol to Toluene. *ChemCatChem* **2017**, *9* (14), 2642–2651. Featured on the journal cover.
5. Goulas, K. A.; Song, Y.; Johnson, G. R.; Chen, J. P.; Gokhale, A. A.; Grabow, L. C.; Toste, F. D. Selectivity Tuning over Monometallic and Bimetallic Dehydrogenation Catalysts: Effects of Support and Particle Size. *Catal. Sci. Technol.* **2018**, *8* (1), 314–327.
6. Guo, S.; Heck, K.; Kasiraju, S.; Qian, H.; Zhao, Z.; Grabow, L. C.; Miller, J. T.; Wong, M. S. Insights into Nitrate Reduction over Indium-Decorated Palladium Nanoparticle Catalysts. *ACS Catal.* **2018**, *8* (1), 503–515.

(III) *Jointly funded by this grant and other grants with relatively minor intellectual contribution from this grant;*

7. Ghorbanpour, A.; Gumidyala, A.; Grabow, L. C.; Crossley, S. P.; Rimer, J. D. Epitaxial Growth of ZSM-5@Silicalite-1: A Core–Shell Zeolite Designed with Passivated Surface Acidity. *ACS Nano* **2015**, *9* (4), 4006–4016.
8. Shuai, J.; Yoo, H. D.; Liang, Y.; Li, Y.; Yao, Y.; Grabow, L. C. Density Functional Theory Study of Li, Na, and Mg Intercalation and Diffusion in MoS₂ with Controlled Interlayer Spacing. *Mater. Res. Express* **2016**, *3* (6), 064001.

Oliver Y. Gutierrez-Tinoco

Mechanism and energetic landscapes of acid-catalyzed alcohol dehydration in condensed phases: towards understanding confinement and solvent effects

Oliver Gutiérrez-Tinoco, Jian Zhi Hu, Andreas Jentys, Mirosław Derewinski, John Fulton, Donghai Mei, Donald M. Camaioni, Johannes A. Lercher
Pacific Northwest National Laboratory

Presentation Abstract

Dehydration of biomass-derived molecules (e.g., ethanol, sugars, polyols and cyclic alcohols) is key to the production of transportation fuels and valuable chemical intermediates; it eliminates oxygen without H₂ consumption (as opposed to metal-catalyzed hydrodeoxygenation and hydrogenolysis) and carbon loss. Herein, we employ rigorous kinetic measurements, calorimetric and adsorption measurements, and density functional theory calculations to understand the nature of the active site, the reaction mechanism and the energy landscape for the dehydration of cyclic alcohols (from reduction of lignin-derived phenolics) in aqueous phase at conditions relevant to biomass upgrading. A variety of acid catalysts have been studied, ranging from homogeneous acids (organic, inorganic) to solid acids (zeolites in particular) with uniform and well-defined acid site structures and a relatively high structural fidelity during reactions in hot liquid water. Differences of more than two orders of magnitude are observed that are attributed to pore confinement rather than acid strength. The results show that the activity (rate normalized to number of acid sites) varies inversely with the size of pore opening (0.55 to 0.74 nm). A complete description of the energy diagram will be furnished and the factors giving rise to these differences will be discussed based on measured enthalpies and entropies of adsorption and activation.

FWP Number 47319: Low-Temperature Catalytic Routes for Energy Carriers via Spatial and Chemical Organization

PI: Johannes Lercher

Postdoc: Hui Shi, Feng Chen

Student: Meng Wang

The Rational Design of Improved Base Metal Catalysts for Carbon Dioxide Valorization and Hydrogen Production

Wesley H. Bernskoetter and Nilay Hazari
University of Missouri; Yale University

Presentation Abstract

The development of catalysts for the conversion of carbon dioxide into more valuable compounds is an important goal due to the potential of this greenhouse gas as a readily available, sustainable, non-toxic, and inexpensive source of carbon. Formic acid and methanol are especially promising targets for the catalytic conversion of carbon dioxide. Both are valuable commodity chemicals, which are synthesized on a large scale, and could also be used as materials for chemical hydrogen storage. Improved catalysts are required for both the hydrogenation of carbon dioxide to formic acid or methanol and also the reverse dehydrogenation of formic acid or methanol to generate hydrogen. In this poster our ongoing research into the development of improved base metal catalysts for these processes and some associated reactions involving carbon dioxide are summarized. This includes: (1) Efforts to design more active catalysts through the modification of the ancillary ligand to increase the lifetime of the catalyst; (2) kinetic studies using stopped-flow to understand the mechanism of CO₂ insertion into a variety of metal-element σ-bonds; and (3) kinetic studies to elucidate the effects of proton shuttles on hydrogen addition and elimination from base metal complexes.

DE-SC0018222: Elucidating the Role of Lewis Acid Co-Catalysts in Base Metal Promoted CO₂ Hydrogenation and Related Processes

Postdoc(s): Upul Jayarathne (Missouri)

Student(s): Julia Curley (Yale); Jessica E. Heimann (Yale); Elizabeth M. Lane (Missouri); Nicholas E. Smith (Yale).

RECENT PROGRESS

Research progress towards the design of more efficient catalysts for reversible base metal catalyzed CO₂ hydrogenation and related reactions is summarized below for selected areas.

1) Ancillary ligand modification

Exploring the effect of isonitrile ancillary ligands on iron pincer catalysts

We have been investigating iron complexes ligated by the bifunctional ligand HN(CH₂CH₂PR₂)₂ (R^{Pr}PN^HP, R= ⁱPr or Cy) for CO₂ hydrogenation and formic acid dehydrogenation (FADH). We demonstrated that for FADH the iron formate complex (ⁱPrPN^HP)Fe(H){OC(O)H}(CO) achieves almost 1,000,000 turnovers (TON) with the addition of a Lewis acid (LA) co-catalyst. The related precatalyst (ⁱPrPNP)Fe(H)(CO) (ⁱPrPNP = N(CH₂CH₂PⁱPr₂)₂⁻) gives a TON of almost 9,000 for CO₂ hydrogenation to formate in the presence of a LA co-catalyst and base (Figure 1a-c). In both cases these are some of the highest TONs observed for first-row transition metal systems. Subsequently,

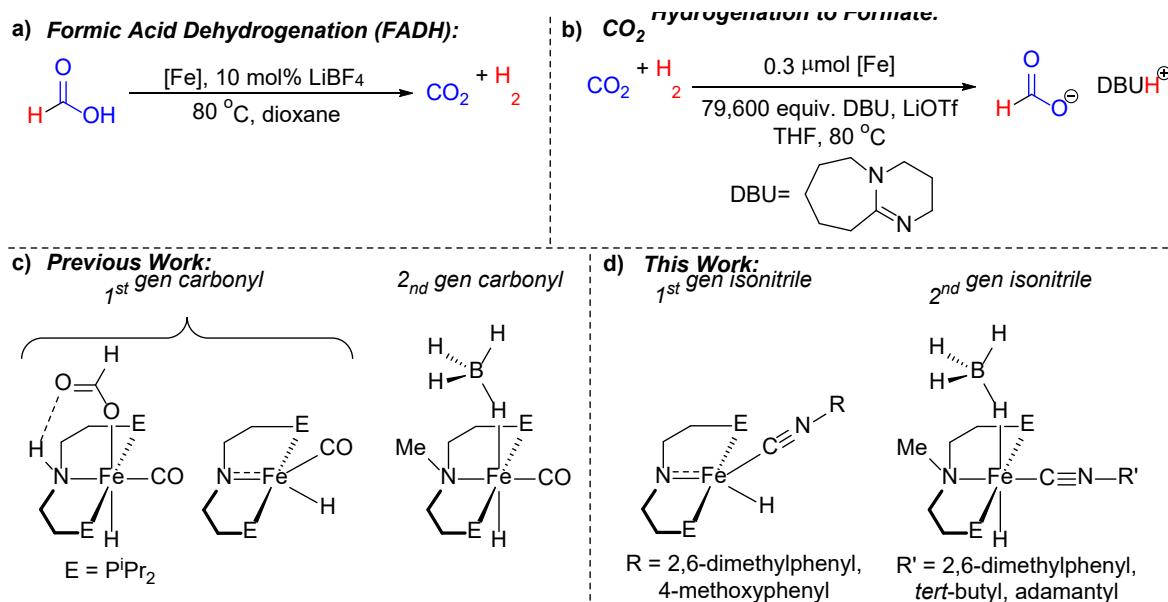


Figure 1: a) Formic acid dehydrogenation (FADH), b) CO₂ hydrogenation to formate, c) Previous PNP iron catalysts studied by our groups, and d) complexes studied in this work. Conditions are standard for 1st generation systems.

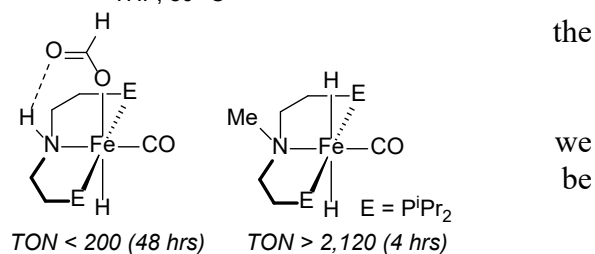
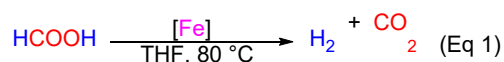
we developed 2nd generation systems in which the bifunctional PNP ligand was replaced with a PNP ligand containing a tertiary amine. Complexes of the form (^RPN^{Me}P)Fe(H)(HBH₃)(CO) (^RPN^{Me}P = CH₃N(CH₂CH₂PR₂)₂, R = ⁱPr or Cy) are an order of magnitude more productive for CO₂ hydrogenation to formate than their 1st generation analogues, affording 60,000 TON in the presence of a LA co-catalyst and base (Figure 1b-c). However, in both the 1st and 2nd generation systems, catalyst decomposition is a major issue, which needs to be addressed in order to develop improved systems.

One strategy to prevent catalyst decomposition is to modify the ancillary ligands around the iron. In particular, the replacement of a carbonyl ligand with an isonitrile ligand provides potential benefits because of the tunable steric and electronic properties of isonitriles. In recent work we have synthesized both 1st and 2nd generation systems with alkyl and aryl isonitrile ancillary ligands instead of carbonyl ligands (Figure 1d). All of these complexes are active catalysts for CO₂ hydrogenation to formate but show decreased activity compared to the 1st generation catalysts. The 2nd generation isonitrile supported species are approximately one order of magnitude more active than 1st generation isonitrile supported species for CO₂ hydrogenation, which suggests that the tertiary amide substituted pincer ligand promotes this reaction. We propose that this is because release of formate from the catalyst is easier for tertiary amide systems because they do not form hydrogen bonding interactions with formate. Further work, will look to investigate alternative substituents on the tertiary amide and explore stronger π-donor ligands such as NO⁺. In preliminary work we have already prepared a number of iron complexes supported by ⁱPrPN^HPhP (ⁱPrPN^HPhP = PhN(CH₂CH₂PⁱPr)₂) ligands.

Tertiary amide containing systems for FADH

The iron formate complex, (ⁱPrPN^HP)Fe(H){OC(O)H}(CO), requires a LA co-catalyst to achieve almost 1,000,000 turnovers (TON) for FADH. This is because the LA is required to assist in the

turnover limiting decarboxylation of the iron formate. We hypothesized that the hydrogen bonding interaction between the N-H group of pincer ligand and the formate ligand makes formate decarboxylation more challenging. By replacing the N-H group with a N-Me group, we postulated that formate decarboxylation would be more facile and that a LA co-catalyst would no longer be required for catalysis. Preliminary experiments indicate that our 2nd generation systems are far more active than our 1st generation systems for FADH in the absence of a LA co-catalyst (Eq 1). Further research will be performed to optimize this reaction and also develop systems that can operate in more concentrated formic acid solutions.



Non-pincer supported systems for CO₂ hydrogenation and FADH

Even though our iron pincer complexes are extremely active for CO₂ hydrogenation and FADH, the pincer ligand is expensive and relatively difficult to synthesize. We have been exploring the chemistry of systems which contain cheaper ligands and are synthetically more accessible.

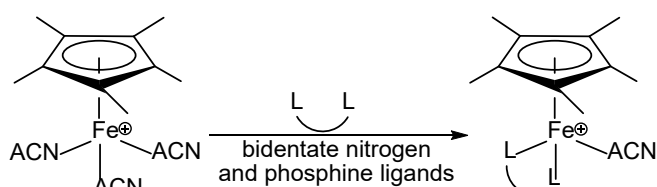


Figure 2: Preparation of iron complexes used for CO₂ hydrogenation and FADH.

Specifically, we are investigating Cp and Cp* supported iron catalysts with bidentate phosphine or nitrogen containing ligands (Figure 2). To date we have shown that using the iron precursors (Cp)Fe(ACN)₃⁺ or (Cp*)Fe(ACN)₃⁺ we can add bidentate nitrogen or phosphine ligands to make our desired complexes. These ligation reactions can be performed either *in situ* or used to generate isolable and well-defined precatalysts. We have demonstrated that some of the complexes we generate using this protocol are active for FADH, as well as for MeOH dehydrogenation. We intend to explore a wide range of bidentate ligands and then perform mechanistic studies on the most active systems.

2) Kinetics of CO₂ insertion into metal-element σ-bonds

Recently, we have been exploring the mechanism of CO₂ insertion into metal hydride bonds using stopped-flow kinetics (see Bernskoetter Abstract). One compound that was evaluated was (PCP)NiH (PCP = 2,6-C₆H₃(CH₂P^tBu₂)₂). It demonstrated that CO₂ insertion into (PCP)NiH was first order with respect to [Ni] and [CO₂] and that the rate of insertion increases as the acceptor number of the solvent increases (Figure 3). Additionally, when the ancillary PCP ligand was modified we showed that more electron rich substituents in the *para*-position of the phenyl backbone of the ligand and less sterically demanding substituents on the phosphine ligands both increased the rate of CO₂ insertion.

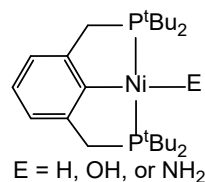


Figure 3: Ni complexes used for stopped-flow studies.

The closely related complexes (PCP)Ni(OH) and (PCP)Ni(NH₂) are also synthetically accessible and insert CO₂ to form the corresponding carbonate and carbamate complexes, respectively. This

allows us to directly compare the kinetics of insertion into a late transition metal hydride, hydroxide, and amide supported by the same ancillary ligand. Using stopped-flow kinetics we were able to show that insertion into (PCP)Ni(OH) and (PCP)Ni(NH₂) is much faster than insertion into (PCP)NiH. In fact, insertion into (PCP)Ni(NH₂) is so fast that we were unable to measure the rate even at low temperature. CO₂ insertion into (PCP)Ni(OH) is first order in [Ni] and [CO₂] but, unlike insertion into (PCP)NiH, there is no correlation between the rate of insertion and the solvent acceptor number. Studies into ligand effects on the rate of insertion into (PCP)Ni(OH) are currently underway.

3) Measuring H₂ addition/release in the presence of proton shuttles

The iron complex (ⁱPrPN^HP)Fe(H){OC(O)H}(CO) is a very active catalyst for methanol dehydrogenation to three equivalents of H₂ and CO₂. The proposed turnover limiting step is 1,2-elimination of H₂ from an iron dihydride species (Figure 4). This reaction is proposed to be facilitated by an equivalent of MeOH, which assists with proton shuttling. However, detailed experimental studies on the role that MeOH plays in this reaction have never been performed. Recently, we developed an experimental setup that enables us to measure the kinetics of 1,2-addition of H₂ to (ⁱPrPNP)Fe(H)(CO), the microscopic reverse process of the 1,2-elimination which occurs in catalysis. Given our ability to measure the kinetics of this reaction we now intend to determine a reaction order in [MeOH] and also probe the ability of higher order alcohols and amines to act as proton shuttles. This will allow us to rationally introduce additives into catalytic reactions.

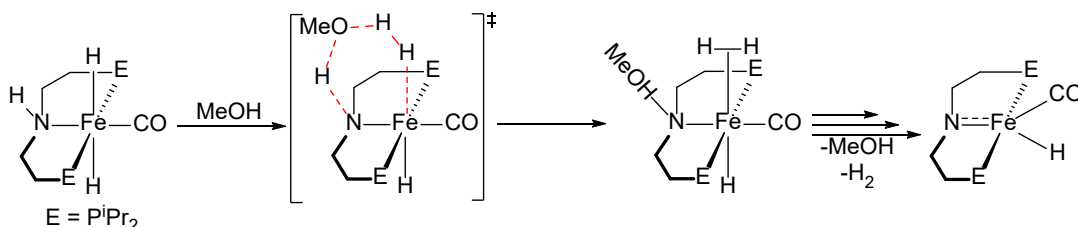


Figure 4: MeOH acts as a proton shuttle to facilitate 1,2-elimination of H₂.

Publications Acknowledging this Grant in 2015-2018

No publications have arisen from this grant to date. However, one publication is submitted:
Heimann, J. E.; Bernskoetter, W. H.; Hazari, N.; Mayer, J. M. 'Acceleration of CO₂ Insertion into Metal Hydrides: Ligand, Lewis Acid, and Solvent Effects on Reaction Kinetics.' Submitted.

Another publication is currently in preparation and will be submitted shortly:

Curley, J. B.; Smith, N. E.; Bernskoetter, W. H.; Hazari, N.; Mercado, B. Q. 'Catalytic Formic Acid Dehydrogenation and CO₂ Hydrogenation Using Iron PN^RP Pincer Complexes with Isonitrile Ligands.' In Preparation.

Performance evaluation of the density-functional tight-binding method for catalysis applications

Ka Hung Lee,^{1,2} Victor Fung,³ De-en Jiang,³ Zili Wu,⁴ and Stephan Irle²

¹Bredesen Center for Interdisciplinary Research and Graduate Education, University of Tennessee, Knoxville, TN 37996; ²Computational Sciences and Engineering Division, Oak Ridge National Laboratory, Oak Ridge, TN 37831; ³Department of Chemistry, University of California, Riverside, CA 92521; ⁴Chemical Sciences Division, Oak Ridge National Laboratory, Oak Ridge, TN 37831

One of our catalysis program goals is to understand the cooperative interactions of metals with active supports and tailor their catalytic activities and/or reaction pathways. “In vivo” surface reconstruction occurring under the pretreatment and reaction conditions may expose or create novel reactive sites responsible for the experimentally observed catalytic activity, but are difficult to investigate theoretically. First principles-based density functional theory (DFT) investigations are typically limited to model systems containing ~1000 atoms and timescales on the order of ~100 picoseconds, and are therefore limited to the study of idealized model systems, causing disconnect between theory and experiment. DFT methods are ill-equipped to handle nanometer-scale unit cells and longer diffusion time scales required to describe complex interfacial catalyst dynamic processes.

The density-functional tight-binding (DFTB) method [1] is an approximation to DFT that reduces the computational effort by 2-3 orders of magnitude, and is therefore better suited for the purpose of predictive surface transformation processes. For instance, it was used for the prediction of the fullerene formation mechanism [2], the Haeckelite formation mechanism on metal surfaces [3], and the existence of a “sweet spot” for the catalyst oxygen content of carbon nanotube formation [4]. As a starting point, this work aims to predict molecular structures and isomer energies of icosahedral and truncated octahedral clusters of Pt atoms containing up to ~3000 atoms using previously reported DFTB parameters for Pt [5] and investigate the effect of spin polarization. This is the first step toward DFTB-based studies of surface reconstruction processes occurring at Pt-clusters on TiO₂ and SrTiO₃ active support interfaces, paving the way for the design of new metal catalysts on active supports.

Research supported by the U.S. Department of Energy, Office of Science, Basic Energy Sciences, Chemical Sciences, Geosciences, and Biosciences Division. This research is part of FWP ERKCC96: Fundamentals of Catalysis and Chemical Transformations. For a full description of recent progress see the Extended Abstract for ERKCC96.

References

- (1) Cui, Q.; Elstner, M. Density functional tight binding: values of semi-empirical methods in an ab initio era, *Phys. Chem. Chem. Phys.* **2014**, *16*, 14368-14377.
- (2) Saha, B.; Irle, S.; Morokuma, K. Hot giant fullerenes can eject and capture C₂ molecules: QM/MD simulations with constant density, *J. Phys. Chem. C* **2011**, *115*, 22707-22716.
- (3) Wang, Y.; Page, A. J.; Nishimoto, Y.; Qian, H.-J.; Morokuma, K.; Irle, S. Template Effect in the Competition Between Haeckelite and Graphene Growth on Ni(111): Quantum Chemical Molecular Dynamics Simulations, *J. Am. Chem. Soc.* **2011**, *133*, 18837-18842.

- (4) Wang, Y.; Song, W.; Jiao, M.; Wu, Z.; Irle, S. Importance of Oxygen in Single-Walled Carbon Nanotube Growth: Insights from QM/MD Simulations, *Carbon* **2017**, *121*, 292-300.
- (5) Shi, H.; Koskinen, P.; Ramasubramaniam, A. Self-Consistent Charge Density-Functional Tight-Binding Parametrization for Pt-Ru Alloys. *J. Phys. Chem. A* **2017**, *121* (12), 2497–2502.

Positioning Active Sites in Catalytic Materials – From Cooperative Catalysis to Cascade Catalysis in Multicompartment Nanoreactors

Seung Soon Jang,¹ Marcus Weck,² Christopher W. Jones¹
¹Georgia Institute of Technology, ²New York University

Presentation Abstract

At any given moment, the cell is carrying out a large number of non-orthogonal (and competing) catalytic transformations simultaneously. This is made possible by compartmentalizing these transformations and catalysts, thereby shielding them from each other. Currently, synthetic analogs to such chemical reaction diversity do not widely exist, though there is significant interest in one-pot, multistep strategies to supersede intermediate work-up procedures. In particular, synthetic multicompartment systems – where individual catalyst particles are tailored to contain multiple, distinct zones or compartments within a single particle that isolate specific active sites, reagents or reactions - are in their infancy. Furthermore, reports of combining non-orthogonal transformations in one pot have been limited to a few examples, none of them allowing for multiple non-orthogonal and enantioselective transformations. An interdisciplinary research team that can probe all aspects of the design, synthesis and characterization of compartmentalizable, catalyst-containing nanoreactors is exploring this topic from both experimental and theoretical points of view. Our prior work began with the design of cooperative catalysts, where multiple active sites work in tandem on a single substrate to catalyze a reaction, and now focuses on cascade catalysis. In particular, researchers at GT and NYU are developing new platforms for use as multicompartment nanoreactors to support a library of catalysts, both transition metal based and organocatalysts, for tandem or multi-step catalysis. Using these model systems, we seek fundamental principles that can be used to understand and design future classes of supported, cooperative and/or tandem catalysts.

N₂ electroreduction catalysis – design of the near surface environment for enhanced selectivity

Michael J. Janik,¹ Lauren Greenlee,² Julie Renner³

1 -Department of Chemical Engineering, Pennsylvania State University

2 – Department of Chemical Engineering, University of Arkansas

3 – Department of Chemical and Biomolecular Engineering, Case Western Reserve University

Presentation Abstract

The overall research goals of this project are to determine key steps and descriptors for the N₂RR reaction mechanism and predict catalyst/ligand environments that enable highly active and selective N₂RR catalysts. To achieve these goals, the objectives of the proposed research are: (1) to design nitrogenase-inspired short-chain peptide sequences with specific regions of hydrophobicity and pK_a (i.e., protonation/deprotonation as a function of pH), (2) to use the peptides as a platform to control the local surface environment of metal/metal hydroxide film catalysts, and (3) to understand N₂/H₂O adsorption/desorption and electrochemical behavior of the films from a coordinated experimental and theoretical standpoint. We have prepared Fe, Ni, and mixed oxide/hydroxide thin film electrodes, and characterized them with XPS, XRD, and SEM. Peptide-modified Au and Fe₂O₃ electrodes were prepared, and their structure and stability probed in electrolyte environments. Density functional theory studies have examined late transition metals to illustrate kinetic limitations to activity and selectivity, and provide insight into how modifying the near surface region can alter elementary N₂RR electrokinetics.

DE-SC0016529: Peptide Control of Electrocatalyst Surface Environment and Catalyst Structure: A Design Platform to Enable Mechanistic Understanding and Synthesis of Active and Selective N₂ Reduction Catalysts

PI: Lauren Greenlee, **Co-PIs:** Julie Renner, Michael Janik

Student(s): Sergio I. Perez Bakovic (Arkansas), Charles Loney (CWRU), Sharad Maheshwari (PSU)

RECENT PROGRESS

Electrodeposited Catalyst Films: Real-Time Monitoring & Chemical Characterization

Our research over the past year has focused on repeatable synthesis of homogeneous, conformal electrodeposited catalyst films with controlled Fe_xNi_y composition. We have now developed a precise electrodeposition methodology using a quartz crystal microbalance (QCM) platform and an optimized electrode pretreatment procedure that produces highly reproducible films of controlled composition and thickness. The technique allows a complete coating of the underlying gold electrode surface. The QCM platform allows real-time measurement of electrodeposited mass and therefore control of film thickness.

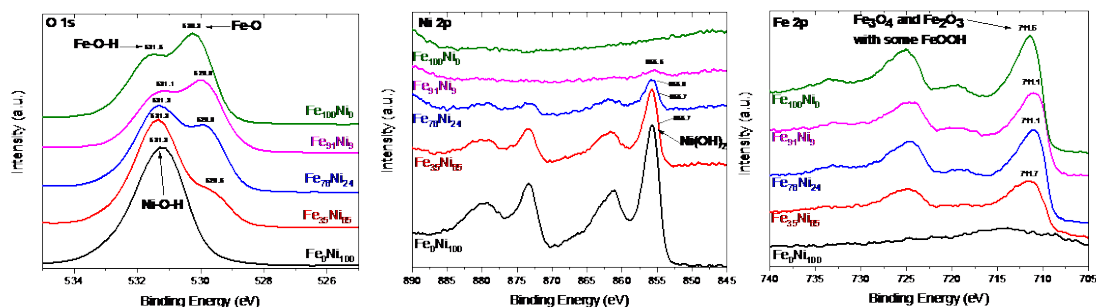


Figure 1. X-ray photoelectron spectroscopy (XPS) is used a primary chemical characterization technique to analyze the surface chemistry of as-synthesized electrodeposited catalyst films. (a) Oxygen 1s binding energy window, (b) nickel 2p binding energy window, and (c) iron 2p binding energy window.

Chemical characterization via x-ray photoelectron spectroscopy (XPS) (Figure 1) has provided detailed information about the chemical composition and speciation of the surface of electrodeposited catalysts. XPS results demonstrate the change in surface chemistry as a function of Fe_xNi_y composition, where the oxygen 1s region is particularly useful in identifying a shift in oxygen chemical environment as the composition of the film changes.

DFT Studies of N_2RR on Late Transition Metals

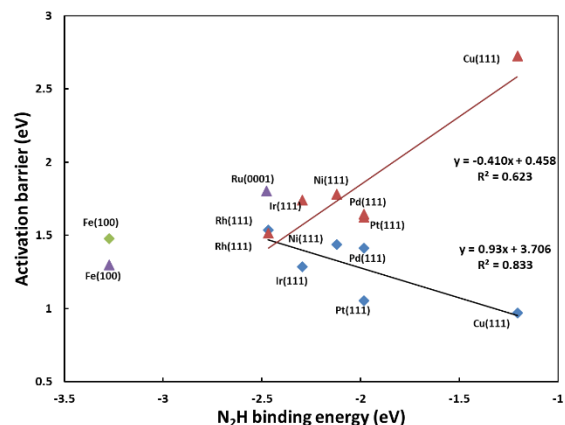


Figure 2. Activation barriers (at 0 V-RHE) for N_2 reduction to N_2H^* (red triangles) and NH^* to NH_2^* (blue diamonds) on close-packed late transition metals show a rough correlation with N_2H^* intermediate binding energy. These correlations results in a “kinetic volcano” with all transition metals having a high barriers requiring large overpotentials. Barriers for Fe(100) (green) and Ru(0001) (purple) are included on the plot, but not in the best fit linear correlations (solid lines).

faradaic efficiency of electrochemical ammonia production by >10X on iron (III) oxide, we discovered using a quartz crystal microbalance (QCM) that 1) that the peptide binds to iron (III) oxide at $\sim 110 \pm 20 \text{ ng/cm}^2$, 2) the thickness of the layer is $1 \pm 0.20 \text{ nm}$ and 3) the peptide layer is stable in 10 mM KOH. Figure 3 shows representative QCM data. Based on the size of the peptide, the QCM analysis reveals that the peptide lays flat in a monolayer at $\sim 85\%$ coverage. We also

Our DFT studies have examined the elementary electrokinetics of N_2 reduction on low index facets of Fe catalysts. By explicitly evaluating all electrokinetic barriers as a function of electrode potential, we have been able to evaluate the reliability of BEP relationships and to estimate kinetic limitations. Key steps have been examined across late transition metals, allowing us to construct the “kinetic volcano” relationship below that illustrates the extreme challenge late transition metals have in surmounting high barriers for the N_2RR . We have also examined how near surface additives (proton transfer agents) can lower these barriers.

Peptide Control of Surface Properties and Selectivity

Over the past year, we have examined the extent that peptides can modulate surface properties of iron (III) oxide and gold. Starting with a peptide that has demonstrated the ability to increase the

were able to characterize the binding affinity (via Scatchard analysis) and chemical nature of the peptide-functionalized iron (III) oxide surface (via XPS), both of which points to a likely chelation with carboxylate groups.

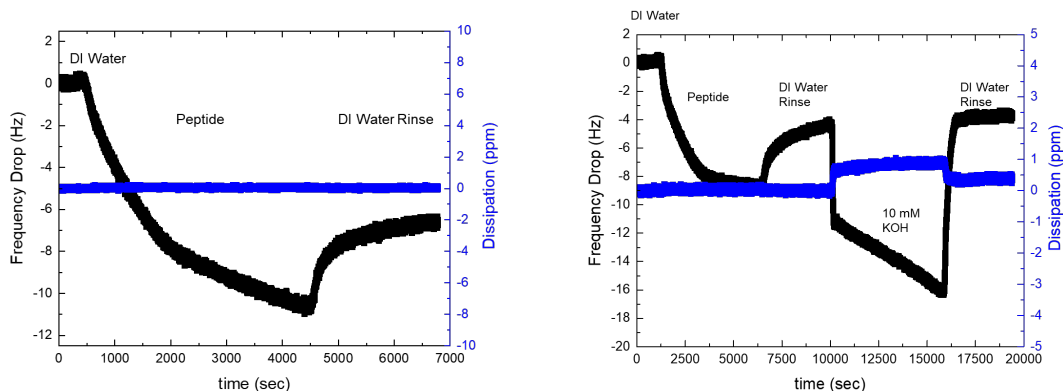


Figure 3: Representative QCM data showing a) peptide binding to iron (III) oxide sensors and b) peptide stability on iron (III) oxide in KOH solution.

Finally, we have studied the ability of a simple tripeptide system to modulate the hydrophobicity of a gold surface and were able to show through contact angle measurements that the system can be used to make the surface significantly more hydrophobic.

Publications Acknowledging this Grant in 2015-2018

I. Exclusively funded by this grant;

1. Greenlee, L.F.; Renner, J.N. Validation of Measurements for Electrocatalytic Ammonia Synthesis from Dinitrogen. *ACS Catalysis*, **2018**, invited viewpoint, submitted.
2. Maheshwari, S.; Rostamikia, G.; Janik, M. J. Elementary kinetics for nitrogen electro-reduction on Fe surfaces. *J. Chem. Phys.* (2018), submitted.

II. Jointly funded by this grant and other grants with leading intellectual contribution from this grant;

3. S.L. Foster, S.I.P. Bakovic, R. Duda, S. Maheshwari, R.D. Milton, S.D. Minter, M.J. Janik, J.N. Renner, L.F. Greenlee. Catalysts for Nitrogen Reduction to Ammonia. *Nature Catalysis* (2018), in press

Transition Metal Activation and Functionalization of C-H and C-C Bonds

William D. Jones
 Department of Chemistry, University of Rochester, Rochester, NY 14450

Presentation Abstract

This project has as its overall goal improvement in the intelligent use of our energy resources, specifically petroleum derived products, and is aimed at the development of new routes for the manipulation of C-H and C-C bonds. During this project period, our research is focused on the following general goals: (1) C-H bond activation reactions in functionalized substrates, including alkylnitriles, ketones, ethers, fluoromethanes, alcohols, and alkynes, and fundamental studies of their effects on metal-carbon bond strengths using trispyrazolylborate-rhodium (TpRh) complexes; (2) Hydrogenation reactions using first-row transition metals; (3) C-CN bond activation in aryl-nitriles and allyl-nitriles; (4) Determination of relative Rh-OR bond strengths; (5) Determination of the lifetime of Tp'Rh(CNR)(σ -alkane) complexes. We have also co-written a report on best practices for benchmarking catalytic reactions, a book chapter on how ligands can affect metal-carbon bond strengths, and a book chapter summarizing the use of pincer-manganese and cobalt complexes for hydrogenation/dehydrogenation reactions.

FG02-86-ER13569: Transition Metal Activation and Functionalization of Carbon-Hydrogen and Carbon-Carbon Bonds

Postdoc(s): Sumit Chakraborty

Student(s): Jing Yuwen, Ahmet Gunay, Yunzhe Jiao, Brett Swartz, Meagan Evans, Lloyd Munjanja

RECENT PROGRESS

The specific accomplishments of the current grant period include:

(1) We have made a breakthrough in our understanding of rhodium-alkoxide bond strengths (eq 1) by the examination of the kinetics and thermodynamics of C-H bond activation in several alcohols such as methanol, ethanol, isopropanol, and t-butanol. This work demonstrates that there is a 1:1 tradeoff between the metal-oxygen bond strength and the hydrogen-oxygen bond strength (Fig. 1). This work was published in *Inorg. Chem.*

$$D_{\text{rel}}(\text{Rh-OR}) = [\Delta H(\text{Rh-OR}) - \Delta H(\text{Rh-Ph})] = \Delta G^\circ + RT \ln(6/\#H) + [\Delta H(\text{RO-H}) - \Delta H(\text{Ph-H})] \quad (1)$$

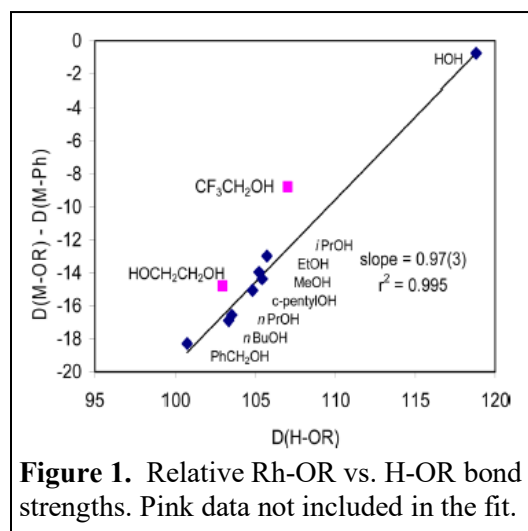
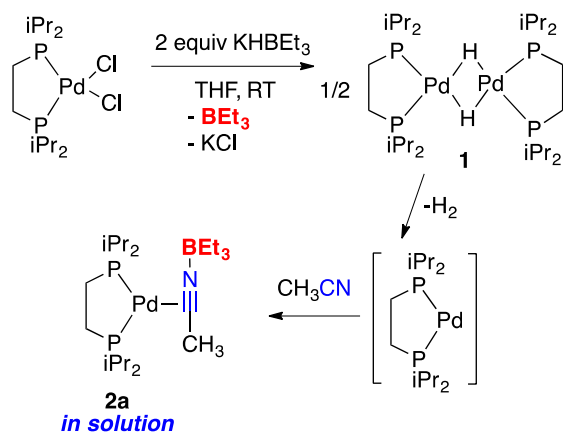


Figure 1. Relative Rh-OR vs. H-OR bond strengths. Pink data not included in the fit.

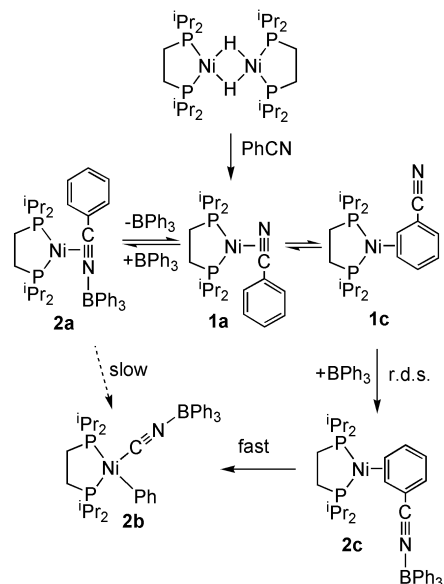
(2) We have published a study of C-C cleavage in acetonitrile and benzonitrile using a palladium-dippe precursor (*Organometallics*). Here, C-CN cleavage occurs with benzonitrile in the presence of BEt_3 as Lewis acid activator (Scheme 1).

(3) We have investigated the use of Lewis acids to assist in the cleavage of C-C bonds using a nickel(0) complex (*SYNLETT*-Special cluster on C-C bond activation) (Scheme 2).

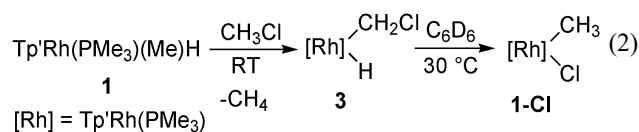
Scheme 1:



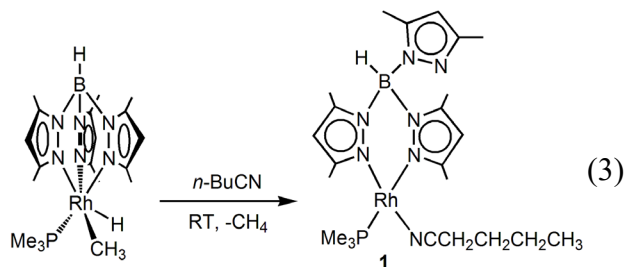
Scheme 2:



(4) We have examined the reaction of MeCl with $\text{Tp}'\text{Rh}(\text{PMe}_3)$, showing that initial C-H activation ultimately leads to C-Cl activation via a methylidene intermediate (eq 2).



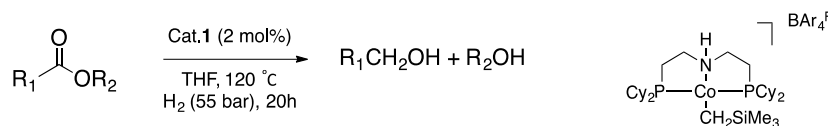
(5) We have demonstrated that $[\text{Tp}'\text{Rh}(\text{PMe}_3)]$ reacts with capronitrile to give the N-bound product, not the methyl C-H activation product as seen with $[\text{Tp}'\text{Rh}(\text{CNneopentyl})]$ (eq 3).



(6) We have published a book chapter on “The Effects of Ancilliary Ligands on Metal-Carbon Bond Strengths,” in *Topics in Organometallic Chemistry: C-H Bond Activation And Catalytic Functionalization* (vol. 56) 2016.

(7) We have investigated the use of a cobalt-PNP catalyst for the hydrogenation of esters (*ACS Catalysis*) (Table 1).

Table 1. Catalytic hydrogenation of esters using the cobalt catalyst 1.^a

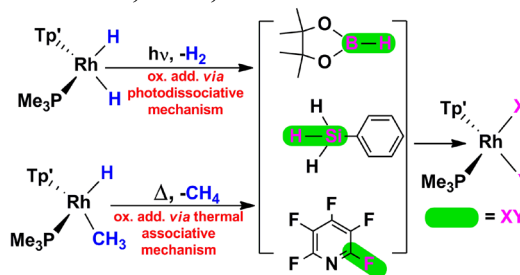


entry	substrate	conv.(%)	product	yield (%) ^b					
1		97	Ph-CH2OH	97	7		91		89
2 ^d		24	Ph-CH2OH	15	8 ^d		100		66 ^c
3		94	Ph-CH2OH	90					35 ^c
4		32	CH3-CH2-CH2OH	30	9 ^d		100		2 ^c
									98 ^c
5		82	CH3-CH2-CH2OH	67	10 ^d		64	MeOH	8
6		45	Cyclohexyl-CH2OH	26	11		0		0

(a) Reaction conditions: substrate (0.5 mmol), catalyst **1** (2 mol%), THF (1.0 mL), H₂ (55 bar), 120 °C, 20 hours. (b) Yields were determined by GC. (c) Product yields are ratios at 100% conversion. Yields of methanol and ethanol are not reported. (d) Toluene was used as solvent.

(8) In a collaborative project with Prof. Robin N. Perutz of the University of York, we examined the reactions of several substrates containing B-H, Si-H, and C-F bonds with various precursors for the [Tp^{*}Rh(PMe₃)] fragment (*J. Am. Chem. Soc.*) (Scheme 4).

Scheme 4: Activation of B-H, Si-H, and C-F bonds

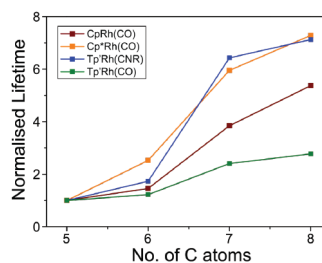


X-Y bond activation favored over C-H bond activation

(9) In collaboration with Mike George (Nottingham) and Mike Hall (Texas A&M) we have examined lifetimes of alkane σ -complexes of Tp^{*}Rh(CNneopentyl)(σ -alkane) (Table 2, Figure 2). The lifetimes vary with the length of the chain, indicating migration.

Table 2. Lifetimes of various alkane σ -complexes **Fig. 2. Plot of lifetime vs. #carbons**

	CpRh(CO) ^d	Cp [*] Rh(CO) ^d	Tp [*] Rh(CNR)	Tp [*] Rh(CO)
<i>c</i> -pentane	5.9 (\pm 0.2)	10.2 (\pm 0.8)	220 (\pm 10)	230 (\pm 10)
<i>c</i> -hexane	8.6 (\pm 0.3)	25.8 (\pm 2.0)	380 (\pm 40)	280 (\pm 15)
<i>c</i> -heptane	22.7 (\pm 0.7)	60.7 (\pm 2.4)	1415 (\pm 50)	550 (\pm 45)
<i>c</i> -octane	31.7 (\pm 0.9)	74.3 (\pm 4.0)	1570 (\pm 70)	640* (\pm 60)



Publications Acknowledging this Grant in 2015-2018

(I) Exclusively funded by this grant:

1. Gunay, A.; Brennessel, W. W.; Jones, W. D. Investigation of C-C Bond Activation of sp^3 C-C Bonds of Acetylene Derivatives via Photolysis of Pt Complexes. *Organometallics* **2015**, *34*, 2233-2239. (DOE)
2. Jiao, Y.; Brennessel, W. W.; Jones, W. D. Oxidative Addition of Chlorohydrocarbons to a Rhodiumtrispyrazolylborate Complex. *Organometallics*, **2015**, *34*, 1552-1566. (DOE)
3. Jiao, Y.; Brennessel, W. W.; Jones, W. D. Nitrile Coordination to Rhodium Does Not Lead to C-H Activation. *Acta Cryst. C*, **2016**, *72*, 850-852. (DOE)
4. Yuwen, J.; Jiao, Y.; Brennessel, W. W.; Jones, W. D. Determination of Rhodium-Alkoxide Bond Strengths in $Tp^*Rh(PMe_3)(OR)H$. *Inorg. Chem.* **2016**, *55*, 9482-9491. (DOE)
5. Yuwen, J.; Chakraborty, S.; Brennessel, W. W.; Jones, W. D. Additive-Free Cobalt-Catalyzed Hydrogenation of Esters to Alcohols. *ACS Catal.* **2017**, *7*, 3735-3740. (DOE).
6. Swartz, B. D.; Brennessel, W. W.; Jones, W. D. Lewis Acid Assisted C-CN Cleavage of Benzonitrile using $[(dippe)NiH]_2$. *SYNLETT*, **2018**, *29*, 747-753. DOI: 10.1055/s-0036-1590801 Special cluster on C-C bond activation. (DOE)

(II) Jointly funded by this grant and other grants with leading intellectual contribution from this grant:

7. Procacci, B.; Jiao, Y.; Evans, M. E.; Jones, W. D.; Perutz, R. N.; Whitwood, A. C. Activation of B-H, Si-H, and C-F bonds with $Tp^*Rh(PMe_3)$: Kinetics, Mechanism and Selectivity. *J. Am. Chem. Soc.* **2015**, *137*, 1258-1272. (DOE)
8. Munjanja, L.; Torres-López, C.; Brennessel, W. W.; Jones, W. D. C-CN Cleavage using Palladium Supported by a Dippe Ligand. *Organometallics* **2016**, *35*, 2010-2013. (NSF, CENTC, DOE)
9. Guan, J.; Wriglesworth, A.; Brothers, E. N.; Zarić, S. D.; Evans, M. E.; Jones, W. D.; Hall, M. E.; George, M. W. Probing the Carbon-Hydrogen Activation of Alkanes Following Photolysis of $Tp^*Rh(CNR)(carbodiimide)$: A Computational and Time-resolved Infrared Spectroscopic Study, *J. Am. Chem. Soc.* **2018**, *140*, 1842-1854. (DOE)

(III) Jointly funded by this grant and other grants with relatively minor intellectual contribution from this grant:

10. Bligaard, T.; Bullock, R. M.; Campbell, C. T.; Chen, J.; Gates, B. C.; Gorte, R. J.; Jones, C. W.; Jones, W. D.; Kitchin, J. R.; Scott, S. L. Towards Benchmarking in Catalysis Science: Best Practices, Opportunities and Challenges. *ACS Catal.* **2016**, *6*, 2590-2602. (DOE)

Confinement of Supported Molecular Active Sites in Cups: A Comparative Study of Homogeneous, Amorphous, and Crystalline Catalysts

Nicolás A. Grosso-Giordano,¹ Christian Schöttle,¹ Andrew Palermo,^{1,2} Erjia Guan,² Alexander Okrut,¹ Andrew Solovyov,¹ Christian Schroeder,³ Hubert Koller,³ Walter Chassé,³ Nebojša Marinković,⁴ Stacey I. Zones,⁵ Bruce C. Gates,² Alexander Katz¹

- (1) Department of Chemical and Biomolecular Engineering, University of California at Berkeley, Berkeley, California 94720, USA
- (2) Department of Chemical Engineering, University of California at Davis, One Shields Avenue, Davis, California 95616, USA
- (3) Institut für Physikalische Chemie, Westfälische Wilhelms-Universität Münster, Münster, Germany
- (4) Department of Chemical Engineering, Columbia University, New York, New York, 10027, United States
- (5) Chevron Energy Technology Company, Richmond, California, 94804, United States

Presentation Abstract

This abstract is divided into two subsections: (i) robust heterogenization of a molecular catalyst active site, bridging homogeneous and heterogeneous catalysis; and (ii) understanding the importance of the solid support as an active outer-sphere ligand in catalysis on solids, comparing amorphous and crystalline silica. In the first subsection, we demonstrate a general approach for stabilization of a nanoscale structure in a supported molecular catalyst, relying on confinement by sterically bulky ligands, which allow transport of reactants and products in the working catalyst but hinder deactivation via aggregation. Our approach is exemplified with the synthesis and characterization of P-bridging calix[4]arene diiridium complex $[\text{Ir}(\text{CO})_2\text{PPhL}]_2$ **1**, and its anchoring on porous silica as a nominally non-interacting support. Our results demonstrate that the silica-supported complex remains robust following hydrogenation catalytic turnover, as evidenced by atomic-resolution scanning transmission electron microscopy (STEM) imaging and extended X-ray absorption fine structure (EXAFS) spectroscopy, providing nanoscale insight into the unique and crucial protective role afforded by the calixarene macrocyclic ligands of **1**. In the second subsection, the effect of outer-sphere environment on alkene epoxidation catalysis using an organic hydroperoxide oxidant is demonstrated for calix[4]arene-TiIV single-sites grafted on amorphous vs. crystalline delaminated zeotype (UCB-4) silicates as supports. A chelating calix[4]arene macrocycle ligand enforces a constant TiIV inner-sphere, as characterized by UV-visible and X-ray absorption spectroscopies, thus enabling the rigorous comparison of outer-sphere environments across different siliceous supports. These outer-sphere environments are characterized by solid-state ¹H NMR spectroscopy to comprise proximally organized silanols confined within 12-membered-ring cups in crystalline UCB-4, and are responsible for up to 5-fold enhancements in rates of epoxidation by Ti(IV) centers.

DE-FG02-05ER15696: Control of Supported Molecular Catalysts Using Metallocalixarene Active Sites

Postdoc(s): Christian Schöttle, Alexander Okrut, Andrew Solovyov

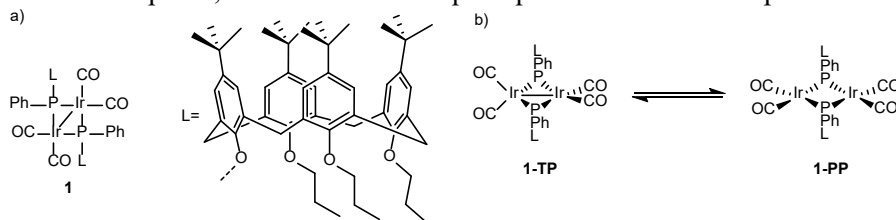
Student(s): Nicolás A. Grosso-Giordano, Andrew Palermo

RECENT PROGRESS

Bulky Calixarene Ligands Stabilize a Silica-Supported Molecular Iridium Dimer Catalyst

The solid-state structure of **1** was elucidated on the basis of single-crystal X-ray diffraction (XRD) crystallography and high-angle annular dark-field (HAADF) STEM (Fig. 1 for schematic representation). To isolate the catalytic sites in this cluster for reaction of gas-phase reactants and avoid solvent effects, we supported cluster **1** on porous, dehydroxylated silica, a nominally non-interacting support. Infrared (IR) spectra of **1-SiO₂** recorded under catalytic ethylene hydrogenation conditions demonstrate that catalytic activation proceeds via dissociation of one of the four CO ligands during the course of the first 24 h on stream. The loss of this CO to open an active site on the cluster core was characterized by EXAFS spectra of **1-SiO₂**, recorded before and after catalysis.

Figure 1. (a) Molecular structure of $[\text{Ir}(\text{CO})_2\text{PPhL}]_2$ (**1**); (b) $[\text{Ir}(\text{CO})_2\text{PPhL}]_2$: Isomer **1-TP**: tetrahedral/square planar coordination sphere; isomer **1-PP**: all-square planar coordination sphere.



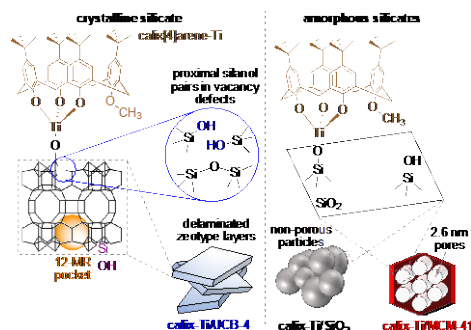
We measured a steady-state turnover frequency (TOF) of 540 h^{-1} for ethylene hydrogenation catalysis at 323 K using **1-SiO₂** as catalyst, which remained stable after more than 90 h on stream, with no decrease in activity observable. HAADF-STEM images recorded before and after catalysis by **1-SiO₂** show the nanoscale integrity of the silica-supported clusters even after catalysis (the heavy Ir atoms on the light SiO₂ support were imaged with atomic resolution, and the dimeric structure of the cluster core is evident in the 0.27 nm distance between the Ir atoms in a cluster). EXAFS data before and after catalysis agrees with the HAADF-STEM data, by demonstrating the integrity of the Ir-Ir and Ir-P coordination sphere following catalysis. In summary, catalyst **1-SiO₂** is a robust nanostructured catalyst that exhibits a stable TOF and does not show any evidence of metal aggregation during hydrogenation catalysis. These results demonstrate a benefit of the bulky calixarene-ligands – they keep the metal centers separated from each other and prevent aggregation. Thus, the data demonstrate a new paradigm for stabilizing supported molecular catalysts, in a manner that does not involve the support.

Outer-Sphere Control of Catalysis on Surfaces: A Comparative Study of Ti(IV) Single-Sites Grafted on Amorphous versus Crystal-line Silicates for Alkene Epoxidation

We demonstrate that outer-sphere environments have profound consequences on the reactivity of Ti(IV) sites supported on siliceous surfaces, the same type of active sites used in industrial propylene epoxidation catalysts. Our approach enforces a constant inner-sphere environment for grafted Ti(IV) single-sites with a chelating macrocyclic calix[4]arene ligand, while maintaining active-site accessibility across crystalline zeolitic versus amorphous outer-sphere environments of identical composition. It is shown in Scheme 1, and is based on a calix[4]arene-Ti surface complex (highlighted in brown) as a Lewis-acid catalytic Ti(IV) center. This is grafted onto a silanol (SiOH) group on the surface of three different siliceous supports, consisting of a crystalline delaminated zeotype UCB-4, and two amorphous silicas,

which comprise Aerosil® 200 fumed silica particles (denoted SiO₂) and MCM-41, a hexagonally ordered silicate with uniform 2.6 nm mesopores. The resulting catalysts comprising grafted calix[4]arene-Ti complexes are denoted **calix-Ti/SUP**, where **SUP** = crystalline UCB-4, amorphous SiO₂, or amorphous MCM-41 indicates the support in Scheme 1.

Scheme 1. Schematic representation of grafted calix[4]arene-Ti(IV) structures (brown). Details of the crystalline SSZ-70 (MWW-type) zeotype framework of UCB-4 is shown in the left panel. Silanol (SiOH) species characterized by NMR spectroscopy on SSZ-70 are represented as a proximal silanol pair in blue, and isolated crystal-plane terminating silanols in purple.



Rate constants normalized by Ti(IV) contents (k_{eff}) for the epoxidation of cyclohexene with tert-butyl hydroperoxide, a common probe reaction for epoxidation activity, are summarized in Table 1 for all **calix-Ti/SUP** catalysts, with epoxide yields uniformly high. Values of k_{eff} are observed to be 4- and 5-fold higher in crystalline **calix-Ti/UCB-4**, as compared to amorphous **calix-Ti/MCM-41** and **calix-Ti/SiO₂**, respectively. Similar enhancements favoring **calix-Ti/UCB-4** are also observed when quantifying turnover numbers for epoxide production, irrespective of whether the amorphous support contains a well-ordered porous system in MCM-41 or not (SiO₂). We surmise that, on a single-site basis, all Ti(IV) centers behave similarly when grafted on amorphous supports, as described previously, but with distinctly lower activity than on crystalline **calix-Ti/UCB-4**. Control experiments were performed to confirm that the high-activity in **calix-Ti/UCB-4** relative to the amorphous catalysts is not due to artifacts of the delamination, acid washing treatment, presence of B(III), or diffusional constraints, is independent of calix[4]arene-Ti(IV) surface density, and is generalizable to other olefins and oxidants. Significantly, calix[4]arene-Ti(IV) sites grafted on fully hydroxylated SiO₂ (**calix-Ti/SiO₂-AW**) exhibit rates equivalent to those of calix-Ti/SiO₂ ($k_{\text{eff}} = 8 \text{ M}^{-2}\text{s}^{-1}$), indicating that silanol pairing as achieved by high local silanol densities on amorphous silicates is alone insufficient for enhancing reactivity. Based on the identical electronic and inner-sphere environments of grafted Ti(IV) for all catalysts (XANES and DR-UV/Vis spectroscopic data), active sites would be expected to display similar epoxidation rates in the absence of outer-sphere effects; however, they are instead observed to be up to 5-fold more active when grafted on the crystalline framework of UCB-4, in comparison to amorphous supports. We conclude that these enhancements in rate are brought about by outer-sphere effects intrinsic to the support in **calix-Ti/UCB-4**.

Publications Acknowledging this Grant in 2015-2018

(I) Exclusively funded by this grant

1. Chung, P.-W.; Charmot, A.; Click, T.; Lin, Y.; Bae, Y.; Chu, J.-W.; Katz, A. Importance of Internal Porosity for Glucan Adsorption in Mesoporous Carbon Materials. *Langmuir* **2015**, *31*, 7288–7295.
2. To, A. T.; Chung, P.-W.; Katz, A. Weak-Acid Sites Catalyze Crystalline-Cellulose Hydrolysis to Glucose in Water: Importance of Carbon Post-Synthetic Surface Functionalization. *Angewandte Chemie International Edition in English* **2015**, *54*, 11050–11053.
3. Chung, P.-W.; Yabushita, M.; To, A. T.; Bae, Y. J.; Jankolovits, J.; Kobayashi, H.; Fukuoka, A.; Katz, A. Long-Chain Glucan Adsorption and Depolymerization in Zeolite-Templated Carbon Catalysts. *ACS Catalysis* **2015**, *5*, 6422–6425.
4. Charmot, A.; Solovyov, A.; Katz, A. Silica-Supported Phosphonic Acids as Thermally and Oxidatively Stable Organic Acid Sites. *Chemistry of Materials* **2016**, *28*, 6166–6177.
5. Yabushita, M.; Li, P.; Kobayashi, H.; Fukuoka, A.; Farha, O. K.; Katz, A. Complete Furanics–Sugar Separations with Metal–Organic Framework NU-1000. *ChemComm* **2016**, *52*, 11791–11794.

6. Yabushita, M.; Techikawara, K.; Kobayashi, H.; Fukuoka, A.; Katz, A. Zeolite-Templated Carbon Catalysts for Adsorption and Hydrolysis of Cellulose-Derived Long-Chain Glucans: Effect of Post-Synthetic Surface Functionalization. *ACS Sustainable Chemistry and Engineering* **2016**, *4*, 6844 – 6851.
 7. Yabushita, M.; Li, P.; Durkin, K. A.; Kobayashi, H.; Fukuoka, A.; Farha, O. K.; Katz, A. Insights into Supramolecular Sites Responsible for Complete Separation of Biomass-Derived Phenolics and Glucose in Metal-Organic Framework NU-1000. *Langmuir* **2017**, *33*, 4129 – 4137.
 8. Yabushita, M.; Li, P.; Islamoglu, T.; Kobayashi, H.; Fukuoka, A.; Farha, O. K.; Katz, A. Selective Metal-Organic Framework Catalysis of Glucose to 5-Hydroxymethylfurfural Using Phosphate-Modified NU-1000. *Ind. Eng. Chem. Res.* **2017**, *56*, 7141 – 7148.
 9. Schottle, C.; Clark, E.; Harker, A.; Solovyov, A.; Bell, A. T.; Katz, A. Nanoporous Gold Assemblies of Calixarene-Phosphine-Capped Colloids. *ChemComm* **2017**, *53*, 10870–10873.
- (II) *Jointly funded by this grant and other grants with leading intellectual contribution from this grant*
1. Winner, L.; Daniloff, G.; Nichiporuk, R. V.; Solovyov, A.; Katz, A. Patterned Grafted Lewis-Acid Sites on Surfaces: Olefin Epoxidation Catalysis Using Tetrameric Ti(IV)-Calix[4]arene Complexes. *Topics in Catalysis* **2015**, *58*, 441–450.
 2. Yabushita, M.; Li, P.; Bernales, V.; Kobayashi, H.; Fukuoka, A.; Gagliardi, L.; Farha, O. K.; Katz, A. Unprecedented Selectivity in Molecular Recognition of Carbohydrates by a Metal-Organic Framework. *ChemComm* **2016**, *52*, 7094–7097.
 3. Grosso-Giordano, N. A.; Solovyov, A.; Hwang, S.; Katz, A. Effect of Coordination Environment in Grafted Single-Site Ti-SiO₂ Olefin Epoxidation Catalysis. *Topics in Catalysis* **2016**, *59*, 1110–1122.
 4. May, E. M.; Solovyov, A.; Guo, Y.; Drapailo, A.; Matveev, Y.; Kalchenko, V.; Nitsche, H.; Katz, A. Unprecedented Increase in Affinity for Eu(III) over Am(III) through Silica Grafting of a Carbamoylmethylphosphine Oxide-Calix[4]arene Site. *European Journal of Inorganic Chemistry* **2016**, *28*, 4542–4545.
 5. Guo, Y.; Solovyov, A.; Grosso-Giordano, N.; Hwang, S.-J.; Katz, A. Stabilizing Single Sites on Solid Supports: Robust Grafted Ti(IV)-Calixarene Olefin Epoxidation Catalysts via Surface Polymerization and Cross-Linking. *ACS Catalysis* **2016**, *6*, 7760–7768.
 6. Palermo, A.; Solovyov, A.; Ertler, D.; Okrut, A.; Gates, B. C.; Katz, A. Dialing in Single-Site Reactivity of a Supported Calixarene-Protected Tetrairidium Cluster Catalyst. *Chemical Science* **2017**, *8*, 4951 – 4960.
 7. Zhang, S. D.; Foyle, A.; Okrut, A.; Solovyov, A.; Katz, A.; Gates, B. C.; Dixon, D. A. *Role of N-Heterocyclic Carbenes as Ligands in Iridium Carbonyl Clusters*. *J. Phys. Chem. A* **2017**, *121*, 5029–5044.
 8. Aigner, M.; Grosso-Giordano, N. A.; Schötle, C.; Okrut, A.; Zones, S. I.; Katz, A. Epoxidation of 1-octene under harsh tail-end conditions in a flow reactor I: a comparative study of crystalline vs. amorphous catalysts. *Reaction Chemistry and Engineering* **2017**, *2*, 842–851.
 9. Aigner, M.; Grosso-Giordano, N. A.; Schötle, C.; Okrut, A.; Zones, S. I.; Katz, A. Epoxidation of 1-octene under harsh tail-end conditions in a flow reactor II: impact of delaminated-zeolite catalyst surface area and structural integrity on catalytic performance. *Reaction Chemistry and Engineering* **2017**, *2*, 852–861.
 10. Grosso-Giordano, N. A.; Schroeder, C.; Okrut, A.; Solovyov, A.; Schottle, C.; Chasse, W.; Marinkoyic, N.; Koller, H.; Zones, S. I.; Katz, A. Outer-Sphere Control of Catalysis on Surfaces: A Comparative Study of Ti(IV) Single-Sites Grafted on Amorphous versus Crystalline Silicates for Alkene Epoxidation. *Journal of the American Chemical Society* **2018**, *140*, 4956 – 4960.

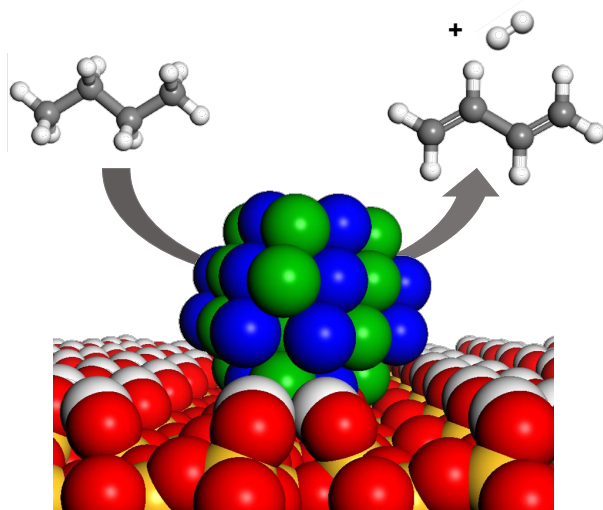
Computational Studies of Bimetallic Nano-Cluster for Non-Oxidative Dehydrogenation of Light Alkanes

Cong Liu,¹ Gokhan Celik,¹ Even Wegner,¹ A. Jeremy Kropf,¹
Magali Ferrandon,¹ Massimiliano Delferro¹

¹Chemical Sciences and Engineering Division, Argonne National Laboratory.

congliu@anl.gov

A series of supported bimetallic nanocatalysts have been developed in our program. The synthesized bimetallic alloy nanoclusters and intermetallic nanoparticles have shown outstanding activity and selectivity for both heterogeneous catalysis of non-oxidative dehydrogenation and hydrogenation. The unique performance of the bimetallic nanocatalysts have motivated us to study computationally in detail the catalytic properties of these systems as compared to pure metal nanocatalysts. In the case of n-butane dehydrogenation using silica supported PtZn alloy clusters, we observed experimentally that the atomic layer deposition of Pt complex precursors on Zn²⁺ modified SiO₂ followed by H₂ treatment results in small PtZn alloy clusters (~1 nm), while that on



SiO₂ leads to larger Pt nanoparticles (~7 nm). Density functional theory (DFT) calculations found that the presence of Zn²⁺ sites on silica creates the anchoring hydroxyl groups that are more acidic than the regular silica hydroxyls, and results in stronger interactions with the Pt precursor complex during the experimental atomic layer deposition (ALD). Such enhanced interactions stabilize Pt sites on SiO₂, resulting in smaller cluster size. The resulting PtZn nanocluster also showed outstanding selectivity towards 1,3-butadiene compared to the larger Pt nanoparticles. Computational mechanism studies found that the smaller PtZn alloy clusters showed a much higher binding interaction with

the first dehydrogenation intermediate 1-butene than Pt nanoparticles, suggesting that olefin dissociation is less energetically favorable on the nanocluster. Hence, the smaller PtZn clusters likely favor a second C-H activation/dehydrogenation to form 1,3-butadiene. Based on these studies, we carried out systematic computational studies on the catalytic properties of PtFe, PtCo, PtNi and PtCu systems, to compare with Pt and PtZn systems, with respect to different cluster/particle size and metal ratio. Detailed mechanistic studies and calculated electronic properties suggest that both the C-H activation barriers and the 1-butene binding energies that are affected by the cluster size and metal composition play important roles in the selectivity and activity of these bimetallic catalysts.

Reforming of Methane on Single Site Catalysts

Ping Liu, Shizhong Liu, Jose A. Rodriguez, and Sanjaya D. Senanayake
Chemistry Department, Brookhaven National Laboratory
Upton, NY 11973

Presentation Abstract

Single site catalysts have drawn considerable attentions due to their superior behaviors in catalysis. However, the origin of promoting effect of single site is not well understood. Here, we take single site Ni_n/Mg(100) catalysts as a case study to elucidate their behaviors under the complex dry reforming of methane (DRM, CO₂ + CH₄ → 2CO + 2H₂) reaction by combining theoretical modeling (Density Functional Theory and kinetic Monte Carlo simulation) and experimental studies. The synergy between single Ni atom and MgO is found to improve the binding property of MgO; yet it is not enough to dissociate CO₂ and CH₄. It can be achieved by the formation of the single site Ni₄/MgO(100) catalyst, enabling the formations of CO, H₂ and H₂O under the DRM conditions. During this process, coking, as observed for bulk-like Ni particles, is completely eliminated. By confining the reaction to occur at the isolated Ni ensemble the single site Ni₄/MgO(100) catalyst is able to balance the CO₂ and CH₄ activations, which is identified as the key for tuning the DRM activity and selectivity of Ni/MgO catalysts. The theory-identified promotion introduced by increasing the size of MgO-supported Ni clusters from Ni₁ to Ni₄ and the MgO-introduced site confinement of single site catalysts is verified by corresponding experimental studies, highlighting the independent roles of confined sites in tuning the performance of single site catalysts during complex catalytic processes.

FWP-BNL-CO040: Catalysis for Advanced Fuel Synthesis and Energy

CO₂-Assisted Ethane Dehydrogenation and Aromatization over Zn-Containing Zeolites

Raul F. Lobo

Center for Catalytic Science and Technology
Department of Chemical and Biomolecular Engineering
University of Delaware, Newark DE 19716

Presentation Abstract

The catalytic properties of Zn-ZSM-5 and Zn-beta for ethane/ethylene aromatization were investigated to understand the impact of the ratio of Lewis acid sites (Zn^{2+}) and BAS (Zn/BAS). For ethane, Zn/BAS < 0.8 favor ethylene formation while higher Zn/BAS increase reaction rates and selectivity to aromatics, revealing that Zn sites have a role in ethane aromatization besides dehydrogenation. The impact of steam and CO₂—over 5% (w/w) Zn-ZSM-5 catalysts prepared by impregnation—show that CO₂ increases the formation rate of ethylene and CO, and steam increases the formation rate of ethylene. In addition, CO₂ decreased the formation rates of methane and aromatics by factors of ~3 and 7, respectively. Hydrogen formed from ethane dehydrogenation reacted with CO₂, via the reverse water gas shift reaction, to form CO and water. It is shown that carbon dioxide can be used to control selectivity and to increase the yield of ethylene by consuming hydrogen.

Grant or FWP Number: DE-SC0014436

Grant Title: Methane Activation over Cu-Containing Zeolite Catalysts

Postdoc: Ali Mehdad

Student: Edward Schreiner

RECENT PROGRESS

Water Gas Shift Reaction over Zn-containing zeolites.

Isolated Zn sites (Zn^{2+} or $Zn(OH)^+$) exchanged into aluminosilicate zeolites, and zinc oxide clusters $(ZnO)_n$ supported on silicalite-1 (MFI) are shown (for the first time) to catalyze the RWGS reaction at temperatures above 723 K. Zn-ZSM-5 samples have lower activation energy (~54 kJ/mol) than the small pore chabazite zeolites (~74 kJ/mol). Reduction of CO₂ in Zn-ZSM-5 proceeds via a formate pathway following a mechanism similar to the one previously proposed for co-conversion of methane and CO₂ to acetic acid on Zn-ZSM-5, and it is shown that formic acid rapidly dehydrates on both Zn-sites and Brønsted acid sites, forming CO, at RWGS reaction conditions. Reaction rates were stable with turn-over-frequencies in the range of 4-8 h⁻¹ per Zn atom in ZSM-5. Figure 1 compares reaction rates for different zeolite catalysts and shows that reaction rates are very stable over a period of 5 hr. ZSM-5 zeolites with high aluminum content and Zn content, catalyze this reaction at the highest reaction rates. Figure 2 displays a suggested reaction mechanism that is analogous to the mechanism previously suggested for methane reaction into acetic acid.

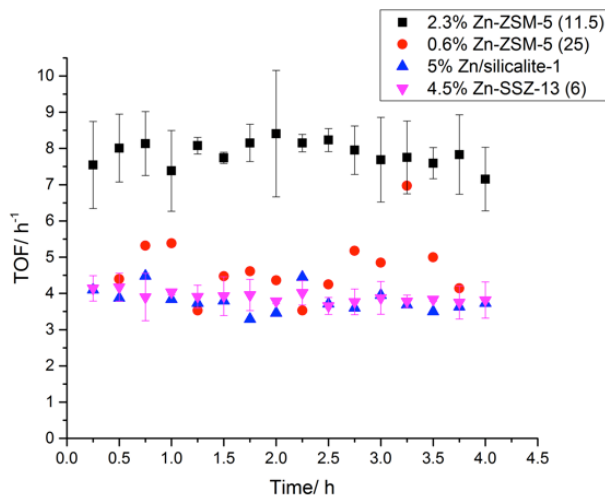


Figure 1. TOF of CO₂ reduction on different catalysts at 723 K. Feed: 5%CO₂/5%H₂/90% He.

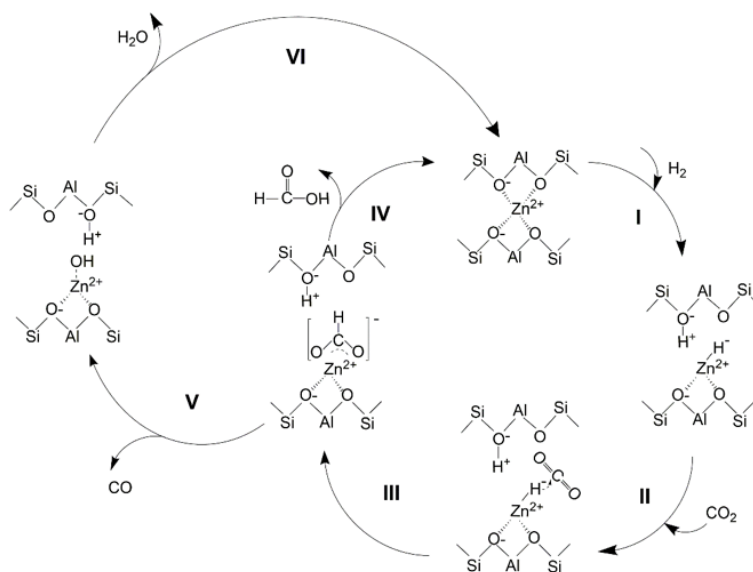


Figure 2: Proposed mechanism for CO₂ hydrogenation is consistent with the selectivity to hydrogen of formic acid decomposition.

Dimethyl ether to Olefins over Fe-beta zeolite catalysts

We have investigated the conversion of dimethyl ether on H-[Fe]beta as an alternative methanol-to-olefins catalysts. It was found that conversion of DME on H-[Fe]beta produced olefins with high selectivity (>90%) and isobutene was the major species produced followed by triptene. While conversion of DME on H-[Al]beta produced paraffins and H-[Fe]beta produced olefins with high selectivity, the product distributions based on carbon number and compound skeletal structure

Schreiner, E.P., Lobo, R. F., “C4 and C7 Olefins via Methanol Homologation over Fe-zeolite beta”, *Applied Catal. A General*, **2018**, *in preparation*.

(II) *Jointly funded by this grant and other grants with leading intellectual contribution from this grant;*

Mehdad, A., Gould, N.S., Xu, B.X., and Lobo, R.F. “Effect of Steam and CO₂ on Ethane Activation in Zn-ZSM-5”, *Catal. Sci. Technol.* **2018**, *8*, 358-366. DOI: 10.1039/c7cy01850a

Atomic-scale Design of Metal and Alloy Catalysts: A Combined Theoretical and Experimental Approach

Manos Mavrikakis,[†] James A. Dumesic,[†] Younan Xia[‡]

[†] Department of Chemical & Biological Engineering, University of Wisconsin – Madison; [‡] School of Chemistry & Biochemistry, Georgia Institute of Technology

Presentation Abstract

The main objective of this combined theoretical and experimental project is to: (i) *design* from first-principles, (ii) *synthesize* using advanced *nanosynthesis* techniques, and (iii) experimentally evaluate *new metal* and *alloy nanoparticles*, with unique *catalytic* properties for a number of important chemical reactions. Measurable impact can be found in a number of applications, including low temperature fuel cells, hydrogen production and purification, fuels/chemicals production, and pollution remediation. The importance of the atomic-scale architecture of these new theoretically-designed catalysts to their unique properties is driving the development of *new inorganic materials synthesis* approaches, which are capable of synthesizing the theoretically determined optimal, and in some cases, metastable, nanoscale catalytic architectures.

Grant or FWP Number: DOE Grant No. DE-FG02-05ER15731 (Atomic-scale Design of Metal and Alloy Catalysts: A Combined Theoretical and Experimental Approach)

PI: Manos Mavrikakis, James A. Dumesic, Younan Xia

Postdoc(s): Florian Göttl (UW) Song Shen (GIT)

Student(s): Yunhai Bai, Ahmed Elnabawy, Sean Tacey, Andrew Gould, Joshua Lin, Saurabh Bhandari, Ellen Murray, Demetrios Kirvassilis (UW)

Legna Figueroa-Cosme, Madeline Vara, Wenxia Wang (GIT)

Affiliations(s): University of Wisconsin-Madison, Georgia Institute of Technology

RECENT PROGRESS

Boron Nitride-supported Sub-nanometer Pd₆ Clusters for Formic Acid Decomposition¹

Sub-nanometer metal clusters of atomic precision show remarkable activity and selectivity for a variety of reactions, such as CO oxidation.^{2,3} Using density functional theory (DFT), we studied the catalytic properties of an *h*-BN-supported Pd₆ sub-nanometer cluster for the decomposition of formic acid (FA), assessing its selectivity for H₂/CO₂ production versus H₂O/CO production.

FA decomposes through two main paths: *i*) the formate-mediated (HCOO) path, where the O–H bond of FA is first broken, and *ii*) the carboxyl-mediated (COOH) path, where the C–H bond of FA is broken first, instead. Interestingly, for the COOH-mediated path, once COOH is formed, subsequent dehydrogenation, COOH → CO₂ + H, is more facile than decarbonylation, COOH → CO + OH, by ~26 kJ mol⁻¹, suggesting that supported Pd₆ may be able to selectively convert FA to H₂ with minimal competing CO formation, even if COOH, usually thought to be a precursor to CO, is formed. This is major reactivity difference between large nanoparticles and sub-nm Pd clusters.

On Pd(111), the COOH-mediated path is dominant; not the HCOO-mediated path.^{4,5} However, on Pd₆, FA decomposition likely via the HCOO-mediated path, as HCOO is much stable than COOH on Pd₆ (Figure 1). This change selectivity is also because HCOO binds much strongly on Pd₆ than on Pd(111). To the best of knowledge, this is a unique feature that can be associated to the highly undercoordinated Pd present in Pd₆.

We also found that the reaction energetics depend strongly on the presence/absence of defects in the support; on pristine *h*-BN the catalyst is more selective towards H₂/CO₂ formation, while the introduction of B-vacancies (formation energy: 16.6 eV) or N-vacancies (formation energy: 12.8 eV) greatly enhance CO formation due to charge transfer and Pd₆ cluster reconstruction.

Synthesis Gas Conversion over Rh-Based Catalysts Promoted by Fe and Mn⁶

We conducted a combined experimental and DFT study of Rh/SiO₂ catalysts promoted with Mn and Fe for converting syngas into oxygenates and light hydrocarbons, to understand how promoters affect this chemistry.

To elucidate the atomistic structure of this complex catalyst, we first modelled the facets and the step edges of a Rh nanoparticle using extended (111) and (211) surfaces, respectively. We then studied different possible *reducing environments* typically encountered under these reaction conditions, Fe is reduced into metallic monomers, which lie in the subsurface of Rh. Mn however is only partially reduced, and exists as a hydroxylated species at the step edges (Figure 2).

We then calculated the vibrational frequencies of CO adsorbed onto these model surfaces, and compared them with experimental infra-red (IR) measurements on the supported catalysts. From this, we showed that the presence of Fe and Mn promoters significantly change the binding of CO compared to the clean Rh(211) surface.

Experimentally, we find that Mn suppresses catalytic processes which are selective towards formation of the unwanted byproduct CH₄, while Fe, when present as subsurface species on the terraces, enhances the selectivity of (111) facets towards ethanol. This

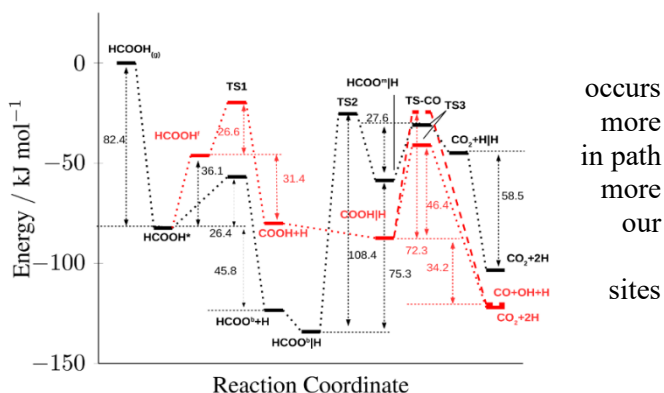


Figure 7. PES for HCOOH decomposition on *h*-BN-supported Pd₆ clusters, through the HCOO–(black) and COOH–mediated (red) paths. The dashed red line is associated with breaking of C–OH of COOH, leading to CO + OH. “|” denotes co-adsorbed states. HCOO^m and HCOO^b indicate monodentate and bidentate formate, respectively. Note that 96.5 kJ mol⁻¹ = 1 eV. Figure from ref. 1.

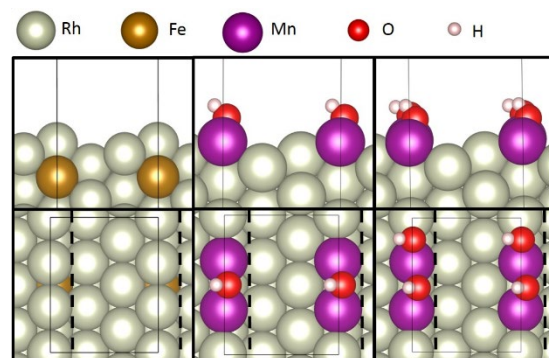


Figure 8. Preferred calculated structures of Fe, Mn promoters on Rh edges under reaction conditions. (Above) Side view. (Below) Top view. Dashed lines indicate step edges. Figure adapted from ref. 6.

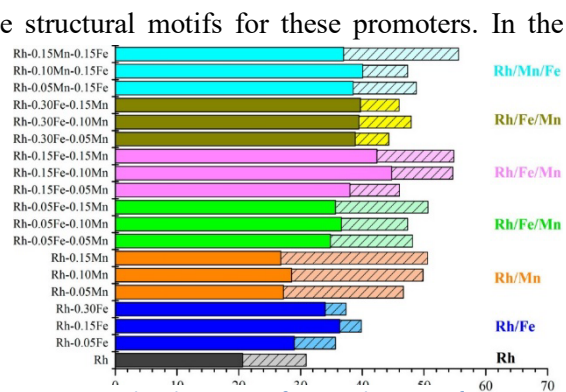


Figure 9 Experimental selectivities for production of oxygenates and C₂₊ hydrocarbons for syngas conversion: Total products (%) over Rh/SiO₂ and Rh-based bimetallic and trimetallic catalysts. Figure from ref. 6.

results in the majority product for trimetallic catalysts being ethanol, with 35% of total carbon going to C₂₊ oxygenates and 10% to C₂₊ hydrocarbons, while the majority product for the monometallic Rh catalyst is CH₄, with only 21% of total carbon going to C₂₊ oxygenates and 10% to C₂₊ hydrocarbons (Figure 3). The carbon balances are closed with CO₂/CH₄ in both cases. Our DFT calculations suggest that these effects are due to fundamental changes in the reaction mechanisms brought about by changes in the binding modes of CO when Mn and Fe are added to Rh.

Kinetics of shape and architectural degradation process of shape-selected nanoparticles^{7,8}

The shape and architecture (e.g. core@shell) of nanocrystals are liable to degrade at the elevated temperatures typical of some industrial catalytic processes. To understand this process, we combined *in situ* high resolution transmission electron microscopy (HRTEM) and DFT calculations.

Shape and architectural stability of Pd@Pt core@shell nanocubes and octahedra⁷

Pd@Pt core@shell nanocubes and octahedra nanocrystals were synthesized. Their shape stabilities were then probed by heating. The cubes lost their shape after heating above 400°C. By contrast, the octahedra preserved their shape even when heated at 700°C.

Diffusion of edge atoms onto the adjacent terraces was proposed to be the dominant mechanism for the loss of nanoparticle shape. As shown in Figure 4, this diffusion is exothermic for cubes and has a moderate barrier of 0.60 eV; for octahedra however, this process is highly endothermic and has a high barrier of 1.99 eV. The higher barriers for edge reconstruction in octahedra as compared to cubes result in their higher shape stability.

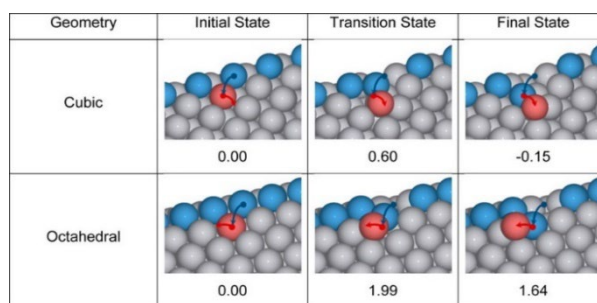


Figure 10. Mechanistic processes for edge degradation in Pd@Pt core@shell cubes and octahedra. Numbers denote energies relative to the initial state, in eV. Color code: Edge atom – blue, displaced terrace atom – red, terrace atoms – grey. All atoms shown are Pt. Figure from ref. 7

Contrary to the trend found for shape stability, the core@shell architecture of the cubes was maintained even after heating up to 600°C for 40 minutes, whereas the octahedra started to alloy at 500°C after an hour of heating. This alloying process involves *diffusion in the bulk* instead of on the surface. We showed that subsurface vacancies of octahedra were more stable than vacancies in the cubes, suggesting that octahedra have a higher concentration of vacancies. Therefore, we propose that vacancy-mediated interatomic diffusion occurs at a higher rate in octahedra, thus explaining why their core@shell architecture is lost at lower temperatures than in cubes.

Shape stability of Pd concave icosahedra⁸

Upon heating, Pd concave icosahedra lose their concavity and revert to regular icosahedra. We were able to temporally resolve this transformation using high-angle annular dark-field scanning transmission electron microscopy (HAADF-STEM), as shown in Figure 5. To understand these processes, we developed a model of the edges of the concave icosahedra. DFT calculations show that removal of the first atom from the step edge is the most activated process and is thus the decisive step that initiates the degradation. The barrier for this removal is 1.04 eV, which is only surmountable at the high temperatures of 200 – 400 °C, at which we experimentally observed these transformations.

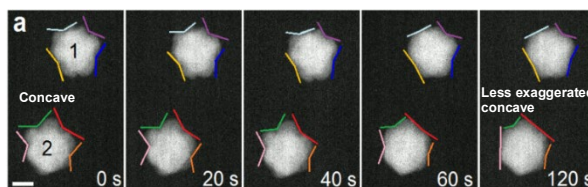


Figure 11. Temporal resolution of the transformation of two concave icosahedra to less exaggerated concave icosahedra, using *in situ* HAADF-STEM. Colored lines denote guesses for the edges of the icosahedra. Figure from ref. 8.

Reaction Mechanism for NO reduction by H₂ on Pt(100)⁹

Nitric oxide (NO) is a pollutant formed by many combustion processes. To understand how NO can be reduced by H₂ on Pt(100), as Pt is a common catalyst for NO remediation, we studied the energetics of NO decomposition via various N–O activation paths, including *direct* and *hydrogen-assisted* N–O bond-breaking paths. We also investigated the formation of three different N-containing products, N₂, N₂O, and NH₃, to determine the major products of this reaction.

Our results are summarized in the PES in Figure 6. NO* dissociation has a lower barrier than NO* hydrogenation to HNO* or NOH*, therefore, the *direct NO dissociation path is predicted to dominate N–O activation* on clean Pt(100). Once the N–O bond is broken, atomic N* can then form N₂O, N₂, or NH₃. N₂O formation via recombination of N* and NO*, as well as NH₃ formation via three successive hydrogenations of N*, are both kinetically more difficult than N₂ formation, suggesting that N₂ is the major product.

We also calculated *ab initio* phase diagrams of NO adsorption on Pt(100), showing that the Pt(100) surface could be covered by ½ ML of NO under realistic reaction conditions, which motivates us to study in the future the same chemistry on Pt(100) covered by ½ ML NO.

References

- (1) Schimmenti, R.; Cortese, R.; Duca, D.; Mavrikakis, M. Boron Nitride-Supported Sub-Nanometer Pd₆ Clusters for Formic Acid Decomposition: A DFT Study. *ChemCatChem* **2017**, *9*, 1610–1620.
- (2) Zhang, C.; Yoon, B.; Landman, U. Predicted Oxidation of CO Catalyzed by Au Nanoclusters on a Thin Defect-Free MgO Film Supported on a Mo(100) Surface. *J. Am. Chem. Soc.* **2007**, *129*, 2228–2229.
- (3) Lee, S.; Fan, C.; Wu, T.; Anderson, S. L. CO Oxidation on Au_n/TiO₂ Catalysts Produced by Size-Selected Cluster Deposition. *J. Am. Chem. Soc.* **2004**, *126*, 5682–5683.
- (4) Herron, J. A.; Scaranto, J.; Ferrin, P.; Li, S.; Mavrikakis, M. Trends in Formic Acid Decomposition on Model Transition Metal Surfaces: A Density Functional Theory Study. *ACS Catal.* **2014**, *4*, 4434–4445.
- (5) Scaranto, J.; Mavrikakis, M. Density Functional Theory Studies of HCOOH Decomposition on Pd(111). *Surf. Sci.* **2016**, *650*, 111–120.
- (6) Liu, Y.; Göelltl, F.; Ro, I.; Ball, M. R.; Sener, C.; Aragão, I. B.; Zanchet, D.; Huber, G. W.; Mavrikakis, M.; Dumesic, J. A. Synthesis Gas Conversion over Rh-Based Catalysts Promoted by Fe and Mn. *ACS Catal.* **2017**, *7*, 4550–4563.
- (7) Vara, M.; Roling, L. T.; Wang, X.; Elnabawy, A. O.; Hood, Z. D.; Chi, M.; Mavrikakis, M.; Xia, Y. Understanding the Thermal Stability of Palladium–Platinum Core–Shell Nanocrystals by In Situ Transmission Electron Microscopy and Density Functional Theory. *ACS Nano* **2017**, *11*, 4571–4581.
- (8) Gilroy, K. D.; Elnabawy, A. O.; Yang, T. H.; Roling, L. T.; Howe, J.; Mavrikakis, M.; Xia, Y. Thermal Stability of Metal Nanocrystals: An Investigation of the Surface and Bulk Reconstructions of Pd Concave Icosahedra. *Nano Lett.* **2017**, *17*, 3655–3661.
- (9) Bai, Y.; Mavrikakis, M. Mechanistic Study of Nitric Oxide Reduction by Hydrogen on Pt(100) (I): A DFT Analysis of the Reaction Network. *J. Phys. Chem. B* **2018**, *122*, 432–443.

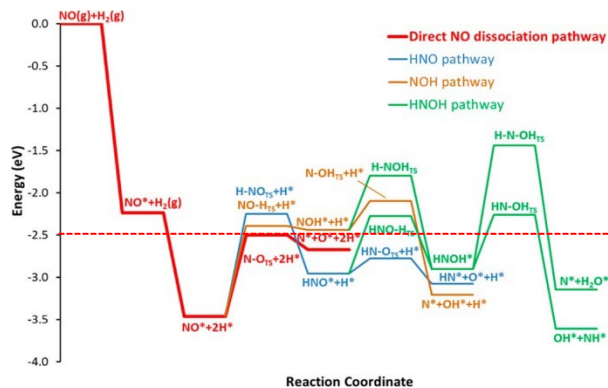


Figure 12. PES of NO reduction by H₂ on Pt(100). “(g)” for gas phase species, superscript “*” for adsorbed species, and subscript “TS” for transition states. The dashed red line denotes the energy of the highest transition state for the direct NO dissociation path. Figure adapted from ref 9.

direct NO dissociation path is predicted to dominate N–O activation on clean Pt(100). Once the N–O bond is broken, atomic N* can then form N₂O, N₂, or NH₃. N₂O formation via recombination of N* and NO*, as well as NH₃ formation via three successive hydrogenations of N*, are both kinetically more difficult than N₂ formation, suggesting that N₂ is the major product.

Publications Acknowledging this Grant in 2015-2018

(I) Exclusively funded by this grant

1. Rangarajan S.; Maravelias C. T.; Mavrikakis M.; **Sequential-Optimization-Based Framework for Robust Modeling and Design of Heterogeneous Catalytic Systems**, *Journal of Physical Chemistry C* **2018**, *121*, 25847-25863
2. Xu L.; Kirvassilis D.; Bai Y.; Mavrikakis M.; **Atomic and molecular adsorption on Fe(110)**, *Surface Science* **2018**, *667*, 54-65
3. Bai Y.; Mavrikakis M.; **A Mechanistic Study of Nitric Oxide Reduction by Hydrogen on Pt(100) (I): A DFT Analysis of the Reaction Network**, *Journal of Physical Chemistry B*, **2018**, *122*, 432-443
4. Chen B. W. J.; Kirvassilis D.; Bai. Y.; Mavrikakis M.; Atomic and Molecular Adsorption on Ag(111), *Journal of Physical Chemistry C*, Article ASAP, DOI: 10.1021/acs.jpcc.7b1162.
5. Rangarajan S.; Mavrikakis M.; **On the Preferred Active Sites of Promoted MoS₂ for Hydrodesulfurization with Minimal Organonitrogen Inhibition**, *ACS Catalysis* **2017**, *7*, 501-509
6. Schimmenti R.; Cortese R.; Duca D.; Mavrikakis M.; **Boron Nitride-supported Subnanometer Pd₆ Clusters for Formic Acid Decomposition: A DFT Study**. *ChemCatChem* **2017**, *9*, 1610-1620
7. Vara M.; Roling L. T.; Wang X.; Elnabawy A. O.; Hood Z. D.; Chi. M.; Mavrikakis M.; Xia Y.; **Understanding the Thermal Stability of Palladium–Platinum Core–Shell Nanocrystals by *In Situ* Transmission Electron Microscopy and Density Functional Theory**, *ACS Nano* **2017**, *11*, 4571-4581
8. Gilroy K. D.; Elnabawy A. O.; Yang T.-H.; Roling L. T.; Howe J.; Mavrikakis M.; Xia Y.; **Thermal Stability of Metal Nanocrystals: An Investigation of the Surface and Bulk Reconstructions of Pd Concave Icosahedra**, *Nano Letters* **2017**, *17*, 3655-3661
9. Roling L. T.; Mavrikakis M.; **Toward Rational Nanoparticle Synthesis: Predicting Surface Intermixing in Bimetallic Alloy Nanocatalysts**, *Nanoscale* **2017**, *9*, 15005-15017
10. Vara M.; Lu P.; Yang X.; Lee C.-T.; Xia Y.; A photochemical, room-temperature, and aqueous route to the synthesis of Pd nanocubes enriched with atomic steps and terraces on the side faces, *Chemistry of Materials* **2017**, *29*, 4563-4571
11. Li S.; Scaranto J.; Mavrikakis M.; **On the Structure Sensitivity of Formic Acid Decomposition on Cu Catalysts**. *Topics in Catalysis* **2016**, *59*, 1580-1588.
12. Roling L. T.; Herron J. A.; Budiman W.; Ferrin P.; and Mavrikakis M.; **Dimethyl Ether Electro-Oxidation on Platinum Surfaces**. *Nano Energy* **2016**, *29*, 428-438
13. Herron J. A.; Morikawa Y.; and Mavrikakis M.; **Ab initio molecular dynamics of solvation effects on reactivity at electrified interfaces**. *Proceedings of the National Academy of Sciences of the United States of America* **2016**, *113*, E4937-E4945.
14. Xu L.; Yao X.; Khan A.; Mavrikakis M.; **Chloroform Hydrodechlorination over Palladium–Gold Catalysts: A First-Principles DFT Study**. *ChemCatChem* **2016**, *8*, 1739-1746.

15. Tacey S. A.; Xu L.; Mavrikakis M.; Schauer J. J.; **Heterogeneous Reduction Pathways for Hg(II) Species on Dry Aerosols: A First-Principles Computational Study.** *Journal of Physical Chemistry A* **2016**, *120*, 2106-2113.
16. Herron J. A.; Ferrin P.; Mavrikakis M.; **On the Structure Sensitivity of Dimethyl Ether Electro-oxidation on Eight FCC Metals: A First-Principles Study.** *Topics in Catalysis* **2015**, *58*, 1159-1173.
17. Celik F. E.; Mavrikakis M.; **Stability of surface and subsurface hydrogen on and in Au/Ni near-surface alloys.** *Surface Science* **2015**, *640*, 190-197.
18. Zhang L.; Roling L. T.; Wang X.; Vara M.; Chi M.; Liu J.; Choi S.; Park J.; Herron J. A.; Xie Z.; Mavrikakis M.; Xia Y.; **Platinum-based nanocages with subnanometer-thick walls and well-defined, controllable facets** *Science* **2015**, *349*, 412-416.
19. Choi S.; Herron J. A.; Scaranto J.; Huang H.; Wang Y.; Xia X.; Lv T.; Park J.; Peng H.; Mavrikakis M.; Xia Y.; **A Comprehensive Study of Formic Acid Oxidation on Palladium Nanocrystals with Different Types of Facets and Twin Defects.** *ChemCatChem* **2015**, *7*, 2077-2084.
20. Herron J. A.; Ferrin P.; Mavrikakis M.; **Electrocatalytic Oxidation of Ammonia on Transition-Metal Surfaces: A First-Principles Study.** *Journal of Physical Chemistry C* **2015**, *119*, 14692-14701.
21. Wang X.; Choi S.; Roling L. T.; Luo M.; Ma C.; Zhang L.; Chi M.; Liu J.; Xie Z.; Herron J. A.; Mavrikakis M.; Xia Y.; **Palladium-platinum core-shell icosahedra with substantially enhanced activity and durability towards oxygen reduction.** *Nature Communications* **2015**, *6*, 7594.
22. Elnabawy A. O.; Rangarajan S.; Mavrikakis M.; **Computational chemistry for NH₃ synthesis, hydrotreating, and NO_x reduction: Three topics of special interest to Haldor Topsøe.** *Journal of Catalysis* **2015**, *328*, 26-35.
23. Park J.; Zhang L.; Choi S.; Roling L. T.; Lu N.; Herron J. A.; Xie S.; Wang J.; Kim M. J.; Mavrikakis M.; Xia Y.; **Atomic Layer-by-Layer Deposition of Platinum on Palladium Octahedra for Enhanced Catalysts toward the Oxygen Reduction Reaction.** *ACS Nano* **2015**, *9*, 2635-2647.

(II) Jointly funded by this grant and others with leading intellectual contribution from this grant

24. Liu Y.; Göttl F.; Ro I.; Ball. M. R.; Sener C.; Aragão I. B.; Zanchet D.; Huber G. W.; Mavrikakis M.; Dumesic J. A.; **Synthesis Gas Conversion over Rh-Based Catalysts Promoted by Fe and Mn,** *ACS Catalysis* **2017**, *7*, 4550-4563
25. Yang X.; Roling L. T.; Vara M.; Elnabawy A. O.; Zhao M.; Hood Z. D.; Bao S.; Mavrikakis M.; Xia Y.; **Synthesis and Characterization of Pt-Ag Alloy Nanocages with Enhanced Activity and Durability towards Oxygen Reduction.** *Nano Letters* **2016**, *16*, 6644-6649.
26. Merte L. R.; Bai Y.; Zeuthen H.; Peng G.; Lammich L.; Besenbacher F.; Mavrikakis M.; Wendt S.; **Identification of O-rich structures on platinum(111)-supported ultrathin iron oxide films.** *Surface Science* **2016**, *652*, 261-268.

27. Kudernatsch W.; Peng G.; Zeuthen H.; Bai Y.; Merte L. R.; Lammich L.; Besenbacher F.; Mavrikakis M.; Wendt S.; **Direct Visualization of Catalytically Active Sites at the FeO–Pt(111) Interface.** *ACS Nano* **2015**, *9*, 7804-7814.

(III) Jointly funded by this grant and other grants with relatively minor intellectual contribution from this grant

28. Tao Z.; Chen C.; Szilvási T.; Keller M.; Mavrikakis M.; Kapteyn H.; Murnane M.; **Direct time-domain observation of attosecond final-state lifetimes in photoemission from solids.** *Science* **2016**, *353*, 62-67.
29. Scaranto J.; Mavrikakis M.; **Density functional theory studies of HCOOH decomposition on Pd(111).** *Surface Science* **2016**, *650*, 111-120.
30. Rangarajan S.; Mavrikakis M.; **DFT Insights into the Competitive Adsorption of Sulfur- and Nitrogen-Containing Compounds and Hydrocarbons on Co-Promoted Molybdenum Sulfide Catalysts.** *ACS Catalysis* **2016**, *6*, 2904-2917.
31. Scaranto J.; Mavrikakis M.; **HCOOH decomposition on Pt(111): A DFT study,** *Surface Science* **2016**, *648*, 201-211.
32. Matyba P.; Carr A.; Chen C.; Miller D. L.; Peng G.; Mathias S.; Mavrikakis M.; Dessau D. S.; Keller M. W.; Kapteyn H. C.; Murnane M.; **Controlling the electronic structure of graphene using surface-adsorbate interactions.** *Physical Review B* **2015**, *92*, 041407.
33. Cattelan M.; Peng G. W.; Cavaliere E.; Artiglia L.; Barinov A.; Roling L. T.; Favaro M.; Píš I.; Nappini S.; Magnano E.; Bondino F.; Gavioli L.; Agnoli S.; Mavrikakis M.; Granozzi G.; **The nature of the Fe-graphene interface at the nanometer level.** *Nanoscale* **2015**, *7*, 2450-2460.

Fundamental Mechanisms of C-X bond Transformations on Complex Molten Surfaces

¹Shizhao Su, ¹Behzad Tangeysh, ²David Mannini, ¹Eric McFarland, ¹Michael Gordon, ²Horia Metiu

¹Department of Chemical Engineering, University of California, Santa Barbara

²Department of Chemistry and Biochemistry, University of California, Santa Barbara

ABSTRACT

We are investigating pathways for transformation of methane on high-temperature liquid surfaces where deactivation by deposited coke will not occur. Work on molten metal alloys has shown composition-dependent activity for methane pyrolysis that can be correlated to changes in the electronic structure and Lewis acidity of the specific alloys. Recent work has focused on the surfaces of molten salts and metals suspended in molten salts. Results are provided for MgF_2 with comparisons of the solid and melt surfaces. The Lewis acidity of MgF_2 was probed by IR spectroscopy of absorbed CO and will be correlated to ongoing DFT and MD-DFT calculations. Strong Lewis basicity is also under investigation for C-H activation of methane using solvated electrons which theory predicts will form a stable reactive pairs. Preliminary work on C-H bond activation on Pt nanoparticles suspended in molten halide salts is also presented whereby the nanofluid system prevents stable carbon deposition on the solid metal surface. Propane dehydrogenation is used as a model reaction.

DE-FG-02-89ER14048: Fundamental Mechanisms of C-X bond Transformations on Complex Molten Surfaces

PI: Eric McFarland, Michael Gordon, Horia Metiu

Postdoc(s): Shizhao Su, Behzad Tangeysh, **Student(s):** Ches Upham, Davide Mannini

RECENT PROGRESS

Methane Activation on Lewis Acidic MgF_2

According to the optical basicity scale of molten salts, fluoride salts have the strongest Lewis acidity among all halide salts¹. MgF_2 was chosen as a catalyst candidate for methane pyrolysis, because its potential Lewis acidity could activate the C-H bond in methane. Our preliminary DFT results show methane dissociation on MgF_2 with H and CH_3 coordinated to 1 and 2 Mg ions respectively (Figure 1). The Lewis acidity of MgF_2 was measured with Diffuse Reflectance Infrared Fourier Transform Spectroscopy (DRIFTS) of CO adsorption and desorption on the MgF_2 surface, Figure 2. The peaks in the CO stretching region are listed in the figure, and are in good agreement with previous research of the IR spectra of CO absorbed on sol-gel prepared MgF_2 .² The bands are shifted towards smaller wavenumbers, indicating that CO is absorbed on the surface acid sites.

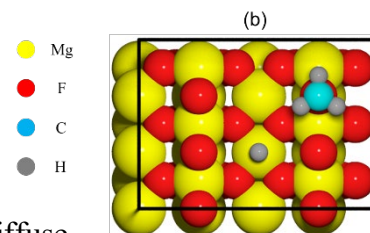


Fig 1.

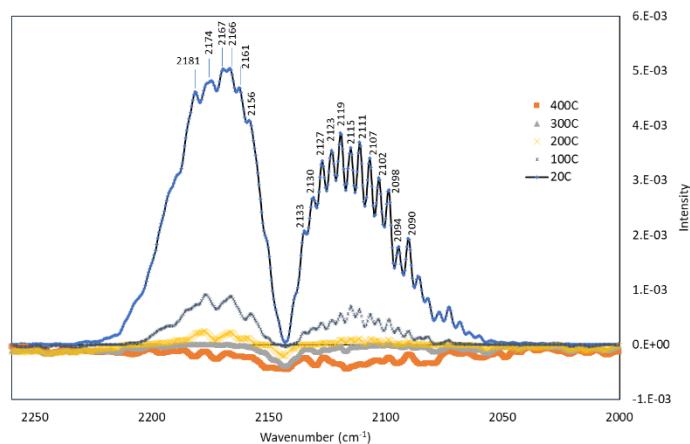


Figure 2: CO stretching region of DRIFTS spectra of absorbed CO on solid MgF₂ at 20°C and subsequently desorbed at higher temperatures up to 400°C.

The catalytic activity of both solid and molten MgF₂ for methane pyrolysis were measured experimentally. The turnover frequency (TOF) on the solid MgF₂ catalyst was calculated based on the methane conversion in a heated packed bed reactor from 650 to 1050°C (Figure 3(a)). In order to measure the reaction activity of molten MgF₂, 87mol% KF was added to MgF₂ to form a eutectic salt with lower melting point. The methane conversion in a 6cm (0.4s residence time) height molten salt bubble column reactor was measured (Figure 3b). In the bubble column, methane within the bubble can react both at the gas-liquid surface or within the gas phase. Further, methyl radicals or other intermediates from the surface will enter into the gas phase reaction network. Although the reaction rate at surface may be greater than in the gas phase, the surface to volume ratio is not large enough to ignore the bulk gas phase reaction. Without deconvolution of the methane decomposition

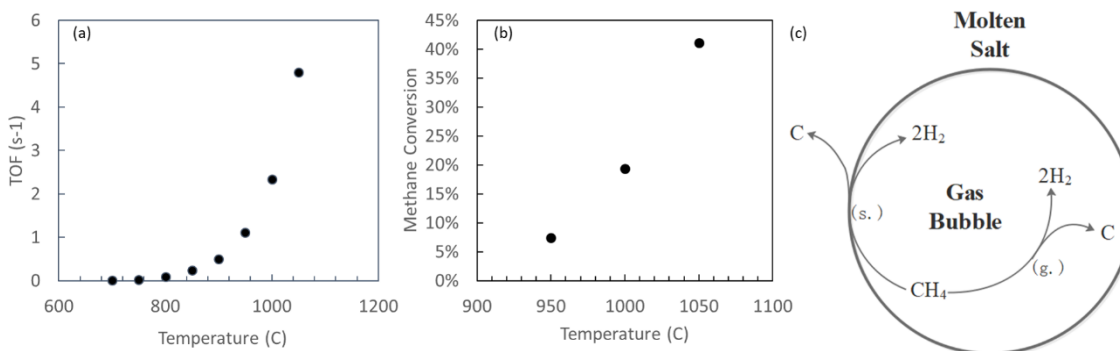


Figure 3. (a) TOF of solid MgF₂ catalyst in a packed bed reactor for methane pyrolysis reaction from 650–1050°C. (b) Methane conversion as a function of temperature for a KF–MgF₂ (%mole= 87:13) molten salt bubble column from 950–1050°C. (c) Reaction paths of methane decomposition in a molten salt bubble column reactor, ‘s.’ represents reaction at the gas-liquid interface, and ‘g.’ represents reaction in the bulk of the gas bubble.

reaction within the two different environments, the effective TOF of the molten KF–MgF₂ bubble column can not be calculated. Both solid and molten MgF₂ show unusually high activity for the methane pyrolysis reaction. The apparent activation energies (E_a) of both solid MgF₂ and molten KF–MgF₂ were measured to be 206kJ/mol and 231kJ/mol, respectively.

The Raman spectra of the carbon formed during methane pyrolysis in the solid MgF_2 packed bed and molten KF-MgF_2 bubble column are shown in Figure 4. The different I_D/I_G ratio indicates that the carbon formed in the solid MgF_2 packed bed was less “graphitic” than the carbon formed in the molten KF-MgF_2 bubble column. It is possible that on the solid MgF_2 surface, CH_3 radicals are formed and desorb which promotes the gas phase pathway. This is a possible explanation for the high TOF on the solid MgF_2 and lack of deactivation in continuous runs of over 24 hours. Carbon does not strongly bind to the MgF_2 surface. We are trying to understand the pathway to more graphitic carbon in the molten KF-MgF_2 bubble column which is also resistant to deactivated during continuous operation where clear phase separation occurs between the solid carbon and the molten salt.

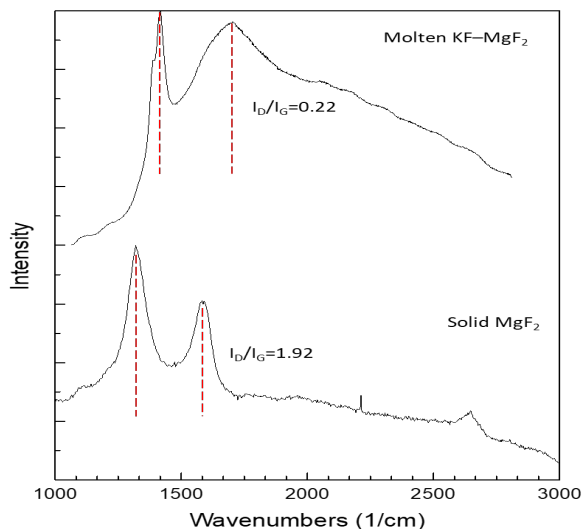
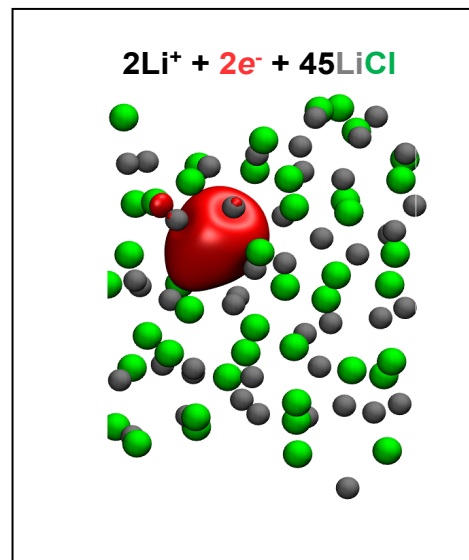


Figure 4. Raman spectra of the carbon formed during the methane pyrolysis in solid MgF_2 packed bed (bottom), and molten KF-MgF_2 bubble column (top). The I_D/I_G ratio was calculated after Lorentz peak fitting and peak integration.

Solvated Electrons as Strong Lewis Base

We have performed *ab initio* constant temperature molecular dynamics to study the electronic structure and the chemistry of the solvated electrons produced when an alkali metal is dissolved in a molten alkali halide. We found that the solvated electrons formed a stable pair, leading to a cavity inside the salt. The surface of equal electron density of this pair is shown at the right. The molten salt containing solvated electrons is a very strong Lewis base. Its work function is ~ 2.5 eV, which is close to that of an alkali metal. The energy of the molecular orbitals, which the solvated electrons occupy, fluctuates very strongly in time, due to the thermal motion of the ions in the melt. The difference between the highest and the lowest energy of this orbital is close to 1 eV. These fluctuations play an important role in any charge-transfer reaction taking place in this system.

The reactivity of Li dissolved in molten LiCl was calculated and found the following: this system dissociates methane to form CH_3^- and H^- ; it converts N_2 to N_2^{2-} ; and it dissociates hydrogen to form 2H^- . The dissolved alkali is a very potent reductant and dissolving RuCl_3 in a lithium-containing LiCl melt results in the formation of Ru



clusters. If there is enough Li dissolved in the salt these clusters become negatively charged, which prevents coarsening. We have found that the negatively charged Ru clusters are chemically active and dissociate N_2 .

Simulations of Na in NaCl have shown that while this system also produces solvated electrons, their chemistry is very different from those produced by Li in LiCl. This indicates that the chemical properties of the solvated electrons can be tuned by changing the alkali metal and the alkali halide.

We expect these alkali metal/molten alkali halide solutions to be exceptionally good base catalysts. The paradigm for these catalysts is that they act by donating an electron to a substrate to form a negative ion, which then reacts with another molecule, forms a product, and returns the electron to the melt. In this system, the electron is the base catalyst.

We plan to perform experiments in which we will produce Li by the electrolysis of molten LiCl/KCl salt and bubble gases through the electrolyte to cause them to react with the dissolved lithium. We will also perform experiments to prepare Ru and other metal clusters by reducing a Ru salt dissolved in molten LiCl-KCl salt. We expect such clusters to be very reactive by analogy with the Rieke metals produced by reduction of salts with potassium dissolved in ether solvents. In our case, the “solvent” is replaced by a molten salt.

Propane Dehydrogenation on Salt Suspended Pt Nanoparticles (PtNPs)

A nanofluid of PtNPs suspended in molten LiCl-LiBr-KBr (%mole= 25:37:38) was formed through thermal decomposition of H_2PtCl_6 , and the activity investigated for propane dehydrogenation. Suspended particles are predicted to favor the gas-liquid interface facilitating dehydrogenation. Melting of the halide host salt results in a colorless liquid (control), while in the presence of H_2PtCl_6 a grey melt was obtained, suggesting the formation of PtNPs, which were confirmed by TEM measurements (Figure 5).

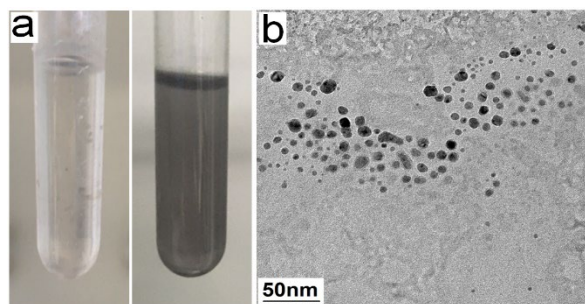


Figure 5. (a) Photographs of the test tubes containing molten LiCl-LiBr-KBr at 500°C with (grey) and without (clear) suspended PtNPs. (b) TEM image of PtNPs produced in molten LiCl-LiBr-KBr through thermal decomposition of H_2PtCl_6 .

At 400°C the suspension was shown to be stable by *In-situ* UV-Vis for over 350 minutes; however, when the temperature was increased further aggregation (as monitored by a decrease in the absorption) was observed. The dehydrogenation activity of the PtNP nanofluid was measured in a bubble column using mass spectroscopy and shown to have higher activity for alkane dehydrogenation than the salt control.

References

1. Duffy, J A., Optical Basicity: A Practical Acid-Base Theory for Oxides and Oxyanions, *Journal of Chemical Education*, **1996**, 73(12), 1138-1142
2. Wuttke, S.; Vimont, A.; Lavalley, J. C.; Daturi, M; Kemnitz, E., Infrared Investigation of the Acid and Basic Properties of a Sol-Gel Prepared MgF_2 , *J. Phys. Chem. C*, **2010**, 114, 5113-5120

Publications Acknowledging this Grant in 2015-2018

(I) Exclusively funded by this grant;

Upham, D. C.; Snodgrass, Z. R.; Zavareh, M. T.; McConnaughey, T. B.; Gordon, M. J.; Metiu, H.; McFarland, E. W., Molten salt chemical looping for reactive separation of HBr in a halogen-based natural gas conversion process. *Chemical Engineering Science* **2017**, *160*, 245-253.

Upham, D. C.; Agarwal, V.; Khechfe, A.; Snodgrass, Z. R.; Gordon, M. J.; Metiu, H.; McFarland, E. W., Catalytic molten metals for the direct conversion of methane to hydrogen and separable carbon. *Science* **2017**, *358* (6365), 917-921.

Kristoffersen, H. H.; Neilson, H. L.; Buratto, S. K.; Metiu, H., Stability of V₂O₅ Supported on Titania in the Presence of Water, Bulk Oxygen Vacancies, and Adsorbed Oxygen Atoms. *The Journal of Physical Chemistry C* **2017**, *121* (15), 8444-8451.

Upham, D. C.; Gordon, M. J.; Metiu, H.; McFarland, E. W., Halogen-Mediated Oxidative Dehydrogenation of Propane Using Iodine or Molten Lithium Iodide. *Catalysis Letters* **2016**, *146* (4), 744-754.

Pradhan, S.; Upham, D. C.; Metiu, H.; McFarland, E. W., Partial oxidation of propane with CO₂ on Ru doped catalysts. *Catalysis Science & Technology* **2016**, *6* (14), 5483-5493.

Kristoffersen, H. H.; Metiu, H., Interaction between Monomeric Vanadium Oxide Clusters Supported on Titania and Its Influence on Their Reactivity. *The Journal of Physical Chemistry C* **2016**, *120* (25), 13610-13621.

Kristoffersen, H. H.; Metiu, H., Structure of V₂O₅·nH₂O Xerogels. *The Journal of Physical Chemistry C* **2016**, *120* (7), 3986-3992.

Kristoffersen, H. H.; Metiu, H., Structure and Oxidizing Power of Single Layer α -V₂O₅. *Topics in Catalysis* **2016**, *59* (8), 809-816.

Huang, C.; Kristoffersen, H. H.; Gong, X.-Q.; Metiu, H., Reactions of Molten LiI with I₂, H₂O, and O₂ Relevant to Halogen-Mediated Oxidative Dehydrogenation of Alkanes. *The Journal of Physical Chemistry C* **2016**, *120* (9), 4931-4936.

Agarwal, V.; Metiu, H., Energy of Oxygen-Vacancy Formation on Oxide Surfaces: Role of the Spatial Distribution. *The Journal of Physical Chemistry C* **2016**, *120* (4), 2320-2323.

Agarwal, V.; Metiu, H., Oxygen Vacancy Formation on α -MoO₃ Slabs and Ribbons. *The Journal of Physical Chemistry C* **2016**, *120* (34), 19252-19264.

Upham, D. C.; Derk, A. R.; Sharma, S.; Metiu, H.; McFarland, E. W., CO₂ methanation by Ru-doped ceria: the role of the oxidation state of the surface. *Catalysis Science & Technology* **2015**, *5* (3), 1783-1791.

Chrétien, S.; Metiu, H., Hydrogen Dissociative Adsorption on Lanthana: Polaron Formation and the Role of Acid-Base Interactions. *The Journal of Physical Chemistry C* **2015**, *119* (34), 19876-19882.

Agarwal, V.; Metiu, H., Hydrogen Abstraction Energies and Ammonia Binding to BEA, ZSM-5, and α -Quartz Doped with Al, Sc, B, or Ga. *The Journal of Physical Chemistry C* **2015**, *119* (28), 16106-16114.

Reuter, K.; Metiu, H., A decade of computational surface catalysis, preface for Section 5 "Surface Catalysis", in *Handbook of Materials Modeling (2nd edition)*, Volume 1, Wanda Andreoni and Sidney Yip, editors in chief, Springer (Invited, submitted and accepted)

Metiu, H.; Agarwal, V.; Kristoffersen, H. H., Oxide catalysis, in *Handbook of Materials Modeling (2nd edition)*, Volume 2, Wanda Andreoni and Sidney Yip, editors in chief, Springer (Invited, submitted and accepted)

H. H. Kristoffersen and H. Metiu, Chemistry of solvated electrons in molten alkali chloride melts, *J. Phys. Chem. C* (submitted)

In preparation

Upham, D. C.; Kristoffersen, H. H.; Snodgrass, Z. R.; Gordon, M. J.; Metiu, H.; McFarland, E. W., Bromine and/or iodine for selective partial oxidation of propane and methane,

Metiu, H.; Agarwal, V.; Kristoffersen, H. H., The role of computations in catalysis, in *Reviews in Computational Chemistry*, Kenny Lipkowitz, editor, Wiley (**Invited**)

Su, S.; Mannini, D.; Metiu, H.; Gordon, M. J.; McFarland, E. W., Catalytic methane pyrolysis on supported transition metals in molten salts,

Upham, D. C.; Snodgrass, Z. R.; Gordon, M. J.; Metiu, H.; McFarland, E. W., Halogen Mediated Partial Combustion of Methane in Molten Salts to Produce CO₂-free Power and Solid Carbon,

Tangeysh, B.; Gordon, M. J.; Metiu, H.; McFarland, E. W., Nanocolloids of transition metal suspensions as catalysts in molten salts

(II) Jointly funded by this grant and other grants with leading intellectual contribution from this grant;

Su, S.; Mannini, D.; Metiu, H.; Gordon, M. J.; McFarland, E. W., Chlorine Production by HCl Oxidation in a Molten Chloride Salt Catalyst. *Industrial & Engineering Chemistry Research* **2018**, *57* (23), 7795-7801.

(III) Jointly funded by this grant and other grants with relatively minor intellectual contribution from this grant;

Parkinson, B.; Tabatabaei, M.; Upham, D. C.; Ballinger, B.; Greig, C.; Smart, S.; McFarland, E., Hydrogen production using methane: Techno-economics of decarbonizing fuels and chemicals. *International Journal of Hydrogen Energy* **2018**, *43* (5), 2540-2555.

Wang, X.; Liu, R.-F.; Cork, J.; Gu, Y.; Upham, D. C.; Laycock, B.; McFarland, E. W., Investigation of the Bromination/Dehydrobromination of Long Chain Alkanes. *Industrial & Engineering Chemistry Research* **2017**, *56* (34), 9411-9418.

Tuning Selectivity on Metal Oxide Catalysts and Supports with Organic Monolayers

J. Will Medlin, Daniel K. Schwartz, Lucas D. Ellis, Pengxiao Hao
University of Colorado Boulder

Presentation Abstract

Developing new strategies for design of surfaces that are more selective in catalyzing reactions of biomass-derived compounds has been a major thrust of heterogeneous catalysis research. One relatively new approach that has been applied on supported metal catalysts is to use organic monolayers or capping ligands to tune the surface and near-surface environment. Here, we describe our recent extension of this approach to metal oxide catalysts and supports such as TiO₂ and Al₂O₃ using alcohol dehydration and hydrodeoxygenation as probe reactions. By applying organophosphonate SAMs to metal oxide powders, these surfaces could be functionalized with various organic species. Phosphonate-modified TiO₂ found to be much more active and selective for alkanol dehydration than the uncoated catalyst. More interestingly, the dehydration activity could be controlled by systematically varying the electron-donating or withdrawing character of the organic ligands, suggesting a new approach for rational design of metal oxide catalysts. Application of organic ligands to metal catalyst supports can also have a strong influence on selectivity, as will be discussed in this presentation.

DE-SC0005239: Organic Monolayers for Bifunctional Catalysis

PI: J. Will Medlin

Postdoc(s): Timothy Van Cleve

Student(s): Lucas Ellis, Pengxiao Hao

RECENT PROGRESS

Control of Metal Oxide Reactivity

Reactivity of molecular catalysts can be controlled by organic ligands that regulate the steric and electronic properties of catalyst sites. This level of control has generally been unavailable for heterogeneous catalysts. We showed that self-assembled monolayers (SAMs) on titania with tunable electronic properties provided fine control over surface reactivity. Controlling the identity of substituents on benzylphosphonic acid SAMs modulated the near-surface electrostatics, enabling regulation of the dehydration activity of 1-propanol and 1-butanol over a wide range, with activities and selectivities of the optimal catalyst far exceeding those of uncoated TiO₂ (Figure 1). The dipole moment of the adsorbed phosphonate was strongly correlated to the dehydration activity; kinetic measurements and computational modeling indicated that the interfacial electric field altered the transition-state structure and energy.

Coating catalysts with SAMs having controllable charge distributions may provide a general

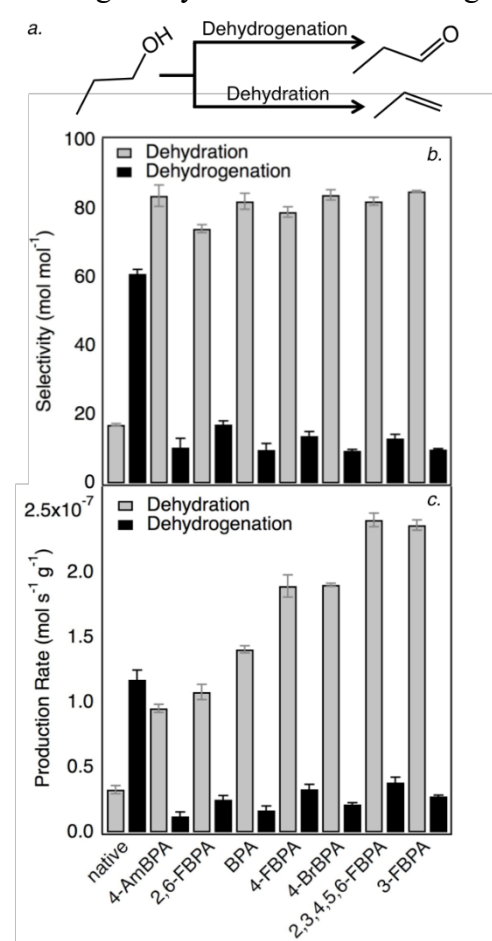


Figure 1: Reaction performance for TiO₂ functionalized with various phosphonates. Reaction pathway (a.), selectivity (b.) and activity (c.) of 1-propanol dehydration and dehydrogenation at 250°C. All columns to the right of the “native” catalyst represent phosphonic acids with different tail groups.

approach to heterogeneous catalyst design analogous to the variation of ligands in molecular catalysts.

Monolayers formed from organophosphonic acids were employed to stabilize porous γ -Al₂O₃, both as a single component and as a support for Pt nanoparticle catalysts, during exposure to hydrothermal conditions. To provide a baseline, structural changes of uncoated γ -Al₂O₃ catalysts under model aqueous phase reforming conditions (liquid water at 200 °C and autogenic pressure) were examined over the course of 20 h. These changes were characterized by X-ray diffraction, NMR spectroscopy, N₂ physisorption, and IR spectroscopy. It was demonstrated that γ -alumina was rapidly converted into a hydrated boehmite (AlOOH) phase with significantly decreased surface area. Deposition of alkyl phosphonate groups on γ -alumina drastically inhibited the formation of boehmite, thereby maintaining its high specific surface area over 20 h of treatment. ²⁷Al MAS NMR spectra demonstrated that hydrothermal stability increased with alkyl tail length despite lower P coverages. Although the inhibition of boehmite formation by the phosphonic acids was attributed primarily to the formation of Al₂O₃-PO_x bonds, it was found that use of longer-chain octadecylphosphonic acids led to the most pronounced effect. Phosphonate coatings on Pt/ γ -Al₂O₃ improved stability without adversely affecting the rate of a model reaction, catalytic hydrogenation of 1-hexene.

Control of Interfacial Reactivity

Numerous important reactions consisting of combinations of steps (for example, hydrogenation and dehydration) have been found to require bifunctional catalysts with both a late-transition metal component and an acidic component. We reported on the development of a method for preparing and controlling bifunctional sites by employing organic acid-functionalized monolayer films tethered to the support as an alternative to traditional ligand-on-metal strategies. This approach was used to create a reactive interface between the phosphonic acid monolayers and metal particles, where active-site properties such as acid strength were manipulated via tuning of the molecular structure of the organic ligands within the monolayer. After surface modification, the resultant catalysts exhibited markedly improved selectivity and activity towards hydrodeoxygenation of aromatic alcohols and phenolics. Moreover, by tuning the ligand of the acidic modifier, the rate of deactivation was significantly reduced.

One route toward the design of cooperative catalysts is to tether two different catalytically active functions so that they are in close proximity while avoiding undesirable interactions that can block active sites. Deposition of carboxylic acid (CA)-functionalized organophosphonate monolayers onto Al₂O₃-supported Pd nanoparticle catalysts to prepare bifunctional catalysts containing both Brønsted acid and metal sites. Modification with phosphonic acids (PAs) improved activity and selectivity for gas-phase deoxygenation (DO) reactions, but the degree of improvement was highly sensitive to both the presence and positioning of the CA group, suggesting a significant contribution from both the PA and CA sites. Short spacer lengths of 1–2 methylene groups between the phosphonate head and CA tail were found to yield the best DO rates and selectivities, whereas longer chains performed similarly to self-assembled monolayers having alkyl tails. Results from a combination of density functional theory and Fourier transform infrared spectroscopy suggested that the enhanced catalyst performance on the optimally positioned CAs was due to the generation of strong acid sites on the Al₂O₃ support adjacent to the metal. Furthermore, the high activity of these sites was found to result from a hydrogen-bonded cyclic structure involving cooperativity between the phosphonate head group and CA tail function. More broadly, these results indicate that functional groups tethered to supports via organic ligands can influence catalytic chemistry on metal nanoparticles.

We also recently have demonstrated the application of organophosphonic acids (PAs) to Pd/Al₂O₃ catalysts for low temperature vanillin HDO. Reaction studies indicated that PA-modification significantly improved the liquid-phase HDO activity; the yield to the desirable product, p-cresol, increased from 2.5% to 87% at 50 °C. This improvement was attributed to the creation of metal/acid bifunctional sites upon PA modification. In addition, HDO activity positively correlated with the Brønsted acidity of the PA modifier, which could be tuned by adjusting the PA tail functionality.

Publications Acknowledging this Grant in 2015-2018

(I) *Exclusively funded by this grant;*

- (1) Hao, P.; Schwartz, D. K.; Medlin, J. W. *Appl. Catal. A Gen.* **2018**, *561*, 1.
- (2) Van Cleve, T.; Underhill, D.; Veiga Rodrigues, M.; Sievers, C.; Medlin, J. W. *Langmuir* **2018**, *34* (12), 3619.
- (3) Ellis, L. D.; Trottier, R. M.; Musgrave, C. B.; Schwartz, D. K.; Medlin, J. W. *ACS Catal.* **2017**, *7* (12), 8351.
- (4) Ellis, L. D.; Pylypenko, S.; Ayotte, S. R.; Schwartz, D. K.; Medlin, J. W. *Catal. Sci. Technol.* **2016**, *6* (14), 5721.
- (5) Hao, P.; Pylypenko, S.; Schwartz, D. K.; Medlin, J. W. *J. Catal.* **2016**, *344*, 722.
- (6) Kahsar, K. R.; Schwartz, D. K.; Medlin, J. W. *J. Mol. Catal. A Chem.* **2015**, *396*, 188.

(II) *Jointly funded by this grant and other grants with leading intellectual contribution from this grant;*

- (7) Zhang, J.; Ellis, L. D.; Wang, B.; Dzara, M. J.; Sievers, C.; Pylypenko, S.; Nikolla, E.; Medlin, J. W. *Nat. Catal.* **2018**, *1* (2), 148.

- (8) Coan, P. D.; Ellis, L. D.; Griffin, M. B.; Schwartz, D. K.; Medlin, J. W. *J. Phys. Chem. C* **2018**, *122* (12), 6637.
- (9) Pang, S. H.; Medlin, J. W. *J. Phys. Chem. Lett.* **2015**, *6* (8), 1348.

Expanding the Chemistry of Molecular Nitrides and Phosphides in Groups 3 and 5 Transition Metals and the Selective Catalytic Monoborylation of Methane

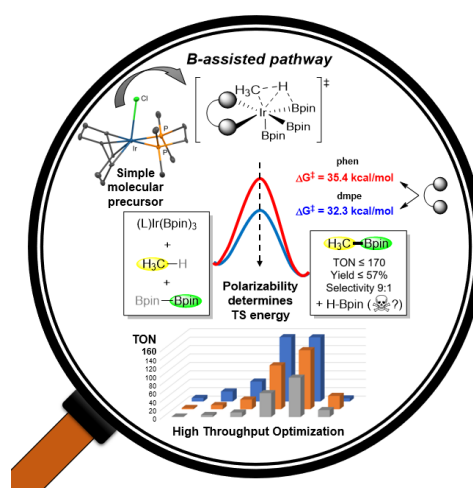
Daniel J. Mindiola, Lauren N. Grant, Dieter Sorsche

Department of Chemistry, University of Pennsylvania, Philadelphia, PA 19104 (USA)

Presentation Abstract

Metal nitrides and phosphides are indispensable archetypes in the context of catalysis and new important materials. Despite this entry to molecular forms of these types of ligands in early transition metals is exceedingly rare. Herein we report how low-valent titanium azides can allow for entry to the nitride group by reductively promoted N_2 extrusion. We have expanded these studies to the heavier congeners Zr and Hf and that similar nitrides (with higher basicities) can be prepared via reduction of tetravalent azide precursors. We also showcase how the phosphoethynolate ligand OCP^- can allow us to investigate new binding modes and new ligands (P-based) on early metals such as Sc, Ti, and V. OCP^- ligand can undergo a series of reactions as radical coupling and decarbonylation to form ligands classes for these early transition metals as P_2^{2-} , P_3^{3-} (via transient phosphido species), $[OCPPCO]^{2-}$. Another component of our research has been the optimization, via high-pressure and high-throughput analysis, of the

selective catalytic monoborylation of the methane to H_3CBpin (pin = pinacolato) using simple to prepare Ir(I) homogeneous pre-catalysts. A combination of high-throughput techniques, synthesis, and theoretical studies have been combined to allow us to understand the mode of operation but also optimize conditions and selectivity with TON of up to 170 and selectivity of 9:1 for the monoborylation (versus diborylation of methane, $H_2C[Bpin]_2$) as shown in the Figure.

found
be alsotypes
The
such
new
such
and

DE-FG02-07ER15893: Synthesis and Exploratory Catalysis of 3d Metals: Atom and Group-Transfer Reactions and the Activation and Functionalization of Small Molecules Including Greenhouse Gases

Grant Title Second Line if Necessary

Postdoc(s): Dieter Sorsche

Student(s): Lauren N. Grant

Publications Acknowledging this Grant in 2015-2018

Please classify your publications into three categories according to the source of support for the work published:

(III) Exclusively funded by this grant:

1. Thompson, R.; Tran, B. L.; Ghosh, S.; Chen, C.-H.; Pink, M.; Gao, X.; Carroll, P. J.; Baik, M.-H.; Mindiola, D. J. Addition of Si-H and B-H Bonds and Redox Reactivity Involving Low-Coordinate Nitrido Vanadium Complexes. *Inorg. Chem.* **2015**, *54*, 3068-3077.
2. Fortier, S.; Jackson, T. A.; Wijeratne, G. B.; Chen, C.-H.; Carroll, P. J.; Zolnhofer, E. M.; Grant, L. N.; Meyer, K.; Krzystek, J.; Ozarowski, A.; Mindiola, D. J.; Telser, J. Electronic Structure and Reactivity of a Well-Defined Mononuclear Complex of Ti(II). *Inorg. Chem.* **2015**, *54*, 10380-10397.
3. Hounjet, L. J.; Adhikari, D.; Pink, M.; Carroll, P. J.; Mindiola, D. J. Synthesis of an Iron(II) Ethyl Complex Accompanied by Formation of an Unusual Dinitrogen-Ligated Iron(I) Hydride. *Zeitschrift für Anorganische und Allgemeine Chemie (Special issue on Reactive Nitrogen-Containing Species: Generation, Characterization and Functionalization)* **2015**, *641*, 45-48.
4. Carroll, M. E.; Pinter, B.; Carroll, P. J.; Mindiola, D. J. Mononuclear and Terminally Bound Titanium Nitrides. *J. Am. Chem. Soc.* **2015**, *137*, 8884-8887.
5. Pinter, B.; Smith, K. T.; Kamitani, M.; Zolnhofer, E. M.; Tran, B. L.; Fortier, S.; Pink, M.; Wu, G.; Manor, B. C.; Meyer, K.; Baik, M.-H.; Mindiola, D. J. Cyclo-P₃ Complexes of Vanadium: Redox Properties and the Origin of the ³¹P NMR Spectroscopic Chemical Shift. *J. Am. Chem. Soc.* **2015**, *137*, 15247-15261.
6. Grant, L. N.; Carroll, M. E.; Carroll, P. J.; Mindiola, D. J. An Unusual Cobalt Azide Adduct that Produces A Nitrene Species for C-H Insertion Chemistry. *Inorg. Chem.* **2016**, *55*, 7997-8002.
7. Grant, L. N.; Pinter, B.; Kurogi, T.; Carroll, M. E.; Wu, G.; Manor, B.; Carroll, P. J.; Mindiola, D. J. Molecular Titanium Nitrides: Nucleophiles Unleashed. *Chem. Sci.* **2017**, *8*, 1209-1224.
8. Grant, L. N.; Pinter, B.; Manor, B. C.; Suter, R.; Grützmacher, H.; Mindiola, D. J. A Planar Ti₂P₂ Core Assembled by Reductive Decarbonylation of ⁻O-C≡P and P-P Radical Coupling. *Chem. Eur. J.* **2017**, *23*, 6272-6276 (selected as a hot paper).
9. Grant, L. N.; Miehllich, M. E.; Meyer, K.; Mindiola, D. J. Arrested Disproportionation in Trivalent, Mononuclear, and Non-Metallocene Complexes of Zr(III) and Hf(III). *Chem. Commun.* **2018**, *54*, 2052-2055.
10. Grant, L. N.; Pinter, B.; Manor, B. C.; Grützmacher, H.; Mindiola, D. J. A Scandium Stabilized Diisoposphaethynolate Ligand, [OCPPCO]⁴⁻. *Angew. Chem. Int. Ed.* **2018**, *57*, 1049-1052.
11. Dieter Sorsche, D.; Miehllich, M. E.; Zolnhofer, E. M.; Carroll, P. J.; Manor, B. C.; Meyer, K.; Mindiola, D. J. Metal-Ligand Cooperativity Promoting Sulfur-Atom Transfer in Ferrous Complexes and Isolation of a Sulfurmethylenephosphorane Adduct. *Manuscript accepted to Inorg. Chem.*
12. Ahn, S.; Sorsche, D.; Ryu, H.; Berritt, S.; Gau, M. R.; Mindiola, D. J. Baik, M.-H. Rational Design of a Catalyst for the Selective Monoborylation of Methane. *Manuscript submitted for publication.*

(II) Jointly funded by this grant and other grants with leading intellectual contribution from this grant;

13. Mullane, K. C.; Ryu, H.; Cheisson, T.; Grant, L. N.; Park, J. Y.; Manor, B. C.; Carroll, P. J.; Baik, M.-H.; Mindiola, D. J.; Schelter, E. J. C–H Bond Addition Across a Transient Uranium Nitrido and Formation of a Parent Uranium Imido Complex. *Manuscript accepted to J. Am. Chem. Soc.*

Surface Chemistry Experiments Related to Fischer-Tropsch Synthesis on Cobalt Deposited on Au(111)

C. Buddie Mullins (Presenter), Edward J. Evans Jr., Michael E. Floto
Mcketta Department of Chemical Engineering and Department of Chemistry
University of Texas at Austin
Austin, TX 78712

Presentation Abstract

We have experimentally studied the interactions of molecules (CO and C₂H₄) with a surface consisting of cobalt deposited on Au(111). Regarding carbon monoxide, we have briefly studied and quantified the dissociative adsorption of CO on a cobalt/gold alloy surface at a temperature of 470K. We also studied the co-adsorption of ethylene and cobalt (evaporated) onto a Au(111) substrate. Here we note that when ethene and Co are co-adsorbed and subsequently annealed higher hydrocarbons are produced. Such production does not occur when ethylene and cobalt are adsorbed separately.

DE-SC0018116: Surface Science Studies of Selective Fischer-Tropsch Chemistry on Cobalt Carbide Surfaces

Postdoc(s): N/A

Student(s): Edward J. Evans Jr., Michael E. Floto, Ryan A. Ciufo, Sungmin Han

Affiliations(s): Same as above.

RECENT PROGRESS

Dissociation of Carbon Monoxide on a Co/Au(111) Surface

A Cobalt/Au(111) surface was prepared by evaporating 15 monolayers (ML) of Co (calibrated by a Quartz Crystal Microbalance (QCM)) onto a Au(111) sample held at 77 K. Prior to surface chemistry experiments, the sample is heated to 450 K to desorb off background gas molecules that are on the surface. The heating step allows for some of the gold in the substrate to diffuse to the top of the deposited cobalt surface, but with a large amount of cobalt on the surface remaining (confirmed by AES). This sample was then exposed to carbon monoxide by a molecular beam followed by a temperature programmed desorption (TPD) measurement of the CO evolving from the sample. CO will molecularly adsorb onto a Co/Au surface at 77 K. As seen in the figure below (red curve), heating a Co/Au(111) sample exposed to CO will cause an increase in the mass 28 (CO) signal at relatively low temperatures, indicating molecular desorption of CO from the surface. For the Co/Au sample exposed to CO at 77 K (red curve in the figure below), the large desorption feature below 200 K is mostly due to weakly bound chemisorbed CO molecules. The second large desorption feature at ~ 300 K is due to more strongly bound molecularly chemisorbed CO molecules on the surface. If the Co/Au surface is held at an elevated temperature, CO

molecules can more readily dissociatively adsorb. To test this hypothesis a Co/Au(111) surface was held at 450 K during exposure by molecular to CO, and then cooled to 77 K. That sample was then heated to 650 K. The TPD plot is shown in the figure below as the black curve. As readily seen, the low temperature desorption peak (likely from background CO molecules physisorbed to the surface once it was cooled) is much smaller than in the same temperature range of the red curve. More importantly, there is no large desorption peak at 300 K, and there is a peak at 600 K. The feature around 600 K is attributed to the recombination of carbon and oxygen atoms left on the surface. These C and O atoms possibly come from dissociation of adsorbed CO while the sample is held at 450 K during adsorption. The absence of the desorption peak at 380 K indicates no strongly bound chemisorbed CO molecules on the surface, and the peak at 600 K can be argued to be a result of the associative desorption of C and O atoms on the surface from the dissociative

adsorption of CO molecules at the elevated temperature.

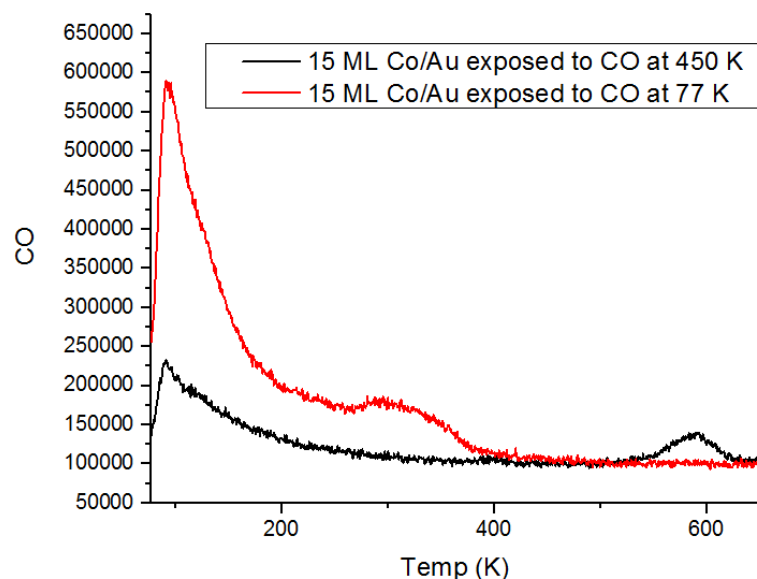


Figure: TPD spectra of 15 ML Co/Au surfaces exposed to CO at 77 K (red curve) and 450 K (black curve).

Synthesis of Higher Hydrocarbons from Simultaneous Deposition of Ethene and Co on Au(111)

We observe the production of various alkanes and alkenes due to the simultaneous co-adsorption of ethylene at a partial pressure of 2×10^{-7} Torr and 4 ML of cobalt on a Au(111) substrate. Notable masses that yielded appreciable signal are shown in the temperature-programmed desorption in the figure below. Considering that hydrocarbons share many masses in their fragmentation patterns, it is difficult to assign certain masses to particular molecules. However, some masses are fairly unique to specific hydrocarbons, allowing us to suggest the production of pentene ($m/z = 55$), butane ($m/z = 56$) and ($m/z = 58$) at ~ 200 K. We also observe alkanes with at least five carbons via $m/z = 57$, which shows an additional desorption feature at ~ 225 K. Very small signals from $m/z = 86$ (hexane) and $m/z = 71$ (heptane) (not shown) were observed at the same desorption temperature as the other hydrocarbons, supporting our claim regarding the production of larger hydrocarbons. Regardless of the hydrocarbon designation, alkane production indicates hydrogenation capability with the H_2 source likely coming from decomposed ethylene molecules or background H_2 . More importantly, products with larger masses indicate C-C bond formation upon co-adsorption of cobalt and ethylene, which is a critical step in olefin production for Fischer Tropsch synthesis. It is worth noting that while ethylene shows the unique characteristic of yielding these other hydrocarbons with concurrent cobalt exposure, co-adsorption of ethane and Co only

yields ethane desorption with some H₂ desorption, mostly due to background H₂. Perhaps co-adsorption of cobalt with other alkenes will provide similar hydrocarbon production. These experiments are currently underway.

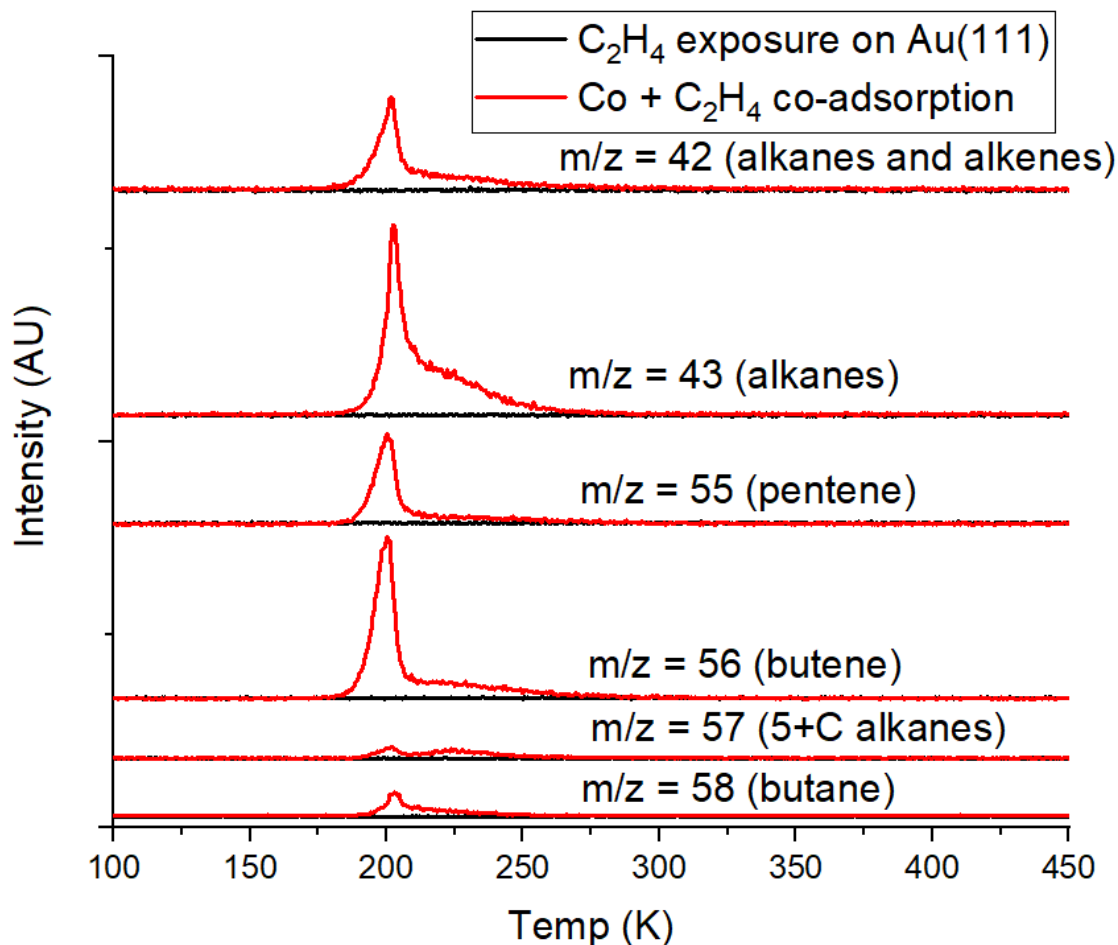


Figure: TPD measurements after C₂H₄ exposure on Au(111) (black) and after cobalt and C₂H₄ co-adsorption on Au(111) (red) at 77 K.

Publications Acknowledging this Grant in 2015-2018 (Grant began in June 2017)

Please classify your publications into three categories according to the source of support for the work published:

(I) *Exclusively funded by this grant;*
None

(II) *Jointly funded by this grant and other grants (Welch Foundation) with leading intellectual contribution from this grant;*

Evans Jr., E. J.; Li, H.; Yu, W.-Y.; Mullen, G. M.; Henkelman, G.; Mullins, C. B. The mechanism and production of hydrogen from ethanol dehydrogenation on Pd-Au model catalysts *Phys. Chem. Chem. Phys.* **2017**, *19*, 30578-30589.

<http://dx.doi.org/10.1039/C7CP05097F>

Mullen, G. M.; Evans Jr., E. J.; Siegert, B. C.; Miller, N. R.; Rosselet, B. K.; Sabsevari, I.; Brush, A.; Duan, Z.; Mullins, C. B. The interplay between ceria particle size, reducibility, and ethanol oxidation activity of ceria-supported gold catalysts. *React. Chem. Eng.* **2018**, *3*, 75-85.

<http://dx.doi.org/10.1039/C7RE00175D>

Han, S.; Mullins, C. B. Surface alloy composition controlled O₂ activation on Pd-Au bimetallic model catalysts. *ACS Catalysis* **2018**, *8*, 3641-3649.

<http://dx.doi.org/10.1021/acscatal.8b00140>

(III) *Jointly funded by this grant and other grants with relatively minor intellectual contribution from this grant;*
None

Matthew Neurock

Elucidating and Controlling Active Sites and their Environments in the Electrocatalytic Reduction of CO₂ over Post Transition Metals

Matthew Neurock¹, Stuart Winikoff¹, John DiMeglio², Joel Rosenthal², Jonnathan Medina-Ramos³, Daniel Lutterman⁴, Robert Sacci⁴

¹*Department of Chemical Engineering and Materials Science, University of Minnesota, Minneapolis, MN.*

²*Department of Chemistry, University of Delaware, Newark Delaware.*

³*Chemical Science and Engineering Division, Argonne National Laboratory, Argonne, IL.*

⁴*Chemical Science Division, Oak Ridge National Laboratory, Oak Ridge TN.*

Presentation Abstract

The direct catalytic conversion of CO₂ to CO or formic acid and their subsequent transformation to fuels and chemical intermediates offers one potentially attractive route toward the development of carbon-neutral sustainable strategies to meet increasing energy demands. Nature carries out these transformations quite exquisitely and can be used to guide the development of heterogeneous electrocatalytic systems. Herein we examine the coupling of non-noble metal catalysts such as Bi and Sn together with different ionic liquids to carry out these reactions with high current densities and Faradaic efficiencies. Novel potential-dependent ab initio methods were used to explore these systems in detail and compare with experimental results. The metal and electrolyte are manipulated to control the selective formation to CO or formic acid. The active sites and the local solution environment that forms upon cathodic polarization resemble those present in enzymes. The results present insights into the mechanisms involved in the controlling proton and electron transfer steps and suggest new ways to potentially engineer the catalyst and its environment.

DE-AC02-05CH11231: Fluid Interface Reactions, Structures & Transport, an Energy Frontier Research Center

PI: Wesolowski, D., Oak Ridge National Laboratory (LEAD of the EFRC)

Postdoc(s): Stuart Winikoff, University of Minnesota

Publications Acknowledging this Grant in 2015-2018

Winikoff, S.G., DiMeglio, J.L., Medina Ramos, J., Neurock, M. Cooperative Electrode-Electrolyte Interactions Drive Efficient Electrocatalytic Reduction of CO₂ to CO, In Review, **2018**. (Exclusively Funded by this grant)

Medina-Ramos, J., Zhang, W.W., Yoon, K., Bai, P., Chemburkar, A., Atifi, A., Lee, S.S. Fister T.T., Ingram, B.J. Hubaud, T. T. Fister, P. Fenter, W. Zhang, K. Yoon, A. van Duin, P. Bai, A.

Chemburkar, W. Tang, Rosenthal, J., Neurock, M., van Duin, A., Fenter, P. Cathodic Corrosion at the Bismuth Ionic Liquid Electrolyte Interface Under Conditions for CO₂ Reduction, *Chem. Mater.*, **2018**, 30, 7, 2362-2373. (Jointly funded by this grant and others).

Atifi, A., Boyce, D.W., DiMeglio, J.L. and Rosenthal, J. Directing the Outcome of CO₂ Reduction at Bismuth Cathodes Using Varied Ionic Liquid Promoters, *ACS Catal.*, **2018**, 8, 4, 2857-2863. (Exclusively funded by this grant)

Medina-Ramos, J., Lee, S.S., Fister, T.T., Hubaud, A.A., Sacci, R.L., Mullins, D.R., DiMeglio, Pupillo, R.C., Velardo, S.M. Lutterman, D.A., Rosenthal, J. Structural Dynamics and Evolution of Bismuth Electrodes during Electrochemical Reduction of CO₂ in Imidazolium Based Ionic Liquid Solutions, *ACS Catal.*, **2017**, 10, 7285-7295, (Jointly funded by this Grant and others).

Zhang, Z., Chi, M., Veith, G.M., Zhang, P., Lutterman, D.A., Rosenthal, J., Overbury, S., Dai, S., Zhu, H. Rational Design of Bi Nanoparticles for Efficient Electrochemical CO₂ Reduction: The Elucidation of Size and Surface Condition Effects *ACS Catal.*, **2016**, 6, 9, 6255-6264. (Jointly funded by this grant and others)

Medina-Ramos, J., Pupillo, R.C., Keane, T.P., DiMeglio, J.L., J. Rosenthal; Efficient Conversion of CO₂ to CO Using Tin and Other Inexpensive and Easily Prepared Post-Transition Metal Catalysts, *J. Am. Chem. Soc.*, **2015**, 137, 15, 5021-5027. (Exclusively funded by this grant)

Winikoff, S.G., Rosenthal, J., Neurock M. "Selective Pathways in Electrocatalytic Reduction of CO₂ over Bi in Imidazolium-Based Ionic Liquids", *J. Am. Chem. Soc.*, Submitted, **2018**. (Exclusively funded by this grant)

Winikoff, S.G., Yoon, K., van Duin, A., Neurock, M., Bismuth Surface Structure in Electrocatalyzed CO₂ Reduction, submitted, *ACS Catal.*, **2018** (Exclusively funded by this grant)

Medina-Ramos, J., DiMeglio, J.L., Rosenthal, J., Efficient Reduction of CO₂ to CO with High Current Density Using in Situ or ex Situ Prepared Bi-Based Materials, *J. Am. Chem. Soc.*, **2014**, 136, 23, 8361-8367. (Exclusively funded by this grant)

Efficient Oxygen Electrocatalysis by Nanostructured Mixed-Metal Oxides

XiangKui Gu, Juliana Carnerio, Samji Samira, Nuwandi M Ariyasingha
and Eranda Nikolla

Department of Chemical Engineering and Materials Sciences, Wayne State University,
Detroit, Michigan-48202 (USA)

Oxygen electrocatalysis plays a critical role in the efficiency of important energy conversion and storage systems. While many efforts have focused on designing efficient electrocatalysts for these processes, optimal catalysts that are inexpensive, active, selective and stable are still being searched. Nonstoichiometric, mixed metal oxides present a promising group of electrocatalysts for these processes due to the versatility of the surface composition and fast oxygen conducting properties. We demonstrate, using a combination of theoretical and experimental studies, the ability to develop design principles that can be used to engineer oxygen electrocatalysis activity of layered, mixed ionic-electronic conducting Ruddlesden-Popper (R-P) oxides. We show that a density function theory (DFT) derived descriptor - O_2 binding energy on a surface oxygen vacancy – can be effective in identifying efficient R-P oxide structures for ORR. Using a controlled synthesis method, well-defined nanostructures of R-P oxides are obtained, which along with thermochemical and electrochemical activity studies are used to validate the design principles. This has led to the identification of a highly active ORR electrocatalyst, nanostructured Co-doped lanthanum nickelate oxide, which when incorporated in solid oxide fuel cell cathodes significantly enhances the performance at intermediate temperatures (~ 550 °C), while maintaining long-term stability. The reported findings demonstrate the effectiveness of the developed design principles to engineer mixed ionic-electronic conducting oxides for efficient oxygen electrocatalysis, and the potential of nanostructured Co-doped lanthanum nickelate oxides as promising catalysts for oxygen electrocatalysis.

DE-SC0014347: Nanostructured, Targeted Layered Metal Oxides as Active and Selective Heterogeneous Electrocatalysts for Oxygen Evolution

PI: Eranda Nikolla

Postdoc(s): XiangKui Gu, Nuwandi M Ariyasingha

Institution: Wayne State University, Detroit, MI

RECENT PROGRESS

DFT Predicted Activity Trend for Oxygen Electrocatalysis

The activity of electrochemical high temperature ORR/OER on R-P oxides is generally governed by the surface oxygen exchange process. The first step in this process is the generation of a surface oxygen vacancy via a surface lattice oxygen diffusion into an interstitial site. The second step involves the dissociation of gas-phase O_2 on this surface oxygen vacancy with one oxygen atom

filling in the surface oxygen vacancy and the other one binding to the surface as an oxygen adatom. In the third step, evolution of the oxygen from the oxide to gas phase occurs via the oxygen adatom association with a surface lattice oxygen, leaving behind a surface oxygen vacancy. Lastly, the interstitial oxygen is transported to a surface oxygen vacancy to close the catalytic cycle. DFT calculations are used to determine the energetics associated with these elementary steps as a function of the B-site composition (B = Fe, Co, Ni, and Cu) on B-site terminated (001) surfaces of these oxides (the most active surfaces for ORR). These studies show that doping the Ni-site of LNO with Cu leads to an increase in the energy barrier for surface oxygen vacancy formation through the diffusion of a surface lattice oxygen into an interstitial site. Conversely, doping it with Fe and Co facilitates this process, with Co-doped LNO exhibiting the lowest barrier of ~ 1.14 eV. The next step involves O₂ dissociation on a surface oxygen vacancy with one O atom filling the vacancy and the other one binding to an adjacent transition metal atom. In the case of the oxides with a mixed B-site, the O atom binds to the transition metal with the highest oxygen affinity, such as Fe and Co. The third step in the catalytic cycle involves oxygen evolution. The energetics of this step can be predicted using the formation energy of a surface oxygen vacancy ($V_o^{\bullet\bullet}$) generated from the desorption of a surface lattice O as 1/2 O₂ in the gas phase. We find that this surface $V_o^{\bullet\bullet}$ formation energy is also linearly correlated to the binding energy of O₂ on a surface oxygen vacancy and becomes lower as O₂ binding becoming weaker. An intersection in the opposite linear trends for the energy of the transition state for O₂ dissociation and surface $V_o^{\bullet\bullet}$ formation energy (O₂ evolution) versus O₂ binding energy is found. The oxides (i.e., Co doped LNO) near this intersection provide the best compromise between the energetics associated with these two steps (the most critical for surface oxygen exchange), and thus are predicted to result in the highest activity for surface oxygen exchange. The last step involves healing of a surface vacancy via oxygen diffusion from an interstitial site, which is generally favorable both kinetically and thermodynamically on these oxides. A microkinetic model is used to determine the qualitative activity trend for this process. A “volcano”-type relationship between the calculated rates and the binding energies of O₂ on a surface O vacancy is found, suggesting that the O₂ binding energy is a good descriptor for predicting the surface oxygen exchange activity of these oxides. This structure-activity relation predicts that oxides near the top of the “volcano” (i.e., Co-doped LNO) provide the optimal oxygen binding strength and should exhibit the highest activity for oxygen reduction and evolution.

Synthesis and catalytic activity of controlled nanostructured R-P oxide electrocatalysts

Undoped La₂NiO_{4+ δ} (LNO) and Fe, Co, and Cu-doped nanostructured lanthanum nickelate oxides are synthesized using a facile reverse microemulsion method. The crystal structures of the synthesized oxides (Co-LNO, Cu-LNO, Fe-LNO and LNO) are analyzed using powder X ray diffraction (XRD) and the spectra are compared with that of the standard bulk LNO, which has a K₂NiF₄ structure within the I4/m space group. The morphology of the LNO and B-site doped LNO nanostructures is analyzed using scanning electron microscopy showing predominantly a nanorod-shaped geometry for all the synthesized oxides (Figure 1). Surface structure characterization of these nanostructures is conducted using HR-STEM-HAADF, LEIS and EDS

elemental mapping. These studies confirm the termination of the nanostructures by (001) transition metal oxide surfaces.

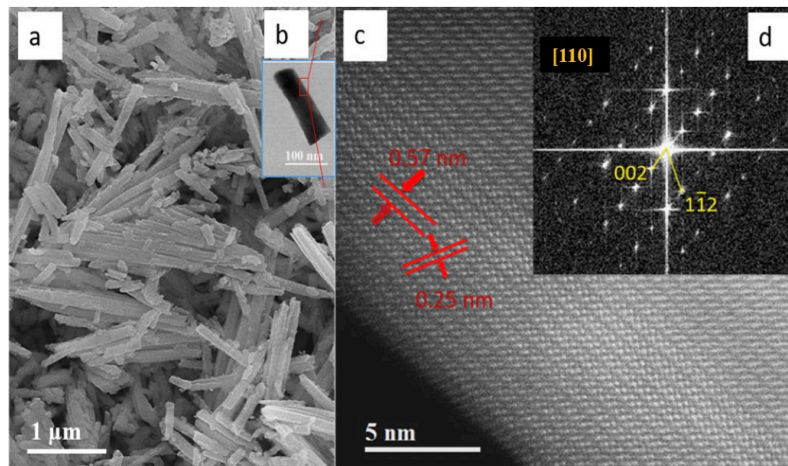


Figure 1. (a) SEM image of the nanorod structures. (b) Bright-field STEM image of a typical nanorod. (c) HAADF-STEM image of nanorod surface from the area outlined by the red square in (b) showing continuous lattice fringes. (d) Corresponding Fast Fourier Transform pattern showing that Co-LNO nanorods with the (001) surfaces perpendicular to the projected zone axis, [110].

The activity toward surface oxygen exchange is determined using $^{18}\text{O}_2$ labeled isotopic experiments on these nanostructured R-P oxides. Among all the catalysts tested, Co-LNO displayed the best performance for the surface oxygen exchange process in terms of the lowest apparent activation energy and highest normalized rates (TOFs) at a particular temperature as compared to the other catalysts. The experimental results indicate that the activity trend for thermochemical surface oxygen exchange follows: Co-LNO > Fe-LNO > LNO > Cu-LNO; consistent with the DFT predictions. To evaluate the potential of the Ni-site doping on improving the electrochemical activity of the R-P oxides toward electrochemical oxygen reduction, the most catalytically active nanostructured Co-doped LNO is tested and compared to LNO nanorods using button cell geometry SOFCs (Figure 2). In these experiments, we have used an anode-supported SOFCs (Ni – YSZ (anode)|YSZ (electrolyte)|YSZ – R-P oxides (cathode)), where the anode is exposed to pure hydrogen (50 ml min^{-1}) and the cathode to atmospheric air. In these cells, the O_2 molecules are reduced ($1/2 \text{ O}_2 + 2\text{e}^- \Rightarrow \text{O}^{2-}$) on the R-P oxide at the cathode generating oxygen ions (O^{2-}), which are transported through the YSZ electrolyte to the anode, where H_2 electro-oxidation ($\text{H}_2 + \text{O}^{2-} \Rightarrow \text{H}_2\text{O} + 2\text{e}^-$) takes place. The electrochemical performance results suggest that doping the Ni-site of nanostructured LNO with Co leads to significant improvement in the overall cell performance at both temperatures. The power densities of the cells containing Co-doped LNO are $\sim 50\%$ higher than the ones with LNO nanorods. No significant changes are observed in the crystal structure of the Co-doped LNO nanorods after electrochemical studies, suggesting that doping the B-site of LNO with small concentration of Co enhances the oxygen reduction activity of the lanthanum nickelate oxide without compromising stability.

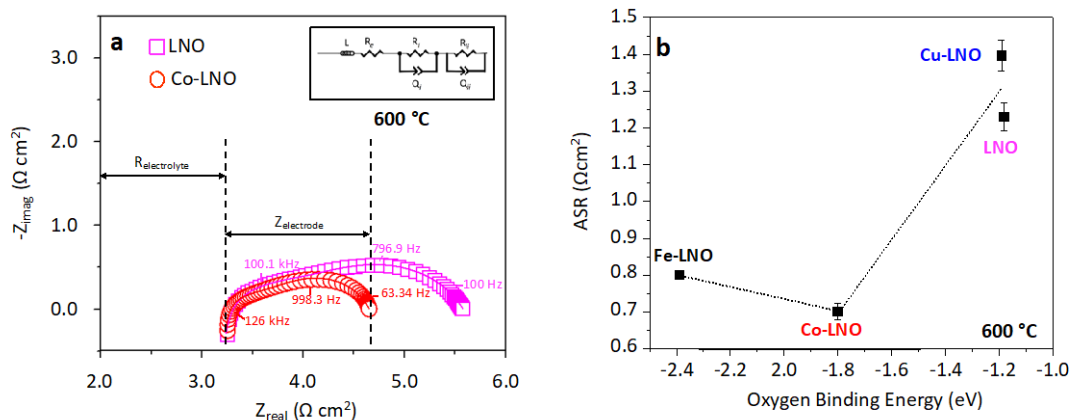


Figure 2. (a) Impedance spectra for R-P oxides–YSZ | YSZ | YSZ–R-P oxides symmetric cells operating at $p\text{O}_2 = 1$ atm and 600 °C. The equivalent circuit used to fit the polarization resistance curves is shown as an inset. (b) Area specific resistance for R-P oxides–YSZ | YSZ | YSZ–R-P oxides symmetric cells as function of O_2 binding energy on a surface oxygen vacancy at 600 °C.

Publications Acknowledging this Grant in 2015-2018

(IV) Exclusively funded by this grant;

- Gu X.,[‡] Carneiro J.,[‡] Samira S., Das A., Ariyasingha N., Nikolla E.*, “Efficient Oxygen Electro-catalysis By Nanostructured Mixed Metal Oxides”, *J. of Amer. Chem. Soc.*, DOI: 10.1021/jacs.7b11138, 2018.
[‡] Equal contributions
- Gu X.; Nikolla E.; “Design of Ruddlesden-Popper Oxides with Optimal Surface Oxygen Exchange Properties for Oxygen Reduction and Evolution from First Principles”, *ACS Catalysis* 7, 5912, 2017.
- Das A.; Xhafa E.; Nikolla E. “Electro- and thermal-catalysis by layered, first series Ruddlesden-Popper oxides”, *Catal. Today - Special Issue on “Catalysis by Mixed Oxides”*, 2277 (2), 2016.

(V) Jointly funded by this grant and other grants with leading intellectual contribution from this grant;

- Gu X.,[‡] Samira S.,[‡] Nikolla E.*, “Oxygen Sponges for Electrocatalysis: Oxygen Reduction/Evolution on Non-stoichiometric, Mixed Metal Oxides”, *“Up and Coming” Series for the Journal of Chemistry of Materials*, 30 (9), pp 2860–2872, 2018. [‡] Equal contributions

Effect of Polarity Matching on Kinetics of Hydrogen Atom Transfer from Transition-Metal Hydrides to Trityl Radicals

Jack R. Norton,¹ Thilina Gunasekara,¹ Graham P. Abramo,¹ Andreas Hansen,² Hagen Neugebauer,² Markus Bursch,² Stefan Grimme²

¹ Department of Chemistry, Columbia University, 3000 Broadway, New York, New York 10027, United States

² Mulliken Center for Theoretical Chemistry, Institut für Physikalische und Theoretische Chemie, Rheinische Friedrich-Wilhelms Universität Bonn, Beringstraße 4, 53115 Bonn, Germany

Presentation Abstract

A useful concept in Hydrogen Atom Transfer (HAT) in organic reaction systems is radical polarity. For example, if radicals are classified as either electrophilic or nucleophilic, an electrophilic species will react more readily with a nucleophilic H• donor than with an electrophilic H• donor (and *vice versa*). Thus, a single-step HAT reaction that is slow because the donor and the acceptor have the same polarity can be replaced with two HAT steps in which the H• donor and acceptor have opposite polarities. This is known as Polarity Reversal Catalysis. We are investigating the applicability of this concept to H• transfer from transition-metal hydrides to radical substrates. As a model system, H• transfer from (C₅Ph₅)Cr(CO)₃H (**1**) to tris(*p*-tert-butylphenyl)methyl radical (**2**) has been studied. The electrophilicity of the radicals has been determined by Density Functional Theory calculations as the global electrophilicity index (ω). Both **1** and **2** have similar electrophilicities, i.e., $\omega = 3.0$ and 6.7 , respectively. The second-order rate constant and the activation energy for the reaction between **1** and **2** are $1.4 \times 10^{-2} \text{ M}^{-1} \text{ s}^{-1}$ and $9.5 \text{ kcal mol}^{-1}$ at 25 °C, respectively. To catalyze this HAT reaction, we have used TEMPO radical (**3**) which is much more electrophilic ($\omega = 15.5$). As expected, H• transfer from **1** to **3** to form TEMPO-H and metalloradical is very fast, with a second-order rate constant of $1.7 \times 10^2 \text{ M}^{-1} \text{ s}^{-1}$ and an activation energy of $2.1 \text{ kcal mol}^{-1}$ at 25 °C. The reaction between TEMPO-H and **2** has a second-order rate constant of $4.1 \times 10^{-2} \text{ M}^{-1} \text{ s}^{-1}$ and an activation energy of $7.2 \text{ kcal mol}^{-1}$ at 25 °C. We then studied the reaction of **1** and **2** in the presence of 25 mol% **3**. Kinetic simulation and experimental results show a noticeable, albeit modest, catalytic effect.

Grant or FWP Number: The Activation of Hydrogen by First-Row Transition-Metal Complexes

PI: Lead PI(s) Name(s) (*include only if different from above*)

Postdoc(s): Thilina Gunasekara

Student(s): Graham P. Abramo (*former graduate student*)

Affiliations(s): (*include only if different from above*)

RECENT PROGRESS

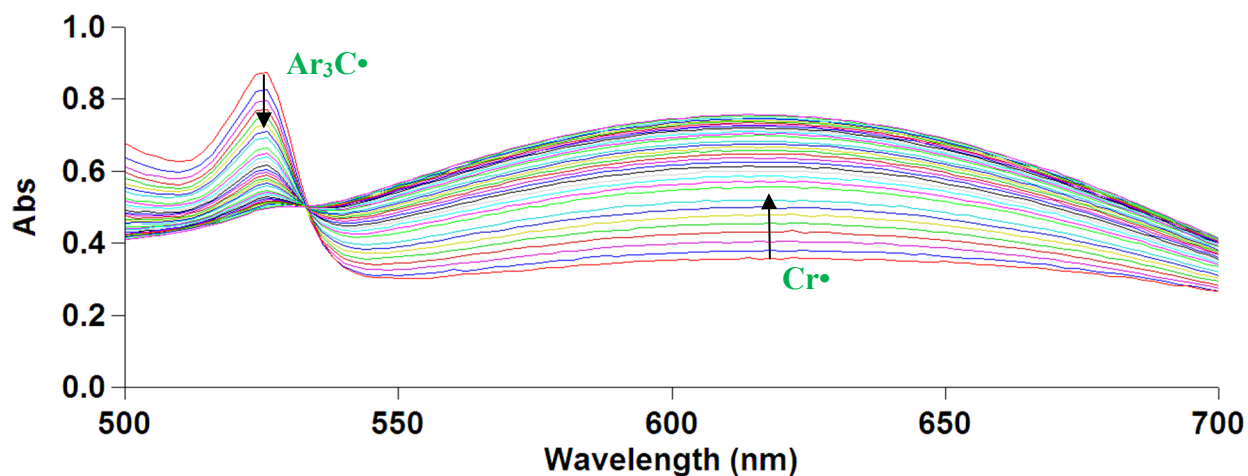
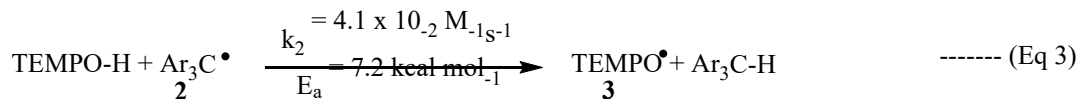
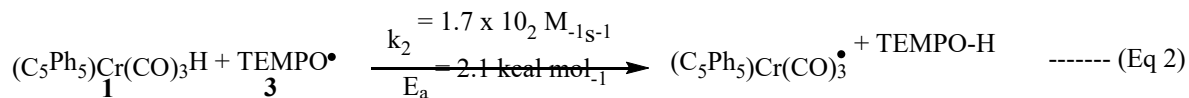
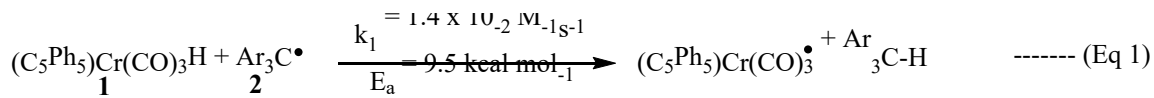


Figure 1. Time profile (0 – 250 minutes) of UV-Visible spectrum for the reaction between **1** and **2** (Eq 1).

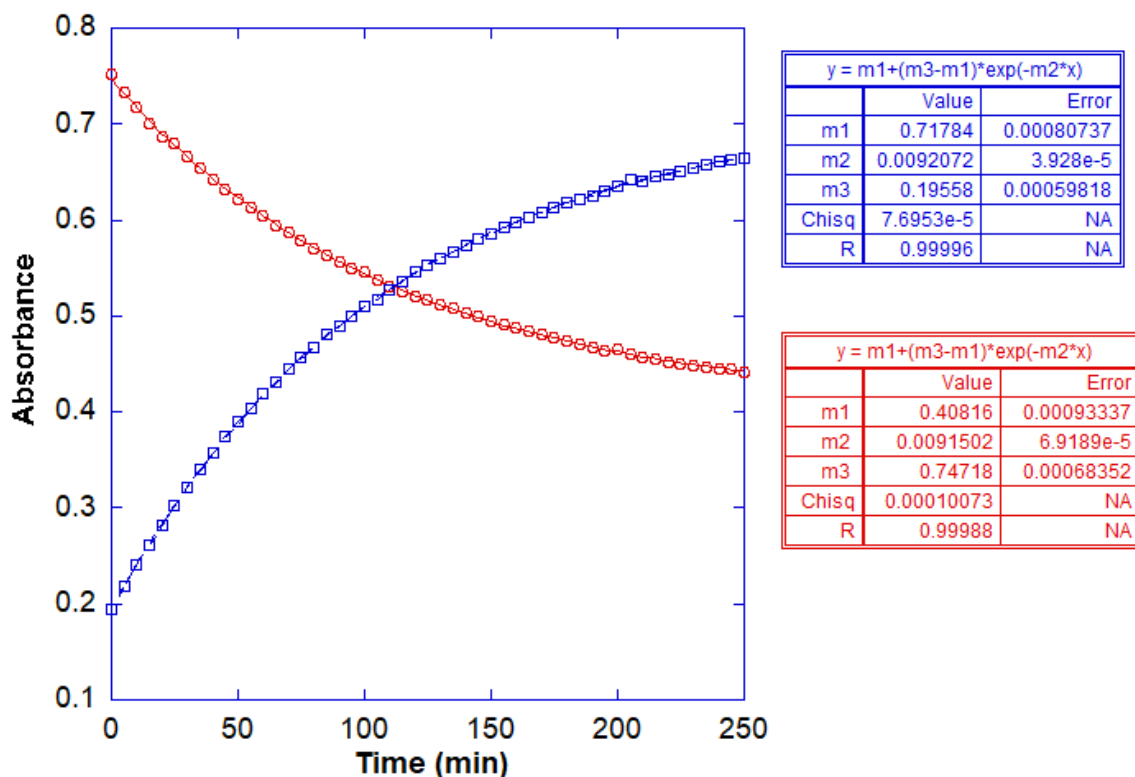


Figure 2. Time profile (0 – 250 minutes) of absorbance at 523 nm (red) and 611 nm (blue) for the reaction between **1** and **2** (Eq 1).

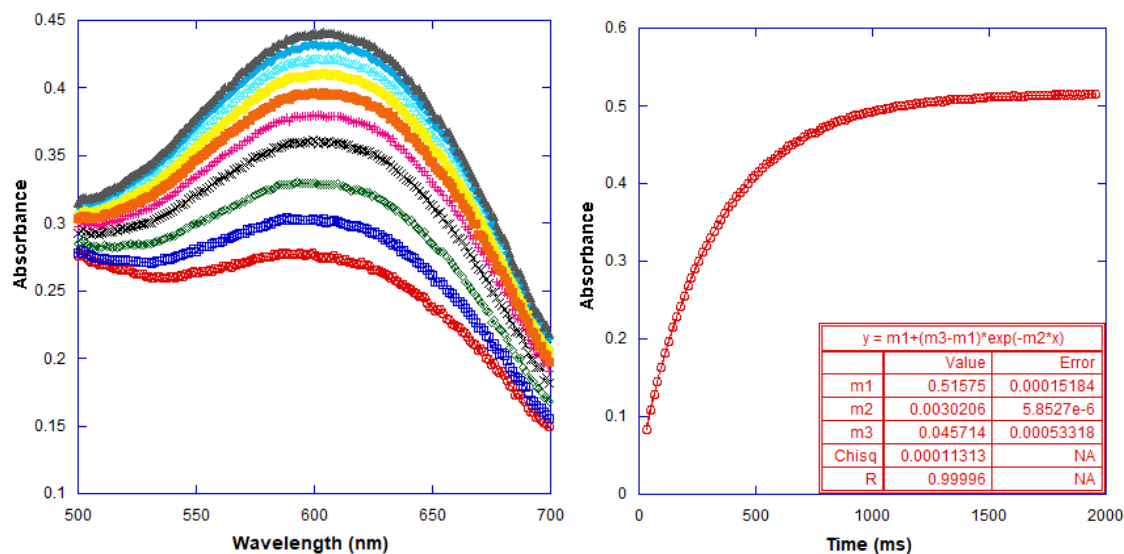


Figure 3. Stopped-flow kinetics for the reaction between **1** and **3** (Eq 2). (left) Time profile (50 – 500 msec) of UV-Visible spectrum; (right) Time profile of absorbance at 611 nm.

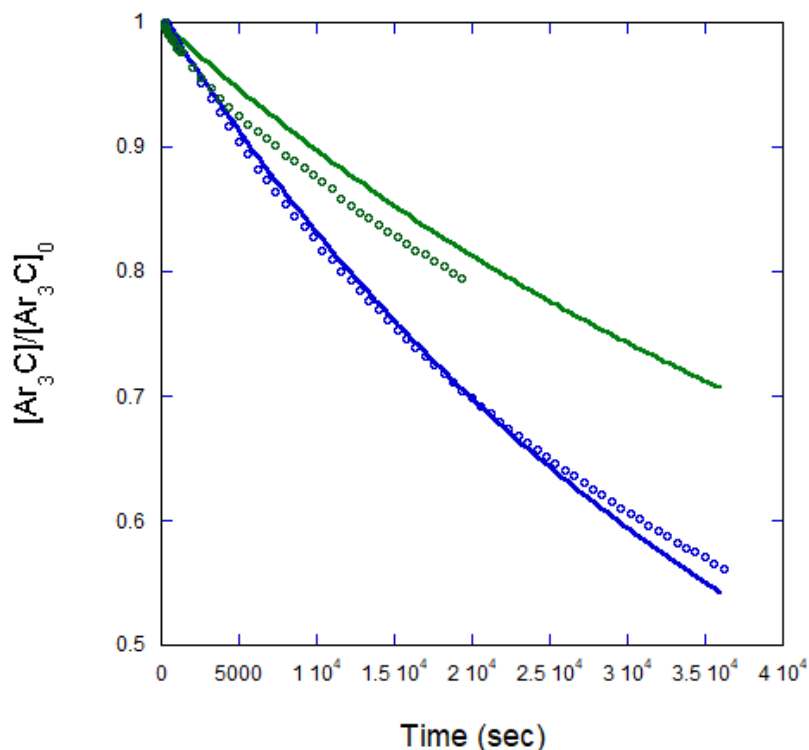


Figure 4. Conversion-time profile of **2** for the reaction between 1.2 mM of **1** and 1.2 mM of **2**. Green; in the absence of TEMPO•. Blue; in the presence of 25 mol% of TEMPO•. Symbols are data, lines are simulation results using ReactLab-KinSim.

Publications Acknowledging this Grant in 2015-2018

(VI) *Exclusively funded by this grant;*

- Liu, S.; Eberhart, M. S.; Norton, J. R.; Yin, X.; Neary, M. C.; Paley, D. W. Cationic Copper Hydride Clusters Arising from Oxidation of $(\text{Ph}_3\text{P})_6\text{Cu}_6\text{H}_6$. *J. Am. Chem. Soc.* **2017**, *139*, 7685-7688.
- Gunasekara, T.; Abramo, G.P.; Hansen, A.; Neugebauer, H.; Bursch, M.; Grimme, S.; Norton, J.R. Effect of Polarity Matching on Kinetics of Hydrogen Atom Transfer from Transition-Metal Hydrides to Trityl Radicals (manuscript in preparation)
- Kuo, J. L.; Gunasekara, T.; Hansen, A.; Grimme, S.; Norton, J. R.; Quinlivan, P. J. Thermodynamics of $[\text{CpV}(\text{CO})_3\text{H}]^-$ and the Implications for Catalysis Under H_2 : Further Evidence for Electron Transfer (manuscript in preparation)

(VII) *Jointly funded by this grant and other grants with leading intellectual contribution from this grant;*

-none-

(VIII) *Jointly funded by this grant and other grants with relatively minor intellectual contribution from this grant;*

-none-

Designing Catalytic Spaces in Organic Semiconductors

Colin Nuckolls

Department of Chemistry, Columbia University, New York, NY 10027

Poster Abstract

This poster will discuss an emerging class of contorted aromatic molecules made from perylene diimide ribbons that can be formed into twistacenes and helicenes. The electron transporting twistacenes and helicenes can be incorporated into rigid macrocyclic structures that form semiconducting materials possessing open and functional spaces in them. We have named these materials “cellular semiconductors”. These spaces allow these cellular semiconducting materials to be useful in a number of applications. In the context of our DOE project the cellular semiconductors are a locus for catalytic chemistry to occur. For example, in an operating transistor, the electrical current can be used to detect and discriminate between guest molecules. Moreover, the open spaces when the semiconductor is under electrical bias can serve as a nanoscale chemical reactor. New, cellular materials with larger pore volumes have been shown to be useful as high performance pseudocapacitors.⁶

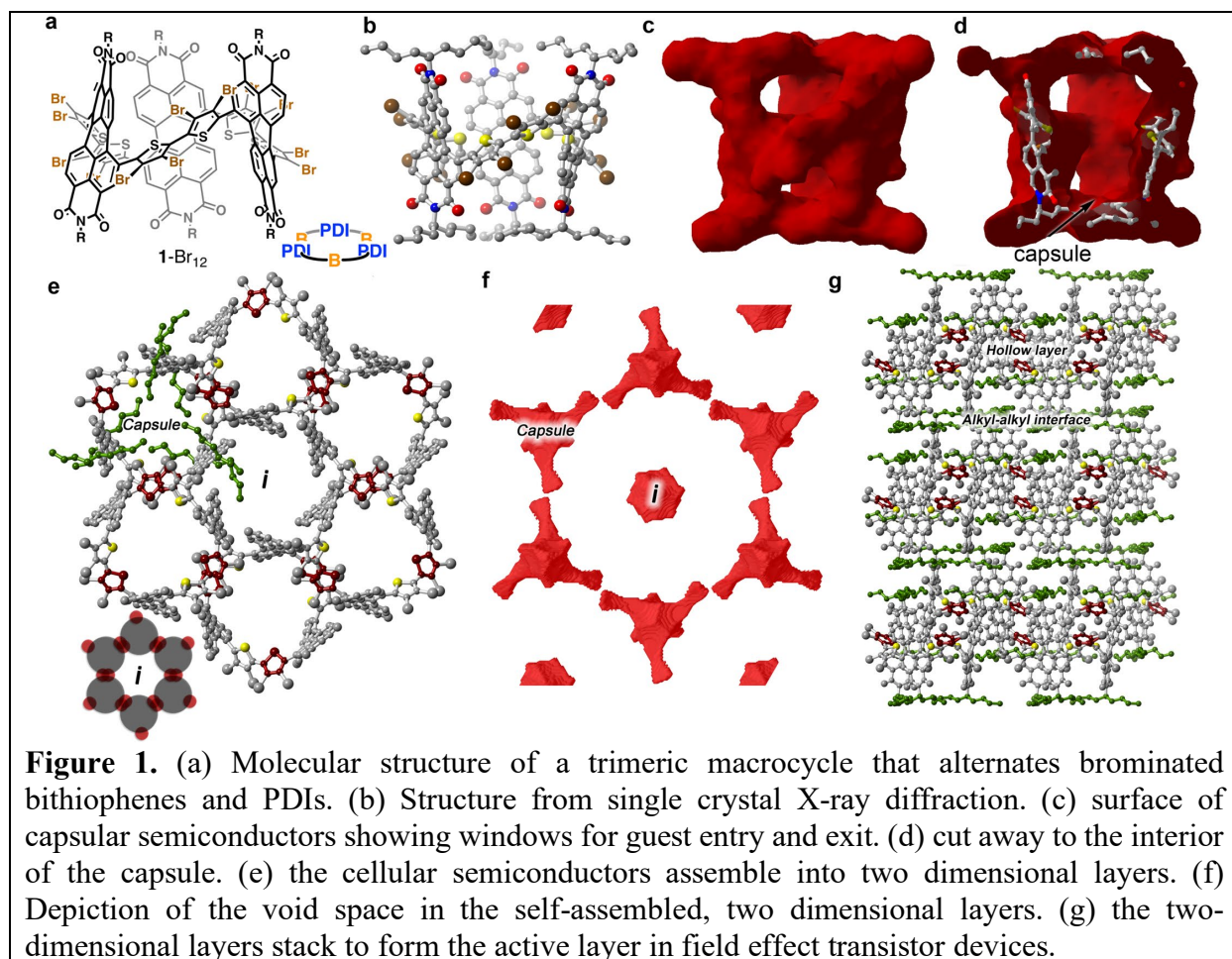
DE-FG02-01ER15264: Catalytic Growth of Molecular Scale Wiring

Postdoc(s): Nathaniel Schuster

Student(s): Grisha Etkin, Melissa Ball, Boyuan Zhang

RECENT PROGRESS

The results described here were recently published in *Nature Communications*, and are built around the molecule shown in Figure 1, which is the union of three tetra-bromobithiophenes and three perylene diimides (PDIs). PDIs are well known as electron transporting materials. Unlike other cyclic molecules we have created that are good electronic materials, the materials in Figure 1 are conformationally locked up to temperatures >260 °C. Meaning it is a rigid molecule that resembles a capsule or vessel. Figure 1b-d show views, where the top and bottom of the capsule are capped with alkyl chains, and the walls are the aromatic moieties (the bithiophenes and PDIs). As shown in Figure 1d, the interior of the macrocycle has space to accommodate host-guest interactions. Remarkably, this structure exhibits robust self-assembly in thin films and in the solid state. There is a strong three-fold halogen bonding interaction between the bromines of the thiophene and the carbonyl of the PDI. The essential point in the context of this proposal is that these assemblies are able to maintain their shape and organization when the films are placed under vacuum or in the presence of vapors.



The self-assembly of this molecule forms the cellular semiconducting phase in thin films and single crystals. The interior space of the capsule is a nanoenvironment that can accommodate a guests (Figure 1c,d). This is where the catalytic chemistry occurs. The capsules are chiral and exist as a mixture of enantiomers, each with an interior volume of $\sim 415 \text{ \AA}^3$. Each of these redox active molecules assembled into two-dimensional layers (Figure 1e,f) held together through the halogen bonding interactions described above. In the solid state and in films, these two-dimensional layers assemble into the three-dimensional crystalline structure (Figure 1g) and they persist even if the material is placed in vacuum.

Another key result for this grant is that this hollow material in Figure 2 is able to form the active layer in field effect transistor devices. This is shown in the near text-book example of an OFET⁴³⁻⁴⁸ in Figure 2a. This material, while under operational conditions of the electric field from the gate and source-drain bias, can be evacuated and back filled with gases and small molecules. These guests can be a reactant in a very unusual nano-environment for catalysis. It is in these spaces that we envision the catalysis will occur. Figure 2b shows the device as it is toggled between vacuum and nitrogen gas. The difference in current in the device for these guests is small but more polarizable guests such as ethanol or hydrocarbons produce much larger effects. This offers the intriguing possibility that the FET could serve as a source of the electric field to influence the reaction trajectory but it could also serve as a reporter of the chemistry that was occurring within

the nano-environment of the cellular semiconducting phase. We utilize each of these modes of action in ongoing studies.

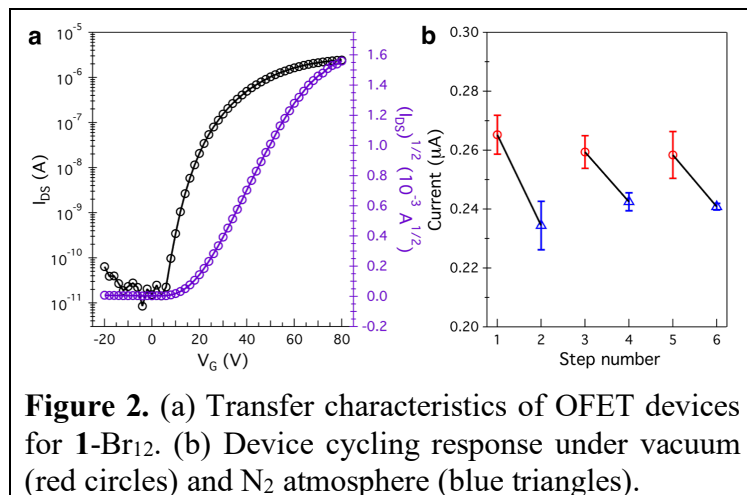


Figure 2. (a) Transfer characteristics of OFET devices for 1-Br₁₂. (b) Device cycling response under vacuum (red circles) and N₂ atmosphere (blue triangles).

This research touches on several areas of contemporary science: organic electronics; cyclic, conjugated molecules; photoredox catalysis; catalysis in electric fields; and conductive covalent/metal organic frameworks.

Publications Acknowledging this Grant in 2015-2018

(I) Exclusively funded by this grant

1. Ball, M.; Fowler, B.; Li, P.; Joyce, L. A.; Li, F.; Liu, T.; Paley, D.; Zhong, Y.; Li, H.; Xiao, S.; et

al. Chiral Conjugated Corrals. *J. Am. Chem. Soc.* **2015**, *137*, 9982–9987.

2. Ball, M.; Zhong, Y.; Fowler, B.; Zhang, B.; Li, P.; Etkin, G.; Paley, D. W.; Decatur, J.; Dalsania, A. K.; Li, H.; et al. Macrocyclization in the Design of Organic N-Type Electronic Materials. *J. Am. Chem. Soc.* **2016**, *138*, 12861–12867.

(II) Jointly funded by this grant and other grants with leading intellectual contribution from this grant

3. Chen, Q.; Trinh, M. T.; Paley, D. W.; Preefer, M. B.; Zhu, H.; Fowler, B. S.; Zhu, X.-Y.; Steigerwald, M. L.; Nuckolls, C. Strain-Induced Stereoselective Formation of Blue-Emitting Cyclostilbenes. *J. Am. Chem. Soc.* **2015**, *137*, 12282–12288.

4. Zhong, Y.; Trinh, M. T.; Chen, R.; Purdum, G. E.; Khlyabich, P. P.; Sezen, M.; Oh, S.; Zhu, H.; Fowler, B.; Zhang, B.; et al. Molecular Helices as Electron Acceptors in High-Performance Bulk Heterojunction Solar Cells. *Nat Commun* **2015**, *6*.

5. Choi, B.; Capozzi, B.; Ahn, S.; Turkiewicz, A.; Lovat, G.; Nuckolls, C.; Steigerwald, M. L.; Venkataraman, L.; Roy, X. Solvent-Dependent Conductance Decay Constants in Single Cluster Junctions. *Chem. Sci.* **2016**, *7*, 2701–2705.

6. Zhang, B.; Trinh, M. T.; Fowler, B.; Ball, M.; Xu, Q.; Ng, F.; Steigerwald, M. L.; Zhu, X.-Y.; Nuckolls, C.; Zhong, Y. Rigid, Conjugated Macrocycles for High Performance Organic Photodetectors. *J. Am. Chem. Soc.* **2016**, *138*, 16426–16431.

7. Sisto, T. J.; Zhong, Y.; Zhang, B.; Trinh, M. T.; Miyata, K.; Zhong, X.; Zhu, X.-Y.; Steigerwald, M. L.; Ng, F.; Nuckolls, C. Long, Atomically Precise Donor–Acceptor Cove-Edge Nanoribbons as Electron Acceptors. *J. Am. Chem. Soc.* **2017**, *139*, 5648–5651.

8. Zhong, Y.; Sisto, T. J.; Zhang, B.; Miyata, K.; Zhu, X.-Y.; Steigerwald, M. L.; Ng, F.; Nuckolls, C. Helical Nanoribbons for Ultra-Narrowband Photodetectors. *J. Am. Chem. Soc.* **2017**, *139*, 5644–5647.

9. Zhang, B.; Hernandez Sanchez, R.; Zhong, Y.; Ball, M. L.; Terban, M. W.; Paley, D. W.; Billinge, S. J. L.; Ng, F.; Steigerwald, M. L.; Nuckolls, C. Hollow Organic Capsules Assemble into Cellular Semiconductors. *Nat. Commun.* **2018**, *9*, 1957.
10. Ball, M.; Zhang, B.; Xu, Q.; Paley, D. W.; Ritter, V. C.; Ng, F.; Steigerwald, M. L.; Nuckolls, C. The Influence of Molecular Conformation on Electron Transport in Giant, Conjugated Macrocycles. *J. Am. Chem. Soc.* **2018**, *Accepted*.

(III) Jointly funded by this grant and other grants with relatively minor intellectual contribution from this grant

11. Hiszpanski, A. M.; Woll, A. R.; Kim, B.; Nuckolls, C.; Loo, Y.-L. Altering the Polymorphic Accessibility of Polycyclic Aromatic Hydrocarbons with Fluorination. *Chem. Mater.* **2017**, *29*, 4311–4316.
12. Gao, J.; Sengar, N.; Wu, Y.; Jockusch, S.; Nuckolls, C.; Clancy, P.; Loo, Y.-L. Contorted Octabenzocircumbiphenyl Sorts Semiconducting Single-Walled Carbon Nanotubes with Structural Specificity. *Chem. Mater.* **2017**, *29*, 595–604.

Functionalization of oxide and zeolite catalysts to improve tolerance to hot liquid water

Tuong Bui, Duong T. Ngo, Gengnan Li, Bin Wang, Daniel E. Resasco
Center for Interfacial Reaction Engineering (CIRE), School of Chemical, Biological and Materials Engineering. University of Oklahoma, Norman

Presentation Abstract

Micro and mesoporous catalysts, such as zeolites, mesoporous silicas, and MgO, used in reactions relevant to biomass conversion, exhibit drastic structural collapse when placed in contact with hot liquid water. The attack is a combination of hydrolysis of Si-O bonds initiated at Si-OH terminal sites and dissolution in liquid water. Functionalization with organosilanes has a dual effect of capping the highly reactive Si-OH sites and preventing the wetting of the surface by water due to enhanced hydrophobicity generated by the functional groups. In this contribution we compared several systems in which the presence of this hydrophobic groups not only protect the oxides and zeolites against structural collapse, but also greatly modify the activity and selectivity of acid- and base-catalyzed reactions. Specifically, we will discuss the following systems:

- a) Organosilane-functionalized HY zeolite catalysts used in the cross condensation of cyclopentanone and acetone.
- b) Organosilane-functionalized MgO catalysts used in the cross condensation of cyclopentanone and acetone.
- c) Organosilane + sulfonic-acid functionalized mesoporous silicas (MCM-41 and SBA-15) for acid catalyzed reactions in aqueous and biphasic systems (alkylation, dehydration).

DE-SC0018284: Hydrophobic Enclosures in Bio-Inspired Nanoreactors for Enhanced Phase Selectivity - A Combined Experimental/Theoretical Approach

PIs: Daniel Resasco, Bin Wang

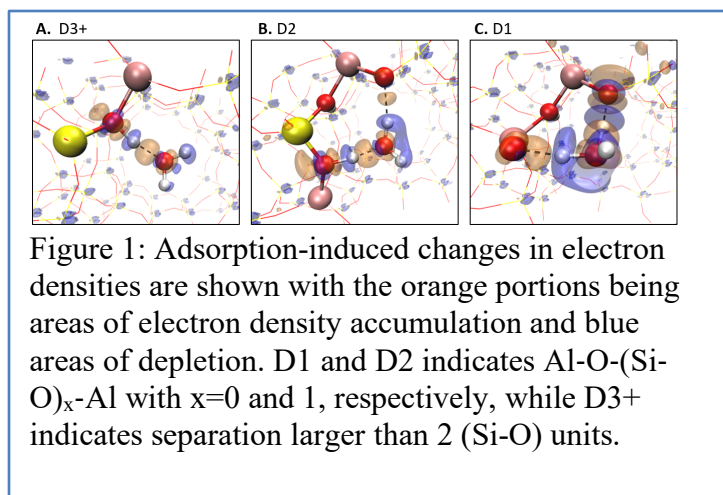
Postdoc(s): Gengnan Li

Student(s): Michael Zeets, Duong T. Ngo, Tuong Bui

RECENT PROGRESS

1. Interaction between water and zeolite.

The presence of water may have detrimental effects on catalysts. Among the most investigated materials for C-C bond forming reactions, zeolites are of special interest because they have a well-defined pore structure, high hydrothermal stability and Brønsted acid strength that can catalyze the coupling of C-C bonds. However, previous studies have shown that the zeolite structure is greatly damaged by the presence of hot liquid water, which are necessary for C-C bond formation. C-C coupling is an important step in the upgrading of biomass-derived compounds, however, the presence of liquid water is practically unavoidable in biomass conversion. Therefore, it is important to investigate methods to deal with its presence.



We recently reported Density functional theory (DFT) calculations, through which we show that the spatial proximity between Brønsted acid sites (BAS) can significantly affect the strength of water adsorption, which can be used as a molecular probe for the local activity. We have shown that the adsorption energy of a water molecule is significantly enhanced when two BAS are in close proximity, such as Al-O-(Si-O)₁-Al, and this enhanced water adsorption results from the increased H-bonding between water and the two

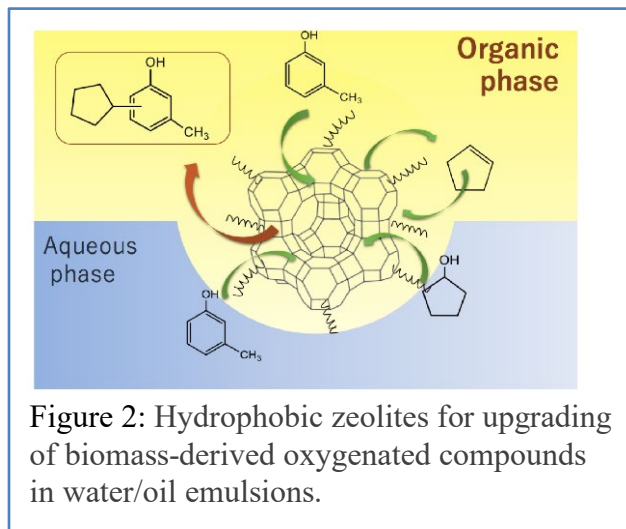
BAS.

This increase of adsorption energy is attributed to enhanced polarization of the water molecule through pronounced interfacial charge transfer. We have observed that the two H atoms of water lose electrons, while the O atom gains electrons, indicating enhanced polarization upon adsorption. However, the extent of this exchange is greatly dependent on site proximity. In some case, we observe that the proton becomes detached from the zeolite framework and forms a hydronium ion. When the site separation distance is larger than that corresponding to Al-O-(Si-O)₂-Al, i.e. two (Si-O) units separating the two BAS, water begins to adsorb at one of the two BAS with only a single H-bond formed. Our results thus suggest that zeolites with adjacent acid sites may provide more effective nucleation centers for water molecules to form clusters and droplets. We expect that the proton delocalization from the zeolite framework into water may be more pronounced when a large water cluster or an aqueous phase is present in the system. Both, the enhanced polarization and proton delocalization may affect activity and selectivity in zeolite-catalyzed reactions.

2. Functionalized acid catalysts with improved stability in biphasic liquid systems.

Surface functionalization of zeolites with silylating agents has emerged as an effective way to improve the catalyst resistance to liquid water and biphasic water-organic systems. Conducting alkylation in biphasic water-organic mixtures is highly advantageous due to the high concentration of water-soluble compounds present in bio-oil and the low water solubility of the targeted products. Besides, biphasic emulsions are promising systems that maximize the interfacial exchange area for simultaneous reaction and separation.

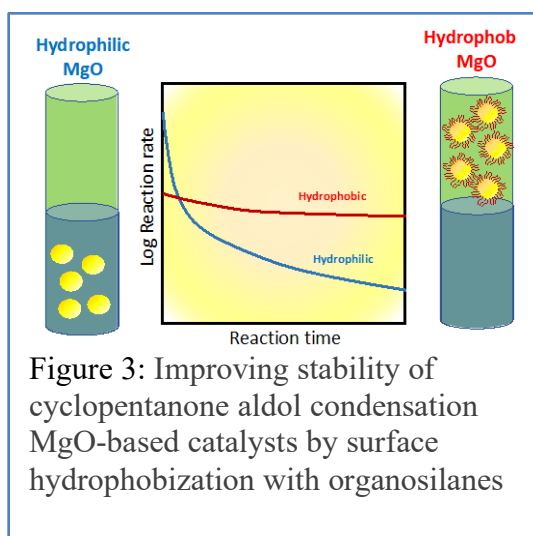
We investigated C-C coupling reactions in biphasic liquid systems over a hydrophobized zeolite. The work was focused on the alkylation of m-cresol with cyclopentanol, as two representative compounds of biomass-derived streams to generate products in the molecular weight range that is appropriate for transportation fuels. This reaction was studied in single and biphasic liquid systems over a hydrophobized H-USY zeolite (Si/Al=30). The effects of functionalization on zeolites with organosilanes of varying alkyl chain length (C2 and C18) to the catalytic performance and structural stability were investigated upon exposure to reaction conditions in water/oil emulsions.



Two oxygenate compounds derived from different bio-oil streams, furfural and m-cresol, were simultaneously converted into longer carbon chain oxygenates via alkylation reaction. The alkylation reaction was performed using OTS-modified H-USY zeolite, in single organic phase (decalin) and biphasic water-decalin emulsions.

The alkylation of m-cresol with cyclopentanol was successfully achieved in single-phase, yielding C-C and C-O alkylation products. It was found that the C-C alkylation was predominant over the C-O alkylation. The temperature and nature of the aromatic

substrate showed a remarkably effect on the product distribution. Activating aromatic substituents such as -OH and -OCH₃, which was the case of guaiacol, improved the rate of alkylation while alkyl substituent -R cannot. The difference in activity with the aromatic substrates was attributed to electro-donating and steric hindrance C-H effects.^[1,56] The rate of alkylation decreased when the reaction was performed in biphasic water-decalin emulsions, showing that water competes with active sites. However, it was clear that the hydrophobic zeolite exhibited a higher catalytic activity in the biphasic system than the untreated zeolite, which was fully deactivated in a short reaction time. Therefore, the grafting of organosilanes onto defect Si-OH groups in zeolite prevents a direct contact of the zeolite with condensed water, decreasing the structural degradation and the loss of catalytic activity. In this sense, the stability of the zeolites to hot liquid water via silylation will enhance their utilization in aqueous phase processes, such as those involved in the bio-oil upgrading reactions.



3. Functionalized base catalysts with improved stability for aldol condensation.

MgO is a typical basic oxide commonly used in aldol condensation. While it is beneficial to enhance the surface area of MgO for higher reaction rates, this enhancement also enhances the uptake of undesirable nucleophiles such as water and product oligomers, which accelerate deactivation, as shown in several studies. Finding catalytic materials that are effective for aldol condensation and at the same time more resistant to deactivation than conventional basic catalyst is an appealing objective. Therefore, the main goal of this contribution has been investigating novel materials with improved stability during aldol condensation.

We have found that MgO modified with mesoporous silica and subsequently grafted with an organosilane (e.g. octodecyltrichlorosilane) renders the surface hydrophobic and greatly improves

catalyst stability. In this case, we have used C-C bond forming reactions of cyclopentanone as a probe reaction. Cyclopentanone is a promising building block in the conversion of biomass to fuels. It can be readily obtained from furanics derived from biomass and can be converted to intermediate products in the molecular weight range compatible with fuels via C-C bond forming reactions. Among them, aldol condensation is a promising route. Conventional MgO catalysts are intrinsically active to catalyze this reaction, but they usually exhibit low surface areas and low stability in the presence of liquid water. The nitrate-citrate combustion method results in high surface area oxides with high condensation activity, but they are still susceptible to water attack.

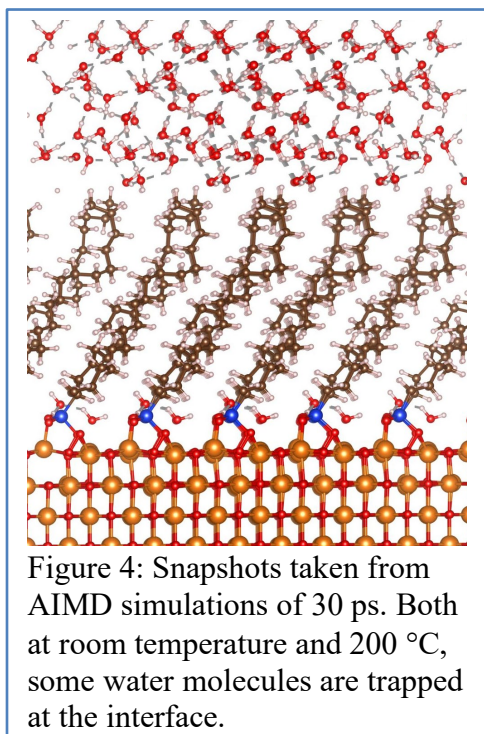


Figure 4: Snapshots taken from AIMD simulations of 30 ps. Both at room temperature and 200 °C, some water molecules are trapped at the interface.

We reach the following conclusions through the combined AIMD simulations and experiments:^[1]^[SEP]

1. While MgO is an active catalyst for aldol condensation of cyclopentanone, it exhibits a low catalyst stability in the liquid phase, particularly in the presence of liquid water.

2. Functionalization with organosilanes increases the hydrophobicity of the surface, which has important effects on activity, selectivity, and stability. Specifically:^[1]^[SEP]a) The catalytic activity is maintained for a much longer time than that of the unfunctionalized material.^[1]^[SEP]b) The resistance to water attack is greatly enhanced. c) The initial rate is significantly reduced, most probably due to the selective titration of the most basic sites on the parent oxide.

3. Hydrophobization is more effective than other methods previously investigated for preventing deactivation of basic catalysts during aldol condensation. For example, while the addition of a hydrogenation catalyst is an effective method for other systems in gas phase, such a method is less effective for cyclopentanone on MgO in the liquid phase. That is, at elevated H₂ pressures, ketone feed

saturation reduces the overall rate of condensation. At low H₂ pressures, catalyst deactivation is significant.

4. Though the hydrophobic functionalization forms a thick hydrophobic barrier for water penetration. However, water, which is either formed through the aldol condensation or diffused driven by gradients of chemical potentials, can be trapped at the MgO/OTS interface, as shown in the AIMD simulations. These water clusters can deactivate the catalysts as well as change the reaction mechanism.

Publications Acknowledging this Grant in 2015-2018

(IX) *Exclusively funded by this grant;*

1. Pino, N.; Bui, T.; Hincapie, G.; Loopez, D.; Resasco, D. E., Hydrophobic zeolites for the upgrading of biomass-derived short oxygenated compounds in water/oil emulsions. *Appl Catal A-Gen* **2018**, *559*, 94-101.
2. Zeets, M.; Resasco, D. E.; Wang, B., Enhanced chemical activity and wettability at adjacent Brønsted acid sites in HZSM-5. *Catalysis Today* **2018**, *312*, 44-50.
3. Ngo, D.; Sooknoi, T.; Resasco, D., Improving stability of cyclopentanone aldol condensation MgO-based catalysts by surface hydrophobization with organosilanes. *Applied Catalysis B: Environmental* **2018**, *237*, 835-843.

**Fundamental Studies of Oxidation Reactions on Model Catalysts:
Product Inhibition and Mechanism for Propylene Epoxidation on Au/TS-1**

Fabio H. Ribeiro and W. Nicholas Delgass

Davidson School of Chemical Engineering, 480 Stadium Mall Drive, West Lafayette, IN 47907

Presentation Abstract

The detailed kinetics of propylene epoxidation by H₂ plus O₂ over Au supported on titanium silicalite-1 (Au/TS-1) catalysts were measured in a CSTR free from temperature and concentration gradients. Apparent reaction orders measured at 473 K for hydrogen (0.7 order), oxygen (0.2), and propylene (0.2) for a series of Au/TS-1 catalysts with varied Au (0.02-0.09 wt%) and Ti (Si/Ti: 75-143) contents were consistent with those reported previously. Co-feeding propylene oxide enabled measurement of the apparent reaction order in propylene oxide (-0.4 to -0.8 order) and the determination that relevant pressures of propylene oxide reversibly inhibit propylene epoxidation over Au/TS-1, while co-feeding carbon dioxide and water had no effect on the propylene epoxidation rate. Analysis of previously proposed two-site reaction mechanisms in light of reaction orders for oxygen (0.4), hydrogen (1), and propylene (0.4), corrected to account for propylene oxide inhibition, provides further evidence that propylene epoxidation over Au/TS-1 occurs via a simultaneous mechanism requiring two distinct, but adjacent, types of sites, and not a sequential mechanism that invokes migration of H₂O₂ formed on Au sites to Ti sites to form PO. Hydrogen oxidation rates are not inhibited by propylene oxide, implying that the sites required for hydrogen oxidation are distinct from those required for propylene epoxidation. In addition to this work, we have begun to probe the site requirements for PO production via density functional theory calculations as well as through the synthesis and characterization of novel materials designed to overcome the technical challenges posed by the very small cluster size of the typical very low gold content Au/TS-1 catalysts.

Grant title: Fundamental Studies of Oxidation Reactions on Model Catalysts

Grant number: DE-FG02-03ER15408

PI: Fabio H. Ribeiro and W. Nicholas Delgass

Student(s): Viktor J. Cybulskis, James Harris, Garrett Mitchell, Jeremy Arvay, and Michael Cordon

RECENT PROGRESS

In our effort to understand the molecular details of this reaction we have used a new continuous stirred tank reactor (CSTR) to focus on the kinetics of propylene epoxidation and hydrogen peroxide production over Au/TS-1 catalysts. Previous literature reports of kinetics over these materials have accounted for the dependence of the rate on the reactants but have not accounted accurately for the effects of the products. While the presence of product inhibition can be detected by analysis of the dependence of the rate on space time⁵ a more precise analysis is afforded by co-feeding products to a CSTR. As discussed in Cybulskis et al. (Cybulskis, V.; Smeltz, A. D.; Zvinevich, Y.; Gounder, R.; Delgass, W. N.; Ribeiro, F. H. *Chem. Eng. Educ.* 50, 202–210 (2016)), this method permits operation at differential conditions and yields the intrinsic kinetic parameters.

The results show significant inhibition by PO (See Figure 1) but no effects of CO₂ or water. This result reveals that all previously measured orders of reaction, none of which account for inhibition, must be corrected (Cybulskis, V. et al., Chem. Eng. Educ. 50, 202–210 (2016)). We have, thus, reevaluated the two-site mechanisms proposed in the literature in light of these corrected orders to differentiate between them. The ‘simultaneous’ mechanism, which requires the Au and Ti (or Au-Ti interface) sites in Au/TS-1 to be neighboring one another, is consistent with all of our measured kinetics, however the ‘sequential’ mechanism, which calls for formation of H₂O₂ on Au followed by its migration to the Ti site to form PO, was found to be incapable of describing any of our measured sets of kinetics. Another important insight gained from this work is the distinction between propylene epoxidation and hydrogen oxidation site ensembles. A lingering question in the literature has been whether the sites primarily responsible for the direct combustion of hydrogen to water are an intrinsic feature of the sites primarily responsible for the epoxidation of propylene, or whether these two site ensembles are separable. Our data show that while PO inhibits propylene epoxidation it does not inhibit hydrogen oxidation, revealing that these two site ensembles are distinct, giving credence to the possibility that a targeted synthetic strategy could be produced in which propylene epoxidation sites could be made *without* making sites which will directly combust hydrogen. Ongoing work will delve further into mechanistic details and effects of catalyst composition on kinetic parameters.

Another goal of this work is the identification of the catalytic sites. One focus is on the use transmission electron microscopy (TEM) to more fully characterize the Au clusters relevant for propylene epoxidation. Development of this skillset has made clear the need for novel materials designed to be amenable to a more complete analysis via TEM. The large crystallites characteristic of conventional Au/TS-1 catalysts obscure signals from the small gold clusters in the interior zeolite pores, preventing analysis. To overcome this technical difficulty, we are working on synthesis of sheet-like Au/Ti MFI catalysts which will enable the direct observation via TEM of gold clusters inhabiting the micropores of MFI catalysts.

To learn more about the structural details that affect activity, we have begun to use updated DFT and molecular dynamics calculations to probe the importance of the size, geometry and mobility of gold clusters located inside the micropores of TS-1. Although this effort is still in its initial stages, preliminary results suggest that the location, size, shape and “fit” of a gold cluster in

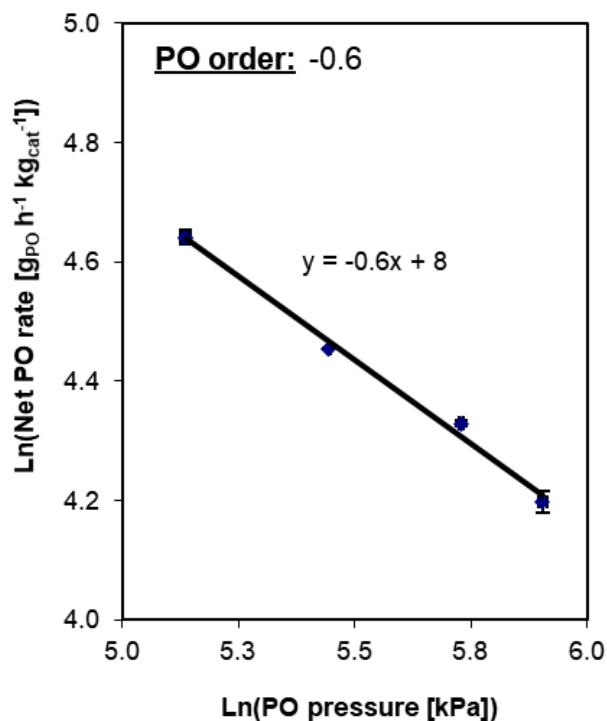


Figure 2- Example propylene epoxidation PO order measurement over Au/TS-1 catalyst (Au wt% = 0.07, Si/Ti = 81). Data collected in CSTR, SV = 26,000 cm³ g_{cat}⁻¹ h⁻¹, T = 473 K, feed = 10% H₂ / 10% O₂ / 10% C₃H₆ / 0-0.24% PO / balance N₂

a zeolite pore structure can affect both its stability and the nature of the active, undercoordinated Au sites. These findings will aid understanding of Au/TS-1 and are also leading us to consider various other frameworks and altered synthesis procedures to indirectly probe the site requirements for propylene epoxidation. Potentially relevant parameters including confinement, pore linearity and diameter, and dimensionality of the pore network, will guide a search for structures that can sufficiently stabilize the optimum Au cluster size, thus allowing synthesis of catalysts with higher activity.

Publications Acknowledging this Grant in 2015-2018

1. Mayr, L.; Shi, X.; Köpfle, N.; Milligan, C. A.; Zemlyanov, D. Y.; Knop-Gericke, A.; Hävecker, M.; Klötzer, B.; Penner, S. Chemical vapor deposition-prepared sub-nanometer Zr clusters on Pd surfaces: promotion of methane dry reforming. *Phys. Chem. Chem. Phys.* **18**, 31586–31599 (2016).
2. Paul, R., Reifenberger, R. G., Fisher, T. S. & Zemlyanov, D. Y. Atomic Layer Deposition of FeO on Pt(111) by Ferrocene Adsorption and Oxidation. *Chem. Mater.* **27**, 5915–5924 (2015).
3. Cybulskis, V. J., Harris, J. W., Zvinevich, Y., Ribeiro, F. H. & Gounder, R. A transmission infrared cell design for temperature-controlled adsorption and reactivity studies on heterogeneous catalysts. *Rev. Sci. Instrum.* **87**, 103101 (2016).
4. Peterson, E. J.; DeLaRiva, A. T.; Lin, S.; Johnson, R. S.; Guo, H.; Miller, J. T.; Hun Kwak, J.; Peden, C. H. F.; Kiefer, B.; Allard, L. F.; Ribeiro, F. H.; Datye, A. K. Low-temperature carbon monoxide oxidation catalysed by regenerable atomically dispersed palladium on alumina. *Nat. Commun.* **5**, (2014).
5. Harris, J. W.; Arvay, J. W.; Mitchell, G.; Delgass, W. N.; Ribeiro, F. H., *J. Catal.*, Propylene

Oxide

Inhibits Propylene Epoxidation over Au/TS-1, *Accepted*

Demystifying atomic environments within heteroatom substituted zeolite frameworks with solid-state nuclear magnetic resonance

Jennifer Lewis, Takayuki Iida, Yuriy Roman-Leshkov
Massachusetts Institute of Technology, Department of Chemical Engineering

The identity of the active sites of hydrophobic Lewis acid zeolites was elucidated by solid-state ^{31}P nuclear magnetic resonance (NMR) spectroscopy following adsorption of trimethylphosphine oxide (TMPO) probe molecules. The adsorption of TMPO on these materials resulted in distinct ^{31}P NMR resonances between $\delta_{\text{iso}} = 59.9$ and 54.9 ppm that correspond to unique chemical environments of the Lewis acidic heteroatoms in the Beta zeolite framework. The ^{31}P NMR resonances were assigned to sites in Sn-Beta zeolites by correlating the variation of ^{31}P NMR spectra during TMPO titration experiments with the corresponding changes in the ^{119}Sn NMR spectra. This method allowed us to establish quantitative relationships between the assignments for each site and the catalytic activity for the glucose isomerization and aldol condensation reactions. The rate of glucose isomerization directly correlated with the combined integrated intensities of ^{31}P MAS NMR resonances at $\delta_{\text{iso}} = 55.8$ and 54.9 ppm, which amounted to 12–33% of total Sn sites. In contrast, the integrated peak area of a different site at $\delta_{\text{iso}} = 58.6$ ppm was shown to correlate with aldol condensation activity. The probing method used to identify and quantify distinct active sites within the framework of low-defect Lewis acidic zeolites developed in this work is applicable to a wide range of microporous materials, regardless of heteroatom identity.

DOE-BES - DE-SC0016214

Title Molecular Understanding of Bifunctional Solid Lewis Acid Zeolites for the C-C Coupling of Alpha Keto Acids

RECENT PROGRESS

Active site speciation with NMR

Phosphorous-31 MAS NMR spectra were acquired after dosing a representative Sn-Beta sample (Si/Sn molar ratio of 300, Sn-Beta-300a) with different loadings of TMPO using a dichloromethane (DCM) solvent-assisted technique. The TMPO occupancy at each site (Table 1) was calculated from the relative peak area normalized by the total P and Sn contents measured by inductively coupled plasma mass spectrometry (ICP-MS). The relative quantity of TMPO occupying different sites in the Sn-Beta zeolite is reflected by the integrated areas of the ^{31}P NMR peaks. At low TMPO loadings (e.g., TMPO/Sn molar ratio = 0.12), two resonances appear at $\delta_{\text{iso}} = 58.6$ and 54.9 ppm at a ratio of ca. 3:1. When the TMPO dosing is increased to TMPO/Sn = 0.48, the areas of these first two resonances increase while maintaining an approximately 3:1 ratio. New resonances with relatively low area (<6%) are observed at $\delta_{\text{iso}} = 63.1, 61.3, 59.9,$ and 57.2 ppm. At TMPO loadings above unity (i.e., TMPO/Sn = 1.09 and 1.14),

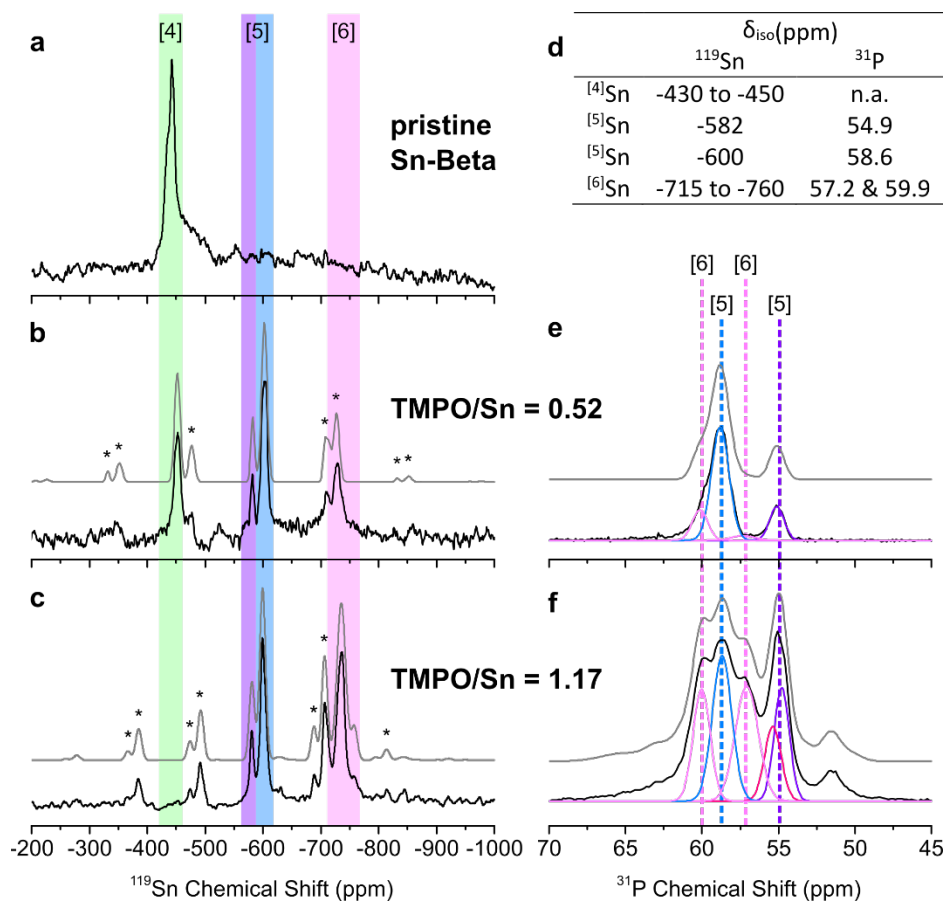


Figure 3. Elucidation of active site speciation in Sn-Beta zeolites using NMR. (a) pristine sample. (b) and (e) dosed with TMPO/Sn = 0.52. (c) and (f) dosed with TMPO/Sn = 1.17. Spinning sidebands for the ^{119}Sn spectra are marked with asterisks. Experimental NMR spectra are shown in black (lower traces), while the simulated spectra are shown in gray (upper traces).

coordinate, pseudo-tetrahedral Sn ($^{[4]}\text{Sn}$) environments in the zeolite framework with approximately a 30:70 ratio (Figure 1a). In addition to these two sharp resonances, a broad component spanning the $^{[4]}\text{Sn}$ region was observed, which could be potentially attributed to disordered Sn distributed randomly throughout the framework. When TMPO was adsorbed onto ^{119}Sn -Beta-300m at a ratio of TMPO/Sn = 0.52 (Figure 1b), the ^{119}Sn MAS NMR spectrum showed a single peak at $\delta_{iso} = -450$ ppm corresponding to pseudo-tetrahedral Sn and two new signals at $\delta_{iso} = -600$ and -582 ppm assigned to penta-coordinated Sn ($^{[5]}\text{Sn}$).^[5, 6] Importantly, the resonances at $\delta_{iso} = -600$ and -582 ppm appeared at a 3:1 ratio and could be clearly assigned to the two sites with ^{31}P MAS NMR resonances at $\delta_{iso} = 58.6$ and 54.9 ppm, respectively, which appeared in approximately the same ratio (4:1, Figure 1e). The spinning sideband manifolds were accounted for in these area ratios due to a considerable chemical shift anisotropy (CSA) contribution observed experimentally and our inability to attenuate the spinning sidebands at moderate spinning frequencies. A minor contribution of six-coordinate Sn ($^{[6]}\text{Sn}$, ~5%, estimated from experiments acquired using multiple spinning frequencies at both 7.1 and 11.7 T) was observed for this sample. Unfortunately, the low S/N and appreciable spinning side bands from

the ^{31}P NMR resonances at $\delta_{iso} = 59.9$ and 57.2 ppm increase in intensity along with a new, relatively high intensity signal (20-25%) at $\delta_{iso} = 55.8$ ppm.

Peak assignments were further refined by using data from ^{119}Sn MAS NMR spectra of ^{119}Sn -enriched Sn-Beta samples with a Si/Sn ratio of ~300 (^{119}Sn -Beta-300m, synthesized with ^{119}Sn -enhanced metal precursor) dosed with TMPO (Figure 1). As expected, pristine, dehydrated ^{119}Sn -Beta-300m exhibits sharp ^{119}Sn resonances at $\delta_{iso} = -434$ and -443 ppm corresponding to two different four-

the ^{51}Sn signals did not allow us to determine the exact chemical shift or concentration of this ^{61}Sn site.

Unlike prior characterization techniques, our TMPO dosing method allows correlating catalytic activity to distinct sites within the zeolite framework. Site time yields (STYs) were plotted against the % integrated peak area normalized by total Sn content showed a linear trend for glucose isomerization only when combining the contributions from the ^{31}P NMR resonances at $\delta_{\text{iso}} = 55.8$ and 54.9 ppm. This combination yielded a relatively good linear fit with an R^2 value of 0.69 and intersected the origin within error. The concentration of this active site ranged from 12 to 33 % of the total Sn content for our samples, which is in remarkable agreement with the 13-33% concentration of active sites calculated with FTIR spectroscopy for a variety of fluoride-synthesized Sn-Beta samples used for glucose isomerization. This site was related to an “open” configuration. In contrast, plots of the STY for aldol condensation versus the peak areas of different ^{31}P MAS NMR resonances showed drastically different trends compared to those found for glucose isomerization. Specifically, linear correlations were only found for the combination of the ^{51}Sn site at $\delta_{\text{iso}} = 58.6$ ppm and either $\delta_{\text{iso}} = 59.9$ or 57.2 ppm of the ^{61}Sn site pair, which is a site correlated with a closed configuration. The difference in Sn-Beta active site assignment for glucose isomerization and aldol condensation is striking and significant. *The current results are especially illuminating, as many theoretical and experimental researchers have previously proposed that the same site, a hydrolyzed “open” site, is the catalytic site for both of these reactions!*

Encapsulation of nanoparticles via concerted demetallation.

We developed a novel synthetic approach was developed to produce PtZnx nanoclusters encapsulated inside zeolite micropores by introducing Pt $^{2+}$ cations into a zincosilicate framework via ion exchange, followed by controlled demetallation and alloying with framework Zn. The resulting zeolites featured nanoclusters with sizes ~ 1 nm, having an interatomic structure corresponding to PtZnx alloy as confirmed by pair distribution function (PDF) analysis. These materials featured simultaneous shape and substrate specificity as demonstrated by the selective production of p-chloroaniline from the competitive hydrogenation of p-chloronitrobenzene and 1,3-dimethyl-5-nitrobenzene.

Publications Acknowledging this Grant in 2015-2018

Exclusively funded by this grant:

1. Iida, T., Zanchet, D., Ohara, K., Wakihara, T., & Román-Leshkov, Y.*, Concerted bimetallic nanocluster synthesis and encapsulation via induced zeolite framework demetallation for shape and substrate selective heterogeneous catalysis. **Angew. Chem. Int. Ed.**, DOI: 10.1002/anie.201800557 (2018).
<https://onlinelibrary.wiley.com/doi/abs/10.1002/ange.201800557>
2. Hunt, S. T. & Román-Leshkov, Y.* Principles and Methods for the Rational Design of Core-Shell Nanoparticle Catalysts with Ultralow Noble Metal Loadings. **Acc. Chem. Res.**, DOI: 10.1021/acs.accounts.7b00510 (2018).
<https://pubs.acs.org/doi/abs/10.1021/acs.accounts.7b00510>

3. Iida, T., Ohara, K., Román-Leshkov, Y.*, & Wakihara, T.* Zeolites with isolated framework and oligomeric extraframework hafnium species characterized with pair distribution function analysis. **PCCP**, 12:7914-7919 (2018).
<http://pubs.rsc.org/en/content/articlehtml/2018/cp/c8cp00464a>
4. Lewis, J.D., Ha, M., Luo, H., Faucher, A., Michaelis, V. K., & Román-Leshkov, Y.* Distinguishing Active Site Identity in Sn-Beta Zeolites using ³¹P MAS NMR of Adsorbed Trimethylphosphine Oxide. **ACS Catal.**, 8:3076-3086 (2018).
<https://pubs.acs.org/doi/10.1021/acscatal.7b03533>
5. Iida, T., Shetty, M., Murugappan, K., Wang, Z., Ohara, K., Wakihara, T., & Román-Leshkov, Y.* Encapsulation of molybdenum carbide nanoclusters inside zeolite micropores enables synergistic bifunctional catalysis for anisole hydrodeoxygenation. **ACS Catal.**, 7:8147-8151 (2017). <https://pubs.acs.org/doi/abs/10.1021/acscatal.7b03175>
6. Garg, A., Milina, M., Ball, M., Hunt, S. T., Dumesic, J. A., & Román-Leshkov, Y.* Transition Metal Nitride Core-Noble Metal Shell Nanoparticles as Highly CO Tolerant Catalysts. **Angew. Chem. Int. Ed.** 56:8828-8833 (2017).
7. Hendon, C. H., Hunt, S. T., Milina, M., Butler, K. T., Walsh, A., & Román-Leshkov, Y.* Realistic Surface Descriptions of Heterometallic Interfaces: The Case of TiWC Coated in Noble Metals. **J. Phys. Chem. Lett.** 7:4475-4482 (2016)
8. Gunther, W. R., Michaelis, V. K., Griffin, R. G., & Román-Leshkov, Y.* Interrogating the Lewis acidity of metal sites in Beta zeolites with ¹⁵N pyridine adsorption coupled with MAS NMR spectroscopy **J. Phys. Chem. C.** 120:28533–28544 (2016).
9. Hunt, S. T., Milina, M., Wang, Z., & Román-Leshkov, Y.* Activating Earth-Abundant Electrocatalysts for Efficient, Low-Cost Hydrogen Evolution/Oxidation: Sub-Monolayer Platinum Coatings on Titanium Tungsten Carbide Nanoparticles. **Energy Environ. Sci.** 9:3290-3301 (2016).

Structural evolution of titanium dioxide during reduction in high pressure hydrogen

Xunhua Zhao, Sencer Selcuk and Annabella Selloni
Department of Chemistry, Princeton University, Princeton, N.J. 08544

Presentation Abstract

The excellent photocatalytic properties of TiO₂ under UV light have long motivated the search for doping strategies capable of extending its photoactivity to the visible, but progress has proven difficult. An alternative approach is high-pressure hydrogenation, which results in reduced “black TiO₂” nanoparticles with a crystalline core and a disordered shell that absorb the whole spectrum of visible light. We have studied the formation mechanism and relevant structural features of black TiO₂ using first-principles-validated reactive force field molecular dynamics simulations of anatase TiO₂ surfaces and nanoparticles (NPs) in high-temperature, high-pressure hydrogen atmosphere. Our simulations show that surface oxygen vacancies (V_{OS}) created upon reaction of H₂ with surface O atoms tend to diffuse toward the bulk but encounter a high barrier for subsurface migration on {001} facets, which initiates the disordering of NP’s surface. Besides supporting the key role of the hydrogenated amorphous shell in the photoactivity of black TiO₂, our results provide insight into the properties of the disordered surface layer that is observed on anatase nanocrystals under reaction conditions relevant to photocatalytic water splitting.

DE-SC0007347: Understanding Surfaces and Interfaces of Photocatalytic Oxide Materials with First Principles Theory and Simulations

Postdocs: Xunhua Zhao

Students: Xiao Shi, Marcos Calegari Andrade

RECENT PROGRESS

Methanol on anatase TiO₂ (101): Mechanistic insights into photocatalysis – We have investigated the photoactivity of methanol adsorbed on the anatase TiO₂ (101) surface by a combination of scanning tunneling microscopy (STM), temperature-programmed desorption (TPD), X-ray photoemission spectroscopy (XPS), and density functional theory (DFT) calculations. Isolated methanol molecules adsorbed at the anatase (101) surface show a negligible photoactivity. Two ways of methanol activation were found. First, methoxy groups formed by reaction of methanol with coadsorbed O₂ molecules or terminal OH groups are photoactive, and turn into formaldehyde upon UV illumination. The methoxy species show an unusual C1s core-level shift of 1.4 eV compared to methanol; their chemical assignment was verified by DFT

calculations with inclusion of the final-state effect. The second way of methanol activation opens at methanol coverages above 0.5 monolayer (ML), and methyl formate is produced in this reaction pathway. The adsorption of methanol in the coverage regime from 0 to 2 ML is described in detail; it is key for understanding the photocatalytic behavior at high coverages. There, a hydrogen-bonding network is established in the adsorbed methanol layer, and consequently methanol dissociation becomes energetically more favorable. DFT calculations show that dissociation of the methanol molecule is always the key requirement for hole transfer from the substrate to the adsorbed methanol. We show that the hydrogen-bonding network established in the methanol layer dramatically changes the kinetics of proton transfer during the photoreaction.

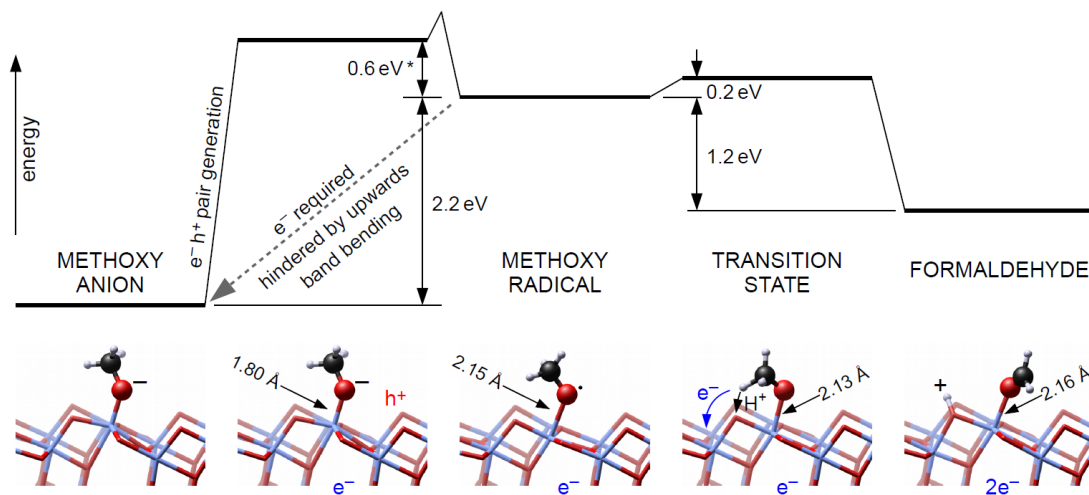


Figure 1. Calculated energy barriers for photoconversion of CH_3O^- (left) into formaldehyde (right). The CH_3O^- first accepts a hole, forming a methoxy radical (middle). This can either convert into formaldehyde with an energy barrier of 0.2 eV, or accept an electron from the n -doped TiO_2 ; the backward reaction is hindered by an activation barrier. We consider that excess electrons are present in the sample by having a Ti atom substituted with a Nb atom, causing the presence of an extra electron (e^-). The energies are based on PBE+U calculations, except for the energy marked by asterisk, which is based on B3LYP.

Electronic Structure and Photoabsorption of Ti^{3+} Ions in reduced Anatase and Rutile TiO_2 . We have investigated the electronic structure and photoabsorption of the reduced anatase TiO_2 (101) and rutile TiO_2 (110) surfaces using two-photon photoemission (2PPE) spectroscopy and first-principles density functional theory calculations. 2PPE measurements on anatase (101) show an excited resonance induced by reduced Ti^{3+} species centered around 2.5 eV above the Fermi level (E_F). While this state is similar to that observed on the rutile (110) surface, the intensity of the 2PPE peak is much weaker. Calculation of the oscillator strengths of the transitions from the occupied gap states to the empty states in the conduction band show peaks between 2.0-3.0 eV above the conduction band minimum (CBM) on both surfaces, confirming the presence of empty Ti^{3+} resonances at these energies. Although the crystal field environment of Ti ions is octahedral in both rutile and anatase, Ti^{3+} ions exhibit distinct d orbital splittings, due to different distortions of the TiO_6 units. This affects the directions of the transition dipoles from the gap states to the conduction band, explaining the polarization dependence of the 2PPE signal in the two materials. Our results show that the Ti^{3+} induced states in the band gap are shallower in anatase than in rutile.

In addition, $d \rightarrow d$ transitions from the occupied gap states to the empty Ti^{3+} excited states in anatase can occur at energies well below 3 eV, consistent with the observed visible-light photocatalytic activity of Ti^{3+} self-doped anatase.

Publications Acknowledging this Grant in 2015-2018

(I) Exclusively funded by this grant;

1. Sencer Selçuk, Xunhua Zhao, Annabella Selloni, Structural evolution of titanium dioxide during reduction in high pressure hydrogen, *Nature Materials*, accepted.
2. Xunhua Zhao, Sencer Selçuk, Annabella Selloni, Formation and stability of reduced TiO_x layers on anatase $TiO_2(101)$: identification of a novel Ti_2O_3 phase, *Phys. Rev. Materials*, **2018**, 2, 015801
3. Sencer Selçuk and Annabella Selloni, Excess Electrons at TiO_2 Anatase Surfaces and Interfaces: insights from first principles simulations, *Journal of Physics D: Applied Physics*, **2017**, 50, 273002.
4. Sencer Selçuk and Annabella Selloni, Facet-dependent trapping and dynamics of excess electrons at anatase TiO_2 surfaces and aqueous interfaces, *Nature Materials*, **2016**, 15, 1107-1112.
5. Ye-Fei Li and Annabella Selloni, Pathway of Photocatalytic Oxygen Evolution on Aqueous TiO_2 Anatase and Insights into the Different Activities of Anatase and Rutile, *ACS Catalysis*, **2016**, 6, 4769-4774.
6. U. Aschauer, A. Selloni, Adsorption of biomedical coating molecules, amino acids, and short peptides on magnetite (110), *J. Chem. Phys.*, **2015**, 143, 044705
7. S. Selcuk, A. Selloni, DFT+U Study of the Surface Structure and Stability of $Co_3O_4(110)$: Dependence on U, *J. Phys. Chem. C*, **2015**, 119, 9973-9979.
8. U. Aschauer, A. Tilocca, A. Selloni, Ab initio simulations of the structure of thin water layers on defective anatase $TiO_2(101)$ surfaces, *Int. J. Quantum Chemistry* **2015**, 115, DOI: 10.1002/qua.24918

(II) Jointly funded by this grant and other grants with leading intellectual contribution from this grant

9. Yue Lu, Wen-Jin Yin, Kai-Lin Peng, Kwan Wang, Qi Hu, Annabella Selloni, Fu-Rong Chen, Li-Min Liu, Man-Ling Sui, Self-hydrogenated shell promoting photocatalytic H_2 evolution on anatase TiO_2 . *Nature Communications*, accepted.
10. Immad M Nadeem, Jon PW Treacy, Sencer Selcuk, Xavier Torrelles, Hadeel Hussain, Axel Wilson, David C Grinter, Gregory Cabailh, Oier Bikondoa, Chris Nicklin, Annabella Selloni, Jörg Zegenhagen, Robert Lindsay, Geoff Thornton, Water Dissociates at the Aqueous Interface with Reduced Anatase $TiO_2(101)$, *J. Phys. Chem. Letters*, **2018**, 9, 3131-3136
11. Bo Wen, Qunqing Hao, Wen-Jin Yin, Le Zhang, Zhiqiang Wang, Tianjun Wang, Chuanyao Zhou, Annabella Selloni, Xueming Yang, Li-Min Liu, Electronic Structure and Photoabsorption of Ti^{3+} Ions in reduced Anatase and Rutile TiO_2 , *Phys. Chem. Chem. Phys.* **2018**, accepted
12. Wen-Jin Yin, Bo Wen, Chuanyao Zhou, Annabella Selloni, Li-Min Liu, Excess Electrons in Reduced Anatase and Rutile TiO_2 , *Surf. Sci. Reports* **2018**, 73, 58-82.
13. Jan Balajka, Ulrich Aschauer, Stijn Mertens, Annabella Selloni, Michael Schmid, and Ulrike Diebold, Surface Structure of TiO_2 Rutile (011) Exposed to Liquid Water, *J. Phys. Chem. C*, **2017**, 121, 26424-26431.
14. M. Setvin, X. Shi, J. Hulva, T. Simschitz, G. S. Parkinson, M. Schmid, C. Di Valentin, A. Selloni, U. Diebold, Methanol on anatase $TiO_2(101)$: Mechanistic insights into photocatalysis, *ACS Catalysis*, **2017**, 7, 7081

15. Honghong Wang, Taicheng An, Annabella Selloni, Effect of reducible oxide-metal cluster charge transfer on the structure and reactivity of adsorbed Au and Pt atoms and clusters on anatase TiO₂, *J. Chem. Phys.* **2017**, *146*, 184703.
16. Martin Setvin, Jan Hulva, Honghong Wang, Thomas Simschitz, Michael Schmid, Gareth S Parkinson, Cristiana Di Valentin, Annabella Selloni, Ulrike Diebold, Formaldehyde adsorption on the anatase TiO₂(101) surface: Experimental and Theoretical Investigation, *J. Phys. Chem. C*, **2017**, *121*, 8914-8922.
17. Xiao Shi, Steven L. Bernasek, and Annabella Selloni, Oxygen Deficiency and Reactivity of Spinel NiCo₂O₄ (001) Surfaces, *J. Phys. Chem. C*, **2017**, *121*, 3929-3937.
18. Francesca Nunzi, Filippo De Angelis, and Annabella Selloni, Ab Initio Simulation of the Absorption Spectra of Photoexcited Carriers in TiO₂ Nanoparticles, *J. Phys. Chem. Lett.*, **2016**, *7*, 3597-3602
19. Martin Setvin, Ulrich Aschauer, Jan Hulva, Thomas Simschitz, Benjamin Daniel, Michael Schmid, Annabella Selloni, and Ulrike Diebold, Following the Reduction of Oxygen on TiO₂ Anatase (101) Step by Step, *J. Am. Chem. Soc.* **2016**, *138*, 9565-9571.
20. Xiao Shi, Steven L. Bernasek, and Annabella Selloni, Formation, Electronic Structure, and Defects of Ni Substituted Spinel Cobalt Oxide: a DFT+U Study, *J. Phys. Chem. C*, **2016**, *120*, 14892-14898
21. He Lin, Guido Fratesi, Sencer Selçuk, Gian Paolo Brivio, and Annabella Selloni, Effects of Thermal Fluctuations on the Structure, Level Alignment, and Absorption Spectrum of Dye-Sensitized TiO₂: A Comparative Study of Catechol and Isonicotinic Acid on the Anatase (101) and Rutile (110) Surfaces, *J. Phys. Chem. C*, **2016**, *120*, 3899–3905.
22. Martin Setvin, Maria Buchholz, Weiyi Hou, Cui Zhang, Bernhard Stöger, Jan Hulva, Thomas Simschitz, Xiao Shi, Jiri Pavelec, Gareth S. Parkinson, Mingchun Xu, Yuemin Wang, Michael Schmid, Christof Wöll, Annabella Selloni, Ulrike Diebold, A Multi-Technique Study of CO Adsorption on the TiO₂ Anatase (101) Surface, *J. Phys. Chem. C*, **2015**, *119*, 21044-21052.
23. Zhiqiang Wang, Bo Wen, Qunqing Hao, Li-Min Liu, Chuanyao Zhou, Xinchun Mao, Xiufeng Lang, Wen-Jin Yin, Dongxu Dai, Annabella Selloni, and Xueming Yang, Localized Excitation of Ti³⁺ Ions in the Photoabsorption and Photocatalytic Activity of Reduced Rutile TiO₂, *J. Am. Chem. Soc.*, **2015**, *137*, 9146–9152.
24. Xiao Shi, Ye-Fei Li, S. L. Bernasek, A. Selloni, Structure of the NiFe₂O₄(001) surface in contact with gaseous O₂ and water vapor, *Surf. Sci.* **2015**, *640*, 73-79.
25. F. Nunzi, S. Agrawal, A. Selloni, F. De Angelis, Structural and Electronic Properties of Photoexcited TiO₂ Nanoparticles from First Principles, *J. Chem. Theory Comput.* **2015**, *11*, 635-645.

(III) *Jointly funded by this grant and other grants with relatively minor intellectual contribution from this grant;*

26. Moritz Müller, Daniel Sánchez-Portal, He Lin, Gian Paolo Brivio, Annabella Selloni, Guido Fratesi, Effect of Structural Fluctuations on Elastic Lifetimes of Adsorbate States: Isonicotinic Acid on Rutile (110), *J. Phys. Chem. C*, **2018**, *122*, 7575-7585
27. Wentao Yuan, Yong Wang, Hengbo Li, Hanglong Wu, Ze Zhang, Annabella Selloni, and Chenghua Sun, Real time observation of reconstruction dynamics on TiO₂ (001) surface under oxygen via an environmental TEM, *Nanolett.*, **2016**, *16*, 132-137.
28. Xiong Xiao, Fumitaka Hayashi, Hiromasa Shiiba, Sencer Selçuk, Kazuhiro Ishihara, Kenta Namiki, Lei Shao, Hiromasa Nishikiori, Annabella Selloni, and Katsuya Teshima, Platy KTiNbO₅ as a Selective Sr Ion Adsorbent: Crystal Growth, Adsorption Experiments, and DFT Calculations, *J. Phys. Chem. C*, **2016**, *120*, 11984-11992.

Wendy J. Shaw

Cooperativity of the outer coordination sphere with the active site for molecular catalysts for small molecule conversions

Wendy J. Shaw, Aaron Walsh, Nilusha Boralugodage, John Linehan, Sriram Katipamula
Pacific Northwest National Laboratory

Presentation Abstract

The performance of molecular catalysts that are being developed for multi-proton and multi-electron reactions still lag the superior catalytic activity and specificity observed in enzymes. Our group has been adding an enzyme-inspired outer coordination sphere to electrocatalysts for H₂ oxidation and to thermal CO₂ hydrogenation catalysts. By incorporating additional functional features from enzymes, we have been able to use proton pathways to lower overpotentials and increase rates, to use functional groups to alter the active site structure either statically or dynamically, and to enable electrochemical reversibility while maintaining fast rates, the highest form of electrochemical efficiency. The simplicity of the functionalities that we introduce demonstrates that the entire scaffold does not need to be recreated for substantial performance improvements. We have demonstrated a clear impact of the outer coordination sphere on both types of catalysts noted above. Of particular importance is the demonstration of features within the first, second, and outer coordination sphere working together to achieve enhanced performance, a cooperativity dominant in enzymes and likely essential to develop the best catalysts. Conversely, we show that a lack of cooperativity can severely diminish performance.

Grant or FWP Number: Low-Temperature Catalytic Routes for Energy Carriers via Spatial and Chemical Organization, 47319

PI: Johannes Lercher

Conversion of Methane over NiO/Ce_xZr_{1-x}O₂ Catalysts

Georgia Institute of Technology – School of Chemical & Biomolecular Engineering

Presentation Abstract

The enormous scale of conventional and non-conventional methane reserves has motivated significant research activities regarding its conversion to fuels and chemicals. Since large amounts of natural gas are located in remote areas and transporting gases in pipelines is difficult, processes for converting methane into denser, preferably liquid, value-added products are highly desirable. Significant efforts have been undertaken to activate and upgrade methane, but in many cases, different temperatures are required for different parts of the catalytic cycle, or expensive oxidants (e.g., H₂O₂ or organic peroxides) are consumed in the process.

To address these challenges, we developed multi-functional NiO/ceria-zirconia (NiO/CZ) catalysts that is capable of activating methane. Depending on activation and reaction conditions, non-oxidative coupling, combustion, reforming, and selective oxidation to alcohols can occur as the dominant reaction path. In the absence of other reactants, methane can be converted to ethane, but the conversion at 350-500 °C remains low due to thermodynamic limitations. Combustion is the dominant reaction in the presence of significant amounts of O₂. When the NiO particles are reduced to Ni prior to reaction, methane is predominantly converted by reforming followed by water-gas-shift. Selective oxidation to alcohols is possible under well controlled reaction conditions with limited O₂ supply. The presence of very small NiO clusters is an essentially prerequisite for the formation of alcohols, while larger NiO or Ni particles tend to form carbonaceous deposits. Consequently, we developed improved synthesis procedures for NiO/CZ with very highly dispersed Ni species.

Grant or FWP Number: DE-SC0016486 (Production of Higher Alcohols from Methane over NiO/Ce_xZr_{1-x}O₂ Catalysts)

Student(s): Chukwuemeka Okolie, Yimeng Lyu

RECENT PROGRESS***Conversion of Methane without Oxygen in the Feed***

The conversion of methane over Ni/NiO on ceria-zirconia in the absence of other reactants was investigated in the temperature range of 350 to 500 °C after activation of the catalysts in nitrogen. Several distinct regimes were observed (Figure 1). In each reaction, the conversion of methane initially increased with increasing time on stream. At 450 and 500 °C, it reached a maximum at $0.64 \pm 0.02\%$ and $1.16 \pm 0.01\%$ after about 10 h, respectively (Figure 1a). Then, the conversion declined and approached the thermodynamic limit for the conversion of methane to ethane. Specifically, the conversions of methane after 4400 min at 500 °C, 450 °C and 350 °C were $0.40 \pm 0.01\%$, $0.22 \pm 0.01\%$ and $0.118 \pm 0.002\%$, respectively.

The increase in methane conversion in the beginning is attributed to activation of the catalyst by progressive reduction of the NiO particles to metallic Ni. In the early stages of the reactions at

450 and 500 °C, some of the methane was converted into aromatics and carbonaceous deposits as indicated by the limited carbon balance closure. This reaction is comparable to the formation of carbon nanotubes that was reported under similar conditions.¹ As the conversion declined after the maximum, ethane became the dominant product. It is suggested that the formation of aromatic deposits is favored over sufficiently large Ni particles. This reaction path ceases as these particles are covered with carbonaceous deposits. In contrast, the sustained production ethane is attributed to the presence of a substantial amount of Ni clusters that are too small to assemble aromatic deposits and consequently retain their activity.

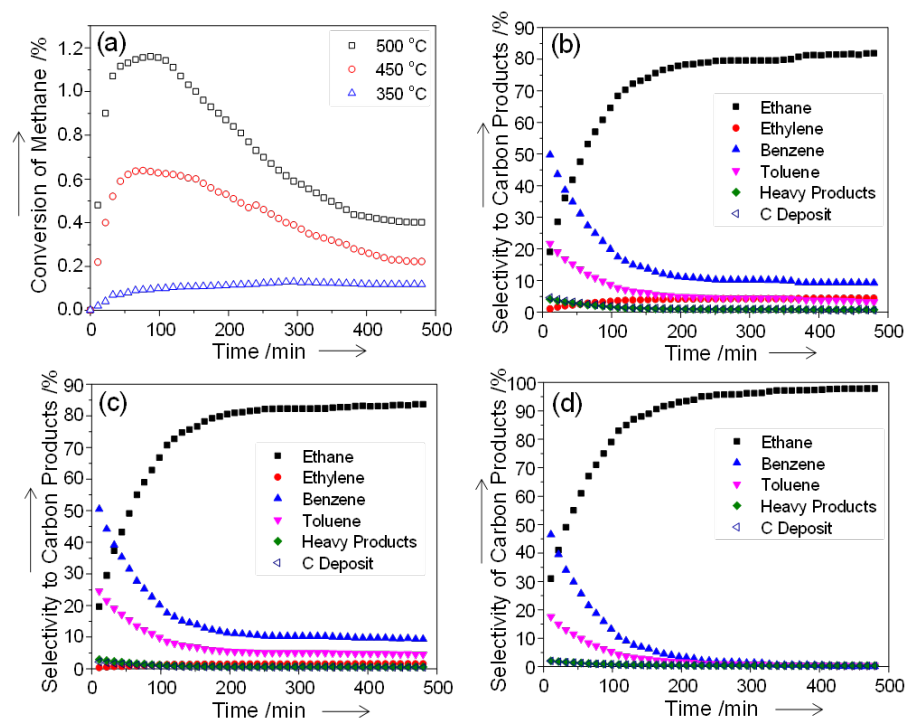


Figure 1. (a) Conversion of methane over NiO/CZ at different temperatures. Selectivity of carbon containing products at (b) 500 °C (c) 450 °C (d) 350 °C.

Influence of Activation and Reaction Conditions on the Performance of NiO/CZ

The conversion of methane in the presence of steam and O₂ over NiO/CZ activated under different conditions was studied at 450 °C. After activation in H₂ at 450 °C, CO₂ and H₂ were observed as the major products along with small amounts of CO. It is safe to assume that the NiO particles were reduced during the activation procedure. It is suggested that methane is converted by steam or oxy-reforming on the reduced Ni particles. The low CO yield is probably due to the presence of excess steam, which shifts the water-gas-shift almost entirely to CO₂ and H₂.

When the catalyst was activated in O₂ or H₂O, methane was converted to CO₂ in both cases. However, the conversion of methane is higher when activated in O₂ than in H₂O. During these activation procedures, the NiO clusters remain in the oxidic state. NiO clusters are capable of activating methane, but this reaction occurs at a lower rate compared to reduced Ni particles. Under the present conditions, catalytic combustion appears to be the dominant reaction path. The results also indicate that methane activation appears to be partially inhibited on by large amounts of steam.

The strong dependence of the performance of NiO/CZ on the activation conditions illustrates that this catalyst can favor very different paths for methane conversion depending on the oxidation state of the Ni/NiO clusters and the nature of surface species in the beginning of the reaction. Selective oxidation to alcohols is possible when the catalyst is reduced in N₂ and a very limited amount of O₂ is fed.

Characterization and Performance of NiO/CZ Catalysts Prepared by Different Synthesis Techniques

Our previous reactivity and characterization studies of NiO/CZ led us to hypothesize that activity of this catalyst for selective oxidation of methane to alcohol depends on the presence of very small NiO clusters. To study this hypothesis, we used different synthesis techniques to prepare NiO/CZ aiming to increase the dispersion of NiO particles compared to the benchmark catalyst prepared by dry impregnation (DI). For strong electrostatic adsorption (SEA), a net surface charge was introduced on the support, which allowed for adsorption of nickel precursors with the opposite charge. This technique is based on the notion that strong adsorption of metal complexes on the surface reduces agglomeration during calcination. Co-precipitation (CP) of Ni, Ce, Zr precursors was also used to prepare NiO/CZ. Since CP is a bulk technique and only a fraction of nickel atoms end up on the surface, several catalysts with different loading of Ni were prepared to find the optimum loading.

The reactivity results for the conversion of methane with steam and oxygen at 450 °C were consistent with the hypothesis. Among the catalysts with 2 wt% Ni, the one prepared by SEA gave the best performance in terms of methane conversion and alcohol selectivity (Figures 2a and b). The conversion of methane over 2NiO/CZ_CP was lower compared to the other catalysts, this samples had the highest selectivity to alcohols. Varying the Ni loading of catalysts prepared by CP showed that the catalyst prepared with 6 wt% Ni loading had the optimal composition, as it provided the best alcohol yield (Figure 2c). All of these observations are consistent with the expected correlation of high dispersion of NiO particles with the formation of alcohols.

Thus, it was essential to rigorously probe the size distribution of the NiO clusters on this catalyst. In our earlier study, EDX mapping showed that most of the NiO in 2 wt% NiO/CZ_DI is present in particles of less than 2 nm, but a higher resolution was not available by this technique or other microscopy methods due to detection/stability limits.² In a less conventional approach, we utilized the Lewis acidity of NiO (in contrast to the very weak Lewis acidity of CZ) to probe the dispersion of Ni. Specifically, the concentration of accessible Lewis acidic sites (LAS) was measured by pyridine adsorption followed by IR spectroscopy and normalized for the amount of Ni in the sample. The highest apparent dispersion of 31% was observed for NiO/CZ_SEA. The lower LAS concentration for the catalyst prepared by CP is not surprising because only a fraction of the Ni is expected to be accessible on the surface. Due to the size of the pyridine molecule, it might not be possible to adsorb two molecules on adjacent sites, but these results clearly show that NiO is highly dispersed. More detailed insight into the distribution of Ni was obtained in recent EXAFS measurements that confirmed the presence of very small NiO clusters in our samples.

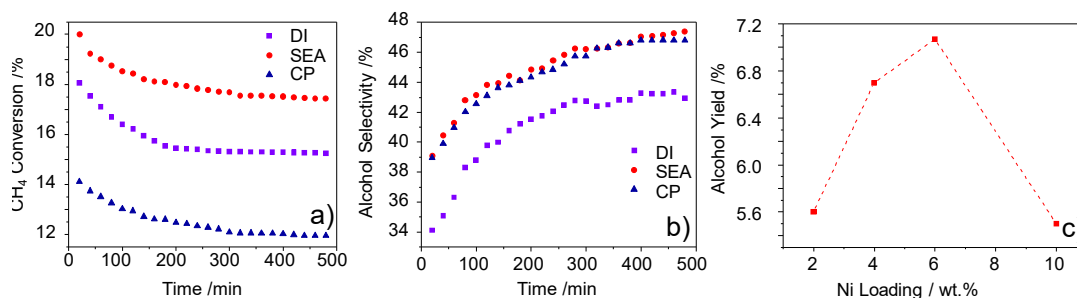


Figure 2. (a) Methane conversion in the presence of steam and oxygen at 450 °C over 2 NiO/CZ prepared by different techniques. (b) Alcohol selectivities over 2 NiO/CZ prepared by different techniques. (c) Alcohol yields over catalysts prepared by CP as a function of Ni loading.

References

1. Takenaka, S.; Shigeta, Y.; Tanabe, E.; Otsuka, K., Methane decomposition into hydrogen and carbon nanofibers over supported Pd–Ni catalysts. *J. Catal.* **2003**, *220* (2), 468-477.
2. Okolie, C.; Belhseine, Y. F.; Lyu, Y.; Yung, M. M.; Engelhard, M. H.; Kovarik, L.; Stavitski, E.; Sievers, C., Conversion of Methane to Methanol and Ethanol over Nickel Oxide on Ceria-Zirconia Catalysts in a Single Reactor. *Angew. Chem. Int. Ed.* **2017**, *56* (44), 13876-13881.

Publications Acknowledging this Grant in 2015-2018

Jointly funded by this grant and other grants with leading intellectual contribution from this grant:

1. Okolie, C.; Belhseine, Y. F.; Lyu, Y.; Yung, M. M.; Engelhard, M. H.; Kovarik, L.; Stavitski, E.; Sievers, C., Conversion of Methane to Methanol and Ethanol over Nickel Oxide on Ceria-Zirconia Catalysts in a Single Reactor. *Angew. Chem. Int. Ed.* **2017**, *56*, 13876-13881.
2. Okolie, C.; Lyu, Y.; Kovarik, L.; Stavitski, E.; Sievers, C., Coupling of Methane to Ethane, Ethylene and Aromatics over Nickel on Ceria-Zirconia at Low Temperatures. *ChemCatChem* **2018**, *10*, 2700-2708.

Electrocatalytic ammonia splitting at ambient temperatures

Reza Ghazfar, Thomas Hamann, Mona Maleka Ashtiani, Faezeh Habib Zadeh, Susanne L. Miller, and Milton R. Smith, III
Michigan State University, Department of Chemistry

Poster Abstract

The combined biological and abiological production of ammonia from N_2 is one of the largest scale chemical syntheses on Earth. The reaction of N_2 and H_2 to make NH_3 is thermoneutral. Thus, very little of the energy in H_2 is lost in NH_3 synthesis. Thus, the regeneration of H_2 and N_2 from NH_3 can potentially generate H_2 efficiently. Since ammonia liquefies at low pressure, has an energy density similar to methanol, has been transported across the U.S. by pipeline for decades, and N_2 is atmosphere abundant, ammonia is an attractive liquid fuel for storing and distributing H_2 .

Compared to NH_3 synthesis, its conversion to N_2 and H_2 has received far less attention. Most reactions require high temperatures, which can exceed those of the Haber-Bosh process. Electrolysis offers the possibility of ‘on demand’ H_2 generation, but the most efficient examples are run in aqueous media using catalysts that are alloys of precious metals.¹

The conversion of liquid NH_3 to H_2 and N_2 at ambient temperatures has never been described with a molecular catalyst. We have designed Ru systems capable of catalyzing these reactions. Synthesis, electrocatalysis, and mechanistic studies will be presented.

Grant or FWP Number: DE-SC0016604

Postdoc(s): Susanne L. Miller

Student(s): Reza Ghazfar, Mona Maleka Ashtiani, and Faezeh Habib Zadeh

1. Little, D. J.; Edwards, D. O.; Smith, M. R., III; Hamann, T. W. As Precious as Platinum: Iron Nitride for Electrocatalytic Oxidation of Liquid Ammonia. *ACS Appl. Mater. Interfaces* **2017**, *9*, 16228-16235.

Jin Suntivich

**Measurements of the Oxygen Electroadsorption on Well-defined IrO₂ and RuO₂:
A Discussion of the Scaling Relation and Sabatier Principle**

Jin Suntivich

Cornell University, Department of Materials Science and Engineering

Presentation Abstract

We present the measurements of hydroxide ('OH_{ad}') and oxide ('O_{ad}') electroadsorption energies on well-defined IrO₂(110) and RuO₂(110) surfaces and discuss the implications of the measurement results on our ability to design electrocatalysts for the oxygen reduction reaction (ORR) and oxygen evolution reaction (OER). The ORR and OER are the major contributor of overpotential in many fuel-cell and electrolyzer devices. A highly active ORR/OER electrocatalyst can reduce this overpotential requirement by stabilizing the ORR/OER intermediates via surface electroadsorption. While this idea has led to a number of new ORR/OER electrocatalysts, the fundamental relationship between the electroadsorption and the oxygen electrochemical kinetics has still not yet been measured on oxides. We present a measurement of this relationship on IrO₂ and RuO₂ grown using molecular-beam epitaxy on TiO₂(110) single crystals. The high quality of the IrO₂ and RuO₂ films affords a measurement of the oxygen electroadsorption energies. We use these measurements to test (1) the scaling relation, an idea that the first surface bond can approximate the trend of the intermediates adsorption, and (2) the Sabatier principle, a concept that a catalyst is most active when the intermediate stabilization is moderate, not too weak such that the surface is inert and ineffective, nor too strong such that the intermediate cannot leave and disrupt the subsequent catalytic cycle.

DE-SC0018029: Rational Selection of Transition-Metal Oxide Electrocatalysts from Structure-Electronic Structure-Activity Relations: The Role of Defects, Strain, and Sub-Surface Layering

Graphite-Conjugated Catalysis

Yogesh Surendranath
Massachusetts Institute of Technology, Department of Chemistry

Presentation Abstract

The interconversion of electrical and chemical energy requires catalysts that can efficiently transfer multiple electrons to or from small molecules. Heterogeneous catalysts have extended band structures with high densities of states at the Fermi level, allowing these surfaces to engage in concerted electron transfer and substrate activation; however, it is difficult, if not impossible, to obtain significant molecular-level understanding for most heterogeneous catalysts because surface active sites are inherently dynamic, difficult to modify at the molecular level, and hard to identify, much less characterize. Recently, we have developed a new class of catalysts that incorporate molecularly well-defined, highly-tunable active sites into heterogeneous graphite surfaces. These graphite-conjugated catalysts (GCCs) feature a unique conjugated linkage between a discrete molecular active site and the delocalized states of graphitic carbons. Electrochemical and spectroscopic investigations establish that GCCs exhibit strong electronic coupling to the electrode, leading to electron transfer (ET) behavior that diverges fundamentally from that of solution phase or surface-tethered analogues. We find that: (1) ET is not observed between the electrode and a redox-active GCC moiety regardless of applied potential. (2) ET is observed at GCCs *only* if the interfacial reaction is ion-coupled. (3) Even when ET is observed, the oxidation state of a transition metal GCC site remains unchanged. From these observations, we construct a mechanistic model for GCC sites in which ET proceeds exclusively through inner-sphere mechanisms. This behavior is identical to that of catalytically active metal surfaces rather than to that of molecules in solution, making GCCs the first platform in which molecular active sites behave as metal surface sites. Our results demonstrate that GCCs provide a versatile platform for investigating and controlling interfacial inner-sphere reactivity in both elementary ET steps and electrocatalysis at the molecular level.

DE-SC0014176: Tunable Oxygen Reduction Electrocatalysis by Phenazine-Modified Carbons

PI: Yogesh Surendranath

Postdoc(s): Tomohiro Fukushima

Student(s): Megan Jackson, Seokjoon Oh, Corey Kaminsky, Travis Marshall-Roth

Affiliations(s): Massachusetts Institute of Technology

RECENT PROGRESS

In the past year, we have also discovered that the unique conjugated linkage formed between GCC sites and carbon electrodes leads to a distinct mechanism of electron transfer. Electrochemical and spectroscopic studies led to three key observations, from which we have constructed a mechanistic model:

(1) ET is not observed between the electrode and GCC sites.

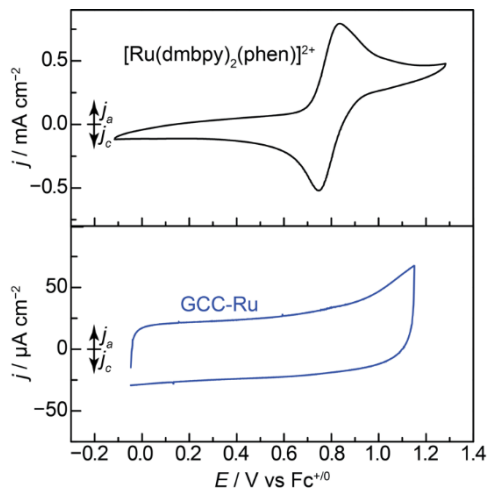


Figure 4. CVs of dissolved $[\text{Ru}^{\text{II}}(\text{dmbpy})_2(\text{phen})]^{2+}$ (5mM, 100 mV s^{-1}) (top) and GCC-Ru (10 mV s^{-1}) (bottom) recorded in acetonitrile electrolyte containing 0.1 M TBAPF₆.

In the absence of bond cleavage or formation, redox features are not observed at GCC sites. Cyclic voltammograms (CVs) of the dissolved complex $[\text{Ru}^{\text{II}}(\text{dmbpy})_2(\text{phen})]^{2+}$ (dmbpy = 4,4'-dimethyl-2,2'-bipyridine, phen = 1,10-phenanthroline) display a reversible Ru(III/II) wave, and the same wave is observed when the molecule is anchored to an electrode surface through an insulating aliphatic linkage. Remarkably, conjugating this Ru center to the graphite surface causes the redox waves to disappear (**Figure 1**). Similarly, CVs of phenazine in aprotic acetonitrile electrolyte show a reversible feature attributed to one-electron reduction and re-oxidation of phenazine, but no wave is observed when a phenazine unit is conjugated to a carbon electrode (**Figure 2**).

The inability to do outer-sphere ET to these GCC sites suggests that varying the potential does not lead to the same change in ET driving force for the conjugated system. This lack of driving force is consistent with double-layer theory if and only if the molecular fragment is electronically coupled to the electrode. In metallic electrodes, the metal atoms are strongly coupled to the band states of the solid, and the effective conductivity of a metal ensures that the Fermi level of the surface-exposed metal atoms is identical to that of the bulk. Upon application of a potential, the ensuing interfacial field gradient raises the Fermi level of the solid *and* the energy levels of surface atoms in synchrony; thus, the energy separation between the donor/acceptor states of the surface atoms and the Fermi level remain the same irrespective of the applied potential. Our data indicate that the same phenomenon is occurring in GCCs. In particular, the inability to observe outer-sphere ET in GCCs indicates that the pyrazine linkage electronically couples the molecular fragment to the electrode. This electronic coupling ensures that the separation between the Fermi level of the carbon and the molecular donor/acceptor states of the appended fragments remain largely invariant with applied potential; i.e., varying the applied potential does not change the *difference* in the potential between the electrode and the GCC site, thereby eliminating the possibility of outer-sphere ET between them (**Figure 3**, bottom).

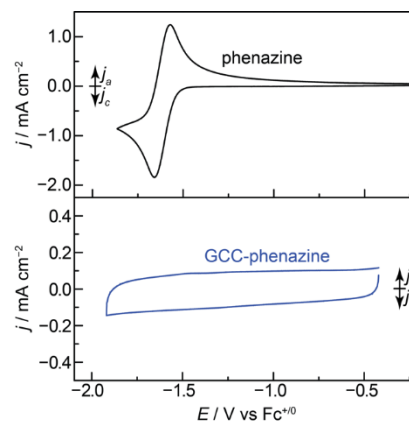


Figure 5. CVs of dissolved phenazine (5 mM, 100 mV s^{-1}) (top) and GCC-phenazine (10 mV s^{-1}) (bottom) recorded in acetonitrile electrolyte containing 0.1 M TBAPF₆.

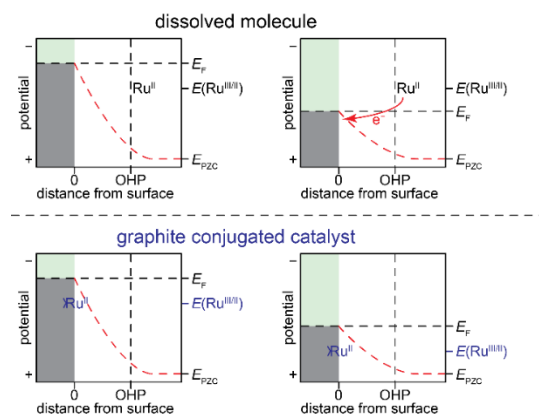


Figure 6. Putative interfacial free energy diagrams for unmodified electrodes with dissolved Ru^{II} molecules (top) and electrodes modified with conjugated Ru^{II} surface sites (bottom). The diagram denotes the Fermi level of the electrode, E_{F} , and the redox potential of the molecule, $E(\text{Ru}^{\text{III/II}})$, upon varying the applied potential (left to right). The electrostatic potential across the electrochemical double layer is indicated by the red dotted line. Varying E_{F} does not impact $E(\text{Ru}^{\text{III/II}})$ for the dissolved molecule, leading to classical outer-sphere ET (top) at the interface. For GCCs (bottom), varying E_{F} simultaneously shifts the energy levels of donor/acceptor states in the conjugated molecule by a similar magnitude, and the driving force for ET remains unchanged.

between the GCC site and the solution. Therefore, varying the applied potential can alter the driving force for *ions* to transfer between the GCC site and the solution, provided that the surface site is able to bind the ion in question. GCC-phenazine can form and break bonds with protons in the presence of a proton donor.

When the applied potential is sufficiently negative, the electric field drives protons to cross the double layer and bind to the N sites. Since protons carry a positive charge, compensating electrons must flow from the external circuit in order to maintain the electrode potential. This compensatory current is observed as a surface redox wave. Since all N sites are expected to bind protons with similar affinity, ET occurs over a relatively narrow potential range, leading to a distinct wave above the background double-layer charging current. Similarly, the Rh in GCC-Rh binds a Cl^- ion, and when the potential is sufficiently negative, the electric field drives this negatively charged ion across the double layer into solution. Again, this ion dissociation leads to compensatory electron flow from the external circuit, which we observe as a redox wave (**Figure 5b**).

(2) ET is observed at GCCs only if the interfacial reaction is ion-coupled.

GCC sites *do* undergo ET if the ET process is coupled to forming or breaking a bond with an ion in solution. Although CVs of GCC-phenazine do not display any redox features in aprotic acetonitrile electrolyte, they display reversible redox waves when tosylic acid is added to solution or when the electrode is scanned in an aqueous electrolyte (**Figure 4**). Additionally, $[\text{Rh}^{\text{III}}\text{Cp}^*(\text{phenda})\text{Cl}]^+$ ($\text{Cp}^* =$ pentamethylcyclopentadienyl) loses a chloride upon reduction of the metal center, and likewise the conjugated Rh molecule gives rise to a redox feature coinciding with loss of halide (**Figure 5**).

We believe in both of these cases, it is the ion transfer that is driving ET. Even though our data suggest that there is negligible potential drop between the electrode and the GCC site, there *is* a potential

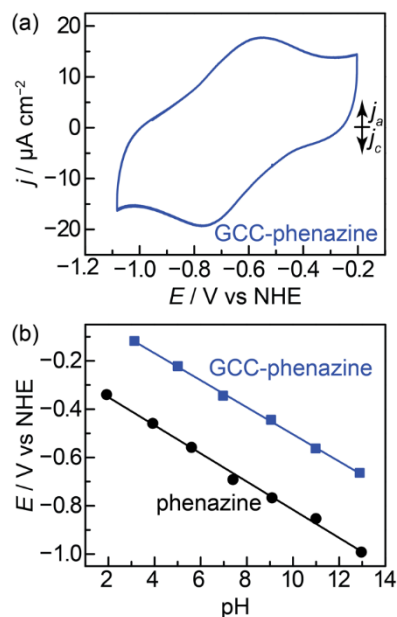


Figure 7. (a) Cyclic voltammogram (10 mV s^{-1}) of GCC phenazine recorded in 0.1 M NaOH. (b) $E_{1/2}$ vs pH for dissolved phenazine (red) and GCC-phenazine (black). Values for dissolved phenazine are re-plotted from literature values obtained from linear sweep voltammograms recorded in 10% ethanolic aqueous electrolyte. CVs of GCC phenazine were recorded at 10 mV s^{-1} in pH-adjusted 0.1 M borate/0.1 M phosphate/0.1 M formate aqueous

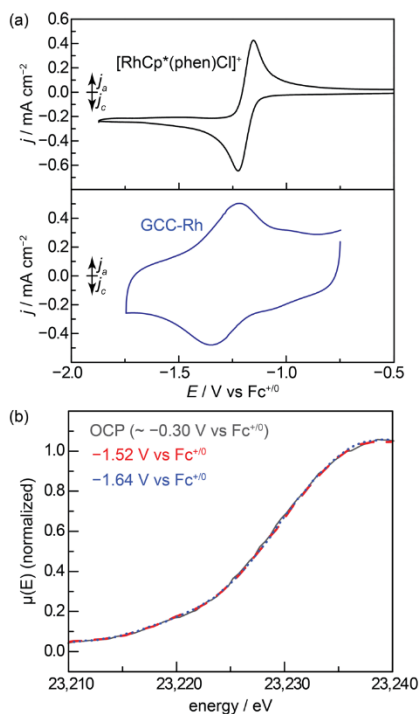


Figure 8. CVs of dissolved $[\text{Rh}^{\text{III}}\text{Cp}^*(\text{phen})\text{Cl}]^+$ (5 mM, 100 mV s^{-1}) (a, top) and GCC-Rh (10 mV s^{-1}) (a, bottom) recorded in acetonitrile electrolyte containing 0.1 M TBACl. (b) in situ Rh K-edge X-ray absorption near edge structure spectra of GCC-Rh recorded in acetonitrile electrolyte containing 0.1 M TBACl and held at the open circuit potential (OCP, $\sim -0.3 \text{ V}$), -1.43 V , and $-1.55 \text{ V vs Fc}^{+/0}$.

(3) Even during ET, the oxidation state of a transition metal GCC site remains unchanged.

Perhaps most surprisingly, in situ X-ray absorption near-edge spectra data (**Figure 5c**) indicate that the oxidation state of the Rh remains constant throughout the redox event for GCC-Rh, suggesting that ET at GCCs is electrode-based rather than metal-based. This observation in particular has important implications on catalyst design. Since the oxidation state of the GCC site can remain constant throughout an ET process, the valency and reduction potential of the molecular analogue do not directly dictate the rate and driving force for elementary and catalytic redox reactions at GCCs. Instead, redox chemistry at GCCs must be driven by the binding strength of substrates and intermediates with the surface sites.

In sum, the reactivity patterns of GCCs mimic those of metallic surface sites. At metal surface sites, ET proceeds exclusively via inner-sphere mechanisms in which electron flow is driven by ions or molecules crossing the double layer. As a result, ET is only observed when bonds are made or broken at metallic surface sites, and no ET occurs in the absence of a species that is able to adsorb to the surface. Our data suggest that ET at graphite-conjugated molecules also proceeds exclusively via inner-sphere pathways, making GCCs mechanistically indistinguishable from authentic metallic surfaces.

Publications Acknowledging this Grant in 2015-2018

(X) Exclusively funded by this grant;

None

(XI) Jointly funded by this grant and other grants with leading intellectual contribution from this grant;

1. Oh, S.; Gallagher, J. R.; Miller, J. T.; Surendranath, Y. Graphite-Conjugated Rhenium Catalysts for Carbon Dioxide Reduction. *J. Am. Chem. Soc.* **2016**, *138*, 1820–1823.
2. Fukushima, T.; Drisdell, W.; Yano, J.; Surendranath, Y. Graphite-Conjugated Pyrazines as Molecularly Tunable Heterogeneous Electrocatalysts. *J. Am. Chem. Soc.* **2015**, *137*, 10926–10929.
3. Chu, S. B.; Fukushima, T.; Surendranath, Y. *Chem. Mater.* **2017**, *29*, 495–498.
4. Murray, A. T.; Surendranath, Y. *ACS Catal.* **2017**, *7*, 3307–3312.

5. Ricke, N. D.; Murray, A. T.; Shepherd, J. J.; Welborn, M. G.; Fukushima, T.; Van Voorhis, T.; Surendranath, Y. *ACS Catal.* **2017**, *7*, 7680-7687.
6. Jackson, M. N.; Oh, S.; Kaminsky, C. J.; Chu, S. B.; Zhang, G.; Miller, J. T.; Surendranath, Y. *J. Am. Chem. Soc.* **2018**, *140*, 1004-1010.

Platinum Single-site Centers through Metal-ligand Self-assembly on Powdered Metal Oxide Supports and their Selective Catalytic Activity

Steven L. Tait
Department of Chemistry, Indiana University

Presentation Abstract

The central hypothesis of this project is that two-dimensional coordination of single-site metals at oxide surfaces will produce metal sites with well-defined chemistry and high selectivity in catalysis. We are developing single-site transition metal centers at oxide surfaces for hydrocarbon chemistries, particularly C-H activation in small alkanes, a prerequisite to selective oxidation, oxidative coupling, and other desirable chemistries for upgrading methane to value-added chemical commodities. Most of this work is accomplished by developing novel synthesis strategies to produce metal-organic complexes on high surface area oxide powders. Much of that design is based on studies in highly-controlled vacuum environments on model single crystal surfaces. The reaction chemistry on powder supports guides the surface science studies and, conversely, studies of model systems have led to highly effective designs for the high surface area catalysts.

The long-term goal of this research is to develop metal-organic complexes as surface catalysts that can be tuned to specific selective alkane functionalization reactions. In the past year, we have made significant advances in demonstrating the single site character of Pt stabilized by tetrazine-based ligands on Al₂O₃, MgO, and CeO₂ powder supports. These are characterized by photoelectron spectroscopy, electron microscopy, CO adsorption, and by X-ray absorption spectroscopy (at Argonne National Laboratory). We have also demonstrated catalytic activity and turnover in a hydrosilylation reaction, where we are able to demonstrate activity and selectivity in the metal-organic single-site catalysts that competes with and exceeds those of the industrial standard catalyst. Our ongoing studies seek to extend these results to other systems and also to develop new coordination geometries.

DE-SC0016367: Single-Site Metal Organic Complexes on Oxide Supports for Selective Alkane Functionalization

Student(s): Iyad Ali, Linxiao Chen, Tobias Morris, Miao Wang, Christopher Williams

RECENT PROGRESS

Oxide-supported Pt single-site catalysts by metal-ligand self-assembly

We have investigated and developed oxide-supported Pt single-site catalysts (SSCs) by metal-ligand self-assembly. This involves a novel synthesis method that we have been developing during this project, which involves a modified wet-impregnation approach to introduce small organic ligands to stabilize single-site Pt centers on the surface of the powdered oxides. The ligands are designed to have excellent coordination sites for the Pt, as well as a strong electron accepting character to induce a redox exchange upon assembly. The wet impregnation method is modified to introduce the ligand at a stage that will achieve a high level of single-site formation through metal-ligand complexation. Impregnating Pt and a ligand 3,6-di-2-pyridyl-1,2,4,5-tetrazine (DPTZ, Figure 1) simultaneously (one-step) creates Pt-DPTZ single-sites on powdered MgO, Al₂O₃, and CeO₂. MgO has the most uniform single-sites due to a strong, non-competitive support-ligand interaction, and a support-metal interaction of appropriate strength. Pt(II) centers are stabilized between the N binding pockets of DPTZ, with minimal metallic nanoparticle formation.

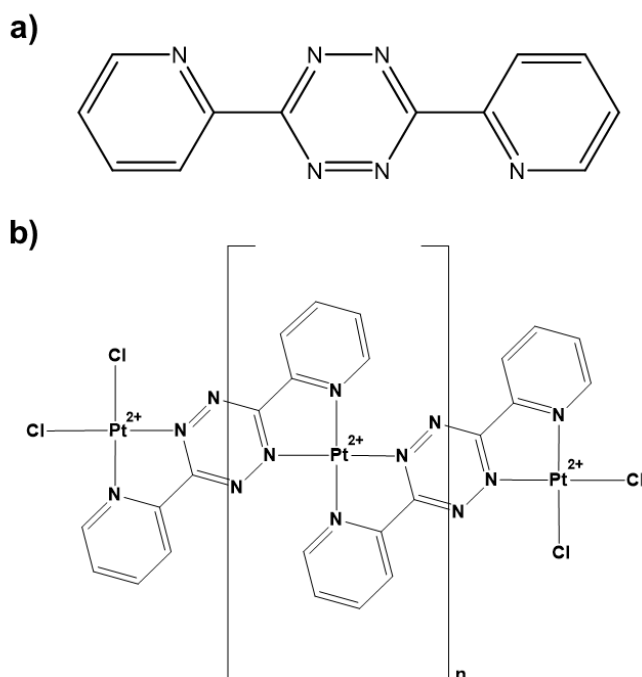


Figure 1. (a) Structure of DPTZ ligand. (b) Potential structure of Pt single-site centers in Pt-DPTZ complexes, illustrating quasi-square planar coordination geometry and likely Cl bonding on some Pt. Pt binding with surface oxygen also exists, but is not included in this drawing.

X-ray Absorption Spectroscopy (XAS) was performed at Argonne National Laboratory to examine the formation of single-sites and elucidate the local coordination structure of MgO and CeO₂-supported Pt-DPTZ SSCs (Figure 2). We find that the coordination sphere of the Pt is chiefly composed of N (ligand), O (oxide support), and some Cl (residual from Pt precursor), but it does not show evidence of Pt-Pt interactions. This system was also characterized by XPS, TEM, XRD, and CO adsorption. Sequential impregnation of Pt and DPTZ (two-step) was also tested on Al₂O₃ and CeO₂, but is not as effective as the one-step method due to limited Pt accessibility and mobility. This work is currently in press for publication in the *Journal of Catalysis*.

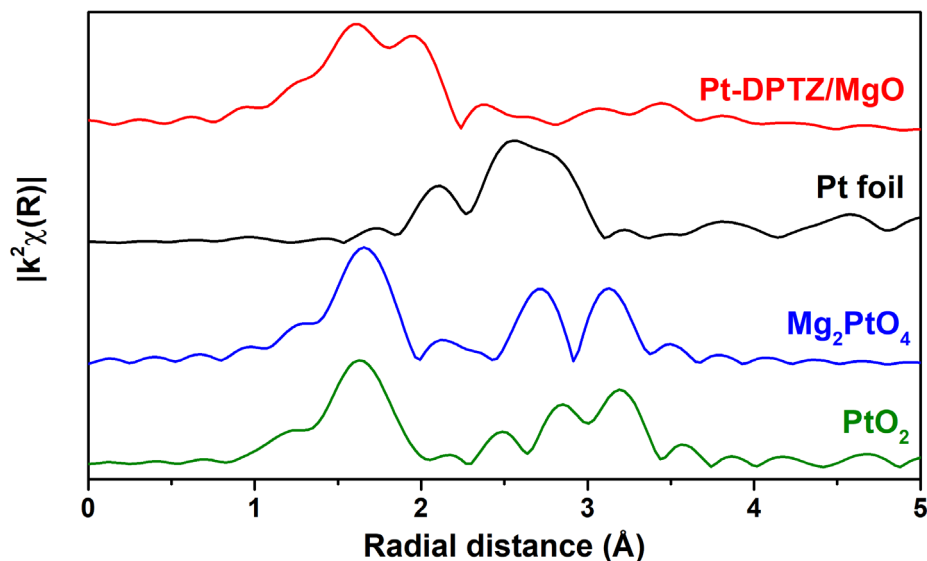


Figure 2. Comparison between EXAFS Fourier transform magnitudes of one-step Pt-DPTZ/MgO, Pt foil, Mg₂PtO₄, and PtO₂. Note the absence of Pt–Pt shell in one-step Pt-DPTZ/MgO, which is the dominant feature in Pt foil.

These SSCs were applied in alkene hydrosilylation reactions, and showed satisfactory activity as well as improved yields over commercial Speier and Karstedt catalysts. Pt-DPTZ SSCs catalyze side reactions (alkene hydrogenation and isomerization) less than commercial catalysts, form less colloidal Pt that lead to deactivation after reactions, and are more tolerant with highly reactive epoxide substrates. We found that, despite some Pt leaching, the reaction is mostly heterogeneous in nature and high yield can be maintained after multiple iterations of recycling the catalyst. Pt-DPTZ SSCs exhibited higher turnover frequency (TOF) than oxide-supported nanoparticles, emphasizing the advantages of single-site catalysis. The activity (and TOF) of Pt SSC is dependent on the nature of the support and ligands.

We also discovered that after H₂ pre-treatment at moderate temperature (150 °C), CeO₂-supported Pt-DPTZ SSC is capable of activate CH₄ at room temperature. The formation of surface –OH and adsorbed –CO after CH₄ exposure was verified by in situ DRIFTS.

Sulfate-promoted selective catalytic reduction of NO by NH₃ (NH₃-SCR) on CeO₂

We discovered that modifying CeO₂ with ligands containing –SO₃H group promotes its NH₃-SCR activity after O₂ activation. The main species that contribute to this promotion effect was proved to be surface sulfates that increase Lewis acidity and suppresses active surface oxygen. We investigated the reaction mechanism using *in situ* DRIFTS, concluding that the reaction has two mechanisms (Langmuir-Hinshelwood and Eley-Rideal). Surface sulfates do not only promote key steps in both mechanisms, also suppress the NH₃ oxidation side reaction. We also compared sulfates with classic inorganic promoter FeO_x, finding out that sulfates outperform FeO_x particularly at high temperature due to its unique capability in oxygen deactivation and facilitating hydrogen extraction from adsorbed NH₃. We are also preparing a manuscript on the sulfate promotion effect in CeO₂-catalyzed NH₃-SCR.

Redox-active complexation by vibrational spectroscopy in highly controlled environments

High Resolution Electron Energy Loss Spectroscopy (HREELS) and other techniques were used to demonstrate that single-site V atoms in metal-organic complexes at surfaces are active and highly selective toward O₂ activation. Dipyridyl-tetrazine (DPTZ) forms ordered complexes with single-site V atoms on Au(100) at RT. After 50 L O₂ exposure at RT, a single V=O stretch mode shows up in HREEL spectra, indicating activity in dissociating O₂ molecules at V single sites. In comparison, O₂ exposure to V nanoparticles induces multiple vibrational modes including V=O stretch and O-V-O bridging modes. Those results clearly show better selectivity of single-site V atoms compared to V nanoparticles. This study of interaction between gas molecules and single metal atoms in metal-organic complexes shows potential catalytic significance and could possibly be mimicked at metal-oxide surfaces in the future. This vibrational spectroscopy work allows us to correlate studies under highly controlled UHV conditions with the high pressure cell DRIFTS measurements. The UHV studies have been very valuable in identifying strong candidates for metal-organic complexation on high surface area oxides.

Publications Acknowledging this Grant in 2015-2018

(XII) Exclusively funded by this grant;

1. Chen, L.; Sterbinsky, G. E.; Tait, S. L. Synthesis of platinum single-site centers through metal-ligand self-assembly on powdered metal oxide supports. *J. Catalysis* **2018**, *in press*.
2. Chen, L.; McCann, J. P.; Tait, S. L. A Re-examination of the Catalyst Activation and Temperature Hysteresis in Methane Combustion on Pt/Al₂O₃. *Appl. Catal. A: General* **2018**, *549*, 19-30.
DOI: [10.1016/j.apcata.2017.09.008](https://doi.org/10.1016/j.apcata.2017.09.008)
3. Williams, C. G.; Wang, M.; Skomski, D.; Tempas, C. D.; Kesmodel, L. L.; Tait, S. L. Metal-Ligand Complexation through Redox Assembly at Surfaces Characterized by Vibrational Spectroscopy. *J. Phys. Chem. C* **2017**, *121*, 13183-13190. DOI: [10.1021/acs.jpcc.7b02809](https://doi.org/10.1021/acs.jpcc.7b02809)
4. Tempas, C. D.; Skomski, D.; Tait, S. L. Lifting of the Au(100) Surface Reconstruction by Pt, Cr, Fe, and Cu Adsorption. *Surf. Sci.* **2016**, *654*, 33-38.
DOI: [10.1016/j.susc.2016.07.012](https://doi.org/10.1016/j.susc.2016.07.012)
5. Williams, C. G.; Wang, M.; Skomski, D.; Tempas, C. D.; Kesmodel, L. L.; Tait, S. L. Dehydrocyclization of Peripheral Alkyl Groups in Porphyrins at Cu(100) and Ag(111) Surfaces. *Surf. Sci.* **2016**, *653*, 130-137. DOI: [10.1016/j.susc.2016.06.013](https://doi.org/10.1016/j.susc.2016.06.013)
6. Skomski, D.; Tempas, C. D.; Bukowski, G. S.; Smith, K. A.; Tait, S. L. Redox-Active On-Surface Polymerization of Single-Site Divalent Cations from Pure Metals by a Ketone-Functionalized Phenanthroline. *J. Chem. Phys.* **2015**, *142*, 101913. DOI: [10.1063/1.4906894](https://doi.org/10.1063/1.4906894)

(XIII) Jointly funded by this grant and other grants with leading intellectual contribution from this grant;

7. Skomski, D.; Tempas, C. D.; Cook, B. J.; Polezhaev, A. V.; Smith, K. A.; Caulton, K. G.; Tait, S. L. **Two and Three Electron Oxidation of Single-site Vanadium Centers at Surfaces by Ligand Design.** *J. Amer. Chem. Soc.* **2015**, *137*, 7898-7902. DOI: [10.1021/jacs.5b03706](https://doi.org/10.1021/jacs.5b03706)

(XIV) Jointly funded by this grant and other grants with relatively minor intellectual contribution from this grant;

8. Goronzy, D. P.; Ebrahimi, M.; Rosei, F.; Arramel; Fang, Y.; De Feyter, S.; Tait, S. L.; Wang, C.; Beton, P. H.; Wee, A. T. S.; Weiss, P. S.; Perepichka, D. F. Supramolecular Assemblies on Surfaces: Nanopatterning, Functionality, and Reactivity. *ACS Nano* **2018**, *in press*.
9. Tempas, C. D.; Morris, T. W.; Wisman, D. L.; Din, N. U.; Le, D.; Williams, C. G.; Wang, M.; Polezhaev, A. V.; Rahman, T. S.; Caulton, K. G.; Tait, S. L. Redox-active Ligand Controlled Selectivity of Vanadium Oxidation on Au(100). *Chem. Sci.* **2018**, *9*, 1674-1685. DOI: [10.1039/c7sc04752e](https://doi.org/10.1039/c7sc04752e)

Water Trapped at the Interface of Hydrophobized Catalysts for C-C Coupling Reactions

Duong T. Ngo, Bin Wang, Daniel Resasco
Center for Interfacial Reaction Engineering (CIRE), School of Chemical, Biological and
Materials Engineering. University of Oklahoma, Norman

Presentation Abstract

The presence of liquid water is practically unavoidable in some reaction systems, such as biomass conversion. Cyclopentanone is a promising building block in the conversion of biomass to fuels. It can be converted to valuable products via C-C bond forming reactions. Among them, aldol condensation is a promising route. Conventional MgO catalysts are intrinsically active to catalyze this reaction, but they usually exhibit low stability in the presence of liquid water. Here, we show that hydrophobic MgO-based catalysts functionalized with octadecyltrichlorosilane (OTS) exhibit remarkable stability in the liquid phase under conditions in which a conventional MgO deactivates in short time. Ab initio molecular dynamics (AIMD) simulations suggest that OTS forms a thick hydrophobic barrier for water penetration. However, these simulations also show that water, which is either formed through the aldol condensation or diffused driven by gradients of chemical potentials, can be trapped at the MgO/OTS interface. These water clusters can deactivate the catalysts as well as change the reaction mechanism.

DE-SC0018284: Hydrophobic Enclosures in Bio-Inspired Nanoreactors for Enhanced Phase Selectivity - A Combined Experimental/Theoretical Approach

PIs: Daniel Resasco, Bin Wang

Postdoc(s): Gengnan Li

Student(s): Michael Zeets, Duong T. Ngo, Tuong Bui

The grant section in extended abstract by Daniel E. Resasco

Robert M. Waymouth

Selective Catalytic Oxidations: Scope and Mechanism

Robert M. Waymouth, Wilson Ho
Department of Chemistry, Stanford University, Stanford, CA 94305

Presentation Abstract

We have developed a versatile Pd catalyst for the chemoselective aerobic oxidation of alcohols, vicinal diols, polyols and carbohydrates. The cationic Pd dimer $[(\text{neocuproine})\text{Pd}(\mu\text{-OAc})]_2[\text{OTf}]_2$ (neocuproine = 2,9-dimethyl-1,10-phenanthroline) is an active catalyst precursor for the oxidation of a variety of primary and secondary alcohols. This complex exhibits modest chemoselectivity for the oxidation of primary alcohols in the presence of secondary alcohols, but terminal 1,2-diols are selectively oxidized to the hydroxyketones. More complex polyols, such as glycerol, threitol and unprotected alkyl pyranosides are also oxidized in high selectivity to the hydroxyketones; for alkyl pyranosides oxidation occurs selectively to afford the 3-ketoses. Mechanistic and kinetics studies have illuminated some of the factors responsible for the reversal in chemoselectivity observed for vicinal diols relative to primary and secondary alcohols.

For aerobic alcohol oxidations, competitive oxidative degradation of the ligand limited the catalyst lifetime. Mechanistic studies, including *in situ* mass spectrometry techniques, provided insights that guided the development of effective strategies for mitigating catalyst deactivation. Specifically, the addition of H-atom donors and appropriate ligand modifications improved the catalyst lifetime, enabling the efficient aerobic oxidations of a variety of polyols on a multigram scale with as little as 0.25 mol% Pd without any appreciable loss in chemoselectivity.

During the course of these studies, we identified the trinuclear species $[(\text{LPd})_3(\mu^3\text{-O})_2]^{2+}$ (L = neocuproine = 2,9-dimethyl-1,10-phenanthroline) as a product of dioxygen activation that is formed during aerobic oxidations catalyzed by $[\text{LPd}(\text{OAc})]_2(\text{OTf})_2$. The role of this compound in catalysis and its mechanism of formation have been investigated by a series of kinetic investigations, isotope labeling, and reactivity studies. The results suggest the trinuclear compound is involved in the decomposition of hydrogen peroxide, the initial product of oxygen reduction during catalysis.

DOE DE-SC00181168: Selective Catalytic Oxidations: Opportunities and Challenges for Selective Conversion of Renewable Resources

PI: Robert M. Waymouth

Postdoc(s): Timothy R. Blake

Student(s): Wilson Ho

Affiliations(s): Department of Chemistry, Stanford University, Stanford CA 94305

hydrogen atom donors. Phenol anti-oxidants such as **H** proved a particularly useful additive for mitigating oxidative degradation of the catalyst. In addition, styrene additives proved to improve catalyst lifetimes by intercepting Pd hydrides, facilitating re-oxidation of the Pd hydride species and mitigating formation of Pd black.⁽¹⁾

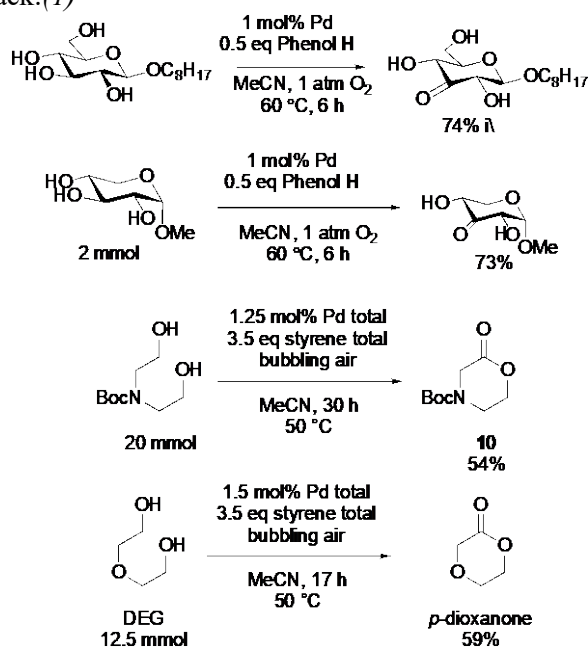


Figure 3. Selective Oxidation of Carbohydrates and 1,5-diols.

These insights enabled us to modify our aerobic oxidation protocols for the aerobic oxidation of a variety of polyols on a multigram scale with catalyst loadings as low as 0.25 mol % Pd (Figure 3). The mechanistic studies on the oxidative degradation of the neocuproine ligand and the strategies we developed for extending catalyst lifetimes were utilized to improve catalytic strategies for the chemoselective oxidation of unprotected carbohydrates, the selective oxidation of glycerol to dihydroxyacetone, and the oxidative lactonization of a variety of 1,5-diols. With these new protocols, the chemoselective oxidation of the unprotected alkyl glucosides can be carried out aerobically with catalyst loadings as low as 1 mol% Pd to afford excellent yields of the 3-ketoses in high chemoselectivity (Figure 3).⁽²⁾

The mechanistic origin of the high selectivities of these oxidations reactions remains unclear and represents one area of active investigation.

Scope and Utility of Chemoselective Catalytic Oxidations: Fundamental investigations to improve the scope of the Pd-catalyzed alcohol oxidations has proven an enabling advance for collaborative studies with the Wender group at Stanford to generate functional polyesters as novel degradable polymers useful for the delivery of messenger RNA in cells and live animals.⁽⁶⁻⁸⁾ The oxidative lactonization of substituted diethanolamines to generate new families of morpholinones (Figure 4),⁽¹⁾ which have proven a versatile class of monomers for generating

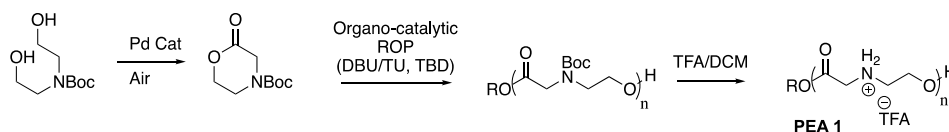


Figure 4. Oxidative lactonization of functionalized diethanolamines and ring-opening polymerization of resulting morpholinones.

functionalized, degradable polyesters. Lactones accessed via the Pd-catalyzed oxidative lactonization of α - ω diols⁽¹⁾ were polymerized (by organocatalytic ROP) to generate functionalized poly(α -aminoester)s (PAEs) of precise molecular weight and low polydispersity. Removal of the Boc protecting group affords novel cationic, water soluble poly(aminoesters) PAEs (Figure 4) that we have shown are efficient vectors for the transfection of cells with mRNA, DNA and other bioactive oligonucleotides.⁽⁶⁻⁸⁾

Publications Acknowledging this Grant in 2015-2018 (publications prior to 08/2017 were funded by prior related DOE Grant DE-SC0005430)

I. Exclusively funded by this grant

1. Ho, W. C., Chung, K.; Ingram, A. J., Waymouth, R. M. "Pd-Catalyzed Aerobic Oxidation Reactions: Strategies to Increase Catalyst Lifetimes", *J. Am. Chem. Soc.*, **2018**, *140*, 748-757. doi: 10.1021/jacs.7b11372.
2. Chung, K., Waymouth, R.M. "Selective Catalytic Oxidation of Unprotected Carbohydrates" *ACS Catalysis*, **2016**, *6*, 4653-4659. DOI: 10.1021/acscatal.6b01501.

II. Jointly funded by this grant and other grants with leading intellectual contribution from this grant;

3. Ingram, A. J.; Walker, K. L.; Zare, R. N.; Waymouth, R. M. "Catalytic Role of Multinuclear Palladium-Oxygen Intermediates in Aerobic Oxidation Followed by Hydrogen Peroxide Disproportionation" *J. Am. Chem. Soc.* **2015**, *137*, 13632-13646, doi: 10.1021/jacs.5b08719
4. Walker, K. L.; Dornan, L.M.; Zare, R. N.; Waymouth, R. M.; Muldoon, M. J. "Catalytic Oxidation of Styrenes with Hydrogen Peroxide in the Presence of Cationic Palladium Complexes" *J. Am. Chem. Soc.*, **2017**, *139*, 12495-12503, doi: 10.1021/jacs.7b05413.

III. Jointly funded by this grant and other grants with relatively minor intellectual contribution from this grant.

5. Zhang, X.; Fevre, M.; Jones, G. O.; Waymouth, R. M. "Catalysis as an Enabling Science for Sustainable Polymers" *Chem. Rev.* **2018**, *118*, 839-885. doi: 10.1021/acs.chemrev.7b00329.
6. McKinlay, C.J.; Benner, N.L.; Haabeth, O.A.; Waymouth, R. M.; Wender, P.A. "Enhanced mRNA delivery into lymphocytes enable by lipid-varied libraries of Charge-Altering Releasable Transporters" *Proc. Nat. Acad. Sci.*, **2018**, published online 06/11/18. doi: 10.1073/pnas.1805358115
7. Benner, N. L.; Near, K. E.; Bachmann, M. H.; Contag, C. H.; Waymouth, R. M.; Paul A. Wender, P. A. "Functional DNA Delivery Enabled by Lipid-Modified Charge-Altering Releasable Transporters (CART)s", *Biomacromolecules*, **2018**, published online 04 May 2018. doi: 10.1021/acs.biomac.8b00401
8. McKinlay, C. J.; Vargas, J. R.; Blake, T. R.; Hardy, J. W.; Kanada, M.; Contag, C. H.; Wender, P. A.; Waymouth, R. M. "Charge-altering Releasable Transporters (CARTs) for the delivery and release of messenger RNA in living animals" *Proc. Natl. Acad. Sci.*, **2017**, *114*, E448-E456, online publication 01/09/17, doi: 10.1073/pnas.1614193114
9. Davis, D.C.; Walker, K. L.; Hu, C.; Zare, R. N.; Waymouth, R. M.; Dai, M. "Catalytic Spirolactonization of Hydroxycyclopropanols: Total Synthesis of Levantenolides" *J. Am. Chem. Soc.*, **2016**, *138*, 10693-10699. doi:10.1020/jac.6b06573.

Size-Selected Metal Oxide Clusters as Model Inverse Catalysts

Michael G. White,^{1,2} Meng Xue,¹ Kenneth R. Goodman,¹ Yilin Ma,¹ Jason Wang¹ and Ping Liu²

¹Department of Chemistry, Stony Brook University, Stony Brook, NY 11794

²Chemistry Division, Brookhaven National Laboratory, Upton, NY 11973

Presentation Abstract

Size-selected cluster deposition is being used to prepare model inverse catalysts of metal oxides on Cu, Cu₂O and Au surfaces that have proved to be highly active for the alcohol dehydration, water-gas-shift and CO₂ hydrogenation. Size-selected cluster deposition is unique in its ability to control cluster stoichiometry which provides a means of introducing oxygen “vacancies” and varying the average cation oxidation state. Recent experiments demonstrated that Ti_nO_{2n} (n = 3, 4, 5) clusters deposited on Cu(111) are active for catalyzing the water-gas-shift under ambient pressure (AP) conditions using the AP-XPS end station at NSLS-II. Under these conditions, we observe reaction-induced O-vacancy formation via the appearance of Ti³⁺ (Ti 2p spectra) as well as the formation of formate intermediates (C 1s spectra). These results show that under elevated pressures, the very small stoichiometric oxide clusters can be reduced and thereby act as active site for water dissociation. STM imaging of Ti₃O_{5,6} clusters deposited on Au and Cu surfaces is also being used to investigate cluster binding sites, morphology and thermal stability towards sintering which is a major concern for small clusters at elevated pressures and temperature. At room temperature, the stoichiometric Ti₃O₆ cluster form small assemblies of 3-5 clusters on Au terraces while individual clusters decorate the step edges with nearly uniform spacing. The assemblies are composed of individual clusters in close contact, but not chemically fused to form larger TiO_x islands. By comparison, the “reduced” Ti₃O₅ cluster forms larger fractal-like assemblies consisting of 10-200 clusters that can extend across steps edges. For annealing temperatures up to 700K, the size of the Ti₃O₆ assemblies remain mostly unchanged, although the appearance of smaller structures above 550K suggest some cluster decomposition. The Ti₃O₅ fractal structures become smaller at higher temperatures, but the individual clusters appear to retain their size and shape. The binding structures and temperature behavior of the metal oxide clusters can be contrasted to similarly-sized metal clusters where agglomeration into larger nanostructures is typical at high coverages and temperature.

This work is funded through FWP-BNL-CO-040: Catalysis for Advanced Fuel Synthesis and Energy

Force/Activity Relationships in Transition Metal-Catalysis

Ross A. Widenhoefer, Stephen L. Craig, Robert G. Carden, Patricia N. Johnson, Liqi Wang,
Yichen Yu
Department of Chemistry, Duke University

Presentation Abstract

Strategies to increase the efficiency of catalytic reactions remain a fundamental need in basic energy sciences. A promising and emerging approach is to reversibly switch ligand geometry within a catalytic cycle, so that the catalyst is optimized for each of multiple elementary reaction steps. Our program is focused on using mechanical force to reversibly perturb the ligand geometry of transition metal complexes, ultimately to bias catalysis. A key effort is directed at identifying quantitative relationships between an applied force of tension and the energetics of elementary steps such as oxidative insertion and reductive elimination within catalytic coupling reactions. These studies are impacting our understanding of ligand geometry effects broadly and inspiring new designs for catalytic approaches that have the potential to reach broadly across the basic energy catalysis spectrum. New catalytic transition metal complexes have been synthesized that have the potential to deterministically direct multiple forms of primary energy input, including acoustic waves, physical deformation, and light, into catalytic cycles through mechanochemical coupling.

DE-SC0018188: Multi-State Catalysts Modulated by Mechanical Force

PIs: Ross A. Widenhoefer, Stephen L. Craig

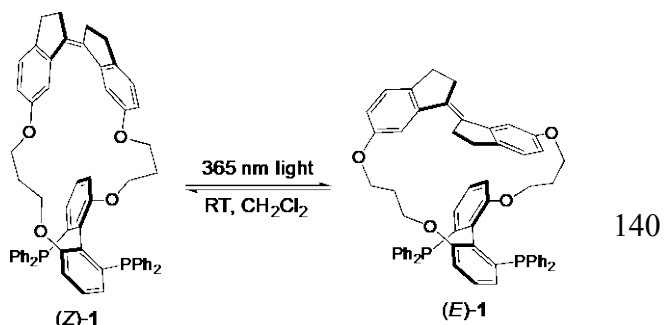
Students: Robert G. Carden, Patricia Johnson, Liqi Wang, Yichen Yu

RECENT PROGRESS

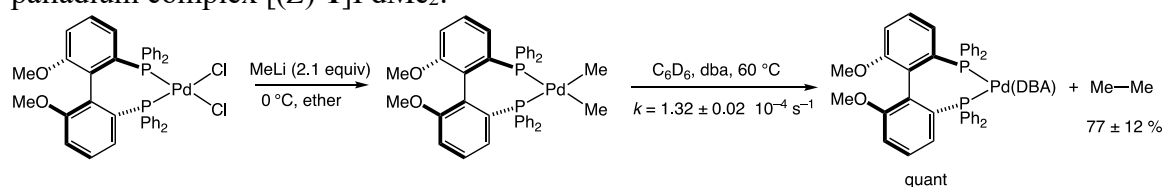
The long-term objective of this project is to funnel mechanical forces to the molecular level and use those forces to improve catalyst activity and/or selectivity. Key questions include: how does an applied force of tension to a ligand affect reactivity in the various elementary steps of a catalytic cycle? What types of ligands, metals, and reactions are most susceptible to mechanical perturbation? How precise must the quantity of delivered force be to achieve a specific outcome? And ultimately, what materials are the most promising supports for bulk multi-state mechanocatalysis? Our current activities are directed toward understanding the fundamental underpinnings required to develop mechanically-responsive catalysts, including the elucidation of force-reactivity relationships, force-modulated catalytic reaction mechanisms, and force-modulated potential energy landscapes, and toward understanding the geometric modulation of flexible catalysts embedded within a bulk elastomeric matrix.

Quantitative force-activity relationships for elementary steps within catalytic coupling reactions

Recent efforts are directed toward understanding and quantifying the effects of applied mechanical force on the energetics of reductive elimination and oxidative addition from palladium bis(phosphine) complexes. These transformations represent two of the most important steps required for synthetically important cross-coupling reactions. Both steps involve significant perturbation of the P–M–P bond angle in the ground state relative to the transition state and, for this reason, are likely to be strongly affected by external mechanical force. Our approach toward this objective employs molecular force-probe ligand **1** and related compounds comprising a stiff stilbene (1,1'-biindane) photoswitch tethered to a MeO-BIPHEP-derived bis(phosphine) ligand. The force delivered to the BIPHEP ligand can be switched photochemically without perturbing the electronic structure of the ligand. For example, DFT calculations at the B3LYP/6-311+G(d) level reveal that ligand (*Z*)-**1** produces 130 pN of compressive force along the O...O coordinate relative to MeO-BIPHEP, while photochemically-generated (*E*)-**1** produces pN of extension force relative to MeO-BIPHEP.



The first step toward our larger objectives is to identify model reactions through which to establish quantitative force-activity relationships. For reductive elimination, systematic screening efforts have led us to focus our efforts on the reductive elimination of ethane from dimethyl palladium complexes of the form (P–P)PdMe₂, where P–P = MeO-BIPHEP and force probe ligands. Here, commercially available MeO-BIPHEP serves as the force-free benchmark against which to quantify the effect of applied mechanical force. We required a synthesis that would provide analytically pure (P–P)PdMe₂ complexes at or below room temperature and on short time scales to avoid the potential decomposition of more reactive complexes and we have identified such conditions. For example, treatment of (MeO-BIPHEP)PdCl₂ with MeLi (2.1 equiv) at –78 °C followed by aqueous/ether extraction and evaporation provides pure (MeO-BIPHEP)PdMe₂ in near quantitative yield. Importantly, thermolysis of (MeO-BIPHEP)PdMe₂ in C₆D₆ containing dibenzylideneacetone as a trapping ligand at 60 °C leads to clean and reproducible first-order decay through ≥3 half lives ($k = 1.32 \pm 0.02 \times 10^{-4} \text{ s}^{-1}$) to form (MeO-BIPHEP)Pd(DBA) as the exclusive phosphine-containing species and ethane as the sole organic product in 77 ± 12% yield (¹H NMR). Concurrent with these efforts, we have synthesized force-probe ligand (*Z*)-**1** and the corresponding dimethyl palladium complex [(*Z*)-**1**]PdMe₂.

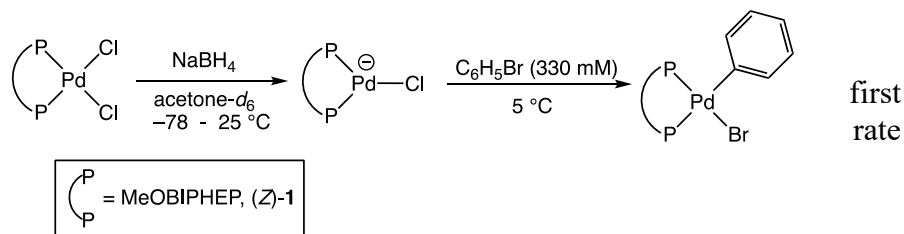


Similar considerations apply to oxidative addition, and we have identified a model system based on the oxidative addition of aryl halides to the anionic, three-coordinate palladium chloride complexes of the form [(P–P)PdCl][–], where P–P = MeO-BIPHEP and **1**. Toward this objective, reduction of (MeO-BIPHEP)PdCl₂ with sodium borohydride in acetone at –78 °C formed (MeO-BIPHEP)PdCl[–] as the exclusive product as evidenced by the single resonance in the ³¹P NMR

spectrum at $\delta = 20.0$. Reaction of (MeO-BIPHEP)PdCl⁻ (33 mM) with excess bromobenzene (330 mM) at 5 °C led to clean pseudo-first-order kinetics to ≥ 3 half lives ($k_{\text{obs}} = 1.21 \pm 0.04 \times 10^{-4} \text{ s}^{-1}$) to form (MeO-BIPHEP)Pd(Ph)Br as the exclusive product. In a similar manner, reduction of the force-probe ligand complex [(Z)-1]PdCl₂ with NaBH₄ generated [(Z)-1]PdCl⁻, which reacted with bromobenzene to form [(Z)-1]Pd(Ph)Br. Importantly, reaction of [(Z)-1]PdCl⁻ with bromobenzene was ~ 16 times faster than was reaction of bromobenzene with (MeO-BIPHEP)PdCl⁻.

This result represents the first demonstration of enhanced reactivity in a transition metal catalyzed reaction via a

mechanically perturbed ligand, and more importantly it provides a quantitation of a force-relationship of this type. Gratifyingly, the methodology should be applicable to a range of



forces and ultimately other substrates, catalysts, and reactions (including reductive elimination, above), but even these early results are raising interesting questions. For example, ³¹P NMR chemical shifts suggest that the electronic structure of the catalyst is trivially perturbed. That is, the change in reactivity is not due to changes in the ground state of the catalyst, but due to the effect of force on restricting catalyst conformation during the reaction. Further experiments will be needed to fully assess this hypothesis, but the nature of quantitative force-activity relationships have the potential to provide new insights into the factors that underlie ligand effects more broadly.

Electrochemical Nitrogen Reduction Reaction on Metal Nitrides

Bingjun Xu¹, Xuan Yang¹, Jared Nash¹, Jacob Anibal¹, Marco Dunwell¹, Shyam Kattel², Eli Staviski³, Klaus Attenkofer³, Yushan Yan¹, and Jingguang Chen²

¹Department of Chemical and Biomolecular Engineering, University of Delaware

²Department of Chemical Engineering, Columbia University

³Chemistry Division, Brookhaven National Laboratory

Presentation Abstract

Ammonia synthesis via the Haber-Bosch process is a pillar of modern agriculture, which converts the abundant but inert dinitrogen in the atmosphere to nitrogen-based fertilizers. Despite more than a century of optimization, the Haber-Bosch process remains energy intensive and carbon intensive. Distributed and modular ammonia synthesis via the electrochemical nitrogen reduction reaction (ENRR) at or close to ambient conditions, powered by renewable electricity is an attractive alternative because it allows as needed production of ammonia, and in turn N-fertilizers, as well as drastically reduces or eliminates the carbon footprint. However, selective ENRR catalyst is lacking.

We developed two transition metal nitride catalysts (VN and Cr₂N) with ammonia production rates and Faradaic efficiencies (FE) 50-200 times higher than precious metals. Catalysts are evaluated in a membrane electrode assembly (MEA) configuration to ensure the performance can be easily reproduced in devices. In particular, we demonstrate that VN nanoparticles are active, selective and stable ENRR catalysts in the membrane electrode assembly configuration with an ENRR rate and Faradaic efficiency (FE) of $3.3 \times 10^{-10} \text{ mol s}^{-1} \text{ cm}^{-2}$ and 6.0% at -0.1 V within 1 h, respectively. An ammonia production rate of $1.1 \times 10^{-10} \text{ mol s}^{-1} \text{ cm}^{-2}$ can be maintained for 116 h, with a steady state turnover number of 431. ENRR with ¹⁵N₂ as the feed indicates that the reaction follows a Mars-van Krevelen mechanism.

Grant: Low temperature, ambient pressure electrochemical ammonia synthesis in alkaline media — Mechanistic studies and catalyst design

Postdoc(s): Xuan Yang

Student(s): Jared Nash, Jacob Anibal

RECENT PROGRESS

ENRR Catalyzed by VN Catalysts

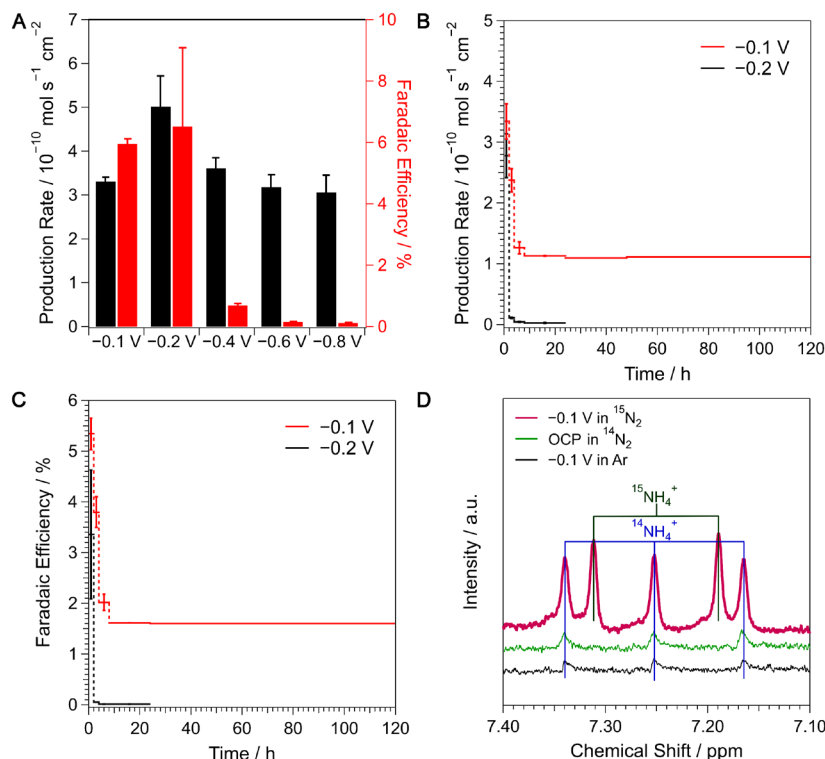


Figure 1. VN is active and selective ENRR catalyst. (A) Production rate and Faradaic efficiency of VN catalysts at different potentials for 1 h tests. Time-dependent production rate (B) and Faradaic efficiency (C) at -0.1 V and -0.2 V, respectively. (D) ^1H nuclear magnetic resonance (NMR) spectra for the post-electrolysis 0.05 M H_2SO_4 at -0.1 V in $^{15}\text{N}_2$ and Ar, and at OCP in $^{14}\text{N}_2$ For 48 h.

ENRR Catalyzed by Noble Metal Catalysts

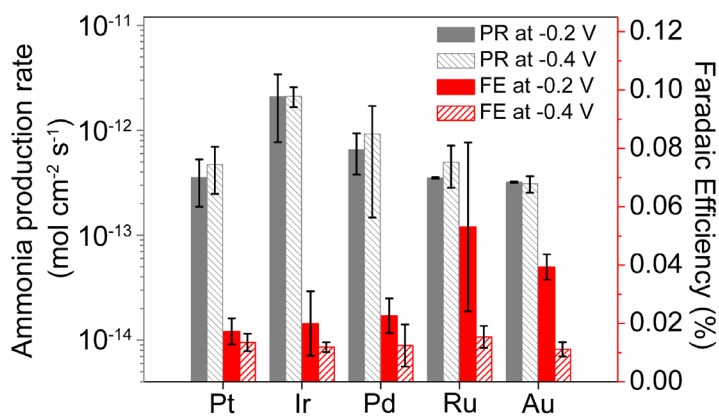


Figure 2. Noble metal catalysts are not selective for ENRR in acid conditions. The ammonia production rate and Faradaic efficiency (FE) on noble metal catalysts tested in PEMELs for 1 h at -0.2 V and -0.4 V. The production rate is normalized by the ECSA.

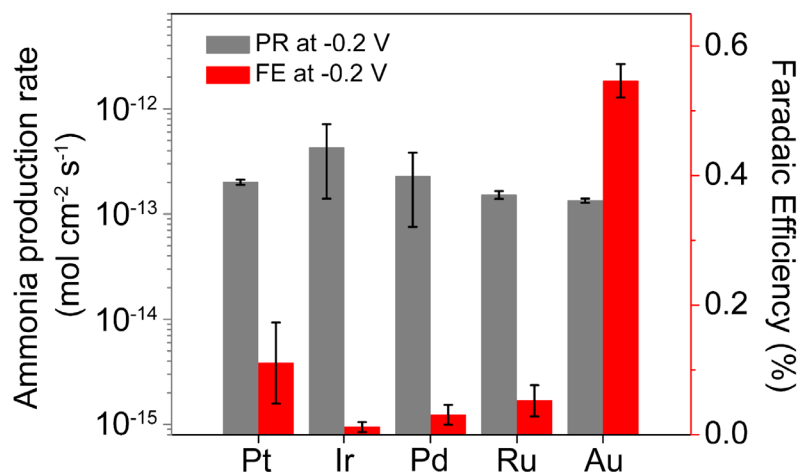


Figure 3. Noble metal catalysts are not selective for ENRR in alkaline conditions. The ammonia production rate and Faradaic efficiency (FE) of different noble metal catalysts in HEMELs at -0.2 V for 1 h. The production rate is normalized by the ECSA.

Publications Acknowledging this Grant in 2015-2018

1. Nash, J.; Yang, X.; Anibal, J.; Wang, J.; Yan, Y.; Xu, B., Electrochemical Nitrogen Reduction Reaction on Noble Metal Catalysts in Proton and Hydroxide Exchange Membrane Electrolyzers, *J. Electrochem. Soc.* **2017**, *164*, F1712-F1716.

Interaction of Hydrogen with CoCrFeNi High Entropy Alloys

Yuxin Fang,¹ Frank McKay,² Philip Sprunger,² John C. Flake,¹ William A. Shelton,¹ and Ye Xu¹
¹Cain Department of Chemical Engineering, ²Department of Physics and Astronomy, Louisiana State University, Baton Rouge, LA 70803

Presentation Abstract

High-entropy alloys (HEAs) are solid solutions of equal or nearly equal quantities of several metals, for which the entropy of mixing is maximized thus contributing notably to the stability of the alloy phase. They often exhibit unique material properties such as high tensile strength and fracture resistance, but their chemical reactivity is incompletely understood. Here we report the findings of our study on the interaction of hydrogen with CoCrFeNi-based HEAs. XPS and EELS spectroscopies, cyclic voltammetry, and mass spectrometry are among the experimental techniques used to characterize the interaction of the HEAs with hydrogen under surface science as well as electrochemical settings, while theoretical KKR-CPA calculations are performed to determine the stability and composition of the alloy surfaces and the adsorption strength of H as a function of bulk composition. The accuracy of our theoretical approach is validated against adsorption on the monometallic alloying components via literature or DFT-GGA calculations.

DE-SC0018408: Toward a universal electronic structure model for catalytic transformations on multi-metallic alloys

PI: Ye Xu

Co-PI: William A. Shelton

Affiliation: Louisiana State University

RECENT PROGRESS

We have begun simulations of the CoCrFeNi-based HEAs using the Korringa–Kohn–Rostoker (KKR) coherent potential approximation (CPA) method. For the parent 4-component bulk alloy in the fcc phase we have found the system to be non-magnetic with a minimum lattice constant of $a=3.447$ Å but near a ferromagnetic transition at approximately $a=3.52$ Å. H and O adsorption studies have been carried out on fcc(111) surfaces. The key advantage of our approach is the use of the CPA within multiple scattering theory. The CPA is a mean-field approximation for the configurational average. It restores the underlying periodicity, which means that surface unit cells of any size that can be constructed for an ordered fcc metal (e.g. Pt) can equally be used for the high-component HEAs.

Publications Acknowledging this Grant in 2015-2018

None to report so far.

Interfacial catalysts for transformations of oxygenates: construction, characterization, catalytic activity and reaction mechanisms

Aaron D. Sadow, Takeshi Kobayashi, Marek Pruski, Igor I. Slowing
Ames Laboratory, U.S. DOE, Iowa State University, Ames, IA 50011-3111

PRESENTATION ABSTRACT

The overarching goal of this collaborative project is to elucidate the key properties that control catalytic phenomena at liquid-solid interfaces and thereby guide the rational design of selective and efficient heterogeneous catalysts for redox conversions of oxygenated compounds. To this end our research team combines expertise in mesoporous and nanostructured catalyst synthesis, organometallic chemistry, kinetics and mechanisms of catalytic reactions, and solid-state (SS)NMR, including the ultrasensitive dynamic nuclear polarization (DNP) technique. Herein, we report the development of novel additive manufacturing methods to produce heterogeneous catalysts, the investigation of binding kinetics and equilibria of phenolics on nanostructured ceria in aqueous media, and the synthesis and electrocatalytic properties of doped ordered mesoporous carbons (OMCs). Precatalytic sites, containing activated Si-H bonds, were prepared to react with mesoporous silica, high surface area ceria, and carbon materials for catalytic hydrosilylations. In addition, a cobalt compound is selectively oxygenated with O₂. We also describe SSNMR studies of the mechanisms of formation and atomic-scale structure of OMC materials, the DNP-enabled characterization of binding of the organometallic ligands to catalyst surface, and the development of improved strategies for DNP-enhanced SSNMR of surfaces.

AL-03-380-011: Homogeneous and Interfacial Catalysis in 3D Controlled Environments

Student(s): Smita Patnaik, Walikadage Boteju, Abhranil Biswas, Zachary Weinstein, Zhuoran Wang, Nishant Praveen, Dilini Singappuli, Pranjali Naik, Juan Manzano.

RECENT PROGRESS

Publications Acknowledging this Grant in 2015-2018

Source of support for the work published:

(XV) *Exclusively funded by this grant*¹⁻¹⁷

(XVI) *Jointly funded by this grant and other grants leading intellectual contribution from this grant*¹⁸⁻⁴⁶

(XVII) *Jointly funded by this grant and other grants with relatively minor intellectual contribution from this grant*⁴⁷⁻⁵⁷

(1) Additive manufacturing of catalytically active materials. A general strategy was developed for 3D printing of structures containing organocatalytic or metal active sites.³³ The approach involved the spatially resolved photopolymerization of substituted alkenes, where the substituent carried the target catalytic activity and was inert to the polymerization conditions (Fig. 1a). Three types of catalytic functionalities were demonstrated: 1) carboxylic acid moieties produced using acrylic acid as a precursor gave 3D architectures catalytically active for a three-component Mannich reaction; 2) primary and secondary allyl amines copolymerized with acrylic acid produced bifunctional 3D structures that acted as cooperative catalysts for an aldol condensation; and 3) Cu^{2+} carboxylate-bearing objects were 3D printed as catalysts for a Huisgen cycloaddition. The value of additive manufacturing for producing catalytic architectures was shown by assembling: 1) a cuvette adaptor for solution UV-Visible spectroscopy that allowed tracking *in situ* the overall kinetics of an acid catalyzed Mannich reaction, and each of its major steps (Fig. 1b); and 2) a millifluidic catalytic reactor with Cu^{2+} active sites homogeneously dispersed on its channel walls (Fig. 1c). This work showed the potential of combining the versatility offered by novel additive manufacturing technologies with the arsenal of chemistries available to the catalysis community.

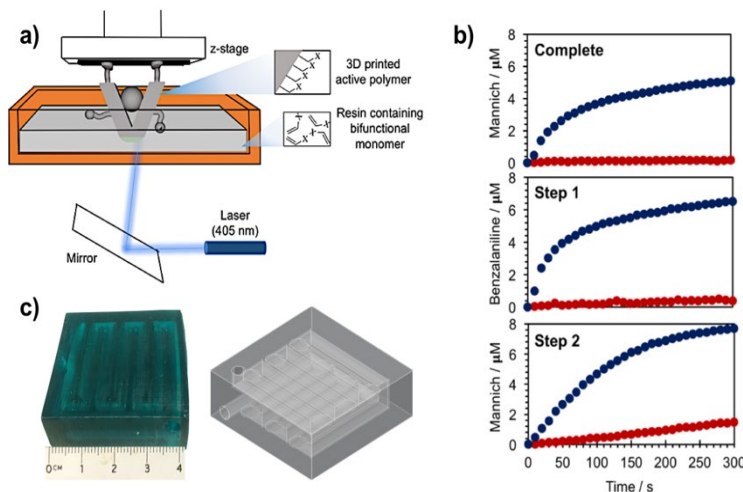


Figure 1. a) Additive manufacturing via laser-guided photopolymerization of functionalized alkene monomers. b) Kinetics of Mannich reaction between aniline, benzaldehyde and cyclohexanone monitored by UV-Visible spectroscopy, with (blue) and without (red) the catalyst. Measurements were enabled by a 3D printed cuvette adaptor containing the catalytic species. c) Cu^{2+} -containing millifluidic reactor (left) and its CAD design (right) used for the catalytic Huisgen cycloaddition *in flow*.

Visible spectroscopy that allowed tracking *in situ* the overall kinetics of an acid catalyzed Mannich reaction, and each of its major steps (Fig. 1b); and 2) a millifluidic catalytic reactor with Cu^{2+} active sites homogeneously dispersed on its channel walls (Fig. 1c). This work showed the potential of combining the versatility offered by novel additive manufacturing technologies with the arsenal of chemistries available to the catalysis community.

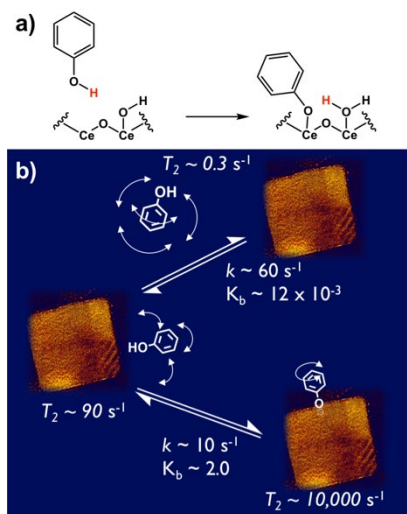


Figure 2. a) Dissociative chemisorption of phenol on oxygen vacancy sites of CeO_2 nanocubes and b) kinetic and equilibrium parameters of the process obtained by T_2 relaxation measurements of ^1H NMR.

(2) Studying the dynamics of phenol binding at water- CeO_2 interfaces. The phenol hydrogenation activity of Pd is much higher when supported on CeO_2 than on carbon, silica, or alumina. This has been attributed to a non-innocent behavior of CeO_2 during substrate binding. Previous studies suggested that phenol binding to oxygen vacancy sites of CeO_2 results in deprotonation to form a phenoxide (Fig. 2a), which is more readily reduced by Pd-activated H.^{34, 58} However, phenol binding is limited by competition with the solvent, especially water. We explored the dynamics of phenol binding to CeO_2 nanocubes in water by following changes in ^1H NMR spin-spin (T_2) relaxation times in aqueous suspension.³¹ To prevent nanoparticle sedimentation during long acquisition times we employed a novel approach using an agarose gel to entrap the nanoparticles (40 – 100 nm) within micron-sized pores.

Control experiments in the absence of CeO₂ demonstrated negligible interactions between the gel and phenol. The measurements revealed a two-step process (Fig. 2b) characterized by a weakly bound state ($R_2 \sim 90 \text{ s}^{-1}$), with 12 mM affinity constant corresponding to relatively mobile phenol molecules at the interface, that favorably transitions ($K \sim 2$) to a strongly bound state ($R_2 10^4 \text{ s}^{-1}$), likely corresponding to the chemisorbed phenoxide. Further experiments are being conducted to characterize the binding in the presence of catalytic Pd and additional competing species, and to examine possible correlations between binding and reaction kinetics.

(3) S-doped ordered mesoporous carbons (OMC) as electrocatalyst for the selective reduction of nitroaromatics.

An S-doped OMC was prepared using thiophenol precursor and SBA-15 type mesoporous silica nanoparticles (MSN) as a hard template (Fig. 3a).²² The high surface area and S-doping (~ 600 and $400 \text{ m}^2/\text{g}$, and 1.5 %S and 0.5%S at 600 and 900 °C pyrolysis temperatures respectively) of the semigraphitic materials allowed their use as metal-free electrocatalysts for the selective reduction of nitro groups in the presence of other reducible moieties (amide, sulfoxide, thiophosphate). The cathodic transition of the nitro group in chloramphenicol to hydroxylamine was obtained with a 7-fold enhancement in peak current and $\sim 170 \text{ mV}$ potential shift (-440 to -267 mV) compared to glassy carbon electrode in a 0.1 M H₂SO₄ solution (Fig. 3b). Transition of the hydroxylamine to aniline using the S-OMC coated electrode was observed at -700 mV . To determine the role of S on the electrocatalytic performance of the material, an N-doped OMC was prepared using aniline as a starting material and the same MSN template. Initial studies comparing the voltammograms of the $[\text{Fe}(\text{CN})_6]^{3-/4-}$ couple showed approximately 50% higher peak currents for the S-doped material suggesting the heteroatom may play a role in the electrochemical process. Additional characterization and reactivity studies will provide more insights into the effect of the dopant on the electrocatalytic behavior of this type of OMC.

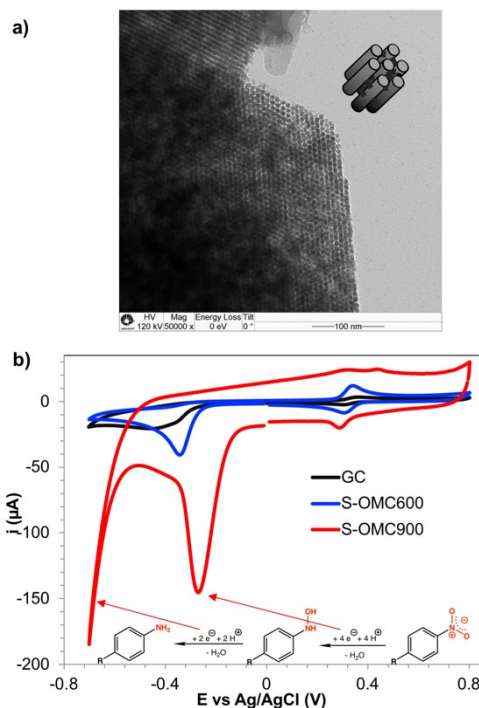


Figure 3. a) TEM image of an S-doped ordered mesoporous carbon (S-OMC), and b) cyclic voltammogram of the electrochemical conversion of chloramphenicol using bare (black) and S-OMC coated glassy carbon electrodes. The numbers by S-OMC correspond to pyrolysis temperatures.

(4) Rare earth homoleptic silazidos for carbonyl hydrosilylation.

We have previously studied MSN supported dimethylamido zirconium(IV), prepared by protonolytic grafting of Zr(NMe₂)₄ at surface silanol sites, in catalytic hydroboration of ketones.¹⁴ Next, we targeted new rare earth silazido compounds of the type Ln{N(SiHMe₂)R}₃⁴ to access sites with increased activity and through new mechanisms for hydroelementation of oxygenates. These compounds contain bridging Ln⁻H-Si, the ¹J_{SiH} of which provide means to characterize the coordination number of surface grafted species. A new silazido ligand N(SiHMe₂)Dipp (Dipp = 2,6-diisopropylphenyl) also reacts with LnX₃ salts to provide homoleptic tris(silazido) rare earth pseudo-organometallic compounds Ln{N(SiHMe₂)Dipp}₃ (Ln = Sc, Y, Lu; Fig. 4) as salt-free and donor-solvent-free coordinatively unsaturated and low electron-count compounds for surface grafting.²³ The steric

bulk of the diisopropylphenyl group favors an unusual planar LnN₃ core, whereas the dissimilar steric properties of dimethylsilyl and diisopropylphenyl substituents lead to highly asymmetric Ln–N(SiHMe₂)Dipp interactions. These include inequivalent Ln–N and Ln–H distances in X-ray structures, SiH stretching modes in the IR, and chemical shifts and ¹J_{SiH} values in low temperature NMR spectra. One of the three bridging Ln–H–Si is notably more activated (¹J_{SiH} = 116 Hz) than the other two (¹J_{SiH} = 141 and 132 Hz). Moreover, one of the three silazido ligands reacts with acetophenone to give a hydrosilylation product, indicating that the combination of bridging SiH and a highly electrophilic metal center can facilitate Si–O bond formation. This step may provide a new mechanism for

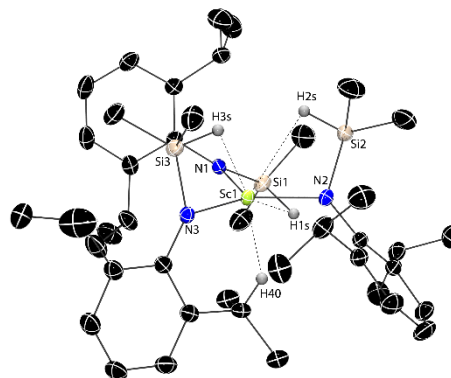
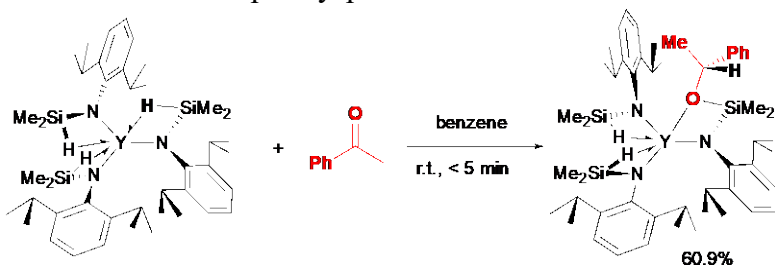
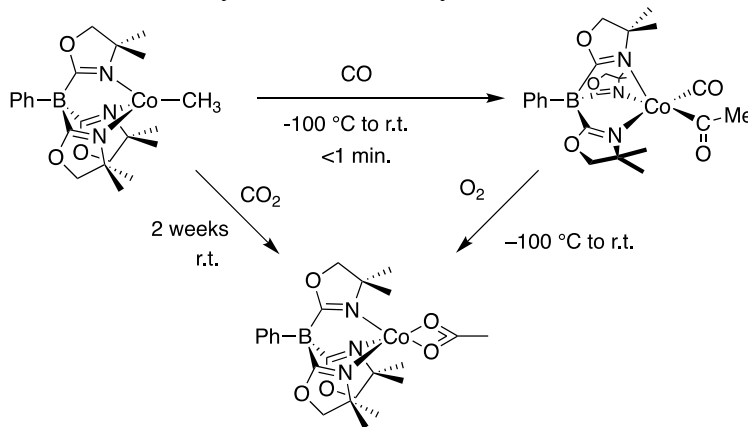


Figure 4. Single crystal X-ray structure of Sc{N(SiHMe₂)Dipp}₃, containing three inequivalent Sc–H–Si and an agostic CH.



catalytic hydrosilylation of carbonyls, to complement late metal catalysts. Our current efforts are exploring supported analogues for interfacial single-site catalysis.

(5) Oxygenation of a cobalt(II) methyl. The oxygenation of a cobalt(II) acetyl, formed from cobalt methyl and CO, by O₂ occurs rapidly in a tris(4,4-dimethyl-2-oxazolonyl)borate-supported compound to give cobalt(II) acetate.³² Acetate is a biological energy carrier and part of the Krebs cycle, which also involves acetyl compounds formed from methyl and CO. In the natural system, methyl and CO are both derived from carbon dioxide. Acetate might also be formed from the direct addition of a methyl group and naturally abundant carbon dioxide, yet nature chooses an energetically less efficient route. Our studies of the synthetic cobalt system indicate that both routes (oxygenation or direct insertion of CO₂) yield acetate, but the pathway involving carbon monoxide is kinetically preferred over carbon dioxide by more than 10⁶ times. Living organisms cannot wait for the slow reaction, and instead enzymes have developed a fast, low temperature, mild alternative. This idea also applies in synthetic catalytic chemistry, in which carboxylate moieties are installed by the combination of carbon monoxide with an organometallic compound followed by oxidation, rather than direct treatment with carbon dioxide. That is, approaches for utilization of carbon dioxide as a C₁ reagent in catalytic synthesis might be advantaged by a three-step process involving reduction to carbon monoxide, reaction with organometallics, followed by oxidation.



(6) Characterization of Catalytic Materials by Solid-State (SS) NMR. SSNMR spectroscopy is extensively developed and used to provide atomic-scale structural information about the catalytic heterogeneous catalysts developed in this project. Our studies take advantage of two state-of-the-art SSNMR technologies: (ultrafast)fast magic angle spinning (MAS) and dynamic nuclear polarization (DNP). The DNP technique, which offers 100-to-1000-fold enhancement in sensitivity, is particularly well-suited for the studies of catalytic systems, because it can efficiently and selectively sensitize surfaces and interfaces, enabling measurements that are off-limits to conventional SSNMR.

We used SSNMR in concert with elemental analysis and textural characterization to detail the structures of OMC materials prepared using Pluronic F127 as template with resorcinol and formaldehyde as polymerizing precursors.² Analysis of ^{13}C MAS spectra provided quantitative distribution of carbon functionalities at various stages of pyrolysis and offered new insights into the pyrolysis mechanisms. The important findings are: (1) the formaldehyde carbons were fully converted to $-\text{CH}_2-$ links between adjacent six-membered rings at temperature below $80\text{ }^\circ\text{C}$, (2) the structural changes upon pyrolysis include the formation of methyl groups (below $300\text{ }^\circ\text{C}$), gradual incorporation of aliphatic carbons into aromatic structures (advanced at temperatures above $300\text{ }^\circ\text{C}$), and the formation of polycyclic aromatic substructures via a series of deoxygenation and radical reactions, and (3) the average sizes of aromatic clusters in samples pyrolyzed at 300 , 400 , and $500\text{ }^\circ\text{C}$ are close to 2, 3 and 4 respectively, whereas one treated at $900\text{ }^\circ\text{C}$ comprises a highly carbonized aromatic network composed of much larger clusters.

The DNP-enhanced ^{17}O SSNMR experiments for characterization of single-site organometallic catalysts were carried out.¹⁹ Until now, the ^{17}O studies used the so-called indirect DNP approach, which relies on the hyperpolarization of ^1H nuclei by DNP and the subsequent transfer of this magnetization to the nearby oxygens. The shortcoming of this approach is that it relies on close proximity (typically less than 0.2 nm) between ^1H and ^{17}O nuclei, thereby precluding the detection of non-protonated oxygens. The novelty of our work is that it uses direct polarization of ^{17}O nuclei by DNP, without the ‘help’ of protons, to observe all oxygen atoms. This enabled, for the first time, the detection of non-protonated catalytically relevant oxygen sites, especially those responsible for binding the organometallic ligands to catalyst surface (Fig. 5).

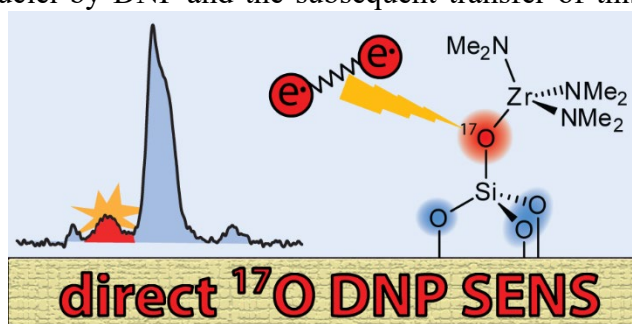


Figure 5. Direct ^{17}O DNP enabled observation of oxygen sites that link the catalyst to the surface.

We improved strategies for DNP-enhanced SSNMR of surfaces, by using ^1H -free solvents to eliminate the solvent-derived correlation signals from the 2D HETCOR spectra of materials.³⁰ This methodology implies that there is no H/D isotope exchange with deuterated solvents and relies upon the sample’s strongly coupled innate protons to mediate the spin diffusion and hyperpolarize the targeted spins on the surface or in the bulk. In samples where such networks of protons exist, the use of proton-free solvents yielded significantly improved 2D HETCOR spectra with no loss in sensitivity. Also, we systematically studied the efficacy of DNP in the studies of alumina, silica,

and OMC) materials with vastly different surface areas, as a function of the biradical concentration.¹⁸ Importantly, our studies show that the use of a “one-size-fits-all” biradical concentration should be avoided when performing DNP experiments and instead an optimal concentration should be selected as appropriate for the type of material studied as well as its surface area. In general, materials with greater surface areas require higher radical concentrations for best possible DNP performance. This result is explained with the use of a thermodynamic model wherein radical-surface interactions are expected to lead to an increase in the local concentration of the polarizing agent at the surface. We also show, using plane-wave density functional theory calculations, that weak radical-surface interactions are the cause of the poor performance of DNP SENS for carbonaceous materials. Finally, we carried out a series of SSNMR studies to elucidate, for the first time, the spatial distributions of functional groups on the surfaces of mesoporous silica materials (see abstract entitled “Spatial distribution of organic functionalities on silica: exploration by conventional and DNP-enhanced homonuclear SSNMR”).

References.

I. Exclusively funded by this grant:

1. Manzano, S.; Singappuli-Arachchige, D.; Parikh, B. L.; Slowing, I. I., Fine-tuning the release of molecular guests from mesoporous silicas by controlling the orientation and mobility of surface phenyl substituents. *Chemical Engineering Journal* **2018**, *340*, 73-80.
2. Wang, Z.; Opembe, N.; Kobayashi, T.; Nelson, N. C.; Slowing, II; Pruski, M., Quantitative atomic-scale structure characterization of ordered mesoporous carbon materials by solid state NMR. *Carbon* **2018**, *131*, 102-110.
3. Nelson, N. C.; Wang, Z. R.; Naik, P.; Manzano, J. S.; Pruski, M.; Slowing, II, Phosphate modified ceria as a Bronsted acidic/redox multifunctional catalyst. *J. Mater. Chem. A* **2017**, *5* (9), 4455-4466.
4. Eedugurala, N.; Wang, Z. R.; Yan, K. K.; Boteju, K. C.; Chaudhary, U.; Kobayashi, T.; Ellern, A.; Slowing, II; Pruski, M.; Sadow, A. D., beta-SiH-Containing Tris(silazido) Rare-Earth Complexes as Homogeneous and Grafted Single-Site Catalyst Precursors for Hydroamination. *Organometallics* **2017**, *36* (6), 1142-1153.
5. Boteju, K. C.; Ellern, A.; Sadow, A. D., Homoleptic organolanthanide compounds supported by the bis(dimethylsilyl)benzyl ligand. *Chem. Commun.* **2017**, *53* (4), 716-719.
6. Kobayashi, T.; Singappuli-Arachchige, D.; Wang, Z. R.; Slowing, II; Pruski, M., Spatial distribution of organic functional groups supported on mesoporous silica nanoparticles: a study by conventional and DNP-enhanced Si-29 solid-state NMR. *Phys. Chem. Chem. Phys.* **2017**, *19* (3), 1781-1789.
7. Perras, F. A.; Wang, Z. R.; Naik, P.; Slowing, II; Pruski, M., Natural Abundance O-17 DNP NMR Provides Precise O-H Distances and Insights into the Bronsted Acidity of Heterogeneous Catalysts. *Angew. Chem. Int. Ed.* **2017**, *56* (31), 9165-9169.
8. Kobayashi, T.; Slowing, II; Pruski, M., Measuring Long-Range C-13-C-13 Correlations on a Surface under Natural Abundance Using Dynamic Nuclear Polarization-Enhanced Solid-State Nuclear Magnetic Resonance. *J. Phys. Chem. C* **2017**, *121* (44), 24687-24691.
9. Nelson, N. C.; Manzano, J. S.; Slowing, II, Deactivation of Ceria Supported Palladium through C-C Scission during Transfer Hydrogenation of Phenol with Alcohols. *J. Phys. Chem. C* **2016**, *120* (49), 28067-28073.

10. Singappuli-Arachchige, D.; Manzano, J. S.; Sherman, L. M.; Slowing, II, Polarity Control at Interfaces: Quantifying Pseudo-solvent Effects in Nano-confined Systems. *ChemPhysChem* **2016**, *17* (19), 2982-2986.
11. Manna, K.; Eedugurala, N.; Sadow, A. D., Zirconium-Catalyzed Desymmetrization of Aminodialkenes and Aminodialkynes through Enantioselective Hydroamination. *J. Am. Chem. Soc.* **2015**, *137* (1), 425-435.
12. Eedugurala, N.; Hovey, M.; Ho, H. A.; Jana, B.; Lampland, N. L.; Ellern, A.; Sadow, A. D., Cyclopentadienyl-bis(oxazoline) Magnesium and Zirconium Complexes in Aminoalkene Hydroaminations. *Organometallics* **2015**, *34* (23), 5566-5575.
13. Bataineh, H.; Pestovsky, O.; Bakac, A., Iron(II) Catalysis in Oxidation of Hydrocarbons with Ozone in Acetonitrile. *ACS Catal.* **2015**, *5* (3), 1629-1637.
14. Eedugurala, N.; Wang, Z. R.; Chaudhary, U.; Nelson, N.; Kandel, K.; Kobayashi, T.; Slowing, II; Pruski, M.; Sadow, A. D., Mesoporous Silica-Supported Amidozirconium-Catalyzed Carbonyl Hydroboration. *ACS Catal.* **2015**, *5* (12), 7399-7414.
15. Kandel, K.; Chaudhary, U.; Nelson, N. C.; Slowing, II, Synergistic Interaction between Oxides of Copper and Iron for Production of Fatty Alcohols from Fatty Acids. *ACS Catal.* **2015**, *5* (11), 6719-6723.
16. Xu, S. C.; Magoon, Y.; Reinig, R. R.; Schmidt, B. M.; Ellern, A.; Sadow, A. D., Organometallic Complexes of Bulky, Optically Active, C-3-Symmetric Tris(4*S*-isopropyl-5,5-dimethyl-2-oxazolanyl)phenylborate (To(P)*). *Organometallics* **2015**, *34* (14), 3508-3519.
17. Nishiyama, Y.; Kobayashi, T.; Malon, M.; Singappuli-Arachchige, D.; Slowing, II; Pruski, M., Studies of minute quantities of natural abundance molecules using 2D heteronuclear correlation spectroscopy under 100 kHz MAS. *Solid State Nucl. Magn. Reson.* **2015**, *66-67*, 56-61.

II. Jointly funded by this grant and other grants leading intellectual contribution from this grant

18. Perras, F. A.; Wang, J. S.; Manzano, J. S.; Chaudhary, U.; Opembe, N.; Johnson, D. D.; Slowing, I. I.; Pruski, M., Optimal Sample Formulations for DNP SENS: The Importance of Radical-Surface Interactions. *Curr. Opin. Colloid Interface Sci.* **2018**, *33*, 9-18.
19. Perras, F. A.; Boteju, K. C.; Slowing, II; Sadow, A. D.; Pruski, M., Direct O-17 dynamic nuclear polarization of single-site heterogeneous catalysts. *Chem. Commun.* **2018**, *54* (28), 3472-3475.
20. Kobayashi, T.; Nishiyama, Y.; Pruski, M., Heteronuclear Correlation SSNMR Spectroscopy with Indirect Detection under Fast Magic Angle Spinning. In *New Developments in Solid-State NMR, No. 15, 'Modern Methods in Solid-State NMR: A practitioner's guide'*, Hodgkinson, P., Ed. Royal Society of Chemistry: London, 2018.
21. Perras, F. A.; Kobayashi, T.; Pruski, M., Growing Signals from the Noise: Challenging Nuclei in Materials DNP. In *Encyclopedia of Magnetic Resonance*, 2018; p in press.
22. Maluta, J. R.; Machado, S. A. S.; Chaudhary, U.; Manzano, J. S.; Kubota, L. T.; Slowing, I. I., Development of a semigraphitic sulfur-doped ordered mesoporous carbon material for electroanalytical applications. *Sens. Actuators, B* **2018**, *257*, 347-353.
23. Boteju, K. C.; Wan, S.; Venkatesh, A.; Ellern, A.; Rossini, A. J.; Sadow, A. D., Rare earth arylsilazido compounds with inequivalent secondary interactions. *Chem. Commun.* **2018**, *54*, 7318 - 7321.

24. Perras, F. A.; Padmos, J. D.; Johnson, R. L.; Wang, L. L.; Schwartz, T. J.; Kobayashi, T.; Horton, J. H.; Dumesic, J. A.; Shanks, B. H.; Johnson, D. D.; Pruski, M., Characterizing Substrate-Surface Interactions on Alumina-Supported Metal Catalysts by Dynamic Nuclear Polarization Enhanced Double-Resonance NMR Spectroscopy. *J. Am. Chem. Soc.* **2017**, *139* (7), 2702-2709.
25. Mouat, A. R.; Kobayashi, T.; Pruski, M.; Marks, T. J.; Stair, P. C., Direct Spectroscopic Evidence for Isolated Silanols in SiO_x/Al₂O₃ and Their Formation Mechanism. *J. Phys. Chem. C* **2017**, *121* (11), 6060-6064.
26. Perras, F. A.; Luo, H.; Zhang, X. M.; Mosier, N. S.; Pruski, M.; Abu-Omar, M. M., Atomic-Level Structure Characterization of Biomass Pre- and Post-Lignin Treatment by Dynamic Nuclear Polarization-Enhanced Solid-State NMR. *J. Phys. Chem. A* **2017**, *121* (3), 623-630.
27. Perras, F. A.; Venkatesh, A.; Hanrahan, M. P.; Goh, T. W.; Huang, W. Y.; Rossini, A. J.; Pruski, M., Indirect detection of infinite-speed MAS solid-state NMR spectra. *J. Magn. Reson.* **2017**, *276*, 95-102.
28. Nelson, N. C.; Boote, B. W.; Naik, P.; Rossini, A. J.; Smith, E. A.; Slowing, II, Transfer hydrogenation over sodium-modified ceria: Enrichment of redox sites active for alcohol dehydrogenation. *J. Catal.* **2017**, *346*, 180-187.
29. Kobayashi, T.; Perras, F. A.; Murphy, A.; Yao, Y.; Catalano, J.; Centeno, S. A.; Dybowski, C.; Zumbulyadis, N.; Pruski, M., DNP-enhanced ultrawideline Pb-207 solid-state NMR spectroscopy: an application to cultural heritage science. *Dalton Trans.* **2017**, *46* (11), 3535-3540.
30. Kobayashi, T.; Perras, F. A.; Chaudhary, U.; Slowing, II; Huang, W. Y.; Sadow, A. D.; Pruski, M., Improved strategies for DNP-enhanced 2D H-1-X heteronuclear correlation spectroscopy of surfaces. *Solid State Nucl. Magn. Reson.* **2017**, *87*, 38-44.
31. Egner, T. K.; Naik, P.; Nelson, N. C.; Slowing, II; Venditti, V., Mechanistic Insight into Nanoparticle Surface Adsorption by Solution NMR Spectroscopy in an Aqueous Gel. *Angew. Chem. Int. Ed.* **2017**, *56* (33), 9802-9806.
32. Reinig, R. R.; Fought, E. L.; Ellern, A.; Windus, T. L.; Sadow, A. D., Rapid and ordered carbonylation and oxygenation of a cobalt(ii) methyl. *Chem. Commun.* **2017**, *53* (80), 11020-11023.
33. Manzano, J. S.; Weinstein, Z. B.; Sadow, A. D.; Slowing, I. I., Direct 3D Printing of Catalytically Active Structures. *ACS Catal.* **2017**, *7* (11), 7567-7577.
34. Nelson, N. C.; Boote, B. W.; Naik, P.; Rossini, A. J.; Smith, E. A.; Slowing, I. I., Transfer hydrogenation over sodium-modified ceria: Enrichment of redox sites active for alcohol dehydrogenation. *J. Catal.* **2017**, *346*, 180-187.
35. Johnson, R. L.; Perras, F. A.; Kobayashi, T.; Schwartz, T. J.; Dumesic, J. A.; Shanks, B. H.; Pruski, M., Identifying low-coverage surface species on supported noble metal nanoparticle catalysts by DNP-NMR. *Chem. Commun.* **2016**, *52* (9), 1859-1862.
36. Perras, F. A.; Chaudhary, U.; Slowing, II; Pruski, M., Probing Surface Hydrogen Bonding and Dynamics by Natural Abundance, Multidimensional, O-17 DNP-NMR Spectroscopy. *J. Phys. Chem. C* **2016**, *120* (21), 11535-11544.
37. Perras, F. A.; Kobayashi, T.; Pruski, M., Magnetic resonance imaging of DNP enhancements in a rotor spinning at the magic angle. *J. Magn. Reson.* **2016**, *264*, 125-130.
38. Kobayashi, T.; Perras, F. A.; Goh, T. W.; Metz, T. L.; Huang, W. Y.; Pruski, M., DNP-Enhanced Ultrawideline Solid-State NMR Spectroscopy: Studies of Platinum in Metal-Organic Frameworks. *J. Phys. Chem. Lett.* **2016**, *7* (13), 2322-2327.

39. Reinig, R. R.; Mukherjee, D.; Weinstein, Z. B.; Xie, W. W.; Albright, T.; Baird, B.; Gray, T. S.; Ellern, A.; Miller, G. J.; Winter, A. H.; Bud'ko, S. L.; Sadow, A. D., Synthesis and Oxidation Catalysis of Tris(oxazolanyl)borato cobalt(II) Scorpionates. *Eur. J. Inorg. Chem.* **2016**, (15-16), 2486-2494.
40. Perras, F. A.; Reinig, R. R.; Slowing, II; Sadow, A. D.; Pruski, M., Effects of biradical deuteration on the performance of DNP: towards better performing polarizing agents. *Phys. Chem. Chem. Phys.* **2016**, *18* (1), 65-69.
41. Webb, J. D.; Seki, T.; Goldston, J. F.; Pruski, M.; Crudden, C. M., Selective functionalization of the mesopores of SBA-15. *Microporous Mesoporous Mater.* **2015**, *203*, 123-131.
42. Perras, F. A.; Kobayashi, T.; Pruski, M., Natural Abundance O-17 DNP Two-Dimensional and Surface-Enhanced NMR Spectroscopy. *J. Am. Chem. Soc.* **2015**, *137* (26), 8336-8339.
43. Perras, F. A.; Kobayashi, T.; Pruski, M., PRESTO polarization transfer to quadrupolar nuclei: implications for dynamic nuclear polarization. *Phys. Chem. Chem. Phys.* **2015**, *17* (35), 22616-22622.
44. Kobayashi, T.; Perras, F. A.; Slowing, II; Sadow, A. D.; Pruski, M., Dynamic Nuclear Polarization Solid-State NMR in Heterogeneous Catalysis Research. *ACS Catal.* **2015**, *5* (12), 7055-7062.
45. Hull, E. A.; West, A. C.; Pestovsky, O.; Kristian, K. E.; Ellern, A.; Dunne, J. F.; Carraher, J. M.; Bakac, A.; Windus, T. L., UV-visible spectroscopy of macrocyclic alkyl, nitrosyl and halide complexes of cobalt and rhodium. Experiment and calculation. *Dalton Trans.* **2015**, *44* (8), 3811-3816.
46. Xu, S. C.; Boschen, J. S.; Biswas, A.; Kobayashi, T.; Pruski, M.; Windus, T. L.; Sadow, A. D., Mild partial deoxygenation of esters catalyzed by an oxazolanylborate-coordinated rhodium silylene. *Dalton Trans.* **2015**, *44* (36), 15897-15904.

III. Jointly funded by this grant and other grants with relatively minor intellectual contribution from this grant

47. Mouat, A. R.; Whitford, C. L.; Chen, B. R.; Liu, S. S.; Perras, F. A.; Pruski, M.; Bedzyk, M. J.; Delferro, M.; Stair, P. C.; Marks, T. J., Synthesis of Supported Pd-0 Nanoparticles from a Single-Site Pd²⁺ Surface Complex by Alkene Reduction. *Chem. Mater.* **2018**, *30* (3), 1032-1044.
48. Khazdozian, H. A.; Manzano, J. S.; Gandha, K.; Slowing, I. I.; Nlebedim, I. C., Recycled Sm-Co bonded magnet filaments for 3D printing of magnets. *AIP Advances* **2018**, *8* (5), 056722.
49. Camacho-Bunquin, J.; Ferrandon, M.; Sohn, H.; Yang, D. L.; Liu, C.; Ignacio-de Leon, P. A.; Perras, F. A.; Pruski, M.; Stair, P. C.; Delferro, M., Chemoselective Hydrogenation with Supported Organoplatinum(IV) Catalyst on Zn(II)-Modified Silica. *J. Am. Chem. Soc.* **2018**, *140* (11), 3940-3951.
50. Kaphan, C.; Klet, R. C.; Perras, F. A.; Pruski, M.; Yang, C.; Kropf, A. J.; Delferro, M., Surface Organometallic Chemistry of Supported Iridium(III) as a Probe for Metal-Support Interactions in C-H Activation. *ACS Catal.* **2018**, *8*, 5363-5373.
51. Klet, R. C.; Kaphan, C.; Liu, C.; Perras, F. A.; Pruski, M.; Hock, A. S.; Delferro, M., Evidence for Redox Mechanisms in Organometallic Chemisorption and Reactivity on Sulfated Metal Oxides. *J. Am. Chem. Soc.* **2018**, *140*, 6308-6316.
52. Garcia, A.; Evans, J. W.; Slowing, I., Pore diameter dependence of catalytic activity: p-nitrobenzaldehyde conversion to an aldol product in amine-functionalized mesoporous silica. *J. Chem. Phys.* **2018**, *Accepted*.

53. Alammar, T.; Slowing, II; Andereg, J.; Mudring, A. V., Ionic-Liquid-Assisted Microwave Synthesis of Solid Solutions of $\text{Sr}_{1-x}\text{Ba}_x\text{SnO}_3$ Perovskite for Photocatalytic Applications. *ChemSusChem* **2017**, *10* (17), 3387-3401.
54. Dairo, T. O.; Nelson, N. C.; Slowing, II; Angelici, R. J.; Woo, L. K., Aerobic Oxidation of Cyclic Amines to Lactams Catalyzed by Ceria-Supported Nanogold. *Catal. Lett.* **2016**, *146* (11), 2278-2291.
55. Batista, A. P. D.; Zahariev, F.; Slowing, II; Braga, A. A. C.; Ornellas, F. R.; Gordon, M. S., Silanol-Assisted Carbinolamine Formation in an Amine-Functionalized Mesoporous Silica Surface: Theoretical Investigation by Fragmentation Methods. *J. Phys. Chem. B* **2016**, *120* (8), 1660-1669.
56. Gu, W. X.; Stalzer, M. M.; Nicholas, C. P.; Bhattacharyya, A.; Motta, A.; Gallagher, J. R.; Zhang, G. H.; Miller, J. T.; Kobayashi, T.; Pruski, M.; Delferro, M.; Marks, T. J., Benzene Selectivity in Competitive Arene Hydrogenation: Effects of Single-Site Catalyst center dot center dot center dot Acidic Oxide Surface Binding Geometry. *J. Am. Chem. Soc.* **2015**, *137* (21), 6770-6780.
57. Mouat, A. R.; George, C.; Kobayashi, T.; Pruski, M.; van Duyne, R. P.; Marks, T. J.; Stair, P. C., Highly Dispersed $\text{SiO}_x/\text{Al}_2\text{O}_3$ Catalysts Illuminate the Reactivity of Isolated Silanol Sites. *Angew. Chem. Int. Ed.* **2015**, *54* (45), 13346-13351.
58. Nelson, N. C.; Manzano, J. S.; Sadow, A. D.; Overbury, S. H.; Slowing, I. I., Selective Hydrogenation of Phenol Catalyzed by Palladium on High-Surface-Area Ceria at Room Temperature and Ambient Pressure. *ACS Catal.* **2015**, *5*, 2051-2061.

FWP50966: Tunable Single-Site Catalysts for Selective Functionalization of Alkanes

Principal Investigators: Massimiliano Delferro (Lead PI),¹ Cong Liu,¹ Larry A. Curtiss,¹ Adam S. Hock,^{1,2} Peter C. Stair^{1,3}

ANL Staff members: Jeremy Kropf (X-ray), Magali Ferrandon (Catalysts testing)

Postdocs: David Kaphan, Ryan R. Langeslay, Gokhan Celik, Evan Wegener

Graduate student: Yiqing Zhao²

Contractor: HackSung Kim³

Affiliations: ¹Chemical Sciences and Engineering Division, Argonne National Laboratory, ²Department of Chemistry, Illinois Institute of Technology,³ Department of Chemistry, Northwestern University

RECENT PROGRESS

Goals

The long-term goal of our current efforts are to understand and manipulate isolated, “homogeneous-in-function” supported single-site catalysts for kinetically-limited transformations (e.g., alkane C–H activation and functionalization) and elucidation of the operant mechanisms. The energy input required to drive such reactions using traditional heterogeneous catalysts could compromise the product selectivity and stability, resulting in a distribution of reaction products and deactivation, respectively. The use of single-site catalysts overcomes these problems. Our group recently developed synthetic control of isolated, single-site catalysts on metal oxide supports (i.e. SiO₂) employing the tools of surface organometallic chemistry (SOMC) and atomic layer deposition (ALD). The nature of these active site support platforms provides efficient and general routes to isolated, single-site surface species that exhibit catalytic activity, selectivity and stability, notably under reaction conditions where their molecular analogs are largely unstable and/or unreactive.

Description of the Results

Our group achieved successes in two major project thrusts in FY16-18. The first project thrust has been focused on control of the reactivity and stability of sensitive single-atom catalysts supported on *tailored metallo-ligand environments/surfaces* (Thrust 1). By employing stepwise synthesis of multicomponent catalyst scaffolds, we successfully developed site-isolated organometallic catalysts on surfaces equipped with metal anchoring sites/promoter ions. In parallel, we have developed *rational design via well-defined, single-site catalysts* on support platforms for controlled hydrocarbon transformations such as non-oxidative dehydrogenation of alkanes to alkenes and its microscopic reverse, alkene hydrogenation (Thrust 2). Our recent achievements cover advances in the (1) synthesis of well-defined, supported organometallic sites using state-of-the-art synthetic techniques (e.g., ALD, surface organometallic synthesis), (2) development of spectroscopic strategies to elucidate operant reaction mechanisms and (3) computationally guided development of supported single-atom catalytic sites.

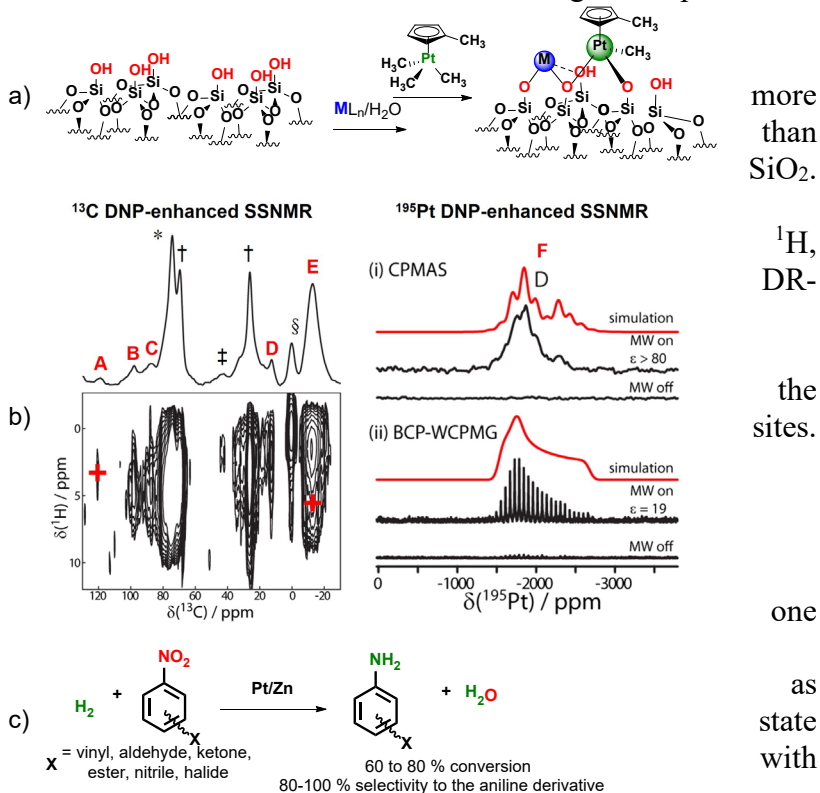
Thrust 1: Promoter and Anchoring Site Effects in Single-Site Catalysts. Single-ion catalysts based on highly reducible noble metals (e.g., Pt) remains challenging due to their susceptibility to sintering. To date, two notable strategies have been shown effective in stabilizing single-ion or

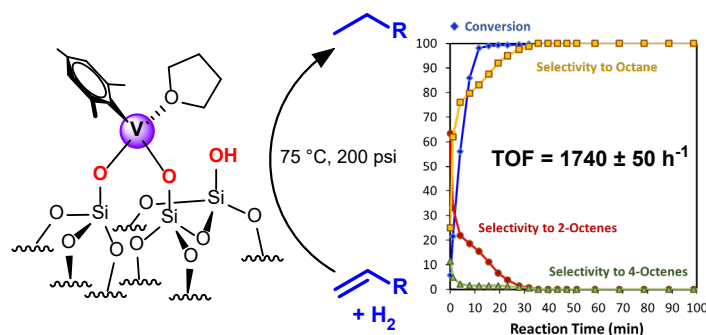
pseudo-single-ion noble metal catalysts on solid supports, which include (1) nucleation on defect sites on bulk oxides and (2) support on carbonaceous surfaces where the surface hydroxyl concentrations are low. Air-stable, well-defined, isolated organoplatinum(IV) precatalysts were deposited on ALD-Zn²⁺(submonolayer)/SiO₂ surfaces, employing solution-phase synthesis conditions under which SiO₂ is largely unreactive (Figure 2). The straightforward deposition of the trimethyl(methylcyclopentadienyl)platinum(IV) [(MeCp)PtMe₃] precursor is attributed to the increased acidity of surface silanols associated to Zn²⁺ cations. DFT modeling of the platinumation reaction suggests that the

metalation of Zn²⁺-bound silanols is thermodynamically favorable ($\Delta G = -12.4$ kcal/mol) with silanols of non-modified SiO₂. The results of a combination of spectroscopic (e.g., XAS, SS ¹³C, and ¹⁹⁵Pt NMR, DRIFTS, UV-Vis) and surface characterization (e.g., TPR) techniques are consistent with presence of site-isolated Pt⁴⁺. The Pt⁴⁺ sites deposited via solution-phase synthesis ((MeCp)PtMe/Zn/SiO₂) are stabilized by a methylcyclopentadienyl ligand, unreacted methyl group, and an anionic siloxy group (Figure 2), confirmed by advanced solid DNP NMR (in collaboration DOE Ames Lab/ Dr. M. Pruski).

Solution-phase, chemoselective hydrogenation of a series of functionalized nitroaryls to the corresponding anilines was achieved under mild conditions employing (MeCp)PtMe/Zn/SiO₂ with excellent tolerance of other hydrogenation-sensitive functionalities (e.g., vinyl, aldehyde, ketone, esters, nitriles and halides). On the other hand, Pt(NP)/SiO₂ (NP = nanoparticles) fully hydrogenated the -NH₂ group and other unsaturated functionalities (i.e., alkene and carbonyl groups). TPR, variable-temperature DRIFTS, and *in situ* XAS experiments under H₂ provided important insights into the precatalyst activation mechanism. In particular for (MeCp)PtMe/Zn/SiO₂, at the reaction temperature of 135 °C, the Pt-CH₃ group undergoes hydrogenolysis to yield a Pt⁴⁺-H species, identified via *in situ* DRIFTS, while the CpMe ligand is not cleaved. This suggests that the ancillary ligand is necessary for the observed chemoselectivity.

Thrust 2: Rational Design of Supported Single-Site Catalysts. Hydrogenation of unsaturated hydrocarbons using noble metals such as Ru, Rh, Pd and Pt has been extensively investigated over the past few decades in both homogeneous and heterogeneous systems. Recently, the utilization of late first-row transition metals (Fe, Co, Ni and Cu) have garnered much attention due to their lower cost and abundance. The hydrogenation activity of early- and mid-first row transition metals

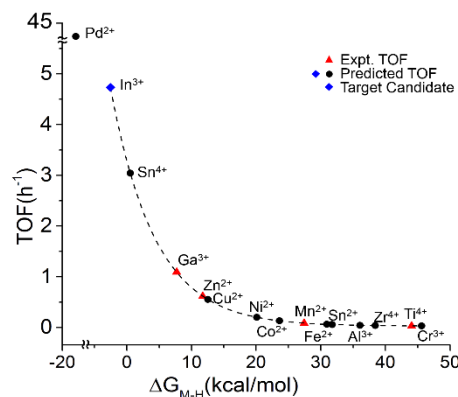




(Sc, Ti, V, Cr, Mn), however, have not been rigorously studied other than for their role as metal ion dopants to hydrogenation catalysts. Our group recently developed a series of well-defined, site-isolated first-row organo-transition metal catalysts (V^{III}, Cr^{III}, Mn^{II}, Co^{II} and Ni^{II}) supported on a catechol-containing porous organic polymer (CatPOP) which are active for

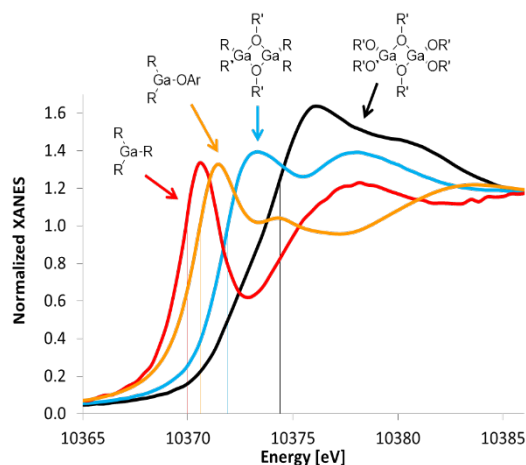
alkyne semi-hydrogenation. Among the catalysts tested, superior hydrogenation activity was observed using the [(CatPOP)V^{III}(Mes)(THF)], with turnover frequency (TOF) 40 times higher than others. As a follow-up study, we incorporated same organovanadium (III) species on the redox-innocent silica support (SiO₂) via surface organometallic synthesis. Through a combination of characterization techniques (ICP, ¹H NMR, TGA-MS, DRIFTS), the presence of one mesityl and one THF donor groups bound to the vanadium center was confirmed. Results of EPR, XPS, DR-UV/Vis and XAS experiments verified isolated V(III) sites. The catalytic performance of the [(SiO₂)V^{III}(Mes)(THF)] catalyst was examined for hydrogenation of diphenylacetylene and 1-octene in the liquid-phase, and hydrogenation of ethylene in the gas-phase. In both cases, the catalyst showed unprecedented high hydrogenation reactivity. Kinetic poisoning experiments were conducted using 2,2'-bipyridine and confirmed that all V sites are active. All of these results show that the redox properties of the support is not a prerequisite to obtain high hydrogenation activity over the [(SiO₂)V^{III}(Mes)(THF)] catalyst.

A series of supported single-site first-row transition metal (V³⁺, Zn²⁺) and main group element (Ga³⁺) hydrogenation catalysts have been developed in our program. The generality of the active site design strategy that we demonstrated encouraged us to pursue rational active site design based on molecular-level understanding of catalytic properties and reaction mechanisms. Thus, we have carried out a combined theoretical and experimental study to demonstrate computationally guided active site design strategy, specifically developing descriptors for single-site catalysts for hydrogenation reactions. Density Functional Theory (DFT) calculations are used to investigate the structures and thermodynamic stabilities of active sites of the type M/SiO₂ (M = Ga³⁺, Zn²⁺, Mn²⁺ and Ti⁴⁺), as well as the periodicity of reaction mechanisms and rate-limiting steps based on representative single-atom catalysts for propylene hydrogenation. A cluster model with six silica rings and up to four hydroxyl groups are used to represent the structure of the M/SiO₂ catalysts. The results show that catalyst activation proceeds through H₂ activation over a M-O bond, resulting in M-H and Si-O-H bond formation. This intermediate can then hydrogenate propylene through two probable metal-dependent mechanisms: Ga³⁺, Mn²⁺ and Ti⁴⁺ ions go through a concerted hydrogenation step, while Zn²⁺ undergoes a stepwise pathway. The calculations also indicate that the stability of the M-H is critical to the kinetics of hydrogenation. This approach generated a computational activity descriptor that closely correlates with the experimental activity observed during catalysis. The experimental activities show a remarkable trend as a function of the calculated ΔG_{M-H} . Specifically, an exponential correlation is observed



between the calculated ΔG_{M-H} and the experimental TOF, enabling the prediction that lower the ΔG_{M-H} gives rise to more active single-site catalysts. Among the cationic sites considered, Pd^{2+} , In^{3+} and Sn^{4+} are predicted to be more active than the experimentally discovered Ga^{3+} catalyst. The validity of this computationally guided active site design strategy has been confirmed by the higher experimental hydrogenation activity of the $\text{In}^{3+}/\text{SiO}_2$ (TOF = 3.4 h^{-1} at 200 °C).

The accessibility of spectroscopic techniques to probe the transformations of supported catalytic sites under reaction conditions remains a grand challenge in fundamental catalysis research. For example, Ga catalysts on solid supports such as zeolites and oxides are employed for a range of industrial alkane activation and functionalization processes. Despite the diverse and rigorous attempts to understand the mechanism of these alkane transformations, the nature of the active Ga species has not been definitively elucidated. Hence, our group postulated that well-defined, homogeneous molecular organometallic complexes that mimic the changes in the Ga^{3+} coordination environment can elucidate the oxidation state of the active Ga species. A series of Ga^{3+} organometallic model compounds have been prepared, and their XANES spectra compared to those of the heterogeneous Ga-SiO₂ catalyst acquired under reducing conditions. The resulting spectra clearly demonstrate that shifts in XANES edge energy cannot be assumed to arise from the change in oxidation state from Ga^{3+} to Ga^+ . This range overlaps with the edge energy range of known Ga^+ compounds. Consequently, XANES edge energy cannot definitively distinguish Ga^{3+} alkyls or hydrides from Ga^+ , thus the formation of Ga^{3+} alkyl or hydride intermediates cannot be ruled out. Comparison of the XANES spectrum of Ga-SiO₂ exposed to hydrogen at high temperature with the XANES spectra of molecular reference compounds further suggests that these catalysts may contain three-coordinate Ga^{3+} dihydride species rather than Ga^+ . Grafting of molecular models to silica support confirms the similarity between spectra of three-coordinate Ga alkyls and *in-situ* spectra of supported Ga-SiO₂ catalysts under reducing conditions. These findings agree with the observation in the literature of the formation of Ga-H species under catalytic conditions, suggesting that Ga^{3+} hydrides are mechanistically relevant. Finally, catalytic activity of Ga-SiO₂ catalysts for olefin hydrogenation – the microscopic reverse of alkane dehydrogenation – is observed at temperatures as low as 110°C, and it is chemically unlikely that Ga^{3+} can be reduced under such mild conditions. Therefore, we believe that Ga^{3+} does not undergo reduction to Ga^+ during alkane dehydrogenation, and that C-H bond activation on Ga^{3+} catalysts instead proceeds via a non-redox, heterolytic cleavage mechanism involving Ga^{3+} alkyl and hydride intermediates.



Publications exclusively funded by this grant in 2015-2018

- 1) Klet, R. C.; Kaphan, D. M.; Liu, C.; Yang, C.; Kropf, A. J.; Perras, F. A.; Pruski, M.; Hock, A. S.; Delferro, M., Evidence for Redox Mechanisms in Organometallic Chemisorption and Reactivity on Sulfated Metal Oxides. *J. Am. Chem. Soc.* **2018**, *140*, 6308–6316 (JACS May 23, 2018 Cover and JACS Spotlights).

- 2) Kaphan, D. M.; Klet, R. C.; Perras, F. A.; Pruski, M.; Yang, C.; Kropf, A. J.; Delferro, M. Surface Organometallic Chemistry of Supported Iridium(III) as a Probe for Organotransition Metal–Support Interactions in C–H Activation. *ACS Catal.* **2018**, *8*, 5363–5373
- 3) Camacho-Bunquin, J.; Ferrandon, M.; Sohn, H.; Yang, D.; Liu, C.; Ignacio-de Leon, P. A.; Perras, F. A.; Pruski, M.; Stair, P. C.; Delferro, M. Chemo-Selective Hydrogenation of Nitro Compounds with Supported Organoplatinum(IV) on Zn(II)/SiO₂ Catalyst. *J. Am. Chem. Soc.* **2018**, *140*, 3940–3951.
- 4) Liu, C.; Camacho-Bunquin, J.; Ferrandon, M.; Savara, A.; Sohn, H.; Yang, D.; Kaphan, D. M.; Langeslay, R. R.; Ignacio-de Leon, P. A.; Liu, S.; Das, U.; Yang, B.; Hock, A. S.; Stair, P. C.; Curtiss, L. A.; Delferro, M. Development of Activity-Descriptor Relationship in Supported Metal Ion Hydrogenation Catalysts on Silica. *Polyhedron* **2018**, DOI: 10.1016/j.poly.2018.06.006 (Invited contribution)
- 5) Zhao, Y.; Sohn, H.; Hu, B.; Niklas, J.; Poluektov, O. G.; Tian, J.; Delferro, M.; Hock, A. S. Zirconium Modification Promotes Catalytic Activity of a Single-Site Cobalt Heterogeneous Catalyst for Propane Dehydrogenation. *ACS Omega* **2018**, accepted.
- 6) Sohn, H.; Camacho-Bunquin, J.; Langeslay, R. R.; Ignacio-de Leon, P. A.; Niklas, J.; Poluektov, O. G.; Liu, C.; Connell, J. G.; Yang, D.; Kropf, J.; Kim, H.; Stair, P. C.; Ferrandon, M.; Delferro, M. Supported Single-Site Organo-Vanadium(III) Catalyst on Silica for Hydrogenation of Alkenes and Alkynes. *Chem. Commun.* **2017**, *53*, 7325–7328 (invited for special issue: ChemComm Emerging Investigators Issue 2017).
- 7) Camacho-Bunquin, J.; Ferrandon, M.; Das, U.; Dogan, F.; Liu, C.; Larsen, C.; Platero-Prats, A. E.; Curtiss, L. A.; Hock, A. S.; Miller, J. T.; Nguyen, S. T.; Marshall, C. L.; Delferro, M.; Stair, P. C. Supported Aluminum Catalysts for Olefin Hydrogenation. *ACS Catal.* **2017**, *7*, 689–694.
- 8) Getsoian A.; Hu B.; Miller J. T.; Hock A. S. Supported Single-Site Sc and Y Alkyl Catalysts for Olefin Hydrogenation. *Organometallics*, **2017**, *36*, 3677–3685.
- 9) Camacho-Bunquin, J.; Aich, P.; Ferrandon, M.; Getsoian, A.; Das, U.; Dogan, F.; Curtiss, L.; Miller, J. T.; Marshall, C. L.; Hock, A. S.; Stair, P. C. Single-Site Zinc on Silica Catalysts for Propylene Hydrogenation and Propane Dehydrogenation. Synthesis and Reactivity Evaluation through Integrated Atomic Layer Deposition-Catalysis Experimentation. *J. Catal.* **2017**, *345*, 170–182 (Editor’s Choice).
- 10) Getsoian, A.; Das, U.; Camacho-Bunquin, J.; Zhang, G.; Gallagher, J. Hu, B.; Schaidle, J.; Ruddy, D. A.; Kraft, S. J.; Henley, J.; Curtiss, L. A.; Miller, J. T.; Hock, A.S. Organometallic model complexes elucidate the active gallium species in alkane dehydrogenation catalysts based on ligand effects in Ga K-edge XANES. *Catal. Sci. Technol.* **2016**, *6*, 6339–6353.
- 11) Das, U.; Zhang, G.; Hu, B.; Hock, A. S.; Redfern, P. C.; Miller, J. T.; Curtiss, L. A. Effect of Siloxane Ring Strain and Cation Charge Density on the Formation of Coordinately Unsaturated

Metal Sites on Silica: Insights from Density Functional Theory (DFT) Studies. *ACS Catal.* **2016**, *5*, 7177-7185.

- 12) Camacho-Bunquin, J.; Shou, H.; Aich, P.; Beaulieu, D. R.; Klotzsch, H.; Bachman, S.; Marshall, C. L.; Hock, A. S.; Stair, P. C. Catalyst Synthesis and Evaluation Using A High-Throughput Atomic Layer Deposition–Catalysis Testing Tool *Rev. Sci. Instrum.* **2015**, *86*, 084103/084101-084103/084107.
- 13) Hu, B.; Schweitzer, N. M.; Zhange, G.; Kraft, S. J.; Childers, D. J.; Lanci, M. P.; Miller, J. T.; Hock, A. S. Isolated Fe^{II} on Silica As a Selective Propane Dehydrogenation Catalyst. *ACS Catal.* **2015**, *5*, 3494-3503.
- 14) Camacho-Bunquin, J.; Siladke, N. A.; Zhang, G.; Niklas, J.; Poluektov, O. G.; Nguyen, S. T.; Miller, J. T.; Hock, A. S. Synthesis and Catalytic Hydrogenation Reactivity of a Chromium Catecholate Porous Organic Polymer. *Organometallics* **2015**, *34*, 947-952.
- 15) Hu, B.; Schweitzer, N. M.; Das, U.; Kim, H. K.; Stair, P. C.; Curtiss, L. A.; Hock, A. S.; Miller, J. T. Selective Propane Dehydrogenation with Single Site Co^{II} on SiO₂ by a Non-redox Mechanism. *J. Catal.* **2015**, *322*, 24-37.

Submitted/In preparation:

- 16) Camacho-Bunquin, J.; Ferrandon, M.; Sohn, H.; Kropf, A. J.; Yang, C.; Wen, J.; Liu, C.; Marshall, C. L.; Stair, P. C.; Delferro, M. Atomically Precise Strategy to PtZn Alloy Nanocluster Catalyst for Deep Dehydrogenation of n-Butane to 1,3-Butadiene. *Submitted*
- 17) Langeslay, R. R.; Sohn, H.; Hu, B.; Mohar, J. S.; Ferrandon, M.; Liu, C.; Kim, H.; Niklas, J.; Poluektov, O. G.; Alp, E. E.; Sattelberger, A. P.; Hock, A. S.; Delferro, M. Nuclearity Effects in Supported, Single-Site Fe(II) Hydrogenation Catalysts. *Submitted*
- 18) Langeslay, R. R.; Kaphan, D. M.; Marshall, C. L.; Sattelberger, A. P.; Stair, P. C.; Delferro, M. Catalytic Applications of Vanadium: A Mechanistic Perspective. *Chem Rev.* **2018** (Invited Contribution; “First Row Metals and Catalysis”). *Submitted*
- 19) Kaphan, D. M.; Langeslay, R. R.; Ferrandon, M.; Liu, C.; Wegner, E.; Kropf, A. J.; Delferro, M. Evidence for an Eley-Rideal Type Mechanism in Supported Organovanadium(III) Catalyzed Olefin Hydrogenation.
- 20) Syed, Z. H.; Kaphan, D. M.; Perras, F. A.; Pruski, M.; Ferrandon, M. S.; Yang, C.; Kropf, A. J.; Goldberg, K. I.; Delferro M. C–H Bond Activation and Functionalization with Supported Pincer-Ir Complexes on Metal Oxides.

Patents

- 21) Multimetallic catalysts for selective hydrogenation of dienes. Camacho-Bunquin, J.; Ferrandon, M.; Delferro, M. U.S. Patent Application Number: 15/484,928.
- 22) Multimetallic catalysts. Camacho-Bunquin, J.; Ferrandon, M.; Delferro, M.; Stair, P. C. U.S. Patent Application Number: 62/402,218.

- 23) Multimetallic catalysts for alkane dehydrogenation and synthesis thereof. Stair, P. C.; Camacho-Bunquin, J.; Marshall, C. L.; Hock A. S. U.S. Patent Application Number: 15/157,109.

Publications jointly funded by this grant and other grants with leading intellectual contribution from this grant in 2015-2018

- 24) Pang, H.; Gallou, F.; Sohn, H.; Bunquin, J. C.; Delferro, M.; Lipshutz B. H. Synergistic effects in Fe nanoparticles doped with ppm levels of (Pd + Ni). A new catalyst for sustainable nitro group reductions. *Green Chem.* **2018**, *20*, 130–135
- 25) Huang, Z.; Liu, D.; Camacho-Bunquin, J.; Zhang, G.; Yang, D.; López-Encarnación, J. M.; Jellinek, J.; Xu, Y.; Ferrandon, M.; Lei, A.; Bunel, E. E.; Delferro, M. Supported Single-Site Ti(IV) on a Metal–Organic Framework for the Hydroboration of Carbonyl Compounds. *Organometallics* **2017**, *36*, 3921-3930
- 26) Cybulskis, V. J.; Pradhan, S. U.; Lovón-Quintana, J. J.; Hock, A. S.; Hu, B.; Zhang, G.; Delgass, W. N.; Ribeiro, F. H.; Miller J. T. The Nature of the Isolated Gallium Active Center for Propane Dehydrogenation on Ga/SiO₂. *Catal. Lett.* **2017**, *147*, 1252-1262.
- 27) Martynowycz, M. W.; Hu, B.; Kuzmenko, I.; Bu, W.; Hock, A.; Gidalevitz, D. Monomolecular Siloxane Film as a Model of Single-Site Catalysts *J. Am. Chem. Soc.* **2016**, *138*, 12432-12439.

In preparation/submitted

- 28) Zhong, H.; Camacho-Bunquin, J.; Sohn, H.; Yang, C.; Delferro, M.; Chirik, P. J. Understanding the Methanol Stability of Bis(phosphine) Cobalt Asymmetric Hydrogenation Catalysts: An XAS Study. *Submitted*
- 29) Zhang, M.; van Dornshuld, E.; J.; Bunquin, J.; Delferro, M.; Webster, C. E.; Hollis, T. K. Synthesis, Characterization, Computation, and Photophysics of Unsymmetric CCC-NHC Pincer Platinum Complexes. PtEP (Platinum (Pt) Electronic Parameter): A Donicity Scale Incorporating Strictly Meridional, Tridentate Ligands. *Submitted*
- 30) Zhang, M.; Autry, S. A.; Dixit, V.; Denny, A. J.; Bunquin, J.; Delferro, M.; Hammer, N. I.; Webster, C. E.; Hollis, T. K. Synthesis, Characterization, Computation, and Photophysics of Unsymmetric CCC-NHC Pincer Platinum Complexes. *Submitted*
- 31) Zhang, M.; Denny, A. J.; Dixit, V.; Autry, S. A.; Zhang, X.; Bunquin, J.; Delferro, M.; Valente, E. J.; Hammer, N. I.; Webster, C. E.; Hollis, T. K. Synthesis, Characterization, Computation, and Photophysics of symmetric CCC-NHC Pincer Platinum Complexes. *Submitted*
- 32) Zhang, M.; Dixit, V.; Autry, S. A.; Denny, A. J.; Bunquin, J.; Delferro, M.; Hammer, N. I.; Webster, C. E.; Hollis, T. K. Comparing N-heterocyclic Carbenes (NHCs) in CCC-NHC pincer Pt complexes: Imidazolyl vs. Benzimidazolyl vs. Triazolyl - Synthesis, Characterization, Computation, and Photophysics. *Submitted*
- 33) Liu, C.; Yang, D.; Ferrandon, M. S.; Tian, J.; Liu, Y.; Barenó, J.; Bunel, E. E.; Delferro, M.; Lei A. Organic-Porous-Cage Encapsulated Ultrasmall Palladium Nano-particles for Selective Hydrogenation of Alkynes. *Submitted*

Jointly funded by this grant and other grants with relatively minor intellectual contribution from this grant in 2015-2018

- 34) Jung, D.; Saleh, L. M. A.; Berkson, Z. J.; El-Kady, M. F.; Hwang, J. Y.; Mohamed, N.; Wixtrom, A. I.; Titarenko, E.; Shao, Y.; McCarthy, K.; Guo, J.; Martini, I. B.; Kraemer, S.; Wegener, E. C.; Saint-Cricq, P.; Ruehle, B.; Langeslay, R. R.; Delferro, M.; Brosmer, J. L.; Hendon, C. H.; Gallagher-Jones, M.; Rodriguez, J.; Chapman, K. W.; Miller, J. T.; Duan, X.; Kaner, R. B.; Zink, J. I.; Chmelka, B. F.; Spokoyny, A. M., A molecular cross-linking approach for hybrid metal oxides. *Nature Mater.* **2018**, *17*, 341-348.
- 35) Halder, A.; Liu, C.; Liu, Z.; Emery, J. D.; Pellin, M. J.; Curtiss, L. A.; Zapol, P.; Vajda, S.; Martinson, A. B. F. Water Oxidation Catalysis via Size-Selected Iridium Clusters. *J. Phys. Chem. C* **2018**, *122*, 9965-9972.
- 36) Canossa, S.; Bellè, E.; Delferro, M.; Predieri, G.; Graiff, C. Structural motifs in heteroleptic copper and cadmium selenites *Inorg. Chim. Acta* **2018**, *470*, 206–212.
- 37) Yang, B.; Liu, C.; Halder, A.; Tyo, E.; Martinson, A. B. F.; Seifert, S.; Zapol, P.; Curtiss, L. A.; Vajda, S. Copper Cluster Size Effect in Methanol Synthesis from CO₂. *J. Phys. Chem. C* **2017**, *121*, 10406–10412.

**In-situ Studies for the Conversion of C-O Bonds
on Complex Metal-Oxide Interfaces**

José A. Rodriguez, Ping Liu, Sanjaya D. Senanayake and Michael G. White
Brookhaven National Laboratory, Chemistry Department

Presentation Abstract

In the area of C1 Chemistry, the water-gas shift reaction (WGS: $\text{CO} + \text{H}_2\text{O} \leftrightarrow \text{H}_2 + \text{CO}_2$) and the hydrogenation of CO_2 to methanol ($\text{CO}_2 + 3\text{H}_2 \rightarrow \text{CH}_3\text{OH} + \text{H}_2\text{O}$) are important processes which involve the formation or cleavage of C-O bonds. Complex metal-oxide interfaces play a fundamental role in materials used to catalyze these processes. Fundamental studies have been performed to investigate the chemistry associated with the WGS reaction and CO_2 hydrogenation on a series of model and powder Cu-ZnO and Cu-CeO₂ catalysts. Several *in-situ* techniques {X-ray diffraction (XRD), pair-distribution function analysis (PDF), X-ray absorption spectroscopy (XAS), environmental scanning tunneling spectroscopy (ESTM), infrared spectroscopy (IR) and ambient-pressure X-ray photoelectron spectroscopy (AP-XPS)} and theoretical calculations {Density Functional Theory and kinetic Monte Carlo} were used to characterize the properties of the active phase in the catalysts and the reaction mechanism. The active phase in these catalysts involved metallic copper in contact with ZnO or CeO_x. The *in-situ* studies indicate that metal-oxide interfaces useful for the WGS and CO_2 hydrogenation are dynamic entities which change with reaction conditions. The highest activity is seen in conditions where the metal and oxide participate in the binding and conversion of key intermediates such as HOCO and HCOO. In general, the highly active WGS and CO_2 hydrogenation catalysts are bifunctional with the metal and oxide catalyzing different parts of the reactions. The complexity of the metal-oxide interface can be modified by the controlled use of alkali metals. The alkali-modified metal-oxide interfaces display a good selectivity for the production of C₂-C₄ alcohols during the hydrogenation of CO_2 .

FWP-BNL-CO040: Catalysis for Advanced Fuel Synthesis and Energy

Co-PIs: Ping Liu, Sanjaya Senanayake, and Michael G. White

Postdoc(s): Zongyuan Liu, Robert Palomino, David Grinter, Mausumi Mahapatra,
Juan Pablo Simonovis

Student(s): Si Luo, Zongyuan Liu, Fang Xu, Dimitriy Vovchok, Zhijun Zuo, Pamela Carrillo, Kenneth Goodman, Rebecca Hamlyn, Yilin Ma, Jason Wang, Meng Xue.

Affiliations(s): All students are from SUNY Stony Brook, Department of Chemistry

RECENT PROGRESS

C1 chemistry involves the conversion of molecules that contain one carbon atom into valuable products. C1 chemistry is expected to become a major area of interest for the transportation fuel and chemical industries in the relatively near future. In general, the feedstocks for C1 chemistry

include natural gas (mostly methane), carbon monoxide, carbon dioxide, methanol and synthesis gas (a mixture of carbon monoxide and hydrogen). Thus, a fundamental understanding of the conversion of C-O and C-H bonds is essential for controlling C1 chemistry. The Catalysis Group at BNL has been quite active in this area. In the period 2015-2018, seventy-one papers have been published in peer-reviewed journals (Science, Angewandte Chemie, Journal of the American Chemical Society).¹⁻⁷¹ Thirteen of them were exclusively funded by this grant and for the other fifty-eight this grant made the major intellectual contribution. The reactions investigated included the oxidation of CO, the water-gas shift, the hydrogenation of CO₂ and the activation of methane and its dry reforming. Experimental and theoretical studies have been performed exploring correlations between the structure and reactivity of typical metal catalysts or catalysts that contain oxides and carbides. Work was done with high-surface area powders and model catalysts. In the last three years, major research achievements within this program have been:

- Discovery of the essential role that complex metal-oxide and metal-carbide interfaces play in the catalysis associated with C1 chemistry.^{9,35,43,48,52}
- Detailed proof through *operando* studies that metal/oxide catalysts are dynamic entities that change as a function of reaction conditions during the water-gas shift, CO₂ hydrogenation and methane dry reforming.^{14,15,38,55,56,70}
- Discovery of the importance of metal-support interactions in active catalysts for C1 chemistry.^{17,18,19,22,36,43}
- Identification of A/CeO_x/TiO₂ and A/MoC (A= Au or Cu) as highly active and stable catalysts for the hydrogenation of CO₂ to methanol.^{18,43,44,50,52,59}
- Identification of HOCO as a key intermediate for the water-gas shift reaction by *In-situ* and theoretical studies.^{18,44,50,59}
- Discovery of the high surface mobility of K as a promoter of the activity of catalysts used for CO oxidation, the water-gas shift and CO₂ hydrogenation.^{45,65}
- Identification of Co-CeO₂ and Ni-CeO₂ as active systems for the low-temperature activation of methane.^{49,58}

A. Studies on the water-gas shift and CO₂ hydrogenation: C-O bond conversion

A.1 *In-situ studies with XRD, PDF, XAFS and AP-XPS: Evolution of metal/oxide catalysts.* In-situ time-resolved X-ray diffraction (XRD), Pair-distribution function (PDF) analysis, X-ray absorption fine structure (XAFS) and ambient-pressure X-ray photoelectron spectroscopy (AP-XPS) were used to study the active phase of a series of metal/oxide powder catalysts (Cu/CeO₂-spheres, Cu/CeO₂-rods, Cu/CeO₂-cubes, Pt/CeO_x/TiO₂, Au/CeO_x/TiO₂, Ce_{1-x}Ni_xO_{2-y}, CeO_x/CuO) used for the hydrogenation of CO₂ and the water gas shift reaction^{44,43,18,50,52,70} Under reaction conditions most of these metal/oxide catalysts underwent chemical transformations that drastically modified their chemical composition with respect to that obtained during the synthesis process. The active phase of catalysts which combine Cu or Au and ceria consisted of metal nano-particles on partially reduced ceria.^{18,70} A typical result is shown in Figure 1 where we displayed the effects of H₂ and a CO₂/H₂ mixture of catalysts generated by dispersing copper of ceria nanorods (CeO₂-NR) and nanospheres (CeO₂-NS).⁷⁰

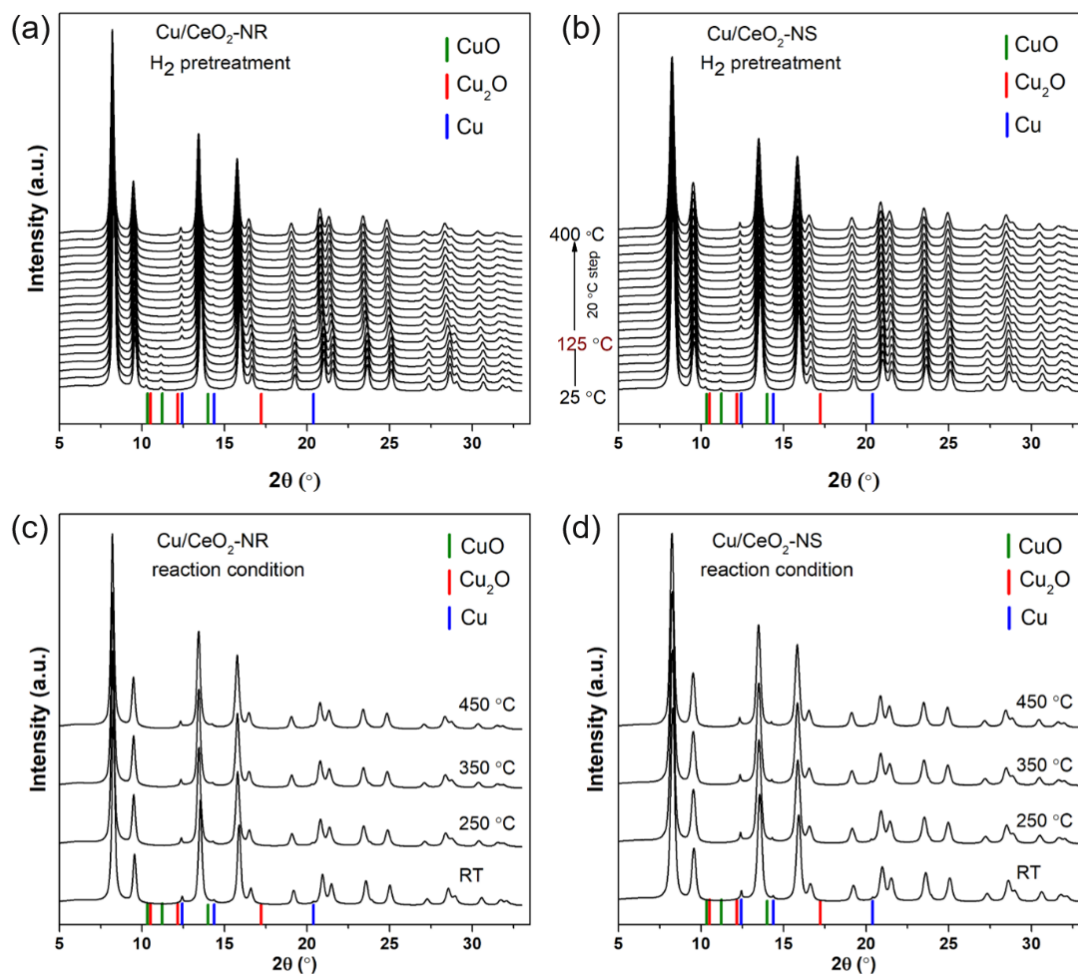


Figure 1. In-situ time-resolved XRD patterns for (a) CuO/CeO₂-NR and (b) CuO/CeO₂-NS catalysts with H₂ pretreatment (50%H₂/He), and pre-reduced (c) CuO/CeO₂-NR and (d) CuO/CeO₂-NS under RWGS reaction condition at different temperature (10%CO₂/50%H₂/ He).⁷⁰

Pulse experiments showed that the oxide was not a simple spectator.^{15,70} Significant differences in chemical and catalytic activity were found when the morphology of the ceria was changed from spheres, to rods, and to cubes.⁷⁰ The order of catalytic activity increased following the sequence: Cu/CeO₂-cubes < Cu/CeO₂-spheres < Cu/CeO₂-rods.⁷⁰ This order matched well trends in the degree of dispersion of copper. Small Cu particles and a strong metal-support interaction were found for the Cu/CeO₂-rods system.⁷⁰ On the opposite end was the Cu/CeO₂-cubes system which exhibited big copper particles and a weak metal-support interaction.^{15,70}

A.2 Importance of metal-oxide interface for the water-gas shift and CO₂ hydrogenation

Inverse oxide/metal catalysts have been quite useful in the study of the conversion of C-O bonds. The CeO_x/Cu(111) and ZnO/Cu(111) systems have shown the important role played by the metal-oxide interface during the WGS and CO₂ hydrogenation reactions.^{14,35,43,63} Cu(111) has problems dissociating the H₂O molecule during the WGS or binding CO₂ during synthesis of methanol. In general, Cu(111) is a poor catalysts for the conversion of C-O bonds.^{35,63} The addition of nanoparticles of CeO_x or ZnO to Cu(111) opens new routes for the WGS and CO₂ hydrogenation

increasing the rates of reaction by 2-3 orders of magnitude.^{35,63} Experiments of ambient-pressure XPS and infrared spectroscopy revealed that the metal-oxide interface is very active for the dissociation of water into OH during the WGS or the binding of CO₂ and the formation of HOCO/HCOO intermediates during CO₂ hydrogenation.^{35,63} Results of DFT calculations indicate that all the important steps of these reactions occur at the metal-oxide interface with the reactants and intermediates bound to metal and O centers. Furthermore, the calculations show a huge reduction in the key energy barriers for the reaction that leads to a very large increase in the rate for the production of hydrogen and CO₂

A.3 Water-gas shift and hydrogenation of CO₂ on metal-carbide interfaces

For small Cu and Au clusters supported on TiC or MoC, strong admetal ↔ C_{surface} interactions induce charge polarization over the surface.^{17,44} As a result, there is a significant enhancement in the catalytic activity when going from metal bulk surfaces to carbide-supported small clusters, and systems such as Au/MoC and Au/TiC display a high catalytic activity for the low-temperature water-gas shift reaction.^{53,57,59}

Experimentally, a promotion in activity and selectivity for CO₂ hydrogenation is observed when depositing small particles of Au, Cu or Ni on TiC(001).^{44,49,52} Although the major product is CO, in the cases of Au/TiC(001) and Cu/TiC(001), a substantial amount of methanol is also produced and no methane is detected. On the other hand, Ni/TiC(001) produces a mixture of CO, methanol, and methane. For all three systems, the highest catalytic activity is found for small 2D particles or clusters of the admetals in close contact with TiC(001). In addition, Cu/TiC is more active for the synthesis of methanol than Au, Ni/TiC and a model for a Cu/ZnO industrial catalysts. DFT calculations show that the charge polarization induced by the Cu-C interaction enhances the CO₂ adsorption via a η³-C,O,O bonding configuration on Cu/TiC(001), and therefore the production of methanol probably involves the hydrogenation of a HCOO intermediate or of the CO generated by the RWGS.

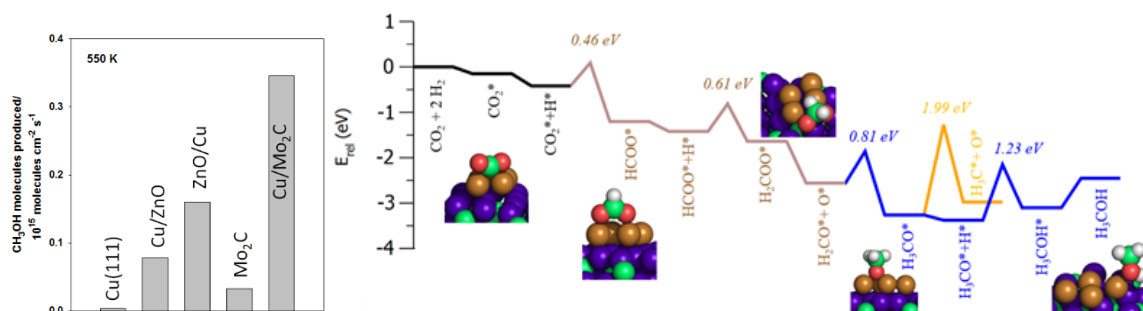


Figure 2 Left: Rates for the production of methanol on Cu(111), Cu/ZnO(000 $\bar{1}$), ZnO/Cu(111), bare β -Mo₂C(001) and Cu/Mo₂C(001). In a batch reactor, the catalysts were exposed to 0.049 MPa (0.5 atm) of CO₂ and 0.441 MPa (4.5 atm) of H₂ at a temperature of 550 K; Right: DFT-calculated energy profile of methanol on a Cu₄/β-Mo₂C(001) surface model.^{44,52}

Depositing Cu clusters on β-Mo₂C(001) increases the methanol production to a level above that seen for a model of a technical catalyst (Figure 2); besides, it lowers the selectivity to methane according to our experimental observations.^{44,51} DFT calculations on surfaces with C- and Mo-terminations corroborate the experimental observations.

A.4 Size-Clusters as

Size (mass)-selected metal oxide and sulfide clusters are being used for the preparation of novel inverse catalysts for C₁ chemistry, where it is possible to investigate the effects of

cluster size and chemical composition with atomic resolution.^{31,32,48} Recent work has focused on the

preparation and characterization of supported sulfide clusters, M_xS_y (M=Fe, Mo, W), as model catalysts for CO₂ activation and CO/CO₂ hydrogenation. This work is motivated by early studies that identified alkali-promoted metal sulfides as promising catalysts for alcohol synthesis, and more recent theoretical studies that suggest small clusters like Mo₆S₈ are active for CO₂ conversion to methanol.²⁷ We have found that the M₆S₈ (M=Mo, W) clusters co-deposited with K-atoms at low coverage on Au(111) reversibly bind CO₂ above 400K (see Figure 3). Different preparation schemes and DFT calculations suggest that the CO₂ binding sites are at the cluster-K interfaces, either at the Au surface or on the cluster itself. More recently we have used a mixed metal target in the cluster source to prepare Fe-Mo sulfide clusters, e.g., Fe₃Mo₂S₅, which bind CO₂ above room temperature without alkali promotion. The latter results open the possibility of using multiple metals to “tune” the reactivity of sulfide (and oxide) clusters with well-defined M₁/M₂/S(O) stoichiometry afforded by cluster sources and mass-selection. Future studies will explore the electronic and reactivity properties of these sulfide cluster surfaces under CO₂ hydrogenation conditions.

A.5 FeRh Alloys for Alcohol Synthesis from CO Hydrogenation

Early and late transition metals are often combined as a strategy to tune the selectivity of catalysts for the conversion of syngas (CO/H₂) to C₂₊ oxygenates, such as ethanol.^{7,30} In a recent study, we were able to show how the use of a highly reducible Fe₂O₃ support for Rh leads to the *in-situ* formation of supported FeRh nanoalloy catalysts that exhibit high selectivity for ethanol synthesis.¹³ *In-situ* x-ray characterization methods show that Rh/Fe₂O₃ undergoes dramatic phase changes under CO hydrogenation conditions including the formation of metallic FeRh nanoalloys and the complete transformation of the iron oxide support to carbide (ε'-Fe_{2.2}C).¹³ The presence of FeRh alloy phases can be correlated with significant increases in selectivity for C₂₊ oxygenates (see Figure 4). The formation of nanoalloys by *in-situ* reduction of a metal oxide support under

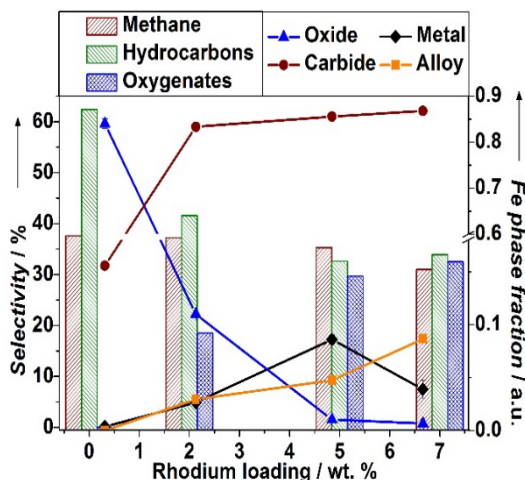


Figure 4: Oxygenate selectivity and iron phase content versus Rh loading for Rh/Fe₂O₃ catalysts studied under CO

Selected Metal Oxide and Sulfide Model Inverse Catalysts

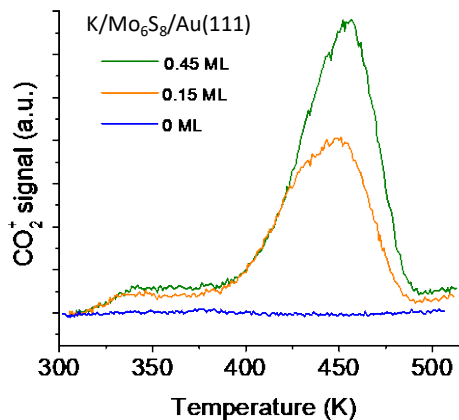
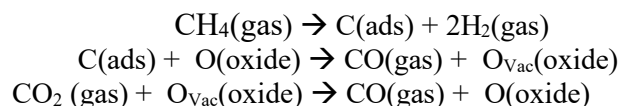


Figure 3: Thermal desorption spectra for CO₂ binding to a Au(111) surface with co-deposited K-atoms and Mo₆S₈ clusters at various coverages.

working conditions represents a simple approach for the preparation bi-metallic catalysts with enhanced catalytic properties.

B. Fundamental studies on the activation and dry reforming of methane: C-H bond conversion

A part of our program is focused on the activation of methane on metal-oxide and metal-carbide surfaces and the conversion of the hydrocarbon through dry reforming with the CO₂ molecule.^{38,58,69} Ceria reacts with methane only at high temperatures (> 500 K). However, the deposition of Ni and Co atoms on CeO₂(111) produces systems that can activate methane at 300 K.^{38,58,69} This is a consequence of strong-metal support interactions which modify the intrinsic properties of Ni and Co. DFT calculations show bonding interactions for methane on Ni/CeO₂(111) and Co/CeO₂(111) which are stronger than those seen on surfaces of pure nickel and cobalt.^{38,58,69} On the other hand, the activation energies for C-H bond cleavage on the metal/oxide systems are well below 1 eV with O sites and the admetal participating in the dissociation of the hydrocarbon. C 1s XPS spectra for the interaction of methane with Ni/CeO₂(111) and Co/CeO₂(111) at 300 K show peaks for adsorbed CH_x and CO_x species.^{38,58,69} Some of the adsorbed methane molecules undergo a quick CH₃ → CH₂ → CH → C transformation on the surface with the produced C atoms reacting with O centers to generate CO_x species. At 300 K, there is only chemisorption of methane on the metal/oxide systems and no significant reduction of the substrate was observed.^{38,58,69} Catalytic activity for methane dry reforming was observed at temperatures above 500 K. At elevated temperatures methane reduced the ceria and on the O vacancies there was dissociation of CO₂ to close the catalytic cycle for methane dry reforming:^{38,58,69}



More details on the work of the BNL Catalysis group on methane activation and conversion will be included in the presentations of Dr. Ping Liu and Dr. Sanjaya Senanayake.

Publications Acknowledging this Grant in 2015-2018

*** Exclusively funded by this grant*

2015:

1. An, W.; Liu, P. Rationalization of Au Concentration and Distribution in AuNi@Pt core-shell nanoparticles for oxygen reduction reaction, *ACS Catal.* **2015**, *5*, 6328-6336.
2. An, W.; Xu, F.; Stacchiola, D.; Liu, P. Potassium-induced Effect on Structure and Chemical Activity of Cu_xO/Cu(111) (x<=2) surface: a combined STM and DFT study, *ChemCatChem*, **2015**, *7*, 3865-3872.

2016:

3. Liu, S.; White, M.G.; Liu, P. Mechanism of Oxygen Reduction Reaction on Pt(111) in Alkaline Solution: Importance of Chemisorbed Water on Surface”, *J. Phys. Chem. C* **2016**, *120*, 15288-15298.
4. An, W.; Liu, P. Complex behavior of Pd₇ cluster supported on TiO₂(110) during CO oxidation: adsorbate-driven promoting effect, *Phys. Chem. Chem. Phys.: Communication* **2016**, *18*, 30881-31340. **(Cover art)**
5. Liu, Z.; Senanayake, S.D.; Rodriguez, J.A. Elucidating the Interaction between Ni and CeOx in Ethanol Steam Reforming Catalysts: A Perspective of Recent Studies over Model and Powder Systems, *Applied Catal. B: Environmental*, **2016**, *197*, 184-199 **(Invited)**.
6. Hoffmann, F.M.; Hrbek, J.; Ma, S. et al. Enhancing the Reactivity of Gold: Nanostructured Au(111) Adsorbs CO, *Surf. Sci.* **2016**, *650*, 17-32.
7. Magee, J. W.; Palomino, R. M.; White, M. G. Infrared Spectroscopy Investigation of Fe-Promoted Rh Catalysts Supported on Titania and Ceria for CO Hydrogenation, *Catal. Lett.* **2016**, *146*, 1771-1779.
8. Pruski, M.; Sadow, A.D.; Slowing, I.I. et al, Virtual Special Issue on Catalysis at the US Department of Energy National Laboratories, *ACS Catal.* **2016**, *6*, 3227.

2017:

9. Rodriguez, J.A.; Grinter, D.C.; Liu, Z.; Palomino, R.M.; Senanayake, S.D. Ceria-based Model Catalysts: Fundamental Studies on the Importance of the Metal-Ceria Interface in CO oxidation, the Water-gas Shift, CO₂ Hydrogenation, and Methane and Alcohol reforming, *Chem. Soc. Reviews* **2017**, *46*, 1824-1833. **(Invited)**
10. Palomino, R.M.; Hamlyn, R.; Liu, Z.; Grinter, D.C.; Waluyo, I.; Rodriguez, J.A.; Senanayake, S.D. Interfaces in Heterogeneous Catalytic Reactions: Ambient Pressure XPS as a Tool to Unravel Surface Chemistry, *J. Electron Spectros. & Related Phen.* **2017**, *221*, 28-43 **(Invited)**.
11. Liu, Z.; Senanayake, S.D.; Rodriguez, J.A. Catalysts for the steam reforming of ethanol and other alcohols”, in *Ethanol: Science and Engineering* (Elsevier) - Editors: Angelo Basile, Adolfo Iulianelli, Nejat T. Veziroglu, April (2017) **(Invited)**

2018:

12. Liu, S.; White, M.G.; Liu, P. Oxygen Reduction Reaction on Ag(111) in Alkaline Solution: A Combined Density Functional Theory and Kinetic Monte Carlo Study, *ChemCatChem* **2018**, *10*, 540-549. **(Cover art)**
13. Carrillo, P.; Shi, R. ; Teeluck, K.; Senanayake, S. D.; White, M. G.; Nano-Fe₂O₃ as Support and Promoter for Rh Catalysts for Ethanol Synthesis from Syngas Conversion, *ACS Catal.* **2018**, in press.

*** Jointly funded by this grant and other grants with leading intellectual contribution from this grant:*

2015:

- 14.** Mudiyansele, K.; Senanayake, S.D.; Ramirez, P.J. et al., Intermediates arising from the Water-Gas Shift Reaction over Cu Surfaces: From UHV to Near Atmospheric Pressure, *Topics in Catalysis*, **2015**, *58*, 271-280.
- 15.** Zhao, F.; Liu, Z.; Xu, W. et al, Pulse Studies to Decipher the Role of Surface Morphology in CuO/CeO₂ Nanocatalysts for the Water Gas Shift Reaction, *Catal. Lett.* **2015**, *145*, 808-815.
- 16.** Carrasco, J.; Lopez-Duran, D.; Liu, Z. et al, *In Situ* and Theoretical Studies for the Dissociation of Water on an Active Ni/CeO₂ Catalyst: Importance of Strong Metal-Support Interactions for the Cleavage of O-H bonds, *Angew. Chem. Int. Ed.* **2015**, *54*, 3917-3921.
- 17.** Posada-Perez, Vines, F.; Rodriguez, J.A.; F. Illas, F. Structure and Electronic Properties of Cu Nanoclusters Supported on Mo₂C(001) and MoC(001) Surfaces, *J. Chem. Phys.* **2015**, *143*, 1114704-1,5
- 18.** Yang, X.; Kattel, S.; Senanayake, S.D. et al, Low Pressure CO₂ Hydrogenation to Methanol over Gold Nanoparticles Activated on a CeO_x/TiO₂ Interface, *J. Am. Chem. Soc.* **2015**, *137*, 10104-10107.
- 19.** Graciani, J.; Yang, F.; Vidal, A.B. et al, When Ruthenia Met Titania: Achieving Extraordinary Catalytic Activity at Low Temperature by Nanostructuring of Oxide, *Phys. Chem. Chem. Phys.* **2015**, *17*, 26813-26818.
- 20.** Xu, W.; Ramirez, P.J.; Stacchiola, D.; Brito, J.L.; J.A. Rodriguez, J.A. The Carburization of Transition Metal Molybdates (M_xMoO₄, M= Cu, Ni or Co) and the Generation of Highly Active Metal/Carbide Catalysts for CO₂ Hydrogenation, *Catal. Lett.* **2015**, *145*, 1365-1373.
- 21.** Asara, G.G.; Ricart, J.M.; Rodriguez, J.A.; Illas, F. Exploring the Activity of Au/TiC(001) model Catalysts towards CO and CO₂ Hydrogenation, *Surf. Sci.* **2015**, *640*, 141-149.
- 22.** Yu, L.; Liu, Y.; Yang, F.; Evans, J.; Rodriguez, J.A.; P. Liu, P. CO Oxidation on Gold-Supported Iron Oxides: New Insights into Strong Oxide-Metal Interactions, *J. Phys. Chem. C*, **2015**, *119*, 16614-16622.
- 23.** Liu, Z.; Xu, W.; Yao, S.; Johnson-Peck, A.C. et al, Superior Performance of Ni-W-Ce Mixed-metal Oxide Catalysts for Ethanol Steam Reforming: Synergistic Effects of W- and Ni-dopants”, *J. Catal.* **2015**, *321*, 90-99.
- 24.** Rodriguez, J.A.; Liu, P.; Stacchiola, D.; Senanayake, S.D.; White, M.G.; Chen, J.G. Hydrogenation of CO₂ to Methanol: Importance of Metal-Oxide and Metal-Carbide Interfaces in the Activation of CO₂, *ACS Catal.* **2015**, *5*, 6696-6706.
- 25.** Liu, Z.; Duchon, T.; Wang, H. et al, Mechanistic Insights of Ethanol Steam Reforming over Ni-CeO_x(111): The Importance of Hydroxyl Groups for Suppressing Coke Formation, *J. Phys. Chem. C*, **2015**, *119*, 18248-18256.
- 26.** Guzmán, H.J.; Xu, W.; Stacchiola, D.; Vitale, G.; Scott, C.E.; Rodríguez, J.A.; Pereira-Almao, P. Formation of β-Mo₂C below 600 °C using MoO₂ nanoparticles as precursor, *J. Catal.* **2015**, *332*, 83-94.
- 27.** Liu, C.; Liu, P. Mechanistic Study of Methanol Synthesis from CO₂ and H₂ on a Modified model Mo₆S₈ cluster, *ACS Catal.* **2015**, *5*, 1004-1012.

28. Zhang, X.; Yu, S.; Qiao, L.; Zheng, W.; Liu, P. Stabilization of Pt Monolayer Catalysts under Harsh Conditions of Fuel Cells, *J. Chem. Phys.* **2015**, *142*, 194710.
29. Kuttiyiel, K.A.; Choi, Y.; Hwang, S.; Park, G.; Yang, T.; Su, D.; Sasaki, K.; Liu, P.; Adzic, R.R. Enhancement of the Oxygen Reduction on Nitride Stabilized Pt-M (M = Fe, Co, and Ni) Core-Shell Nanoparticle Electrocatalysts, *Nano Energy*, **2015**, *13*, 442-449.
30. Palomino, R.; Magee, J. W.; Llorca, J.; Senanayake, S. D.; White, M. G. The Effects of Fe-Rh Alloying on CO Hydrogenation to C₂₊ Oxygenates, *J. Catal.* **2015**, *329*, 87–94.
31. Vajda, S.; White, M. G. “Catalysis Applications of Size-selected Cluster Deposition,” *ACS Catal.*, **2015**, *5*, 7152–7176.
32. Nakayama, M.; Xue, M.; An, W.; Liu, P.; White, M. G. “Influence of Cluster-Support Interactions on Reactivity of Size-Selected Nb_xO_y Clusters,” *J. Phys. Chem. C* **2015**, *119*, 14756-14768.
- 2016**
33. Grinter, D.C.; Park, J.B.; Agnoli, S. et al, Water-gas Shift Reaction over Gold Nanoparticles Dispersed on Nanostructured CeO_x-TiO₂(110) Surfaces: Effects of High Ceria Coverage, *Surf. Sci.* **2016**, *650*, 34-46.
34. Senanayake, S.D.; Pappoe, N.A.; Nguyen-Phan, T.D. et al, Interfacial Cu⁺ Promoted Surface Reactivity: Carbon Monoxide Oxidation Reaction over Polycrystalline Copper-Titania Catalysts, *Surf. Sci.* **2016**, *652*, 206-218.
35. Senanayake, S.D.; Ramírez, P.J.; Waluyo, I. et al, Hydrogenation of CO₂ to Methanol on CeO_x/Cu(111) and ZnO/Cu(111) Catalysts: Role of the Metal-Oxide Interface and Importance of Ce³⁺ Sites, *J. Phys. Chem. C*, **2016**, *120*, 1778-1784.
36. Posada-Pérez, S.; Ramírez, P.J.; Gutiérrez, R.A. et al, The Conversion of CO₂ to Methanol on orthorhombic β-Mo₂C and Cu/β-Mo₂C Catalysts: Mechanism for Admetal-induced Change in the Selectivity and Activity, *Catal. Sci. & Tech.* **2016**, *6*, 6766-6772.
37. Jimenez-Orozco, C.; Florez, E.; Moreno, A.; Liu, P.; Rodriguez, J.A. Systematic Theoretical Study of Ethylene Adsorption on δ-MoC(001), TiC(001), and ZrC(001) Surfaces, *J. Phys. Chem. C*, **2016**, *120*, 13531-13536.
38. Liu, Z.; Grinter, D.C.; Lustemberg, P. et al. Dry Reforming of Methane on a Highly-Active Ni-CeO₂ Catalyst: Effects of Metal-Support Interactions on C–H Bond Breaking, *Angew. Chem. Int. Ed.* **2016**, *55*, 7455-7459.
39. Rodriguez, J.A.; Rousseau, R.; Stacchiola, D. et al, Catalytic Chemistry of Oxide Nanostructures, in: *Oxide Materials at the Two Dimensional Limit*, First ed.; F. Netzer, Fortunelli, A., Eds. Springer International: New York, 2016; pp 251-280. **(Invited)**
40. Liu, Z.; Duchon, T.; Wang, H.R. et al, Ambient pressure XPS and IRRAS investigation of ethanol steam reforming on Ni- CeO₂(111) catalysts: an in situ study of C-C and O-H bond scission, *Phys. Chem. Chem. Phys.* **2016**, *18*, 16621-16625.
41. Mudiyansele, K.; Luo, S.; Kim, H.Y. et al, How to Stabilize Highly Active Cu⁺ Cations in a Mixed-oxide Catalyst. *Catal. Today* **2016**, *263*, 4-17.

42. Nguyen-Phan, T.; Baber, A.E.; Rodriguez, J.A.; Senanayake, S.D. Au and Pt Nanoparticle Supported Catalysts Tailored for H₂ Production: From Models to Powder Catalysts, *Applied Catalysis A: Gen.* **2016**, *518*, 18-32.
43. Plata, J.J.; Graciani, J.; Evans, J.; Rodriguez, J.A.; Fernandez-Sanz, J. Cu Deposited on CeO_x-Modified TiO₂(110): Synergistic Effects at the Metal– Oxide Interface and the Mechanism of the WGS Reaction. *ACS Catal.* **2016**, *6*, 4608.
44. Posada-Pérez, S.; Ramírez, P.J.; Evans, J.; Viñes, F.; Liu, P.; Illas, F.; Rodriguez, J. A. Highly Active Au/ δ -MoC and Cu/ δ -MoC Catalysts for the Conversion of CO₂: The Metal/C Ratio as a Key Factor Defining Activity, Selectivity, and Stability, *J. Am. Chem. Soc.* **2016**, *138*, 8269-8274.
45. Grinter, D.; Remensal, E.R.; Luo, S. et al. Potassium and Water Co-Adsorption on TiO₂(110): OH-Induced Anchoring of Potassium and the Generation of Single-Site Catalysts, *J. Phys. Chem. Lett.* **2016**, *7*, 3866-3870.
46. Zuo, Z.; Ramirez, P.J.; Senanayake, S.D.; Liu, P.; Rodriguez, J.A. The Low-temperature Conversion of Methane to Methanol on CeO_x/Cu₂O Catalysts: Water Controlled Activation of the C-H Bond, *J. Am. Chem. Soc.* **2016**, *138*, 13810-13814.
47. Lustemberg, P.; Ramirez, P.J.; Liu, Z. et al, Room Temperature Activation of Methane and Dry Reforming with CO₂ on Ni-CeO₂(111) Surfaces: Effect of Ce³⁺ Sites and Metal-Support Interactions on C-H bond Cleavage, *ACS Catal.* **2016**, *6*, 8184-8189.

2017

48. Xue, M.; Nakayama, M.; Liu, P.; White, M.G. Electronic Interactions of Size-Selected Oxide Clusters on Metallic and Thin Film Oxide Supports, *J. Phys. Chem. C*, **2017**, *121*, 22234–22247.
49. Posada-Pérez, S.; Viñes, F.; Valero, R.; Rodriguez, J.A.; Illas, F. Adsorption and dissociation of molecular hydrogen on orthorhombic β -Mo₂C and cubic α -MoC(001) surfaces, *Surf. Sci.* **2017**, *656*, 24-29.
50. Luo, S.; Barrio, L; Nguyen-Phan, T.-D. et al, Importance of Low Dimensional CeO_x Nanostructures in Pt/CeO_x-TiO₂Catalysts for the Water–Gas Shift Reaction, *J. Phys, Chem. C*, **2017**, *121*, 6635-6640.
51. Jimenez-Orozco, C.; Florez, E.; Moreno, A.; Liu, P.; Rodriguez, J.A. Acetylene Adsorption on δ -MoC(001), TiC(001) and ZrC(001) Surfaces: A Comprehensive Periodic DFT Study, *Phys. Chem. Chem. Phys.* **2017**, *19*, 1571-1576.
52. Posada-Perez, S.; Ramirez, P.J.; Gutierrez R.A. et al, The Conversion of CO₂ to Methanol on Orthorhombic β -Mo₂C and Cu/ β -Mo₂C Catalysts: Mechanism for Admetal Induced Change in the Selectivity and Activity, *Catal. Sci. & Technol.* **2016**, *6*, 6766-6774.
53. Rodriguez, J.A.; Ramirez, P.J.; Gutierrez, R.A. Highly Active Pt/MoC and Pt/TiC Catalysts for the Low-Temperature Water-gas Shift Reaction: Effects of the Carbide Metal/Carbon Ratio on the Catalyst Performance, *Catal. Today* **2017**, *289*, 47-58.

- 54.** Guild, C.J.; Vovchok, D.; Kriz, D.A. et al, Water-Gas-Shift over Metal-Free Nanocrystalline Ceria: An Experimental and Theoretical Study, *Chem. Cat. Chem.* **2017**, *9*, 1373.
- 55.** Palomino, R.; Stavitski, E.; Waluyo, I. et al, New In-Situ and Operando Facilities for Catalysis Science at NSLS-II: The Deployment of Real-Time, Chemical, and Structure-Sensitive X-ray Probes, *Synchrotron Radiation News*, **2017**, *30*, 30-44 (**Invited**).
- 56.** Vovchok, D.; Guild, C.J.; Llorca, J. et al, Cu Supported on Mesoporous Ceria: Water-gas Shift Activity at Low Cu Loadings through Metal–Support Interactions, *Phys. Chem. Chem. Phys.* **2017**, *19*, 17708-17713.
- 57.** Yao, S.; Zhang, X.; Xhou, W. et al, Atomic layered Au clusters on α -MoC as catalyst for the low temperature water gas shift reaction, *Science*, **2017**, *357*, 389-393.
- 58.** Liu, Z.; Lustemberg, P.; Gutierrez, R.A. et al, In-situ Investigation of Methane Dry Reforming on M-CeO₂(111) {M= Co, Ni, Cu} Surfaces: Metal-Support Interactions and the activation of C-H bonds at Low Temperature, *Angew. Chem. Int. Ed.* **2017**, *56*, 13041-13045.
- 59.** Posada-Pérez, S.; Gutiérrez, R.A.; Zuo, Z. et al, Highly active Au/ δ -MoC and Au/ β -Mo₂C catalysts for the Low-temperature Water Gas Shift Reaction: Effects of the Carbide Metal/Carbon Ratio on the Catalyst Performance, *Catal. Sci. & Technol.* **2017**, *7*, 5332-5339.
- 60.** An, W.; Men, Y.; Wang, J.; Liu, P. Interfacial and Alloying Effects on Activation of Ethanol from First Principles, *J. Phys. Chem. C*, **2017**, *121*, 5603–5611.
- 61.** Lu, F.; Zhang, Y.; Liu, S. et al, Surface Proton Transfer Promotes Four-Electron Oxygen Reduction on Gold Nanocrystal Surfaces in Alkaline Solution, *J. Am. Chem. Soc.* **2017**, *139*, 7310–7317.
- 62.** Vukmirovic, M.B.; Teeluck, K.M.; Liu, P.; Adzic R.R. Single Platinum Atoms Electrocatalysts: Oxygen Reduction and Hydrogen Oxidation Reactions, *Croatica Chemica Acta*, **2017**, *90*, 1-6.
- 2018**
- 63.** Palomino, R.M.; Ramirez, P.J.; Liu, Z. et al, Hydrogenation of CO₂ on ZnO/Cu(100) and ZnO/Cu(111) Catalysts: Role of Copper Structure and Metal-Oxide Interface in Methanol Synthesis, *J. Phys. Chem. B*, **2018**, *122*, 794-798.
- 64.** Jimenez-Orozco, C.; Florez, E.; Moreno, A.; Liu P.; Rodriguez, J.A. Acetylene and Ethylene Adsorption on a β -Mo₂C(100) Surface: A Periodic DFT Study on the Role of C- and Mo-terminations for Bonding and Hydrogenation Reactions, *J. Phys. Chem. C*, **2017**, *121*, 19786-19791.

65. Rodriguez, J.A.; Grinter, D.C.; Ramírez, P.J. et al, High Activity of Au/K/TiO₂(110) for CO Oxidation: Alkali Enhanced Dispersion of Au and Bonding of CO, *J. Phys. Chem. C*, **2018**, *122*, 4324-4328.
66. Hamlyn, R.C.E.; Mahapatra, M.; Grinter, D.C. et al, Imaging the Ordering of a Weakly Adsorbed Two-Dimensional Condensate: Ambient-Pressure Microscopy and Spectroscopy of CO₂ Molecules on Rutile TiO₂(110), *Phys. Chem. Chem. Phys.* **2018**, in press, DOI: 10.1039/C8CP01614C.
67. Kunkel, C.; Viñes, F.; Ramírez, P.J.; Rodriguez, J.A.; Illas, F. Combining Theory and Experiment for Multitechnique Characterization of Activated CO₂ on Transition Metal Carbide (001) Surfaces, *J. Phys. Chem. C*, **2018**, in press, DOI: 10.1021/acs.jpcc.7b12227.
68. Vovchok, D.; Guild, C.; Senanayake, S.D. et al, Characterization of Mesoporous Co/CeO₂ Catalysts for the High Temperature Water-Gas Shift, *J. Phys. Chem. C*, **2018**, in press.
69. Zhang, F.; Liu, Z.; Zhang, S. et al, *In-situ* Elucidation of the Active State of Co-CeO₂ Catalysts in the Dry Reforming of Methane: The Important Role of the Reducible Oxide Support and Interactions with Cobalt, *ACS Catal.* **2018**, in press.
70. Lin, L.; Yao, S.; Liu, Z. et al, *In-situ* Characterization of Cu/CeO₂ Nanocatalysts for CO₂ Hydrogenation: Morphological Effects of Nanostructured Ceria on the Catalytic Activity, *J. Phys. Chem. C*, **2018**, in press.
71. Ma, Z.; Zhang, Y.; Liu, S. et al, Reaction Mechanism for Oxygen Evolution on RuO₂, IrO₂, and RuO₂@IrO₂ Core-shell Nanocatalysts, *J. Electroanal. Chem.* **2018**, *819*, 296-305.

FWP ERKCC96: Fundamentals of Catalysis and Chemical Transformations

PIs: Zili Wu, Miaofang Chi, Sheng Dai, De-en Jiang (UC-Riverside), Stephan Irlle, David R. Mullins, Aditya (Ashi) Savara, Huiyuan Zhu

Postdoc(s): Zhenghong Bao, Guo Shiou Foo, Runhong Huang (UC-Riverside), Felipe Polo Garzon, Chengcheng Tian, Yafen Zhang,

Student(s): Victor Fung (UC-Riverside), Michelle Lukosi

Affiliation (s): Oak Ridge National Laboratory

RECENT PROGRESS

The overarching goal of this project is to understand how to control reaction pathways through tuning synergism in multi-functional catalysts with well-defined structures. The vision of our research is that by fundamentally understanding the composition, structure and interaction of catalytic sites and the reaction pathways, we will be able to precisely assemble different catalytic sites/entities into a synergistic catalyst to achieve the desired level of selectivity and activity in multi-step reactions. Specifically, we will elucidate the synergism among site geometry, surface and bulk composition, acid-base and redox sites, and metal-support interactions in controlling reactivity, selectivity and stability in reactions catalyzed by oxide surfaces and supported metal particles. We summarize here our recent progress along these lines. To understand the catalytic consequence of composition and structure of oxides, we choose perovskites as the model ternary oxides because of the wide tunability of the A and B cations in ABO_3 perovskites that can result in tunable catalytic chemistry. One of the foci of our research is to understand surface reconstruction behaviors of complex oxides by investigating both model single crystal, thin film surfaces and nanoshaped particles of perovskites. From these studies, we learned about the importance of the synergy among different surface sites and between surface and subsurface in catalyzing acid-base and redox reactions and how to take advantage of surface reconstruction to achieve the synergism. We have also investigated how to tune the synergism at the interface between metal and support to stabilize metal particles and enhance their catalytic reactivity. These include utilizing perovskite as a support to stabilize single atoms and bimetallic particles, core-shell structures to enhance metal-support interactions and utilizing interfacial charge flow from novel support to metal nanoparticles for enhanced catalysis.

Composition and structure effect in oxide catalysis

The goal of this part of work is to achieve a fundamental understanding of how acid-base and redox sites on oxide surfaces work synergistically to control reaction pathways and catalytic selectivity. We hypothesize that this can be achieved via tuning the surface structure and composition of oxides and probed by studying the adsorption and reaction of oxygenates and hydrocarbons over ternary oxides including perovskites and mixed oxides where both surface and bulk structure and composition can be widely tuned. We have used the comparison of oriented film vs shaped nanocrystals to probe structure-function relationships in oxide catalysis. A key focus was to understand the impact of *surface reconstruction* of complex oxides on both acid-base and redox reactions. For nanoshaped particles, similar reactions were studied via reaction kinetic measurements, DRIFTS/Raman, microcalorimetry, and inelastic neutron scattering (INS). We probed the surface species over thin film surfaces with ambient pressure x-ray photoelectron

spectroscopy (AP-XPS) and the desorption products in TPD. DFT has enhanced our understanding of the reaction mechanism, the surface structure and composition of perovskites and provided predictive catalytic descriptors. Together these studies have led to a detailed description of reaction pathways of model oxygenates and understanding of the synergism among various catalytic sites over complex oxides where surface reconstruction cannot be underestimated.

Surface reconstruction overrides facet effect of perovskite in acid-base catalysis. Shape-controlled nanocrystals of oxides have shown to be good models for understanding oxide catalysis because they display specific crystallographic faces. However, such studies have been focused primarily on single component oxides and have not been reported for complex oxides. We studied *for the first time* the acid-base reactivity of the (001) and (110) crystal facets of a model perovskite, strontium titanate by using dehydrogenation of ethanol as a probe reaction over various shape-controlled SrTiO₃ (STO) nanocrystals (Foo *et al.*, 2018).²⁴ Cubes, Truncated Cubes, Dodecahedra, and Etched Cubes STO with varying ratios of (001) and (110) crystal facets are synthesized and their surface acid-base properties were characterized. Kinetic, isotopic, and spectroscopy methods show that the dehydrogenation of ethanol proceeds through the facile dissociation of the alcohol group, followed by the cleavage of the C_α-H bond over an acid-base pair. Rigorous turnover rates, obtained through kinetic measurements and chemical titration of active sites, allow the comparison of activity between the various shape-controlled STO nanocrystals. The results show that ethanol turnover rate is not directly correlated to the percentage of either surface facet ((001) or (110)) of the STO nanocrystals. Instead, the reaction rate is found to increase with the strength of acid sites but decrease with the strength of base sites (**Figure 1**). The acid-base property is directly related to the surface composition as a result of different surface reconstruction behaviors of the three shaped STO nanocrystals. The finding here underscores the importance of characterizing the top surface compositions and sites properties ideally under reaction conditions when assessing the catalytic performance of shape-controlled complex oxides such as perovskites.

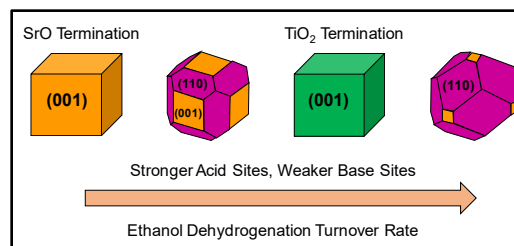


Figure 1. Illustration of ethanol reactivity trend over shape-controlled STO particles.

Surface reconstruction of perovskites improves redox catalysis. Taking advantage of our understanding of surface reconstruction behavior of perovskites from acid-base catalysis, we investigated the impact that the reconstruction of surface and subsurface monolayers of perovskite catalysts has on redox reaction such as methane combustion, using SrTiO₃ (STO) as a model perovskite. Several STO samples obtained through different synthesis methods and subjected to different post-synthesis-treatments were tested for methane combustion. Through top surface characterization, kinetic experiments (including isotope labelling experiments) and density functional theory (DFT) calculations, it is shown that both surface segregation of Sr and creation of step-surfaces of STO (**Figure 2**) can impact the rate of methane combustion over an order of magnitude. Applying these STO catalysts to oxidative coupling of methane also shows that surface segregation of Sr and the co-existence of Sr-O-Ti moiety at the subsurface play an important role in determining the C₂ including ethane and ethene selectivity. This work highlights the possibility of utilizing and tuning the surface reconstruction of perovskites for efficient methane activation and conversion.

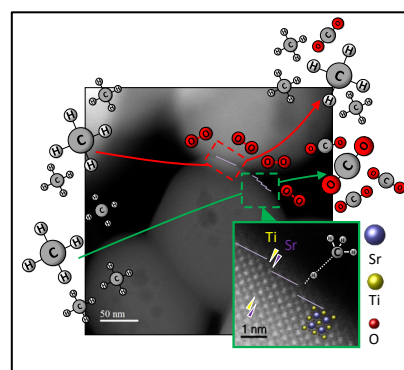


Figure 2. Illustration of methane activation on reconstructed STO surfaces.

Descriptors of catalytic activity of perovskites for methane activation from DFT prediction. Parallel to our experimental effort in understanding methane conversion over a limited selection of perovskites, our DFT effort aims at finding general principles for methane activation over a wide range of perovskites. By building upon the compositional diversity of the perovskites, we establish catalytic descriptors based on DFT to correlate with the key reaction steps of methane activation on the oxide surfaces. From the analysis of first and second C-H activation energies and their correlation with the hydrogen adsorption energy on a variety of ABO_3 perovskites, general trends emerge that an optimal range of hydrogen adsorption energy strikes the right balance between easy first C-H activation and difficult second C-H activation energies to avoid further oxidation. Moreover, the tradeoff between first C-H bond breaking and methyl desorption suggests a sweet-spot in oxygen reactivity for oxidative methane coupling. This study (Fung *et al.*, 2018)²⁵ presents an initial attempt toward addressing the compositional diversity of perovskites in the context of energetic descriptors as well as methane activation. Experimental verification of the predicted trend is underway using methane combustion as the model reaction.

Effect of surface reconstruction on the catalytic behavior of perovskite thin films. Doping an

additional A -cation (A') into the perovskite lattice can alter the catalytic behavior of the non-doped perovskite by altering the strain of the lattice, changing the oxidation state of B or introducing O -vacancies if A and A' have different oxidation states, or through different compositional terminations at the surface. We explored this

effect by synthesizing a series Sr-doped $La_{1-x}Sr_xMnO_3(001)$ ($x = 0, 0.3, 0.7$) (LSMO) thin films grown on single crystal $SrTiO_3(001)$ by pulsed laser deposition (PLD). The catalytic oxidation of methanol, ethanol and 2-propanol, and acetic acid was characterized by temperature programmed desorption/decomposition (TPD) and temperature programmed reaction (TPR) in an ultrahigh vacuum environment. TPD of all three alcohols indicated that the LSMO was essentially unreactive with only the adsorbed alcohol desorbing below 300 K. $LaMnO_3$ (LMO) was much more reactive and the activity increased as the size of the alcohol increased, i.e. 2-propanol > ethanol > methanol. The product distribution indicated that the LMO was primarily redox in behavior with ethanol and 2-propanol producing primarily acetaldehyde and acetone, respectively. TPR produced very different results from the TPD. As shown in **Figure 3**, both surfaces demonstrated 2-propanol oxidation activity (similar behavior was observed for methanol and ethanol). LMO is clearly more active than LSMO. Further, the reaction products primarily indicated dehydration to propylene rather than dehydrogenation to acetone as observed in TPD. The relative activity of the two surfaces and the change in product distribution between TPD and TPR can be ascribed to the different surface

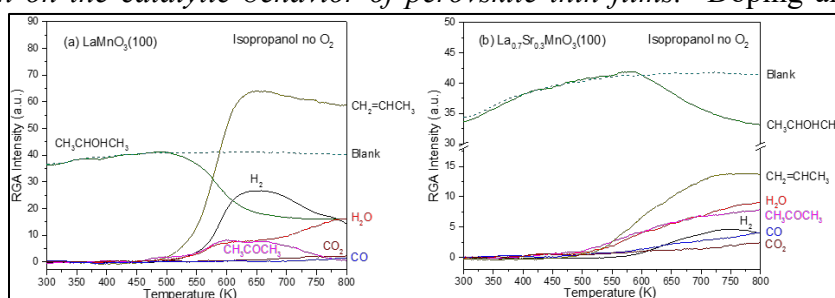
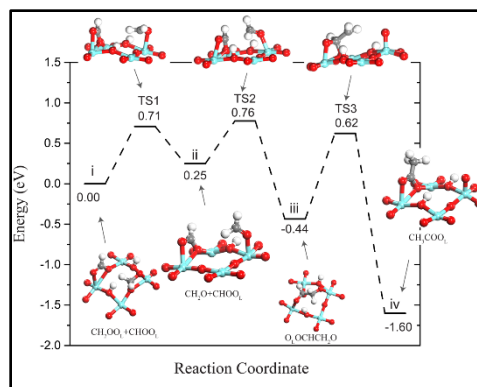


Figure 3. Temperature programmed reaction of 2-propanol on (a) $LaMnO_3(100)$ and (b) $La_{0.7}Sr_{0.3}MnO_3(100)$

effect by synthesizing a series Sr-doped $La_{1-x}Sr_xMnO_3(001)$ ($x = 0, 0.3, 0.7$) (LSMO) thin films grown on single crystal $SrTiO_3(001)$ by pulsed laser deposition (PLD). The catalytic oxidation of methanol, ethanol and 2-propanol, and acetic acid was characterized by temperature programmed desorption/decomposition (TPD) and temperature programmed reaction (TPR) in an ultrahigh vacuum environment. TPD of all three alcohols indicated that the LSMO was essentially unreactive with only the adsorbed alcohol desorbing below 300 K. $LaMnO_3$ (LMO) was much more reactive and the activity increased as the size of the alcohol increased, i.e. 2-propanol > ethanol > methanol. The product distribution indicated that the LMO was primarily redox in behavior with ethanol and 2-propanol producing primarily acetaldehyde and acetone, respectively. TPR produced very different results from the TPD. As shown in **Figure 3**, both surfaces demonstrated 2-propanol oxidation activity (similar behavior was observed for methanol and ethanol). LMO is clearly more active than LSMO. Further, the reaction products primarily indicated dehydration to propylene rather than dehydrogenation to acetone as observed in TPD. The relative activity of the two surfaces and the change in product distribution between TPD and TPR can be ascribed to the different surface



reconstruction-resulted terminations of LMO (enriched in Mn) and LSMO (enriched in Sr) as probed by energy dependent XPS analysis. The reducible, weakly acidic MnO₂ is more active than the non-reducible, more basic SrO, which explains well the TPD and TPR results.

DFT insights into C-C coupling over perovskite surface. Understanding how different surface sites work to direct the interaction of difference surface species is essential for designing catalysts for coupling reactions. C-C coupling of oxygenates is relevant to many important processes such as methanol-to-olefin and ethanol-to-higher-alcohols. Although zeolites and transition metals are commonly used for the conversion, oxides such as perovskites are much less explored. Especially, the tunability of the perovskite composition provides a great many opportunities for exploring oxygenate chemistry. To this end, we recently observed by surprise formation of acetate on the SrTiO₃(100) surface from C-C coupling of methanol via ambient-pressure XPS.²⁵ To understand how this coupling takes place and how it relates to the termination of the SrTiO₃(100) surface, we have performed a detailed DFT study of the surface chemistry of methanol on both the A and B terminations of the SrTiO₃(100) surface (Huang *et al.*, 2018).²⁸ We were able to find out the most likely pathways for the coupling reactions, and more important, we found that the B termination can greatly facilitate the acetate formation from coupling of the CH₂O and CHO intermediates (**Figure 4**). Our findings can well explain the observations from the ambient-pressure XPS spectrum and shed new light on designing perovskite surfaces for oxygenate coupling reactions.

Figure 4. The reaction pathway of C-C coupling between CH₂O and CHO groups on the SrTiO₃(100) B termination. Color code: Ti, cyan; O, red; C, dark gray; H, white. Only the surface layer is shown.

Neutron spectroscopy of surface chemistry on mixed oxide catalysts. In the conversion of hydrocarbon and oxygenates over oxide surfaces, hydrogen transfer is commonly involved in the dehydration, dehydrogenation and oxidation reactions. To understand how an oxide manages surface hydrogen, we studied CO₂ hydrogenation – reverse water gas shift reaction (RWGS) and forward WGS over a commercial CuCrFeOx catalyst with various in situ spectroscopy including neutron spectroscopy (INS), IR and AP-XPS. The reaction mechanism of high temperature (HT) WGS over CuCrFeOx remains unclear and has no spectroscopic support for either redox or associative pathways (via formate HCOO or COOH intermediate). Both IR and AP-XPS did not show strong evidence for any H-containing surface species during the reaction. Interestingly, INS gave clear signal for surface hydride and OH species (see **Figure 5**) and possible presence of surface formate species. Combined with SSITKA study of the CO – H₂O and CO- H₂¹⁸O switches at steady state condition at different reaction temperatures, we are able to conclude that the HTWGS reaction proceed mostly via a redox mechanism with less contribution from the associative route, which is currently under verification by DFT calculations. This is for the first time the reaction mechanism is clearly revealed for the important HTWGS reaction over a commercial CuCrFeOx catalyst.

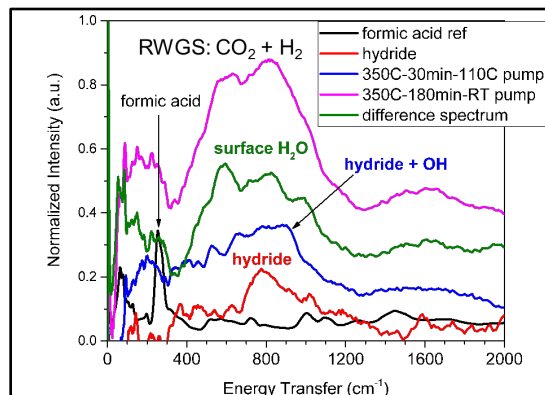


Figure 5. INS spectra collected at 10 K over CuCrFeOx catalyst after RWGS at 350°C. Reference spectra from water, hydride and formic acid are also shown for comparison.

Tuning metal-support interface for enhanced stability and catalysis

The goal of this part of work is to understand how synergism can be tailored at the metal-support interface to control catalytic activity and selectivity and stability. Our hypothesis is the long-range synergism arising from the chemical and electronic interactions between metal nanoparticles and oxides can provide an amplification of catalytic activity, selectivity and/or stability of the supported metal centers. In the past year, we have explored various ways to tailor the interfacial structure and electronic property to achieve highly stable metal single atoms and nanoparticles (NPs) with enhanced catalytic reactivity and selectivity.

Ultra-stable and active single Au atoms and AuPd intelligent particles on perovskite support. We hypothesize that the unique ability of perovskites in stabilizing noble metal NPs can be extended to stabilize single atoms (SAs). We have recently shown that small Au NPs supported on LaFeO₃-MCF (mesoporous cellular foam silica) displayed high sintering-resistance, catalytic activity and stability for CO oxidation, thanks to the strong interfacial interaction from the heterostructured perovskite. The observed ultrastability of the supported metal NPs prompted us to investigate how the strong interfacial interactions can be utilized to anchor the often-unstable SAs on perovskite supports to form a highly stable and reactive catalytic active center with desired catalytic performance. We found that it is possible stabilize even single atom Au over the heterostructured LaFeO₃ surface up to 700 °C. DFT calculations showed Au single atom bind to the LaFeO₃ surface much stronger than to the TiO₂ surface, supporting the observation of high sintering resistance. The designed Au single-atom catalysts not only demonstrated sintering-resistance but also showed high catalytic activity and unique “reversible” self-regeneration under reaction conditions, suggesting great potential for practical applications. Mechanistic studies confirmed that the surface Au active sites are predominately positively charged and the reaction pathways over this Au SAC system follow both redox and Langmuir-Hinshelwood (LH) mechanisms for CO oxidation.

Pd/perovskite is a well-known intelligent catalytic system with reversible movement of Pd species in and out of perovskite a function of oxidizing/reducing conditions at high temperatures. We hypothesize that an intelligent bimetallic system can be made based on Pd to control catalytic activity and selectivity. We recently demonstrated the intelligent behaviors of AuPd bimetallic systems supported on the heterostructured LaFeO₃ surface (**Figure 6**). Different reduction and oxidation conditions were systematically applied to induce the migration of Pd species to interfaces for controlling AuPd particle compositions. The catalytic consequence of alloying was probed with selective hydrogenation of acetylene. Due to the drastic difference in ability to activate H₂ between Pd and Au, the alloying and de-alloying of Pd with Au NPs were found to impact the activity and selectivity significantly, confirming the intelligent behavior of the bimetallic AuPd system as also supported by STEM and EXAFS studies. We envision that the new type of intelligent bimetallic catalysts can be utilized to tune the catalytic chemistry and reaction pathways in more complex reactions.

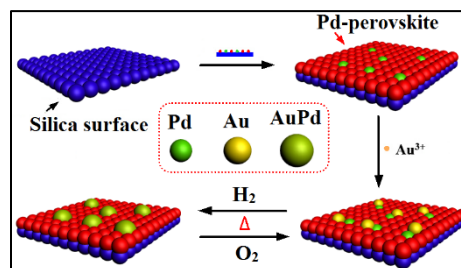


Figure 6. Schematic illustration of the AuPd-LaFeO₃-MCF preparation and intelligent behavior.

Stabilization of single metal sites through high entropy oxide. In addition to perovskite support, we also explored new strategy to stabilize active metal centers. Our hypothesis was that introduction of noble metals into an appropriate mixed metal oxide solid solution would afford a randomly dispersed, homogeneous system of single atoms which are entropically stabilized at elevated temperatures. Recently, we report (Chen *et al.*, 2018)²³ the successful preparation of an entropy-stabilized, single-phase, mixed oxide (NiMgCuZnCoOx) supported Pt high-temperature catalyst as shown in **Figure 7**. The single-phase and entropically-driven stability of the PtNiMgCuZnCoOx (0.3 wt% Pt) endowed the catalyst with a superior activity for CO oxidization, even after treatment at 900 °C. We expect that this exciting new synthetic approach will hold great promise for the development of stabilized single atom materials for high temperature reactions such as methane oxidative coupling which is currently under study.

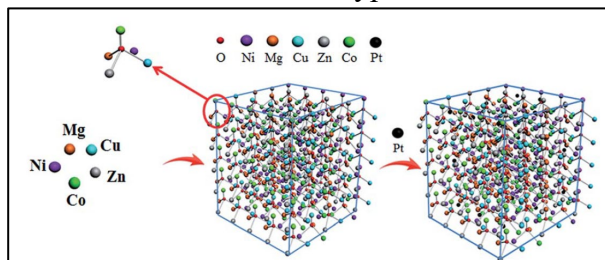


Figure 7. Scheme of the formation of 0.3 wt% PtNiMgCuZnCoOx entropy-stabilized metal oxide solid solution.

Stabilization of metal particles through core-shell nanoarchitectures. Although Metal – oxide core-shell architectural strategy has been employed for inhibition of metal sintering, it often results in a decrease of activity of the metal centers due to physical blockage by the oxide. We recently developed a “double confinement” strategy, which both enhanced metal oxide interaction via solid solution and core-shell confinement, through confinement of ultrathin Pd-CeOx nanowire (2.4 nm) within SiO₂ (Peng *et al.*, 2018).⁵⁶ These “doubly confined” catalysts enable CH₄ total oxidation at a low temperature of 350 °C, much lower than that of a commercial Pd/Al₂O₃ catalyst (425 °C). Importantly, unexpected stability was observed even under harsh conditions (800 °C, water vapor, and SO₂), owing to the confinement and shielding effect of the porous silica shell together with the promotion of CeO₂. This strategy can lead to the design of more active and stable metal catalysts for use under severe conditions.

Controlling catalytic selectivity with a yolk-shell system. The yolk-shell structure is generally used to stabilize metal centers, here we demonstrate that it is also possible to utilize such structure to control catalytic selectivity. By developing a unique structure of yolk-shell Pd-FeO_x system, we explored the catalytic consequence on catalytic hydrogenation of acetylene in such a confined system because it not only introduces the electronic effect (change of d-band center of Pd by FeO_x) but also geometric effect (the spatial confinement) at the interface (**Figure 8**). Several parameters have been controlled, including the shell thickness and the volume of the voids to allow the accessibility of the Pd sites. The optimized structure shows a highly selective hydrogenation of acetylene to ethylene under mild conditions as compared to supported Pd catalyst. The FeO_x oxide shell may constrain core expansion, suppressing the formation of β-hydride as confirmed by neutron spectroscopy study, while voids in the shell still provide abundant active sites for adsorption, leading to the highly selective hydrogenation to ethylene.

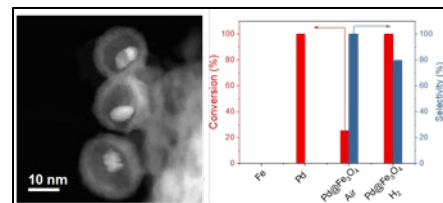


Figure 8. The unique Pd-FeO_x yolk-shell structure demonstrates high selectivity in C₂H₂ hydrogenation.

Controlling the degree of charge transfer at metal – support interface. Surface charge state of metal catalysts plays a vital role in heterogenous catalysis as it regulates the adsorption and activation of reactants and intermediates. To date, it remains obscure as how to maneuver the surface charge state of metal catalysts to improve catalytic activity and selectivity. We recently demonstrated a scenario of “Mott-Schottky modulated catalysis” on Pt nanoparticles (NPs) via an electron-donating carbon nitride (CN) support (**Figure 9**). The Fermi level of CNs were controlled by our synthetic conditions. By adjusting the relative Fermi levels of CNs and Pt NPs, we can control the degree of charge transfer from CN to Pt. Exemplified by the CO oxidation catalysis, in which the excess negative charge on Pt acts as a double-edged sword: on the one hand, the negatively-charged Pt brings in an enhanced CO activation and dissociative adsorption of O₂, on the other hand, Pt–CO bond is strengthened, leading to a “CO poisoning” on Pt; here we discovered that a properly-charged Pt by CN is an excellent catalyst for CO oxidation with an initial conversion temperature as low as 25 °C and a total CO conversion below 85 °C. Additionally, we

found that the deeply charged Pt NPs by CN with a higher Fermi level is opposite to the improvement of catalysis, proving an indispensable role of the degree of charge transfer. This study shed light on how to regulate the degree of charge transfer at metal-support interface to impact catalytic activity. The follow-up study will be focused on how to utilize the charge transfer at the interface to control reaction pathways in multi-step reactions.

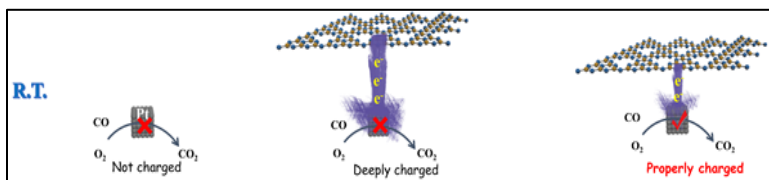


Figure 9. Schematics of a “Mott–Schottky modulated catalysis” on Pt nanoparticles via an electron–donating carbon nitride support with a tunable Fermi level.

DFT prediction of charge transfer at metal – support interface. To explore novel routes to control the charge transfer at metal – support interface and thus catalytic activity and selectivity, we propose an interface-engineering design where the transition-metal surface is covered by a monolayer of two-dimensional atomically thin material such as hexagonal boron nitride (h-BN). We show from first principles DFT that this h-BN layer can effectively suppress hydrogen adsorption, but adsorption of some oxygen-containing intermediates channel is not affected due to the charge transfer between h-BN and the underlying metal that provides the binding site for the oxygen-containing intermediates (Hu *et al.*, 2018).²⁶ Specifically, we predict h-BN/Ni and h-BN/Co to be very good catalysts for CO₂ reduction to HCOOH, while filtering out the hydrogen evolution channel. This charge-transfer interface design could be very instrumental for experimental efforts in controlling catalytic selectivity using supported metal catalysts.

Publications Acknowledging this Grant in the past three years (July 2015 – June 2018)

(XVIII) Exclusively funded by this grant:

1. Zhang, P.; Lu, H.; Zhou, Y.; Zhang, L.; Wu, Z.; Yang, S.; Shi, H.; Zhu, Q.; Chen, Y.; Dai, S., Mesoporous Mncox Solid Solutions for Low Temperature and Selective Oxidation of Hydrocarbons. *Nature Communications* **2015**, *6*, 8446.
2. Zhu, H.; Wu, Z.; Su, D.; Veith, G. M.; Lu, H.; Zhang, P.; Chai, S.-H.; Dai, S., Constructing Hierarchical Interfaces: TiO₂-Supported PtFe–FeOx Nanowires for Room Temperature CO Oxidation. *Journal of the American Chemical Society* **2015**, *137*, 10156-10159.

3. Zhu, H.; Zhang, P.; Dai, S., Recent Advances of Lanthanum-Based Perovskite Oxides for Catalysis. *ACS Catalysis* **2015**, *5*, 6370–6385.
4. Beste, A.; Overbury, S. H., Dehydrogenation of Methanol to Formaldehyde Catalyzed by Pristine and Defective Ceria Surfaces. *Physical Chemistry Chemical Physics* **2016**, *18*, 9990-9998.
5. Lukosi, M.; Zhu, H. Y.; Dai, S., Recent Advances in Gold-Metal Oxide Core-Shell Nanoparticles: Synthesis, Characterization, and Their Application for Heterogeneous Catalysis. *Frontiers of Chemical Science and Engineering* **2016**, *10*, 39-56.
6. Mullins, D. R., The Interaction of Carbon Monoxide with Rhodium on Potassium-Modified CeO₂(111). *Surface Science* **2016**, *652*, 238-246.
7. Mullins, D. R., SO₂ Adsorption on CeO₂(100) and CeO₂(111). *Topics in Catalysis* **2016**, 1-9.
8. Savara, A., Comment on "Equilibrium Constants and Rate Constants for Adsorbates: Two-Dimensional (2D) Ideal Gas, 2D Ideal Lattice Gas, and Ideal Hindered Translator Models". *J Phys Chem C* **2016**, *120*, 20478-20480.
9. Savara, A., Simulation and Fitting of Complex Reaction Network Tpr: The Key Is the Objective Function. *Surface Science* **2016**, *653*, 169-180.
10. Tian, C. C.; Zhu, X.; Abney, C. W.; Tian, Z. Q.; Jiang, D. E.; Han, K. S.; Mahurin, S. M.; Washton, N. M.; Dai, S., Use of Steric Encumbrance to Develop Conjugated Nanoporous Polymers for Metal-Free Catalytic Hydrogenation. *Chemical Communications* **2016**, *52*, 11919-11922.
11. Wu, Z.; Hu, G.; Jiang, D.E.; Mullins, D. R.; Zhang, Q.-F.; Allard, L. F.; Wang, L.-S.; Overbury, S. H., Diphosphine-Protected Au₂₂ Nanoclusters on Oxide Supports Are Active for Gas-Phase Catalysis without Ligand Removal. *Nano Letters* **2016**, *16*, 6560-6567.
12. Yue, Y. F.; Zhang, L.; Chen, J. H.; Hensley, D. K.; Dai, S.; Overbury, S. H., Mesoporous xEr₂O₃.CoTiO₃ Composite Oxide Catalysts for Low Temperature Dehydrogenation of Ethylbenzene to Styrene Using CO₂ as a Soft Oxidant. *RSC Adv.* **2016**, *6*, 32989-32993.
13. Beste, A., Methanol Adsorption and Dissociation on LaMnO₃ and Sr Doped LaMnO₃ (001) Surfaces. *Surface Science* **2017**, *664*, 155-161.
14. Foo, G. S.; Hu, G.; Hood, Z. D.; Li, M.; Jiang, D.E.; Wu, Z., Kinetics and Mechanism of Methanol Conversion over Anatase Titania Nanoshapes. *ACS Catalysis* **2017**, *7*, 5345-5356.
15. Foo, G. S.; Polo-Garzon, F.; Fung, V.; Jiang, D.E.; Overbury, S. H.; Wu, Z., Acid–Base Reactivity of Perovskite Catalysts Probed Via Conversion of 2-Propanol over Titanates and Zirconates. *ACS Catalysis* **2017**, *7*, 4423-4434.
16. Fung, V.; Jiang, D.E., Exploring Structural Diversity and Fluxionality of Pt_n (n = 10–13) Clusters from First-Principles. *The Journal of Physical Chemistry C* **2017**.
17. Gill, L.; Beste, A.; Chen, B.; Li, M.; Mann, A. K. P.; Overbury, S. H.; Hagaman, E. W., Fast Mas 1h Nmr Study of Water Adsorption and Dissociation on the (100) Surface of Ceria Nanocubes: A Fully Hydroxylated, Hydrophobic Ceria Surface. *The Journal of Physical Chemistry C* **2017**, *121*, 7450-7465.
18. Hu, G.; Tang, Q.; Lee, D.; Wu, Z.; Jiang, D.E., Metallic Hydrogen in Atomically Precise Gold Nanoclusters. *Chemistry of Materials* **2017**, *29*, 4840-4847.
19. Mullins, D. R., Variations in the Surface Chemistry of Methanol with CeO₂(100) at Low and Elevated Pressures. *Surf. Interface Anal.* **2017**, DOI: 10.1002/sia.6266.
20. Polo-Garzon, F.; Yang, S.-Z.; Fung, V.; Foo, G. S.; Bickel, E. E.; Chisholm, M. F.; Jiang, D. E.; Wu, Z., Controlling Reaction Selectivity Via Surface Termination of Perovskite Catalysts. *Angewandte Chemie International Edition* **2017**, *56*, 9820-9824.
21. Tian, C., et al., Toward the Design of a Hierarchical Perovskite Support: Ultra-Sintering-Resistant Gold Nanocatalysts for CO Oxidation. *ACS Catalysis* **2017**, *7*, 3388-3393.
22. Zhang, Y.; Savara, A.; Mullins, D. R., Ambient-Pressure Xps Studies of Reactions of Alcohols on SrTiO₃(100). *The Journal of Physical Chemistry C* **2017**, *121*, 23436-23445.
23. Chen, H.; Fu, J.; Zhang, P.; Peng, H.; Abney, C. W.; Jie, K.; Liu, X.; Chi, M.; Dai, S., Entropy-Stabilized Metal Oxide Solid Solutions as CO Oxidation Catalysts with High-Temperature Stability. *Journal of Materials Chemistry A* **2018**.

24. Foo, G. S.; Hood, Z. D.; Wu, Z., Shape Effect Undermined by Surface Reconstruction: Ethanol Dehydrogenation over Shape-Controlled SrTiO₃ Nanocrystals. *ACS Catalysis* **2018**, *8*, 555-565.
25. Fung, V.; Polo-Garzon, F.; Wu, Z.; Jiang, D.E., Exploring Perovskites for Methane Activation from First Principles. *Catalysis Science & Technology* **2018**, *8*, 702-709.
26. Hu, G.; Wu, Z.; Dai, S.; Jiang, D.E., Interface Engineering of Earth-Abundant Transition Metals Using Boron Nitride for Selective Electroreduction of CO₂. *ACS Applied Materials & Interfaces* **2018**, *10*, 6694-6700.
27. Hu, G.; Wu, Z.; Jiang, D.E., Stronger-Than-Pt Hydrogen Adsorption in a Au₂₂ Nanocluster for the Hydrogen Evolution Reaction. *Journal of Materials Chemistry A* **2018**.
28. Huang, R.; Fung, V.; Zhang, Y.; Mullins, D. R.; Wu, Z.; Jiang, D. E., Understanding Methanol Coupling on SrTiO₃ from First Principles. *The Journal of Physical Chemistry C* **2018**, *122*, 7210-7216.
29. Polo-Garzon, F.; Wu, Z., Acid-Base Catalysis over Perovskites: A Review. *Journal of Materials Chemistry A* **2018**, *6*, 2877-2894.
30. Prati, L.; Villa, A.; Jouve, A.; Beck, A.; Evangelisti, C.; Savara, A., Gold as Modifier of Metal Nanoparticles: Effect on Structure and Catalysis. *Faraday Discussions* **2018**, DOI: 10.1039/C7FD00223H.
31. Wu, Z.; Mullins, D. R.; Allard, L. F.; Zhang, Q.; Wang, L., CO Oxidation over Ceria Supported Au₂₂ Nanoclusters: Shape Effect of the Support. *Chinese Chemical Letters* **2018**, DOI: 10.1016/j.ccllet.2018.01.038.

(XIX) *Jointly funded by this grant and other grants with leading intellectual contribution from this grant:*

32. Binder, A. J.; Toops, T. J.; Unocic, R. R.; Parks, J. E.; Dai, S., Low-Temperature CO Oxidation over a Ternary Oxide Catalyst with High Resistance to Hydrocarbon Inhibition. *Angewandte Chemie International Edition* **2015**, *54*, 13263-13267.
33. Lin, Y.; Wu, Z.; Wen, J.; Ding, K.; Yang, X.; Poeppelmeier, K. R.; Marks, L. D., Adhesion and Atomic Structures of Gold on Ceria Nanostructures: The Role of Surface Structure and Oxidation State of Ceria Supports. *Nano Letters* **2015**, *15*.
34. D'Angelo, A. M.; Wu, Z.; Overbury, S. H.; Chaffee, A. L., Cu-Enhanced Surface Defects and Lattice Mobility of Pr-CeO₂ Mixed Oxides. *The Journal of Physical Chemistry C* **2016**, *120*, 27996-28008.
35. Li, H. Y.; Meng, B.; Chai, S. H.; Liu, H. L.; Dai, S., Hyper-Crosslinked Beta-Cyclodextrin Porous Polymer: An Adsorption-Facilitated Molecular Catalyst Support for Transformation of Water-Soluble Aromatic Molecules. *Chemical Science* **2016**, *7*, 905-909.
36. Liu, F. J.; Liu, C.; Kong, W. P.; Qi, C. Z.; Zheng, A. M.; Dai, S., Design and Synthesis of Micro-Meso-Macroporous Polymers with Versatile Active Sites and Excellent Activities in the Production of Biofuels and Fine Chemicals. *Green Chemistry* **2016**, *18*, 6536-6544.
37. Liu, F. J.; Wu, Q.; Liu, C.; Qi, C. Z.; Huang, K.; Zheng, A. M.; Dai, S., Ordered Mesoporous Polymers for Biomass Conversions and Cross-Coupling Reactions. *ChemSuschem* **2016**, *9*, 2496-2504.
38. Pruski, M., et al., Virtual Special Issue on Catalysis at the U.S. Department of Energy's National Laboratories. *ACS Catalysis* **2016**, *6*, 3227-3235.
39. Savara, A.; Rossetti, I.; Chan-Thaw, C. E.; Prati, L.; Villa, A., Microkinetic Modeling of Benzyl Alcohol Oxidation on Carbon-Supported Palladium Nanoparticles. *Chemcatchem* **2016**, *8*, 2482-2491.
40. Wu, P. W.; Zhu, W. S.; Chao, Y. H.; Zhang, J. S.; Zhang, P. F.; Zhu, H. Y.; Li, C. F.; Chen, Z. G.; Li, H. M.; Dai, S., A Template-Free Solvent-Mediated Synthesis of High Surface Area Boron Nitride Nanosheets for Aerobic Oxidative Desulfurization. *Chemical Communications* **2016**, *52*, 144-147.
41. Yue, Y., et al., Hierarchically Superstructured Metal Sulfides: Facile Perturbation-Assisted Nanofusion Synthesis and Visible Light Photocatalytic Characterizations. *ChemNanoMat* **2016**, *2*, 1104-1110.
42. Zhan, W. C., et al., A Sacrificial Coating Strategy toward Enhancement of Metal-Support Interaction for Ultrastable Au Nanocatalysts. *Journal of the American Chemical Society* **2016**, *138*, 16130-16139.

43. Zhu, W.; Gao, X.; Li, Q.; Li, H.; Chao, Y.; Li, M.; Mahurin, S. M.; Li, H.; Zhu, H.; Dai, S., Controlled Gas Exfoliation of Boron Nitride into Few-Layered Nanosheets. *Angewandte Chemie International Edition* **2016**, *55*, 10766-10770.
44. Doughty, B.; Goverapet Srinivasan, S.; Bryantsev, V. S.; Lee, D.; Lee, H. N.; Ma, Y.-Z.; Lutterman, D. A., Absolute Molecular Orientation of Isopropanol at Ceria (100) Surfaces: Insight into Catalytic Selectivity from Interfacial Structure. *The Journal of Physical Chemistry C* **2017**, *121*, 14137-14146.
45. Savara, A.; Chan-Thaw, C. E.; Sutton, J. E.; Wang, D.; Prati, L.; Villa, A., Molecular Origin of the Selectivity Differences between Palladium and Gold-Palladium in Benzyl Alcohol Oxidation: Different Oxygen Adsorption Properties. *ChemCatChem* **2017**, *9*, 253-257.
46. Tan, S.; Gray, M. B.; Kidder, M. K.; Cheng, Y.; Daemen, L. L.; Lee, D.; Lee, H. N.; Ma, Y.-Z.; Doughty, B.; Lutterman, D. A., Insight into the Selectivity of Isopropanol Conversion at Strontium Titanate (100) Surfaces: A Combination Kinetic and Spectroscopic Study. *ACS Catalysis* **2017**, *7*, 8118-8129.
47. Wang, T.; Zhang, P.; Sun, Y.; Liu, B.; Liu, Y.; Qiao, Z.-A.; Huo, Q.; Dai, S., New Polymer Colloidal and Carbon Nanospheres: Stabilizing Ultrasmall Metal Nanoparticles for Solvent-Free Catalysis. *Chemistry of Materials* **2017**, *29*, 4044-4051.
48. Wu, Z.; Cheng, Y.; Tao, F.; Daemen, L.; Foo, G. S.; Nguyen, L.; Zhang, X.; Beste, A.; Ramirez-Cuesta, A. J., Direct Neutron Spectroscopy Observation of Cerium Hydride Species on a Cerium Oxide Catalyst. *Journal of the American Chemical Society* **2017**, *139*, 9721-9727.
49. Zhan, W.; Shu, Y.; Sheng, Y.; Zhu, H.; Guo, Y.; Wang, L.; Guo, Y.; Zhang, J.; Lu, G.; Dai, S., Surfactant-Assisted Stabilization of Au Colloids on Solids for Heterogeneous Catalysis. *Angewandte Chemie International Edition* **2017**, *56*, 4494-4498.
50. Zhan, W., et al., Crystal Structural Effect of Au-Cu Alloy Nanoparticles on Catalytic CO Oxidation. *Journal of the American Chemical Society* **2017**, *139*, 8846-8854.
51. Zhan, W.; Yang, S.; Zhang, P.; Guo, Y.; Lu, G.; Chisholm, M. F.; Dai, S., Incorporating Rich Mesoporosity into a Ceria-Based Catalyst Via Mechanochemistry. *Chemistry of Materials* **2017**, *29*, 7323-7329.
52. Zhu, W., et al., Taming Interfacial Electronic Properties of Platinum Nanoparticles on Vacancy-Abundant Boron Nitride Nanosheets for Enhanced Catalysis. *Nature Communications* **2017**, *8*, 15291.
53. Ding, S.; Tian, C.; Zhu, X.; Wang, H.; Wang, H.; Abney, C. W.; Zhang, N.; Dai, S., Engineering Nanoporous Organic Frameworks to Stabilize Naked Au Clusters: A Charge Modulation Approach. *Chemical Communications* **2018**, *54*, 5058-5061.
54. Dong, H.; Li, Y.; Jiang, D.E., First-Principles Insight into Electrocatalytic Reduction of CO₂ to CH₄ on a Copper Nanoparticle. *The Journal of Physical Chemistry C* **2018**, *122*, 11392-11398.
55. Huang, W.; Wu, Z.; Tang, J.; Wei, W. D.; Guo, X., Surface Chemistry Connecting Heterogeneous Catalysis, Photocatalysis and Plasmonic Catalysis. *Chinese Chemical Letters* **2018**, *29*, 725-726.
56. Peng, H.; Rao, C.; Zhang, N.; Wang, X.; Liu, W.; Mao, W.; Han, L.; Zhang, P.; Dai, S., Confined Ultrathin Pd-Ce Nanowires with Outstanding Moisture and SO₂ Tolerance in Methane Combustion. *Angewandte Chemie International Edition* **2018**, doi:10.1002/anie.201803393.
57. Xiao, W., et al., Facile Synthesis of Highly Porous Metal Oxides by Mechanochemical Nanocasting. *Chemistry of Materials* **2018**, *30*, 2924-2929.

(XX) *Jointly funded by this grant and other grants with relatively minor intellectual contribution from this grant:*

58. Dong, Y.; Brooks, J. D.; Chen, T.-L.; Mullins, D. R.; Cox, D. F., Methylene Migration and Coupling on a Non-Reducible Metal Oxide: The Reaction of Dichloromethane on Stoichiometric Al-Cr₂O₃(0001). *Surface Science* **2015**, *632*, 28-38.
59. Jang, G. G.; Jacobs, C. B.; Ivanov, I. N.; Joshi, P. C.; III, H. M. M.; Kidder, M.; Armstrong, B. L.; Datskos, P. G.; Graham, D. E.; Moon, J.-W., In Situ Capping for Size Control of Monochalcogenide (Zns, Cds and Sns) Nanocrystals Produced by Anaerobic Metal Reducing Bacteria. *Nanotechnology* **2015**, *26*, 325602.

60. Mathis, J.; Kidder, M.; Li, Y.; Zhang, J.; Paranthaman, M., Controlled Synthesis of Mesoporous Codoped Titania Nanoparticles and Their Photocatalytic Activity. *Advances in Nano Research* **2016**, *4*, 157-165.
61. Mathis, J. E.; Lieffers, J. J.; Mitra, C.; Reboredo, F. A.; Bi, Z.; Bridges, C. A.; Kidder, M. K.; Paranthaman, M. P., Increased Photocatalytic Activity of TiO₂ Mesoporous Microspheres from Codoping with Transition Metals and Nitrogen. *Ceramics International* **2016**, *42*, 3556-3562.
62. Moon, J.-W., et al., Manufacturing Demonstration of Microbially Mediated Zinc Sulfide Nanoparticles in Pilot-Plant Scale Reactors. *Applied Microbiology and Biotechnology* **2016**, *100*, 7921-7931.
63. Wen, J.; Lin, Y.; Sheng, H.; Wang, L.; Miller, D. J.; Wu, Z.; Poepelmeier, K. R.; Marks, L. D., Atomic Surface Structures of Oxide Nanoparticles with Well-Defined Shapes. *Microscopy and Microanalysis* **2016**, *22*, 360-361.
64. Zhang, Y.; Kidder, M.; Ruther, R. E.; Nanda, J.; Foo, G. S.; Wu, Z.; Narula, C. K., Promotional Effects of in on Non-Oxidative Methane Transformation over Mo-ZSM-5. *Catalysis Letters* **2016**, *146*, 1903-1909.
65. Abney, C. W.; Patterson, J. T.; Gilhula, J. C.; Wang, L.; Hensley, D. K.; Chen, J.; Foo, G. S.; Wu, Z.; Dai, S., Controlling Interfacial Properties in Supported Metal Oxide Catalysts through Metal-Organic Framework Templating. *Journal of Materials Chemistry A* **2017**, *5*, 13565-13572.
66. Bugnet, M.; Overbury, S.; Wu, Z.; Aires, F.; Epicier, T., Atomic Scale Environmental Transmission Electron Microscopy Study of the Surface Mobility of Ceria Nanocubes. *Microscopy and Microanalysis* **2017**, *23*, 898-899.
67. Bugnet, M.; Overbury, S. H.; Wu, Z. L.; Epicier, T., Direct Visualization and Control of Atomic Mobility at {100} Surfaces of Ceria in the Environmental Transmission Electron Microscope. *Nano Letters* **2017**, *17*, 7652-7658.
68. Ding, S.; Tian, C.; Zhu, X.; Abney, C. W.; Tian, Z.; Chen, B.; Li, M.; Jiang, D.E.; Zhang, N.; Dai, S., Pd-Metalated Conjugated Nanoporous Polycarbazoles for Additive-Free Cyanation of Aryl Halides: Boosting Catalytic Efficiency through Spatial Modulation. *ChemSuschem* **2017**, *10*, 2348-2351.
69. Kwak, K.; Choi, W.; Tang, Q.; Kim, M.; Lee, Y.; Jiang, D.E.; Lee, D., A Molecule-Like PtAu₂₄(SC₆H₁₃)₁₈ Nanocluster as an Electrocatalyst for Hydrogen Production. *Nature Communications* **2017**, *8*, 14723.
70. Lepore, A. W.; Li, Z.; Davison, B. H.; Foo, G. S.; Wu, Z.; Narula, C. K., Catalytic Dehydration of Biomass Derived 1-Propanol to Propene over M-ZSM-5 (M = H, V, Cu, or Zn). *Industrial & Engineering Chemistry Research* **2017**, *56*, 4302-4308.
71. Li, Z.; Lepore, A. W.; Salazar, M. F.; Foo, G. S.; Davison, B. H.; Wu, Z.; Narula, C. K., Selective Conversion of Bio-Derived Ethanol to Renewable BTX over Ga-ZSM-5. *Green Chemistry* **2017**, *19*, 4344-4352.
72. Liu, J.; Olds, D.; Peng, R.; Yu, L.; Foo, G. S.; Qian, S.; Keum, J.; Guiton, B. S.; Wu, Z.; Page, K., Quantitative Analysis of the Morphology of {101} and {001} Faceted Anatase TiO₂ Nanocrystals and Its Implication on Photocatalytic Activity. *Chemistry of Materials* **2017**, *29*, 5591-5604.
73. Narula, C. K.; Allard, L. F.; Wu, Z., Ab Initio Density Functional Calculations and Infra-Red Study of Co Interaction with Pd Atoms on Θ -Al₂O₃ (010) Surface. *Scientific Reports* **2017**, *7*, 6231.
74. Sutton, J. E.; Danielson, T.; Beste, A.; Savara, A., Below-Room-Temperature C-H Bond Breaking on an Inexpensive Metal Oxide: Methanol to Formaldehyde on CeO₂(111). *The Journal of Physical Chemistry Letters* **2017**, *8*, 5810-5814.
75. Wang, B.; Di, J.; Zhang, P.; Xia, J.; Dai, S.; Li, H., Ionic Liquid-Induced Strategy for Porous Perovskite-Like PbBiO₂Br Photocatalysts with Enhanced Photocatalytic Activity and Mechanism Insight. *Applied Catalysis B: Environmental* **2017**, *206*, 127-135.
76. Wu, P.; Yang, S.; Zhu, W.; Li, H.; Chao, Y.; Zhu, H.; Li, H.; Dai, S., Tailoring N-Terminated Defective Edges of Porous Boron Nitride for Enhanced Aerobic Catalysis. *Small* **2017**, *13*, 1701857.

77. Yao, Q.; Feng, Y.; Fung, V.; Yu, Y.; Jiang, D.E.; Yang, J.; Xie, J., Precise Control of Alloying Sites of Bimetallic Nanoclusters Via Surface Motif Exchange Reaction. *Nature Communications* **2017**, *8*, 1555.
78. Yao, Q.; Yuan, X.; Fung, V.; Yu, Y.; Leong, D. T.; Jiang, D.E.; Xie, J., Understanding Seed-Mediated Growth of Gold Nanoclusters at Molecular Level. *Nature Communications* **2017**, *8*, 927.
79. Zhang, P.; Li, W.; Yang, S.; Schott, J. A.; Liu, X.; Mahurin, S. M.; Huang, C.; Zhang, Y.; Fulvio, P. F.; Chisholm, M. F.; Dai, S., Solid-State Synthesis of Ordered Mesoporous Carbon Catalysts Via a Mechanochemical Assembly through Coordination Cross-Linking. *Nature Communications* **2017**, *8*, 15020.
80. Artyushkova, K.; Mullins, D. R.; Gregoratti, L.; Yu, X. Y., Foreword to Special Section on “near Ambient and Synchrotron Surface Analysis (NAXPS)”. *Surface and Interface Analysis* **2018**, *0*, doi:10.1002/sia.6383.
81. Hossain, S.; Ono, T.; Yoshioka, M.; Hu, G.; Hosoi, M.; Chen, Z.; Nair, L. V.; Niihori, Y.; Kurashige, W.; Jiang, D. E.; Negishi, Y., Thiolate-Protected Trimetallic Au₂₀Ag₄Pd and Au₂₀Ag₄Pt Alloy Clusters with Controlled Chemical Composition and Metal Positions. *The Journal of Physical Chemistry Letters* **2018**, *9*, 2590-2594.
82. Kim, M.; Tang, Q.; Narendra Kumar, A. V.; Kwak, K.; Choi, W.; Jiang, D. E.; Lee, D., Dopant-Dependent Electronic Structures Observed for M₂Au₃₆(SC₆H₁₃)₂₄ Clusters (M = Pt, Pd). *The Journal of Physical Chemistry Letters* **2018**, *9*, 982-989.
83. Liu, F.; Huang, K.; Zheng, A.; Xiao, F.-S.; Dai, S., Hydrophobic Solid Acids and Their Catalytic Applications in Green and Sustainable Chemistry. *ACS Catalysis* **2018**, *8*, 372-391.
84. Yao, Q.; Fung, V.; Sun, C.; Huang, S.; Chen, T.; Jiang, D.E.; Lee, J. Y.; Xie, J., Revealing Isoelectronic Size Conversion Dynamics of Metal Nanoclusters by a Noncrystallization Approach. *Nature Communications* **2018**, *9*, 1979.

FWP 47319: Transdisciplinary Approaches to Realize Novel Catalytic Pathways to Energy Carriers

PI: Johannes Lercher

Subtask PI's: Aaron M. Appel, Zdenek Dohnálek, Johannes A. Lercher, Roger Rousseau, János Szanyi

Co-PIs and Key Personnel: S. Thomas Autrey, R. Morris Bullock, Mirosław Derewinski, David A. Dixon, John L. Fulton, Feng Gao, Bojana Ginovska, Vassiliki-Alexandra Glezakou, Oliver Gutiérrez-Tinoco, Jian Zhi Hu, Enrique Iglesia, Andreas Jentys, Abhijeet Karkamkar, Bruce D. Kay, Greg A. Kimmel, Libor Kovarik, John C. Linehan, Donghai Mei, Nikolay G. Petrik, Gregory K. Schenter, Wendy J. Shaw, Huamin Wang, Yong Wang, Eric S. Wiedner

RECENT PROGRESS

The central goal of this BES Catalysis Sciences research program, “Transdisciplinary approaches to realize novel catalytic pathways to energy carriers” is to develop insight into novel approaches for designing catalytic centers and their environments. We aim to catalyze C-C and C-H bond formation and C-O bond cleavage on acid-base and hydrogenation sites with rates that exceed the current state-of-the-art by at least an order of magnitude and with selectivities that match the best currently known. We target the fundamental catalysis of these reactions because high rates for these reactions at mild reaction conditions coupled with high selectivity is one of the keys for more flexible production of fuels and chemicals.

We are convinced that in order to enhance the rates and selectivity of acid-base catalyzed C-C coupling and metal-catalyzed hydrogen addition to C-O bonds, the nature of active sites has to be understood at a level of complexity that markedly exceeds the current state. We acquire and use new insights for the design of active sites by placing specific emphasis on both, (1) the nature, nuclearity, and local environment of active centers and (2) the extended chemical and structural environment around the active center to support suitable self-organization of reactants and solvents and to stabilize transition states. Our work is rooted in the knowledge that the nature of the active center (its electronic properties, spatial arrangement, and nuclearity) determines the chemical specificity and intrinsic reactivity and is guided by the fundamental hypothesis that activity along selected pathways for metal and acid-base catalyzed reactions can be markedly enhanced by (i) positioning of functional groups around the active center, (ii) adjusting the available space around the active center to match that of the rate-limiting transition state, and (iii) self-organization of solvent and reactant molecules around the active center. This environment can have the form of a void (maximizing van der Waals contacts with minimal distortions of the host and the guest in the transition state), a functional group aiding the stabilization of reactants along the reaction path, and solvent/reactant molecules engulfing the active center.

To achieve our goal of enhancing rates and selectivities for our target reactions, the program is organized into two thrusts that focus on “Tailoring acid-base sites for controlled C-C bond formation” and “Enhancing H₂ addition rates by designing the metal center and its environment.” To gain molecular level insight into catalysis on both types of sites, computational catalysis is integrated in the crosscutting subtask, “Novel theoretical approaches to describe catalysts and catalysis,” and will support, enhance, and guide experimental efforts. The first thrust explores the impact of the geometric and electronic properties of Lewis and Brønsted acid-base sites on C-C bond formation by combining precision synthesis of homotopic active sites of chosen nuclearity and the stabilization of such sites in homogeneous catalysts, inert substrates, faceted oxides, mesoporous solids, and zeolites. Spectroscopic characterization of these sites and the catalytic transformations allow for directed cross coupling of the obtained insights. The second thrust addresses the fundamentals of hydrogen addition to CO groups in molecules such as CO₂, alcohols, aldehydes, ketones, and carboxylic acids. We will exploit novel, highly active sites comprised of single metal atoms and small clusters of defined nuclearity supported on homogeneous scaffolds of increasing complexity and heterogeneous supports, such as graphene and faceted oxides, as well as in micropores. We designed our program structure to promote cross-disciplinary collaborations within and across thrusts and subtasks. The structure-activity relationships dominated by the acid-base or metal center are highlighted in the first subtasks in each thrust, while the second subtasks feature the impact of the environment (ligands, confinement, solvent, and reactant molecules).

Examples of Recent Results

Hydroalkylation to Adjust the Size of Alkanes. Acid-catalyzed C-C coupling of phenols with alcohols yields alkylated phenols with carbon-numbers in the same range as transportation fuels. In zeolites, the catalytic activity, mechanism, and reaction pathways (C- or O-alkylation) depend on the concentration and strength of acid sites, space constraints for the reaction, and alkylating agent. Detailed kinetic analyses and in situ ^{13}C Magic Angle Spinning Nuclear Magnetic Resonance (MAS NMR) spectroscopy in non-polar media show that phenol alkylation with cyclohexanol does not appreciably occur before a majority of cyclohexanol has been dehydrated to cyclohexene. Figure 1 shows that alkylation reactions are retarded when cyclohexanol and cyclohexene are present. In contrast, alkylation products are readily formed when the solution initially contains just phenol and cyclohexene. The strict reaction sequence is not posed by competitive adsorption (phenol and cyclohexanol show similar adsorption strengths) but by the absence of a reactive electrophile. This is due to the preferential formation of protonated dimers of cyclohexanol at Brønsted acid sites, which hinders the adsorption of cyclohexene. At low coverage of the acid sites by protonated dimers, cyclohexene adsorption and protonation yield cyclohexyl carbenium ions, which perform an electrophilic attack on phenol to produce alkylated products. This further implies that carbenium ions are formed at much lower concentrations, if at all, from the protonated dimer.

The rate of alkylation is much lower in water than in decalin. We attribute this to the generation of the cyclohexyl cation from cyclohexanol being energetically more demanding in the aqueous phase and the olefin protonation by the hydronium ion having a significantly higher barrier than protonation by a framework-bound proton. These insights have important implications for process design, emphasizing the importance of maintaining low concentrations of water and alcohol during alkylation and hence the use of back-mixed reactors operated at high conversions.

Key Roles of Lewis Acid–base Pairs on $\text{Zn}_x\text{Zr}_y\text{O}_z$ in Direct Ethanol/acetone-to-Isobutene Conversion. In this effort, we have been focusing on the effects of surface acid-base properties on the cascade ethanol-to-isobutene conversion using $\text{Zn}_x\text{Zr}_y\text{O}_z$ catalysts. The ethanol-to-isobutene reaction was found to be limited by the secondary reaction of the key intermediate, acetone, namely the acetone-to-isobutene reaction. Although catalysts with coexisting Brønsted acidity could catalyze the rate-limiting acetone-to-isobutene reaction, the presence of Brønsted acidity is also detrimental. First, secondary isobutene isomerization is favored, producing a mixture of butene isomers. Second, undesired polymerization and coke formation prevail, leading to rapid catalyst deactivation. Most importantly, both steady-state and kinetic reaction studies as well as Fourier

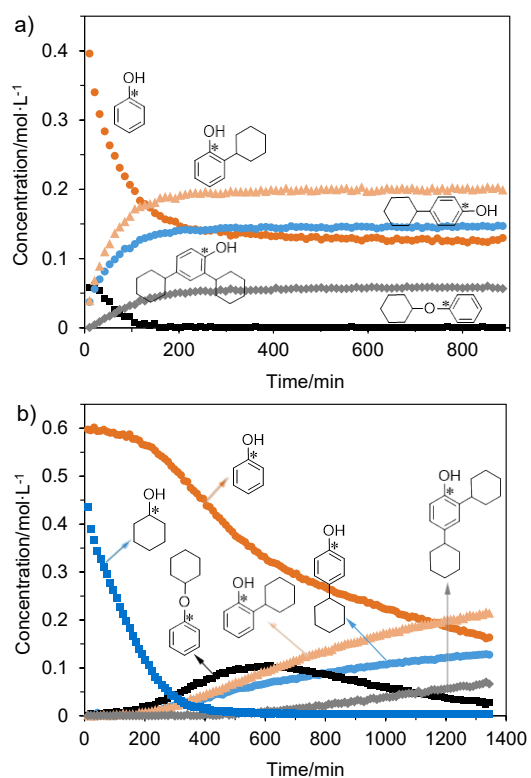


Figure 9. Concentration profiles, monitored by in situ NMR, during the alkylation of phenol with cyclohexene only (a) and with equimolar concentrations of cyclohexene and cyclohexanol (b) at 127 °C.

transform infrared spectroscopy (FTIR) analysis of adsorbed acetone-d₆ and D₂O unambiguously showed that a highly active and selective nature of balanced Lewis acid-base pairs was masked by the coexisting Brønsted acidity in the aldolization and self-deoxygenation of acetone to isobutene. As a result, Zn_xZr_yO_z catalysts with only Lewis acid-base pairs were discovered, on which nearly a theoretical selectivity to isobutene (~88.9 percent) was successfully achieved. Moreover, the absence of Brønsted acidity in such Zn_xZr_yO_z catalysts also eliminates the side isobutene isomerization and undesired

polymerization/coke reactions, resulting in the production of high purity isobutene with significantly improved catalyst stability (< 2 percent activity loss after 200 h time-on-stream). Our integrated experimental and theoretical work suggested that Lewis acid-base pairs on a ZrO₂ catalyst can catalyze the acetone aldolization reaction to form mesityl oxide. The formed mesityl oxide strongly adsorbs and blocks the Lewis acid-base active site, resulting in the dominant acetone decomposition (Figure 2, red highlighted pathway), as well as other possible side reactions, such as polymerization. However, adding ZnO significantly modifies the properties of surface Lewis acid-base pairs. As a result, the cascade acetone aldolization and self-deoxygenation reactions are significantly accelerated, leading to the highly active and stable Zn_xZr_yO_z catalyst for both acetone-to-isobutene and ethanol-to-isobutene reactions.

Phenylalkanol Deoxygenation Pathways on Rutile TiO₂(110). In this work, we focus on the deoxygenation of biomass-derived alcohols. In this regard, the role of radicals in the reaction mechanisms leading to functionalized aromatics has been extensively argued. The involvement of radical species has been firmly established for a number of simpler reactions on high surface area oxide catalysts, such as oxidative coupling of methane and selective oxidation of propylene. However, the formation of free radicals is rarely demonstrated. In this work, the reaction pathways of simple lignin-derived aromatic alcohols (i.e., phenol, phenylmethanol, and 2-phenylethanol) on a prototypical model oxide surface, rutile TiO₂(110), are studied using a combination of molecular beam dosing and temperature programmed desorption (TPD). For phenylmethanol, the coverage dependent TPD data show that about 40% of molecules adsorbed on the surface at a saturation coverage are converted to reaction products, indicating that the reactions proceed on regular five-fold coordinated Ti sites. This is in contrast to aliphatic alcohols where the reactions are shown to proceed exclusively on bridging oxygen vacancy defect sites. The

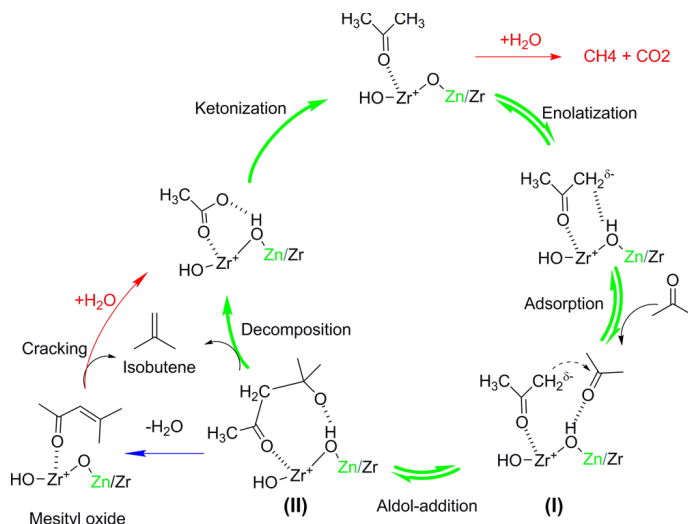


Figure 10. Proposed acetone-to-isobutene reaction mechanism over Zn_xZr_yO_z catalyst.

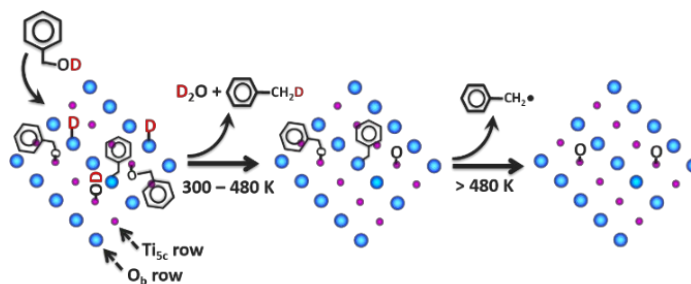


Figure 11. Reaction pathways for the conversion of phenylmethanol on TiO₂(110).

studies of OD-labelled phenylmethanol demonstrate that a fraction of OD hydrogen is transferred to the benzyl group to form toluene that desorbs between 300 K and 480 K (Figure 3). In the competing reaction, the OD hydrogen is converted to water at ~350 K. Once the OD hydrogen is depleted above 480 K, the remaining phenylmethoxy surface species dissociate yielding benzyl radicals in the gas phase. Combined, these results show that the conversion of phenylmethanol on TiO₂(110) proceeds via a unique chemistry. In contrast, both phenol and 2-phenylethanol exhibit expected surface chemistry analogous to that of aliphatic alcohols. These findings reveal for the first time the formation of free radical species from the interaction of phenylmethanol with TiO₂(110) and demonstrate a new direct mechanism for deoxygenation of lignin-derived benzylic alcohols to aromatics on TiO₂.

Comparing Cobalt and Rhodium Complexes for the Hydrogenation of CO₂.

Using an exceptionally active class of catalysts that we have identified for the hydrogenation of CO₂, we performed systematic studies of a series of M(diphosphine)₂H (M = Co, Rh) complexes with an aim to understand how to design active catalysts that work under ambient conditions. The catalytic turnover frequency was correlated to thermodynamic driving force of the three catalyst steps: (1) hydride transfer, (2) H₂ addition, and (3) deprotonation (Figure 4). This analysis demonstrated that the most active catalyst, Co(dmpe)₂H, has the optimal balance in driving force for the three reaction steps. Hydride transfer for the Co catalysts was found to be rate-limiting, so catalysts with extra driving force in the other steps are not as active. The Rh catalysts have a much stronger driving force for hydride transfer, but this comes at the cost of too little driving force for H₂ addition and deprotonation, which are rate-limiting in the Rh catalysts.

This analysis demonstrated that the most active catalyst, Co(dmpe)₂H, has the optimal balance in driving force for the three reaction steps. Hydride transfer for the Co catalysts was found to be rate-limiting, so catalysts with extra driving force in the other steps are not as active. The Rh catalysts have a much stronger driving force for hydride transfer, but this comes at the cost of too little driving force for H₂ addition and deprotonation, which are rate-limiting in the Rh catalysts.

Designing New Catalytic Cycles and Mechanisms in Water.

Through the fundamental understanding of the impact of solvent gained through our initial studies in aqueous solution, we have been able to design a new catalytic cycle that involves an alternate mechanism in water, resulting in a highly active, nonprecious metal catalyst for the hydrogenation of CO₂ in

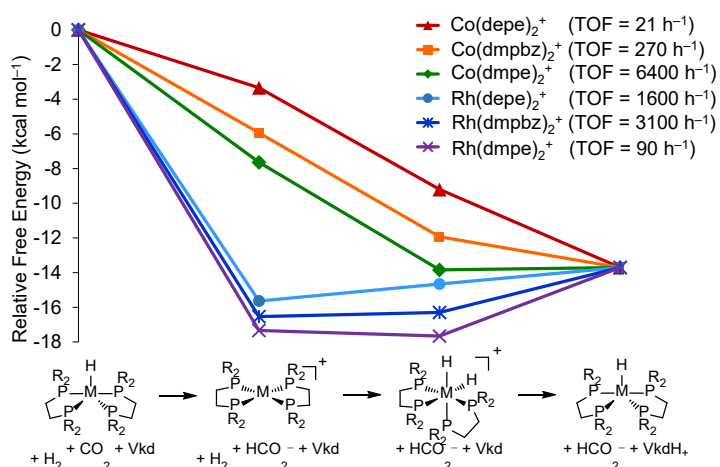


Figure 12. The tradeoff between driving force and rate must be balanced for every step in a catalytic cycle to obtain the most active catalyst.

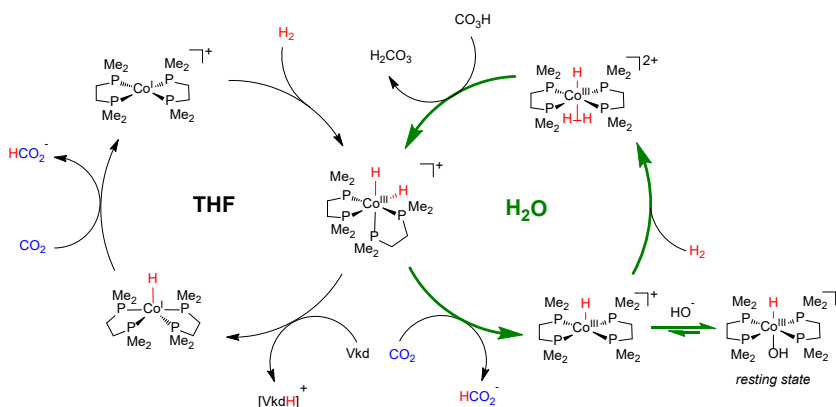


Figure 13. By understanding the impact of solvent upon reduction of CO₂ using cobalt complexes, we have redesigned a catalyst to work in water using cheaper reagents.

water. Using solvent-dependent hydricity, we have demonstrated that $\text{Co}(\text{dmpe})_2(\text{H})_2^+$ is an active catalyst for aqueous hydrogenation of CO_2 , and it operates by different mechanisms in water and organic solvent, as illustrated in Figure 5. Previous studies in tetrahydrofuran solvent demonstrated that $\text{Co}(\text{dmpe})_2(\text{H})_2^+$ must be deprotonated by a strong organic base, such as Verkade's superbase, before it can transfer a hydride to carbon dioxide. In water, direct hydride transfer from $\text{Co}(\text{dmpe})_2(\text{H})_2^+$ to carbon dioxide is thermodynamically favorable. As a result of the change in mechanism, $\text{Co}(\text{dmpe})_2(\text{H})_2^+$ can be regenerated using NaHCO_3 instead of a strong organic base. This cobalt catalyst is more active than all of the other base-metal catalysts that hydrogenate carbon dioxide in water.

Controlling the Selectivity of CO_2 Reduction over Metal/ $\gamma\text{-Al}_2\text{O}_3$ Catalysts.

The focus of our work has been understanding the factors that govern product selectivity in CO_2 hydrogenation over $\text{Pd}/\gamma\text{-Al}_2\text{O}_3$ catalysts. To this end, we have conducted SSITKA/operando FTIR measurements on $\text{Pd}/\gamma\text{-Al}_2\text{O}_3$ catalysts in order to identify the nature and the kinetics of surface species present on the catalysts under steady-state conditions. These studies were built in our prior investigations in which we have identified the nature and reactivity of surface species formed over these catalysts in well-controlled adsorption^{1,2} and in situ transient kinetic experiments. The activation energies of CO and CH_4 formation estimated from the real mean surface residence times were identical to those determined from the IR intensities of alumina-bound bidentate formates and Pd-adsorbed CO, respectively. These results let us conclude that the key intermediate in CO formation is formate, while that in CH_4 formation it is strongly adsorbed CO. The selectivities toward CO and CH_4 productions were governed by the balance between the reaction rate of adsorbed formate reduction to CO, and the rate of strongly held CO hydrogenation to CH_4 . At low reaction temperature, the methanation rate is low, while the formate hydrogenation rate is relatively high. Therefore, the Pd particles are populated with both strongly and weakly adsorbed CO, and most of the weakly held CO desorbed into the gas phase. This results in a high selectivity toward CO and low selectivity toward CH_4 formations. In contrast, at high temperature where the methanation rate is higher than the formate reduction rate, most of the CO produced in the formate reduction will adsorb strongly on the Pd particles, and will further be reduced to CH_4 . Under these conditions, the pool of weakly adsorbed CO is only partially full, or empty. This results in high CH_4 formation, but low CO formation selectivities. This hypothesis was tested on $\text{Pd}/\text{Al}_2\text{O}_3$ catalysts with Pd loadings of 2.5, 5, and 10 wt%, but with very similar particle size distribution (Figure 6). The catalyst with the lowest Pd loading exhibited the highest CO selectivity, while the catalyst with the highest metal content showed the highest CH_4 selectivity. The pool of the key intermediate to adsorbed CO formation (formate) is full in all three cases. However, the pool of sites that can hold adsorbed CO (sites on Pd clusters) varies strongly with metal loading. At low Pd loading, the pool of adsorbed CO is small, so a lot of the CO from the reduction of adsorbed formates ends up at weak adsorption sites and desorb into the gas phase (high CO selectivity). On the other hand, at high metal loading, due

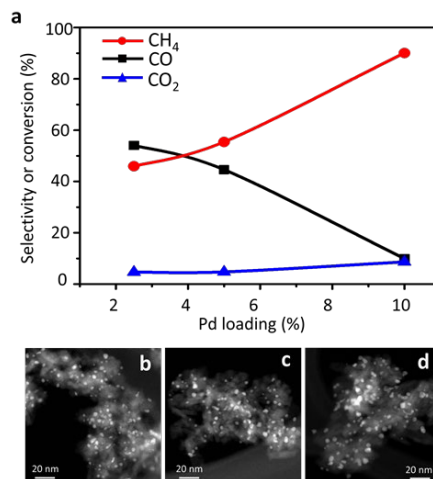


Figure 14. Controlling selectivities in CO_2 reduction by tailor-made catalysts through mechanistic understanding: **a**: CH_4 and CO selectivities and CO_2 conversion as a function of Pd loading at 573 K. **b, c, d**: TEM images of the 2.5, 5, and 10 wt% $\text{Pd}/\text{Al}_2\text{O}_3$ catalysts.

to the large pool of adsorption sites on Pd clusters, most of the CO from formate reduction is bound to strong adsorption sites and can be further reduced to CH₄. As a result, this catalyst produces CH₄ with high selectivity. This demonstrates our ability to prepare materials with controlled properties toward specific reactivity and selectivity, which is critical for future research efforts of this subtask.

Formation of Supported Graphene Oxide. Graphene functionalization is a promising approach in the preparation of well-defined model systems with a broad range of applications in many disciplines. In catalysis, a variety of functional groups anchored on or embedded in graphene films can provide a reliable attachment point via further reactions or nucleation. In this work, we employed temperature-dependent STM imaging with parallel large-scale DFT calculations to map out the relative stability of various atomic oxygen (AO) species in different regions of defect-free graphene (Gr) supported on Ru (0001). Differences in the Gr/Ru lattices result in the superstructure, which offers an array of distinct adsorption sites.

In contrast with the expectations, we reveal that for strongly-bound Gr on Ru(0001), terminally bound enolate oxygen species are preferred over the bridge-bonded epoxy species that dominate on free-standing Gr, nanotubes, and graphite. The AO diffusion is utilized to show that in the regions that are close to the metal substrate, the terminally bonded enolate groups are strongly preferred over bridge-bonded epoxy configurations. No oxygen species are observed on the graphene regions that are far from the underlying Ru, indicating their low relative stability. DFT calculations further provide a clear fundamental basis for understanding the local structural and electronic factors and C-Ru bond strengthening/weakening processes that affect the stability of enolate and epoxy species, Figure 7. The preferred enolate binding sites that are periodic in nature with distances of ~3 nm should allow for future engineering of ordered arrays of well-defined catalytic materials.

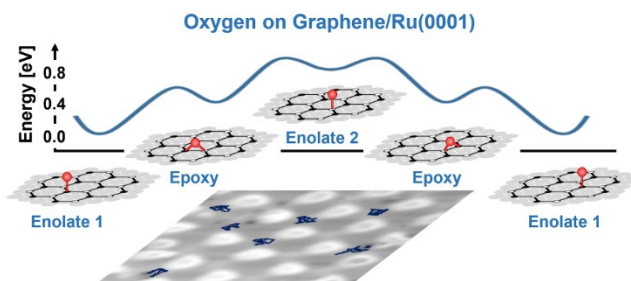


Figure 15. Combined STM and DFT studies demonstrate the critical role of metal-C contacts in controlling surface functionalization of Gr oxide with terminal-bonded (enolate) being the preferred configuration.

Subsequently, the thermal stability of physical vapor deposited Pd (sub-monolayer to multilayer coverages) was investigated on pristine Gr and O-Gr on Ru(0001) using X-ray photoelectron and FTIR spectroscopies. The IR spectra of adsorbed CO indicated that Pd deposited at 300 K formed small clusters. On Gr, Pd clusters readily agglomerate when the temperature is increased to 900 K and form large Pd particles. In contrast, when the Gr was pre-oxidized by AO prior to Pd deposition, the agglomeration was strongly suppressed. The Pd atoms deposited at 300 K spread on the O-Gr layer without the formation of large metal clusters. However, between 900 and 1100 K, Pd was found to intercalate between the Gr layer and the Ru(0001) substrate on both the pristine and oxidized Gr. At even higher temperature, Pd desorbs, and at >1300 K the Gr dissolves into the Ru substrate. These findings provide critical insight into the stability of metal particles on C-based supports that, in turn, will guide our proposed work on the preparation of highly dispersed metal on carbon-based supports.

Publications Acknowledging this Grant in 2015-2018

Publications exclusively funded by this grant

2015

1. Chase, Z. A.; Kasakov, S.; Shi, H.; Vjunov, A.; Fulton, J. L.; Camaioni, D. M.; Balasubramanian, M.; Zhao, C.; Wang, Y.; Lercher, J. A., State of Supported Nickel Nanoparticles during Catalysis in Aqueous Media. *Chem. Eur. J.* **2015**, *21*, 16541–16546. DOI: [10.1002/chem.201502723](https://doi.org/10.1002/chem.201502723).
2. Connelly, S. J.; Wiedner, E. S.; Appel, A. M., Predicting the Reactivity of Hydride Donors in Water: Thermodynamic Constants for Hydrogen. *Dalton. Trans.* **2015**, *44*, 5933–5938. DOI: [10.1039/C4DT03841J](https://doi.org/10.1039/C4DT03841J).
3. Deshlahra, P.; Carr, R. C.; Chai, S.; Iglesia, E., Mechanistic Details and Reactivity Descriptors in Oxidation and Acid Catalysis of Methanol. *ACS Catal.* **2015**, *5*, 666–682. DOI: [10.1021/cs501599y](https://doi.org/10.1021/cs501599y).
4. Fang, Z.; Wang, Y.; Dixon, D. A., Computational Study of Ethanol Conversion on Al₈O₁₂ as a Model for γ -Al₂O₃. *J. Phys. Chem. C* **2015**, *119*, 23413–23421. DOI: [10.1021/acs.jpcc.5b05887](https://doi.org/10.1021/acs.jpcc.5b05887).
5. Ginovska, B.; Autrey, T.; Parab, K.; Bowden, M. E.; Potter, R. G.; Camaioni, D. M., Heterolysis of H₂ Across a Classical Lewis Pair, 2,6-Lutidine-BCl₃: Synthesis, Characterization, and Mechanism. *Chem. Eur. J.* **2015**, *21*, 15713–15719. DOI: [10.1002/chem.201501899](https://doi.org/10.1002/chem.201501899).
6. Henderson, M. A., Photochemical Outcomes of Adsorbed Oxygen: Desorption, Dissociation, and Passivation by Coadsorbed Water. *J. Phys. Chem. C* **2015**, *119*, 19976–19986. DOI: [10.1021/acs.jpcc.5b05972](https://doi.org/10.1021/acs.jpcc.5b05972).
7. Henderson, M. A.; Dahal, A.; Dohnálek, Z.; Lyubinetsky, I., Strong Temperature Dependence in the Reactivity of H₂ on RuO₂(110). *J. Phys. Chem. Lett.* **2016**, *7*, 2967–2970. DOI: [10.1021/acs.jpcclett.6b01307](https://doi.org/10.1021/acs.jpcclett.6b01307).
8. Hu, J. Z.; Xu, S.; Li, W.-Z.; Hu, M. Y.; Deng, X.; Dixon, D. A.; Vasiliu, M.; Craciun, R.; Wang, Y.; Bao, X.; Peden, C. H. F., Investigation of the Structure and Active Sites of TiO₂ Nanorod Supported VO_x Catalysts by High-Field and Fast-Spinning 51V MAS NMR. *ACS Catal.* **2015**, 3945–3952. DOI: [10.1021/acscatal.5b00286](https://doi.org/10.1021/acscatal.5b00286).
9. Kasakov, S.; Zhao, C.; Baráth, E.; Chase, Z. A.; Fulton, J. L.; Camaioni, D. M.; Vjunov, A.; Shi, H.; Lercher, J. A., Glucose- and Cellulose-Derived Ni/C-SO₃H Catalysts for Liquid Phase Phenol Hydrodeoxygenation. *Chem. Eur. J.* **2015**, *21*, 1567–1577. DOI: [10.1002/chem.201405242](https://doi.org/10.1002/chem.201405242).
10. Kovarik, L.; Bowden, M.; Shi, D.; Washton, N. M.; Andersen, A.; Hu, J. Z.; Lee, J.; Szanyi, J.; Kwak, J.-H.; Peden, C. H. F., Unraveling the Origin of Structural Disorder in High Temperature Transition Al₂O₃: Structure of θ -Al₂O₃. *Chem. Mater.* **2015**, *27*, 7042–7049. DOI: [10.1021/acs.chemmater.5b02523](https://doi.org/10.1021/acs.chemmater.5b02523).
11. Li, W.-Z.; Gao, F.; Li, Y.; Walter, E. D.; Liu, J.; Peden, C. H. F.; Wang, Y., Nanocrystalline Anatase Titania-Supported Vanadia Catalysts: Facet-Dependent Structure of Vanadia. *J. Phys. Chem. C* **2015**, *119*, 15094–15102. DOI: [10.1021/acs.jpcc.5b01486](https://doi.org/10.1021/acs.jpcc.5b01486).
12. Li, Y.; Wei, Z.; Gao, F.; Kovarik, L.; Baylon, R. A. L.; Peden, C. H. F.; Wang, Y., Effect of Oxygen Defects on the Catalytic Performance of VO_x/CeO₂ Catalysts for Oxidative Dehydrogenation of Methanol. *ACS Catal.* **2015**, *5*, 3006–3012. DOI: [10.1021/cs502084g](https://doi.org/10.1021/cs502084g).
13. Miller, D. L.; Boro, B. J.; Grubel, K.; Helm, M. L.; Appel, A. M., Synthesis and Characterization of a Triphos Ligand Derivative and the Corresponding Pd^{II} Complexes. *Eur. J. Inorg. Chem.* **2015**, *2015*, 5781–5785. DOI: [10.1002/ejic.201500791](https://doi.org/10.1002/ejic.201500791).
14. Mu, R.; Cantu, D. C.; Glezakou, V.-A.; Lyubinetsky, I.; Rousseau, R.; Dohnalek, Z., Deprotonated Water Dimers: The Building Blocks of Segmented Water Chains on Rutile RuO₂(110). *J. Phys. Chem. C* **2015**, *119*, 23552–23558. DOI: [10.1021/acs.jpcc.5b07158](https://doi.org/10.1021/acs.jpcc.5b07158).
15. Novotny, Z.; Netzer, F. R.; Dohnálek, Z., Cerium Oxide Nanoclusters on Graphene/Ru (0001): Intercalation of Oxygen via Spillover. *ACS Nano* **2015**, *9*, 8617–8626. DOI: [10.1021/acsnano.5b03987](https://doi.org/10.1021/acsnano.5b03987).

16. Priyadarshani, N.; Ginovska, B.; Bays, J. T.; Linehan, J. C.; Shaw, W. J., Photoswitching a Molecular Catalyst to Regulate CO₂ Hydrogenation. *Dalton. Trans.* **2015**, *44*, 14854-14864. DOI: [10.1039/C5DT01649E](https://doi.org/10.1039/C5DT01649E).
 17. Sun, J.; Karim, A. M.; Mei, D.; Engelhard, M.; Bao, X.; Wang, Y., New Insights into Reaction Mechanisms of Ethanol Steam Reforming on Co-ZrO₂. *Appl.Catal. B* **2015**, *162*, 141-148. DOI: [10.1016/j.apcatb.2014.06.043](https://doi.org/10.1016/j.apcatb.2014.06.043).
 18. Vjunov, A.; Fulton, J. L.; Camaioni, D. M.; Hu, J. Z.; Burton, S. D.; Arslan, I.; Lercher, J. A., Impact of Aqueous Medium on Zeolite Framework Integrity. *Chem. Mater.* **2015**, *27*, 3533-3545. DOI: [10.1021/acs.chemmater.5b01238](https://doi.org/10.1021/acs.chemmater.5b01238).
 19. Vjunov, A.; Fulton, J. L.; Huthwelker, T.; Pin, S.; Mei, D.; Schenter, G. K.; Govind, N.; Camaioni, D. M.; Hu, J. Z.; Lercher, J. A., Correction to "Quantitatively Probing the Al Distribution in Zeolites." *J. Am. Chem. Soc.* **2015**, *137*, 2409-2409. DOI: [10.1021/ja513077w](https://doi.org/10.1021/ja513077w).
 20. Wang, X.; Shi, H.; Kwak, J. H.; Szanyi, J., Mechanism of CO₂ Hydrogenation on Pd/Al₂O₃ Catalysts: Kinetics and Transient DRIFTS-MS Studies. *ACS Catal.* **2015**, *5*, 6337-6349. DOI: [10.1021/acscatal.5b01464](https://doi.org/10.1021/acscatal.5b01464).
 21. Wang, Z.-T.; Henderson, M. A.; Lyubinetsky, I., Origin of Coverage Dependence in Photoreactivity of Carboxylate on TiO₂(110): Hindering by Charged Coadsorbed Hydroxyls. *ACS Catal.* **2015**, *5*, 6463-6467. DOI: [10.1021/acscatal.5b01819](https://doi.org/10.1021/acscatal.5b01819).
 22. Whittemore, S. M.; Autrey, T., Kinetic and Thermodynamic Study of the Reduction of 1,1-Diphenylethylene by a Thermally Frustrated Diethyl Ether-BCF Lewis Pair. *Isr. J. Chem.* **2015**, *55*, 196-201. DOI: [10.1002/ijch.201400142](https://doi.org/10.1002/ijch.201400142).
 23. Whittemore, S. M.; Edverson, G.; Camaioni, D. M.; Karkamkar, A.; Neiner, D.; Parab, K.; Autrey, T., Catalytic reduction of polar substrates without metals: A thermodynamic and kinetic study of heterolytic activation of hydrogen by vacancies in frustrated Lewis pairs. *Catal. Today* **2015**, *251*, 28-33. DOI: [10.1016/j.cattod.2014.10.040](https://doi.org/10.1016/j.cattod.2014.10.040).
 24. Yi, C.-W.; Szanyi, J., The thermal behavior of Pd on graphene/Ru(0001). *Surf. Sci.* **2015**, *641*, 154-158. DOI: [10.1016/j.susc.2015.06.005](https://doi.org/10.1016/j.susc.2015.06.005).
 25. Yoon, Y.; Wang, Y.-G.; Rousseau, R.; Glezakou, V.-A., Impact of Nonadiabatic Charge Transfer on the Rate of Redox Chemistry of Carbon Oxides on Rutile TiO₂(110) Surface. *ACS Catal.* **2015**, *5*, 1764-1771. DOI: [10.1021/cs501873m](https://doi.org/10.1021/cs501873m).
 26. Zall, C. M.; Linehan, J. C.; Appel, A. M., A Molecular Copper Catalyst for Hydrogenation of CO₂ to Formate. *ACS Catal.* **2015**, *5*, 5301-5305. DOI: [10.1021/acscatal.5b01646](https://doi.org/10.1021/acscatal.5b01646).
 27. Zhang, S.; Bullock, R. M., Molybdenum Hydride and Dihydride Complexes Bearing Diphosphine Ligands with a Pendant Amine: Formation of Complexes with Bound Amines. *Inorg. Chem.* **2015**, *54*, 6397-6409. DOI: [10.1021/acs.inorgchem.5b00728](https://doi.org/10.1021/acs.inorgchem.5b00728).
 28. Zhao, Z. C.; Xu, S. C.; Hu, M. Y.; Bao, X. H.; Peden, C. H. F.; Hu, J. Z., Investigation of Aluminum Site Changes of Dehydrated Zeolite H-Beta during a Rehydration Process by High-Field Solid-State NMR. *J. Phys. Chem. C* **2015**, *119*, 1410-1417. DOI: [10.1021/jp509982r](https://doi.org/10.1021/jp509982r).
 29. Zhi, Y.; Shi, H.; Mu, L.; Liu, Y.; Mei, D.; Camaioni, D. M.; Lercher, J. A., Dehydration Pathways of 1-Propanol on HZSM-5 in the Presence and Absence of Water. *J. Am. Chem. Soc.* **2015**, *137*, 15781-15794. DOI: [10.1021/jacs.5b09107](https://doi.org/10.1021/jacs.5b09107).
- 2016**
30. Baylon, R. A. L.; Sun, J.; Martin, K. J.; Venkitasubramanian, P.; Wang, Y., Beyond Ketonization: Selective Conversion of Carboxylic Acids to Olefins over Balanced Lewis Acid-base Pairs. *Chem. Commun.* **2016**, *52*, 4975-4978. DOI: [10.1039/C5CC10528E](https://doi.org/10.1039/C5CC10528E).
 31. Baylon, R. A. L.; Sun, J.; Wang, Y., Conversion of Ethanol to 1,3-butadiene over Na Doped Zn_xZr_yO_z Mixed Metal Oxides. *Catal. Today* **2016**, *259, Part 2*, 446-452. DOI: [10.1016/j.cattod.2015.04.010](https://doi.org/10.1016/j.cattod.2015.04.010).

32. Chen, L.; Smith, R. S.; Kay, B. D.; Dohnálek, Z., Adsorption of Small Hydrocarbons on Rutile TiO₂(110). *Surf. Sci.* **2016**, *650*, 83-92. DOI: [10.1016/j.susc.2015.11.002](https://doi.org/10.1016/j.susc.2015.11.002).
33. Deshlahra, P.; Iglesia, E., Reactivity and Selectivity Descriptors for the Activation of C-H Bonds in Hydrocarbons and Oxygenates on Metal Oxides. *J. Phys. Chem. C* **2016**, *120*, 16741-16760. DOI: [10.1021/acs.jpcc.6b04604](https://doi.org/10.1021/acs.jpcc.6b04604).
34. Deshlahra, P.; Iglesia, E., Toward More Complete Descriptors of Reactivity in Catalysis by Solid Acids. *ACS Catal.* **2016**, *6*, 5386-5392. DOI: [10.1021/acscatal.6b01402](https://doi.org/10.1021/acscatal.6b01402).
35. Fang, Z.; Zetterholm, P.; Dixon, D. A., 1,2-Ethanediol and 1,3-Propanediol Conversions over (MO₃)₃ (M = Mo, W) Nanoclusters: A Computational Study. *J. Phys. Chem. A* **2016**, *120*, 1897-1907. DOI: [10.1021/acs.jpca.6b00158](https://doi.org/10.1021/acs.jpca.6b00158).
36. Henderson, M. A.; Mu, R.; Dahal, A.; Lyubinetzky, I.; Dohnálek, Z.; Glezakou, V.-A.; Rousseau, R., Light Makes a Surface Banana-Bond Split: Photodesorption of Molecular Hydrogen from RuO₂(110). *J. Am. Chem. Soc.* **2016**, *138*, 8714-8717. DOI: [10.1021/jacs.6b05083](https://doi.org/10.1021/jacs.6b05083).
37. Hu, J. Z.; Xu, S.; Kwak, J. H.; Hu, M. Y.; Wan, C.; Zhao, Z.; Szanyi, J.; Bao, X.; Han, X.; Wang, Y.; Peden, C. H. F., High Field ²⁷Al MAS NMR and TPD Studies of Active Sites in Ethanol Dehydration using Thermally Treated Transitional Aluminas as Catalysts. *J. Catal.* **2016**, *336*, 85-93. DOI: [10.1016/j.jcat.2016.01.006](https://doi.org/10.1016/j.jcat.2016.01.006).
38. Knaeble, W.; Iglesia, E., Acid Strength and Metal-acid Proximity Effects on Methylcyclohexane Ring Contraction Turnover Rates and Selectivities. *J. Catal.* **2016**, *344*, 817-830. DOI: [10.1016/j.jcat.2016.08.007](https://doi.org/10.1016/j.jcat.2016.08.007).
39. Knaeble, W.; Iglesia, E., Kinetic and Theoretical Insights into the Mechanism of Alkanol Dehydration on Solid Brønsted Acid Catalysts. *J. Phys. Chem. C* **2016**, *120*, 3371-3389. DOI: [10.1021/acs.jpcc.5b11127](https://doi.org/10.1021/acs.jpcc.5b11127).
40. Novotny, Z.; Netzer, F. P.; Dohnálek, Z., Ceria Nanoclusters on Graphene/Ru(0001): A New Model Catalyst System. *Surf. Sci.* **2016**, *652*, 230-237. DOI: [10.1016/j.susc.2016.03.020](https://doi.org/10.1016/j.susc.2016.03.020).
41. Petrik, N. G.; Kimmel, G. A.; Shen, M.; Henderson, M. A., Quenching of electron transfer reactions through coadsorption: A study of oxygen photodesorption from TiO₂(110). *Surf. Sci.* **2016**, *652*, 183-188. DOI: [10.1016/j.susc.2015.12.038](https://doi.org/10.1016/j.susc.2015.12.038).
42. Pruski, M.; Sadow, A. D.; Slowing, I. I.; Marshall, C. L.; Stair, P.; Rodriguez, J.; Harris, A.; Somorjai, G. A.; Biener, J.; Matranga, C.; Wang, C.; Schaidle, J. A.; Beckham, G. T.; Ruddy, D. A.; Deutsch, T.; Alia, S. M.; Narula, C.; Overbury, S.; Toops, T.; Bullock, R. M.; Peden, C. H. F.; Wang, Y.; Allendorf, M. D.; Nørskov, J.; Bligaard, T., Virtual Special Issue on Catalysis at the U.S. Department of Energy's National Laboratories. *ACS Catal.* **2016**, *6*, 3227-3235. DOI: [10.1021/acscatal.6b00823](https://doi.org/10.1021/acscatal.6b00823).
43. Rahman, M. M.; Davidson, S. D.; Sun, J. M.; Wang, Y., Effect of Water on Ethanol Conversion over ZnO. *Top. Catal.* **2016**, *59*, 37-45. DOI: [10.1007/s11244-015-0503-9](https://doi.org/10.1007/s11244-015-0503-9).
44. Ramasamy, K. K.; Gray, M.; Job, H.; Santosa, D.; Li, X. S.; Devaraj, A.; Karkamkar, A.; Wang, Y., Role of Calcination Temperature on the Hydrotalcite Derived MgO-Al₂O₃ in Converting Ethanol to Butanol. *Top. Catal.* **2016**, *59*, 46-54. DOI: [10.1007/s11244-015-0504-8](https://doi.org/10.1007/s11244-015-0504-8).
45. Robinson, S. J.; Zall, C. M.; Miller, D. L.; Linehan, J. C.; Appel, A. M., Solvent influence on the thermodynamics for hydride transfer from bis(diphosphine) complexes of nickel. *Dalton. Trans.* **2016**, *45*, 10017-10023. DOI: [10.1039/c6dt00309e](https://doi.org/10.1039/c6dt00309e).
46. Sun, J.; Baylon, R. A. L.; Liu, C.; Mei, D.; Martin, K. J.; Venkitasubramanian, P.; Wang, Y., Key Roles of Lewis Acid-Base Pairs on Zn_xZr_yO_z in Direct Ethanol/Acetone to Isobutene Conversion. *J. Am. Chem. Soc.* **2016**, *138*, 507-517. DOI: [10.1021/jacs.5b07401](https://doi.org/10.1021/jacs.5b07401).
47. Wan, C.; Hu, M. Y.; Jaegers, N. R.; Shi, D.; Wang, H.; Gao, F.; Qin, Z.; Wang, Y.; Hu, J. Z., Investigating the Surface Structure of γ -Al₂O₃ Supported WOX Catalysts by High Field ²⁷Al MAS NMR and Electronic Structure Calculations. *J. Phys. Chem. C* **2016**, *120*, 23093-23103. DOI: [10.1021/acs.jpcc.6b09060](https://doi.org/10.1021/acs.jpcc.6b09060).
48. Wang, H.; Wang, Y., Characterization of Deactivated Bio-oil Hydrotreating Catalysts. *Top. Catal.* **2016**, *59*, 65-72. DOI: [10.1007/s11244-015-0506-6](https://doi.org/10.1007/s11244-015-0506-6).

49. Wang, X.; Hong, Y. C.; Shi, H.; Szanyi, J., Kinetic modeling and transient DRIFTS-MS studies of CO₂ methanation over Ru/Al₂O₃ catalysts. *J. Catal.* **2016**, *343*, 185-195. DOI: [10.1016/j.jcat.2016.02.001](https://doi.org/10.1016/j.jcat.2016.02.001).
50. Wang, Y. G.; Cantu, D. C.; Lee, M. S.; Li, J.; Glezakou, V. A.; Rousseau, R., CO Oxidation on Au/TiO₂: Condition-Dependent Active Sites and Mechanistic Pathways. *J. Am. Chem. Soc.* **2016**, *138*, 10467-10476. DOI: [10.1021/jacs.6b04187](https://doi.org/10.1021/jacs.6b04187).
51. Yi, C. W.; Szanyi, J., Pd overlayer on oxygen pre-covered graphene/Ru(0001): Thermal stability. *Surf. Sci.* **2016**, *648*, 271-277. DOI: [10.1016/j.susc.2015.12.018](https://doi.org/10.1016/j.susc.2015.12.018).
52. Zall, C. M.; Linehan, J. C.; Appel, A. M., Triphosphine-Ligated Copper Hydrides for CO₂ Hydrogenation: Structure, Reactivity, and Thermodynamic Studies. *J. Am. Chem. Soc.* **2016**, *138*, 9968-9977. DOI: [10.1021/jacs.6b05349](https://doi.org/10.1021/jacs.6b05349).
53. Zhao, Z.; Xu, S.; Hu, M. Y.; Bao, X.; Hu, J. Z., In Situ High Temperature High Pressure MAS NMR Study on the Crystallization of AlPO₄-5. *J. Phys. Chem. C* **2016**, *120*, 1701-1708. DOI: [10.1021/acs.jpcc.5b11294](https://doi.org/10.1021/acs.jpcc.5b11294).
- 2017**
54. Boralugodage, N. P.; Arachchige, R. J.; Dutta, A.; Buchko, G. W.; Shaw, W. J., Evaluating the Role of Acidic, Basic, and Polar Amino Acids and Dipeptides on a Molecular Electrocatalyst for H₂ Oxidation. *Catal. Sci. Technol.* **2017**, *7*, 1108-1121. DOI: [10.1039/c6cy02579j](https://doi.org/10.1039/c6cy02579j).
55. Burgess, S. A.; Appel, A. M.; Linehan, J. C.; Wiedner, E. S., Changing the Mechanism for CO₂ Hydrogenation Using Solvent-Dependent Thermodynamics. *Angew. Chem.* **2017**, *129*, 15198-15201. DOI: [10.1002/ange.201709319](https://doi.org/10.1002/ange.201709319).
56. Burgess, S. A.; Grubel, K.; Appel, A. M.; Wiedner, E. S.; Linehan, J. C., Hydrogenation of CO₂ at Room Temperature and Low Pressure with a Cobalt Tetrphosphine Catalyst. *Inorg. Chem.* **2017**, *56*, 8580-8589. DOI: [10.1021/acs.inorgchem.7b01391](https://doi.org/10.1021/acs.inorgchem.7b01391).
57. Chen, J.; Sun, J.; Wang, Y., Catalysts for Steam Reforming of Bio-oil: A Review. *Ind. Eng. Chem. Res.* **2017**, *56*, 4627-4637. DOI: [10.1021/acs.iecr.7b00600](https://doi.org/10.1021/acs.iecr.7b00600).
58. Chen, L.; Smith, R. S.; Kay, B. D.; Dohnálek, Z., Direct Deoxygenation of Phenylmethanol to Methylbenzene and Benzyl Radicals on Rutile TiO₂(110). *ACS Catal.* **2017**, *7*, 2002-2006. DOI: [10.1021/acscatal.6b03225](https://doi.org/10.1021/acscatal.6b03225).
59. Dahal, A.; Dohnálek, Z., Formation of Metastable Water Chains on Anatase TiO₂(101). *J. Phys. Chem. C* **2017**, *121*, 20413-20418. DOI: [10.1021/acs.jpcc.7b08122](https://doi.org/10.1021/acs.jpcc.7b08122).
60. Glezakou, V.-A.; Rousseau, R.; Elbert, S. T.; Franz, J. A., Trends in Homolytic Bond Dissociation Energies of Five- and Six-Coordinate Hydrides of Group 9 Transition Metals: Co, Rh, Ir. *J. Phys. Chem. A* **2017**, *121*, 1993-2000. DOI: [10.1021/acs.jpca.6b11655](https://doi.org/10.1021/acs.jpca.6b11655).
61. Henderson, M. A.; Shen, M. M., Electron-Scavenging Chemistry of Benzoquinone on TiO₂(110). *Top. Catal.* **2017**, *60*, 440-445. DOI: [10.1007/s11244-016-0707-7](https://doi.org/10.1007/s11244-016-0707-7).
62. Hong, Y.; Wang, Y., Elucidation of Reaction Mechanism for m-cresol Hydrodeoxygenation over Fe Based Catalysts: A Kinetic Study. *Catal. Commun.* **2017**, *100*, 43-47. DOI: [10.1016/j.catcom.2017.06.028](https://doi.org/10.1016/j.catcom.2017.06.028).
63. Hong, Y.; Zhang, S.; Tao, F.; Wang, Y., Stabilization of Iron-based Catalysts against Oxidation: An in situ Ambient Pressure XPS Study. *ACS Catal.* **2017**, *7*, 3639-3643. DOI: [10.1021/acscatal.7b00636](https://doi.org/10.1021/acscatal.7b00636).
64. Houghton, A. Y.; Autrey, T., Calorimetric Study of the Activation of Hydrogen by Tris(pentafluorophenyl)borane and Trimesitylphosphine. *J. Phys. Chem. A* **2017**, *121*, 8785-8790. DOI: [10.1021/acs.jpca.7b08582](https://doi.org/10.1021/acs.jpca.7b08582).
65. Hu, J. Z.; Wan, C.; Vjunov, A.; Wang, M.; Zhao, Z.; Hu, M. Y.; Camaioni, D. M.; Lercher, J. A., ²⁷Al MAS NMR Studies of HBEA Zeolite at Low to High Magnetic Fields. *J. Phys. Chem. C* **2017**, *121*, 12849-12854. DOI: [10.1021/acs.jpcc.7b03517](https://doi.org/10.1021/acs.jpcc.7b03517).
66. Jaegers, N. R.; Hu, M. Y.; Hoyt, D. W.; Wang, Y.; Hu, J. Z. *Development and Application of In Situ High-Temperature, High-Pressure Magic Angle Spinning NMR in Modern Magnetic Resonance*; Webb, G. A., Ed.; Springer International Publishing: Cham, 2017; pp 1-19.

67. Jaegers, N. R.; Wan, C.; Hu, M. Y.; Vasiliu, M.; Dixon, D. A.; Walter, E.; Wachs, I. E.; Wang, Y.; Hu, J. Z., Investigation of Silica-Supported Vanadium Oxide Catalysts by High-Field ^{51}V Magic-Angle Spinning NMR. *J. Phys. Chem. C* **2017**, *121*, 6246-6254. DOI: [10.1021/acs.jpcc.7b01658](https://doi.org/10.1021/acs.jpcc.7b01658).
68. Li, W.-Z.; Nie, L.; Cheng, Y.; Kovarik, L.; Liu, J.; Wang, Y., Surface Enrichment of Pt in Stable Pt-Ir Nanoalloy Particles on MgAl_2O_4 Spinel in Oxidizing Atmosphere. *Catal. Commun.* **2017**, *93*, 57-61. DOI: [10.1016/j.catcom.2017.01.012](https://doi.org/10.1016/j.catcom.2017.01.012).
69. Liu, Y. S.; Vjunov, A.; Shi, H.; Eckstein, S.; Camaioni, D. M.; Mei, D. H.; Barath, E.; Lercher, J. A., Enhancing the Catalytic Activity of Hydronium Ions through Constrained Environments. *Nat. Commun.* **2017**, *8*, 14113. DOI: [10.1038/ncomms14113](https://doi.org/10.1038/ncomms14113).
70. Mei, D. H.; Lercher, J. A., Mechanistic Insights into Aqueous Phase Propanol Dehydration in H-ZSM-5 Zeolite. *AIChE J.* **2017**, *63*, 172-184. DOI: [10.1002/aic.15517](https://doi.org/10.1002/aic.15517).
71. Mu, R.; Dahal, A.; Wang, Z.-T.; Dohnálek, Z.; Kimmel, G. A.; Petrik, N. G.; Lyubnitsky, I., Adsorption and Photodesorption of CO from Charged Point Defects on $\text{TiO}_2(110)$. *J. Phys. Chem. Lett.* **2017**, *8*, 4565-4572. DOI: [10.1021/acs.jpcclett.7b02052](https://doi.org/10.1021/acs.jpcclett.7b02052).
72. Nguyen, M.-T.; Mu, R.; Cantu, D. C.; Lyubnitsky, I.; Glezakou, V.-A.; Dohnálek, Z.; Rousseau, R., Dynamics, Stability, and Adsorption States of Water on Oxidized $\text{RuO}_2(110)$. *J. Phys. Chem. C* **2017**, *121*, 18505-18515. DOI: [10.1021/acs.jpcc.7b03280](https://doi.org/10.1021/acs.jpcc.7b03280).
73. Shi, H.; Eckstein, S.; Vjunov, A.; Camaioni, D. M.; Lercher, J. A., Tailoring Nanoscopic Confines to Maximize Catalytic Activity of Hydronium Ions. *Nat. Commun.* **2017**, *8*, 15442. DOI: [10.1038/ncomms15442](https://doi.org/10.1038/ncomms15442).
74. Vasiliu, M.; Peterson, K. A.; Arduengo, A. J.; Dixon, D. A., Characterization of Carbenes via Hydrogenation Energies, Stability, and Reactivity: What's in a Name? *Chem. Eur. J.* **2017**, *23*, 17556-17565. DOI: [doi:10.1002/chem.201703539](https://doi.org/10.1002/chem.201703539).
75. Wang, M.; Shi, H.; Camaioni, D. M.; Lercher, J. A., Palladium-Catalyzed Hydrolytic Cleavage of Aromatic C-O Bonds. *Angew. Chem., Int. Ed.* **2017**, *56*, 2110-2114. DOI: [10.1002/anie.201611076](https://doi.org/10.1002/anie.201611076).
76. Wang, X.; Shi, H.; Szanyi, J., Controlling selectivities in CO_2 reduction through mechanistic understanding. *Nat. Commun.* **2017**, *8*, 513. DOI: [10.1038/s41467-017-00558-9](https://doi.org/10.1038/s41467-017-00558-9).
77. Wang, Z. T.; Wang, Y. G.; Mu, R.; Yoon, Y. H.; Dahal, A.; Schenter, G. K.; Glezakou, V. A.; Rousseau, R.; Lyubnitsky, I.; Dohnálek, Z., Probing Equilibrium of Molecular and Deprotonated Water on $\text{TiO}_2(110)$. *Proc. Natl. Acad. Sci. U. S. A.* **2017**, *114*, 1801-1805. DOI: [10.1073/pnas.1613756114](https://doi.org/10.1073/pnas.1613756114).
78. Zhang, S.; Appel, A. M.; Bullock, R. M., Reversible Heterolytic Cleavage of the H-H Bond by Molybdenum Complexes: Controlling the Dynamics of Exchange Between Proton and Hydride. *J. Am. Chem. Soc.* **2017**, *139*, 7376-7387. DOI: [10.1021/jacs.7b03053](https://doi.org/10.1021/jacs.7b03053).
79. Zhao, Z.; Shi, H.; Wan, C.; Hu, M. Y.; Liu, Y.; Mei, D.; Camaioni, D. M.; Hu, J. Z.; Lercher, J. A., Mechanism of Phenol Alkylation in Zeolite H-BEA Using In Situ Solid-State NMR Spectroscopy. *J. Am. Chem. Soc.* **2017**, *139*, 9178-9185. DOI: [10.1021/jacs.7b02153](https://doi.org/10.1021/jacs.7b02153).
- 2018**
80. Baylon, R. A. L.; Sun, J.; Kovarik, L.; Engelhard, M.; Li, H.; Winkelman, A. D.; Martin, K. J.; Wang, Y., Structural Identification of $\text{Zn}_x\text{Zr}_y\text{O}_z$ Catalysts for Cascade Aldolization and Self-Deoxygenation Reactions. *Appl. Catal. B.* DOI: [10.1016/j.apcatb.2018.04.051](https://doi.org/10.1016/j.apcatb.2018.04.051).
81. Liu, Y.; Baráth, E.; Shi, H.; Hu, J.; Camaioni, D. M.; Lercher, J. A., Solvent-determined Mechanistic Pathways in Zeolite-H-BEA-catalysed Phenol Alkylation. *Nat. Catal.* **2018**, *1*, 141-147. DOI: [10.1038/s41929-017-0015-z](https://doi.org/10.1038/s41929-017-0015-z).
82. Shi, D.; Wang, H.; Kovarik, L.; Gao, F.; Wan, C.; Hu, J. Z.; Wang, Y., WO_x supported on $\gamma\text{-Al}_2\text{O}_3$ with different morphologies as model catalysts for alkanol dehydration. *J. Catal.* **2018**, *363*, 1-8. DOI: [10.1016/j.jcat.2018.04.004](https://doi.org/10.1016/j.jcat.2018.04.004).

83. Wang, M.; Gutiérrez, O. Y.; Camaioni, D. M.; Lercher, J. A., Palladium Catalyzed Reductive Insertion of Alcohols in Aryl Ether Bonds. *Angew. Chem., Int. Ed.* **2018**. DOI: [10.1002/anie.201709445](https://doi.org/10.1002/anie.201709445).
84. Wiedner, E. S.; Linehan, J. C., Making a Splash in Homogeneous CO₂ Hydrogenation: Elucidating the Impact of Solvent on Catalytic Mechanisms. *Chem. Eur. J.* **2018**. DOI: [10.1002/chem.201801759](https://doi.org/10.1002/chem.201801759).
85. Yun, D.; Wang, Y.; Herrera, J., 1.Ethanol partial oxidation over VO_x/TiO₂ catalysts: the role of titania surface oxygen on the vanadia reoxidation in the Mars-van Krevelen mechanism. *ACS Catal* **2018**. DOI: [10.1021/acscatal.7b03327](https://doi.org/10.1021/acscatal.7b03327)

Publications jointly funded by this grant and other grants with leading intellectual contribution from this grant

2015

86. Dutta, A.; Lense, S.; Roberts, J. A. S.; Helm, M. L.; Shaw, W. J., The Role of Solvent and the Outer Coordination Sphere on H₂ Oxidation Using [Ni(P^{Cy}₂N^{Py}₂)₂]²⁺. *Eur. J. Inorg. Chem.* **2015**, 2015, 5218–5225. DOI: [10.1002/ejic.201500732](https://doi.org/10.1002/ejic.201500732). (A Dutta, S Lense, and WJ Shaw designed and performed the experiments, analyzed and interpreted data, and wrote the paper.)
87. Foraita, S.; Fulton, J. L.; Chase, Z. A.; Vjunov, A.; Xu, P.; Baráth, E.; Camaioni, D. M.; Zhao, C.; Lercher, J. A., Impact of the Oxygen Defects and the Hydrogen Concentration on the Surface of Tetragonal and Monoclinic ZrO₂ on the Reduction Rates of Stearic Acid on Ni/ZrO₂. *Chem. Eur. J.* **2015**, 21, 2423–2434. DOI: [10.1002/chem.201405312](https://doi.org/10.1002/chem.201405312). (JL Fulton, ZA Chase, A Vjunov, DM Camaioni, and JA Lercher were funded by this BES project, with JLF, ZAC, and AV performing XAFS measurements and related work, DMC contributing to manuscript preparation, and JAL directing the work and manuscript preparation.)
88. Hensley, A. J. R.; Wang, Y.; McEwen, J.-S., Phenol Deoxygenation Mechanisms on Fe(110) and Pd(111). *ACS Catal.* **2015**, 5, 523–536. DOI: [10.1021/cs501403w](https://doi.org/10.1021/cs501403w). (Y Wang participated in the interpretation of results and drafting of paper.)
89. Ho, M.-H.; O’Hagan, M.; Dupuis, M.; DuBois, D. L.; Bullock, R. M.; Shaw, W. J.; Raugel, S., Water-assisted Proton Delivery and Removal in Bio-inspired Hydrogen Production Catalysts. *Dalton. Trans.* **2015**, 44, 10969–10979. DOI: [10.1039/C5DT00782H](https://doi.org/10.1039/C5DT00782H). (WJ Shaw assisted in NMR data collection and interpretation and co-wrote the paper.)
90. Hu, J. Z.; Hu, M. Y.; Zhao, Z.; Xu, S.; Vjunov, A.; Shi, H.; Camaioni, D. M.; Peden, C. H. F.; Lercher, J. A., Sealed Rotors for In situ High Temperature High Pressure MAS NMR. *Chem. Commun.* **2015**, 51, 13458–13461. DOI: [10.1039/C5CC03910J](https://doi.org/10.1039/C5CC03910J). (Supported by the BES project, JZ Hu, A Vjunov, H Shi, DM Camaioni, CH Peden, and JA Lercher contributed to the parts of this work concerning molecular sieve crystallization under hydrothermal conditions and the zeolite-catalyzed dehydration of cyclohexanol in hot liquid water.)
91. Kasakov, S.; Shi, H.; Camaioni, D.; Zhao, C.; Barath, E.; Jentys, A.; Lercher, J. A., Reductive Deconstruction of Organosolv Lignin Catalysed by Zeolite Supported Nickel Nanoparticles. *Green Chem.* **2015**, 17, 5079–5090. DOI: [10.1039/C5GC02160J](https://doi.org/10.1039/C5GC02160J). (S Kasakov, H Shi, DM Camaioni, and JA Lercher were supported by the project. JA Lercher directed the work, S Kasakov performed the experimental work, and H Shi and DM Camaioni participated in the interpretation of the results and in the drafting of the manuscript.)
92. Kong, J.; He, M.; Lercher, J. A.; Zhao, C., Direct Production of Naphthenes and Paraffins from Lignin. *Chem. Commun.* **2015**, 51, 17580–17583. DOI: [10.1039/C5CC06828B](https://doi.org/10.1039/C5CC06828B). (JA Lercher was supported by this project. He directed the work and participated both in the interpretation of the results and in the drafting of the manuscript.)
93. Nandasiri, M. I.; Shutthanandan, V.; Manandhar, S.; Schwarz, A. M.; Oxenford, L.; Kennedy, J. V.; Thevuthasan, S.; Henderson, M. A., Instability of Hydrogenated TiO₂. *J. Phys. Chem. Lett.* **2015**, 6, 4627–4632. DOI: [10.1021/acs.jpcclett.5b02219](https://doi.org/10.1021/acs.jpcclett.5b02219). (MA Henderson was funded by this FWP to design and interpret the experiments and to write this article.)
94. Perea, D. E.; Arslan, I.; Liu, J.; Ristanović, Z.; Kovarik, L.; Arey, B. W.; Lercher, J. A.; Bare, S. R.; Weckhuysen, B. M., Determining the Location and Nearest Neighbours of Aluminium in Zeolites with Atom Probe Tomography. *Nat. Commun.* **2015**, 6, 7589. DOI: [10.1038/ncomms8589](https://doi.org/10.1038/ncomms8589). (JA Lercher was involved in the initial discussions of the experiments and contributed to the discussion and manuscript preparation.)

95. Petrik, N. G.; Henderson, M. A.; Kimmel, G. A., Insights into Acetone Photochemistry on Rutile TiO₂(110). 1. Off-Normal CH₃ Ejection from Acetone Diolate. *J. Phys. Chem. C* **2015**, *119*, 12262-12272. DOI: [10.1021/acs.jpcc.5b02477](https://doi.org/10.1021/acs.jpcc.5b02477). (MA Henderson was funded by this FWP to design and interpret the experiments and to contribute to writing of the manuscript. NG Petrik was supported by this program to perform experiments, analyze data, and help prepare the manuscript. GA Kimmel was funded by CPIMS, experimental design, data analysis and manuscript preparation.)
96. Petrik, N. G.; Henderson, M. A.; Kimmel, G. A., Insights into Acetone Photochemistry on Rutile TiO₂(110). 2. New Photodesorption Channel with CH₃ Ejection along the Surface Normal. *J. Phys. Chem. C* **2015**, *119*, 12273-12282. DOI: [10.1021/acs.jpcc.5b02478](https://doi.org/10.1021/acs.jpcc.5b02478). (MA Henderson was funded by this FWP to design and interpret the experiments and to contribute to writing of the manuscript. NG Petrik was supported by this program to perform experiments, analyze data, and help prepare the manuscript. GA Kimmel was funded by CPIMS, experimental design, data analysis and manuscript preparation.)
97. Rodriguez-Maciá, P.; Dutta, A.; Lubitz, W.; Shaw, W. J.; Rüdiger, O., Direct Comparison of the Performance of a Bio-inspired Synthetic Nickel Catalyst and a [NiFe]-Hydrogenase, Both Covalently Attached to Electrodes. *Angew. Chem., Int. Ed.* **2015**, *54*, 12303-12307. DOI: [10.1002/anie.201502364](https://doi.org/10.1002/anie.201502364). (A Dutta and WJ Shaw initiated the collaboration, provided the molecular complex, interpreted data, and co-wrote the paper.)
98. Schwenzler, B.; Cosimbescu, L.; Glezakou, V.-A.; Karkamkar, A. J.; Wang, Z.; Weber, R. S., Use of Solvatochromism to Assay Preferential Solvation of a Prototypic Catalytic Site. *Top. Catal.* **2015**, *58*, 258-270. DOI: [10.1007/s11244-015-0367-z](https://doi.org/10.1007/s11244-015-0367-z). (Theoretical studies by V-A Glezakou were supported by this program.)
99. Shi, H.; Lercher, J. A.; Yu, X.-Y., Sailing Into Uncharted Waters: Recent Advances in the In Situ Monitoring of Catalytic Processes in Aqueous Environments. *Catal. Sci. Technol.* **2015**, *5*, 3035–3060. DOI: [10.1039/C4CY01720J](https://doi.org/10.1039/C4CY01720J). (H Shi and JA Lercher were supported by this project and participated in the drafting of this literature review.)
100. Song, W.; Liu, Y.; Barath, E.; Zhao, C.; Lercher, J. A., Synergistic Effects of Ni and Acid Sites for Hydrogenation and C–O Bond Cleavage of Substituted Phenols. *Green Chem.* **2015**, *17*, 1204–1218. DOI: [10.1039/C4GC01798F](https://doi.org/10.1039/C4GC01798F). (JA Lercher was supported by this project and participated in the interpretation of the results, in the postulation of hypotheses ultimately confirmed, and in the drafting of the manuscript.)
101. Sun, J.; Karim, A. M.; Li, X. S.; Rainbolt, J.; Kovarik, L.; Shin, Y.; Wang, Y., Hierarchically structured catalysts for cascade and selective steam reforming/hydrodeoxygenation reactions. *Chem. Commun.* **2015**, *51*, 16617-16620. DOI: [10.1039/C5CC07244A](https://doi.org/10.1039/C5CC07244A). (J Sun performed the catalyst testing, YWang participated in the interpretation of the results and led the effort to draft the paper.)
102. Szanyi, J.; Kwak, J. H., Photo-catalytic oxidation of acetone on a TiO₂ powder: An in situ FTIR investigation. *J. Mol. Catal. A-Chem.* **2015**, *406*, 213-223. DOI: [10.1016/j.molcata.2015.05.025](https://doi.org/10.1016/j.molcata.2015.05.025). (J Szanyi was supported by this program to conduct all the experiment, analyze data and prepare the manuscript.)
103. Thanthiriwatte, K. S.; Vasiliu, M.; Battey, S. R.; Lu, Q.; Peterson, K. A.; Andrews, L.; Dixon, D. A., Gas Phase Properties of MX₂ and MX₄ (X = F, Cl) for M = Group 4, Group 14, Cerium, and Thorium. *J. Phys. Chem. A* **2015**, *119*, 5790-5803. DOI: [10.1021/acs.jpca.5b02544](https://doi.org/10.1021/acs.jpca.5b02544). (DA Dixon, KS Thanthiriwatte, and M Vasiliu supported by this program for computational work on Group 4 and 14 compounds and writing the manuscript.)
104. Vjunov, A.; Derewinski, M. A.; Fulton, J. L.; Camaioni, D. M.; Lercher, J. A., Impact of Zeolite Aging in Hot Liquid Water on Activity for Acid-Catalyzed Dehydration of Alcohols. *J. Am. Chem. Soc.* **2015**, *137*, 10374–10382. DOI: [10.1021/jacs.5b06169](https://doi.org/10.1021/jacs.5b06169). (All authors were supported by the BES project, M Derewinski was partially supported by the Materials Synthesis and Simulation Across Scales (MS3 Initiative) conducted under Laboratory Directed Research & Development Program at PNNL. His support under that program enabled the synthesis of several zeolites that were used in this work. Under the BES project, he participated in the interpretation of the results, in the postulation of hypotheses, and in the drafting of the manuscript.)
105. Wang, Y.-G.; Mei, D.; Glezakou, V.-A.; Li, J.; Rousseau, R., Dynamic formation of single-atom catalytic active sites on ceria-supported gold nanoparticles. *Nat. Commun.* **2015**, *6*. DOI: [10.1038/ncomms7511](https://doi.org/10.1038/ncomms7511). (J Li and Y-G Wang were also financially supported by NKBRFSF (2011CB932400) and NSFC of China.)

106. Wang, Z.-T.; Garcia, J. C.; Deskins, N. A.; Lyubinetsky, I., Ability of TiO₂(110) surface to be fully hydroxylated and fully reduced. *Phys. Rev. B* **2015**, *92*, 081402. (I Lyubinetsky and Z-T Wang were funded by this program to carry out experimental studies and prepare the manuscript.)
107. Wei, Z.; Karim, A.; Li, Y.; Wang, Y., Elucidation of the Roles of Re in Aqueous-Phase Reforming of Glycerol over Pt–Re/C Catalysts. *ACS Catal.* **2015**, *5*, 7312-7320. DOI: [10.1021/acscatal.5b01770](https://doi.org/10.1021/acscatal.5b01770). (Z Wei performed catalytic activity measurement, Y Wang participated in the interpretation of the results, and both Z Wei and Y Wang led the effort to draft the paper.)
108. Weiss, C. J.; Wiedner, E. S.; Roberts, J. A. S.; Appel, A. M., Nickel phosphine catalysts with pendant amines for electrocatalytic oxidation of alcohols. *Chem. Commun.* **2015**, *51*, 6172-6174. DOI: [10.1039/C5CC01107H](https://doi.org/10.1039/C5CC01107H). (CJ Weiss, ES Wiedner, and AM Appel were supported by this program to perform experiments, interpret results, and prepare the manuscript.)
109. Xu, S.; Walter, E. D.; Zhao, Z.; Hu, M. Y.; Han, X.; Hu, J. Z.; Bao, X., Dynamic Structural Changes of SiO₂ Supported Pt–Ni Bimetallic Catalysts over Redox Treatments Revealed by NMR and EPR. *J. Phys. Chem. C* **2015**, *119*, 21219-21226. DOI: [10.1021/acs.jpcc.5b06344](https://doi.org/10.1021/acs.jpcc.5b06344). (JZ Hu, S Xu, Z Zhao, and M Hu were supported by this program for conducting the NMR experiments and participate in the preparation of the manuscript. In particular, JZ Hu provided the NMR mentorship to S Xu.)
110. Yang, Y.; Mei, D.; Peden, C. H. F.; Campbell, C. T.; Mims, C. A., Surface-Bound Intermediates in Low-Temperature Methanol Synthesis on Copper: Participants and Spectators. *ACS Catal.* **2015**, *5*, 7328-7337. DOI: [10.1021/acscatal.5b02060](https://doi.org/10.1021/acscatal.5b02060). (D Mei and CHF Peden were supported by this program. CT Campbell acknowledges the Department of Energy, Office of Basic Energy Sciences, Chemical Sciences Division, CAM partial support as a visiting professor and the National Science and Engineering Research Council (Canada).)
111. Yoon, Y.; Du, Y.; Garcia, J. C.; Zhu, Z.; Wang, Z.-T.; Petrik, N. G.; Kimmel, G. A.; Dohnálek, Z.; Henderson, M. A.; Rousseau, R.; Deskins, N. A.; Lyubinetsky, I., Anticorrelation between Surface and Subsurface Point Defects and the Impact on the Redox Chemistry of TiO₂(110). *ChemPhysChem* **2015**, *16*, 313-321. DOI: [10.1002/cphc.201402599](https://doi.org/10.1002/cphc.201402599). (Y Yoon, ZT Wang, NG Petrik, GA Kimmel, Z Dohnálek, MA Henderson, R Rousseau, and I Lyubinetsky were funded by this FWP. I Lyubinetsky designed the experiments, ZT Wang carried out the STM experiments, Y Yoon and R Rousseau contributed to the DFT calculations; NG Petrik, GA Kimmel, Z Dohnálek, MA Henderson, R Rousseau, and I Lyubinetsky wrote the manuscript.)
- 2016**
112. Alexopoulos, K.; Lee, M.-S.; Liu, Y.; Zhi, Y.; Liu, Y.; Reyniers, M.-F.; Marin, G. B.; Glezakou, V.-A.; Rousseau, R.; Lercher, J. A., Anharmonicity and Confinement in Zeolites: Structure, Spectroscopy, and Adsorption Free Energy of Ethanol in H-ZSM-5. *J. Phys. Chem. C* **2016**, *120*, 7172–7182. DOI: [10.1021/acs.jpcc.6b00923](https://doi.org/10.1021/acs.jpcc.6b00923). (MS Lee, VA Glezakou, R Rousseau, and JA Lercher were supported by the BES project. MS Lee and VA Glezakou performed calculations. R Rousseau and JA Lercher participated in the interpretation of the results, in the postulation of hypotheses, and in the drafting of the manuscript.)
113. Asthagiri, A.; Dixon, D. A.; Dohnálek, Z.; Kay, B. D.; Rodriguez, J. A.; Rousseau, R.; Stacchiola, D. J.; Weaver, J. F. *Catalytic Chemistry on Oxide Nanostructures in Oxide Materials at the Two-Dimensional Limit*; Netzer, P. F., Fortunelli, A., Eds.; Springer International Publishing: Cham, 2016; pp 251-280. (DA Dixon, Z Dohnálek, BD Kay, and R Rousseau were supported by this program for the preparation of this book chapter.)
114. Cardenas, A. J. P.; Ginovska, B.; Kumar, N.; Hou, J.; Raugei, S.; Helm, M. L.; Appel, A. M.; Bullock, R. M.; O'Hagan, M., Controlling Proton Delivery through Catalyst Structural Dynamics. *Angew. Chem., Int. Ed.* **2016**, *55*, 13509-13513. DOI: [10.1002/anie.201607460](https://doi.org/10.1002/anie.201607460). (BB Ginovska was supported by this program for doing MD simulations and manuscript preparation.)
115. Comish, A. J.; Ginovska, B.; Thelen, A.; da Silva, J. C. S.; Soares, T. A.; Raugei, S.; Dupuis, M.; Shaw, W. J.; Hegg, E. L., Single-Amino Acid Modifications Reveal Additional Controls on the Proton Pathway of FeFe–Hydrogenase. *Biochemistry* **2016**, *55*, 3165-3173. DOI: [10.1021/acs.biochem.5b01044](https://doi.org/10.1021/acs.biochem.5b01044).
116. Dutta, A.; Ginovska, B.; Raugei, S.; Roberts, J. A.; Shaw, W. J., Optimizing Conditions for Utilization of an H₂ Oxidation Catalyst with Outer Coordination Sphere Functionalities. *Dalton Trans* **2016**, *45*, 9786-993.

- DOI: [10.1039/c6dt00280c](https://doi.org/10.1039/c6dt00280c). (A Dutta, B Ginovska, WJ Shaw designed and performed the experiments, analyzed and interpreted data, and wrote the paper.)
117. Fang, Z. T.; Both, J.; Li, S. G.; Yue, S. W.; Apra, E.; Keceli, M.; Wagner, A. F.; Dixon, D. A., Benchmark Calculations of Energetic Properties of Groups 4 and 6 Transition Metal Oxide Nanoclusters Including Comparison to Density Functional Theory. *J. Chem. Theory Comput.* **2016**, *12*, 3689-3710. DOI: [10.1021/acs.jctc.6b00464](https://doi.org/10.1021/acs.jctc.6b00464). (DA Dixon, Z Fang, and J Both were supported by this program for most of the computational work and writing the manuscript.)
118. Fang, Z. T.; Lee, Z.; Peterson, K. A.; Dixon, D. A., Use of Improved Orbitals for CCSD(T) Calculations for Predicting Heats of Formation of Group IV and Group VI Metal Oxide Monomers and Dimers and UCl_6 . *J. Chem. Theory Comput.* **2016**, *12*, 3583-3592. DOI: [10.1021/acs.jctc.6b00327](https://doi.org/10.1021/acs.jctc.6b00327). (DA Dixon and Z Fang were supported by this program for computational work on Group 4 and 6 compounds and writing the manuscript.)
119. Fang, Z.; Thanthiriwatte, K. S.; Dixon, D. A.; Andrews, L.; Wang, X., Properties of Cerium Hydroxides from Matrix Infrared Spectra and Electronic Structure Calculations. *Inorg. Chem.* **2016**, *55*, 1702-1714. DOI: [10.1021/acs.inorgchem.5b02619](https://doi.org/10.1021/acs.inorgchem.5b02619). (DA Dixon and Z Fang were supported by this program for computational work on Ce compounds and writing the manuscript.)
120. Feller, D.; Peterson, K. A.; Dixon, D. A. The Impact of Larger Basis Sets and Explicitly Correlated Coupled Cluster Theory on the Feller-Peterson-Dixon Composite Method in Annual Reports in Computational Chemistry; Dixon, D. A., Ed.; Elsevier: Amsterdam, 2016; Vol. 12. (DA Dixon was supported by this program for the preparation of this book chapter.)
121. Finney, B.; Fang, Z.; Francisco, J. S.; Dixon, D. A., Energetic Properties and Electronic Structure of $[Si,N,S]$ and $[Si,P,S]$ Isomers. *J. Phys. Chem. A* **2016**, *120*, 1691-1697. DOI: [10.1021/acs.jpca.6b00918](https://doi.org/10.1021/acs.jpca.6b00918). (DA Dixon and Z Fang were supported by this program for computational work on title compounds and writing the manuscript.)
122. Ginovska, B.; Raugei, S.; Shaw, W. J. Molecular Dynamics Studies of Proton Transport in Hydrogenase and Hydrogenase Mimics in Computational Approaches for Studying Enzyme Mechanism, Pt B; Voth, G. A., Ed., 2016; Vol. 578; pp 73-101.
123. Haiges, R.; Vasiliu, M.; Dixon, D. A.; Christe, K. O., The niobium oxoazides $[NbO(N_3)_3]$, $[NbO(N_3)_3 \cdot 2CH_3CN]$, $[(bipy)NbO(N_3)_3]$, $Cs_2[NbO(N_3)_5]$ and $[PPh_4]_2[NbO(N_3)_5]$. *Dalton Trans* **2016**, *45*, 10523-9. DOI: [10.1039/c6dt01479h](https://doi.org/10.1039/c6dt01479h). (DA Dixon and M Vasiliu were supported by this program for all computational work and writing the manuscript.)
124. Henderson, M. A.; Chen, J. G.; Dohnálek, Z., Editorial: Insights into Surface Phenomena: In Honor of John T. Yates Jr. *Surf. Sci.* **2016**, *652*, 1. DOI: [10.1016/j.susc.2016.06.017](https://doi.org/10.1016/j.susc.2016.06.017). (Z Dohnálek and MA Henderson were funded by this FWP to prepare this editorial.)
125. Kelley, S. P.; McCrary, P. D.; Flores, L.; Garner, E. B.; Dixon, D. A.; Rogers, R. D., Structural and Theoretical Study of Salts of the $B_9H_{14}^-$ Ion: Isolation of Multiple Isomers and Implications for Energy Storage. *Chempluschem* **2016**, *81*, 922-925. DOI: [10.1002/cplu.201600270](https://doi.org/10.1002/cplu.201600270). (DA Dixon, L Flores, and EB Garner were supported by this program for all computational work and writing the manuscript.)
126. Kwak, J. H.; Lee, J.; Szanyi, J.; Peden, C. H. F., Modification of the acid/base properties of $\gamma-Al_2O_3$ by oxide additives: An ethanol TPD investigation. *Catal. Today* **2016**, *265*, 240-244. DOI: [10.1016/j.cattod.2015.07.042](https://doi.org/10.1016/j.cattod.2015.07.042). (J Szanyi was supported by this program to participate in the experimental design, data interpretation, and in the preparation of the manuscript.)
127. Laminack, W.; Gole, J. L.; White, M. G.; Ozdemir, S.; Ogden, A. G.; Martin, H. J.; Fang, Z.; Wang, T.-H.; Dixon, D. A., Synthesis of nanoscale silicon oxide oxidation state distributions: The transformation from hydrophilicity to hydrophobicity. *Chem. Phys. Lett.* **2016**, *653*, 137-143. DOI: [10.1016/j.cplett.2016.04.079](https://doi.org/10.1016/j.cplett.2016.04.079). (DA Dixon, TH Wang, and Z Fang were supported by this program for all computational work and writing the manuscript.)
128. Lao, D. B.; Galan, B. R.; Linehan, J. C.; Heldebrant, D. J., The steps of activating a prospective CO_2 hydrogenation catalyst with combined CO_2 capture and reduction. *Green Chem.* **2016**, *18*, 4871-4874. DOI: [10.1039/c6gc01800a](https://doi.org/10.1039/c6gc01800a). (JC Linehan and BR Galan were supported by this program to perform operando catalysis studies and interpret the corresponding data.)

129. Lee, M. S.; Um, W.; Wang, G.; Kruger, A. A.; Lukens, W. W.; Rousseau, R.; Glezakou, V. A., Impeding $^{99}\text{Tc(IV)}$ mobility in novel waste forms. *Nat. Commun.* **2016**, *7*, 12067. DOI: [10.1038/ncomms12067](https://doi.org/10.1038/ncomms12067). (M-S Lee contributed to the planning and executed the simulations and analysed the data, W Um, G Wang, and WW Lukens performed the experiments and related data analysis. R Rousseau provided pseudopotentials for the calculations and contributed to the analysis of the data. V-A Glezakou planned and supervised the research. M-S Lee, R Rousseau, and V-A Glezakou jointly wrote the manuscript with input from all authors.)
130. Peroni, M.; Mancino, G.; Baráth, E.; Gutiérrez, O. Y.; Lercher, J. A., Bulk and $\gamma\text{Al}_2\text{O}_3$ -supported Ni_2P and MoP for Hydrodeoxygenation of Palmitic Acid. *Appl.Catal. B* **2016**, *180*, 301–311. DOI: [10.1016/j.apcatb.2015.06.042](https://doi.org/10.1016/j.apcatb.2015.06.042). (Supported by the BES project, JA Lercher participated in the interpretation of the results, in the postulation of hypotheses, and in the drafting of the manuscript.)
131. Priyadarshani, N.; Dutta, A.; Ginovska, B.; Buchko, G. W.; O'Hagan, M.; Rauei, S.; Shaw, W. J., Achieving Reversible H_2/H^+ Interconversion at Room Temperature with Enzyme-Inspired Molecular Complexes: A Mechanistic Study. *ACS Catal.* **2016**, *6*, 6037–6049. DOI: [10.1021/acscatal.6b01433](https://doi.org/10.1021/acscatal.6b01433). (N Priyadarshani, A Dutta, B Ginovska, GW Buchko, and WJ Shaw designed and performed the experiments, analyzed and interpreted data, and wrote the paper.)
132. Prodinge, S.; Derewinski, M. A.; Vjunov, A.; Burton, S. D.; Arslan, I.; Lercher, J. A., Improving Stability of Zeolites in Aqueous Phase via Selective Removal of Structural Defects. *J. Am. Chem. Soc.* **2016**, *138*, 4408–4415. DOI: [10.1021/jacs.5b12785](https://doi.org/10.1021/jacs.5b12785). (A Vjunov, SA Burton, I Arslan, and JA Lercher were supported by this program. SA Burton contributed to NMR measurements, A Vjunov participated in the preparation of the manuscript, I Arslan carried out TEM measurements, and JA Lercher participated in data evaluation and manuscript preparation.)
133. Reback, M. L.; Ginovska, B.; Buchko, G. W.; Dutta, A.; Priyadarshani, N.; Kier, B. L.; Helm, M. L.; Rauei, S.; Shaw, W. J., Investigating the Role of Chain and Linker Length on the Catalytic Activity of an H_2 Production Catalyst Containing Beta-hairpin Peptide. *J. Coord. Chem.* **2016**, *69*, 1730–1747. DOI: [10.1080/00958972.2016.1188924](https://doi.org/10.1080/00958972.2016.1188924). (B Ginovska, GW Buchko, A Dutta, N Priyadarshani, and WJ Shaw designed and performed the calculations and supporting experiments, analyzed and interpreted data, and wrote the paper.)
134. Rodriguez-Macia, P.; Priyadarshani, N.; Dutta, A.; Weidenthaler, C.; Lubitz, W.; Shaw, W. J.; Rudiger, O., Covalent Attachment of the Water-insoluble $\text{Ni}(\text{P}^{\text{Cy}2}\text{N}^{\text{Ph}2})_2$ Electrocatalyst to Electrodes Showing Reversible Catalysis in Aqueous Solution. *Electroanalysis* **2016**, *28*, 2452–2458. DOI: [10.1002/elan.201600306](https://doi.org/10.1002/elan.201600306). (A Dutta and WJ Shaw provided the molecular complex, assisted in interpreting data, and co-wrote the paper.)
135. Schreiber, M. W.; Rodriguez-Nino, D.; Gutiérrez, O. Y.; Lercher, J. A., Hydrodeoxygenation of Fatty Acid Esters Catalyzed by Ni on Nano-sized MFI Type Zeolites. *Catal. Sci. Technol.* **2016**, *6*, 7976–7984. DOI: [10.1039/c6cy01598k](https://doi.org/10.1039/c6cy01598k). (Funded by this BES project, JA Lercher participated in the interpretation of the results, in the postulation of hypotheses, and in the drafting of the manuscript.)
136. Song, W.; Liu, Y.; Baráth, E.; Wang, L. L.; Zhao, C.; Mei, D.; Lercher, J. A., Dehydration of 1-Octadecanol over H-BEA: A Combined Experimental and Computational Study. *ACS Catal.* **2016**, *6*, 878–889. DOI: [10.1021/acscatal.5b01217](https://doi.org/10.1021/acscatal.5b01217). (LL Wang, D Mei, and JA Lercher were supported by the BES project. LL Wang and D Mei performed first-principal computations. JA Lercher participated in the interpretation of the results, in the postulation of hypotheses, and in the drafting of the manuscript.)
137. Song, Y.; Gutiérrez, O. Y.; Herranz, J.; Lercher, J. A., Aqueous Phase Electrocatalysis and Thermal Catalysis for the Hydrogenation of Phenol at Mild Conditions. *Appl.Catal. B* **2016**, *182*, 236–246. DOI: [10.1016/j.apcatb.2015.09.027](https://doi.org/10.1016/j.apcatb.2015.09.027). (Supported by this project, JA Lercher participated in the interpretation of the results, in the postulation of hypotheses, and in the drafting of the manuscript.)
138. Wang, W. Y.; Wu, K.; Liu, P. L.; Li, L.; Yang, Y. Q.; Wang, Y., Hydrodeoxygenation of p-Cresol over $\text{Pt}/\text{Al}_2\text{O}_3$ Catalyst Promoted by ZrO_2 , CeO_2 , and $\text{CeO}_2\text{-ZrO}_2$. *Ind. Eng. Chem. Res.* **2016**, *55*, 7598–7603. DOI: [10.1021/acs.iecr.6b00515](https://doi.org/10.1021/acs.iecr.6b00515). (Y Wang participated in the interpretation of results and writing the paper.)
139. Wiedner, E. S.; Chambers, M. B.; Pitman, C. L.; Bullock, R. M.; Miller, A. J. M.; Appel, A. M., Thermodynamic Hydricity of Transition Metal Hydrides. *Chem. Rev.* **2016**, *116*, 8655–8692. DOI: [10.1021/acs.chemrev.6b00168](https://doi.org/10.1021/acs.chemrev.6b00168). (ES Wiedner and AM Appel were supported by this program to tabulate thermochemical values and participate in the manuscript preparation.)

140. Xu, S.; Zhao, Z.; Hu, M. Y.; Han, X.; Hu, J. Z.; Bao, X., Investigation of water assisted phase transformation process from $\text{AlPO}_4\text{-5}$ to $\text{AlPO}_4\text{-tridymite}$. *Microporous Mesoporous Mat.* **2016**, *223*, 241-246. DOI: [10.1016/j.micromeso.2015.10.039](https://doi.org/10.1016/j.micromeso.2015.10.039). (JZ Hu, S Xu, Z Zhao, and M Hu were supported by this program for conducting the NMR experiments and participate in the preparation of the manuscript. In particular, JZ Hu provided the NMR mentorship to S Xu.)
141. Yu, X. J.; Zhang, Z. R.; Yang, C. W.; Bebensee, F.; Heissler, S.; Nefedov, A.; Tang, M. R.; Ge, Q. F.; Chen, L.; Kay, B. D.; Dohnálek, Z.; Wang, Y. M.; Woll, C., Interaction of Formaldehyde with the Rutile $\text{TiO}_2(110)$ Surface: A Combined Experimental and Theoretical Study. *J. Phys. Chem. C* **2016**, *120*, 12626-12636. DOI: [10.1021/acs.jpcc.6b03689](https://doi.org/10.1021/acs.jpcc.6b03689). (L Cheng, BD Kay, and Z Dohnálek were funded by this FWP. L Cheng carried out the TPD measurements, BD Kay and Z Dohnálek guided TPD experiments, put forward data interpretations, and contributed to the manuscript preparation.)
142. Zhang, S. G.; Li, H. X.; Appel, A. M.; Hall, M. B.; Bullock, R. M., Facile P-C/C-H Bond-Cleavage Reactivity of Nickel Bis(diphosphine) Complexes. *Chem.-Eur. J.* **2016**, *22*, 9493-9497. DOI: [10.1002/chem.201601469](https://doi.org/10.1002/chem.201601469). (SG Zhang, AM Appel, and RM Bullock were supported by this project to perform and interpret all experimental data, as well as prepare the manuscript.)
- 2017**
143. Agirrezabal-Telleria, I.; Iglesia, E., Stabilization of active, selective, and regenerable Ni-based dimerization catalysts by condensation of ethene within ordered mesopores. *J. Catal.* **2017**, *352*, 505-514. DOI: [10.1016/j.jcat.2017.06.025](https://doi.org/10.1016/j.jcat.2017.06.025). (I Agirrezabal-Telleria stipend was covered by a Marie Curie Fellowship. Most of the materials expenses and all of E Iglesia's time were covered by this project.)
144. Burgess, S. A.; Kendall, A. J.; Tyler, D. R.; Linehan, J. C.; Appel, A. M., Hydrogenation of CO_2 in Water Using a Bis(diphosphine) Ni-H Complex. *ACS Catal.* **2017**, *7*, 3089-3096. DOI: [10.1021/acscatal.7b00350](https://doi.org/10.1021/acscatal.7b00350). (SA Burgess, JC Linehan, and AM Appel were supported by this project to perform and interpret all catalytic and thermodynamic data, as well as prepare the manuscript.)
145. Chen, M.; Dixon, D. A., Modeling the formation of TiO_2 ultra-small nanoparticles. *Nanoscale* **2017**, *9*, 7143-7162. DOI: [10.1039/C7NR01749A](https://doi.org/10.1039/C7NR01749A). (DA Dixon was supported by this program for data analysis and writing the manuscript.)
146. Christe, K. O.; Haiges, R.; Rahm, M.; Dixon, D. A.; Vasiliu, M., Misconceptions on fluoronium ions and hypervalent fluorine cations. *J. Fluorine Chem.* **2017**, *204*, 6-10. DOI: [10.1016/j.jfluchem.2017.09.011](https://doi.org/10.1016/j.jfluchem.2017.09.011). (DA Dixon and M Vasiliu were supported by this program for most of the computational work and writing the manuscript.)
147. Christe, K. O.; Haiges, R.; Vasiliu, M.; Dixon, D. A., Formation Mechanism of NF_4^+ Salts and Extraordinary Enhancement of the Oxidizing Power of Fluorine by Strong Lewis Acids. *Angew. Chem., Int. Ed.* **2017**. DOI: [10.1002/anie.201701784](https://doi.org/10.1002/anie.201701784). (DA Dixon and M Vasiliu were supported by this program for all computational work and writing the manuscript.)
148. Eckstein, S.; Hintermeier, P. H.; Olarte, M. V.; Liu, Y.; Baráth, E.; Lercher, J. A., Elementary Steps and Reaction Pathways in the Aqueous Phase Alkylation of Phenol with Ethanol. *J. Catal.* **2017**, *352*, 329-336. DOI: [10.1016/j.jcat.2017.06.002](https://doi.org/10.1016/j.jcat.2017.06.002). (Funded by this BES project, JA Lercher contributed to the interpretation of the data and manuscript preparation.)
149. Fang, Z. T.; Vasiliu, M.; Peterson, K. A.; Dixon, D. A., Prediction of Bond Dissociation Energies/Heats of Formation for Diatomic Transition Metal Compounds: CCSD(T) Works. *J. Chem. Theory Comput.* **2017**, *13*, 1057-1066. DOI: [10.1021/acs.jctc.6b00971](https://doi.org/10.1021/acs.jctc.6b00971). (DA Dixon and M Vasiliu were supported by this program for all computational work and writing the manuscript.)
150. Feng, R. L.; Vasiliu, M.; Peterson, K. A.; Dixon, D. A., Acidity of $\text{M(VI)O}_2(\text{OH})_2$ for M = Group 6, 16, and U as Central Atoms. *J. Phys. Chem. A* **2017**, *121*, 1041-1050. DOI: [10.1021/acs.jpca.6b11889](https://doi.org/10.1021/acs.jpca.6b11889). (DA Dixon and M Vasiliu were supported by this program for computational work on Group 6 and 16 and writing the manuscript.)
151. Foraita, S.; Liu, Y.; Haller, G. L.; Barath, E.; Zhao, C.; Lercher, J. A., Controlling Hydrodeoxygenation of Stearic Acid to n-Heptadecane and n-Octadecane by Adjusting the Chemical Properties of Ni/SiO₂-ZrO₂ Catalyst. *Chemcatchem* **2017**, *9*, 195-203. DOI: [10.1002/cctc.201601162](https://doi.org/10.1002/cctc.201601162). (Supported by this project to

- explore oxidic supports for deoxygenation, JA Lercher participated in the interpretation of the results, in the postulation of hypotheses, and in the drafting of the manuscript.)
152. Gentil, S.; Lalaoui, N.; Dutta, A.; Nedellec, Y.; Cosnier, S.; Shaw, W. J.; Artero, V.; Le Goff, A., Carbon-Nanotube-Supported Bio-Inspired Nickel Catalyst and Its Integration in Hybrid Hydrogen/Air Fuel Cells. *Angew. Chem., Int. Ed.* **2017**, *56*, 1845-1849. DOI: [10.1002/anie.201611532](https://doi.org/10.1002/anie.201611532). (A Dutta and WJ Shaw provided the molecular complex, assisted in interpreting data, and co-wrote the paper.)
 153. Hintermeier, P. H.; Eckstein, S.; Mei, D.; Olarte, M. V.; Camaioni, D. M.; Baráth, E.; Lercher, J. A., Hydronium-Ion-Catalyzed Elimination Pathways of Substituted Cyclohexanols in Zeolite H-ZSM5. *ACS Catal.* **2017**, *7*, 7822–7829. DOI: [10.1021/acscatal.7b01582](https://doi.org/10.1021/acscatal.7b01582). (Supported by this project, JA Lercher participated in the interpretation of the results, in the postulation of hypotheses, and in the drafting of the manuscript.)
 154. Jeletic, M. S.; Hulley, E. B.; Helm, M. L.; Mock, M. T.; Appel, A. M.; Wiedner, E. S.; Linehan, J. C., Understanding the Relationship Between Kinetics and Thermodynamics in CO₂ Hydrogenation Catalysis. *ACS Catal.* **2017**, *7*, 6008-6017. DOI: [10.1021/acscatal.7b01673](https://doi.org/10.1021/acscatal.7b01673). (MS Jeletic, AM Appel, ES Wiedner, and JC Linehan were supported by this program to perform catalysis and thermodynamic measurements, and to prepare the manuscript.)
 155. Li, W. Z.; Kovarik, L.; Cheng, Y. W.; Nie, L.; Bowden, M. E.; Liu, J.; Wang, Y., Stabilization and transformation of Pt nanocrystals supported on ZnAl₂O₄ spinel. *Rsc Advances* **2017**, *7*, 3282-3286. DOI: [10.1039/c6ra26159k](https://doi.org/10.1039/c6ra26159k). (W Li performed most experimental studies, Y Wang and J Liu participated in the interpretation of the results and drafting the manuscript.)
 156. Mu, R.; Zhao, Z.-j.; Dohnálek, Z.; Gong, J., Structural motifs of water on metal oxide surfaces. *Chem. Soc. Rev.* **2017**, *46*, 1785-1806. DOI: [10.1039/C6CS00864J](https://doi.org/10.1039/C6CS00864J). (Z Dohnálek was funded by this FWP to contribute to this review.)
 157. Nie, L.; Mei, D.; Xiong, H.; Peng, B.; Ren, Z.; Isidro Pereira Hernandez, X.; DeLaRiva, A.; Wang, M.; Engelhard, M.; Kovarik, L.; Datye, A.; Wang, Y., Activation of surface lattice oxygen in single-atom Pt/CeO₂ for low-temperature CO oxidation. *Science* **2017**, *358*, 1419-1423. DOI: [10.1126/science.aao2109](https://doi.org/10.1126/science.aao2109). (D Mei performed DFT calculations and Y Wang participated in the interpretation of results.)
 158. Novotny, Z.; Zhang, Z.; Dohnálek, Z., Imaging Chemical Reactions One Molecule at a Time. *Reference Module in Chemistry, Molecular Sciences and Chemical Engineering* **2017**. DOI: [10.1016/B978-0-12-409547-2.12844-6](https://doi.org/10.1016/B978-0-12-409547-2.12844-6). (Z Dohnálek was funded by this FWP to contribute to this review.)
 159. Peroni, M.; Lee, I.; Huang, X.; Baráth, E.; Gutiérrez, O. Y.; Lercher, J. A., Deoxygenation of Palmitic Acid on Unsupported Transition-Metal Phosphides. *ACS Catal.* **2017**, *7*, 6331–6341. DOI: [10.1021/acscatal.7b01294](https://doi.org/10.1021/acscatal.7b01294). (Supported by this project to explore nonoxidic supports for deoxygenation, JA Lercher participated in the interpretation of the results, in the postulation of hypotheses, and in the drafting of the manuscript.)
 160. Prodingler, S.; Shi, H.; Eckstein, S.; Hu, J. Z.; Olarte, M. V.; Camaioni, D. M.; Derewinski, M. A.; Lercher, J. A., Stability of Zeolites in Aqueous Phase Reactions. *Chem. Mater.* **2017**, *29*, 7255–7262. DOI: [10.1021/acs.chemmater.7b01847](https://doi.org/10.1021/acs.chemmater.7b01847). (S Hui, H Eckstein, JZ Hu, MV Olarte, DM Camaioni, and JA Lercher were supported by this program for exploring acidic supports for deoxygenation reactions and NMR experiments. S Hui participated in catalytic tests, H Eckstein contributed to measurement of sorption properties, JZ Hu participated in the NMR measurements, MV Olarte was involved in catalytic measurements, and JA Lercher in data interpretation and preparation of the manuscript.)
 161. Resende, K. A.; Hori, C. E.; Noronha, F. B.; Shi, H.; Gutiérrez, O. Y.; Camaioni, D. M.; Lercher, J. A., Aqueous Phase Hydrogenation of Phenol Catalyzed by Pd and PdAg on ZrO₂. *Applied Catalysis. A, General* **2017**, p. 128–135. DOI: [10.1016/j.apcata.2017.08.005](https://doi.org/10.1016/j.apcata.2017.08.005). (S Hui, OY Gutiérrez, DM Camaioni, and JA Lercher were supported by this program and participated in the interpretation of the results, in the postulation of hypotheses ultimately confirmed, and in the drafting of the manuscript. KA Resende and CE Hori were supported by the National Council for Scientific and Technological Development (CNPq, Conselho Nacional de Desenvolvimento Científico e Tecnológico) of the Brazilian federal government under the Ministry of Science and Technology.)

162. Vasiliu, M.; Peterson, K. A.; Dixon, D. A., Benchmark-Quality Atomization Energies for BeH and BeH₂. *J. Chem. Theory Comput.* **2017**, *13*, 649-653. DOI: [10.1021/acs.jctc.6b01154](https://doi.org/10.1021/acs.jctc.6b01154). (DA Dixon and M Vasiliu were supported by this program for most of the computational work and writing the manuscript.)
163. Vjunov, A.; Wang, M.; Govind, N.; Huthwelker, T.; Shi, H.; Mei, D.; Fulton, J. L.; Lercher, J. A., Tracking the Chemical Transformations at the Brønsted Acid Site upon Water-Induced Deprotonation in a Zeolite Pore. *Chem. Mater.* **2017**, *29*, 9030–9042. DOI: [10.1021/acs.chemmater.7b02133](https://doi.org/10.1021/acs.chemmater.7b02133). (A Vjunov, JL Fulton, D Mei, H Shi, and JA Lercher were supported by the BES project. A Vjunov and JA Lercher performed X-ray absorption spectroscopy measurements. A Vjunov performed Infrared spectroscopy measurements. D Mei performed first principle calculations. JA Lercher and JL Fulton contributed to the interpretation of the results, in the postulation of hypotheses, and in the drafting of the manuscript.)
164. Wagenhofer, M. F.; Barath, E.; Gutiérrez, O. Y.; Lercher, J. A., Carbon-Carbon Bond Scission Pathways in the Deoxygenation of Fatty Acids on Transition-Metal Sulfides. *ACS Catal.* **2017**, *7*, 1068–1076. DOI: [10.1021/acscatal.6b02753](https://doi.org/10.1021/acscatal.6b02753). (JA Lercher was supported by this program. MF Wagenhofer, E Barath, and OY Gutiérrez were support by the German Federal Ministry of Food and Agriculture.)
165. Wei, R.; Li, Q.; Gong, Y.; Andrews, L.; Fang, Z.; Thanthiriwatte, K. S.; Vasiliu, M.; Dixon, D. A., Infrared Spectroscopic and Theoretical Studies on the OMF₂ and OMF (M = Cr, Mo, W) Molecules in Solid Argon. *J. Phys. Chem. A* **2017**, *121*, 7603-7612. DOI: [10.1021/acs.jpca.7b08088](https://doi.org/10.1021/acs.jpca.7b08088). (DA Dixon, KS Thanthiriwatte, and M Vasiliu were supported by this program for all computational work and writing the manuscript.)
166. Xu, C.-Q.; Lee, M.-S.; Wang, Y.-G.; Cantu, D. C.; Li, J.; Glezakou, V.-A.; Rousseau, R., Structural Rearrangement of Au–Pd Nanoparticles under Reaction Conditions: An ab Initio Molecular Dynamics Study. *ACS Nano* **2017**. DOI: [10.1021/acsnano.6b07409](https://doi.org/10.1021/acsnano.6b07409). (The authors M-S Lee, Y-G Wang, DC Cantu, V-A Glezakou, and R Rousseau were supported by this program; C-Q Xu and J Li were financially sponsored by NSFC and NKBRSF of China.)

2018

167. Burks, D. B.; Vasiliu, M.; Dixon, D. A.; Papish, E. T., Thermodynamic Acidity Studies of 6,6'-Dihydroxy-2,2'-bipyridine: A Combined Experimental and Computational Approach. *J. Phys. Chem. A* **2018**, *122*, 2221-2231. DOI: [10.1021/acs.jpca.7b11441](https://doi.org/10.1021/acs.jpca.7b11441). (DA Dixon and M Vasiliu were supported by this program for all of the computational work and writing the manuscript.)
168. Feller, D.; Dixon, D. A., Density Functional Theory and the Basis Set Truncation Problem with Correlation Consistent Basis Sets: Elephant in the Room or Mouse in the Closet? *J. Phys. Chem. A* **2018**, *122*, 2598-2603. DOI: [10.1021/acs.jpca.8b00392](https://doi.org/10.1021/acs.jpca.8b00392). (DA Dixon was supported by this program for writing the manuscript.)
169. Frederick, R. T.; Novotny, Z.; Netzer, F. P.; Herman, G. S.; Dohnálek, Z., Growth and Stability of Titanium Dioxide Nanoclusters on Graphene/Ru(0001). *J. Phys. Chem. B* **2018**, *122*, 640-648. DOI: [10.1021/acs.jpcc.7b05518](https://doi.org/10.1021/acs.jpcc.7b05518). (Z Novotny and Z Dohnálek were funded by this FWP. Z Novotny took part in the STM measurements, Z Dohnálek guided the experiments and contributed to the manuscript preparation.)
170. Hensley, A. J. R.; Wang, Y.; Mei, D.; McEwen, J.-S., Mechanistic Effects of Water on the Fe-Catalyzed Hydrodeoxygenation of Phenol. The Role of Brønsted Acid Sites. *ACS Catal.* **2018**, *8*, 2200-2208. DOI: [10.1021/acscatal.7b02576](https://doi.org/10.1021/acscatal.7b02576). (D Mei performed DFT calculations and Y Wang participated in the interpretation of results and writing the manuscript.)
171. Prodinge, S.; Vjunov, A.; Hu, J. Z.; Fulton, J. L.; Camaioni, D. M.; Derewinski, M. A.; Lercher, J. A., Elementary Steps of Faujasite Formation Followed by in Situ Spectroscopy. *Chem. Mater.* **2018**, *30*, 888–897. DOI: [10.1021/acs.chemmater.7b04554](https://doi.org/10.1021/acs.chemmater.7b04554). (A Vjunov and JL Fulton were supported by this program to perform XAFS measurements and contributed to the interpretation of the data, JZ Hu participated in NMR measurements and data evaluation, DM Camaioni and JA Lercher were supported by this program and participated in the evaluation of the data and manuscript preparation.)
172. Yu, Z.; Wang, Y.; Sun, Z.; Li, X.; Wang, A.; Camaioni, D. M.; Lercher, J. A., Ni₃P as a High-Performance Catalytic Phase for the Hydrodeoxygenation of Phenolic Compounds. *Green Chem.* **2018**, *20*, 609–619. DOI: [10.1039/C7GC03262E](https://doi.org/10.1039/C7GC03262E). (Supported by this project to explore nonoxidic supports for deoxygenation, JA

Dercher and DM Camaioni participated in the interpretation of the results, in the postulation of hypotheses, and in the drafting of the manuscript.)

Publications jointly funded by this grant and other grants with relatively minor intellectual contribution from this grant

2015

173. Allayarov, S. R.; Gordon, D. A.; Henderson, P. B.; Fernandez, R. E.; Jackson, V. E.; Dixon, D. A., Photochemistry of long-lived $[(CF_3)_2CF]_2C \cdot C_2F_5$ radicals. *J. Fluorine Chem.* **2015**, *180*, 240-247. DOI: [10.1016/j.jfluchem.2015.10.003](https://doi.org/10.1016/j.jfluchem.2015.10.003). (DA Dixon and VE Jackson were supported by this program for all computational work and writing the manuscript.)
174. Bayram, E.; Linehan, J. C.; Fulton, J. L.; Szymczak, N. K.; Finke, R. G., Determination of the Dominant Catalyst Derived from the Classic $[RhCp^*Cl_2]_2$ Precatalyst System: Is it Single-Metal Rh_1Cp^* -Based, Subnanometer Rh_4 Cluster-Based, or $Rh(0)_n$ Nanoparticle-Based Cyclohexene Hydrogenation Catalysis at Room Temperature and Mild Pressures? *ACS Catal.* **2015**, *5*, 3876-3886. DOI: [10.1021/acscatal.5b00315](https://doi.org/10.1021/acscatal.5b00315). (JC Linehan, JL Fulton, and NK Szymczak were supported by this project to design, perform, and interpret experiments based on operando catalysis.)
175. Christe, K. O.; Dixon, D. A.; Vasiliu, M.; Wagner, R. I.; Haiges, R.; Boatz, J. A.; Ammon, H. L., Are DTTO and iso-DTTO Worthwhile Targets for Synthesis? *Propellants, Explosives, Pyrotechnics* **2015**, *40*, 463-468. DOI: [10.1002/prep.201400259](https://doi.org/10.1002/prep.201400259). (DA Dixon and M Vasiliu were supported by this program for all computational work and writing the manuscript.)
176. Haiges, R.; Skotnitzki, J.; Fang, Z.; Dixon, D. A.; Christe, K. O., The Molybdenum(V) and Tungsten(VI) Oxoazides $[MoO(N_3)_3]$, $[MoO(N_3)_3 \cdot 2 CH_3CN]$, $[(bipy)MoO(N_3)_3]$, $[MoO(N_3)_5]^{2-}$, $[WO(N_3)_4]$, and $[WO(N_3)_4 \cdot CH_3CN]$. *Angew. Chem., Int. Ed.* **2015**, *54*, 15550-15555. DOI: [10.1002/anie.201505418](https://doi.org/10.1002/anie.201505418). (DA Dixon and Z Fang were supported by this program for all computational work and writing the manuscript.)
177. Haiges, R.; Skotnitzki, J.; Fang, Z.; Dixon, D. A.; Christe, K. O., The First Molybdenum(VI) and Tungsten(VI) Oxoazides $MO_2(N_3)_2$, $MO_2(N_3)_2 \cdot 2 CH_3CN$, $(bipy)MO_2(N_3)_2$, and $[MO_2(N_3)_4]^{2-}$ (M=Mo, W). *Angew. Chem., Int. Ed.* **2015**, *54*, 9581-9585. DOI: [10.1002/anie.201504629](https://doi.org/10.1002/anie.201504629). (DA Dixon and Z Fang were supported by this program for all computational work and writing the manuscript.)
178. Haiges, R.; Vasiliu, M.; Dixon, D. A.; Christe, K. O., The Vanadium(V) Oxoazides $[VO(N_3)_3]$, $[(bipy)VO(N_3)_3]$, and $[VO(N_3)_5]^{2-}$. *Angew. Chem., Int. Ed.* **2015**, *54*, 9101-9105. DOI: [10.1002/anie.201503985](https://doi.org/10.1002/anie.201503985). (DA Dixon and M Vasiliu were supported by this program for all computational work and writing the manuscript.)
179. Hensley, A. J. R.; Schneider, S.; Wang, Y.; McEwen, J.-S., Adsorption of Aromatics on the (111) surface of PtM and PtM₃ (M = Fe, Ni) Alloys. *RSC Advances* **2015**, *5*, 85705-85719. DOI: [10.1039/C5RA13578H](https://doi.org/10.1039/C5RA13578H). (Y Wang participated in the interpretation of results and drafting of the paper.)
180. Kim, B.; Kay, B. D.; Dohnalek, Z.; Kim, Y. K., Ammonia Formation from NO Reaction with Surface Hydroxyls on Rutile TiO₂(110)-1 x 1. *J. Phys. Chem. C* **2015**, *119*, 1130-1135. DOI: [10.1021/jp5109619](https://doi.org/10.1021/jp5109619). (BD Kay and Z Dohnalek were funded by this FWP to guide the experiments, provide interpretation, and prepare the manuscript.)
181. Leclerc, M. C.; Bayne, J. M.; Lee, G. M.; Gorelsky, S. I.; Vasiliu, M.; Korobkov, I.; Harrison, D. J.; Dixon, D. A.; Baker, R. T., Perfluoroalkyl Cobalt(III) Fluoride and Bis(perfluoroalkyl) Complexes: Catalytic Fluorination and Selective Difluorocarbene Formation. *J. Am. Chem. Soc.* **2015**, *137*, 16064-16073. DOI: [10.1021/jacs.5b12003](https://doi.org/10.1021/jacs.5b12003). (DA Dixon and M Vasiliu were supported by this program for all computational work and writing the manuscript.)
182. Lee, J.; Jeon, H.; Oh, D. G.; Szanyi, J.; Kwak, J. H., Morphology-dependent phase transformation of γ -Al₂O₃. *Appl. Catal. A* **2015**, *500*, 58-68. DOI: [10.1016/j.apcata.2015.03.040](https://doi.org/10.1016/j.apcata.2015.03.040). (J Szanyi was supported by this program to participate in the design of the experiments and in the preparation of the manuscript.)
183. Lee, M.-S.; McGrail, B. Peter; Rousseau, R.; Glezakou, V.-A., Structure, dynamics and stability of water/scCO₂/mineral interfaces from ab initio molecular dynamics simulations. *Scientific Reports* **2015**, *5*,

14857. DOI: [10.1038/srep14857](https://doi.org/10.1038/srep14857). (This work was supported by the US Department of Energy, Office of Fossil Energy (M-S Lee, BP McGrail, and V-A Glezakou) and the Office of Basic Energy Science, Division of Chemical Sciences, Geosciences and Biosciences (R Rousseau).)
184. Miranda, B. C.; Chimentão, R. J.; Szanyi, J.; Braga, A. H.; Santos, J. B. O.; Gispert-Guirado, F.; Llorca, J.; Medina, F., Influence of copper on nickel-based catalysts in the conversion of glycerol. *Appl. Catal. B* **2015**, *166–167*, 166-180. DOI: [10.1016/j.apcatb.2014.11.019](https://doi.org/10.1016/j.apcatb.2014.11.019). (J Szanyi was supported by this program to participate in the design of the experiments, carried out the IR measurements, contributed to data interpretation and to the preparation of the manuscript.)
185. Zhang, Z.; Tang, M.; Wang, Z.-T.; Ke, Z.; Xia, Y.; Park, K. T.; Lyubinetsky, I.; Dohnálek, Z.; Ge, Q., Imaging of Formaldehyde Adsorption and Diffusion on TiO₂(110). *Top. Catal.* **2015**, *58*, 103-113. DOI: [10.1007/s11244-014-0349-6](https://doi.org/10.1007/s11244-014-0349-6). (ZT Wang, I Lyubinetsky, and Z Dohnálek were funded by this FWP. ZT Wang took part in the STM measurements, I Lyubinetsky, and Z Dohnálek guided the experiments and contributed to the preparation of the manuscript.)
186. Zhu, K.; Xia, Y.; Tang, M.; Wang, Z.-T.; Jan, B.; Lyubinetsky, I.; Ge, Q.; Dohnálek, Z.; Park, K. T.; Zhang, Z., Tracking Site-Specific C-C Coupling of Formaldehyde Molecules on Rutile TiO₂(110). *J. Phys. Chem. C* **2015**, *119*, 14267-14272. DOI: [10.1021/acs.jpcc.5b04781](https://doi.org/10.1021/acs.jpcc.5b04781). (ZT Wang, I Lyubinetsky, and Z Dohnálek were funded by this FWP. ZT Wang took part in the STM measurements, I Lyubinetsky, and Z Dohnálek guided the experiments and contributed to the preparation of the manuscript.)
187. Zhu, K.; Xia, Y.; Tang, M.; Wang, Z.-T.; Lyubinetsky, I.; Ge, Q.; Dohnálek, Z.; Park, K. T.; Zhang, Z., Low-Temperature Reductive Coupling of Formaldehyde on Rutile TiO₂(110). *J. Phys. Chem. C* **2015**, *119*, 18452-18457. DOI: [10.1021/acs.jpcc.5b05639](https://doi.org/10.1021/acs.jpcc.5b05639). (ZT Wang, I Lyubinetsky, and Z Dohnálek were funded by this FWP. ZT Wang took part in the STM measurements, I Lyubinetsky, and Z Dohnálek guided the experiments and contributed to the manuscript preparation.)
- 2016**
188. Bligaard, T.; Bullock, R. M.; Campbell, C. T.; Chen, J. G. G.; Gates, B. C.; Gorte, R. J.; Jones, C. W.; Jones, W. D.; Kitchin, J. R.; Scott, S. L., Toward Benchmarking in Catalysis Science: Best Practices, Challenges, and Opportunities. *ACS Catal.* **2016**, *6*, 2590-2602. DOI: [10.1021/acscatal.6b00183](https://doi.org/10.1021/acscatal.6b00183). (RM Bullock was supported by this program and participated in writing and revising the article, which resulted from discussions at a Catalysis Science PI meeting (DOE-BES).)
189. Callini, E.; Atakli, Z. O. K.; Hauback, B. C.; Orimo, S.; Jensen, C.; Dornheim, M.; Grant, D.; Cho, Y. W.; Chen, P.; Hjorvarsson, B.; de Jongh, P.; Weidenthaler, C.; Baricco, M.; Paskevicius, M.; Jensen, T. R.; Bowden, M. E.; Autrey, T. S.; Zuttel, A., Complex and liquid hydrides for energy storage. *Appl. Phys. A-Mater. Sci. Process.* **2016**, *122*. DOI: [10.1007/s00339-016-9881-5](https://doi.org/10.1007/s00339-016-9881-5). (T Autrey contributed to section of complex hydrides for this review article.)
190. Deokar, P.; Leitz, D.; Stein, T. H.; Vasiliu, M.; Dixon, D. A.; Christe, K. O.; Haiges, R., Preparation and Characterization of Antimony and Arsenic Tricyanide and Their 2,2'-Bipyridine Adducts. *Chem.-Eur. J.* **2016**, *22*, 13251-13257. DOI: [10.1002/chem.201602436](https://doi.org/10.1002/chem.201602436). (DA Dixon, TH Stein, and M Vasiliu were supported by this program for all computational work and writing the manuscript.)
191. Deokar, P.; Vasiliu, M.; Dixon, D. A.; Christe, K. O.; Haiges, R., The Binary Group 4 Azides [PPh₄]₂[Zr(N₃)₆] and [PPh₄]₂[Hf(N₃)₆]. *Angew. Chem., Int. Ed.* **2016**, *55*, 14348-14352. DOI: [10.1002/anie.201609195](https://doi.org/10.1002/anie.201609195). (DA Dixon, TH Stein, and M Vasiliu were supported by this program for all computational work and writing the manuscript.)
192. Du, Y.; Li, G.; Peterson, E. W.; Zhou, J.; Zhang, X.; Mu, R.; Dohnálek, Z.; Bowden, M.; Lyubinetsky, I.; Chambers, S. A., Iso-oriented monolayer α -MoO₃(010) films epitaxially grown on SrTiO₃(001). *Nanoscale* **2016**, *8*, 3119-3124. DOI: [10.1039/C5NR07745A](https://doi.org/10.1039/C5NR07745A). (R Mu, I Lyubinetsky, and Z Dohnálek were funded by this FWP. R Mu took part in the STM measurements, I Lyubinetsky and Z Dohnálek contributed to the manuscript preparation.)
193. Kaneza, N.; Zhang, J.; Liu, H.; Archana, P. S.; Shan, Z.; Vasiliu, M.; Polansky, S. H.; Dixon, D. A.; Adams, R. E.; Schmehl, R. H.; Gupta, A.; Pan, S., Electrochemical and Spectroscopic Properties of Boron Dipyrromethene–Thiophene–Triphenylamine-Based Dyes for Dye-Sensitized Solar Cells. *J. Phys. Chem. C*

- 2016**, 120, 9068-9080. DOI: [10.1021/acs.jpcc.6b01611](https://doi.org/10.1021/acs.jpcc.6b01611). (DA Dixon, SH Polansky, and M Vasiliu were supported by this program for all computational work and writing the manuscript.)
194. Kim, B.; Dohnálek, Z.; Szanyi, J.; Kay, B. D.; Kim, Y. K., Temperature-programmed desorption study of NO reactions on rutile TiO₂(110)-1 × 1. *Surf. Sci.* **2016**, 652, 148-155. DOI: [10.1016/j.susc.2016.01.032](https://doi.org/10.1016/j.susc.2016.01.032). (J Szanyi was supported by this program to participate in the data interpretation and in the preparation of the manuscript.)
195. Kwak, J. H.; Lee, J.; Szanyi, J.; Peden, C. H. F., Modification of the acid/base properties of γ -Al₂O₃ by oxide additives: An ethanol TPD investigation. *Catal. Today* **2016**, 265, 240-244. DOI: [10.1016/j.cattod.2015.07.042](https://doi.org/10.1016/j.cattod.2015.07.042). (J Szanyi was supported by this program to participate in the experimental design, data interpretation and in the preparation of the manuscript.)
196. Liu, X. G.; Zhang, Y. Z.; Li, B.; Zakharov, L. N.; Vasiliu, M.; Dixon, D. A.; Liu, S. Y., A Modular Synthetic Approach to Monocyclic 1,4-Azaborines. *Angew. Chem., Int. Ed.* **2016**, 55, 8333-8337. DOI: [10.1002/anie.201602840](https://doi.org/10.1002/anie.201602840). (DA Dixon and M Vasiliu were supported by this program for all computational work and writing the manuscript.)
197. Matthiesen, J. E.; Carraher, J. M.; Vasiliu, M.; Dixon, D. A.; Tessonnier, J. P., Electrochemical Conversion of Muconic Acid to Biobased Diacid Monomers. *ACS Sustain. Chem. Eng.* **2016**, 4, 3575-3585. DOI: [10.1021/acssuschemeng.6b00679](https://doi.org/10.1021/acssuschemeng.6b00679). (DA Dixon and M Vasiliu were supported by this program for all computational work and writing the manuscript.)
198. Smith, M. F.; Cassidy, S. J.; Adams, I. A.; Vasiliu, M.; Gerlach, D. L.; Dixon, D. A.; Rugar, P. A., Substituent Effects on the Properties of Borafluorenes. *Organometallics* **2016**, 35, 3182-3191. DOI: [10.1021/acs.organomet.6b00537](https://doi.org/10.1021/acs.organomet.6b00537). (DA Dixon and M Vasiliu were supported by this program for all computational work and writing the manuscript.)
199. Sun, J.; Cai, Q. X.; Wan, Y.; Wan, S. L.; Wang, L.; Lin, J. D.; Mei, D. H.; Wang, Y., Promotional Effects of Cesium Promoter on Higher Alcohol Synthesis from Syngas over Cesium-Promoted Cu/ZnO/Al₂O₃ Catalysts. *ACS Catal.* **2016**, 6, 5771-5785. DOI: [10.1021/acscatal.6b00935](https://doi.org/10.1021/acscatal.6b00935). (D Mei performed DFT calculations and Y Wang participated in the interpretation of results and writing the manuscript.)
200. Tapu, D.; Buckner, O. J.; Boudreaux, C. M.; Norvell, B.; Vasiliu, M.; Dixon, D. A.; McMillen, C. D., A benzothiadiazole-supported N-heterocyclic carbene and its rhodium and iridium complexes. *J. Organomet. Chem.* **2016**, 823, 40-49. DOI: [10.1016/j.jorganchem.2016.09.016](https://doi.org/10.1016/j.jorganchem.2016.09.016). (DA Dixon and M Vasiliu were supported by this program for all computational work and writing the manuscript.)
201. Whittemore, S. M.; Bowden, M.; Karkamkar, A.; Parab, K.; Neiner, D.; Autrey, T.; Ishibashi, J. S. A.; Chen, G.; Liu, S. Y.; Dixon, D. A., Blending materials composed of boron, nitrogen and carbon to transform approaches to liquid hydrogen stores. *Dalton. Trans.* **2016**, 45, 6196-6203. DOI: [10.1039/c5dt04276c](https://doi.org/10.1039/c5dt04276c). (DA Dixon was supported by this program for all computational work and writing the manuscript.)
- 2017**
202. Cammarota, R. C.; Vollmer, M. V.; Xie, J.; Ye, J.; Linehan, J. C.; Burgess, S. A.; Appel, A. M.; Gagliardi, L.; Lu, C. C., A Bimetallic Nickel–Gallium Complex Catalyzes CO₂ Hydrogenation via the Intermediacy of an Anionic d10 Nickel Hydride. *J. Am. Chem. Soc.* **2017**, 139, 14244-14250. DOI: [10.1021/jacs.7b07911](https://doi.org/10.1021/jacs.7b07911). (JC Linehan, SA Burgess, and AM Appel were supported by this project to help collect and interpret high pressure NMR spectroscopy data.)
203. Gates, B. C.; Flytzani-Stephanopoulos, M.; Dixon, D. A.; Katz, A., Atomically dispersed supported metal catalysts: perspectives and suggestions for future research. *Catal. Sci. Technol.* **2017**, 7, 4259-4275. DOI: [10.1039/C7CY00881C](https://doi.org/10.1039/C7CY00881C). (DA Dixon was supported by this program for writing this review.)
204. Goldberg, J. M.; Goldberg, K. I.; Heinekey, D. M.; Burgess, S. A.; Lao, D. B.; Linehan, J. C., Detection of an Iridium–Dihydrogen Complex: A Proposed Intermediate in Ionic Hydrogenation. *J. Am. Chem. Soc.* **2017**, 139, 12638-12646. DOI: [10.1021/jacs.7b06480](https://doi.org/10.1021/jacs.7b06480). (JC Linehan and SA Burgess were supported by this project for the high pressure NMR spectroscopy and corresponding mechanistic studies.)
205. Iglesia, E.; Wang, S.; Agirrezabal-Telleria, I.; Bhan, A.; Simonetti, D.; Takanabe, K., Catalysis for Fuels Introductory Lecture: Catalytic routes to fuels from C1 and oxygenate molecules. *Faraday Discuss.* **2017**.

- DOI: [10.1039/C7FD00018A](https://doi.org/10.1039/C7FD00018A). (This is a review paper that includes as one of the examples, the I Agirrezabal-Telleria work on intrapore liquid effects on transition state stability.)
206. Lee, J.; Szanyi, J.; Kwak, J. H., Ethanol dehydration on γ -Al₂O₃: Effects of partial pressure and temperature. *Molecular Catalysis* **2017**, *434*, 39-48. DOI: [10.1016/j.mcat.2016.12.013](https://doi.org/10.1016/j.mcat.2016.12.013). (J Szanyi was supported by this program to participate in the design of the experiments and in the preparation of the manuscript.)
207. Li, Z.; Yang, X.; Tsumori, N.; Liu, Z.; Himeda, Y.; Autrey, T.; Xu, Q., Tandem Nitrogen Functionalization of Porous Carbon: Toward Immobilizing Highly Active Palladium Nanoclusters for Dehydrogenation of Formic Acid. *ACS Catal.* **2017**, *7*, 2720-2724. DOI: [10.1021/acscatal.7b00053](https://doi.org/10.1021/acscatal.7b00053). (T Autrey contributed to analysis of the results and writing of this paper.)
208. Liu, Z.; Ishibashi, J. S. A.; Darrigan, C.; Dargelos, A.; Chrostowska, A.; Li, B.; Vasiliu, M.; Dixon, D. A.; Liu, S.-Y., The Least Stable Isomer of BN Naphthalene: Toward Predictive Trends for the Optoelectronic Properties of BN Acenes. *J. Am. Chem. Soc.* **2017**, *139*, 6082-6085. DOI: [10.1021/jacs.7b02661](https://doi.org/10.1021/jacs.7b02661). (DA Dixon and M Vasiliu were supported by this program for most of the computational work and writing the manuscript.)
- 2018**
209. Andrella, N. O.; Liu, K.; Gabidullin, B.; Vasiliu, M.; Dixon, D. A.; Baker, R. T., Metal Heptafluoroisopropyl (M-hfip) Complexes for Use as hfip Transfer Agents. *Organometallics* **2018**, *37*, 422-432. DOI: [10.1021/acs.organomet.7b00837](https://doi.org/10.1021/acs.organomet.7b00837). (DA Dixon and M Vasiliu were supported by this program for all of the computational work and writing the manuscript.)
210. Lee, M.-S.; McGrail, B. P.; Rousseau, R.; Glezakou, V.-A., Molecular Level Investigation of CH₄ and CO₂ Adsorption in Hydrated Calcium–Montmorillonite. *J. Phys. Chem. C* **2018**, *122*, 1125-1134. DOI: [10.1021/acs.jpcc.7b05364](https://doi.org/10.1021/acs.jpcc.7b05364). (This work was supported by the US Department of Energy, Office of Fossil Energy (M-SL, BPM, and V-A Glezakou) and the Office of Basic Energy Science, Division of Chemical Sciences (RR).)

Catalyzing electrochemical transformations involving H₂O, O₂, H₂, and H₂O₂

Zhihua Chen, Shuchung Chen, Pong Chakthranont, Thomas Hellstern, Felix Studt, Jakob Kibsgaard, Yi Cui, Bruce M. Clemens, Frank Abild-Pedersen, Christopher Hahn, Laurie A. King, Drew Higgins, Samira Siahrostami, Xiaolin Zheng, Zhenan Bao, Jens K. Nørskov, Thomas F. Jaramillo

SLAC National Accelerator Laboratory and Stanford University

Presentation Abstract

In recent years, the price of renewable electricity has dropped to extraordinarily competitive levels, leading to widespread market penetration. This has created a substantial opportunity to develop new technologies that make use of low-cost, carbon-free electricity for productive purposes. One particular area with significant potential is using electricity to produce fuels and chemicals; another is converting fuels into electricity, especially for transportation applications. In both of these cases, a key technological challenge is the development of catalyst that can execute such transformations with high efficiency, selectivity, and stability. This presentation will describe efforts to understand and develop catalysts along these lines, focusing on several key transformations including: H₂O₂ production by means of oxygen reduction or water oxidation, water electrolysis for the production of H₂, and oxygen reduction to water.

SUNCAT FWP

FWP Number: KC0302010

SLAC National Accelerator Laboratory

PIs, co-PIs: *Thomas Jaramillo (Director), Thomas Bligaard (Co-Director); Jens K. Nørskov (Founding Director); Frank Abild-Pedersen, Zhenan Bao, Simon Bare, Stacey Bent, Matteo Cargnello, Johannes Voss, Karen Chan, Michal Bajdich, Melis S. Duyar, Drew C. Higgins*

RECENT PROGRESS

We seek to establish a systematic theory of heterogeneous catalysis by integrating the work in the four tasks below.

1. Theory of Catalysis and Electrocatalysis (Jens Nørskov, Karen Chan)

The overarching goal of Task 1 is the development of a systematic theory of heterogeneous catalysis. The primary developments in FY2018 have been in fundamental electrocatalysis, which pose significant new challenges on top of gas-phase catalysis. Our primary focus has been on extending our methods beyond a simplistic surface-science approach towards a detailed description of the electrochemical interface, including ions and solvent explicitly in our model systems. Given the importance of ion charge to the energetics and potential dependence of electrochemical activation energies, we have performed extensive studies of the charge of protons

and hydroxide ions at the interface. Using our recently developed schemes to obtain barriers at constant potential we have obtained acidic and alkaline barriers for both hydrogen evolution and 2- and 4-electron oxygen reduction processes towards an understanding of the pH dependence of these processes.

From the applied perspective we have examined, from a thermochemical perspective, the trends in oxygen evolution on oxides and perovskites, and in the 2-electron reduction of oxygen on oxides and defected carbons. Based on these trends we have in collaboration with experimentalists developed new active electrocatalysts for these processes. We have also studied the trends and activity descriptors for syngas conversion towards valuable C_{2+} oxygenated products on transition metals and methane activation on zeolites.

2. Computational Catalysis (*Frank Abild-Pedersen, Michal Bajdich*)

An understanding of the breaking and making of chemical bonds at a solid surface is the starting point for any fundamental description of reactions at the solid-gas or solid-liquid interface. It is particularly important to understand which properties of the surface determine its chemical activity. The description and understanding of activation energies for elementary surface reactions is a prime focus of this task. In addition to activity of catalysts we also focus our attention on the loss of active surface area through either strong metal-support interactions or sintering. The ability to prevent such side-reactions from happening would greatly enhance catalyst life-times and increase the activity/mass ratio significantly. This task is divided into two very general areas: reactivity of transition metal surfaces and transition metal- oxide surfaces.

The surface reactivity of transition metal oxides is also the main determinant of their activity for oxygen evolution reaction (OER). Big part of this task is also focused on achieving a better understanding of the underlying fundamental barriers that limit the performance of the OER catalysts and to identify ways to overcome them.

When it comes to our effort on the chemistry of transition metals, we have made significant advances in describing metal-metal interactions on mono-metallic as well as bi-metallic nanoparticle structures and we have built a framework in which thermodynamic stability on a single-atom swap basis can be predicted with very high accuracy. This allows for fast screening of stable particle structures based on little input from DFT. We have also made significant progress in linking this site stability to the chemistry thus providing a mapping between surface structure and reactivity.

We have extended our scaling relations to involve activated structures. This enables us to extract transition state energies using limited input from DFT. In addition, the similarities between the local nature of the bond breaking and hence the electronic structure variations for specific reactions, C-H, N-H and O-H activation provides a way to classify reactions and through that obtain kinetic information from analysis of ONE member of the class only.

For our effort on the chemistry of transition metal-oxides, we have made significant progress in identification of active sites for oxygen evolution reaction in layered Li_xCoO_2 . The presence of under-coordinated Co-metal site at the surface and its local chemical environment were shown to

be the most important factor determining OER activity. Next, we have investigated the role of metal support in the growth and stabilization of cobalt oxide nanostructures on common fcc(111) surfaces by means of high-resolution scanning tunneling microscopy and DFT calculations. The metal-edges of the Co-oxide nanostripes were found to be the active sites for water dissociation and OER. Additionally, we have benchmarked the ability of DFT/GGA+U and DFT/GGA+EXX methods to capture the adsorption energetics and the structure of dissociatively adsorbed H₂O and HCOOH molecules to careful single crystal calorimetry of Charles T. Campbell.

3. *Experimental catalysis* (Thomas Jaramillo, Stacey Bent, Matteo Cargnello, Zhenan Bao, Simon Bare, Melis S. Duyar, Drew C. Higgins)

Experimental catalysis efforts are focused on synthesis, characterization and testing of catalysts for both thermal heterogeneous catalysis as well as electrocatalysis. The work is closely coupled to the theoretical tasks. Fundamental studies identifying active site motifs and mechanisms and establishing kinetics are core to the program. In situ and operando investigations play a key role in understanding the structure and properties of the catalysts under operating conditions. Novel catalyst synthesis routes are also a key feature as is the use of spectroscopy and microscopy techniques for catalyst characterization. A tightly coupled theory-experiment feed-back loop for catalyst discovery is one of the main defining features of the effort.

We have expanded our work on transition metal phosphide catalysts for CO/CO₂ hydrogenation and examined MoP catalysts under working conditions using operando XAS, XRD and DRIFTS. We used colloidal synthesis techniques to study the effects of different supports on methanol synthesis activity on MoP catalysts. Based on insight from synthesis parametric studies and support/promoter effects we developed a carbon supported MoP catalyst with improved activity and selectivity towards higher alcohols. We studied the phase formation and stability of this catalyst under reaction conditions using XAS and XRD while following product formation from CO and CO₂ hydrogenation. We have discovered a new RuP catalyst for methanol synthesis from syngas. While a Ru analogue of this catalyst shows negligible activity towards methanol, phosphide formation activates methanol synthesis on the RuP catalyst. We have also studied sulfur incorporation onto well-defined Rh surfaces, known to have selectivity to higher oxygenates. New work showed that S atoms not only block Rh sites, but Rh_xS_y clusters exist that are present on the catalyst surface are much more active towards the synthesis of higher oxygenates compared to Rh metal sites. At SSRL we have designed a suite of in-situ cells that are compatible with the full complement of catalysts being developed at SUNCAT and designed a second portable feed manifold with associated on-line analytical tools. In parallel to these efforts, we started the systematic study of activity and stability of Pd-based materials for methane activation, looking in particular at methane combustion as a starting point. Uniform nanocrystals were used as starting materials to show how Pd oxidation state and morphology affects its activity, and how Pd/Pt materials can provide water resistance and improved thermal stability. In-situ and operando spectroscopic techniques helped us characterize the working state of the catalysts. A novel deactivation process has been unveiled with the use of these materials, where particle density and interparticle distance have been directly correlated with the stability of Pd catalysts under reaction conditions. Additionally, new efforts in the development of selective catalysts for oxidation of hydrocarbons have been started by looking at uniform alloys in the diluted regime. Structure-property relationships utilizing x-ray absorption spectroscopy and kinetic characterization have

been used to demonstrate the high activity and selectivity of single Pd atoms embedded within Au nanocrystals.

We have also made progress developing and investigating new core-shell electrocatalyst configurations, including understanding the role and effects gold cores had on the activity of metal-oxide shells towards the oxygen evolution reaction. Advances have been made to identify the active site structures present in nanostructured carbon that are selective for the two- electron oxygen reduction reaction to form hydrogen peroxide. Advancement of electrochemical cell designs and experimental techniques for conducting *in situ* synchrotron (x-ray diffraction, x-ray absorption) characterization in situ characterization of electrocatalysts under reaction conditions. Methods for characterizing nanoparticles, in addition to surface sensitive approaches to characterize thin film electrocatalysts are ongoing efforts, providing an experimental understanding of the electrocatalyst surface that will be crucial input for theoretical investigations.

4. Data and Computational Infrastructure (Thomas Bligaard, Johannes Voss, Karen Chan)

Current catalyst search or design studies have been highly successful in finding new catalyst leads for a number of reactions based on few simulations. It would; however, be strongly desirable if we were able to accurately investigate orders of magnitude more systems in a design study than we currently are. This would for example allow us to investigate reaction networks of a more realistic complexity, and in particular to carry out such an analysis over many (thousands to millions) of facet structures and material compositions in parallel. It would also open for the possibility of utilizing a range of more advanced approaches for calculating free energy contributions to the surface reaction energetics. Such a big-data revolution will soon occur in the computational catalysis field, provided we establish the enabling technologies. This will require a transformation in the way we create and manage simulations, and in the way we featurize the simulations for machine learning purposes. It will transform the way we perform analysis of data and it will deepen the scientific questions that we can address based on simulations. In this Task we aim to lay a foundation for this future - radically more data-rich - computational heterogeneous catalysis and electrocatalysis approach.

We have in FY18 finalized a novel GGA-based functional with the minimally code-sensitive D3-BJ van der Waals force field. This will make the use of error estimation functionals less computationally demanding, especially for small systems, and will drastically reduce the dependence of BEEF-results between different codes and choices of pseudopotential/PAW-setup hardness.

We have developed a method for using surrogate machine learning models to accelerate the search for ground state structures and for determining NEB-paths. This methodology speeds up DFT ground state structure simulations by approximately a factor of two and NEB calculations by a factor of 20. This will be key to enable the construction of automated mapping of large and complex reaction networks.

We have established a cloud-based web-hosting service for catalysis-related apps that we call the Catalysis-hub.org. An app on this site has been established to host electronic structure simulations

of surface chemical properties such as adsorption energies and reaction barriers. This is a deeper data base with more meta data than the earlier used CatApp, and as such takes over from CatApp as SUNCAT's online adsorption and reaction energy service. We have calculated more than 10,000 new adsorption energies which are served through the app.

Collaborations

Malte Behrens (University of Duisburg-Essen), Charles T. Campbell (University of Washington), Ib Chorkendorff (Technical University of Denmark), Yi Cui (Stanford), Søren Dahl (Haldor Topsoe A/S), Alexander Föhlisch (Helmholtz Zentrum Berlin), Jeffrey Greeley (Purdue University), Avetik R. Harutyunyan (Honda Research Institute), Francesc Illas (University of Barcelona), Karsten W. Jacobsen (Technical University of Denmark), Anker D. Jensen (Technical University of Denmark), Sarp Kaya (Koc University Turkey), Anders Nilsson (Stockholm University), Dennis Nordlund (SLAC), Henrik Öström (University of Stockholm), Mats Persson (University of Liverpool), Lars G. M. Pettersson (University of Stockholm), Nichols A. Romero (Argonne National Laboratory), Ansgar Schäfer (BASF), Robert Schlögl (Fritz-Haber Institute Berlin), Renu Sharma (Center for Nanoscale Science and Technology / NIST), Robert Sinclair (Stanford), Muhkles Sowwan (OIST), Felix Studt (KIT), Joel B. Varley (Lawrence Livermore National Laboratory), Aleksandra Vojvodic (University of Pennsylvania), Martin Wolf (Fritz-Haber Institute Berlin), Wilfried Wurth (University of Hamburg), Hongliang Xin (Virginia Tech.), Xiaolin Zheng (Stanford)

Publications Acknowledging this Grant in 2015-2018

Category I

1. Yang, N.; Liu, X.; Asundi, A. S.; Nørskov, J.K.; Bent, S. F. The Role of Sodium in Tuning Product Distribution in Syngas Conversion by Rh Catalysts. *Catalysis Letters*, **2018**, *148*, 289
2. Roling, L.T.; Abild-Pedersen, F. Structure-Sensitive Scaling Relations: Adsorption Energies from Surface Site Stability. *ChemCatChem*, **2018**, *10*, 1643-1650.
3. Schumann, J.; Medford, A. J.; Yoo, J. S.; Zhao, Z.-J.; Bothra, P.; Cao, A.; Studt, F.; Abild-Pedersen, F.; Nørskov, J. K. Selectivity of synthesis gas conversion to C₂+ oxygenates on fcc (111) transition metal surfaces. *ACS Catalysis*, **2018**, *8*, 3447-3453.
4. Yu, L.; Vilella, L.; Abild-Pedersen, F. Generic approach to access barriers in dehydrogenation reactions. *Communications Chemistry*, **2018**, *1*, 2.
5. Lu, Z.; Chen, G.; Siahrostami, S.; Chen, Z.; Liu, K.; Xie, J.; Liao, L.; Wu, T.; Lin, D.; Liu, Y.; Jaramillo, T. F.; Nørskov, J. K.; Cui, Y. High-efficiency oxygen reduction to hydrogen peroxide catalysed by oxidized carbon materials. *Nature Catalysis*, **2018**, 156-162.
6. Jackson, A.; Strickler, A.; Higgins, D.; Jaramillo, T. F. Engineering Ru@Pt Core-Shell Catalysts for Enhanced Electrochemical Oxygen Reduction Mass Activity and Stability. *Nanomaterials*, **2018**, *8*, 38.
7. Dickens, C.F.; Nørskov, J. K. A Theoretical Investigation into the Role of Surface Defects for Oxygen Evolution on RuO₂. *J. Phys. Chem. C*, **2017**, *121*, 18516-18524.

8. Mendes, L. V. P.; Snider, J. L.; Fleischman, S.D., Kibsgaard, J.; McEnaney, J.M.; Aranda, D. A. G.; Jaramillo, T.F. Polyol Synthesis of Cobalt–Copper Alloy Catalysts for Higher Alcohol Synthesis from Syngas. *Catalysis Letters*, **2017**, *147*, 5399-5409.
9. Chakthranont, P.; Kibsgaard, J.; Gallo, J.; Park, J.; Mitani, M.; Sokaras, D.; Kroll, T.; Sinclair, R.; Mogensen, M. B.; Jaramillo, T.F. Effects of Gold Substrates on the Intrinsic and Extrinsic Activity of High-Loading Nickel-Based Oxyhydroxide Oxygen Evolution Catalysts. *ACS Catalysis*, **2017**, *7*, 5399-5409.
10. Aljama, H.; Nørskov, J.K.; Abild-Pedersen, F. Theoretical Insights into Methane C–H Bond Activation on Alkaline Metal Oxides. *J. Phys. Chem. C*, **2017**, *121*, 16440-16446.
11. Yang, N.; Yoo, J. S.; Schumann, J.; Bothra, P.; Singh, J.A.; Valle, E.; Abild-Pedersen, F.; Nørskov, J. K.; Bent, S. F. Rh-MnO Interface Sites Formed by Atomic Layer Deposition Promote Syngas Conversion to Higher Oxygenates. *ACS Catalysis*, **2017**, *7*, 5746-5757.
12. Latimer, A. A.; Abild-Pedersen, F.; Nørskov, J. K. A Theoretical Study of Methanol Oxidation on RuO₂(110): Bridging the Pressure Gap. *ACS Catalysis*, **2017**, *7*, 4527-4534.
13. Gauthier, J.A.; Dickens, C. F.; Chen, L. D.; Doyle, A.D.; Nørskov, J. K. Solvation Effects for Oxygen Evolution Reaction Catalysis on IrO₂(110). *J. Phys. Chem. C*, **2017**, *121*, 11455-11463.
14. Hellstern, T.R.; Kibsgaard, J.; Tsai, C.; Palm, D. W.; King, L. A.; Abild-Pedersen, F., Jaramillo, T.F. Investigating Catalyst–Support Interactions To Improve the Hydrogen Evolution Reaction Activity of Thiomolybdate [Mo₃S₁₃]²⁻ Nanoclusters. *ACS Catalysis*, **2017**, *7*, 7126-7130.
15. Shi, X.; Siahrostami, S.; Li, G.-L.; Zhang, Y.; Chakthranont, P.; Studt, F.; Jaramillo, T.F.; Zheng, X.; Nørskov, J.K. Understanding Activity Trends in Electrochemical Water Oxidation to form Hydrogen Peroxide. *Nature Communications*. **2017**, *8*, 701.
16. Sharada, S.M.; Bligaard, T.; Luntz, A. C.; Kroes, G.-J.; Nørskov, J. K. SBH10: A Benchmark Database of Barrier Heights on Transition Metal Surfaces. *J. Phys. Chem. C* **2017**, *121*, 19807.
17. Montoya, J. H.; Doyle, A.; Nørskov, J.K.; Vojvodic, A. Trends in adsorption of electrocatalytic water splitting intermediates on cubic ABO₃ oxides. *Phys. Chem. Chem. Phys*, **2018**, *20*, 3813-3818. Lu, Z.; Chen, G.; Li, Y.; Wang, H.; Xie, J.; Liao, L.; Liu, C.; Liu, Y.; Wu, T.; Li, Y.; Luntz, A. C.; Bajdich, M.; Cui, Y. Identifying the active surfaces of electrochemically tuned LiCoO₂ for oxygen evolution reaction. *JACS* **2017**, *139*, 6270–6276.
18. Tsai, C.; Li, H.; Park, S.; Park, J.; Han, H. S.; Nørskov, J. K.; Zheng, X.; Abild-Pedersen, F. Electrochemical generation of sulfur vacancies in the basal plane of MoS₂ for hydrogen evolution. *Nature Communications* **2017**, *8*, 15113.
19. Stegmaier, S.; Voss, J.; Reuter, K.; Luntz, A. C. Li⁺ Defects in a Solid-State Li Ion Battery: Theoretical Insights with a Li₃OCl Electrolyte. *Chem. Mater.* **2017**, *29*, 4330–4340.
20. Ulissi, Z. W.; Medford, A. J.; Bligaard, T.; Nørskov, J. K. To address surface reaction network complexity using scaling relations machine learning and DFT calculations. *Nature Communications* **2017**, *8*, 14621.
21. Doyle, A. D.; Bajdich, M.; Vojvodic, A. Theoretical Insights to Bulk Activity Towards Oxygen Evolution in Oxyhydroxides. *Catal. Lett.* **2017**, *147*.

22. Fields, M.; Tsai, C.; Chen, L. D.; Abild-Pedersen, F.; Nørskov, J. K.; Chan, K. Scaling Relations for Adsorption Energies on Doped Molybdenum Phosphide Surfaces. *ACS Catalysis* **2017**, *7*, 2528–2534.
23. Chen, Z.; Chen, S.; Siahrostami, S.; Chakhranont, P.; Hahn, C.; Nordlund, D.; Dimosthenis, S.; Nørskov, J. K.; Bao, Z.; Jaramillo, T. F. Development of a reactor with carbon catalysts for modular-scale, low-cost electrochemical generation of H₂O₂. *Reaction Chemistry & Engineering* **2017**,
24. Latimer, A. A.; Aljama, H.; Kakekhani, A.; Yoo, J. S.; Kulkarni, A.; Tsai, C.; Garcia-Melchor, M.; Abild-Pedersen, F.; Nørskov, J. K. Mechanistic insights into heterogeneous methane activation. *Phys. Chem. Chem. Phys.* **2017**, *19*, 3575–3581.
25. Yu, L.; Abild-Pedersen, F. Bond Order Conservation Strategies in Catalysis Applied to the NH₃ Decomposition Reaction. *ACS Catalysis* **2017**, *7*, 864–871.
26. Strickler, A.; Jackson, A.; Jaramillo, T. Active and Stable Ir@Pt Core-Shell Catalysts for Electrochemical Oxygen Reduction. *ACS Energy Letters* **2016**, *2*, 224–229.
27. Zhao, W.; Bajdich, M.; Carey, S.; Vojvodic, A.; Nørskov, J. K.; Campbell, C. T. Water Dissociative Adsorption on NiO(111): Energetics and Structure of the Hydroxylated Surface. *ACS Catalysis* **2016**, *6*, 7377–7384.
28. Wang, H.; Xu, S.; Tsai, C.; Li, Y.; Liu, C.; Zhao, J.; Liu, Y.; Yuan, H.; Abild-Pedersen, F.; Prinz, F. B.; Nørskov, J. K.; Cui, Y. Direct and continuous strain control of catalysts with tunable battery electrode materials. *Science* **2016**, *354*, 1031–1036.
29. To, J. W. F. et al. High-performance oxygen reduction and evolution carbon catalysis: From mechanistic studies to device integration. *Nano Research* **2016**, 1–15.
30. Kulkarni, A. R.; Zhao, Z.-J.; Siahrostami, S.; Nørskov, J. K.; Studt, F. Monocopper Active Site for Partial Methane Oxidation in Cu-Exchanged 8MR Zeolites. *ACS Catalysis* **2016**, *6*, 6531–6536.
31. Aljama, H.; Yoo, J. S.; Nørskov, J. K.; Abild-Pedersen, F.; Studt, F. Methanol Partial Oxidation on Ag(111) from First Principles. *ChemCatChem* **2016**, *8*, 1–6.
32. Plessow, P. N.; Abild-Pedersen, F. Sintering of Pt Nanoparticles via Volatile PtO₂: Simulation and Comparison with Experiments. *ACS Catalysis* **2016**, *6*, 7098–7108
33. Garcia-Pintos, D.; Voss, J.; Jensen, A. D.; Studt, F. Hydrodeoxygenation of phenol to benzene and cyclohexane on Rh (111) and Rh (211) surfaces: Insights from density functional theory. *J. Phys. Chem. C* **2016**, *120*, 18529–18537.
34. Lundgaard, K. T.; Wellendorff, J.; Voss, J.; Jacobsen, K. W.; Bligaard, T. mBEEF-vdW: Robust fitting of error estimation density functionals. *Phys. Rev. B* **2016**, *93*, 235162.
35. Zhang, S.; Plessow, P. N.; Willis, J. J.; Dai, S.; Xu, M.; Graham, G. W.; Cargnello, M.; Abild-Pedersen, F.; Pan, X. Dynamical Observation and Detailed Description of Catalysts under Strong Metal-Support Interaction. *Nano Lett.* **2016**, *16*, 4528–4534.
36. Kibsgaard, J.; Jackson, A.; Jaramillo, T. Mesoporous platinum nickel thin films with double gyroid morphology for the oxygen reduction reaction. *Nano Energy* **2016**, *29*, 243–248.
37. Plessow, P. N.; Bajdich, M.; Greene, J.; Vojvodic, A.; Abild-Pedersen, F. Trends in the Thermodynamic Stability of Ultrathin Supported Oxide Films. *J. Phys. Chem. C* **2016**, *120*, 10351–10360.
38. Zhao, Z.-J.; Kulkarni, A.; Vilella, L.; Nørskov, J. K.; Studt, F. Theoretical Insights into the Selective Oxidation of Methane to Methanol in Copper-Exchanged Mordenite. *ACS Catalysis* **2016**, *6*, 3760–3766.

39. Pruski, M. et al. Virtual Special Issue on Catalysis at the U.S. Department of Energy's National Laboratories. *ACS Catalysis* **2016**, *6*, 3227–3235.
40. Jaffe, A.; Lin, Y.; Beavers, C. M.; Voss, J.; Mao, W. L.; Karunadasa, H. I. High-Pressure Single-Crystal Structures of 3D Lead-Halide Hybrid Perovskites and Pressure Effects on their Electronic and Optical Properties. *ACS Central Science* **2016**, *2*, 201–209.
41. Ulissi, Z. W.; Singh, A. R.; Tsai, C.; Nørskov, J. K. Automated Discovery and Construction of Surface Phase Diagrams Using Machine Learning. *J. Phys. Chem. Lett.* **2016**, *7*, 3931.
42. Bertheussen, E.; Verdaguer-Casadevall, A.; Ravasio, D.; Montoya, J. H.; Trimarco, D. B.; Roy, C.; Meier, S.; Wendland, J.; Nørskov, J. K.; Stephens, I. E. L.; Chorkendorff, I. Acetaldehyde as an Intermediate in the Electroreduction of Carbon Monoxide to Ethanol on Oxide-Derived Copper. *Angew. Chem. Int. Ed.* **2016**, *55*, 1450.
43. Zhang, B. et al. Homogeneously-Dispersed Multi-Metal Oxygen- Evolving Catalysts. *Science* **2016**, *352*, 333–337.
44. Chakthranont, P.; Pinaud, B.; Seitz, L.; Forman, A.; Jaramillo, T. Improving the Photoelectrochemical Performance of Hematite by Employing a High Surface Area Scaffold and Engineering Solid-Solid Interfaces. *Advanced Materials Interfaces* **2016**, *3*, 1500626.
45. Reinecke, B. N.; Kuhl, K. P.; Ogasawara, H.; Li, L.; Voss, J.; Abild-Pedersen, F.; Nilsson, A.; Jaramillo, T. F. Elucidating the electronic structure of supported gold nanoparticles and its relevance to catalysis by means of hard X-ray photoelectron spectroscopy. *Surf. Sci.* **2016**, *650*, 24–33.
46. Wolcott, C. A.; Medford, A. J.; Studt, F.; Campbell, C. T. Degree of rate control approach to computational catalyst screening. *J. Catal.* **2015**, *330*, 197–207.
47. Luntz, A.; Voss, J.; Reuter, K. Interfacial Challenges in Solid-State Li Ion Batteries. *J. Phys. Chem. Lett.* **2015**, *6*, 4599–4604.
48. Yoo, J. S.; Zhao, Z.-J.; Nørskov, J. K.; Studt, F. Effect of Boron Modifications of Palladium Catalysts for the Production of Hydrogen from Formic Acid. *ACS Catalysis* **2015**, *5*, 6579–6586.
49. Chen, L. D.; Nørskov, J. K.; Luntz, A. C. Al-Air Batteries: Fundamental Thermodynamic Limitations from First-Principles Theory. *J. Phys. Chem. Lett.* **2015**, *6*, 175–179.
50. Wellendorff, J.; Silbaugh, T. L.; Garcia-Pintos, D.; Nørskov, J. K.; Bligaard, T.; Studt, F.; Campbell, C. T. A benchmark database for adsorption bond energies to transition metal surfaces and comparison to selected DFT functionals. *Surf. Sci.* **2015**, *640*, 36–44.
51. Öberg, H. et al. Optical laser-induced CO desorption from Ru(0001) monitored with a free- electron X-ray laser: DFT prediction and X-ray confirmation of a precursor state. *Surf. Sci.* **2015**, *640*, 80–88.
52. Jauho, T. S.; Olsen, T.; Bligaard, T.; Thygesen, K. S. Improved description of metal oxide stability: Beyond the random phase approximation with renormalized kernels. *Phys. Rev. B* **2015**, *92*, 115140.
53. Li, L.; Abild-Pedersen, F.; Greeley, J.; Nørskov, J. K. Surface Tension Effects on the Reactivity of Metal Nanoparticles. *J. Phys. Chem. Lett.* **2015**, *6*, 3797–3801.
54. Tsai, C.; Latimer, A. A.; Yoo, J. S.; Studt, F.; Abild-Pedersen, F. Predicting Promoter-Induced Bond Activation on Solid Catalysts Using Elementary Bond Orders. *J. Phys. Chem. Lett.* **2015**, *6*, 3670–3674.

55. Chen, L. D.; Nørskov, J. K.; Luntz, A. C. Theoretical Limits to the Anode Potential in Aqueous Mg-Air Batteries. *J. Phys. Chem. C* **2015**, *119*, 19660–19667.
56. Kunkes, E. L.; Studt, F.; Abild-Pedersen, F.; Schlögl, R.; Behrens, M. Hydrogenation of CO₂ to methanol and CO on Cu/ZnO/Al₂O₃: Is there a common intermediate or not? *J. Catal.* **2015**, *328*, 43–48.
57. Santos, E. J. G.; Nørskov, J. K.; Vojvodic, A. Screened Hybrid Exact Exchange Correction Scheme for Adsorption Energies on Perovskite Oxides. *J. Phys. Chem. C* **2015**, *119*, 17662–17666.
58. Singh, V. D.; Cassidy, C.; Abild-Pedersen, F.; Kim, J.-H.; Aranishi, K.; Kumar, S.; Lal, C.; Gspan, C.; Grogger, W.; Sowwan, M. Engineering high-performance Pd core-MgO porous shell nanocatalysts via heterogeneous gas-phase synthesis. *Nanoscale* **2015**, *7*, 13387–13392.
59. Zhou, M.; Cai, L.; Bajdich, M.; Garcia-Melchor, M.; Li, H.; He, J.; Wilcox, J.; Wu, W.; Vojvodic, A.; Zheng, X. Enhancing Catalytic CO oxidation over Co₃O₄ Nanowires by Substituting Co²⁺ with Cu²⁺. *ACS Catalysis* **2015**, *5*, 4485–4491.
60. Ng, M. L.; Abild-Pedersen, F.; Kaya, S.; Mbuga, F.; Ogasawara, H.; Nilsson, A. Low Barrier Carbon Induced CO Dissociation on Stepped Cu. *Phys. Rev. Lett.* **2015**, *114*, 246101
61. Montoya, J. H.; Tsai, C.; Vojvodic, A.; Nørskov, J. K. The Challenge of Electrochemical Ammonia Synthesis: A New Perspective on the Role of Nitrogen Scaling Relations. *ChemSusChem* **2015**, *8*, 2180–2186.
62. Medford, A. J.; Vojvodic, A.; Voss, J.; Abild-Pedersen, F.; Studt, F.; Bligaard, T.; Nilsson, A.; Nørskov, J. K. From the Sabatier Principle to a Predictive Theory of Transition Metal Heterogeneous Catalysis. *Journal of Catalysis* **2015**, *328*, 36–42.
63. Koitz, R.; Nørskov, J. K.; Studt, F. A systematic study of metal-supported boron nitride materials for the oxygen reduction reaction. *Phys. Chem. Chem. Phys.* **2015**, *17*, 12722–12727.
64. Plessow, P. N.; Abild-Pedersen, F. Examining the Linearity of Transition State Scaling Relations. *J. Phys. Chem. C* **2015**, *119*, 10448–10453.
65. Pandey, M.; Vojvodic, A.; Thygesen, K. S.; Jacobsen, K. W. Two-Dimensional Metal Dichalcogenides and Oxides for Hydrogen Evolution: A Computational Screening Approach. *J. Phys. Chem. Lett.* **2015**, *6*, 1577–1585.
66. Viswanathan, V.; Hansen, H. A.; Nørskov, J. K. Selective Electrochemical Generation of Hydrogen Peroxide from Water Oxidation. *J. Phys. Chem. Lett.* **2015**, *6*, 4224.
67. Nørskov, J. K.; Niemantsverdriet, H. The Impact Of Haldor Topsoe On Catalysis. *J. Catal.* **2015**, *328*, 1.
68. Bajdich, M.; Nørskov, J. K.; Vojvodic, A. Surface Energetics of Alkaline-Earth Metal Oxides: Trends in Stability and Adsorption of Small Molecules. *Phys. Rev. B* **2015**, *91*, 155401.
69. Wang, C.-M.; Brogaard, R.; Xie, Z.-K.; Studt, F. Transition-state Scaling Relations in Zeolite Catalysis: Influence of Framework Topology and Acid-site Reactivity. *Catalysis Science & Technology* **2015**, *5*, 2814–2820.
70. Studt, F.; Behrens, M.; Kunkes, E. L.; Thomas, N.; Zander, S.; Tarasov, A.; Schumann, J.; Frei, E.; Varley, J. B.; Abild-Pedersen, F.; Nørskov, J. K.; Schlögl, R. The Mechanism of CO and CO₂ Hydrogenation to Methanol over Cu-Based Catalysts. *ChemCatChem* **2015**, *7*, 1105–1111.

71. Öström, H. et al. Probing the Transition State Region in Catalytic CO Oxidation on Ru. *Science* **2015**, *347*, 978–982.
72. Vojvodic, A.; Nørskov, J. K. New Design Paradigm for Heterogeneous Catalysts. *National Science Review* **2015**, *2*, 140–149.
73. Walton, A. S.; Fester, J.; Bajdich, M.; Arman, M. A.; Osiecki, J.; Knudsen, J.; Vojvodic, A.; Lauritsen, J. V. Interface Controlled Oxidation States in Layered Cobalt Oxide Nano-Islands on Gold. *ACS Nano* **2015**, *9*, 2445–2453.
74. Medford, A. J.; Shi, C.; Hoffmann, M. J.; Lausche, A. C.; Fitzgibbon, S. R.; Bligaard, T.; Nørskov, J. K. CatMAP: A Software Package for Descriptor-Based Microkinetic Mapping of Catalytic Trends. *Catal. Lett.* **2015**, *145*, 794–807.
75. Luntz, A. C. Beyond Lithium Ion Batteries. *J. Phys. Chem. Lett.* **2015**, *6*, 300–301.
76. Yoo, J. S.; Khan, T. S.; Abild-Pedersen, F.; Nørskov, J. K.; Studt, F. On the role of the surface oxygen species during A-H (A = C, N, O) bond activation: a density functional theory study. *Chem. Commun.* **2015**, *51*, 2621–2624.

Category II

77. Chen, L.D.; Bajdich, M.; Martirez, J. M. P.; Krauter, C. M.; Gauthier, J. A.; Carter, E. A.; Luntz, A.C.; Chan, K.; Nørskov, J.K. Understanding the apparent fractional charge of protons in the aqueous electrochemical double layer. *Nature Communications*. **2018**. In Press
78. Hedström, S.; Santos, E.C.D.; Liu, C.; Chan, K.; Abild-Pedersen, F.; Pettersson, L.G.M. Spin Uncoupling in Chemisorbed OCCO and CO₂ – Two High-Energy Intermediates in Catalytic CO₂ Reduction. *J. Phys. Chem. C* **2018**. In Press.
79. Kulkarni, A.; Zhao, Z.-J.; Siahrostami, S.; Nørskov, J. K.; Studt, F. Cation-exchanged zeolites for the selective oxidation of methane to methanol. *Catalysis Science & Technology*. **2018**, *8*, 114-123.
80. Willis, J. J.; Gallo, A.; Sokaras, D.; Aljama, H.; Nowak, S.H.; Goodman, E.D.; Wu, L.; Tassone, C. J.; Jaramillo, T.F.; Abild-Pedersen, F.; Cargnello, M. Systematic Structure–Property Relationship Studies in Palladium-Catalyzed Methane Complete Combustion. *ACS Catalysis*, **2017**, *7*, 7810-7821.
81. Siahrostami, S.; Li, G.-L.; Viswanathan, V.; Nørskov, J. K. One- or Two-electron Water Oxidation, Hydroxyl Radical or H₂O₂ Evolution. *J. Phys. Chem. Lett.* **2017**, *8*, 1157–1160.
82. Li, L.; Plessow, P. N.; Rieger, M.; Sauer, S.; Sanchez, R.; Schaefer, A.; Abild-Pedersen, F. Modeling the Migration of Platinum Nanoparticles on Surfaces Using a Kinetic Monte Carlo Approach. *J. Phys. Chem. C* **2017**, *121*, 4261–4269.
83. Nilsson, A.; LaRue, J.; Öberg, H.; Ogasawara, H.; Dell’Angela, M.; Beye, M.; Öström, H.; Gladh, J.; Nørskov, J. K.; Wurth, W.; Abild-Pedersen, F.; Pettersson, L. G. Catalysis in Real Time using X-ray Lasers. *Chem. Phys. Lett.* **2017**, *675*, 145–173.
84. Fester, J.; Garcia-Melchor, M.; Walton, A.; Bajdich, M.; Li, Z.; Lammich, L.; Vojvodic, A.; Lauritsen, J. V. Edge reactivity and water-assisted dissociation on cobalt oxide nanoislands. *Nature Communications* **2017**,
85. Frydendal, R.; Seitz, L. C.; Sokaras, D.; Weng, T.-C.; Nordlund, D.; Chorkendorff, I.; Stephens, I. E.; Jaramillo, T. F. Operando investigation of Au-MnOx thin films with improved activity for the oxygen evolution reaction. *Electrochim. Acta* **2017**, *230*, 22–28.

86. Seh, Z.; Kibsgaard, J.; Dickens, C. F.; Chorkendorff, I.; Nørskov, J. K.; Jaramillo, T. F. Combining theory and experiment in electrocatalysis: Insights into materials design. *Science* **2017**, *355*.
87. Latimer, A. A.; Kulkarni, A. R.; Aljama, H.; Montoya, J. H.; Yoo, J. S.; Tsai, C.; Abild-Pedersen, F.; Studt, F.; Nørskov, J. K. Understanding trends in C-H bond activation in heterogeneous catalysis. *Nature Materials* **2017**, *16*, 225–229.
88. Montoya, J.; Seitz, L.; Chakthranont, P.; Vojvodic, A.; Jaramillo, T.; Nørskov, J. Materials for solar fuels and chemicals. *Nature Materials* **2017**, *16*, 70–81.
89. Fester, J.; Bajdich, M.; Walton, A. S.; Sun, Z.; Plessow, P. N.; Vojvodic, A.; Lauritsen, J. V. Comparative Analysis of Cobalt Oxide Nanoisland Stability and Edge Structures on Three Related Noble Metal Surfaces: Au(111), Pt(111) and Ag(111). *Top. Catal.* **2016**,
90. Seitz, L.; Dickens, C.; Nishio, K.; Hikita, Y.; Montoya, J.; Doyle, A.; Kirk, C.; Vojvodic, A.; Hwang, H.; Nørskov, J.; Jaramillo, T. A highly active and stable IrOx/SrIrO3 catalyst for the oxygen evolution reaction. *Science* **2016**, *353*, 1011–1014.
91. Beye, M. et al. Chemical Bond Activation Observed with an X-ray Laser. *J. Phys. Chem. Lett.* **2016**, *7*, 3647–3651.
92. Siahrostami, S.; Tsai, C.; Karamad, M.; Koitz, R.; Garcia-Melchor, M.; Bajdich, M.; Vojvodic, A.; Abild-Pedersen, F.; Nørskov, J. K.; Studt, F. Two-Dimensional Materials as Catalysts for Energy Conversion. *Catal. Lett.* **2016**, *46*, 1917–1921.
93. Seh, Z.; Fredrickson, K.; Anasori, B.; Kibsgaard, J.; Strickler, A.; Lukatskaya, M.; Gogotsi, Y.; Jaramillo, T.; Vojvodic, A. Two-Dimensional Molybdenum Carbide (MXene) as an Efficient Electrocatalyst for Hydrogen Evolution. *ACS Energy Letters* **2016**, *1*, 589–594.
94. Plessow, P. N.; Sanchez-Carrera, R. S.; Li, L.; Rieger, M.; Sauer, S.; Schaefer, A.; Abild-Pedersen, F. Modeling the Interface of Platinum and α -Quartz(001): Implications for Sintering. *J. Phys. Chem. C* **2016**, *120*, 10340–10350.
95. Ng, J.; Garcia-Melchor, M.; Bajdich, M.; Chakthranont, P.; Kirk, C.; Vojvodic, A.; Jaramillo, T. Gold-supported cerium-doped NiOx catalysts for water oxidation. *Nature Energy* **2016**, *1*, 16053.
96. Yoo, J. S.; Christensen, R.; Vegge, T.; Nørskov, J. K.; Studt, F. Theoretical Insight into the Trends that Guide the Electrochemical Reduction of Carbon Dioxide to Formic Acid. *ChemSusChem* **2016**, *9*, 358.
97. Seitz, L.; Nordlund, D.; Gallo, A.; Jaramillo, T. Tuning Composition and Activity of Cobalt Titanium Oxide Catalysts for the Oxygen Evolution Reaction. *Electrochim. Acta* **2016**, *193*, 240–245.
98. Varley, J. B.; Wang, Y.; Chan, K.; Studt, F.; Nørskov, J. K. Mechanistic insights into nitrogen fixation by nitrogenase enzymes. *Phys. Chem. Chem. Phys.* **2015**, *17*, 29541–29547.
99. Li, H.-J.; Lausche, A. C.; Peterson, A. A.; Hansen, H. A.; Studt, F.; Bligaard, T. Using microkinetic analysis to search for novel anhydrous formaldehyde production catalysts. *Surf. Sci.* **2015**, *641*, 105–111. Kibsgaard, J.; Tsai, C.; Chan, K.; Benck, J. D.; Nørskov, J. K.; Abild-Pedersen, F.; Jaramillo, T. F. Designing an improved transition metal phosphide catalyst for hydrogen evolution using experimental and theoretical trends. *Energy & Environmental Science* **2015**, *8*, 3022–3029.

100. Tsai, C.; Chan, K.; Nørskov, J. K.; Abild-Pedersen, F. Theoretical Insights into the Hydrogen Evolution Activity of Layered Transition Metal Dichalcogenides. *Surf. Sci.* **2015**, *640*, 133–140.
101. Santos, E. J. G.; Nørskov, J. K.; Harutyunyan, A. R.; Abild-Pedersen, F. Toward Controlled Growth of Helicity-Specific Carbon Nanotubes. *J. Phys. Chem. Lett.* **2015**, *6*, 2232–2237.
102. To, J. W. F.; Chen, Z.; Yao, H.; He, J.; Kim, K.; Chou, H.-H.; Pan, L.; Wilcox, J.; Cui, Y.; Bao, Z. Ultrahigh Surface Area Three-Dimensional Porous Graphitic Carbon from Conjugated Polymeric Molecular Framework. *ACS Central Science* **2015**, *1*, 68–76.
103. Rasmussen, D. B.; Christensen, J. M.; Temel, B.; Studt, F.; Moses, P. G.; Rossmeisl, J.; Riisager, A.; Jensen, A. D. Ketene as a Reaction Intermediate in the Carbonylation of Dimethyl Ether to Methyl Acetate over Mordenite. *Angewandte Chemie International Edition* **2015**, *54*, 7261–7264.
104. Xin, H. et al. Strong Influence of Coadsorbate Interaction on CO Desorption Dynamics Probed by Ultrafast X-ray Spectroscopy and Ab Initio Simulations. *Phys. Rev. Lett.* **2015**, *114*, 156101.
105. Wang, H.; Tsai, C.; Kong, D.; Chan, K.; Abild-Pedersen, F.; Nørskov, J. K.; Cui, Y. Transition Metal Doped Edge Sites in Vertically Aligned MoS₂ Catalysts for Enhanced Hydrogen Evolution. *Nano Research* **2015**, *8*, 566–575.
106. Doyle, A. D.; Montoya, J. H.; Vojvodic, A. Improving Oxygen Electrochemistry Through Nanoscopic Confinement. *ChemCatChem* **2015**, *7*, 738–742.
107. Montoya, J. H.; Garcia-Mota, M.; Nørskov, J. K.; Vojvodic, A. Theoretical evaluation of the surface electrochemistry of perovskites with promising photon absorption properties for solar water splitting. *Phys. Chem. Chem. Phys.* **2015**, *17*, 2634–2640.
108. Tsai, C.; Chan, K.; Nørskov, J. K.; Abild-Pedersen, F. Rational design of MoS₂ catalysts: tuning the structure and activity via transition metal doping. *Catalysis Science & Technology* **2015**, *5*, 246–253.
109. Siahrostami, S.; Vojvodic, A. Influence of Adsorbed Water on the Oxygen Evolution Reaction on Oxides. *J. Phys. Chem. C* **2015**, *119*, 1032–1037.

Category III

110. Singh, A.; Montoya, J.H.; Rohr, B.A.; Tsai, C.; Vojvodic, A.; Nørskov, J.K.. Computational Design of Active Site Structures with Improved Transition-State Scaling for Ammonia Synthesis. *ACS Catalysis*, **2018**, *8*, 4017-4024.
111. Higgins, D.; Wette, M.; Gibbons, B.M.; Siahrostami, S.; Hahn, C.; Escudero-Escribano, M.; Garcia-Melchor, M.; Ulissi, Z.; Davis, R.C.; Mehta, A.; Clemens, B.M.; Nørskov, J.K.; Jaramillo, T.F. Copper Silver Thin Films with Metastable Miscibility for Oxygen Reduction Electrocatalysis in Alkaline Electrolytes. *ACS Applied Energy Materials*, **2018**, *1*, 1990-1999.
112. Chen, S.; Chen, Z.; Siahrostami, S.; Kim, T. R.; Nordlund, D.; Sokaras, D.; Nowak, S.; To, J. W. F., Higgins, D.; Sinclair, R.; Nørskov, J.K.; Jaramillo, T.F.; Bao, Z.

- Defective Carbon-Based Materials for the Electrochemical Synthesis of Hydrogen Peroxide. *ACS Sustainable Chemistry & Engineering*, **2018**, *6*, 311-317.
113. Zhao, W.; Doyle, A.D.; Morgan, S.E.; Bajdich, M.; Nørskov, J.K.; Campbell, C.T. Formic Acid Dissociative Adsorption on NiO(111): Energetics and Structure of Adsorbed Formate. *J. Phys. Chem. C*, **121**, 28001-28006.
114. Siahrostami, S.; Jiang, K.; Karamad, M.; Chan, K.; Wang, H.; Nørskov, J. K. Theoretical Investigations into Defected Graphene for electrochemical Reduction of CO₂. *ACS Sustainable Chemistry and Engineering*, **2017**, *5*, 11080-11085.
115. LaRue, J.; Krejci, O.; Yu, L.; Beye, M.; Ng, M. L.; Oberg, H.; Xin, H.; Mercurio, G.; Turner, J. J.; Nordlund, D.; Coffee, R.; Minitti, M.P.; Wurth, W.; Pettersson, L.G.M.; Ostrom, H.; Nilsson, A.; Abild-Pedersen, F.; Ogasawara, H. Real-time elucidation of catalytic pathways in CO hydrogenation on Ru. *J. Phys. Chem. Lett.*, **2017**, *8*, 3820-3825.
116. Singh, A. R.; Rohr, B. A.; Schwalbe, J. A.; Cargnello, M.; Chan, K.; Jaramillo, T. F.; Chorkendorff, I.; Nørskov, J. K. Electrochemical Ammonia Synthesis - The Selectivity Challenge. *ACS Catalysis* **2017**, *7*, 706-709.
117. Chen, L. D.; Urushihara, M.; Chan, K.; Nørskov, J. K. Electric Field Effects in Electrochemical CO₂ Reduction. *ACS Catalysis* **2016**, *6*, 7133-7139.
118. Hoffmann, M. J.; Medford, A.; Bligaard, T. Framework for Scalable Adsorbate-Adsorbate Interaction Models. *J. Phys. Chem. C* **2016**, *120*, 13087-13094.

Catalysis Research P.I. Meeting

July 30-August 1, 2018

Participant List

Aaron Appel
Pacific Northwest National Laboratory
Aaron.Appel@pnnl.gov

Simon Bare
SLAC National Accelerator Laboratory
simon.bare@slac.stanford.edu

Bart Bartlett
University of Michigan
bartmb@umich.edu

Wesley Bernskoetter
University of Missouri
bernskoetterwh@missouri.edu

Guy Bertrand
University of California, San Diego
guybertrand@ucsd.edu

Thomas Bligaard
SLAC National Accelerator Laboratory
Bligaard@stanford.edu

Suzanne Blum
University of California, Irvine
blums@uci.edu

Chris Bradley
U.S. Department of Energy/BES
chris.bradley@science.doe.gov

Phillip Britt
Oak Ridge National Laboratory
brittpf@ornl.gov

Charlie Campbell
University of Washington
campbell@chem.washington.edu

Miaofeng Chi
Oak Ridge National Laboratory
chim@ornl.gov

Chris Chang
UC Berkeley/LBNL
chrischang@berkeley.edu

Jingguang Chen
Columbia University/BNL
jgchen@columbia.edu

Amy Cordones-Hahn
SLAC National Accelerator Laboratory
acordon@slac.stanford.edu

David Cox
Virginia Technical Institute
dfcox@vt.edu

Richard Crooks
University of Texas
crooks@cm.utexas.edu

Abhaya Datye
University of New Mexico
datye@unm.edu

Massimiliano Delferro
Argonne National Laboratory
delferro@anl.gov

Zdenek Dohnalek
Pacific Northwest National Laboratory
zdenek.dohnalek@pnnl.gov

Melis Duyar
SLAC National Accelerator Laboratory
melis@stanford.edu

Catalysis Research P.I. Meeting

July 30-August 1, 2018

Participant List

Dan Ess
Brigham Young University
dhe@chem.byu.edu

Chris Fecko
U.S. Department of Energy/BES
Christopher.Fecko@science.doe.gov

Gregory Fiechtner
U.S. Department of Energy/BES/CPIMS
gregory.fiechtner@science.doe.gov

Josh Figueroa
UC San Diego
jsfig@ucsd.edu

Richard Finke
Colorado State University
rfinke@lamar.colostate.edu

Alison Fout
University of Illinois at Urbana-Champaign
fout@illinois.edu

Bruce Gates
University of California Davis
bcgates@ucdavis.edu

Vanda Glezakou
Pacific Northwest National Laboratory
vanda.glezakou@pnl.gov

Raymond Gorte
University of Pennsylvania
gorte@seas.upenn.edu

John Gregoire
CalTech
gregoire@caltech.edu

Oliver Yair Gutierrez Tinoco
Pacific Northwest National Laboratory
oliver.gutierrez@pnnl.gov

Alexander Harris
Brookhaven National Laboratory
alexh@bnl.gov

Nilay Hazari
Yale University
nilay.hazari@yale.edu

Andreas Heyden
University of South Carolina
heyden@cec.sc.edu

Stephan Irle
Oak Ridge National Laboratory
irles@ornl.gov

Seung Soon Jang
Georgia Institute of Technology
seungsoon.jang@mse.gatech.edu

Michael Janik
Penn State University
mjj13@psu.edu

Tom Jaramillo
SLAC National Accelerator Laboratory
jaramillo@stanford.edu

Cynthia Jenks
Argonne National Laboratory
cjenks@anl.gov

Chris Jones
Georgia Institute of Technology
christopher.jones@chbe.gatech.edu

Bill Jones
University of Rochester
wjones@ur.rochester.edu

Alex Katz
UC Berkeley
askatz@berkeley.edu

Catalysis Research P.I. Meeting

July 30-August 1, 2018

Participant List

Paul King
NREL
Paul.King@nrel.gov

John Kitchin
Carnegie Mellon University
jkitchin@andrew.cmu.edu

Johannes Lercher
Pacific Northwest National Laboratory
Johannes.Lercher@pnnl.gov

Cong Liu
Argonne National Laboratory
congliu@anl.gov

Ping Liu
Brookhaven National Laboratory
pingliu3@bnl.gov

Raul Lobo
University of Delaware
lobo@udel.edu

Manos Mavrikakis
University of Wisconsin
manos@engr.wisc.edu

Eric McFarland
UC Santa Barbara
ewmcfar@engineering.ucsb.edu

Will Medlin
University of Colorado-Boulder
medlin@colorado.edu

Dan Mindiola
University of Pennsylvania
mindiola@sas.upenn.edu

Raul Miranda
U.S. Department of Energy/BES
raul.miranda@science.doe.gov

Karl Mueller
Pacific Northwest National Laboratory
karl.mueller@pnnl.gov

Buddie Mullins
UT Austin
mullins@che.utexas.edu

Matthew Neurock
University of Minnesota
mneurock@umn.edu

Eranda Nikolla
Wayne State University
erandan@wayne.edu

Jack Norton
Columbia University
jrn11@columbia.edu

Colin Nuckolls
Columbia University
cn37@columbia.edu

Ted Oyama
Virginia Technical Institute
oyama@vt.edu

Marek Pruski
Ames Laboratory
marek@ameslab.gov

Daniel Resasco
University of Oklahoma
resasco@ou.edu

Fabio Ribeiro
Purdue University
fabio@purdue.edu

Jose Rodriguez
Brookhaven National Laboratory
rodriguez@bnl.gov

Catalysis Research P.I. Meeting

July 25-28, 2017

Participant List

Yuriy Roman
Massachusetts Institute of Technology
yroman@mit.edu

Aaron Sadow
Ames Laboratory
sadow@iastate.edu

Melanie Sanford
University of Michigan
mssanfor@umich.edu

William Schneider
University of Notre Dame
wschneider@nd.edu

Viviane Schwartz
U.S. Department of Energy/BES/Catalysis
viviane.schwartz@science.doe.gov

Annabella Selloni
Princeton University
aselloni@princeton.edu

Sanjaya Senanayake
Brookhaven National Laboratory
ssenanay@bnl.gov

Carsten Sievers
Georgia Institute of Technology
carsten.sievers@chbe.gatech.edu

Igor Slowing
Ames Laboratory
islowing@iastate.edu

Milton Smith
Michigan State University
smithmil@msu.edu

Robert Stack
U.S. Department of Energy
Robert.Stack@science.doe.gov

Steve Suib
University of Connecticut
Steven.Suib@uconn.edu

Jin Suntivich
Cornell University
jsuntivich@cornell.edu

Yogi Surendranath
MIT
yogi@mit.edu

Wendy Shaw
Pacific Northwest National Laboratory
wendy.shaw@pnnl.gov

Charlie Sykes
Tufts University
Charles.Sykes@tufts.edu

Steve Tait
Indiana University
tait@indiana.edu

Bob Waymouth
Stanford University
waymouth@stanford.edu

Ross Widenhoefer
Duke University
ross.widenhoefer@duke.edu

Bin Wang
University of Oklahoma
wang_cbme@ou.edu

Michael White
Brookhaven National Laboratory
mgwhite@bnl.gov

Zili Wu
Oak Ridge National Laboratory
wuz1@ornl.gov

Catalysis Research P.I. Meeting

July 30-August 1, 2018

Participant List

Bingjun Xu
University of Delaware
bxu@udel.edu

Ye Xu
Louisiana State University
yexu@lsu.edu

Cover images courtesy of: Ged Parkin (Columbia), Jingguang Chen (BNL),
Suzanne Blum (UC Irvine), and Charlie Sykes (Tufts).



U.S. DEPARTMENT OF
ENERGY

Office of
Science